ISBN 0-315-69404-1

DOLOMITIZATION, BRECCIATION AND ZINC MINERALIZATION AND THEIR PARAGENETIC, STRATIGRAPHIC AND STRUCTURAL RELATIONSHIPS IN THE UPPER ST. GEORGE GROUP (ORDOVICIAN) AT DANIEL'S HARBOUR, WESTERN NEWFOUNDLAND

THOMAS EDWARD LANE, M.Sc.

NOTICE

The quality of this microform is heavily dependent upon the quality of the original thesis submitted for microfilming. Every effort has been made to ensure the highest quality of reproduction possible.

If pages are missing, contact the university which granted the degree.

Some pages may have indistinct print especially if the original pages were typed with a poor typewriter ribbon or if the university sent us an inferior photocopy.

Reproduction in full or in part of this microform is governed by the Canadian Copyright Act, R.S.C. 1970, c. C-30, and subsequent amendments.

AVIS

La qualité de cette microforme dépend grandement de la qualité de la thèse soumise au microfilmage. Nous avons tout fait pour assurer une qualité supérieure de reproduction.

S'il manque des pages, veuillez communiquer avec l'université qui a conféré le grade.

La qualité d'impression de certaines pages peut laisser à désirer, surtout si les pages originales ont été dactylographiées à l'aide d'un ruban usé ou si l'université nous a fait parvenir une photocopie de qualité inférieure.

La reproduction, même partielle, de cette microforme est soumise à la Loi canadienne sur le droit d'auteur, SRC 1970, c. C-30, et ses amendements subséquents.

ISBN 0-315-69404-1

DOLOMITIZATION, BRECCIATION AND ZINC MINERALIZATION AND THEIR PARAGENETIC, STRATIGRAPHIC AND STRUCTURAL RELATIONSHIPS IN THE UPPER ST. GEORGE GROUP (ORDOVICIAN) AT DANIEL'S HARBOUR, WESTERN NEWFOUNDLAND

by

(c) Thomas Edward Lane, M.Sc.

A thesis submitted to the School of Graduate Studies in partial fulfillment of the requirements for the degree of Doctor of Philosophy

Department of Earth Sciences
Memorial University of Newfoundland

January 1990

St. John's, Newfoundland

ABSTRACT

The sphalerite deposit at Newfoundland Zinc Mines near Daniels Harbour, western Newfoundland is situated in the upper part of the Lower Ordovician St. George Group, a complex of dolostones, limestones and breccias in the middle of a Lower Paleozoic shallow-water, carbonate platform sequence. It is a zinc-dominated Mississippi Valley Type (MVT) deposit, a subtype of MVTs that is characteristic of the Appalachians. This study shows that zinc mineralization occurred during one phase of a complex history of repeated dolomitization and fracturing of the host carbonates along northeast-trending lineaments. This history is interpreted through an integrated analysis of the sedimentologic, stratigraphic and structural framework, petrography, cathodoluminescence and geochemistry.

The upper St. George Group carbonates were deposited along the edge of the tropical Iapetus Ocean during Early to early Middle Ordovician time when the passive continental margin began to experience the initial effects of plate convergence. Shallow subtidal muddy carbonates (Catoche Formation) shallowed upwards into restricted-water, rhythmically interbedded peloidal grainstones and mudstones (Peloidal or Costa Bay Member) and peritidal laminites and burrow-mottled mudstones (Aguathuna Formation). Deformation and fragmentation of the platform and marine regression during early Middle Ordovician time resulted in the regional St. George Unconformity and the formation of rock-matrix breccias from subsurface karst. The mine stratigraphy records a minimum

of 5 stages of faulting, subsurface dissolution and erosion of the platform at this time. The platform was gradually flooded during Middle Ordovician time as the upper member of the Aguathuna Formation and limestones of the Table Point Formation were deposited over the St. George Unconformity. Continued convergence of the continental margin caused collapse of the platform and generation of a foreland basin in which a thick sequence of siliciclastic flysch was deposited and eventually overridden by Taconic thrust sheets.

Seven dolomite crystal types or generations (I through VII) crystallized in four major settings. Microcrystalline, **syngenetic** dolostones (I) with enriched ^{18}O replaced subtidal to peritidal mudstones at or near the surface. Some of these dolostones were then incorporated as clasts in conglomerates and solution breccias. Composite **diagenetic** crystals (II) grew during burial forming turbid, replacive cores near surface and clear rims at depths where pressure solution (>300 m) was active. Pore-filling, clear, zoned dolomite cements (III) sealed most remaining porosity in early dolostones.

Epigenetic coarse dolostone/sphalerite (D/S) complexes overprinted the earlier dolomites. They formed around fracture systems as extensive stratabound bodies within, and local discordant bodies across the Catoche Formation. Their development occurred in 5 main stages: (1) Regional compression generated linear, stratabound fracture zones along faults and around rock-matrix breccias. (2) Xenotopic pre-ore dolomites (IV) replaced dolostone-mottled limestones and formed zebra fabrics along fractures. (3) Hydrothermal (140°C mode) ore fluids caused extensive dissolution of carbonates. (4) Sulphides precipitated in two

stages along fracture zones as fracturing, faulting and dissolution continued. (5) Post-ore hydrothermal dolomites (V, VI), dominated by replacive and pore-filling saddle dolomites with depleted ^{18}O, crystallized around widespread, dilatant fractures forming spar breccias, pseudobreccias and coarse sparry dolostones. Faults associated with regional uplift displaced the D/S complexes and formed fluid conduits creating a fourth and final environment for late fault-related, turbid dolomites (VII) which replaced limestones.

The genesis of epigenetic dolostones and sulphides is interpreted to be the result of regional fracturing during the initial stages of the Siluro-Devonian Acadian Orogeny. Rising geothermal gradients generated by structural thickening of the crust probably caused warming of basinal fluids, the release of metals and sulphur from minerals in the sediments and basement and the formation of hydrothermal convection in the sedimentary pile. Steep fractures penetrated the base of the sedimentary pile and enabled fluids to rise directly from basement depths of 4 to 6 km. At the deposit site the warm, buoyant fluids rose to the top of fracture aquifers where they displaced cooler formation waters. Cooling, loss of CO_2, sulphate reduction and/or increased pH probably accounted for sulphide precipitation.

ACKNOWLEDGEMENTS

I wish to thank a number of people who made this study possible. Noel James enthusiastically supervised the thesis. His extensive background in the geology of carbonate rocks and western Newfoundland influenced the direction and scope of this study. He provided partial financial support for laboratory analyses and field work through his NSERC grant. Don Sangster initiated the study in the interest of documenting Canadian carbonate-hosted Pb-Zn deposits. He supplied constant enthusiastic support and brought along experienced MVT geologists during several visits to the mine. Through his authority the Geological Survey of Canada supported the early phases of research. David Strong and Bob Stevens, other members of my advisory committee, strongly supported the work and lent helpful advice during visits to the field area.

Teck Explorations Ltd. and Newfoundland Zinc Mines Ltd. financially and technically supported the majority of the work. Matthew Blecha and John May of Teck Explorations Ltd. gave me an extended leave of absence to carry out the study. The personnel at the mine were exceptionally cooperative in providing access to all areas of the operation. The documentation would not have been possible without the resources of several long-resident geologists on the project: Matthew Blecha, the exploration manager since 1972; Roland Crossley, mine geologist since 1975; and Gerry O'Connell, an exploration geologist since 1974. Active

mining, drilling programs and a compilation project provided new data during the progress of the study. In particular, a drilling program devised by William Bergey of the Teck Corporation helped define the geometry of poorly known rock-matrix breccias.

Mario Coniglio and Doug Haywick provided guidance in the study and description of dolomites and their isotopic chemistry. Doug's work established the regional framework and petrographic guidelines for this study. Eric Mountjoy enthusiastically provided critical and constructive comments. Ian Knight spent many hours in the field and in discussion and critically read the text. Sheila Stenzel carefully edited much of the text and provided useful comments on carbonate sedimentology. Kathi Stait studied the conodont biostratigraphy of the mine area. Russell Quick analyzed the carbon content of some dolostones and discussed ideas on behaviour of oil-field brines in basins. Scott Swinden pursued the analysis and interpretation of the lead isotopic composition of the galenas. Darcy Taylor helped with much of the drafting. Brian Sears and Wilf Marsh contributed their photographic skills. Nancy Fagan and Betty Ann McWilliams typed most of the text. Trevor Payne and Jerome Bennett did essential muscle work of hauling hose and washing underground walls.

I also had the good fortune of many esteemed geologists who visited the essential outcrops. To acknowledge a few: the late Helmut Wedow, the late Wolfgang Krebs, Alan Hoagland, Phil Choquette, Dave Leach, Lanier Rowan, Jon Viets, Joe Briskey, Neil Williams, Ted Muraro, Dwight Bradley, John Grotzinger, Art Slingsby, Dave Symons, Paul Hoffman, Peter Cawood and Tyson Birkett.

The time spent during this study was particularly enjoyable because of the good people of the Daniel's Harbour area and the staff, faculty and students at Memorial University. In particular I want to mention my housemates Paul Myrow, Sheila Stenzel and Sue Webb and Flemming Mengel and Russell Quick, who kept me running and in good health.

TABLE OF CONTENTS

LIST OF TABLES

LIST OF FIGURES

LIST OF PLATES

CHAPTER 1 INTRODUCTION

1.1 GENERAL INTRODUCTION AND SETTING

This study investigates the complex history of dolomitization, brecciation and sulphide mineralization at Newfoundland Zinc Mines (NZM) near the coastal community of Daniel's Harbour in western Newfoundland, Canada (Fig.1.1). The NZM ore body is a typical example of a sphalerite-rich, Mississippi Valley-type (MVT) deposit classified within a subgroup of zinc-rich types characteristic of the Appalachians (Brown, 1967; Hoagland, 1976; Ohle, 1980; Anderson and MacQueen, 1982; Sangster, 1983). Such accumulations are stratabound within sequences of carbonate sedimentary rocks and precipitated from low temperature hydrothermal fluids during post-sedimentary epigenesis of areas hundreds of square kilometres in extent. The Daniel's Harbour deposit is an typical case where the ore is situated adjacent to breccia bodies and collapsed stratigraphy immediately below a regional unconformity. In addition the sphalerite is hosted entirely within dolostones which are dominated by an exceptional abundance of megacrystalline, white sparry dolomite, commonly referred to as baroque or saddle dolomite.

The NZM ore bodies lay within dolostone complexes of the upper Catoche Formation of the Lower Ordovician upper St. George Group, part of a Lower Paleozoic platformal sequence of shallow-water carbonate sedimentary rocks. The sediments accumulated on an extensive carbonate platform, more than 50 km inside the shallow water margin of the "Laurentian" continent. A regional unconformity occurs near the top of

Figure 1.1 Location and Geologic Map of Western Newfoundland showing main geologic terranes, areas of stratigraphic study and locales of main Pb-Zn showings. The distribution of the St. George Group is indicated in vertical stripes. Important Pb-Zn occurrences include Newfoundland Zinc Mines, Trapper (T) prospect, Pikes Feeder Pond (PF), Eddies Cove East (EC), Cape Norman, Twin Ponds (TP), Round Pond (RP), Salmon River (SR) and Goose Arm (GA) in the south. A Pb showing occurs in Silurian carbonates at Turner Ridge (TR) in the White Bay area.

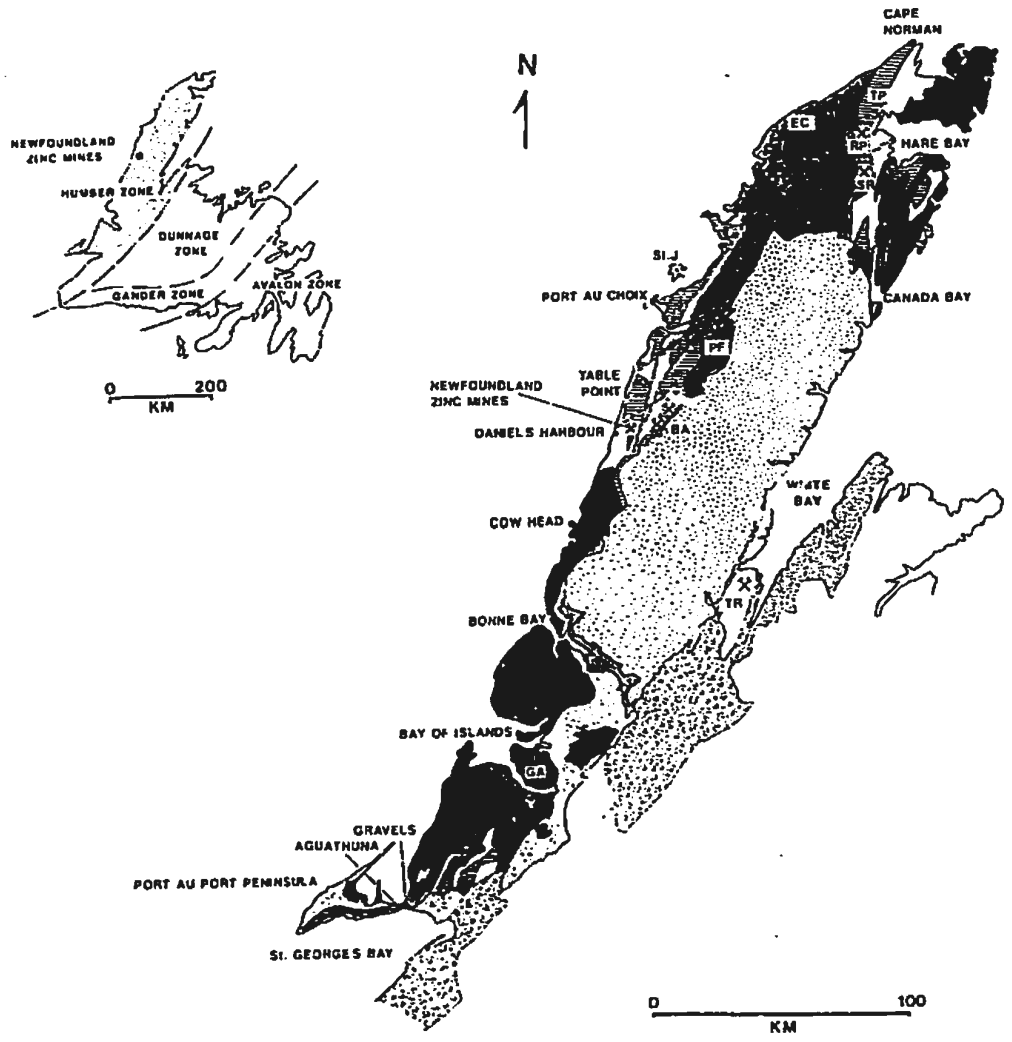

LEGEND

CARBONIFEROUS

- TERRIGENOUS CLASTICS

ALLOCHTHON

- CAMBRO-ORDOVICIAN OPHIOLITES, TERRIGENOUS CLASTICS, CARBONATES

AUTOCHTHON .

- CAMBRO-ORDOVICIAN UNDIVIDED
- ORDOVICIAN CARBONATES/ST. GEORGE GROUP
- CAMBRIAN CARBONATES& TERRIGENOUS CLASTICS
- PRECAMBRIAN GNEISS AND GRANITOIDS
- FLEUR DE LYS SUPERGROUP HADRYNIAN-EARLY ORDOVICIAN ?

the St. George Group beneath the Middle Ordovician Table Head Group. South of NZM the St. George Group is buried beneath Middle Ordovician carbonates of the Table Head Group, siliciclastic rocks of the Goose Tickle Group and imbricated thrust sheets of the Humber Arm Allochthon, which were emplaced during the Middle Ordovician Taconic Orogeny (Fig. 1.2).

Geographically, NZM is situated on the coastal plain of the Great Northern Peninsula of western Newfoundland (Fig. 1.1). The Cambro-Ordovician carbonate rocks and shales underlie a lowland coastal plain which stands 30 to 150 m above sea level and extends from the Gulf of St. Lawrence at Daniel's Harbour 25 km inland to the Long Range Mountains. The Mountains are an inlier of granitoid and gneissic basement of Precambrian age which abruptly rises 600 m above sea level from a fault contact with sedimentary rocks of the coastal plain; and they extend 60 km to the east coast of the Northern Peninsula. Steep faults define the elongate, northeast-trending mountain range which is 200 km long by 60 km wide.

The zinc deposits, 10 km northeast of Daniel's Harbour, are located in an area where the host upper St. George Group is extensively exposed (Fig. 1.3). The coastal plain to the north and east is largely underlain by rocks of the lower St. George Group and of older Cambrian age. In the mine area the upper St. George Group and associated zinc deposits dip gently to the southwest below the Table Head Group to depths greater than 700 m beneath Daniel's Harbour. This monoclinal structure is interrupted by steep, north to northeast-trending faults which vertically displace stratigraphy up to 1000 m.

Figure 1.2 Stratigraphy of the Autochthonous Platformal Rocks of the Humber Zone and Detailed Stratigraphy of Zinc-hosting Rocks in the Daniel's Harbour Mine Area. Enlarged section (right) shows that the sphalerite at Daniel's Harbour occurs within coarse dolostones of the upper Catoche Formation of the St. George Group. Finely crystalline dolostones of the overlying Aguathuna Formation contain several disconformities which correlate with the Sauk/Tippecanoe sequence boundary.

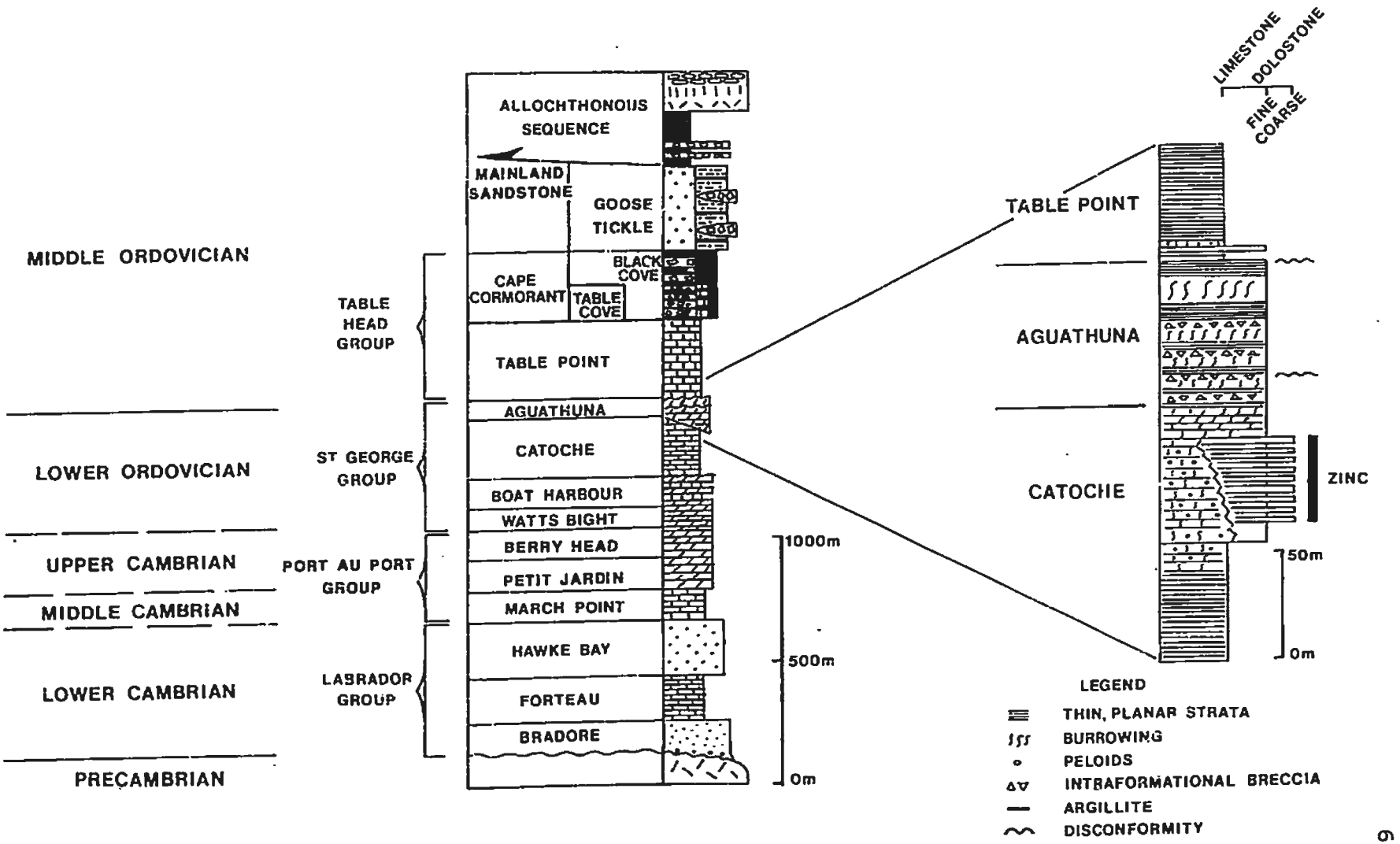
MIDDLE ORDOVICIAN
LOWER ORDOVICIAN
UPPER CAMBRIAN
MIDDLE CAMBRIAN
LOWER CAMBRIAN
PRECAMBRIAN
TABLE HEAD GROUP
ST GEORGE GROUP
PORT AU PORT GROUP
LABRADOR GROUP
ALLOCHTHONOUS SEQUENCE
MAINLAND SANDSTONE
GOOSE TICKLE
BLACK COVE
CAPE CORMORANT
TABLE COVE
TABLE POINT
AGUATHUNA
CATOCHE
BOAT HARBOUR
WATTS BIGHT
BERRY HEAD
PETIT JARDIN
MARCH POINT
HAWKE BAY
FORTEAU
BRADORE
1000m
500m
0m
LIMESTONE
DOLOSTONE
FINE
COARSE
TABLE POINT
AGUATHUNA
CATOCHE
ZINC
50m
0m
LEGEND
THIN, PLANAR STRATA
BURROWING
PELOIDS
INTRAFORMATIONAL BRECCIA
ARGILLITE
DISCONFORMITY

Figure 1.3 Geologic Map and Cross-section of the Daniel's Harbour Region compiled from geologic maps of Newfoundland Zinc Mines, Knight (1985, 1986), Cawood and Williams (1986) and Grenier (1990). FP-1 is the location of a deep drill hole which penetrates the entire St. George Group.

Zinc occurrences are designated as follows:

NZM - Newfoundland Zinc Mines

BD - Black Duck

T - Trapper Prospect

BA - Bill Adam's Showing

PF - Pikes Feeder Pond

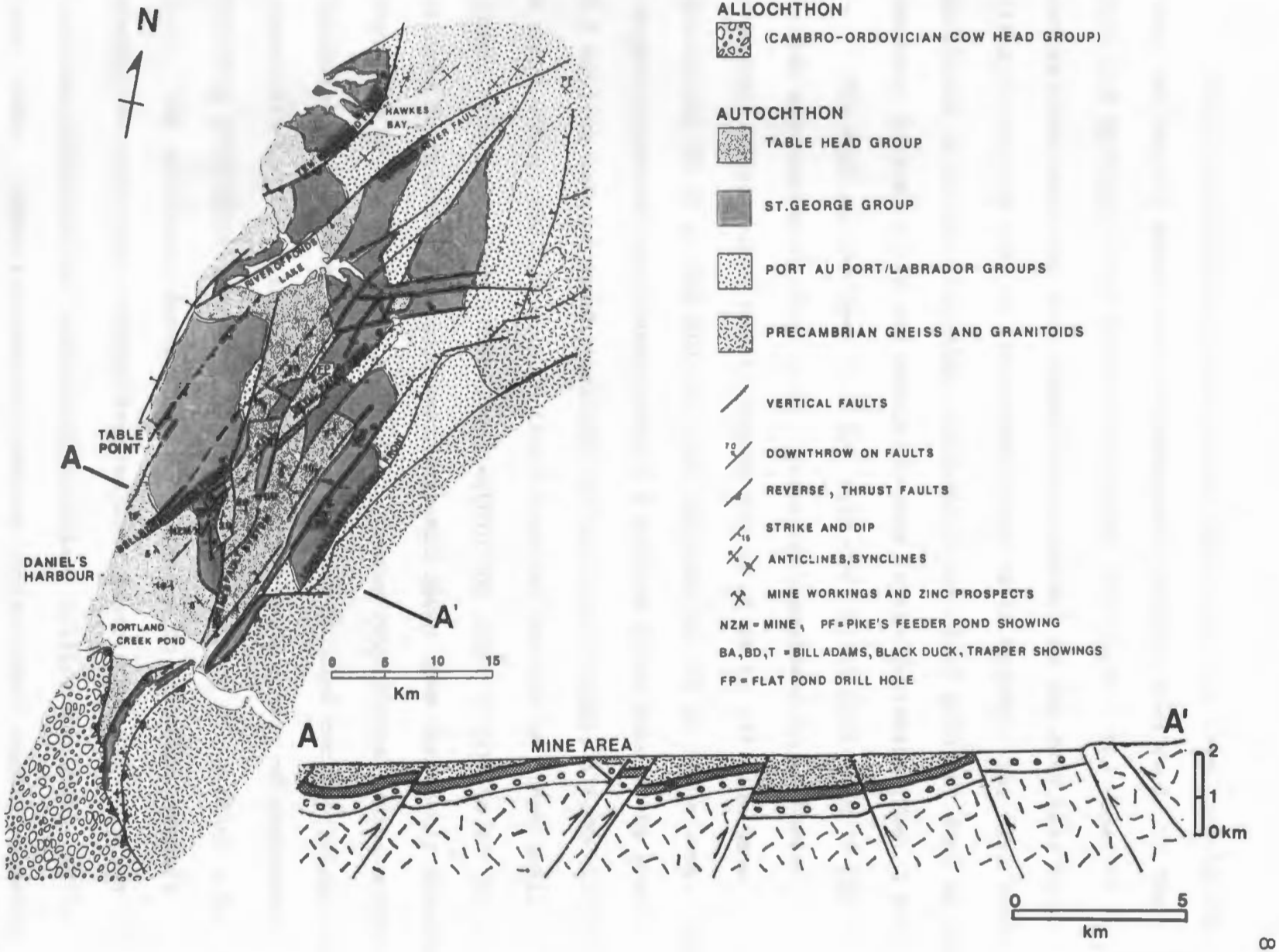
N
HAWKES BAY
RIVER FAULT
RIVER OF PONDS
LAKE
TABLE POINT
A
A'
DANIEL'S HARBOUR
PORTLAND CREEK POND
0 5 10 15
Km
ALLOCHTHON
(CAMBRO-ORDOVICIAN COW HEAD GROUP)
AUTOCHTHON
TABLE HEAD GROUP
ST.GEORGE GROUP
PORT AU PORT/LABRADOR GROUPS
PRECAMBRIAN GNEISS AND GRANITOIDS
VERTICAL FAULTS
DOWNTHROW ON FAULTS
REVERSE , THRUST FAULTS
STRIKE AND DIP
ANTICLINES,SYNCLINES
MINE WORKINGS AND ZINC PROSPECTS
NZM = MINE , PF = PIKE'S FEEDER POND SHOWING
BA,BD,T = BILL ADAMS, BLACK DUCK, TRAPPER SHOWINGS
FP = FLAT POND DRILL HOLE
A
MINE AREA
A'
2
1
0km
0 5
km

NZM is situated in a fault block defined by the coastline to the west, Bellburn's Brook Fault to the north, Brian's Pond Fault to the east and Portland Creek Pond to the south (Fig. 1.3). The upper St. George Group and some zinc deposits are exposed on the Mike Lake Anticline, 2 to 3 km west of the Brian's Pond Fault System. The Mike Lake Anticline is a north-trending, asymmetric open fold with 20° dips on the eastern, faulted flank and gentle 5° dips to the southwest (Fig. 1.4).

The mine encompasses a 16 km^2 area over which more than 15 ore lenses are scattered (Fig. 1.4). These northeastward to eastward-oriented, curvilinear, pencil-shaped bodies of 3% to 12% zinc have dimensions of 10 to 30m wide by 3 to 30m high by 500 to 1000m long. The largely mined-out ore lenses total 7.2 million short tons of 8% zinc, 5.5 million tons of which occurred in the L and T Zones, 470,000 in the A and K Zones, 450,000 tons in the C Zone and 760,000 in other small zones. The bodies are stratabound within the upper 10 to 40m of the Catoche Formation and plunge southwestward 5000m down the gently dipping west limb of the Mike Lake Anticline. Coarse crystalline, white sparry dolomites described as pseudobreccias in vein-riddled rocks envelope the sphalerite bodies which are located around the periphery of northeast-trending structural depressions, faults and fracture zones (Fig. 1.4, 1.5). The structural depressions are elongate to circular, synsedimentary to early post-sedimentary features associated with solution breccias, described as rock-matrix breccias (Collins and Smith, 1975; Lane, 1984). These rock-matrix breccias contain small vague fragments to angular metre-scale blocks of dolostone witha a fine to medium crystalline gray dolomite matrix. Low grade mineralized zones, small

Figure 1.4 Map of Newfoundland Zinc Mines. A map of the distribution of ore zones (black), subeconomic zinc mineralization (stippled), rock-matrix breccias (shaded) and faults of the upper Catoche Formation. Over a dozen ore zones named by letters, lie along faults and the margins of rock-matrix breccias. Structural contours indicate the position of the top of the Catoche Formation (worms marker bed) relative to a datum plane 106 m above sea level. The axis of the north-trending Mike Lake Anticline occurs in the middle of the mine area. Two major steep faults bound the area to the north and east. Ore bodies to the east and west of the anticline plunge below the surface at 5 to 10 degrees. Local stratigraphic collapse occurs over rock-matrix breccias. Section A-A' across the Trout Lake rock-matrix breccia and the main ore body, the L Zone, is illustrated in Fig. 1.5.

Locations are indicated for drill holes A-1, 66, 965, UG 1001 and 1254 from which detailed stratigraphic sections were constructed.

AREA OF NEWFOUNDLAND ZINC MINES

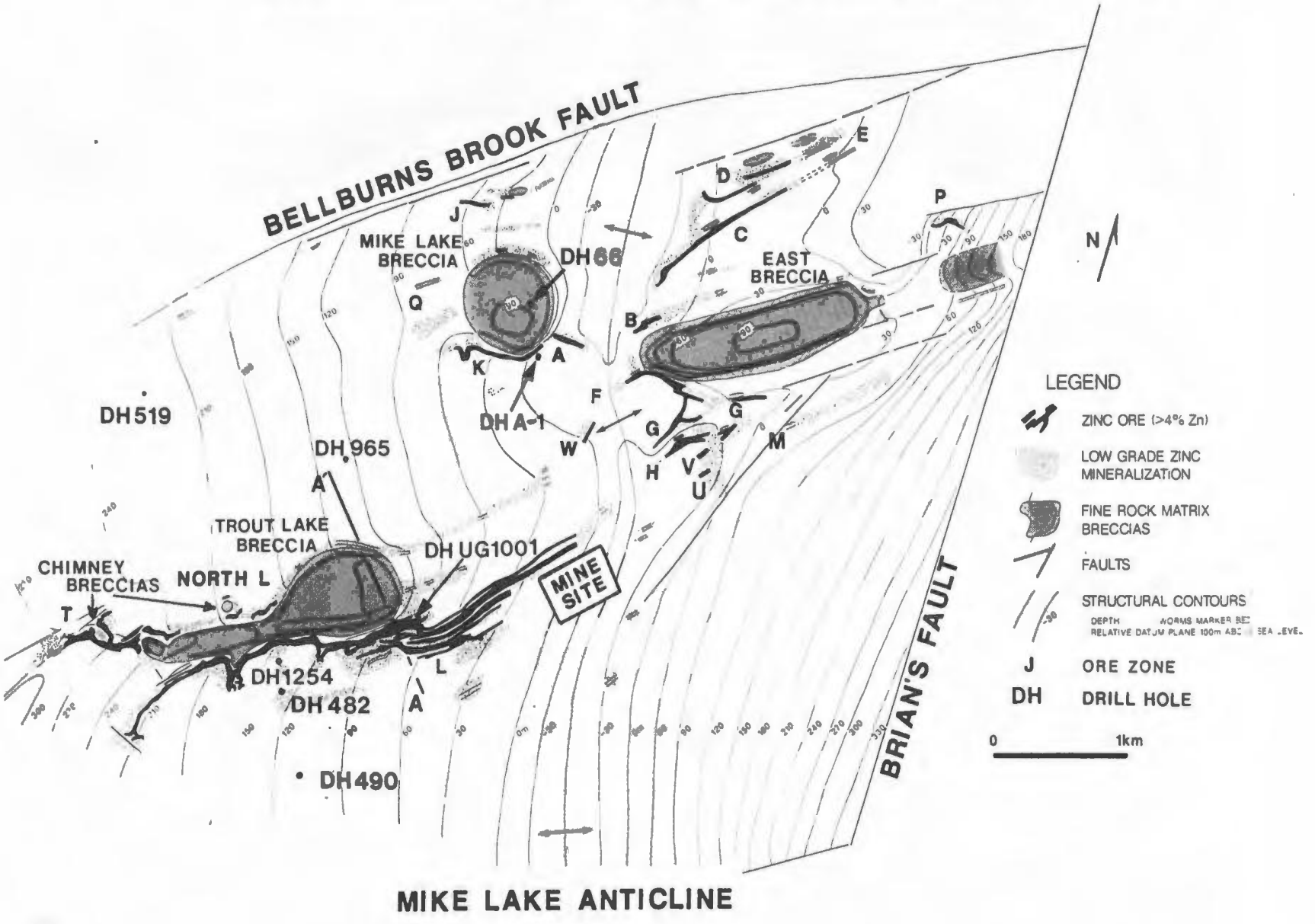

Figure 1.5 Cross-section of the Mine Area

A complex of dolostone bodies comprises most of the upper St. George Group in the mine area. The cross-section transects the L Zone ore body and the Trout Lake rock-matrix breccia (Fig. 1.4). Early dolostone bodies include most of the Aguathuna Formation, rock-matrix breccias and discordant dolostones. Late stratabound, coarse dolostone bodies of pseudobreccia and coarse sparry dolostone in the upper Catoche Formation are associated with zinc sulphides. Discordant, late fault - related dolostones surround faults which displace the other dolostone bodies.

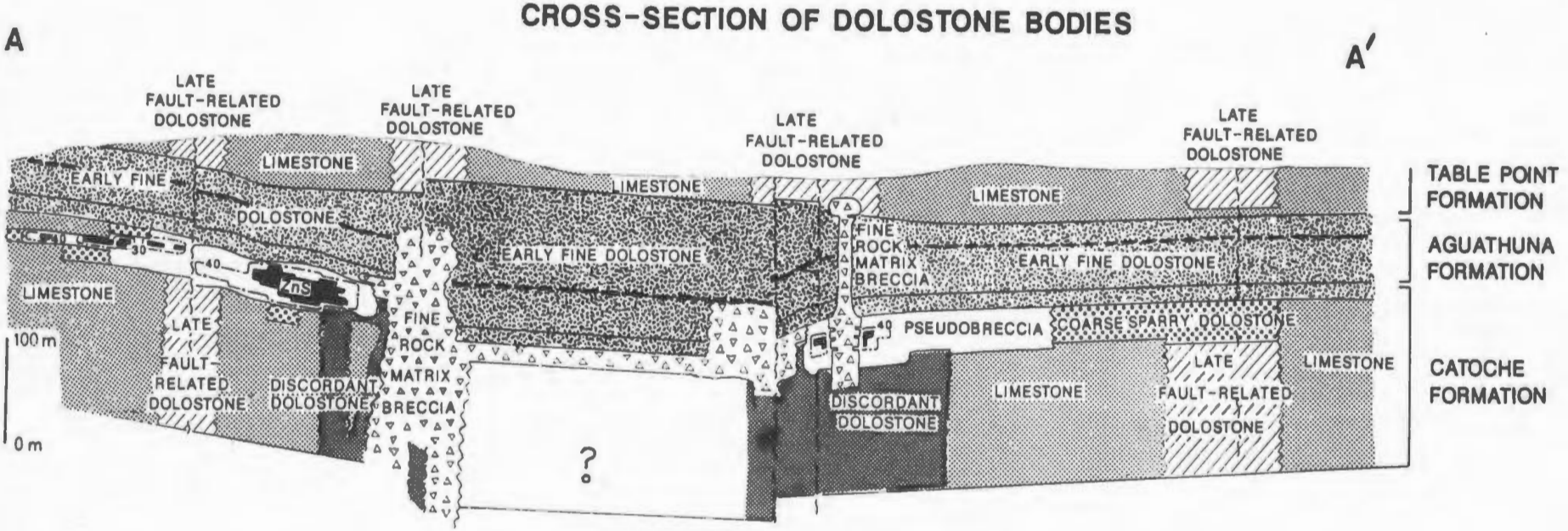
CROSS-SECTION OF DOLOSTONE BODIES
A
A′
LATE FAULT-RELATED DOLOSTONE
LATE FAULT-RELATED DOLOSTONE
LATE FAULT-RELATED DOLOSTONE
LATE FAULT-RELATED DOLOSTONE
LIMESTONE
LIMESTONE
LIMESTONE
EARLY FINE DOLOSTONE
DOLOSTONE
EARLY FINE DOLOSTONE
FINE ROCK MATRIX BRECCIA
EARLY FINE DOLOSTONE
LIMESTONE
30
40
ns
FINE ROCK MATRIX BRECCIA
40
PSEUDOBRECCIA
COARSE SPARRY DOLOSTONE
100 m
0 m
LATE FAULT-RELATED DOLOSTONE
DISCORDANT DOLOSTONE
DISCORDANT DOLOSTONE
LIMESTONE
LATE FAULT-RELATED DOLOSTONE
LIMESTONE
?
TABLE POINT FORMATION
AGUATHUNA FORMATION
CATOCHE FORMATION

scattered occurrences of sphalerites and widespread coarse crystalline saddle dolomites continue 12 km to the northeast and 5 km to the southwest of the mine area along the trend of mineralization.

1.2 History of Mining, Exploration and Previous Study

In 1962 Leitch Gold Mines and Amax Inc. jointly reconnoitered the Cambro-Ordovician carbonate terrain of western Newfoundland for Pb-Zn mineralization similar to regions of Tennessee, Virginia and Pennsylvania. Their efforts resulted in the discovery of the NZM deposits in 1963 when Mike Labchuk found sphalerite outcrops on a lakeshore which became the A Zone. Ira Watson of Leitch Gold Mines introduced much of the local terminology and was responsible for discovery of most of the ore lenses during soil surveys and drilling between 1963 and 1965. Cominco Ltd. optioned the property between 1968 and 1971. Their personnel reexamined drill core and defined a stratigraphic framework for further exploration. During this time period Cumming (1968) of the GSC provided the first published descriptions of the host rock and the regional unconformity. Three years later a Cominco geologist, Jon Collins (1971), described the relationship of sphalerite mineralization to stratigraphy and emphasized the importance of karst breccia bodies. As a result of publications by Collins (1971, 1972) and Collins and Smith (1975) the deposit became a type example of a karst-related ore deposit.

The Teck Corporation acquired Leitch Gold Mines share of the deposit in 1972 and together with Amax Inc. brought the mine into

production in 1975. Mining and exploration drilling continued through 1990 during which time 7.2 million tons were milled. During the early stages of mining Coron (1982) studied the host rocks and the isotopic geochemistry of the sulphides and carbonates. At the same time Dillon (1978) analyzed the trace element geochemistry of the deposit. During the late 1970's and early 1980's comprehensive regional studies of sedimentology, stratigraphy, diagenesis and dolomitization at Memorial University and Newfoundland Department of Mines (Levesque, 1978; Pratt, 1979; Haywick, 1984; Knight and James, 1987) established a regional context with which to relate the NZM deposit.

1.3 Purpose of the Study

The most critical aspect for interpretation of MVT deposits is the understanding of the timing of mineralization. This sense of the temporal also has important implications for the interpretation of dolomitization. This study attempts to put the history of dolomitization, brecciation and sulphide mineralization in perspective through a careful reconstruction of the sedimentary and diagenetic events which produced the complex rocks of the upper Catoche Formation. This approach differs from most previous descriptions of this and other MVT deposits. Those studies largely focus on the geology and geochemistry of the ore-stage rocks. In this study, in contrast, a detailed analysis of the crystal cement history incorporates the ore-stage within a broad spectrum of events which produced the host dolostones.

Dolostones are described and interpreted in a new manner as the

product of several generations of dolomite crystals. This treatment separates the events that occurred during the burial history. In addition, detailed petrography and geochemistry in conjunction with underground mapping and analysis of numerous drill cores have also enabled a revealing reconstruction of the period of ore deposition as a multistage history of structural deformation, brecciation, dolomitization, dissolution and sulphide deposition.

This study should, thus, be an important contribution to the understanding of dolostones, carbonate breccias and MVT deposits. Fifteen or more years of mining and surface drilling and exceptional access to mine workings have allowed the collection of a rare and invaluable record of an MVT deposit. The thorough analysis of the stratigraphy and dolomitization, built on a wealth of previous studies, provides an unusual understanding of the framework of an MVT deposit. The structural setting, probably underemphasized in other MVT deposits, is also highlighted. The study also has important implications for other subjects: (1) cyclic sedimentation on a shallow carbonate platform, (2) regional unconformities and karstification, (3) the origin and classification of dolostones, (4) the origin of carbonate breccias and zebra dolostones and (5) replacement dolomitization by saddle dolomites.

1.4 Organization of the Document

The complex nature of the geology and multistaged nature of the diagenetic history requires the presentation of the subject in six parts, each of which contains several chapters which deal with specific

aspects of the larger topic. The interrelationship of these chapters to the evolution of the deposit is summarized in Fig. 1.6. Part one places NZM within the regional context. The second part establishes the sedimentary and stratigraphic framework of the host rocks, resulting in a new interpretation of shallow carbonate platform sedimentation under the influence of tectonics and eustasy. Part three presents the petrographic and geochemical attributes the various crystal types of dolomites, sulphides and sulphates. This part of the study elaborates a clear, paragenetic sequence of diagenetic events which can generally be grouped into an Ordovician phase of karst formation and dolomitization and a later Siluro-Devonian phase of deep burial dolomitization and ore emplacement. This temporal subdivision provides a convenient framework for the following two sections which cover the nature and interpretation of the rock bodies. Part four outlines the multistage formation and karstification of early dolostones during Ordovician sedimentation and burial. Part five describes and interprets the origin of the economically important sphalerite / dolomite complexes. The final segment, part six, integrates all information into a concise synthesis.

Figure 1.6 Framework of the Study

This graphic relates dolostone development, sphalerites, dolomite/ sphalerite crystal types and breccias to time, sedimentation, burial, pressure solution, solution events and faulting / fracturing. Four major settings are indicated on the event column on the left: (1) Sedimentation was associated with the formation of early fine dolostones, an unconformity and karst breccias. (2) The transition to 1000 m burial (termed early burial) was characterized by the development of stylolites and zoned dolomite crystals to form early burial dolostones and dolostone mottles in limestones. (3) During late burial epigenetic, hydrothermal coarse dolostones and sphalerites formed stratabound bodies around faults and vein systems. (4) During regional uplift late fault-related dolostones replaced limestones along faults. Chapters which describe various aspects of this evolution are indicated on the figure.

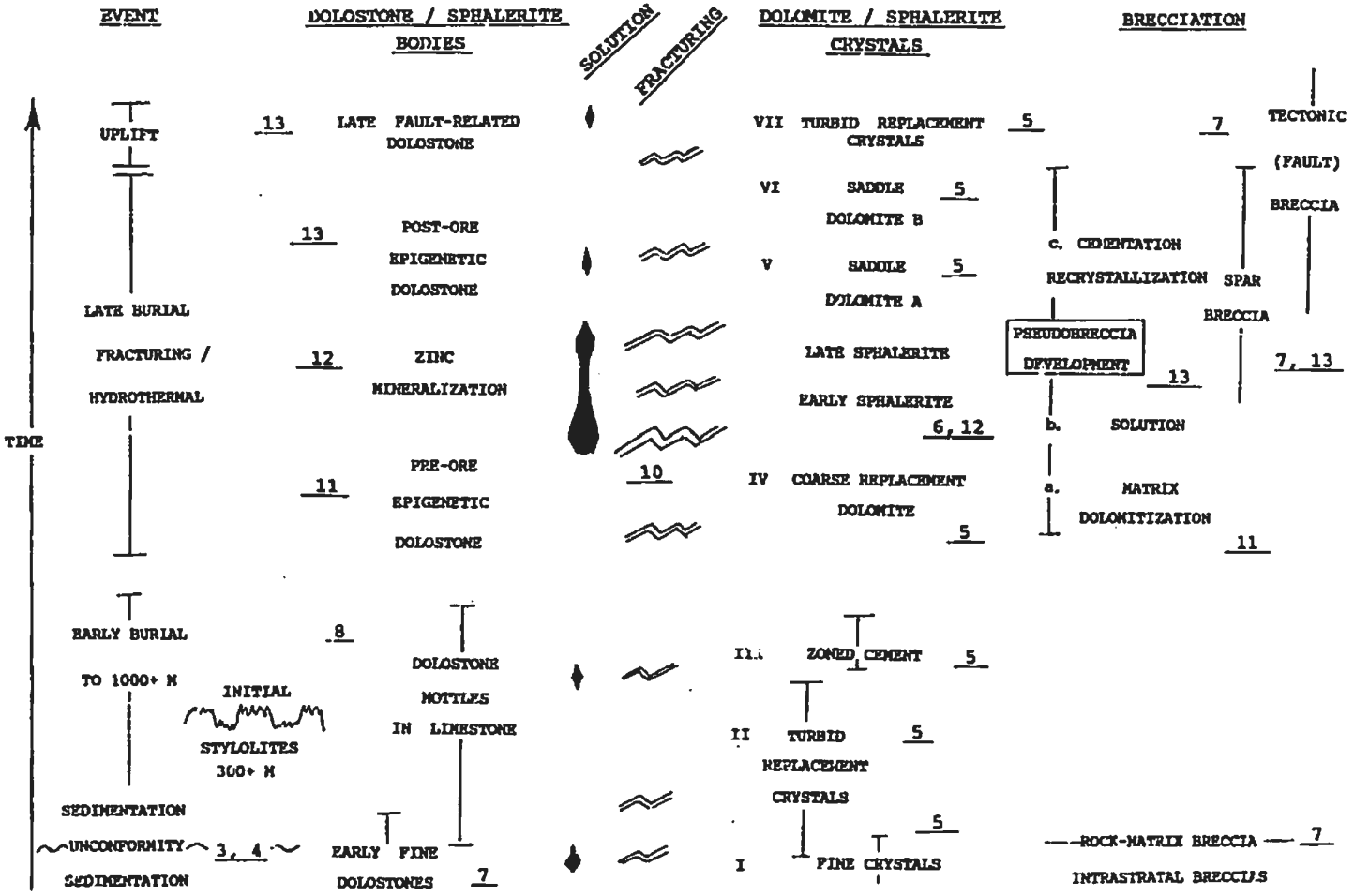
EVENT
DOLOSTONE / SPHALERITE BODIES
SOLUTION
FRACTURING
DOLOMITE / SPHALERITE CRYSTALS
BRECCIATION
TIME
UPLIFT
13
LATE FAULT-RELATED DOLOSTONE
VII TURBID REPLACEMENT CRYSTALS
5
7
TECTONIC (FAULT) BRECCIA
VI SADDLE DOLOMITE B
5
13
POST-ORE EPIGENETIC DOLOSTONE
V SADDLE DOLOMITE A
5
c. CEMENTATION RECRYSTALLIZATION
SPAR BRECCIA
LATE BURIAL FRACTURING / HYDROTHERMAL
12
ZINC MINERALIZATION
LATE SPHALERITE
EARLY SPHALERITE
6, 12
PSEUDOBRECCIA DEVELOPMENT
13
7, 13
b. SOLUTION
10
11
PRE-ORE EPIGENETIC DOLOSTONE
IV COARSE REPLACEMENT DOLOMITE
5
a. MATRIX DOLOMITIZATION
11
EARLY BURIAL
TO 1000+ M
8
DOLOSTONE MOTTLES IN LIMESTONE
III ZONED CEMENT
5
INITIAL STYLOLITES 300+ M
II TURBID REPLACEMENT CRYSTALS
5
SEDIMENTATION
UNCONFORMITY
3, 4
SEDIMENTATION
EARLY FINE DOLOSTONES
7
5
I FINE CRYSTALS
ROCK-MATRIX BRECCIA
7
INTRASTRATAL BRECCIAS

PART I

THE POSITION OF NEWFOUNDLAND ZINC MINES

IN THE REGIONAL SETTING

CHAPTER 2 - REGIONAL SETTING

2.1 Location

The Newfoundland Zinc Mines deposit near Daniel's Harbour lies stratabound within the upper part of the Lower Ordovician St. George Group. These sedimentary carbonates are distributed along the northwest coast of Newfoundland (Fig. 1.1). The St. George Group is part of an autochthonous or parautochthonous sequence of Cambro-Ordovician shallow water platformal sediments which rest unconformably on ca. 1 billion year old Grenvillian basement of high grade granite-gneiss. An allochthonous assemblage of Middle Ordovician Taconic thrust slices of coeval deep-water sediments and ophiolites locally covers the autochthon in the vicinities of the Bay of Islands and Hare Bay (Figs. 1.1, 1.2). This Lower Paleozoic tectono-stratigraphic terrane is referred to as the Humber Zone (Williams, 1978).

Siluro-Devonian Acadian structures deform this tectono-stratigraphic sequence. The Long Range Inlier consists of basement rocks that were uplifted as a northeast-oriented fault block. Paleozoic sediments in surrounding lowlands are gently folded, locally thrusted and dissected by numerous steep faults. Allochthons occupy structural depressions north and south of this basement inlier. Resistant-weathering ophiolites form spectacular table-top highlands in these terrains. Carboniferous sediments unconformably overlie the Lower Paleozoic terrane in the south. They fill pull-apart basins that developed in the vicinity of Deer Lake and St. George Bay (Knight, 1983; Hyde et al, 1988) (Fig. 1.1).

Zinc mineralization as sphalerite is widely scattered throughout the autochthonous Cambro-Ordovician carbonates and in distinctive calcite veins in Carboniferous sediments (Fig. 1.1) (Saunders and Strong, 1986). Sphalerite in the Cambro-Ordovician carbonates is generally associated with coarse dolostones with Newfoundland Zinc Mines as the type example. Here sphalerite occurs in association with megacrystalline white dolomite. The sulphides and dolomites occur in the proximity of faults and in association with a variety of carbonate breccias, some of which are interpreted as karst-related collapse features (Collins and Smith, 1975). The succeeding chapters lay out the nature, framework and relative age of the sulphides and related features.

2.2 Relation of the St. George Group to the Evolution of the Platform

Between latest Precambrian and the Middle Ordovician time, western Newfoundland formed part of the tropical continental margin of ancestral Laurentia. During the Early Ordovician this margin faced south along the Iapetus Ocean (Scotese et al., 1979). Sediments exposed today as the St. George Group accumulated in shallow marine water, probably 50 to 100 km in from the platform margin which possessed a steep edge that shed breccia debris into a deep water basin (James and Stevens, 1986).

The St. George Group records the late history of the rift-drift development of this margin which originated in the late Precambrian when a megacontinent split apart to form the Iapetus Ocean (Williams and Stevens, 1974). Attenuated continental crust subsided as it cooled and

marine sediments onlapped early rift-phase terrestrial siliciclastics (Labrador Group) during rapid early subsidence (Hiscott and Williams, 1978) (Fig. 1.2). Subsequent shallow water, dominantly carbonate, sedimentation kept pace with continued subsidence over the next 50 million years. The platform evolved through three phases (James et al., 1988, 1989): (1) an Early Cambrian ramp covered with abundant terrigenous sediment (Labrador Group); (2) a Middle to Upper Cambrian narrow, 200 km wide platform rimmed by an outer belt of high-energy carbonate sands (Port au Port Group); and (3) a mature, low-energy Lower Ordovician platform characterized by a rimmed margin and extensive carbonate mud deposition over a broad "epeiric" sea (James et al., 1988, 1989).

The Lower Ordovician platform evolved through two sequences or megacycles of progressive deepening followed by shallowing and emergence (Knight and James, 1987). Two worldwide eustatic fluctuations in sea level were probably responsible for these megacycles (Fortey, 1984). Variations in subsidence rates, carbonate production and local tectonism, however, also influenced the development of the sequences. Carbonate production, for example, outpaced subsidence during times of shallow water; and both uplift and faulting accentuated unconformities (Knight and James, 1987).

The upper St. George Group constituted the younger megacycle. Major marine inundation onlapped an emergent platform and the Laurentian craton leaving an upward-deepening sequence of peritidal and subtidal carbonates (upper Boat Harbour and lower Catoche Formations). After maximum transgression the Catoche Formation shallowed upwards into early

dolomitized, peritidal sediments of the Aguathuna Formation.

The stratigraphy of the upper St. George Group and the overlying Table Head and Goose Tickle Groups records convergence of the oceanic lithosphere with the continent. The platform responded by fragmenting, foundering and being buried beneath deep-water sediments and transported rocks of the allochthons. A regional unconformity near the top of the St. George Group coincides with faulting of the platform (Lane, 1984; Knight and James, 1987; Stenzel and James, 1987). Shallow subtidal carbonate sedimentation (Table Head Group) continued during subsidence of a block-faulted platform prior to abruptly foundered into deep water. A succession of deep-water carbonates, shales, conglomerates and sands (upper Table Head Group and Goose Tickle Group) partially filled a foredeep before emplacement of the allochthons (Stenzel and James, 1988).

2.3 Deformational History of the Platform

2.3.1 The Taconic Orogeny and Burial of the St. George Group

Stratigraphy and sedimentology tightly constrain the chronology of the Taconic Orogeny in western Newfoundland. Lower to Middle Ordovician synorogenic sandstones (e.g. Goose Tickle Group) contain detritus which records the progressive westward migration of thrust sheets of oceanic crust (Stevens, 1970). Faulting and foundering of the early Middle Ordovician platform reflects the response of the lithosphere to this westward migration. Emplacement of allochthons is constrained to a 10 million year period between the deposition of foredeep sandstones and unconformable overlap of the Late Ordovician Long Point Group onto the

Humber Arm Allochthon (Stevens, 1970).

Taconic deformation is largely confined to the allochthon (Stevens, 1970). Most deformation occurs along thrust-bounded shale melanges and only penetrates the autochthon far to the east near the Baie Verte Lineament (Cawood et al., 1988).

Burial of the St. George Group reached a maximum between the Late Ordovician and Late Silurian prior to uplift during the Acadian Orogeny. Thermal maturation of conodonts to a CAI of 2 to 2 1/2 implies that the St. George Group at Daniel's Harbour was buried to a depth of 2 to 3 km (Nowlan and Barnes, 1987). A composite overburden of Middle Ordovician sediments (700 m), allochthon (1 - 2 km) and an unknown thickness of Upper Ordovician-Silurian sediment probably account for this maturation. An alternative possibility of shallow burial but an anomalous geothermal gradient has been suggested (Nowlan and Barnes, 1987).

2.3.2 The Acadian Orogeny

Acadian faults and folds affect both the basement and allochthon. Basement thrusts are emergent as the Long Range Front in the Daniel's Harbour area and buried to the south beneath a synclinorium containing the Humber Arm Allochthon (Cawood and Williams, 1986). In the supracrustal rocks steep reverse and normal faults cut asymmetric open folds.

The age of Acadian deformation in western Newfoundland is poorly known. U/Pb ages of zircons in central Newfoundland record Silurian deformation older than 423+/-3 Ma (Dunning et al., 1988). The age of metamorphism near Baie Verte supports a Silurian age of tectonism

(Dallmeyer, 1977; Dallmeyer and Hibbard, 1984). Continued deformation in the Devonian is implied by the Round Head Thrust on the Port au Port Peninsula. This thrust marks the western limit of Acadian deformation since it deforms the Late Silurian (Pridolian) Clam Bank Formation (Williams, 1985). Undeformed early Carboniferous (Visean) are the oldest known sediments to overlap Acadian structures in western Newfoundland (Hyde, 1983).

2.3.3 Carboniferous Structure

High-angle, dip-slip to strike-slip faults dominate Carboniferous structures. Strike slip faults trend northeast and north-northeast. Terrestrial to marine sediments fill moderate-sized basins (the St. Lawrence) and linear "pull-apart" basins (e.g. the Deer Lake and St. George Basins) (Bradley, 1982; Knight, 1983; Hyde et al., 1988).

2.4 Carbonate Diagenesis, Dolomitization and Sulphide Mineralization

Diagenesis and dolomitization affects all carbonate units of the Humber Zone (Pratt, 1979; James and Klappa, 1983; Coniglio, 1985; Haywick, 1984; Chow, 1986; Knight, 1986; Stenzel, in prep.). A relatively uniform pattern of cementation and recrystallization is recognized. Synsedimentary radial fibrous cements are widely observed in specific facies. Early lithification occurs by equant to prismatic calcite cements and widespread neospar recrystallization. Fine crystalline dolostones pre-date compaction (Haywick, 1984; Coniglio, 1985). The onset of pressure solution usually marks the dividing line between

near surface and deep burial diagenesis (cf., Mattes and Mountjoy, 1980). Some fracture-filling blocky calcite spar and most coarse crystalline dolomites post-date and overprint stylolites. Some medium crystalline dolomites line contemporaneous stylolites (Haywick, 1984). Later medium to coarse crystalline dolostones surround late joints and faults and, locally, pervasively replace strata (Haywick, 1984). Distinctive megacrystalline white saddle dolomites are the latest dolomite phases and form the gangue of most lead-zinc occurrences. Late calcite fills vugs and fractures, locally, in association with Carboniferous lead-zinc (Saunders and Strong, 1986).

Regional sulphide mineralization occurs in three settings in western Newfoundland: (1) massive and disseminated sulphides of volcanic exhalatives in Lower Ordovician ocean basin sediments and subsurface stockworks of the Bay of Islands Complex (Swinden et al, 1988); (2) epigenetic, dolomite-hosted, zinc-rich sulphides in the Cambrian to Silurian carbonates of the Humber Zone (Knight, 1984; Saunders and Strong, 1986); and (3) epigenetic lead-zinc sulphides in Carboniferous calcite-healed veins and breccias (Knight, 1983; Saunders and Strong, 1986).

The Daniel's Harbour deposit belongs to the second type of sulphides. This mineralization-type is widely distributed throughout the autochthonous carbonates and cross-cuts into the allochthonous Cow Head Group (Coniglio, 1985). The sulphides are associated with saddle dolomites throughout the stratigraphy (Saunders and Strong, 1986). Mineralization is widespread along particular stratigraphic intervals characterized by coarse dolomites, veins and breccias. Three main

mineralized intervals include: (1) galena and sphalerite in the lower part of the Port-au-Port Group, (2) sphalerite and minor galena at the base of the Boat Harbour Formation and (3) sphalerite at the base and top of the Catoche Formation. Minor sphalerite also occurs in other parts of the Catoche Formation and the base of the Table Head Group (Fig. 1.2) (Knight, 1984; Saunders and Strong, 1986).

2.5 Lithostratigraphy and Sedimentology of the St. George Group

2.5.1 Introduction

The original St. George Series of Schuchert and Dunbar (1934) is redefined and given group status by Knight and James (1987). Burrowed, fossiliferous, muddy carbonates and fine crystalline, peritidal dolostones of the St. George Group are distinguished from the Cambrian Port au Port Group and the Middle Ordovician Table Head Group. The Port au Port Group is poorly fossiliferous, partially siliciclastic and possesses high-energy oolitic facies. The Table Head Group also stands apart. Its rubbly weathering, muddy, skeletal carbonates abruptly overlie peritidal St. George dolostones.

The St. George Group is divided into four formations, in ascending order: the Watts Bight, Boat Harbour, Catoche and Aguathuna Formations (Fig. 2.1) Subtidal to intertidal deposits of the Watts Bight and Catoche Formations underlie peritidal sediments of the Boat Harbour and Aguathuna Formations. Karst unconformities within upper portions of the peritidal units define the tops of the two onlap-offlap megacycles (Knight and James, 1987). The composition and depositional environment

Figure 2.1 Stratigraphy of the St. George Group in the mine area compiled from three drill holes (Flat Pond DDH-1, DDH A-1, DDH 1001) (see Figs. 1.3, 1.4 for drill hole location). Detailed stratigraphy of the upper St. George Group (right) shows key marker beds. Vertical scales measure depth in metres from the top of the St. George Group.

ST.GEORGE GROUP STRATIGRAPHY

(FROM U.S. BORAX DDH-1 FLAT POND,
NZM DDH-A1, UNDERGROUND DDH 1001)

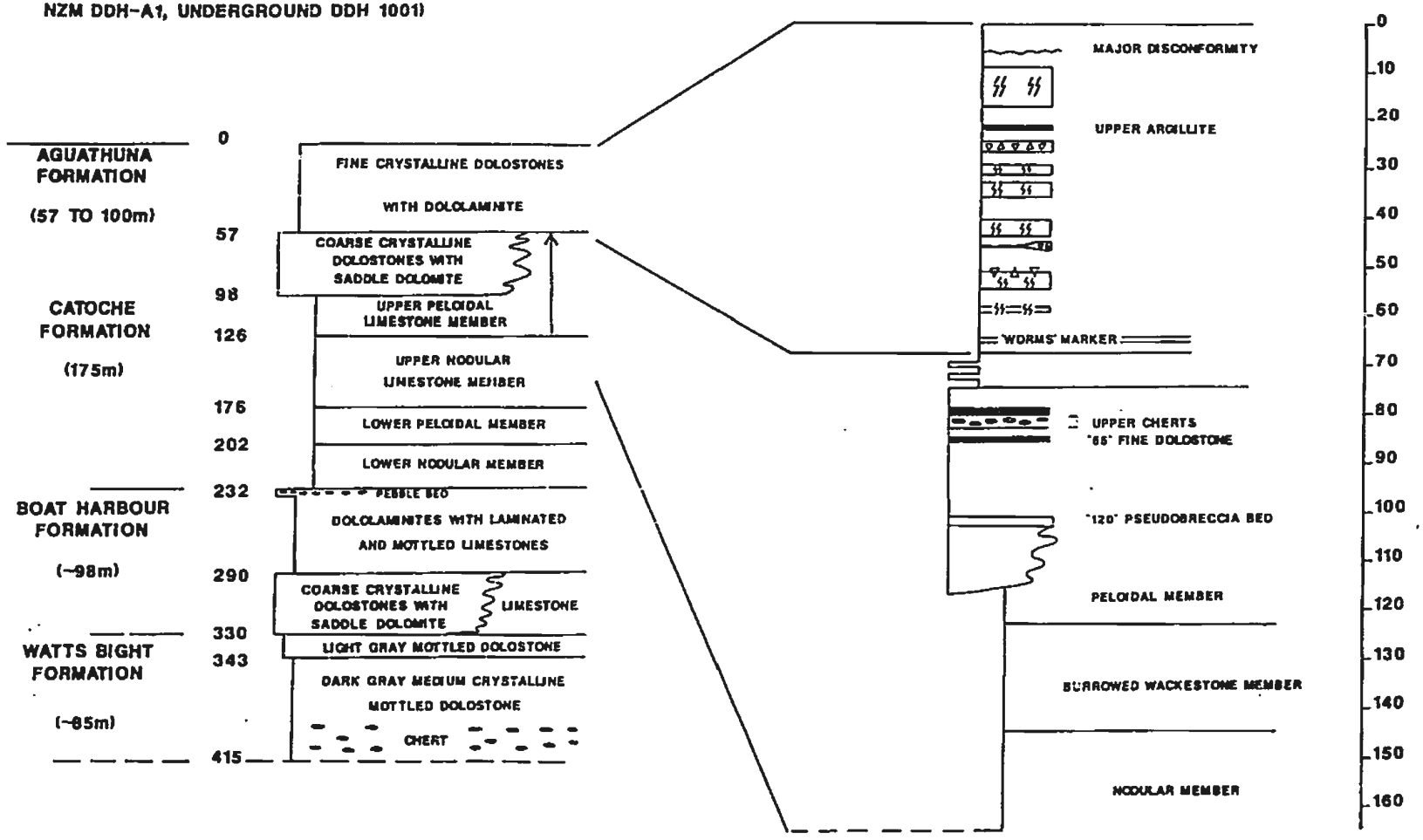

UPPER ST.GEORGE GROUP STRATIGRAPHY

of each formation is summarized below.

2.5.2 Watts Bight Formation (70 - 90 m)

The Watts Bight Formation is characterized by burrow-mottled mudstones and wackestones, some grainstones and common stromatolite and thrombolite mound complexes and associated cherts. Prominent Lichenaria-Renalcis bioherms occur at Green Head (Pratt and James, 1982) on the Port-au-Port Peninsula. The dolomite content of the formation varies from pervasive coarse to fine dolostones on the northwest Northern Peninsula to selective dolomitization on the Port-au-Port Peninsula to 100% limestone at Canada Bay.

Depositional Environment - Quiet subtidal sedimentation of burrowed mudstone and cryptalgal-thrombolite mounds on an open shelf was punctuated by deposition of high energy grainstones. Peritidal mounds formed the base and top of the formation during early marine transgression and late offlap.

2.5.3 Boat Harbour Formation (98 - 156 m)

The Boat Harbour Formation comprises metre-thick repetitive peritidal sequences that grade upwards from bioturbated lime mudstones and wackestones to thrombolites and stromatolites, thinly laminated and lenticular bedded mudstones, thrombolites and stromatolites and locally dololaminite tops. A regional disconformity 17 to 36 metres below the top of the formation is characterized by a lag of chert concretions and pebbles (Knight and James, 1987). The surface is underlain by stratigraphic dolostones, cross-cutting fractures and solution cavities filled

with dolomite-chert breccias (Knight and James, 1987). Peritidal cycles, which overlie the disconformity (the Barbace Cove Member) have distinctive basal grainstones and possess only minor, small mounds. The basal 30 to 50 m of the formation on the Northern Peninsula is extensively brecciated with fine and coarse crystalline dolomite matrix and coarse saddle dolomites which locally host sphalerite.

Depositional Environment - The Boat Harbour Formation is the product of peritidal deposition. Low-energy, muddy sedimentation locally interrupted by cryptalgal or microbial boundstone mounds ranged from subtidal to supratidal environments. Repeated flooding and tidal flat accretion generated shallowing upward cycles. Pratt and James (1986) emphasize the importance of lateral accretion by migrating tidal islands. The platform was exposed, karstified and dolomitized during a eustatic regression. Subsequent marine inundation established mixed sand and mud flats in open shallow-water.

2.5.4 Catoche Formation (160 - 180 m)

The Catoche Formation is a sequence of shallow subtidal carbonates characterized by fossiliferous bioturbated lime mudstones to packstones interrupted by skeletal, intraclast grainstone lenses, thrombolites and algal-metazoan mounds. An abundant benthonic fauna includes trilobites, brachiopods, cephalopods, gastropods and eocrinoids (Fortey, 1979; Knight and James, 1987). Rudstone-filled channels and some mudcracked laminites occur near the base of the formation. Mounds which are locally common in the middle of the formation (Knight, 1986) dominate over 120 metres of section to the east in Hare Bay (Stevens and James,

1976). Characteristic Catoche lithofacies are overlain by 15 to 20 metres of distinctive peloidal and fenestral limestones (Costa Bay Member) on the Port-au-Port Peninsula and the Northern Peninsula (Knight, 1986; Knight and James, 1987).

Portions of the Catoche Formation are pervasively dolomitized. Coarse dolostones that are associated with sphalerites replace the upper 30 to 60 m of the formation on the Northern Peninsula. Elsewhere, individual beds and mottles are selectively dolomitized. The entire formation is dolomitized near fault zones (Knight, 1985, 1986). Rock-matrix breccias within dolostone complexes are associated with collapsed upper St. George stratigraphy related to karst (Collins and Smith, 1975; Lane, 1984; Knight and James, 1987).

Depositional Environment - The Catoche Formation was characterized by quiet, muddy deposition on a shallow subtidal open shelf which was frequently interrupted by storm-deposited thin skeletal, intraclastic grainstones. Algal-metazoan mound complexes formed an energy-dissipating barrier on the outer shelf, while scattered thrombolite mounds flourished on the muddy leeward platform. As the platform shoaled burrowed peloidal wackestone to packstones and fenestral mudstones accumulated in low energy environments and formed shallow water subtidal to peritidal cycles.

2.5.5 Aguathuna Formation (5 - 110 m)

The Aguathuna Formation consists of a sequence of cyclic peritidal sediments including burrowed lime to dolomitic mudstones, dololaminites, mud-cracked dolomitic green shales, stratabound breccias and cherts.

The entire formation is dolomitized in the Daniel's Harbour area, but only partially altered at Port-au-Port. The various lithologies are repeated in the following upward sequence: chert and breccia, laminites with shales, partially burrow-mottled and burrow-mottled mudstones. Based on this pattern, Collins and Smith (1975) termed the formation the "Cyclic Dolomites".

Several disconformities interrupt the formation. Erosional surfaces, thin shales and chert pebbles are associated with intraformational breccias (Collins and Smith, 1975; Lane, 1984; Knight, 1985). A regional disconformity, 5 to 15 m below the top of the formation also marks a significant biostratigraphic break (Stait, 1988). This disconformity is well exposed at Aguathuna Quarry, Port-au-Port, as an erosional surface with 16 m of relief (Cumming, 1968; Pratt, 1979; Haywick, 1984; James et al., 1988). A distinctive 3 to 50 m thick unit of fine crystalline, calcareous dolostone, quartz pebble beds, limestones and shales overlies this disconformity in the Daniel's Harbour area and is informally referred to as the upper member of the Aguathuna Formation. The extreme variations in thickness of the formation are related to one or more phenomena: (1) differential rates of sedimentation on a faulted platform, (2) erosion of faulted stratigraphy and (3) filling of a karst topography.

Depositional Environment - During deposition of the Aguathuna Formation periodic flooding and vertical and lateral sediment accretion on a peritidal platform produced cyclic repetition of lithologies and exposure surfaces. Varying rates of sedimentation and erosion on a block faulted platform produced the variable (0 to 110 m) formational

thicknesses. Much or all of the formation was altered to fine crystalline dolomites of syngenetic or near surface origin.

2.6 Biostratigraphy of the St. George Group

The biostratigraphy of the St. George Group is based on correlation of its mid-continent trilobite and conodont faunas with the Ibex area of Utah. In the western U.S.A. the Ross-Hintze trilobite zones (Hintze, 1951) have a parallel conodont stratigraphy (Ethington and Clark, 1981; Ross et al, 1982). This biostratigraphy is correlated with and supported by numerous North American localities (Ethington and Clark, 1981; Ross et al., 1982).

The St. George Group ranges in age from early Canadian (Gasconadian) through early Whiterockian (Fig. 2.2). Rare zone fossils in the Watts Bight Formation are Gasconadian (Boyce, 1983). Trilobites of the Boat Harbour Formation correlate with Ross-Hintze trilobite zones E and F in New York and Utah, indicating a Middle Canadian (Demingian) age (Fig. 2.2) (Boyce, 1983). The disconformity near the top of the Boat Harbour Formation coincides with the absence of Ross-Hintze trilobite zone G, (Boyce, 1983). The upper 20 m of the Boat Harbour Formation contains upper zone G_2 trilobite Benthamaspis hintzei. Trilobite fauna of the Catoche Formation include diagnostic Ross-Hintze zone G2 and H species: Benthamaspis gibberula Billings, Carolinites genacinaca, Strigigenalis caudata Billings (Fortey, 1979; Boyce, 1985). These fossils give the Catoche Formation a late Canadian (Cassinian) age.

Diagnostic zonal shelly fossils are rare or lacking in the upper

Figure 2.2 Biostratigraphy of the St. George Group

The biostratigraphy of graptolites, brachiopods, trilobites and conodonts is related to the lithostratigraphy of the St. George Group and lower Table Point Formation and Ordovician chronostratigraphic units.

STAGE
GRAPTOLITES
ZONE
LOCAL FOSSILS
BRACHIOPODS
ZONE
LOCAL FOSSILS
TRILOBITES
ZONE
LOCAL FOSSILS
CONODONTS
ZONE
LOCAL FOSSILS
LITHOSTRATIGRAPHY
LLANVIRN
WHITEROCKIAN
UPPER
LOWER
ARENIG
CANADIAN
IBEXIAN
Paraglossograptus "tetragonis" (tentaculatus)
Isograptus victoriae
Didymograptus bifidus
Didymograptus protobifidus
Tetragraptus fruticosus
Tetragraptus accrescens
Diplograptus decoratus
Didymograptus (Expansograptus) extensus
Glossograptus ciliata (Hall)
ORTHIDIELLA
ANOMALORTHIS
Acanthobole expansa
Acanthobole aurora Billings
N
M
L
K
J
I
H
G2
G1
F
E
D
C
B
Bathenia cyclops
Pseudagnostus barrandei
Acidaspis cf. A. speciosa
Bathenia diminutiva Hintze
Ptychagnostus gibbus
Peltabellia gracilis
Bathenia sibirica
Ptychagnostus atavus
Hypagnostus parvifrons
Ptychagnostus punctuosus
Ptychagnostus intermedius
Ptychagnostus praecurrens
Goniagnostus nathorsti
Triarthrus eatoni
Triarthrus spinosus
Triarthrus beckii
Triarthrus sp. A
Triarthrus sp. B
Triarthrus sp. C
Triarthrus sp. D
Triarthrus sp. E
Triarthrus sp. F
Triarthrus sp. G
Triarthrus sp. H
Triarthrus sp. I
Triarthrus sp. J
Triarthrus sp. K
Triarthrus sp. L
Triarthrus sp. M
Triarthrus sp. N
Triarthrus sp. O
Triarthrus sp. P
Triarthrus sp. Q
Triarthrus sp. R
Triarthrus sp. S
Triarthrus sp. T
Triarthrus sp. U
Triarthrus sp. V
Triarthrus sp. W
Triarthrus sp. X
Triarthrus sp. Y
Triarthrus sp. Z
Triarthrus sp. AA
Triarthrus sp. AB
Triarthrus sp. AC
Triarthrus sp. AD
Triarthrus sp. AE
Triarthrus sp. AF
Triarthrus sp. AG
Triarthrus sp. AH
Triarthrus sp. AI
Triarthrus sp. AJ
Triarthrus sp. AK
Triarthrus sp. AL
Triarthrus sp. AM
Triarthrus sp. AN
Triarthrus sp. AO
Triarthrus sp. AP
Triarthrus sp. AQ
Triarthrus sp. AR
Triarthrus sp. AS
Triarthrus sp. AT
Triarthrus sp. AU
Triarthrus sp. AV
Triarthrus sp. AW
Triarthrus sp. AX
Triarthrus sp. AY
Triarthrus sp. AZ
Triarthrus sp. BA
Triarthrus sp. BB
Triarthrus sp. BC
Triarthrus sp. BD
Triarthrus sp. BE
Triarthrus sp. BF
Triarthrus sp. BG
Triarthrus sp. BH
Triarthrus sp. BI
Triarthrus sp. BJ
Triarthrus sp. BK
Triarthrus sp. BL
Triarthrus sp. BM
Triarthrus sp. BN
Triarthrus sp. BO
Triarthrus sp. BP
Triarthrus sp. BQ
Triarthrus sp. BR
Triarthrus sp. BS
Triarthrus sp. BT
Triarthrus sp. BU
Triarthrus sp. BV
Triarthrus sp. BW
Triarthrus sp. BX
Triarthrus sp. BY
Triarthrus sp. BZ
Triarthrus sp. CA
Triarthrus sp. CB
Triarthrus sp. CC
Triarthrus sp. CD
Triarthrus sp. CE
Triarthrus sp. CF
Triarthrus sp. CG
Triarthrus sp. CH
Triarthrus sp. CI
Triarthrus sp. CJ
Triarthrus sp. CK
Triarthrus sp. CL
Triarthrus sp. CM
Triarthrus sp. CN
Triarthrus sp. CO
Triarthrus sp. CP
Triarthrus sp. CQ
Triarthrus sp. CR
Triarthrus sp. CS
Triarthrus sp. CT
Triarthrus sp. CU
Triarthrus sp. CV
Triarthrus sp. CW
Triarthrus sp. CX
Triarthrus sp. CY
Triarthrus sp. CZ
Triarthrus sp. DA
Triarthrus sp. DB
Triarthrus sp. DC
Triarthrus sp. DD
Triarthrus sp. DE
Triarthrus sp. DF
Triarthrus sp. DG
Triarthrus sp. DH
Triarthrus sp. DI
Triarthrus sp. DJ
Triarthrus sp. DK
Triarthrus sp. DL
Triarthrus sp. DM
Triarthrus sp. DN
Triarthrus sp. DO
Triarthrus sp. DP
Triarthrus sp. DQ
Triarthrus sp. DR
Triarthrus sp. DS
Triarthrus sp. DT
Triarthrus sp. DU
Triarthrus sp. DV
Triarthrus sp. DW
Triarthrus sp. DX
Triarthrus sp. DY
Triarthrus sp. DZ
Triarthrus sp. EA
Triarthrus sp. EB
Triarthrus sp. EC
Triarthrus sp. ED
Triarthrus sp. EE
Triarthrus sp. EF
Triarthrus sp. EG
Triarthrus sp. EH
Triarthrus sp. EI
Triarthrus sp. EJ
Triarthrus sp. EK
Triarthrus sp. EL
Triarthrus sp. EM
Triarthrus sp. EN
Triarthrus sp. EO
Triarthrus sp. EP
Triarthrus sp. EQ
Triarthrus sp. ER
Triarthrus sp. ES
Triarthrus sp. ET
Triarthrus sp. EU
Triarthrus sp. EV
Triarthrus sp. EW
Triarthrus sp. EX
Triarthrus sp. EY
Triarthrus sp. EZ
Triarthrus sp. FA
Triarthrus sp. FB
Triarthrus sp. FC
Triarthrus sp. FD
Triarthrus sp. FE
Triarthrus sp. FF
Triarthrus sp. FG
Triarthrus sp. FH
Triarthrus sp. FI
Triarthrus sp. FJ
Triarthrus sp. FK
Triarthrus sp. FL
Triarthrus sp. FM
Triarthrus sp. FN
Triarthrus sp. FO
Triarthrus sp. FP
Triarthrus sp. FQ
Triarthrus sp. FR
Triarthrus sp. FS
Triarthrus sp. FT
Triarthrus sp. FU
Triarthrus sp. FV
Triarthrus sp. FW
Triarthrus sp. FX
Triarthrus sp. FY
Triarthrus sp. FZ
Triarthrus sp. GA
Triarthrus sp. GB
Triarthrus sp. GC
Triarthrus sp. GD
Triarthrus sp. GE
Triarthrus sp. GF
Triarthrus sp. GG
Triarthrus sp. GH
Triarthrus sp. GI
Triarthrus sp. GJ
Triarthrus sp. GK
Triarthrus sp. GL
Triarthrus sp. GM
Triarthrus sp. GN
Triarthrus sp. GO
Triarthrus sp. GP
Triarthrus sp. GQ
Triarthrus sp. GR
Triarthrus sp. GS
Triarthrus sp. GT
Triarthrus sp. GU
Triarthrus sp. GV
Triarthrus sp. GW
Triarthrus sp. GX
Triarthrus sp. GY
Triarthrus sp. GZ
Triarthrus sp. HA
Triarthrus sp. HB
Triarthrus sp. HC
Triarthrus sp. HD
Triarthrus sp. HE
Triarthrus sp. HF
Triarthrus sp. HG
Triarthrus sp. HH
Triarthrus sp. HI
Triarthrus sp. HJ
Triarthrus sp. HK
Triarthrus sp. HL
Triarthrus sp. HM
Triarthrus sp. HN
Triarthrus sp. HO
Triarthrus sp. HP
Triarthrus sp. HQ
Triarthrus sp. HR
Triarthrus sp. HS
Triarthrus sp. HT
Triarthrus sp. HU
Triarthrus sp. HV
Triarthrus sp. HW
Triarthrus sp. HX
Triarthrus sp. HY
Triarthrus sp. HZ
Triarthrus sp. IA
Triarthrus sp. IB
Triarthrus sp. IC
Triarthrus sp. ID
Triarthrus sp. IE
Triarthrus sp. IF
Triarthrus sp. IG
Triarthrus sp. IH
Triarthrus sp. II
Triarthrus sp. IJ
Triarthrus sp. IK
Triarthrus sp. IL
Triarthrus sp. IM
Triarthrus sp. IN
Triarthrus sp. IO
Triarthrus sp. IP
Triarthrus sp. IQ
Triarthrus sp. IR
Triarthrus sp. IS
Triarthrus sp. IT
Triarthrus sp. IU
Triarthrus sp. IV
Triarthrus sp. IW
Triarthrus sp. IX
Triarthrus sp. IY
Triarthrus sp. IZ
Triarthrus sp. JA
Triarthrus sp. JB
Triarthrus sp. JC
Triarthrus sp. JD
Triarthrus sp. JE
Triarthrus sp. JF
Triarthrus sp. JG
Triarthrus sp. JH
Triarthrus sp. JI
Triarthrus sp. JJ
Triarthrus sp. JK
Triarthrus sp. JL
Triarthrus sp. JM
Triarthrus sp. JN
Triarthrus sp. JO
Triarthrus sp. JP
Triarthrus sp. JQ
Triarthrus sp. JR
Triarthrus sp. JS
Triarthrus sp. JT
Triarthrus sp. JU
Triarthrus sp. JV
Triarthrus sp. JW
Triarthrus sp. JX
Triarthrus sp. JY
Triarthrus sp. JZ
Triarthrus sp. KA
Triarthrus sp. KB
Triarthrus sp. KC
Triarthrus sp. KD
Triarthrus sp. KE
Triarthrus sp. KF
Triarthrus sp. KG
Triarthrus sp. KH
Triarthrus sp. KI
Triarthrus sp. KJ
Triarthrus sp. KK
Triarthrus sp. KL
Triarthrus sp. KM
Triarthrus sp. KN
Triarthrus sp. KO
Triarthrus sp. KP
Triarthrus sp. KQ
Triarthrus sp. KR
Triarthrus sp. KS
Triarthrus sp. KT
Triarthrus sp. KU
Triarthrus sp. KV
Triarthrus sp. KW
Triarthrus sp. KX
Triarthrus sp. KY
Triarthrus sp. KZ
Triarthrus sp. LA
Triarthrus sp. LB
Triarthrus sp. LC
Triarthrus sp. LD
Triarthrus sp. LE
Triarthrus sp. LF
Triarthrus sp. LG
Triarthrus sp. LH
Triarthrus sp. LI
Triarthrus sp. LJ
Triarthrus sp. LK
Triarthrus sp. LL
Triarthrus sp. LM
Triarthrus sp. LN
Triarthrus sp. LO
Triarthrus sp. LP
Triarthrus sp. LQ
Triarthrus sp. LR
Triarthrus sp. LS
Triarthrus sp. LT
Triarthrus sp. LU
Triarthrus sp. LV
Triarthrus sp. LW
Triarthrus sp. LX
Triarthrus sp. LY
Triarthrus sp. LZ
Triarthrus sp. MA
Triarthrus sp. MB
Triarthrus sp. MC
Triarthrus sp. MD
Triarthrus sp. ME
Triarthrus sp. MF
Triarthrus sp. MG
Triarthrus sp. MH
Triarthrus sp. MI
Triarthrus sp. MJ
Triarthrus sp. MK
Triarthrus sp. ML
Triarthrus sp. MM
Triarthrus sp. MN
Triarthrus sp. MO
Triarthrus sp. MP
Triarthrus sp. MQ
Triarthrus sp. MR
Triarthrus sp. MS
Triarthrus sp. MT
Triarthrus sp. MU
Triarthrus sp. MV
Triarthrus sp. MW
Triarthrus sp. MX
Triarthrus sp. MY
Triarthrus sp. MZ
Triarthrus sp. NA
Triarthrus sp. NB
Triarthrus sp. NC
Triarthrus sp. ND
Triarthrus sp. NE
Triarthrus sp. NF
Triarthrus sp. NG
Triarthrus sp. NH
Triarthrus sp. NI
Triarthrus sp. NJ
Triarthrus sp. NK
Triarthrus sp. NL
Triarthrus sp. NM
Triarthrus sp. NN
Triarthrus sp. NO
Triarthrus sp. NP
Triarthrus sp. NQ
Triarthrus sp. NR
Triarthrus sp. NS
Triarthrus sp. NT
Triarthrus sp. NU
Triarthrus sp. NV
Triarthrus sp. NW
Triarthrus sp. NX
Triarthrus sp. NY
Triarthrus sp. NZ
Triarthrus sp. OA
Triarthrus sp. OB
Triarthrus sp. OC
Triarthrus sp. OD
Triarthrus sp. OE
Triarthrus sp. OF
Triarthrus sp. OG
Triarthrus sp. OH
Triarthrus sp. OI
Triarthrus sp. OJ
Triarthrus sp. OK
Triarthrus sp. OL
Triarthrus sp. OM
Triarthrus sp. ON
Triarthrus sp. OO
Triarthrus sp. OP
Triarthrus sp. OQ
Triarthrus sp. OR
Triarthrus sp. OS
Triarthrus sp. OT
Triarthrus sp. OU
Triarthrus sp. OV
Triarthrus sp. OW
Triarthrus sp. OX
Triarthrus sp. OY
Triarthrus sp. OZ
Triarthrus sp. PA
Triarthrus sp. PB
Triarthrus sp. PC
Triarthrus sp. PD
Triarthrus sp. PE
Triarthrus sp. PF
Triarthrus sp. PG
Triarthrus sp. PH
Triarthrus sp. PI
Triarthrus sp. PJ
Triarthrus sp. PK
Triarthrus sp. PL
Triarthrus sp. PM
Triarthrus sp. PN
Triarthrus sp. PO
Triarthrus sp. PP
Triarthrus sp. PQ
Triarthrus sp. PR
Triarthrus sp. PS
Triarthrus sp. PT
Triarthrus sp. PU
Triarthrus sp. PV
Triarthrus sp. PW
Triarthrus sp. PX
Triarthrus sp. PY
Triarthrus sp. PZ
Triarthrus sp. QA
Triarthrus sp. QB
Triarthrus sp. QC
Triarthrus sp. QD
Triarthrus sp. QE
Triarthrus sp. QF
Triarthrus sp. QG
Triarthrus sp. QH
Triarthrus sp. QI
Triarthrus sp. QJ
Triarthrus sp. QK
Triarthrus sp. QL
Triarthrus sp. QM
Triarthrus sp. QN
Triarthrus sp. QO
Triarthrus sp. QP
Triarthrus sp. QQ
Triarthrus sp. QR
Triarthrus sp. QS
Triarthrus sp. QT
Triarthrus sp. QU
Triarthrus sp. QV
Triarthrus sp. QW
Triarthrus sp. QX
Triarthrus sp. QY
Triarthrus sp. QZ
Triarthrus sp. RA
Triarthrus sp. RB
Triarthrus sp. RC
Triarthrus sp. RD
Triarthrus sp. RE
Triarthrus sp. RF
Triarthrus sp. RG
Triarthrus sp. RH
Triarthrus sp. RI
Triarthrus sp. RJ
Triarthrus sp. RK
Triarthrus sp. RL
Triarthrus sp. RM
Triarthrus sp. RN
Triarthrus sp. RO
Triarthrus sp. RP
Triarthrus sp. RQ
Triarthrus sp. RR
Triarthrus sp. RS
Triarthrus sp. RT
Triarthrus sp. RU
Triarthrus sp. RV
Triarthrus sp. RW
Triarthrus sp. RX
Triarthrus sp. RY
Triarthrus sp. RZ
Triarthrus sp. SA
Triarthrus sp. SB
Triarthrus sp. SC
Triarthrus sp. SD
Triarthrus sp. SE
Triarthrus sp. SF
Triarthrus sp. SG
Triarthrus sp. SH
Triarthrus sp. SI
Triarthrus sp. SJ
Triarthrus sp. SK
Triarthrus sp. SL
Triarthrus sp. SM
Triarthrus sp. SN
Triarthrus sp. SO
Triarthrus sp. SP
Triarthrus sp. SQ
Triarthrus sp. SR
Triarthrus sp. SS
Triarthrus sp. ST
Triarthrus sp. SU
Triarthrus sp. SV
Triarthrus sp. SW
Triarthrus sp. SX
Triarthrus sp. SY
Triarthrus sp. SZ
Triarthrus sp. TA
Triarthrus sp. TB
Triarthrus sp. TC
Triarthrus sp. TD
Triarthrus sp. TE
Triarthrus sp. TF
Triarthrus sp. TG
Triarthrus sp. TH
Triarthrus sp. TI
Triarthrus sp. TJ
Triarthrus sp. TK
Triarthrus sp. TL
Triarthrus sp. TM
Triarthrus sp. TN
Triarthrus sp. TO
Triarthrus sp. TP
Triarthrus sp. TQ
Triarthrus sp. TR
Triarthrus sp. TS
Triarthrus sp. TT
Triarthrus sp. TU
Triarthrus sp. TV
Triarthrus sp. TW
Triarthrus sp. TX
Triarthrus sp. TY
Triarthrus sp. TZ
Triarthrus sp. UA
Triarthrus sp. UB
Triarthrus sp. UC
Triarthrus sp. UD
Triarthrus sp. UE
Triarthrus sp. UF
Triarthrus sp. UG
Triarthrus sp. UH
Triarthrus sp. UI
Triarthrus sp. UJ
Triarthrus sp. UK
Triarthrus sp. UL
Triarthrus sp. UM
Triarthrus sp. UN
Triarthrus sp. UO
Triarthrus sp. UP
Triarthrus sp. UQ
Triarthrus sp. UR
Triarthrus sp. US
Triarthrus sp. UT
Triarthrus sp. UU
Triarthrus sp. UV
Triarthrus sp. UW
Triarthrus sp. UX
Triarthrus sp. UY
Triarthrus sp. UZ
Triarthrus sp. VA
Triarthrus sp. VB
Triarthrus sp. VC
Triarthrus sp. VD
Triarthrus sp. VE
Triarthrus sp. VF
Triarthrus sp. VG
Triarthrus sp. VH
Triarthrus sp. VI
Triarthrus sp. VJ
Triarthrus sp. VK
Triarthrus sp. VL
Triarthrus sp. VM
Triarthrus sp. VN
Triarthrus sp. VO
Triarthrus sp. VP
Triarthrus sp. VQ
Triarthrus sp. VR
Triarthrus sp. VS
Triarthrus sp. VT
Triarthrus sp. VU
Triarthrus sp. VV
Triarthrus sp. VW
Triarthrus sp. VX
Triarthrus sp. VY
Triarthrus sp. VZ
Triarthrus sp. WA
Triarthrus sp. WB
Triarthrus sp. WC
Triarthrus sp. WD
Triarthrus sp. WE
Triarthrus sp. WF
Triarthrus sp. WG
Triarthrus sp. WH
Triarthrus sp. WI
Triarthrus sp. WJ
Triarthrus sp. WK
Triarthrus sp. WL
Triarthrus sp. WM
Triarthrus sp. WN
Triarthrus sp. WO
Triarthrus sp. WP
Triarthrus sp. WQ
Triarthrus sp. WR
Triarthrus sp. WS
Triarthrus sp. WT
Triarthrus sp. WU
Triarthrus sp. WV
Triarthrus sp. WW
Triarthrus sp. WX
Triarthrus sp. WY
Triarthrus sp. WZ
Triarthrus sp. XA
Triarthrus sp. XB
Triarthrus sp. XC
Triarthrus sp. XD
Triarthrus sp. XE
Triarthrus sp. XF
Triarthrus sp. XG
Triarthrus sp. XH
Triarthrus sp. XI
Triarthrus sp. XJ
Triarthrus sp. XK
Triarthrus sp. XL
Triarthrus sp. XM
Triarthrus sp. XN
Triarthrus sp. XO
Triarthrus sp. XP
Triarthrus sp. XQ
Triarthrus sp. XR
Triarthrus sp. XS
Triarthrus sp. XT
Triarthrus sp. XU
Triarthrus sp. XV
Triarthrus sp. XW
Triarthrus sp. XX
Triarthrus sp. XY
Triarthrus sp. XZ
Triarthrus sp. YA
Triarthrus sp. YB
Triarthrus sp. YC
Triarthrus sp. YD
Triarthrus sp. YE
Triarthrus sp. YF
Triarthrus sp. YG
Triarthrus sp. YH
Triarthrus sp. YI
Triarthrus sp. YJ
Triarthrus sp. YK
Triarthrus sp. YL
Triarthrus sp. YM
Triarthrus sp. YN
Triarthrus sp. YO
Triarthrus sp. YP
Triarthrus sp. YQ
Triarthrus sp. YR
Triarthrus sp. YS
Triarthrus sp. YT
Triarthrus sp. YU
Triarthrus sp. YV
Triarthrus sp. YW
Triarthrus sp. YX
Triarthrus sp. YY
Triarthrus sp. YZ
Triarthrus sp. ZA
Triarthrus sp. ZB
Triarthrus sp. ZC
Triarthrus sp. ZD
Triarthrus sp. ZE
Triarthrus sp. ZF
Triarthrus sp. ZG
Triarthrus sp. ZH
Triarthrus sp. ZI
Triarthrus sp. ZJ
Triarthrus sp. ZK
Triarthrus sp. ZL
Triarthrus sp. ZM
Triarthrus sp. ZN
Triarthrus sp. ZO
Triarthrus sp. ZP
Triarthrus sp. ZQ
Triarthrus sp. ZR
Triarthrus sp. ZS
Triarthrus sp. ZT
Triarthrus sp. ZU
Triarthrus sp. ZV
Triarthrus sp. ZW
Triarthrus sp. ZX
Triarthrus sp. ZY
Triarthrus sp. ZZ
P. serratus (= richtri)
H. holodentata
INTERVAL
P. grandis
J. lanceolatus
INTERVAL
J. canadensis
B. sulcatus
INTERVAL
O. communis
M. marathonensis
INTERVAL
S. deltatus
M. dianae
INTERVAL
4
2-3
1
2
1
E
D
C
Histiodella tablehadensis
Multioistodus mibertatus
Leptochirognathus sp.
Oistodus multicornutus
Scolopodicodus gracilicostatus
Periodon (Tonkicola) communis
Acodus deltatus
Macerodus dianae
Serratognathus extensus
Serpoli
Microzarkodina ozarkodentata (Bradshaw)
TABLE COVE FORMATION
TABLE POINT FORMATION
upper AGUATHUNA FORMATION
HIATUS
middle
lower
AGUATHUNA FORMATION
upper CATOCHE FORMATION
CATOCHE FORMATION
BOAT HARBOUR FORMATION
HIATUS
BOAT HARBOUR FORMATION
WATTS BIGHT FORMATION

Catoche and Aguathuna Formations. The trilobite, Benthamaspis diminutiva Hintze, known from Ross-Hintze zones I and J, occurs 20 metres below the top of the Catoche Formation (Boyce, 1985). A monospecific assemblage of graptolites Didymograptus (Expansograptus) nitidus (Hall, 1958) from the lowest beds of the Aguathuna Formation at Table Point compare with graptolites from Bed 11 of the Cow Head Group, which contains trilobites of Ross-Hintze zone I (Williams et al, 1987).

Whiterockian fauna (trilobites Bathyurus perplexus, Acidiphorus cf. A. pseudobathyurus and the ostracod Eoleperiditia bivia White) occur within dolostones of the upper member of the Aguathuna Formation (Knight, 1984; Boyce, 1985; Williams et al, 1987; Knight and James, 1987). These fossils have a coincident range over Ross-Hintze trilobite zones L and M, which are Whiterockian (Ross et al, 1982). Aporthophyla brachiopods of the Table Point Formation correlate with the upper Whiterockian Anomalorthis Zone and suggest that the shelly fauna of the upper Aguathuna Formation belongs either to Lower or basal Upper Whiterockian (Ross and James, 1987).

Gaps in trilobite stratigraphy are augmented by conodonts found throughout the Catoche and Aguathuna Formations. Lower Ordovician biostratigraphy is known only in a preliminary fashion (Ethington and Clark, 1971, 1981). Stouge (1982) conducted a reconnaissance survey of the St. George Group. Stait (1988) studied the upper St. George Group at Daniel's Harbour and Table Point. Ji (1989) examined conodont biostratigraphy of the St. George Group at Port-au-Port.

The presence of midcontinent Fauna D (Acodus deltatus assemblage zone) and Fauna E (Prioniodus (Oepikodus) communis assemblage zone)

affirms the late Canadian age of the lower to middle Catoche Formation (Stouge, 1982). An abrupt introduction of species (Stouge's Fauna 5) occurs at a lithological change to very shallow water sediments 75 metres below the top of the formation. Among the first-occurring species, Jumudontus gananda, Oistodus multicorrugatus and Semiacontiodus asymmetricus are identified in J. gananda - Reutterodus andinus assemblage zone of lower Midcontinent Fauna 1 (Sweet et al., 1971; Ethington and Clark, 1981) (Data from Stait, 1988; Nolan pers. comm., 1984). At Ibex, Utah, J. gananda occurs in strata of Ross-Hintze trilobite zones H and I (Ethington and Clark, 1981).

Small conodont populations within the lower Aguathuna Formation are dominated by peritidal facies-specific hyaline forms including Drepanoistodus angulensis, D. cf. inequalis and D. venustusi (Stait, 1988). Pteracontiodus cryptodens and Oepikodus intermedius of Midcontinent Fauna 2 suggest that much of the lower Aguathuna Formation is early Whiterockian (Stait, 1988).

Conodonts change abruptly in the upper Aguathuna Formation above the regional unconformity. A facies-specific assemblage belongs to the peritidal/lagoonal Trigonodus - Eoneoprionidus biofacies of the lower 25 m of the Table Head Group (Stouge, 1980; Stait, 1988). Midcontinent Fauna 4 in these beds correlates with the upper Whiterockian Anomalorthis Zone. Several reported diagnostic fossils no older than Fauna 4 include Histiodella tableheadensis = holodentata, Paraprioniodus costatus, Multioistodus subdentatus and Leptochirognathus quadrata (Stait, 1988).

Conodonts and shelly fossils collectively suggest that the uncon-

formity correlates with the Arenig/Llanvirn boundary, a world-scale break (Fortey, 1984). The unconformity probably represents a hiatus of 2 to 5 million years, which encompasses the zone of Midcontinent Fauna 3, part of the Lower Whiterockian Stage (Stait, 1988). Answers about this time span and the base of the Whiterockian, however, remain indefinite because of the limited number and diversity of species in the peritidal lower Aguathuna Formation.

2.7 Lithostratigraphy and Sedimentology of the Table Head Group

2.7.1 Introduction

The Table Head Group, which was described by Schuchert and Dunbar (1934) and Whittington and Kindle (1963), is defined by Klappa et al. (1980). Stenzel et al. (1990) have re-examined the regional lithostratigraphy. The group is subdivided into three formations: (1) Table Point; (2) Table Cove; and (3) Cape Cormorant; which respectively are distinguish by bioturbated gray limestone, ribbon limestone and limestone megabreccia (Fig. 1.2). The boundaries of the group are placed at the top of the St. George dolostones and at the base of black shales, siltstones and sandstones of the Goose Tickle Group (Fig. 1.2).

2.7.2 Table Point Formation (40 - 260 m)

The Table Point Formation comprises shallow subtidal muddy carbonates with an abundant and diverse fauna. It includes dominantly bioturbated bioclastic wackestones and packstones intercalated with lime

mudstones, peloidal grainstones, small slump beds and minor dolostones. Peritidal sediments of the basal 25 to 50 m are called the Spring Inlet Member (Ross and James, 1987) and include (1) argillaceous nodular wackestones to packstones, (2) bioturbated wackestones, (3) fenestral mudstones, (4) dololaminites, (5) limestone conglomerates and (6) coquina limestones (Knight, 1985, 1986; Ross and James, 1987). A downcutting erosional surface occurs within these sediments west of Hare Bay (Knight, 1986). The formation is dolomitized along faults (Knight, 1985).

Depositional Environment - The peritidal to subtidal carbonates of the Table Point Formation record the gradual drowning of the Newfoundland Platform during marine transgression and platform subsidence. Sedimentation rates equalled subsidence as carbonate mud deposition continued on a shallow open shelf. Variable rates of subsidence on a block faulted platform however controlled the local rate of sedimentation and ultimately formational thicknesses. High-energy sand deposits and "seismic" slumps periodically disturbed the substrate (Stenzel and James, 1988).

2.7.3 Table Cove Formation (0 - 94 m)

The Table Cove Formation is a deep water slope deposit of ribbon limestone consisting of thin intercalations of black shale, bioturbated bioclastic wackestones and calcareous mud turbidites. Large scale slump folds are common.

Depositional Environment - The Table Cove Formation was laid down as a veneer of lime and silicic black mud in deep water on a foundered

platform slope.

2.7.4 Cape Cormorant Formation (0 -200 m)

The Cape Cormorant Formation is characterized by lime megabreccias associated with siltstones, sandstones, black shales and calciturbidites. Clasts and olistostromes include lithologies ranging from Cambrian to dominant Table Point/Table Cove clasts.

Depositional Environment - The Cape Cormorant Formation consists of resedimented breccias intermixed with deep water hemipelagic muds and sand/silt turbidites. The megabreccias originated from erosion of platform carbonates uplifted along faults during the foundering of the platform.

2.8 Biostratigraphy of the Table Head Group

The Table Head Group is dated as upper Whiterockian age on the basis of trilobites (Whittington and Kindle, 1963), conodonts (Fahraeus, 1970; Stouge, 1980), graptolites (Finney and Skevington, 1979) and other fossils. Trilobite, Bathyurus perplexis, of Ross-Hintze Zones L to M in the basal Table Point Formation indicates a lower to upper Whiterockian age (Williams et al., 1987). Strata bearing the trilobite, Pseudomera barrendei, 56 metres above the formation's base belong to Whiterockian trilobite Zone M (Whittington and Kindle, 1963). The Table Cove Formation contains slightly younger Zone N trilobites. The brachipods, Aporthophyla superstes n.sp. and Aporthophyla aurora (Billings), of the

Table Point Formation belong to the upper Whiterockian Anomalorthis Zone (Ross and James, 1987). The upper Whiterockian conodont, Histiodella tableheadensis, of Midcontinent Fauna 4 (Sweet et al., 1971) occurs throughout at the Table Point Formation (Stouge, 1980). Conodonts of the North Atlantic middle Llanvirn Eoplacognathus suecicus Zone are limited to the Table Cove Formation (Stouge, 1980). The graptolite Diplograptus decoratus ranges from 46 m above the base of the Table Point Formation to the top of the Table Cove Formation. D. decoratus correlates with the upper Whiterockian Paraglossograptus tentaculatus ("etheridgei") zone.

PART II

STRATIGRAPHY AND SEDIMENTOLOGY OF THE DANIEL'S HARBOUR AREA

INTRODUCTION TO PART II

In Part II the primary sedimentary aspects of the mine stratigraphy are described. This description shows that the ore horizons in the upper part of the Catoche Formation and finely crystalline cap rocks of the Aguathuna Formation acquired their distinctive character as the composition of sediments changed during upward shallowing of the carbonate platform. Newly recognized upward deepening sedimentary sequences result in a new interpretation of shallow water carbonate sedimentation. The St. George Unconformity is put into its stratigraphic context as new informal members of the Aguathuna Formation are defined. This stratigraphy demonstrates that the unconformity formed during a chain of tectonic events which also influenced subsurface karst and sedimentation of the middle and upper members of the Aguathuna Formation.

CHAPTER 3 STRATIGRAPHY AND SEDIMENTOLOGY OF THE CATOCHE FORMATION

3.1 Introduction to the Local Stratigraphy

The following discussion describes the stratigraphy and sedimentology of the upper St. George Group and lower 50 metres of the Table Head Group in the mine area. Lateral relationships are determined on the basis of excellent marker control and extensive drill hole data. This stratigraphy establishes a framework for the following discussion of dolostones, sulphides, breccias and structural evolution.

Continuous exposure of the upper 20 metres of the Catoche Formation, the whole Aguathuna Formation and Table Head Group at the Table Point-Freshwater Cove coastal section is correlated with core at the mine (Fig. 1.3). Three deep drill holes penetrate the St. George Group into the Watts Bight Formation and are designated DDH A-1, Underground DDH 1001 and US Borax Flat Pond-DDH 1 (Figs. 1.3, 1.4). The upper 105 metres of the St. George Group in the mine area is cored by many drill hole fences oriented north-northwest (150°-330°) with holes spaced 20 to 90 metres apart. Over 2600 holes have been drilled in a 250 square kilometre area that extends beyond the mine. Three hundred drill holes in down dip areas penetrate the Table Head Group. Map locations and logs of these drill holes are kept on file at the Newfoundland Department of Mines and Energy, St. John's, Newfoundland. Figures 2.1 and 3.1 summarize the local stratigraphy of the St. George Group.

Figure 3.1 Detailed Stratigraphy of the Upper St. George Group at Newfoundland Zinc Mines

A detailed bed-to-bed log of the upper St. George Group is compiled from three drill holes. The middle Catoche Formation is logged from underground drill hole 1001; the upper Catoche Formation from DDH 1254; and the Aguathuna Formation from DDH 965. The locations of the drill holes are indicated on Fig. 1.4.

LEGEND FOR DETAILED STRATIGRAPHY

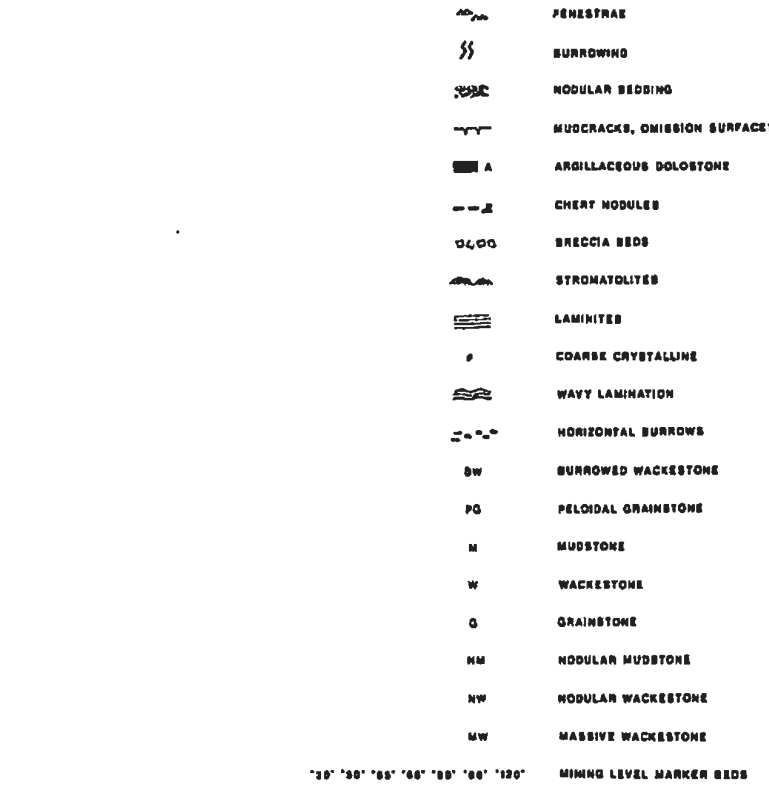

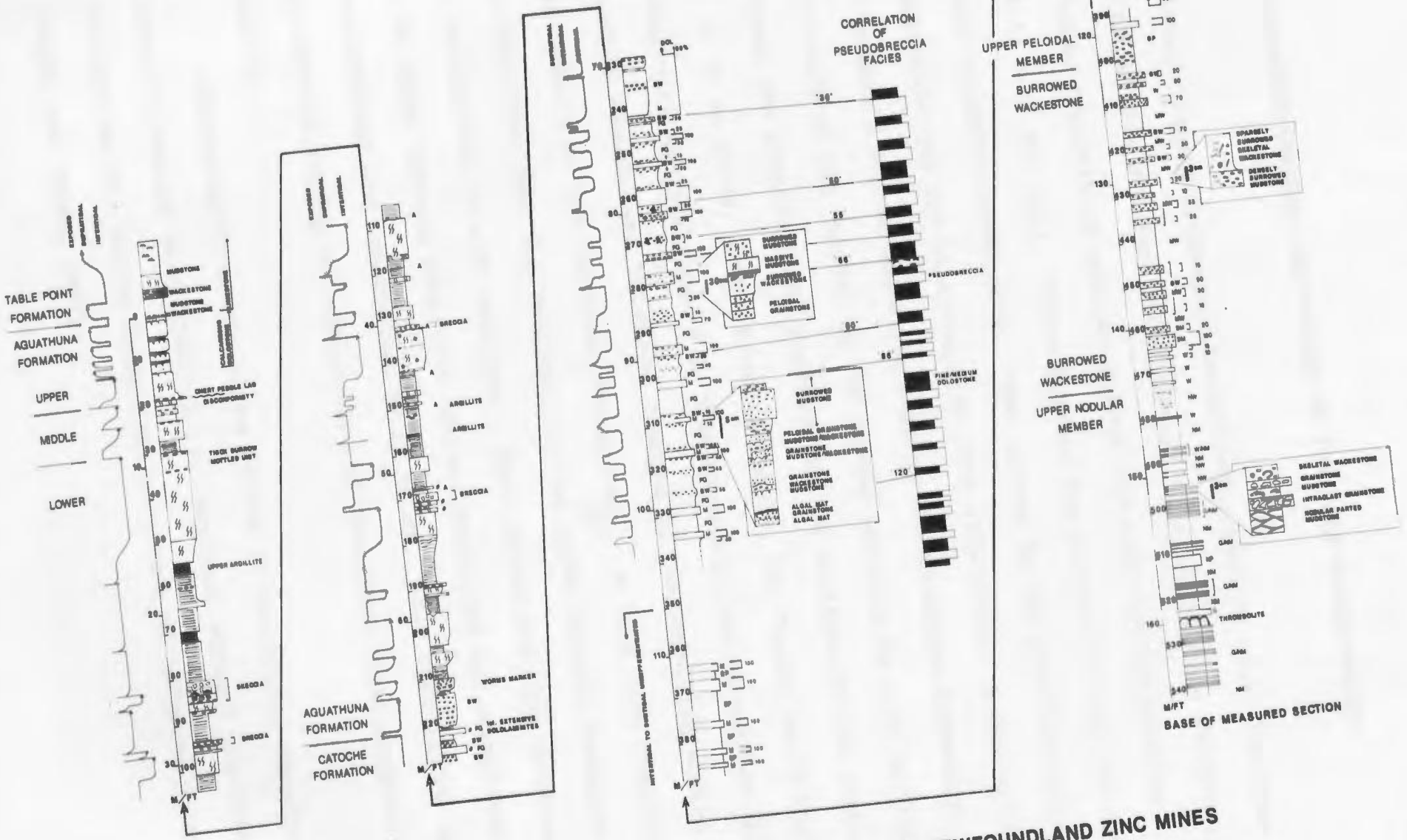

DETAILED STRATIGRAPHY OF THE UPPER ST. GEORGE GROUP AT NEWFOUNDLAND ZINC MINES

3.2 Stratigraphic Control and Review of Previous Nomenclature

Numerous lithostratigraphic marker beds, such as chert horizons, shales, distinctive burrowed intervals and fine crystalline dolostones within coarse crystalline mottled strata, are used for correlation (Figs. 2.1, 3.1, Pl. 3.1). These markers are correlated over the entire 250 square kilometre study area. Most strata in the Aguathuna Formation are distinctive and can be correlated over wide areas. A distinctive burrow marker, 2 metres above the base of the Aguathuna Formation, is locally known as the "worms" or "X" marker and used by mine geologists to measure the stratigraphic position of ore horizons in the mine (Pl. 3.1). A 50 cm-thick, green dolomitic shale, the "upper argillite", together with an overlying, 4 to 7 metre thick, burrow-mottled dolostone is used to demonstrate thickness changes of the overlying middle and upper members of the Aguathuna Formation. A very fine crystalline, dark dolostone bed, the "66" bed, in the upper Catoche Formation is used for correlation in mine workings. Most coarse and fine dolostone beds in the upper Catoche Formation can be identified and correlated between mine workings and exploration drill holes. This correlation is commonly utilized in mining and exploration of important stratigraphic ore levels.

Stratigraphic nomenclature varies in geological reports on the Daniel's Harbour area (Table 3.1). Regional workers previously sub-divided the St. George Group into a variety of informal units (see Knight and James, 1987).

Plate 3.1 Marker Beds

(up in all photographs is toward the top of the page)

a. The dark, gray-green Upper Argillite marker is an argillaceous dolostone containing quartz silt. Fine laminations range from mm to cm-scale. Typical of all drill holes. The scale is in centimetres.

b. The "worms" or X marker bed occurs just above the base of the Aguathuna Formation. Concentrated burrows at the base grade upwards into scattered "worm-shaped" traces with white, saddle dolomite in the centres. Outcrop photographed at the Table Point coastal section. The lens cap is 50 mm in diameter.

c. A kidney-shaped chert nodule within an upper Catoche limestone preserves burrow fabric. The cherts commonly occur 17 m and 21 m below the "worms" marker. Drill core sample from DDH 1254, 16.8 m below the worms marker (b.w.m.). The scale is in centimetres.

PLATE 3.1

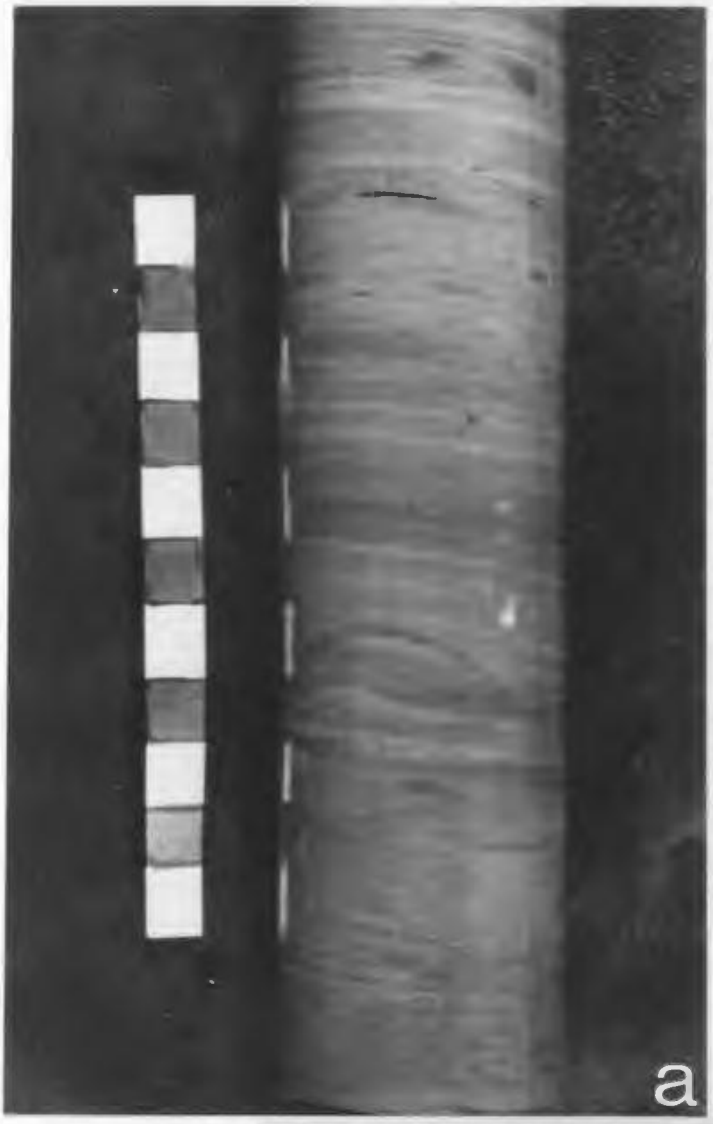

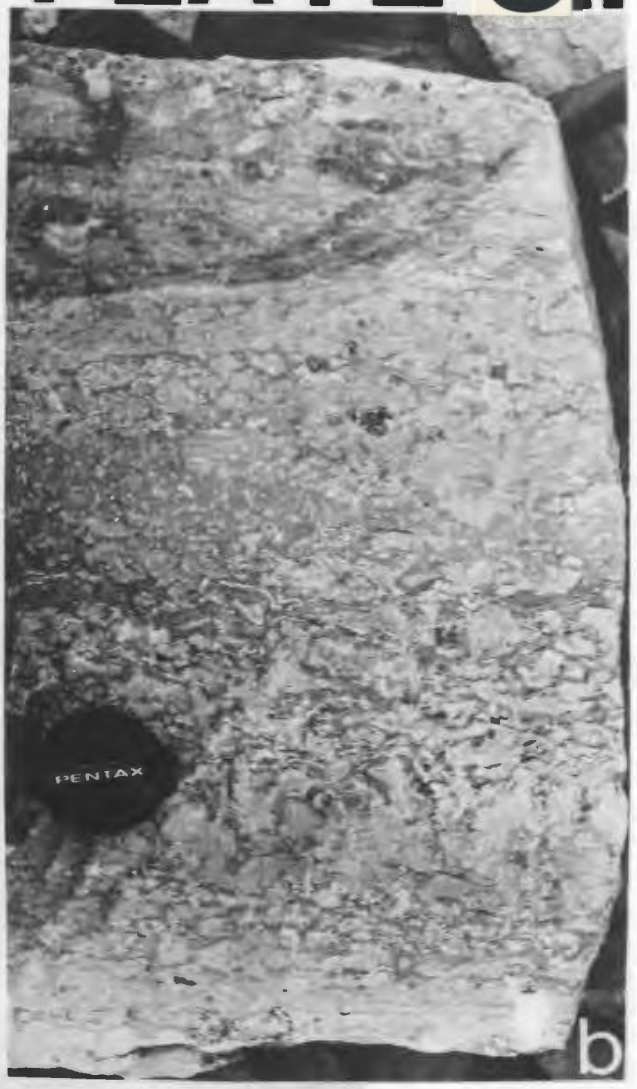

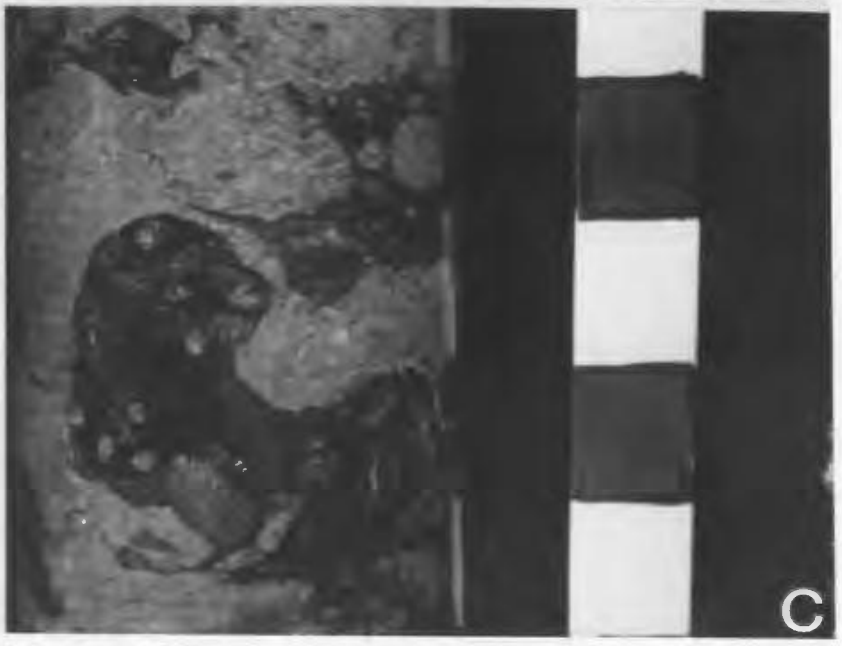

TABLE 3.1
STRATIGRAPHIC NOMENCLATURE

	KNIGHT & JAMES 1987	THIS STUDY	MINE TERMINOLOGY	CORON 1982
ST. GEORGE GROUP		Upper Member		
		Middle Member	Siliceous Dolomite	Bellburns
	AGUATHUNA FORMATION	upper argillite	(Cyclic Dolomites -Collins and Smith, 1975)	Facies
		Lower Member		
	x or worms marker		Dark Gray Dolomite	
	COSTA BAY MEMBER	Peloidal Member	Pseudobreccia Interval	Mike Lake Facies
		Burrowed Wackestone Member		
	CATOCHE FORMATION	Upper Nodular Member	Lower Limestone	Daniel's Harbour Facies
	BOAT HARBOUR FORMATION		Lower Dolomites	
	WATTS BIGHT FORMATION			

3.3 Introduction to the Upper Catoche Formation

The Catoche Formation is characterized by shallow water lithofacies such as fossiliferous burrowed wackestones, skeletal grainstones and thrombolites (Pratt and James, 1986; Knight and James, 1987). The Catoche Formation in deep drill holes is subdivided into five members (A through E, Fig. 2.1). Members A (the lower nodular mudstone) and B (the lower burrowed wackestone) are similar to members C (the upper nodular mudstone) and D (the upper burrowed wackestone). The peloidal member (E) is distinctive and gradational with the overlying Aguathuna Formation. The following discussion is restricted to the upper three members, the lithologies which characterize the entire formation. The detailed stratigraphy for the upper St. George Group is illustrated in Figure 3.1.

3.4 Member C - Upper Nodular Mudstone (50 m)

3.4.1 Lithologies

Four main lithologies characterize this member. Nodular mudstones and burrowed wackestones are the dominant ones. An open marine fauna includes both North Atlantic and North American midcontinental species of trilobites and conodonts (Fortey, 1979; Stait, 1988).

(1) Nodular mudstone - Thin centimetre-scale lime mudstones with few skeletal fragments and rare burrows are parted by millimetre-thin partly dolomitized, black argillaceous laminations (Pl. 3.2a,d). The fabric is generally nodular to fitted, but is locally evenly parted.

Plate 3.2 Middle Catoche Formation

(Up in the photographs is toward the top of the page)

a. A nodular mudstone comprising a structureless mudstone parted by an irregular, dark layer of very fine crystalline dolomite. Sample from DDH 1001, 73 m below the worms marker (b.w.m.). 1 cm scale.

b. A burrowed, skeletal wackestone from Member D contains cross-sections of cylindrical burrows (arrow). Skeletal particles include trilobites and crinoids. Sample from DDH 1001, 58 m b.w.m. 1 cm scale.

c. An intraclastic grainstone overling a burrowed, skeletal wackestone. Sample from DDH 1001, 73 m b.w.m. 1 cm scale.

d. Burrowed wackestone and mudstone with dark argillaceous, dolomitic and stylolitic partings. This core is from the middle Catoche Formation. Sample from DDH 631, 60 m b.w.m. Scale in centimetres.

PLATE 3.2

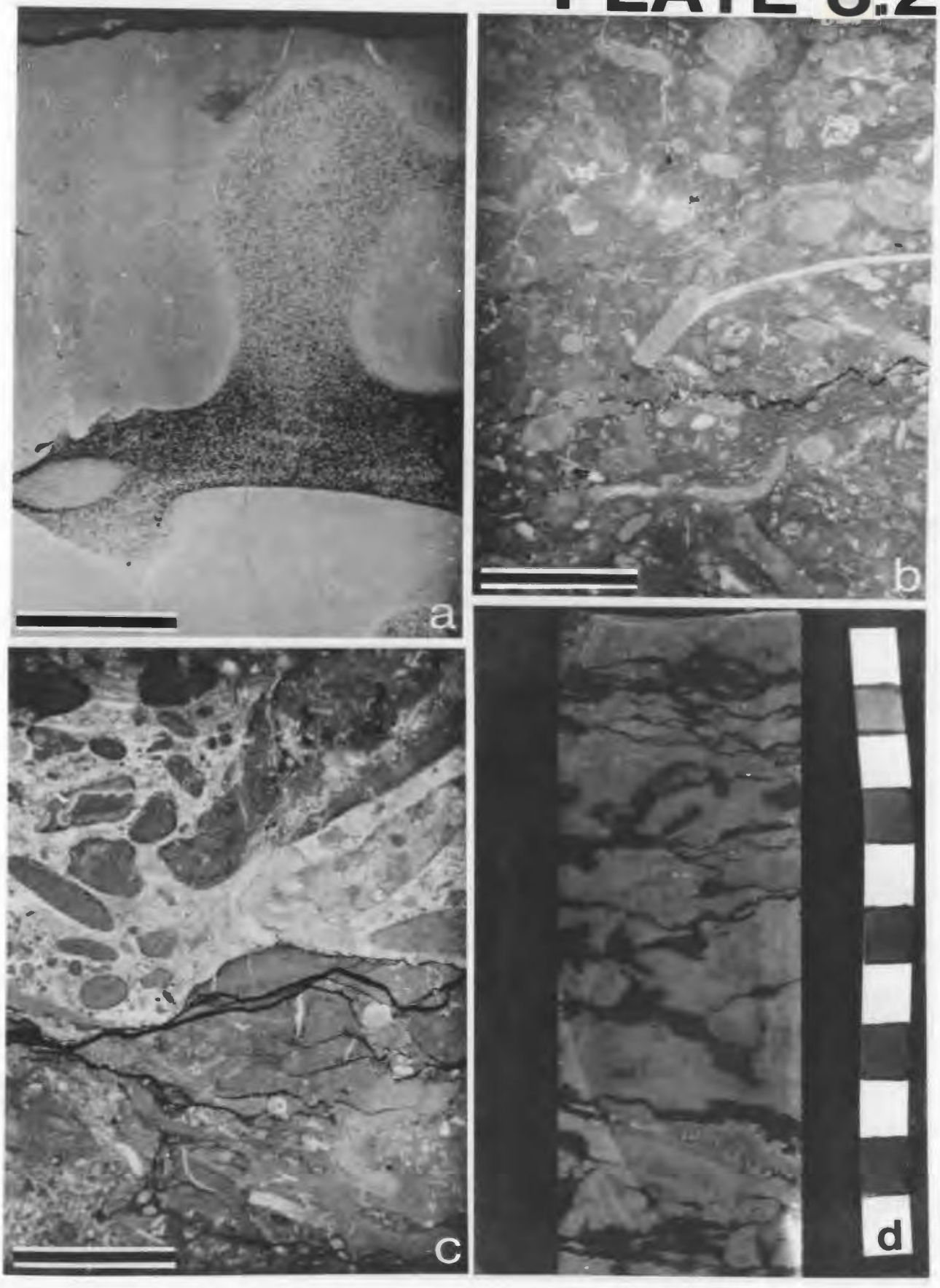

Nodular mudstones are typical of subtidal to deep marine environments (e.g. Wilson, 1975; Ruppel, 1977). Argillaceous, terrigenous laminations and minor bioturbation are associated with skeletal-poor muds. Turbid waters from the influx of terrigenous mud probably restricted habitation by benthonic organisms (e.g. Ruppel, 1977). Increased salinities also could have inhibited burrowing when temporary lagoonal conditions developed leeward of mound banks.

(2) Burrowed skeletal wackestones - These wackestones and packstones are rich in skeletal fragments of trilobites, brachiopods, ostracods and pelmatozoans (Pl. 3.2c). Common, minute, subhorizontal burrows, 1 to 2 mm in cross-section, are recrystallized to microspar. These subtidal wackestones are interpreted to have accumulated in low energy conditions.

(3) Grainstones to Rudstones - These grainstones are thin, 1 to 3 cm-thick, lenses composed of coarse 1 mm to 2 cm-size mudstone intraclasts, pelmatozoans and trilobite fragments (Pl. 3.2c) Intraclasts are similar in composition to underlying strata. These gravelly sands, probably tempestites, were eroded from algal-sponge mud mounds and partially lithified substrates, then entrained and deposited in shallow depressions (Pratt 1979; Knight and James, 1987).

(4) Thrombolites - Metre-thick thrombolite mounds with characteristic clotted fabrics are scattered throughout this member (Pratt, 1979). Complex reef frameworks include Renalcis, Lichenaria and a

diverse associated benthonic fauna (Pratt and James, 1982; Knight and James, 1987). Skeletal-intraclast grainstones are commonly associated with mounds. Thrombolites probably accreted in the shallow, subtidal photic zone where Renalcis and a benthonic fauna flourished (Pratt and James, 1982). The mounds and associated fauna contributed to the surrounding grainstones.

3.4.2 Vertical Distribution of Lithologies

The nodular mudstones, bioturbated wackestones and fossiliferous grainstones are all intercalated (Fig. 3.1). Grainstones occur through portions of the section at 30 to 50 cm intervals. Some of these grainstones occur around thrombolites and are associated there with intercalated mudstone. Uninterrupted nodular mudstone units may reach 8 m in thickness. Wackestones are generally centimetres in thickness.

3.4.3 Depositional Environment

This member is interpreted to have accumulated on an open shelf where a muddy bottom with a diverse benthonic fauna was repeatedly affected by storms and by the influx of terrigenous muds, as indicated by intraclast grainstones and nodular mudstones. Storms ripped up partially lithified muds and deposited the thin grainstones/rudstones. Local bioherms also contributed skeletal debris to grainstones. Periodic influx and deposition of terrigenous muds clouded the waters and temporarily reduced the growth of skeletal organisms.

3.5 Member D - Upper Burrowed Wackestone (20 m)

3.5.1 Lithology

This unit is composed largely of one lithology, burrowed wackestone, and is similar to lithology 2 in Member C (Pl. 3.2b). The burrows, however, are less abundant and the wackestones are vertically continuous for up to 10 m. Abundant skeletal clasts include trilobites and pelmatozoans. Partially dolomitized beds of unfossiliferous burrowed mudstone, 30 to 60 cm thick, rhythmically punctuate the wackestones (Fig. 3.1). Small horizontal tubular burrows, 1 to 4 mm in diameter, penetrate most of these mudstones. A very shallow water (Midcontinent) conodont fauna differs from the open marine fauna with North Atlantic species in the nodular mudstone member (Stouge, 1982; Stait, 1988).

3.5.2 Depositional Environment

These sediments accreted in very shallow subtidal settings. Widespread shallowing of the platform seems to have restricted the conodont fauna to midcontinent species, but marine benthonic organisms still flourished. Significant hydrographic changes caused the abrupt disappearance of intraclast grainstones and nodular mudstones. Either offshore shoals or regional shallowing attenuated wave energy. Burrowing organisms persisted as muds accumulated slowly in clear waters devoid of the muddy turbidity of the open platform. Thin fossil-poor muds accumulated during periodic shallowing into the intertidal (?) zone.

3.6 Member E - Peloidal Member

3.6.1 Lithologies

Peloidal grains form a dominant component of burrowed limestones of the upper Catoche Formation. This member is the local equivalent of the Costa Bay Member (Knight and James, 1987).

(1) Peloidal Packstone/Grainstone - Bimodal packstones and grainstones comprise 50 to 500 μm-size peloids, rounded, 1 to 10 mm-diameter micrite intraclasts, minor skeletal fragments and molds of algal filaments (Pl. 3.3a). Intraclasts and peloids commonly preserve micritized skeletal grains, tubular and "structure grumeleuse" fabrics of Girvanella, boring algae and other unknown calcified algae (Pratt, 1979). Skeletal fragments include gastropods, orthocone cephalopods, trilobites, brachiopods, lithistid sponges, ostracods and a few pelmatozoans. Matrix is largely altered to 10 μm microspar and 20 to 50 μm neospar.

The grainstone beds which are 1 to 2 m thick have a heterogeneous fabric. Irregular layers of micrite and peloidal packstone, 1 to 5 mm thick, interrupt the grainstone (Fig. 3.1; Pl. 3.3a). Relict fabrics of calcified and filamentous algae, and grainstone-filled vertical burrows indicate early binding and lithification. Intraclasts of similar composition suggest local fragmentation. Original layering is partially disrupted by bioturbation, desiccation(?) and fracturing during diagenesis. Cross-cutting infaunal burrows, 2 to 5 mm in diameter, are filled with microspar-supported peloids or 20 to 500 μm neospar.

Plate 3.3 Peloidal Member

a. Peloidal grainstone (above arrow) intercalated with mudstone (M) and peloidal packstone (P) layers. Burrows (light areas) penetrate all lithologies and grainstone fills a dwelling burrow (arrow) in the underlying mudstone layer. Veinlets of coarse calcite cement cut the mudstone and are truncated by stylolites. Sample from DDH 1254, 29 m below worms marker (b.w.m.) 1 cm scale.

b. Burrowed wackestone show abundant horizontal burrows and mottles (arrow) of probable lithstid sponges. These limestone burrows and mottles are outlined by stylolites and surrounded by compacted micrite partially replaced by finely crystalline dolomite. Sample from DDH 1254, 20 m b.w.m. 1 cm scale.

c. The weathered, upper surface of a dolomitized, burrowed wackestone at Table Point exhibits a dense network of horizontal burrows of Planolites and Paleophycus. Bar is 10 cm.

d. A core sample illustrating the abrupt transition from a burrowed wackestone (bottom) upwards into a fine crystalline dolostone (black) with mm-sized burrows (gray). Sample from DDH 1254, 9 m b.w.m. The scale is in centimetres.

PLATE 3.3

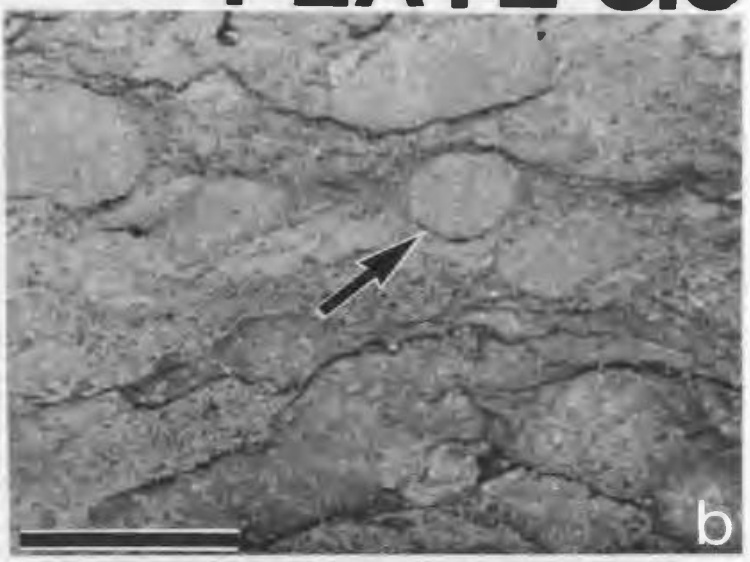

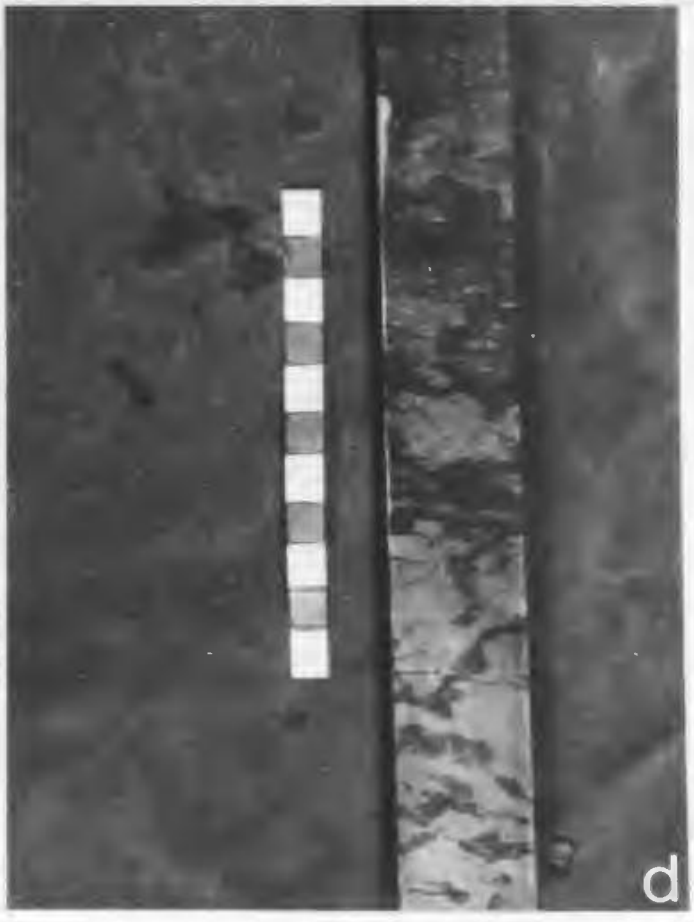

The collective presence of peloids, the calcified microbe Girvanella, a limited, low diversity fauna and burrows indicate shallow subtidal to intertidal deposition. The abundant peloids and intraclasts probably had several origins. Peloids could have been produced by calcified and boring algae microbes that are known to abound in shallow, low energy waters (cf. Moore, 1977; Coniglio and James, 1985) and by infaunal burrowers and skeletal organisms. Intraclasts were probably produced by erosion of lithified crusts in the nearshore (cf. Persian Gulf, Shinn, 1986). Similar peloidal wackestones with an abundant algal fauna are also interpreted as very shallow, nearshore sediments in other Lower Paleozoic sequences in the Appalachians (Walker and Laporte, 1970; Benedict, 1977; Moore, 1977).

(2) Burrowed Wackestone - Burrowed peloidal and skeletal wackestones are characterized by concentrations of horizontal burrows of Paleophycus, Planolites and Chondrites, 3 to 8 mm-wide (Pl.3.3b,c). The burrows which have distinct circular to oval boundaries penetrate the matrix which is selectively dolomitized. The interior of burrows is composed of 10 to 100 μm calcite neospar and microspar surrounding remnants of precursor peloidal wackestone. Spar-filled molds of planispiral gastropods (Maclurites) and orthoconic cephalopods are scattered on bedding planes.

The burrowed wackestones were probably deposited in subtidal settings characteriterized by slow deposition and marine lithification of muddy sediments. This created a nutrient-rich substrate which was inhabited and thoroughly reworked by lateral deposit feeders (Narbonne,

1984). Flattened Planolites probably mined an early soupy substrate, whereas later burrowers of a firmer sediment left circular, less compacted structures (Ekdale et al., 1984). This ichnoassemblage is typical of Lower Paleozoic intertidal to subtidal carbonates (e.g. Narbonne, 1984) but does not specify water depth.

(3) Mudstones - Former beds of mudstone from 30 to 100 cm thick are now finely crystalline (100 to 300 μm) dolostone. Conodonts occur, but no macrofossils are present. Most beds are thoroughly bioturbated and include small, horizontal Chondrites burrows (1 to 3 mm in diameter) (Pl. 3.3d). Bed contacts are normally sharp. Several beds, for example those 7 to 9 m and 19 to 20 m below the "worms" marker, are dark gray, argillaceous at their base and nearly structureless. Very finely crystalline dololaminites locally occur at the base of the 20 m bed above a bed containing white nodular cherts. Beds toward the top of the Catoche Formation tend to be pale gray, massive and locally laminated. A laterally extensive breccia with fine dolomite matrix occurs at the base of a bed 9 m below the "worms" marker.

These beds are interpreted as very shallow subtidal to intertidal deposits. Conodonts and burrows indicate the marine origin of most beds and the abrupt bed contacts and argillaceous to laminated lower portions suggest sudden flooding and deposition above lower surfaces. Deep level burrowers probably formed the Chondrites traces after partial compaction and dewatering (Ekdale et al., 1984). Local chert and laminite bases suggest that the muds and, in particular, their lower surfaces were sometimes exposed.

(4) Cherts - Two types of chert occur along bedding planes. White nodules of 50 to 500 μm megaquartz and 10 to 20 μm microquartz, which occur beneath the base of a dolomitized mudstone, 20 m below the "worms" marker, and are scattered through the wackestones of the peloidal member. Black to brown microcrystalline chert nodules replace burrows within wackestones along horizons, 17 and 21 m below the "worms" marker (Fig. 3.1; Pl. 3.1c).

Both types of chert are diagenetic and concentrated below the mudstone units. The silica may have formed in the immediate subsurface during high intertidal deposition. The white nodular, chert 20 m below the "worms" marker is particularly suggestive of cauliflower cherts which replace evaporites (cf. Chowns and Elkins, 1974).

3.6.2 Distribution of Lithologies

A sequence of lithologies is repeated more than 10 times in the stratigraphy of the peloidal member. Key beds and these sequences are correlated laterally over more than 200 km^2. Each sequence is composed from bottom to top of the following units (Fig. 3.2).

(1) A non-depositional surface. An abrupt surface occurs at the contact between an underlying burrowed wackestone and an overlying mudstone bed.

(2) Mudstone bed. A 20 to 100 cm thick bed of mostly structureless, dark gray carbonate mud wasdeposited in very shallow water during flooding of the underlying surface. Local preservation of laminites suggests periodic deposition in the intertidal zone.

Figure 3.2 Vertical Distribution of Lithologies of the Peloidal Member of the Catoche Formation

The peloidal member is composed of a dozen or more repeated lithological sequences. Each sequence has five distinctive components. Fine dolostone (formerly mudstone) is the basal bed (unit 2) resting abruptly upon a non-depositional surface (1). These dolostones commonly have dark gray argillaceous bases. Burrowed wackestone, unit 3, sharply overlies the dolostone. Peloidal grainstones and packstones (4) dominate the middle portion of limestone beds, where they are intercalated with mudstone laminations and thin beds of burrowed wackestone. Burrowed wackestone, unit 5, also caps sequences at the top of limestone beds.

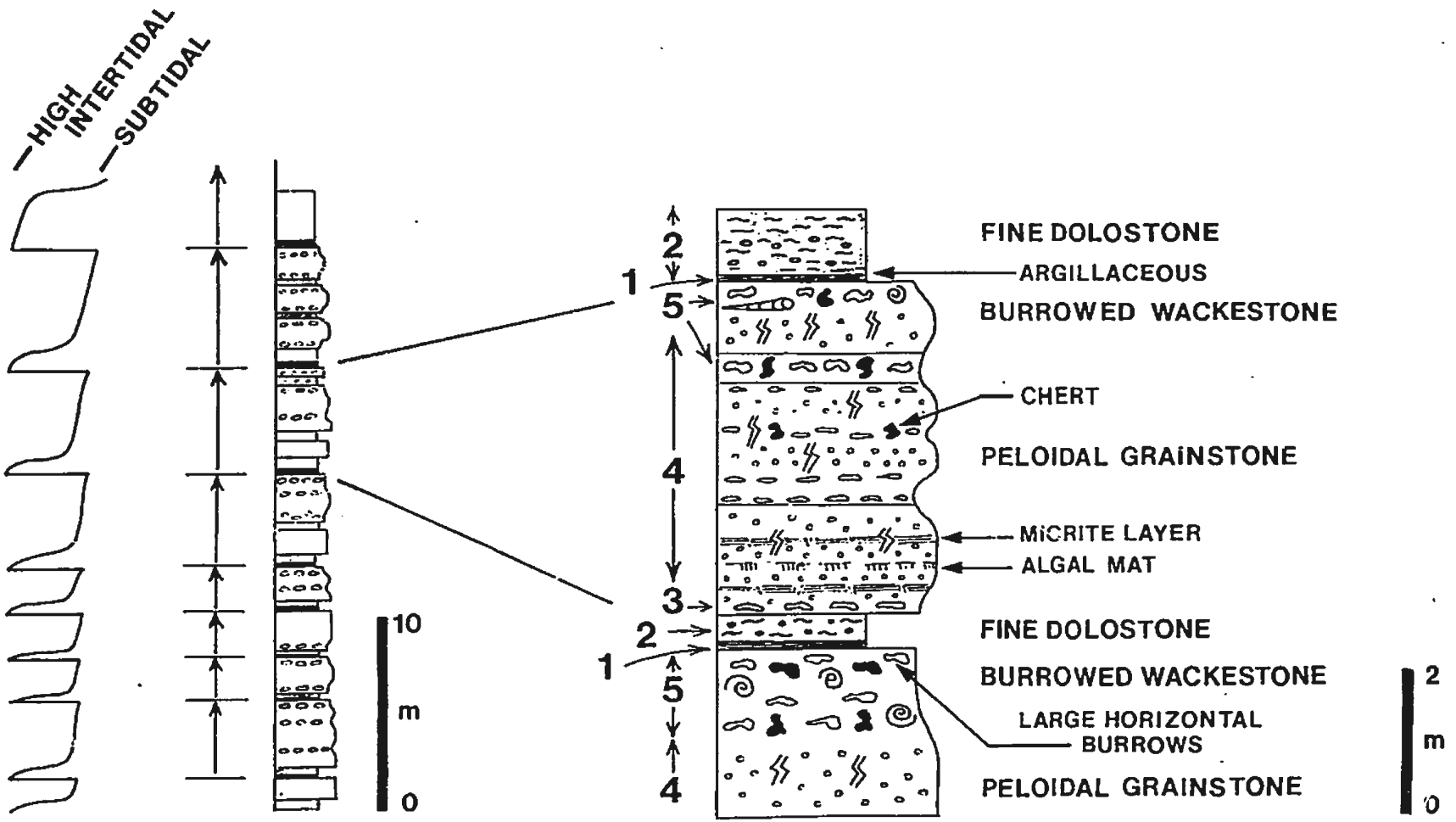
HIGH INTERTIDAL
SUBTIDAL
10
m
0
2
1
5
4
3
2
1
5
4
FINE DOLOSTONE
ARGILLACEOUS
BURROWED WACKESTONE
CHERT
PELOIDAL GRAINSTONE
MICRITE LAYER
ALGAL MAT
FINE DOLOSTONE
BURROWED WACKESTONE
LARGE HORIZONTAL BURROWS
PELOIDAL GRAINSTONE
2
m
0

(3) Burrowed wackestone. This sediment abruptly overlies the upper surface of the mudstone and pass gradationally upwards into peloidal grainstone. The wackestone was deposited subtidally.

(4) Peloidal packstone and grainstone. These lithologies laid down in shallow subtidal conditions dominate a composite unit with alternating cm-thick layers of mudstone, grainstone, packstone and wackestone. Burrowing and sparse skeletal fragments occur throughout the unit. Thin beds of densely burrowed wackestone are intercalated within the unit.

(5) Burrowed wackestone. Shallow subtidal, burrowed wackestones gradationally overlie the peloidal beds and caps a typical sequence. These muddy carbonates commonly contain commonly large fossils of orthoconic cephalopods and planispiral gastropods. Cherts which locally replace mottles in the upper 20 cm may reflect migration of silica-saturated waters beneath an exposed surface at the top of the sequence.

3.6.3 Depositional Environment

During deposition of the peloidal member water depths varied cyclically from very shallow subtidal to intertidal. Peloidal sands and burrowed muds accumulated in very shallow subtidal waters and beds of mud accreted in shallowest conditions. A typical cycle is interpreted to have developed as follows (Fig. 3.2).

(1) A non-depositional surface formed at the top of the burrowed subtidal muds as water shallowed. The muds became locally emergent and rare evaporites, now represented by chert nodules, precipitated in the upper layer of sediment.

(2) As sea level rise drowned the substrate, mud deposition preceded the onlap of grainy, peloidal sediments. Early sedimentation of muds varied from shallow subtidal, storm deposits which were burrowed by Chondrites infauna to intertidal accumulations of structureless muds and laminites in the upper part of the member.

(3) Burrowed peloidal muds and sands were deposited as the shallow subtidal substrate deepened. These sediments also may represent the buildup of the "carbonate factory" (James, 1984) as infauna and other organisms became established and contributed peloidal grains. Cohesive mud laminations, algal mats and early lithification locally stabilized the substrate and left vague, thinly-bedded units. A macrofauna of gastropods, nautiloids and soft-bodied organisms inhabited and reworked the sediments. Abundant algae, deposit feeders and erosion of lithified mud contributed abundant peloids and intraclasts which may have accumulated as washover deposits on stabilized mud laminations.

(4) Peloidal sands graded upwards into burrowed muds in response either to deepening and/or slowed deposition preceding the cessation of sedimentation and the return to stage 1. Slowed deposition was probably a response to isolation behind buildups in the outer platform. Deepening implies that rapid sea level drop caused the subsequent emergence of non-depositional surfaces.

CHAPTER 4 STRATIGRAPHY AND SEDIMENTOLOGY OF THE AGUATHUNA FORMATION AND TABLE POINT FORMATION

4.1 Introduction to the Stratigraphy of the Aguathuna Formation

The Aguathuna Formation at Daniel's Harbour is an assemblage of peritidal dolostones in which buff-weathering, very finely crystalline dololaminite is the most distinctive lithology. Buff-weathering dolostones comprise more than 80% of the section. At the Table Point type section the base of the formation is placed 2.5 m below the "worms" marker at the base of a tan, partially laminated, fine dolostone (Knight and James, 1987). The top of the formation is drawn at the abrupt transition with Table Point limestones. Thin dololaminites interbedded with limestone above this boundary are included within the Table Point Formation. The Aguathuna Formation in the Daniel's Harbour - Table Point area is informally subdivided into lower, middle and upper members (Fig. 4.1). Collins' (1971) thesis at Queen's University, Kingston, Ontario contains a detailed photographic log of the formation from DDH 482 (Fig. 1.4). The stratigraphy of this log is given in Appendix H.

4.2 The Lower Member

4.2.1 Lithologies

The lower member is a unit, approximately 60 m thick, in which

many beds can be correlated beyond the mine area over more than 300 km² (Fig. 4.1, 4.2). Seven peritidal lithofacies comprise the member (Figs. 3.1, 4.1).

(1) Burrowed-mottled to Massive Dolomite: These units, up to one metre thick, are partially to completely burrowed and possess a two-tone texture of gray-brown, very finely (10 μm) crystalline matrix and buff-tan, finely (10-50 μm) crystalline burrow mottles (Pl. 4.1d,e). The distinctive, Thalassinoides (Sheehan and Schiefelbein, 1984) burrows comprise networks of filled passageways which completely rework beds. They are up to 5 cm wide in cross-section, although elongated horizontally, penetrate vertically 1-5 cm (Pl. 4.1d,e). These lithologies also contain minor conodonts of restricted Midcontinental type (Stait,1988). Collins (1971) reported rare fragments of brachiopods, pelecypods, gastropods and bryozoans. Beds are commonly amalgamated into units 3 to 10 m thick (Pl. 4.1f).

The basal contacts of beds vary from abrupt to gradational; tops are always sharp. Beds occur either (1) abruptly above argillaceous finely laminated dolostones or coarse centimetre-scale dololaminites, or (2) gradationally above partially mottled massive to coarse laminated dolostone (Pl. 4.1a). The upper several centimetres are densely burrowed and coarsely crystalline (Pl. 4.1d). Erosional surfaces commonly form the tops of burrowed beds, which locally are capped by thin (3 to 10 cm) dololaminites.

The thoroughly burrowed mud units are similar to modern day low intertidal to shallow subtidal sediments mined by Callianassa shrimp

Figure 4.1 Correlation of the Lower Member of the Aguathuna Formation in the Mine Area

4.1a A profile of the Aguathuna Formation is drawn between seven representative drill holes and the Table Point type section across the 250 km^2 study area (Fig. 4.2). DDH's 1295 and 1575 were drilled 18 km east of the mine. The other holes occur around the mine. The lower member varies little in thickness. The middle member thickens over structural depressions and elsewhere is only a veneer or eroded. Both members are gently folded beneath the St. George Unconformity and the overlying upper member generally forms a veneer and locally thickens over dolines and at Table Point.

4.1b Beds of the lower member are correlated. DDH's 965, 1295, 1575 and 1863 represent normal tidal flat localities. The profile between DDH's 1863, 1868, 1865 and 498 shows an increased proportion of burrowed lithologies at margins of later dolines (1868) and within them (1865 and 498). This implies that subtle subsidence occurred along the same structures during deposition of the lower member.

Key beds and horizons are correlated between all drill holes. These units include thick burrowed beds, exposure horizons of breccia and/or shale. Note, in particular, the extensive correlation of the Upper Argillite and the overlying thick burrowed unit.

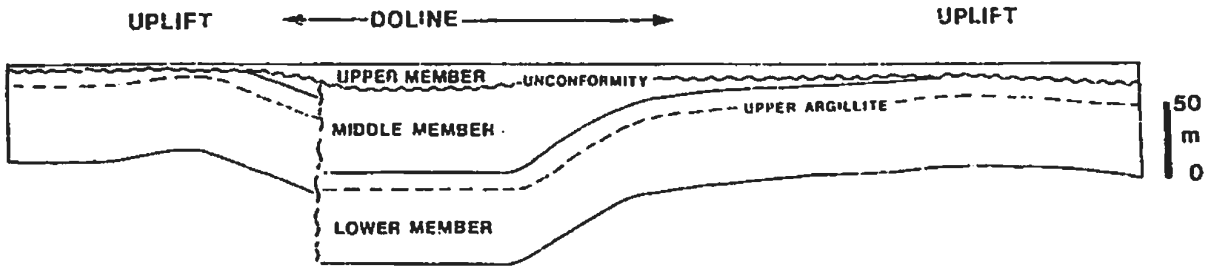

A. CROSS-SECTION OF THE AGUATHUNA FORMATION

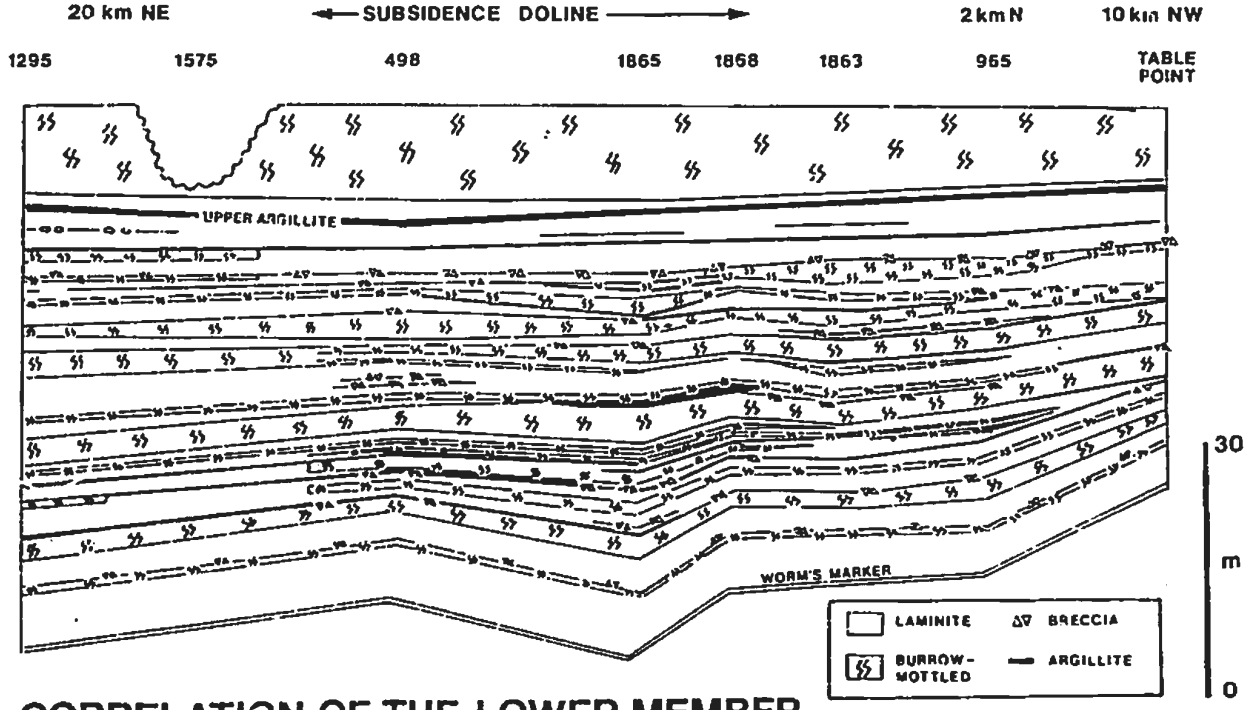

B. CORRELATION OF THE LOWER MEMBER

Figure 4.2 Location Map for Correlation of the Aguathuna Formation

The drill holes correlated in Fig.4.1 form a section approximately 35 km long. The Table Point type section occurs 10 km north of the mine. DDH 965 with stratigraphy characteristic of the region is situated 2 km north of the mine. A series of northeast-trending faults control several dolines, grabens and areas of uplift and erosion. DDH's 498, 1863, 1865 and 1868 represent a longitudinal section across a margin of a doline. The section between DDH's 1295 and 1575 is 18 km northeast of the mine.

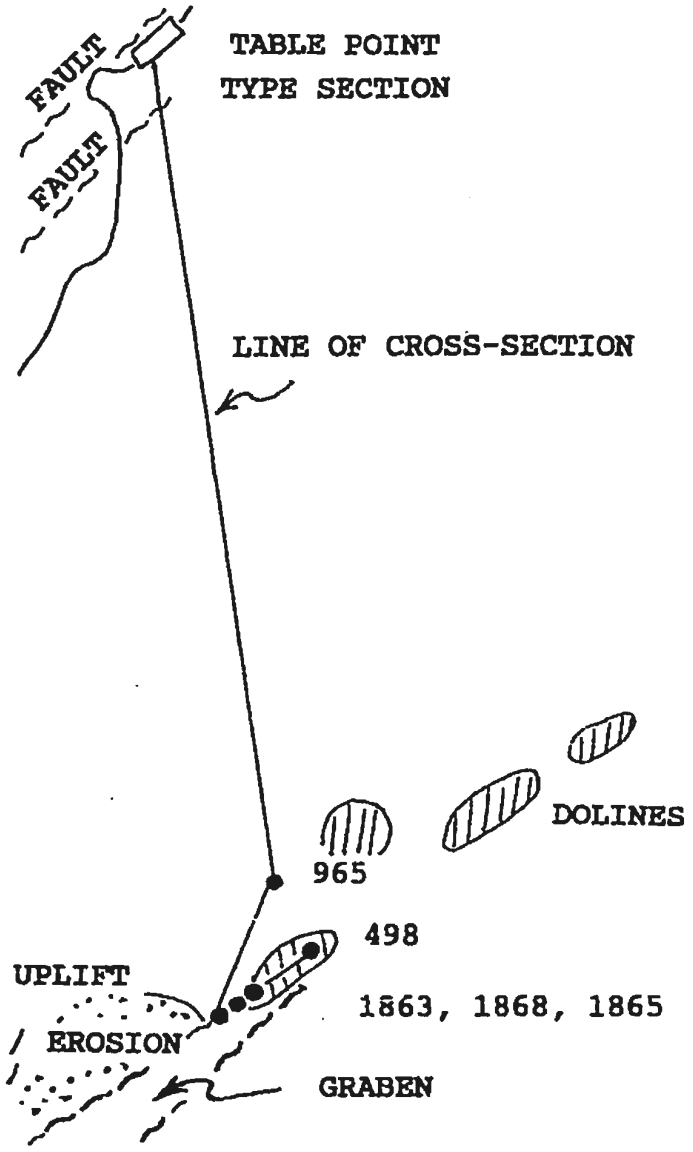

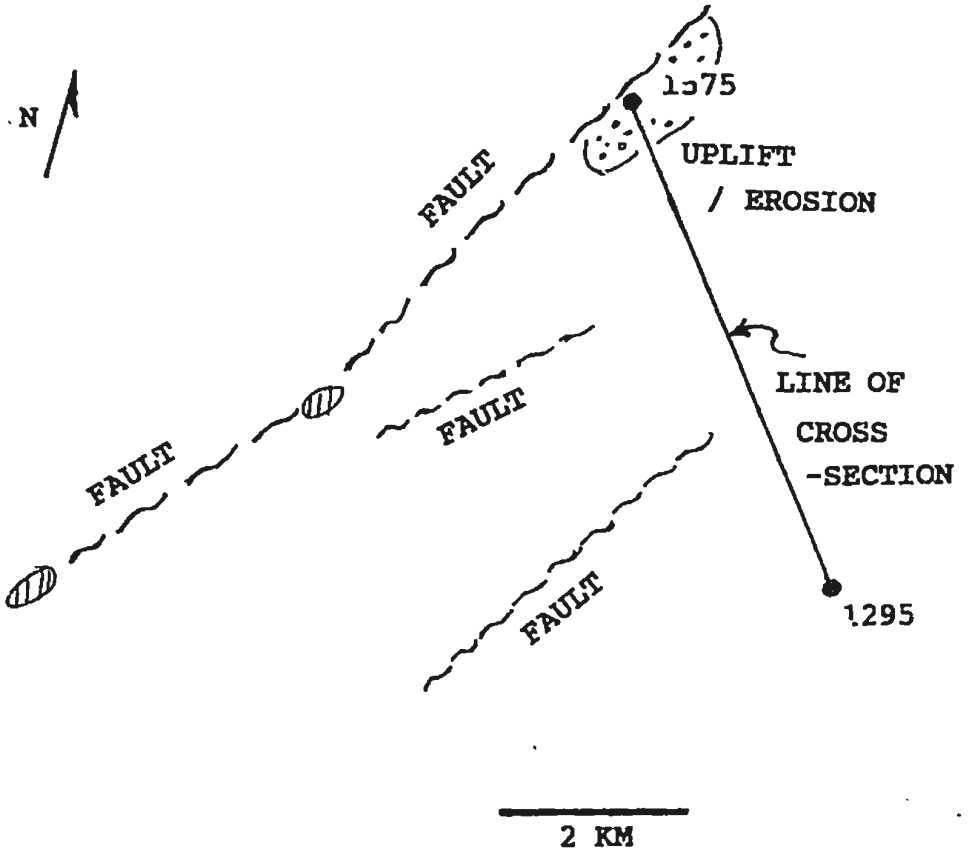

PALEOGEOGRAPHY AND LOCATION OF DRILL HOLE SECTIONS
OF THE AGUATHUNA FORMATION

Plate 4.1 Aguathuna Formation

- Laminites, Shales and Burrow-mottled Beds

(Up is toward the top of the page in all photographs)

a. Finely laminated, cryptalgal dolostones grade upwards into a thick burrow-mottled bed. NW Gravels, Port au Port. The scale is in centimetres.

b. Coarse, cm-thick dololaminites have abrupt,locally scoured bases and planar to wavy upper surfaces. Dark gray, argillaceous laminations and flasers part light gray dolostones. Table Point. The pen measures 14 cm.

c. Argillaceous dolostones contain mud cracks, tepee structures and contorted laminations (arrow). Wavy, stromatolitic dolostones overlie the shales. Table Point. The pen measures 14 cm.

d. The upper portion of a burrowed bed containing large burrows interpreted as Thalassinoides (arrow). It is capped by a 60 cm-thick laminite (above the lens cap). An irregular erosion surface separates the laminite from the overlying burrowed bed. Table Point. The lens cap measures 5 cm.

e. Typical burrow-mottled fabric of dolostone composed of a thorough vertical and horizontal network of burrows (dark gray). Drill core (DDH 1868) from the mine. The scale is in millimetres.

f. A typical burrowed bed, 80 cm thick, displays crude bedding. Large burrows dominate the upper portion of this bed. Table Point. The scale is 20 cm.

PLATE 4.1

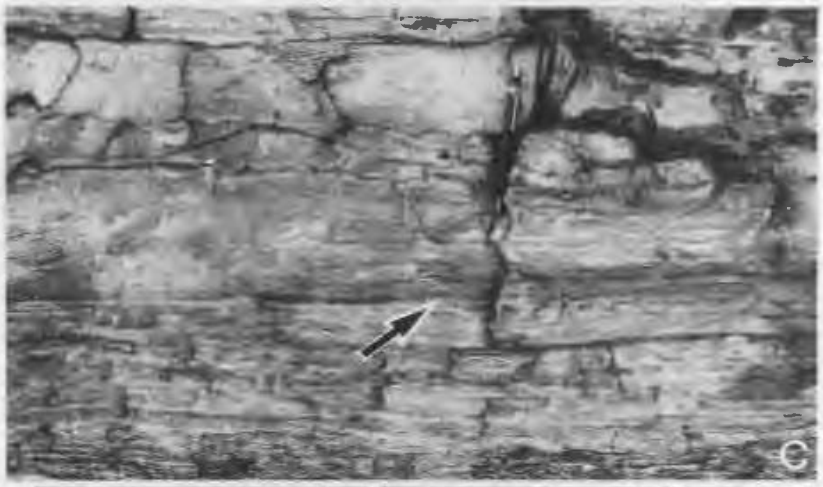

(Shinn, 1968). Unknown organisms bulldozed open galleries through the sediment (Sheehan and Schiefelbein, 1984). In modern analogues theupper limit of burrow homogenization of sediment occurs on low intertidal flats in the humid Bahamas (Hardie, 1977) and in subtidal sediments of Quaternary hypersaline areas (Logan et al., 1974). The exposed tops of these units imply that they accumulated in very shallow water. The paucity of marine megafossils and very limited numbers of conodonts imply that this environment, and probably the entire platform was very shallow and restricted, unlike the modern analogues cited. Hypersaline sea water may have been partially responsible for this situation.

(2) Dololaminites: Dololaminites consist of planar laminations that vary in thickness from fine (millimetre) to coarse (centimetre) size and are grouped in couplets. Thin laminations (0.1 to 1.0 mm-thick) of medium (40 to 60 μm) crystalline dolomite rest on an abrupt base and grade upwards into fine (10 to 20 μm) crystalline, mm to cm-thick laminations (Pl. 4.1a,b). Two types of laminites occur; they are defined as physical and cryptalgal. Physical laminites have small ripple cross-lamination, wavy to lenticular form and graded even layering with local erosional bases and a secondary nodular fabric. Cryptalgal laminites possess very fine mm-sized, wavy to crinkly laminations. Other sedimentary structures associated with the laminites include tepees, desiccation cracks, prism cracks, individual burrow-mottled laminations, "patterned" mottling, nodular chert, intraformational breccias, fissile argillaceous dolostone and post-sedimentary fractures. No macrofossils or conodonts (Stait,1988) occur in the

dololaminites, except for graptolites recovered from a bed at the base of the formation (Williams et al. 1987).

Planar stromatolites and mud/silt laminations indicate accumulation on upper intertidal to supratidal dry mud flats devoid of burrowing organisms (e.g. Kendall and Skipwith, 1969; Shinn et al., 1969; Logan et al., 1970, 1974). Abundant graded plane beds and small ripples imply that much of the sediment accreted during flood tides. Desiccation features and intraformational breccias indicate periodic exposure. Some nodular cherts and "patterned" dolomites are probable remnants of former evaporites (cf. Dixon, 1976; Chowns and Elkins, 1974; see discussion of cherts).

(3) Massive/very fine crystalline dolostone: These rocks are structureless with only faint indications of coarse lamination and/or mottling due to the lack of colour contrast. They generally lie transitionally between underlying laminites and overlying burrow-mottled units.

Since massive beds commonly include evidence of lamination and/or burrow-mottling and occupy their transitional position they probably represent deposition between high and low intertidal flats.

(4) Shales - Gray to green, fissile, dolomitic shales with up to 25% angular quartz silt and fine sand appear as (1) thin veneers at the base of breccia layers; and (2) as 30 to 60 cm thick beds within dololaminites. The first type drapes irregular erosional or solution contacts and is closely associated with chert pebbles and nodules (Pl.

4.2b,c). The second type generally grades upwards into dololaminites. Most shales are extensive and individual units can be correlated between most drill holes in the region (Fig. 4.1). Shale units at Table Point abruptly overlie nodular chert horizons and contain tepees and incomplete desiccation crack polygons and tepees (Pl. 4.1c). The shales contain no conodonts (Stait, 1988). In contemporaneous supratidal sediments of the Romaine Formation, Mingan Islands, Quebec, the same lithology preserves halite casts (Desrochers, 1985); casts are not present at Table Point.

The association of shales with exposure surfaces, mudcracks, dololaminites and chert nodules implies that the silicic silty mud was deposited on exposed flats. The muds may have laid down following extensive short-lived flooding. Local ponds are precluded by the extensive nature of the units. More likely the muds accumulated during periods of extensive flooding or exposure when abundant wind blown silt collected on the flats (cf. Dalrymple et al., 1985). The silts were probably only trapped when the flats were flooded (cf. Persian Gulf, Park, 1976). Mudcracks and tepees imply that desiccation interrupted episodes of flooding. Underlying nodular cherts likely replaced nodular displaced sulphate evaporites which precipitated within the muds. A good analogue for the shales is the grey-green silty dolostone of the Upper Devonian Duperow Formation of the Williston Basin (Wilson, 1967). The Duperow silty dolostones are interstratified with 'sabkha' evaporites and lie above peritidal laminites.

(5) Cherts - Chert is commonly associated with breccia horizons, the base of shales, dololaminites and the upper portions of burrow-mottled beds (Fig. 3.1). Abundant chert is distributed in the upper 10 to 20 metres of the lower member. Pratt (1979) described six main types of chert in the St. George Group:

(1) Cryptoquartz - Nearly isotropic quartz has minute crystals less than 4 μm in size.

(2) Microquartz - Equant anhedral interlocking quartz crystals are up to 20 μm in size (Pl. 4.2e).

(3) Limpid Megaquartz - Anhedral to euhedral crystals that range widely from 20 μm to 3000 μm in size (Pl. 4.2f).

(4) Flamboyant Megaquartz - Masses of large elongate anhedral crystals, up to several millimetres in length, have a coarse radiating habit.

(5) Quartzine - This rare length-slow, coarsely fibrous quartz commonly appears as radial fibrous spherulites that replace anhydrite.

(6) Chalcedony - This length-fast fine to coarsely fibrous quartz occurs as a brown, layered botryoidal pore-filling cement (Pl. 4.2e).

Four chert-lithofacies associations are present in the Aguathuna Formation at Table Point and NW Gravels, Port au Port.

(1) Polymict chert pebble-cobble conglomerates overlying erosional surfaces are composed of nodule-shaped clasts of amber cryptoquartz, banded gray microquartz and white megaquartz. Banded microquartz cobbles exhibit relic lathe textures (Pl. 4.2e), spherulites and pores

Plate 4.2 Aguathuna Formation - Breccia Beds and Cherts

a. A pebble conglomerate-breccia bed at NW Gravels rests disconformably upon the eroded top of a burrow-mottled limestone bed. Argillaceous dolostone forms the base and matrix around white quartz cobbles. Thin-bedded laminites collapse over the bed and are locally incorporated as breccia fragments. The scale is in centimetres.

b. A core sample from the mine area exhibits an exposure horizon developed upon a burrowed bed and overlain by a thin shale, a chert layer and a brecciated dololaminite. The scale is in millimetres.

c. A breccia bed in core from the mine area consists of fragments of the overlying dolostone encased in a dark gray dolomite rock-matrix. Overlying fractures are cemented by late saddle dolomite. The scale is in centimetres and inches.

d. Brecciated dolostone beds and multiple exposure horizons at Table Point. The head of the hammer rests on a lower exposure surface eroded into the top of a burrowed bed. The second surface (arrow) cuts a dololaminite bed. A regolith of dolostone cobbles above this surface is cemented by chert. The overlying beds are fractured and partially collapsed. The hammer handle is 40 cm long.

e. A photomicrograph of a banded, microquartz cobble exhibits relic lathe structure (arrow) of evaporites in the microquartz. Botryoidal chalcedony cements pore space. Gravels section, Port au Port. The scale bar is 1 mm.

f. Megaquartz crystals exhibit a ghost fibrous texture suggesting replacement of evaporites. Table Point section. The scale bar is 1 mm.

PLATE 4.2

partially cemented by chalcedony. Megaquartz pebbles locally preserve fibrous fabrics (Pl. 4.2f). Late megaquartz partially cements and replaces the matrix of these conglomerates.

(2) Biscuit to cauliflower-shaped nodules of white limpid megaquartz ranging from 1 to 5 cm in diameter are scattered within dololaminite and burrow-mottled beds down to depths of .3 m below exposure surfaces.

(3) Layers of small, 0.5 to 1.0 cm-wide, cauliflower nodules of flamboyant white megaquartz and microquartz occur in dololaminites. Lathes occur within the microquartz nodules.

(4) Gray to amber nodules of cryptoquartz with flat pancake shapes incorporate rhombs of dolomite in concentric, outer growth bands. These also locally preserve lathe textures. They occur within dololaminites, particularly beneath the St. George unconformity, and also occur as pebbles which lie on the unconformity.

Most cherts occur at or below exposure surfaces. Most of the quartz is diagenetic, but sedimentary clasts indicate very early formation of some of the chert. Lathe textures, spherulites, cauliflower morphologies, displacive nodules and fibrous fabrics are interpreted to be relic sulphate fabrics (cf.Chowns and Elkins, 1974). The stratigraphic position at or beneath exposure surfaces supports origin by replacement of sabkha-like evaporites (cf. Kendall,1984). Lack of evaporite relics in most chert, however, suggests that sulphate replacement was minor and silica precipitated by another process such as reflux of silica-saturated ground water and crystallization from local changes in CO_2, SiO_2 or Na concentrations (cf. Lovering and Patten, 1962). This

process may be similar to active silica precipitation in dolomitic carbonates at the Coorong Lakes of south Australia (Muir et al., 1980). The concentration of cherts beneath the unconformity also suggests that elevated CO_2 concentrations in meteoric water caused silicification (cf. Banks, 1970).

(6) Breccia and coarsely crystalline dolostone - Beds of breccia, 5 to 50 cm thick, occur at eight or more levels in the lower member (Figs. 3.1, 4.1; Pl. 4.2). Most of these occur at the top of coarsely recrystallized burrow-mottled dolostones, but a few are associated with shales in dololaminite units. Breccia horizons can be correlated over 300 km^2 in the vicinity of the mine.

Breccias directly overlie planar to irregular erosional surfaces that are locally scalloped by erosional gullies (Fig. 4.3). The breccias themselves, however, are complex units, the products of multiple events. Several erosion surfaces occur in some breccia beds (Fig. 4.3; Pl.4.2b). These surfaces are commonly covered with centimetre-thick green to black shales (Pl. 4.2b) and scattered cobbles of white and gray banded cherts; the latter exhibits precursor sulphate fabrics (Pl. 4.2e). Angular breccias, 5 to 50 cm thick, commonly overlie the shales and cobbles (Pl. 4.2a,d; Fig. 4.3). The breccias are composed of a monomict to oligomict assortment of angular, 1 to 5 cm-sized fragments of dolostone and chert. Most dolostone clasts represent collapsed portions of overlying dololaminites (Fig. 4.3; Pl. 4.2c). A clast-supporting matrix is variably composed of (1) rock "flour" recrystallized to fine to medium crystalline dolomite; (2) black to green argillaceous material; (3) 1 to 5 mm-sized dolostone and chert

Figure 4.3 Multigenerational breccia beds at Table Point

Three outcrops of erosional contacts are associated with varying amounts of chert and breccia. Symbols are identified opposite Fig. 3.1.

(A) Erosional surfaces on burrowed beds are overlain by chert cobbles and thin, coarse crystalline dolostone beds.

(B) Secondary gullies cut down into an earlier breccia bed. A shale veneer covers the gully surfaces. Chert cobbles and angular fragments of overlying beds fill them, suggesting a subsurface origin.

(C) A minimum of two erosional surfaces occur in this breccia complex. A thin shale and chert cobbles cover the lower surface. The subsurface origin of the angular breccias is implied by sagging and partial collapse of intercalated and overlying beds.

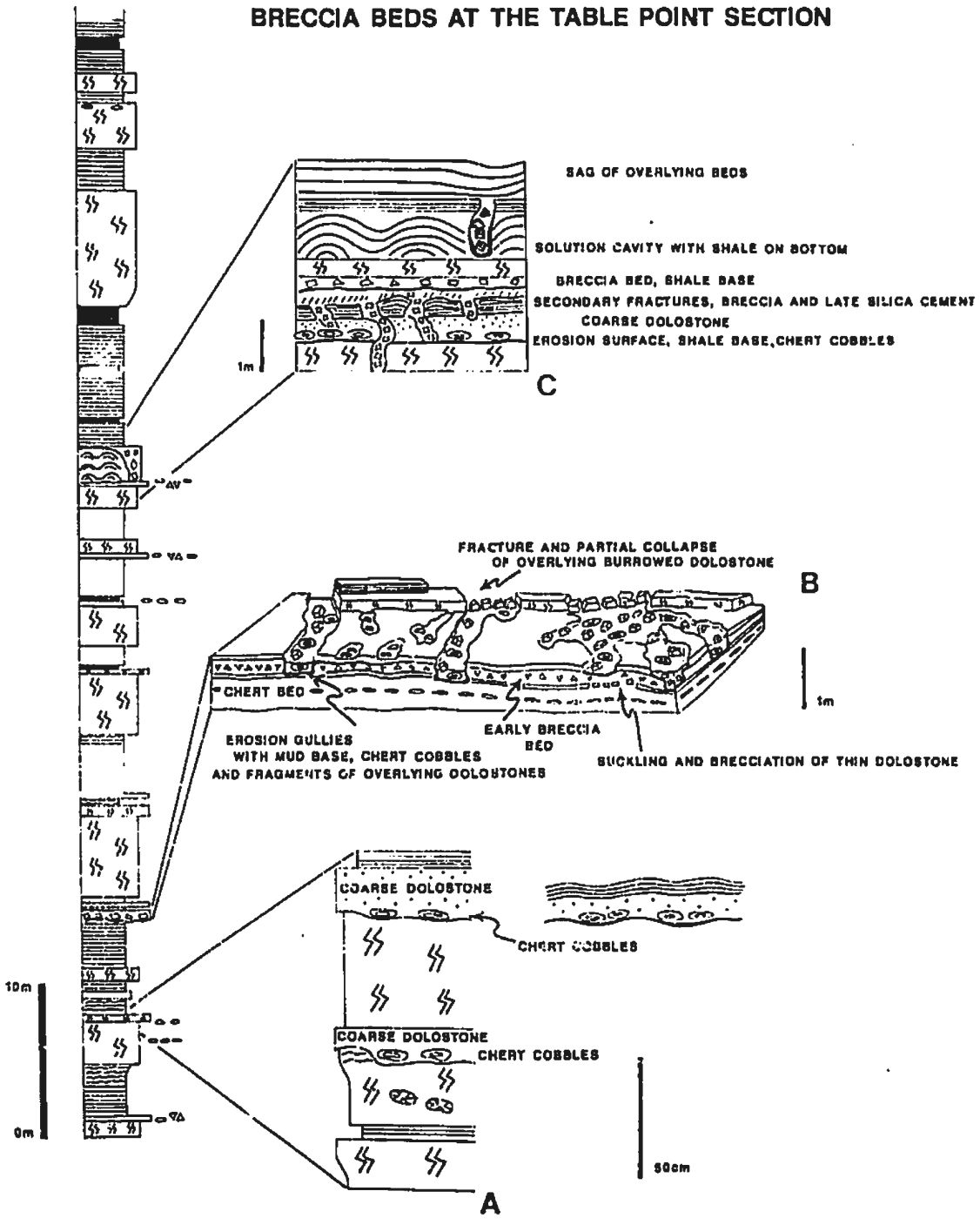
BRECCIA BEDS AT THE TABLE POINT SECTION
SAG OF OVERLYING BEDS
SOLUTION CAVITY WITH SHALE ON BOTTOM
BRECCIA BED, SHALE BASE
SECONDARY FRACTURES, BRECCIA AND LATE SILICA CEMENT
COARSE DOLOSTONE
EROSION SURFACE, SHALE BASE, CHERT COBBLES
1m
C
FRACTURE AND PARTIAL COLLAPSE OF OVERLYING BURROWED DOLOSTONE
B
1m
CHERT BED
EROSION GULLIES WITH MUD BASE, CHERT COBBLES AND FRAGMENTS OF OVERLYING DOLOSTONES
EARLY BRECCIA BED
BUCKLING AND BRECCIATION OF THIN DOLOSTONE
COARSE DOLOSTONE
CHERT COBBLES
COARSE DOLOSTONE
CHERT COBBLES
10m
0m
50cm
A

clasts; (4) up to 30% late silica cement; and (5) late megacrystalline, white saddle dolomite.

The post-sedimentary origin of the breccias is demonstrated by several features: Breccia-filled veins cut beds. Overlying beds collapse and contribute fragments. Beds 5 to 10 m above breccias sag over them (Fig. 4.3).

Most breccia beds are products of multiple events that reflect sedimentation to burial diagenesis. The bases of beds are irregular disconformities upon which probable wind blown silts settled and evaporites crystallized from salt pans or discharging ground water (Kendall, 1984). Evaporites appear to have been rapidly replaced by chert, which then weathered out as pebble beds. Stromatolites and thin mudstones covered the conglomerate beds. Repeated erosion locally cut down through these beds. Later subsurface solution produced strata-bound cavities followed by brecciation, collapse and sag of overlying strata (Fig. 4.3). Throughout burial subsurface fluids repeatedly dolomitized and silicified the matrix of these permeable beds.

(7) Domal stromatolites - Laterally-linked-hemispheroidal stromatolites occur at one horizon at Table Point although identification in nearby cores is difficult. Similar stromatolites are, however, distributed throughout the Aguathuna Formation on the Port-au-Port Peninsula and constitute an important key to environmental interpretation. Characteristically, domal stromatolites 10 to 100 cm in thickness lie immediately above shales at the base of burrow-mottled units and some laminated beds.

Smooth laminated, domal stromatolites form over a broad environmental range in moderate to high energy subtidal to supratidal zones (cf. Shark Bay, Australia, Logan et al., 1974). They commonly occur on "wet" flats in the upper intertidal zone and along supratidal ponds (cf. Grotzinger, 1986; Hardie, 1986). The association of Aguathuna stromatolites with breccia beds and shales implies that they grew high on tidal flats probably at the margin of supratidal ponds. Their position at the base of burrowed beds also suggests that stromatolites mark onlap or intermittent flooding of the flats.

4.2.2 Distribution of Lithologies

Lithologies of the lower member are distributed vertically in 8 or more distinctive repetitive sequences. Each sequence generally consists of a 1 to 3 m-thick burrow-mottled unit with an erosional, conglomeratic cap overlain by 2 to 8 m of dololaminites with shales (Fig. 4.1). A typical sequence consists of four sedimentary components arranged in a consistent order (Fig. 4.4).

(1) The base of the sequence is drawn at the abrupt upper surface of a burrowed unit. The surface is either a flat, irregular karsted or erosional contact with shale-filled cracks.

(2) A pebble-conglomerate bed, 5 to 20 cm thick, covers this surface. Each bed has a basal millimetre to centimetre-thick green shale (Pl. 4.2b). Cobbles, pebbles and layers of chert and megaquartz, some with relic evaporitic textures, cover the thin shales (Pl. 4.2a,b). Stromatolites and planar cryptalgal laminites cap the pebble bed. Many of these beds are brecciated due to collapse.

Figure 4.4 Vertical Distribution of Lithologies of the Lower Member of the Aguathuna Formation

The lower member is composed of seven or more repeated lithological sequences (refer to Fig. 3.1 for the legend). Each sequence has four main components:

(1) An abrupt erosional contact at the top of burrowed beds.

(2) A thin shale forms the base of pebble-conglomerate units and commonly is the only feature between (1) and (3). Pebble-conglo- merate beds overlie the thin shales. Quartz pebbles and cobbles are overprinted by post-depositional, intraformational breccias.

(3) Laminites dominate 2 to 8 m of section which also contains shale beds, cherts and thin burrowed beds. The laminites locally grade upwards into overlying burrowed beds. Otherwise the contact is abrupt.

(4) Thick burrowed units vary from 1 to 4 m in thickness and are anomalously thick (10 m) at the top of the member. The beds tend to thin upwards and upper beds, in particular, shallow upwards into erosional caps.

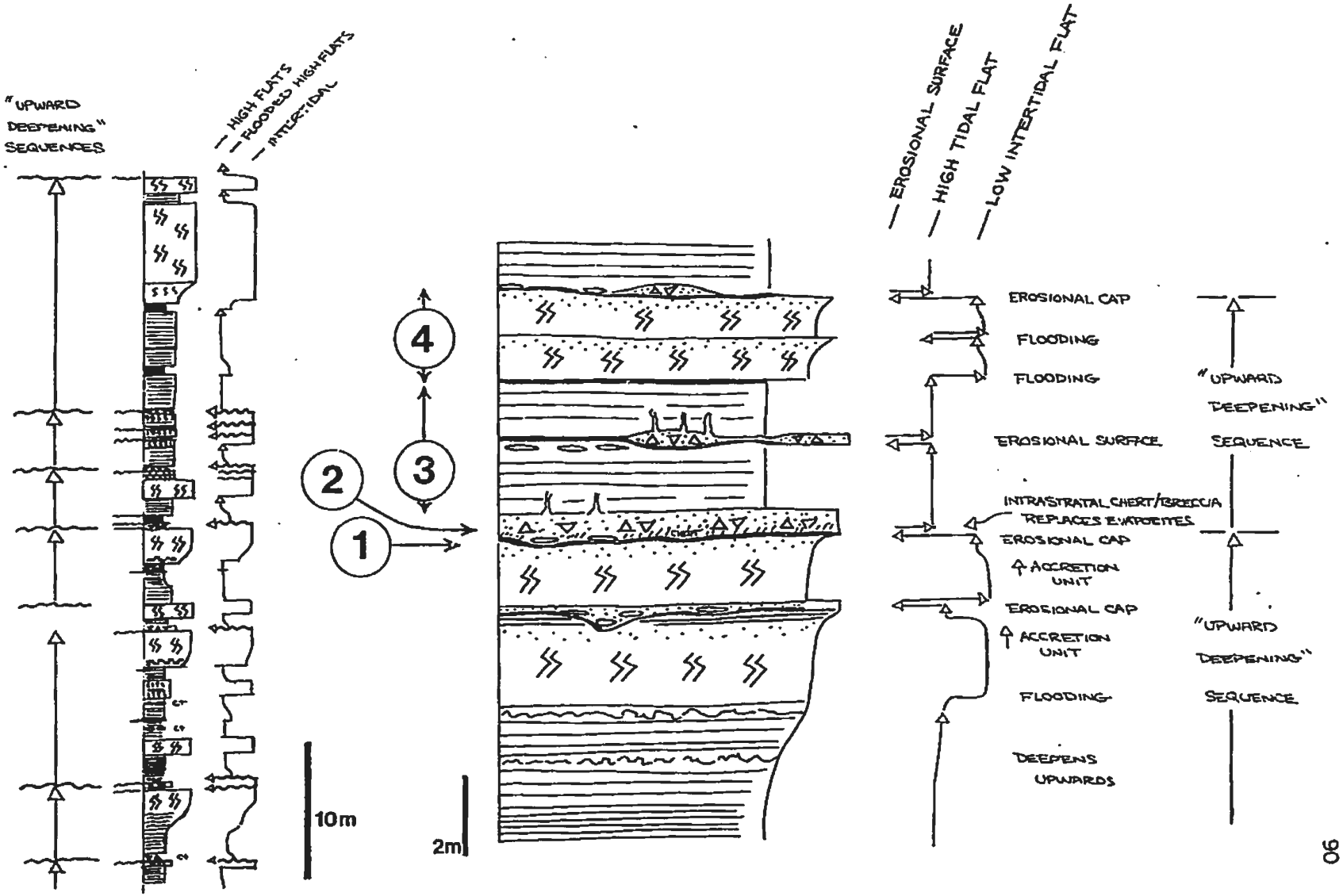
"UPWARD DEEPENING" SEQUENCES
HIGH FLATS
FLOODED HIGH FLATS
INTERTIDAL
10m
2m
1
2
3
4
EROSIONAL SURFACE
HIGH TIDAL FLAT
LOW INTERTIDAL FLAT
EROSIONAL CAP
FLOODING
FLOODING
EROSIONAL SURFACE
INTRASTRATAL CHERT/BRECCIA REPLACES EVAPORITES
EROSIONAL CAP
ACCRETION UNIT
EROSIONAL CAP
ACCRETION UNIT
FLOODING
DEEPENS UPWARDS
"UPWARD DEEPENING" SEQUENCE
"UPWARD DEEPENING" SEQUENCE

(3) Dololaminites dominate a 2 to 7 m thick unit which varies in composition from millimetre-thin cryptalgal laminations to centimetre-thick, partially burrowed beds. Some units grade upward into nodular, massive or burrowed upper portions, whereas others have abrupt contacts with overlying burrowed units. Bases of some units are locally argillaceous. Intercalated desiccation-cracked shales, 10 to 30 cm thick, tend to have abrupt bases above dololaminites with chert nodules and grade upward into laminites. Metre-scale burrowed beds occur locally as part of small-scale shallowing-upward cycles.

(4) Burrow-mottled dolostones in units 3 to 12 m thick consist of amalgamated 10 to 200 cm thick beds. The basal contact is either abrupt or transitional. The lower portion commonly has a fabric of horizontal burrows or vague mottles. Metre-thick basal beds thin upwards to repeated 10 to 20 cm-thick beds with erosional upper surfaces capped by chert-pebble conglomerates (Fig. 4.3A). Thin laminite caps occur locally (Pl. 4.1d). The upper 5 to 20 cm of burrowed units contain large burrows, cauliflower megaquartz and coarse crystalline dolostone. A prominent erosional surface forms the top of most burrowed units.

Most packages can be correlated throughout the 300 km^2 study area but they change in thickness laterally with some units pinching out (Fig. 4.1). Thick burrowed units, their erosional caps and shale beds are extensive. Laminite units are locally dominated by burrowed beds around the margins of synsedimentary faults (Fig. 4.1).

The thickness of sequences varies from 6 to 10 m in the lower 40 m of the lower member. An 18 m thick sequence which forms the top of the member is composed of an 8 m laminite/shale unit overlain by a 10 m

burrowed bed. The Upper Argillite marker bed occurs in the upper part of the 8 m laminite unit (Figs. 3.1, 4.1).

This vertical stratigraphy is compared to the Table Point type section and the NW Gravels section 200 km to the south at Port au Port (Fig. 1.1, 4.5). The lower member at Table Point is only 44 m thick compared to 60 m at the mine and it exhibits general thinning throughout the section. All sequences, however, are present in both areas.

The 60 m thick section at NW Gravels differs in composition from the Daniel's Harbour area. Key beds, however, are present. They include major burrowed units, shale beds, some erosional caps and the thick laminite-burrowed sequence at the top of the member. The detailed sequential stratigraphy is complicated by metre-scale intercalations of varied lithologies: laminites, thick shales, Thalassinoides beds and stromatolitic beds with burrowed to laminated tops. These lithologies are arranged in sequences, 4 to 10 m thick, with 1 to 3 m thick shale bases, 1 to 4 m thick stromatolitic to laminated mid-sections and 2 to 3 m burrowed upper portions (Fig. 4.5). They compare closely to those at Daniel's Harbour.

Correlation with other sections of the lower member at Bonne Bay and Hare Bay has not been made. Sequences within these sections possess shallowing-upward cycles with common intertidal lithologies (Knight, 1986; Stenzel, pers. comm. 1988). The thick laminite-burrowed sequence occurs, however, in an anomalously thick Aguathuna Formation at Bonne Bay (Stenzel, pers. comm. 1988). North of Daniel's Harbour the lower member is either thin or not present (Knight 1985, 1986).

Figure 4.5 Correlation of the Lower Member of the Aguathuna Formation Between Newfoundland Zinc Mines, Table Point and Northwest Gravels

Drill Hole 965 represents typical stratigraphy of the lower member at the mine area. This same stratigraphy is present at Table Point. The thickness of the member at the type section thins, however, from 60 to 44 m. Key burrowed beds from these sections can be correlated with the Northwest Gravels section on the Port au Port Peninsula 200 km to the south. Sequences, 4 to 10 m thick, compare to those at Daniel's Harbour. They are composed of shale beds at the bottom overlain by stromatolitic and laminated units capped by burrowed beds. Breccia beds are minor. Symbols are identified in the legend of Fig. 3.1.

TABLE POINT MINE (DDH 965) NW GRAVELS

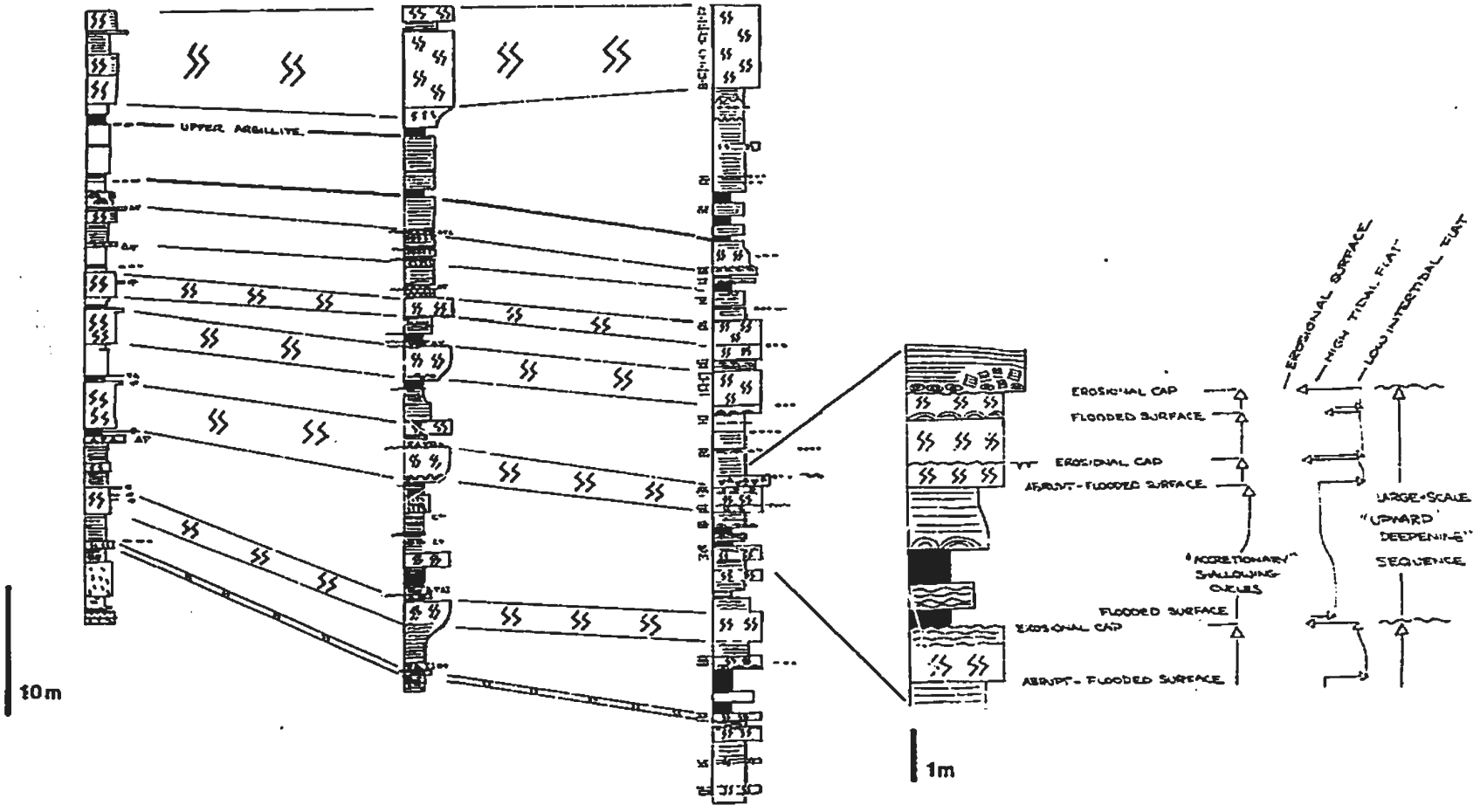

These regional correlations of the lower member have important implications for the origin of the metre-scale cycles. The extensive nature of the intertidal units and of the sequences in the study area and their correlation with the NW Gravels section implies that marine onlap and offlap operated over broad areas.

4.2.3 Depositional Environment

Supratidal laminites dominated high peritidal flats which were grazed by burrowers and covered by silicic muds during periodic flooding and marine onlap. Abrupt offlaps exposed the burrowed substrates and subjected the local platform to erosion and precipitation of evaporites and cherts. Evaporites, mud cracks and laminites suggest an arid or restricted setting for the mud-dominated, low energy platform which contrasted with the grainy substrates of the upper Catoche Formation deposited under more humid (?) conditions.

Overall, the sequences are interpreted as upward deepening overall although internal smaller-scale packages commonly shallow upwards, eg. shales to laminites and burrowed beds with erosional or laminite caps. The deepening upwards sequences are interpreted to have developed in four stages:

(1) Extensive subtidal to intertidal flats emerged as a subaerial surface without an offlap cap of laminites.

(2) A veneer of wind-blown silt covered the subaerial surface and probably settled out in hypersaline pools or as a residue of evaporite dissolution. Thin evaporite beds and nodules precipitated on and beneath the surface from refluxed brines and hypersaline pools. Silica

also precipitated from the brines; partially replaced sulphates; and cemented coeval dolomites. Erosion and deflation then incorporated quartz pebbles and cobbles into lag deposits.

The evaporites probably precipitated from sea water that flooded the erosional surfaces and largely evaporated in the mine area. Longer-lived flooding at Northwest Gravels resulted in the accumulation of muds (shale beds) which shallowed upwards into stromatolites and supratidal laminites. Similar sequences occurred locally in the area of the mine.

(3) Supratidal carbonate sediments onlapped the subaerial platform as subsidence and marine inundation of the outboard platform initiated carbonate production. Tidal flat sedimentation persisted and kept pace with subsidence as tides and winds accumulated thick beds of laminite and shale. Silicic muds at the base and middle of units probably accumulated during extensive, periodic flooding of the high flats (cf. Wilson, 1967; Park, 1976). They graded upwards into supratidal laminites.

(4) Extensive flooding or migration of the intertidal zone over the region occurred gradually or abruptly as the rate of sea level rise (eustatic rise + subsidence) exceeded that of sedimentation. These platform-wide events resulted in regionally extensive subtidal to intertidal units. Subtidal to intertidal conditions dominated during the deposition of the 2 to 4 m thick units as burrowing Thalassinoides infauna excavated a firm mudflat. Accretion and/or sea level fluctuations repeatedly exposed successive beds toward the tops of sequences. Minor elevation differences between present day exposed surfaces and burrowed flats (1 to 2 m, Shinn, 1986), however, suggest that sea level

changes were not dramatic. The general lack of laminite caps implies, however, that external eustatic or tectonic forces caused the emergence of the tidal flats.

4.2.4 Interpretation of the Cyclic Stratigraphy

Introduction - The cyclic peritidal stratigraphy within the upper St. George Group (peloidal member of the Catoche Formation and the lower member of the Aguathuna Formation) records fluctuations of sea level. Incomplete shallowing upward sequences imply that eustasy or episodic tectonism constrained normal shoreline progradation. Vertical continuity of tidal flat lithologies also indicates that carbonate sedimentation remained in near equilibrium with subsidence and eustasy.

Any sedimentary model must account for five distinctive features of the lower member: (1) Most beds can be correlated throughout the study area and some subtidal/intertidal units may extend over more than 200 km. (2) Repeated burrowed beds within intertidal units are capped by exposure surfaces. (3) Thick laminite and burrowed units record prolonged periods of supratidal and subtidal/intertidal sedimentation, respectively. (4) The laminite units are not classical tidal flat caps. They are thick; rest on exposure surfaces and subaerial conglomerates; and locally grade upwards into intertidal units. (5) The alternation of laminite and burrowed units express long period rhythms that can be related to seismicity or climate-controlled Milankovitch cycles. The significance and interpretation of these four aspects are first considered; then, eustatic and tectonic models are evaluated.

Interpretation of Subtidal/Intertidal Units - The widespread subtidal/intertidal units are interpreted to have resulted from regional, and possibly larger scale flooding, of the platform. The stratigraphy of these units implies that sedimentation occurred during periods when sea level fluctuation constrained accretion processes. The subtidal to low-intertidal burrowed beds tend to thin upwards within amalgamated units and upper beds display repeated exposure caps. This stratigraphy implies that during sedimentary accretion of the intertidal flats rapid and repeated sea level change caused emergence and flooding without upper tidal flat sedimentation (the standard laminite cap). Stranding and exposure of subtidal substrates in the Alpine Triassic reflects possibly similar, but much higher amplitude sea level fluctuations (Lofer cyclothems, Fischer, 1964; Latemar Limestone and Dolomia Principale, Hardie et al., 1986; Goldhammer et al., 1987). These sequences display a similar upward thinning of subtidal beds which has been modelled as eustatic Milanko-vitch cycles (Goldhammer et al., 1987). Alternatively this upward thinning reflects the decrease in base level during tidal flat accretion.

Estimated Time Period of Tidal Flat Sedimentation -The alternating sequences of thick (2 to 10 m) units of laminites and burrowed beds accumulated over long periods of time to form the deepening upward cycles. If deposition of the 60 m thick lower member spanned nearly 3 ma.(based on the biostratigraphy, Chapter 2), then rates of sedimentation were relatively slow at approximately 2 to 3 cm/ 1000 years. Individual units, thus, accumulated over periods between 60,000 and 500,000 years and 5 to 7 m-thick, deepening upward sequences developed

in 150,000 to 350,000 years. The laminite units, thus, are not typical laminite caps above intertidal beds, but, rather, represent long periods of upper tidal flat sedimentation.

Significance of Orders of Cycles - Three orders or scales of cyclicity occur in the upper St. George Group.

(1) The first order scheme is overall shallowing on the formational scale. This cycle is interpreted as a general slowing of subsidence on the platform relative to sedimentation.

(2) The second order packaging is deepening upward sequences 2 to 10 m thick. Their composition reflects varying rates of sea level change and sedimentation. Long period sea level oscillations or episodic seismicity occurred over 150,000 to 350,000 year intervals. Subtidal/ intertidal burrowed units accumulated during sea level maxima when significant marine oscillations caused dramatic emergence and flooding of the subtidal flats and prevented upper tidal flat sedimentation. The erosional caps of burrowed units probably marked significant hiatuses during sea level minima. Following sea level minima offshore flooding reestablished carbonate production and inshore upper tidal flat sedimentation which continued in equilibrium with regional subsidence and gradual sea level rise.

(3) Third order metre-scale cycles within second order packages mostly shallow upwards and are commonly arrested. These essentially represent episodes of sedimentary accretion following flooding. Within upper tidal flat units thin shales, burrowed beds or former evaporites grade upwards into stromatolites and supratidal dololaminites. In

subtidal/ intertidal units burrowed beds are capped by thin laminites or erosional surfaces. The characteristic arrested tops suggest either that moderate sea level oscillation or gradual "background" uplift of the platform exposed the flats.

Eustasy, episodic tectonism or a combination of the two generated the sea level changes which controlled this cyclicity.

The Tectonic Model- Regional tectonism related to plate convergence fragmented the platform and caused portions to subside differentially during Late Early to Early Middle Ordovician time (Stenzel and James, 1987, 1988). Condensed stratigraphy of the lower member north of the mine and subtidal facies along synsedimentary faults at the mine indicate tectonic effects on subsidence (Fig. 4.1). Variable rates of subsidence over entire fault blocks or larger areas of the platform possibly accounted for the extensive nature of some beds and cycles. Under this tectonic scenario subtidal conditions existed during seismic episodes of rapid subsidence punctuated by intermittent uplift. Pronounced tectonism in the Daniel's Harbour area produced abundant exposure surfaces. Laminites accreted during intervening, stable periods of gradual subsidence. The thick, upward deepening unit at the top of the lower member reflected regional deepening prior to faulting and uplift of the platform, a predicted effect of the migration through the area of a peripheral bulge during plate convergence (Quinlan and Beaumont, 1984).

The Eustatic Model - Eustasy[1] is also a viable and likely cause of this stratigraphy. Local tectonism on a block-faulted platform does not explain the extensive correlation of the stratigraphy 200 km to the south nor does it adequately account for rhythmic sea level fluctuations. Three criteria imply that eustasy played a role. Firstly, correlation of the stratigraphy suggests that sea level fluctuations affected the entire platform. Secondly, high to moderate amplitude sea level oscillation related to climate-controlled eustasy is a logical means of forming erosional caps on repeated subtidal/intertidal beds (Read et al., 1986; Goldhammer et al., 1987). Thirdly, the periodicity and duration of deepening upward sequences compares to long period Milankovitch rhythms of 100,000 to 300,000 years (Imbrie and Imbrie, 1980; Hardie, 1986).

Under a eustatic scenario a typical sequence would be interpreted as follows: Laminite units accreted as sedimentation kept pace with a gradual eustatic rise. Burrowed beds onlapped the platform during sea level maxima. Moderate amplitude, short period oscillations associated with these maxima caused repeated flooding and emergence of the platform. Erosional caps and breccia beds at tops of subtidal units developed during the fall of the long period sea level cycles and probably lasted throughout the minima. Peritidal sedimentation was renewed as sea level rise in the outboard platform restored production of carbonate sediment. This sedimentation phase commonly began after flooding when evaporite precipitation and silicic mud deposition was

[1]. Eustasy, here, also pertains to large scale fluctuations of sea level on the craton that result from tectonism or isostasy and is not necessarily a world-wide phenomena.

followed by accretion of laminites. Repeated flooding and silicic mud deposition interrupted laminite deposition during short period sea level oscillations. The thick deepening upward unit at the top of the lower member recorded a high amplitude cycle prior to the occurrence of the St. George Unconformity, an anomalous eustatic minimum.

In conclusion, the stratigraphy of the lower member is interpreted to be the result of combined tectonic and eustatic effects. Regional tectonism profoundly affected the platform at the end of the Early Ordovician (James et al., 1988). Shallowing upward of the upper St. George Group, a first order cycle, records decreased subsidence relative to the rate of sedimentation. This is a natural phenomenon of most platforms (Wilson, 1975), but in this case gradual uplift of the margin during lithospheric flexure probably generated shoaling and formation of the St. George Unconformity (Knight et al., in press). The deepening upward second order sequences record long period rhythms which are interpreted to record sea level fluctuations from climate-controlled Milankovitch cycles or pulses of seismicity. The climate-controlled (eustatic) model is preferred for several reasons: (1) the widespread nature of the cycles independent of sedimentation rates and facies changes, (2) repeated subtidal beds with erosional caps are simply explained by high to moderate amplitude sea level oscillations and (3) the estimated periodicity of these sequences is comparable to long period (100,000 to 300,000 year) climatic cycles. Third order metre-scale, shallowing cycles represent normal sedimentary processes of flooding and accretion.

Tectonism altered these processes in several ways: (1) gradual

movement along synsedimentary faults resulted in local changes in subsidence rates and facies, (2) arrested tops of second and third order cycles possibly reflect subtle uplift of the platform which affected late stages of accretion cycles and (3) the abundant breccias and erosional surfaces in the mine area suggest that they are the pronounced effects of local tectonic movements.

4.3 The Middle Member

4.3.1 Nature and Distribution of Lithologies

The middle member, in contrast to the uniformly thick lower member, varies in thickness from 70 m over structural depressions to 7 m at Table Point to less than 2 m in many areas (Figs. 4.6, 4.7). The greatest thicknesses fill areas of solution collapse or down faulting. Areas of solution collapse are underlain by rock-matrix breccias (see Chapter 7). These subsurface karst features fill former caves and occur along faults and are locally stratabound within the Catoche Formation (Fig. 4.6). In the mine area, recognition of the middle member is significant. It marks the beginning of significant faulting and karstification of the platform and indicates that these processes began prior to the regional unconformity as sedimentation continued.

Lithologies are identical to those of the lower member. Burrow-mottled beds are intercalated with tan dololaminites and dark gray, cryptalgal laminites. Metre-scale burrow-mottled beds shallow upwards into laminite caps, in contrast to the lower member where such caps are uncommon. Cherts are locally abundant, particularly at the top of the

member. Thick burrow-mottled facies in the thickest sections are laterally transitional to dololaminite facies where the member thins (Fig. 4.6). Burrow-mottled beds are brecciated and thinned near faults and karst breccias (Fig. 4.6).

4.3.2 Depositional Environment

Peritidal deposits similar to those of the lower member formed a 1 to 10 m-thick veneer over the platform in this region. Contemporaneous faults and subsurface karst created subsiding areas a kilometre or more in width. Peritidal sediments that filled these areas imply that sedimentation rate kept pace with subsidence. Local subsidence, however, was great enough to allow local development of subtidal, burrowed facies.

4.4 The St. George Unconformity

The existence of a regional unconformity was not fully recogniized until the stratigraphy and sedimentology of the drill core was carefully examined. This led to a re-examination and re-interpretation of the Table Point type section. The unconformity is a subtle contact in most drill core and a disconformity at Table Point. In the mine area, tan, massive to laminated dolostones of the middle member are abruptly overlain either by a thin quartz pebble conglomerate, a thin green shale or massive, blue-gray dolostone. At Table Point an irregular surface cuts down into tan laminites with abundant chert nodules and is overlain by a 50 cm-thick shale bed.

Figure 4.6 Stratigraphy of the Upper St. George Group Across a Doline

The lower member of the Aguathuna Formation drops down over the Trout Lake Rock-Matrix Breccia (a subsurface karst breccia) in the upper Catoche Formation (location in Fig.1.4). Gradual thickening of the middle member from 7 to 60 m corresponds to the lateral extent of stratabound oligomict breccias (partial dissolution of beds of the upper Catoche Formation). Burrowed beds of the middle member occur locally within these areas. The upper member generally forms a 7 m-thick veneer over the St. George Unconformity, but it abruptly thickens up to 50 m where it fills sinkhole troughs, 50 to 100 m wide and up to 1000 m long, where the underlying members are down-faulted and collapsed to form polymict breccias in former caves in the Catoche Formation. The middle member is reduced in thickness to 5 to 10 m of solution breccias beneath these sinkholes. Argillaceous limestones with fossil debris and abundant conodonts comprise the sinkhole deposits.

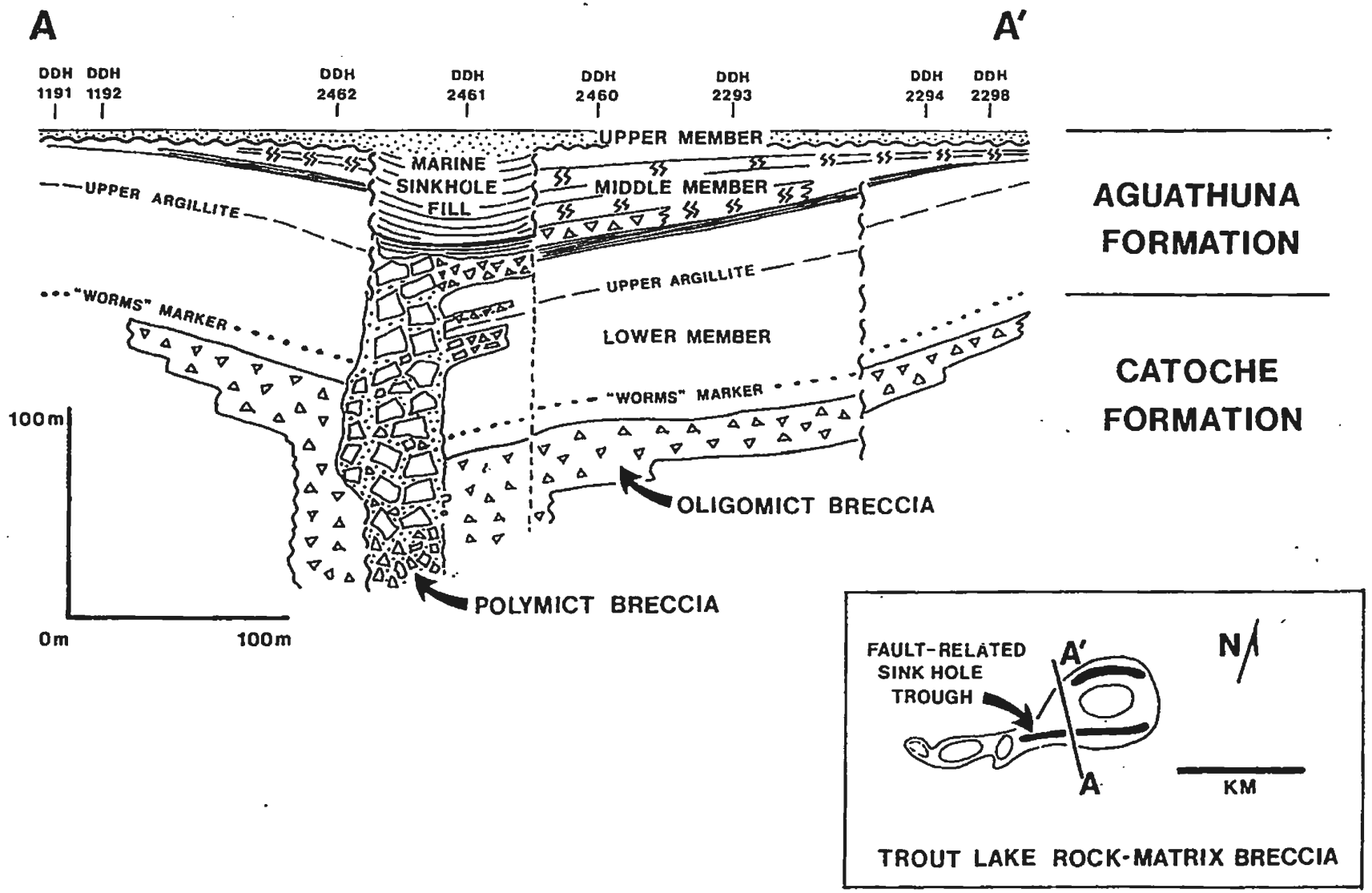
A
A'
DDH 1191
DDH 1192
DDH 2462
DDH 2461
DDH 2460
DDH 2293
DDH 2294
DDH 2298
UPPER MEMBER
MARINE SINKHOLE FILL
MIDDLE MEMBER
UPPER ARGILLITE
"WORMS" MARKER
UPPER ARGILLITE
LOWER MEMBER
"WORMS" MARKER
AGUATHUNA FORMATION
CATOCHE FORMATION
100m
0m
100m
OLIGOMICT BRECCIA
POLYMICT BRECCIA
FAULT-RELATED SINK HOLE TROUGH
A'
A
N
KM
TROUT LAKE ROCK-MATRIX BRECCIA

Figure 4.7 Isopach Map of the Middle and Upper Members of the Aguathuna Formation over a Doline and Structural Depression to the Southwest

An isopach map between two definite stratigraphic markers, the "worms" marker and the base of the Table Point Formation, demonstrates the thickness variation of the middle and upper members of the Aguathuna Formation. Thicknesses greater than 30 m fill areas of solution collapse. Thicknesses between 21 and 30 m define both the subsided 30 to 100 m-wide rim of the collapse zone and, also, a broad area of structural subsidence to the southwest of the collapse zone. Figure 4.2 gives a regional perspective.

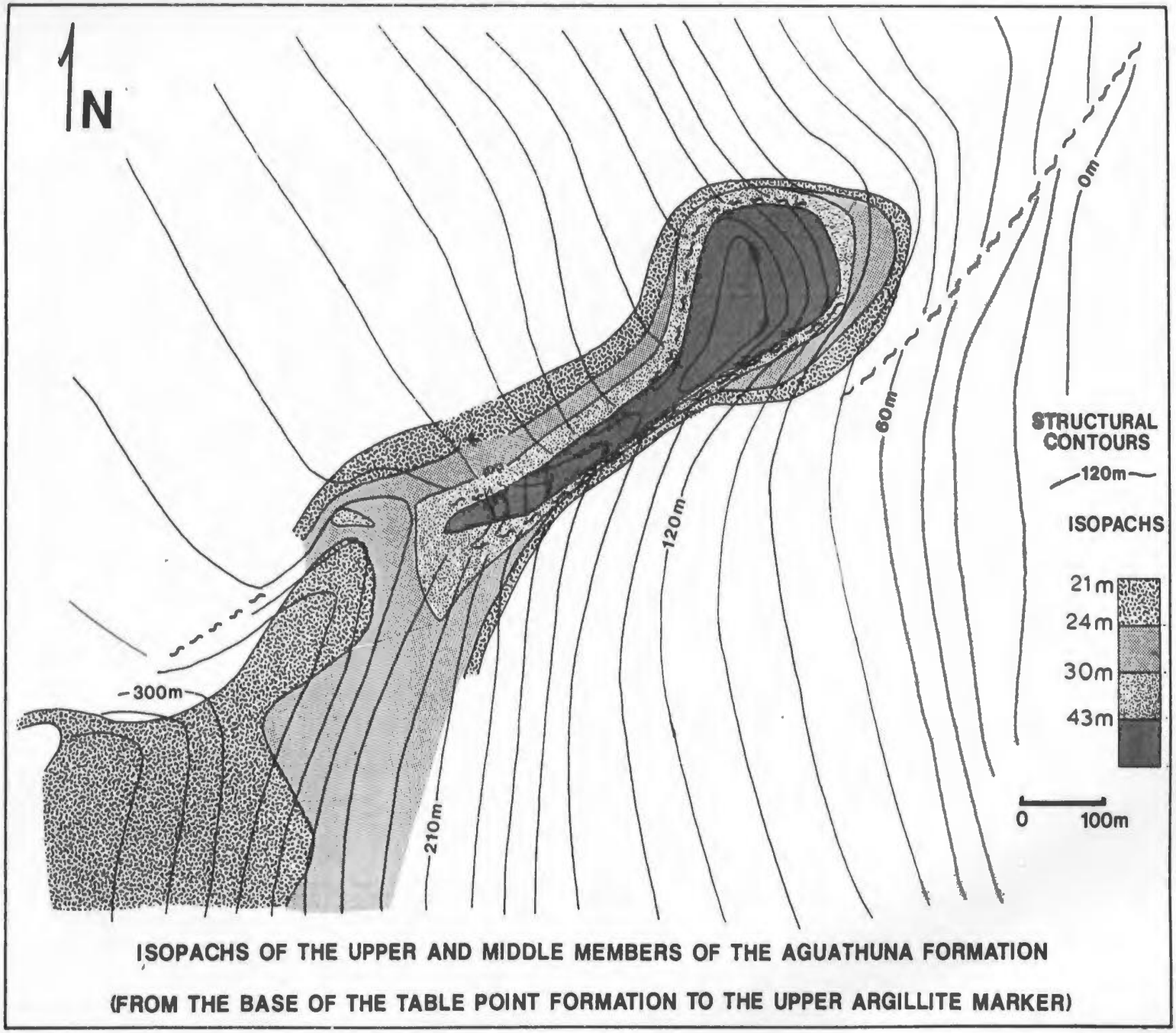

ISOPACHS OF THE UPPER AND MIDDLE MEMBERS OF THE AGUATHUNA FORMATION

(FROM THE BASE OF THE TABLE POINT FORMATION TO THE UPPER ARGILLITE MARKER)

Significant erosional relief of up to 10 m occurs at Aguathuna Quarry at Port au Port and in the mine area. At Aguathuna Quarry an erosional surface, 7 m deep, cuts into the gently folded middle member and is filled with limestones coeval with the upper member (James et al., 1988; Stait, 1988). In the mine area the lower and middle members are tilted and displaced along faults oriented northeast-southwest (Fig. 4.1). A subhorizontal, erosional surface bevels the stratigraphy north of the mine and locally cuts down more than 10 m into the lower member. The lower member dramatically disappears north of the Torrent River Fault (Fig. 1.3), 35 km north of the mine, where the unconformity rests on the Catoche Formation (Knight, 1985; Knight et al., in press).

Several sinkholes occur on the unconformity surface in the mine area. They are steep-sided, elongate troughs, 100 m wide x 1000 m long x 50 m deep, which occur over fault-controlled rock-matrix breccias (Fig. 4.6). Similar sinkholes are documented in east Tennessee (Laurence, 1944; Bridge, 1955).

The history of the unconformity is interpreted as follows: After deposition of the middle member the platform was gently folded and faulted. Contemporaneous or subsequent erosion truncated the deformed stratigraphy and left a microtopography which varied from a nearly level karsted surface to valleys more than 7 m in relief. Local solution collapse over fault-related caves created sinkhole troughs up to 50 m deep.

4.5 The Upper Member

4.5.1 Introduction

A distinctive unit of blue-gray, partly calcareous, finely crystalline dolostone comprises the upper 6 to 15 m of the Aguathuna Formation. Abundant microfossils indicate a distinct difference between the upper and underlying members of the Aguathuna Formation. The unit locally thickens up to 60 m where it fills in sinkholes. In the mine area it rests disconformably upon either the middle member or the upper part of the lower member. At Port au Choix it lies on the Catoche Formation. A basal quartz pebble conglomerate collects the erosional residues of the unconformity.

The biostratigraphy indicates a time break of 1 to 3 ma. at the unconformity (refer to section 2.3.6). The upper member contains a Whiterockian fauna of abundant conodonts, rare trilobites, brachiopods and ostracods (Williams et al., 1987; Stait, 1988). These fossils are the same age as those in the basal Table Point Formation. One or more conodont zones are missing between the upper member and underlying strata (Stait, 1988). The unconformity, thus, probably represents an hiatus of 1 or more million years. Differences in conodont assemblages in basal beds of the upper member in western Newfoundland also suggest that these sediments diachronously onlapped the unconformity from sinkholes in the mine area to the surrounding area and later over Port au Choix (Stait, 1988). The youngest onlap may be recorded near Cape Norman and Burnt Island, Pistolet Bay where the Table Point Formation locally overlies the Catoche Formation (Knight et al., in press).

4.5.2 Lithologies

(1) Massive, finely crystalline dolostone - These blue-gray, partly calcareous beds, 1 to 3 m thick, constitute most of the upper member. They contain a very shallow marine fauna of abundant conodonts and the minor macrofauna noted above. The beds have dark gray to slightly argillaceous bases which grade upwards in colour to light gray dolostone. A few beds are faintly burrow-mottled. Vertical epifaunal burrows and irregular solution (?) pits penetrate abrupt tops and are filled by overlying dark sediments. Pratt (1979) identifies some of these dwellings as Diplocraterion. Some surfaces are desiccation-cracked and eroded.

These beds are interpreted to have been deposited in intertidal environments. The conodont-rich sediment probably originated in the subtidal or intertidal zones and was transported onto high flats during storms. Bed tops were lithified, burrowed, desiccated and karstified in the lower intertidal to shallow subtidal zones (cf. Persian Gulf, Shinn, 1986).

(2) Gray-green dolomitic shales - Desiccation-cracked, quartz silt-rich shales, 1 to 50 cm thick, are similar to shales of the lower member. They were deposited during flooding of tidal flats.

(3) Nodular limestones - One or two thin, 10 to 20 cm bioclastic wackestones similar to those in the overlying Table Point Formation occur locally. They contain trilobites and ostracods and probably accumulated in the subtidal zone.

(4) Pebbly mudstones, quartz sandstones and quartz pebble conglomerates- Pebbly mudstone and sandstone beds (Pl. 4.3a,b,c) possess a

basal lag of millimetre to centimetre-sized chert and dolostone pebbles. The clasts are dispersed and fine upwards in the lower 1 to 10 cm of coarse quartz sandstones or massive dolostone beds. Quartz pebble conglomerates (Pl. 4.3c) up to 1 m thick occur locally on the unconformity. Some clasts reach 6 cm in diameter.

Provenance of the clasts is generally local. Fine dolostone and chert clasts are identical to underlying lithologies (Pl. 4.6a). Haywick (1984), however, reported exotic oolitic and metamorphic clasts.

The quartz pebbles are interpreted to be residual material from erosion at the unconformity. The clasts were entrained in storm floods and deposited within graded pebbly mudstones and sandstones. Conglomerates accumulated along erosional escarpments (James et al., 1988). Exotic clasts suggest that seasonal rivers or floods carried sediment over 100 km from the craton.

(5) Dark gray, argillaceous limestone - This lithology occurs locally within sinkholes. The basal beds are massive argillites. They are overlain by finely laminated limestones, up to 50 m thick, which are millimetre-scale, graded silt-mud rhythmites. Burrows are absent. Thin skeletal grainstones of ostracod fragments and intraclast wackestones are intercalated with the rhythmites. The laminations exhibit variable inclinations in contrast to uniform dips of the underlying stratigraphy.

Dark muds and debris of fossils and intraclasts are interpreted to have filled terrestrial to subtidal sinkholes along karsted fault zones. Anaerobic conditions or rapid sedimentation inhibited benthonic organisms. The rhythmites probably accumulated slowly as thin seasonal deposits and slumped as faulting and solution collapse occurred in the

Plate 4.3 Chert Pebble Beds above the St. George Unconformity

(Up is toward the top of the page.)

a. Quartz pebble conglomerates at the base of the Middle Ordovician Table Point Formation overlie the St. George Unconformity at Aguathuna Quarry. In situ chert nodules occur just beneath this surface in the underlying dololaminites of the middle member of the Aguathuna Formation. They are the main source of the pebbles. The pen measures 13.5 cm.

b. Quartz and dolostone pebbles are dispersed in fine quartz sands which are intermixed with dolostone (originally mudstone). A centimetre-thick coarse pebble lag forms the irregular base of a bed approximately 3 m above the unconformity. Six beds similar to this one occur in the lower 5 m of the upper member at Table Point. The scale is in centimetres.

c. Quartz pebble conglomerate from the base of the upper member at Portland Creek Pond (collected by Ian Knight). The scale is in centimetres.

PLATE 4.3

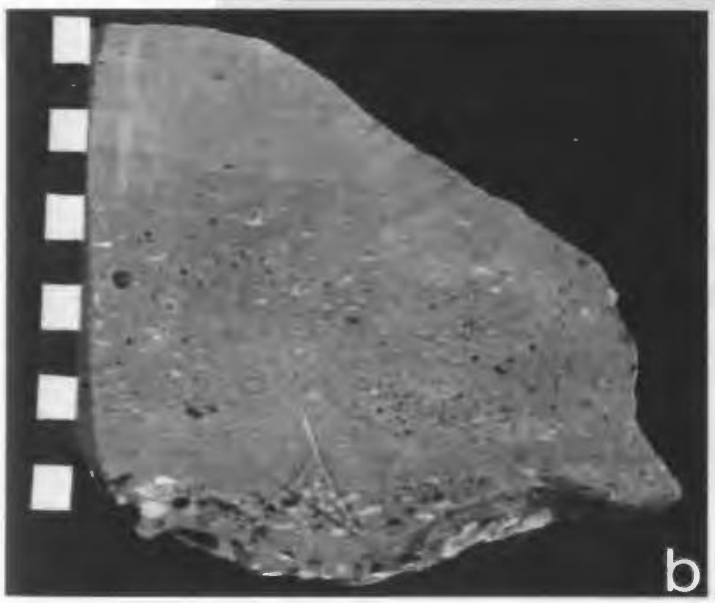

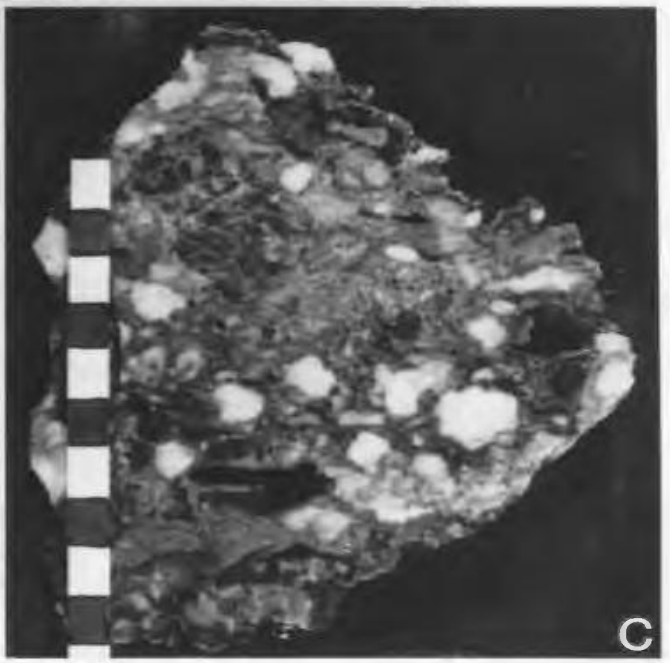

subsurface.

4.5.3 Distribution of Lithologies

Although massive dolostone comprises most of the upper member, subtidal nodular, bioclastic limestones, storm deposits of pebbly mudstone or beds of dark gray mudstone form the lower portions of thememberr. Quartz pebbles are especially common at the base of the upper member, but at Table Point they appear at the base of 6 dolostone beds in the lower 5 m of the member. Desiccation cracks and shale drapes, as well as burrows and microkarst occur on the upper surfaces of some dolostone beds. Unlike the lower member, beds and surface features can not be correlated laterally.

Typical massive dolostones are locally transitional into sinkhole deposits of argillaceous limestone where the upper member thickens from 7 to 50 m. Lithologies within sinkholes change upwards from non-marine (?) argillite at the base to middle portions of marine rhythmites with intercalations of bioclasts and intraclasts, all capped by stylolitic limestones and typical massive dolostones.

4.5.4 Depositional Environment

Sediments of the upper member of the Aguathuna Formation were deposited during the Middle Ordovician transgression of the St. George Unconformity. The thickest deposits accreted over faults or collapse breccias where local ponded sinkholes filled with black muds. The unconformity was locally veneered by chert sand and gravel, the erosional residue of the St. George Unconformity, and this was reworked by non-

marine sheet floods over the hard carbonate landscape. During marine transgression of the platform, however, marine storm processes incorporated the quartz pebbles into muddy peritidal sediments. The muddy tidal flats diachronously onlapped an irregular topography. The tidal flats accreted in repeated episodes of deposition of 1 to 3 m of mud in the intertidal zone. Intermittent exposure of upper surfaces left mud cracks and/or a cover of wind-blown silt. Many of these surfaces were lithified and burrowed by organisms during marine submersion and karsted during emergence in the intertidal zone. Rare subtidal bioclastic wackestones covered these surfaces during the deepest submersion of the flats.

4.6 The Lower Table Point Formation

4.6.1 Introduction

The lower 50 metres of the Table Point Formation contains distinctive light gray fenestral limestones which serve to distinguish it from overlying nodular or rubbly, largely subtidal, limestones. This unit is called the Spring Inlet Member (Ross and James, 1987).

4.6.2 Stratigraphic Markers

Seven key laterally extensive beds are used for correlation in the Daniel's Harbour mine area. The position of the seven beds relative to the base of the formation is as follows:

(1) two thin nodular limestones at the base of the formation;

(2) a burrow mottled bed at 6 to 8 m;

(3) a fenestral unit at 12 to 17 m;

(4) thick nodular strata at 17 to 30 m;

(5) a chert horizon at 28 m;

(6) a fenestral unit at 30 to 50 m;

(7) a thin calcareous sandstone at 50 metres in DDH 519 that can be correlated with the Table Point section.

4.6.3 Lithologies

Three lithologies dominate the Spring Inlet Member.

(1) Nodular limestones - Nodular limestones consist of centimetre-thick lumps or nodules of bioclastic wackestone, separated by millimetre-thin dolomitized argillaceous laminations and thin beds. They are organized into nodular or fitted fabrics (Coniglio, 1985). A restricted, low diversity fauna of leperditid ostracods, high-spired gastropods, brachiopods and conodonts imply that the carbonates accumulated in very shallow water (Stouge, 1980; Ross and James,1987). The fossiliferous beds are interpreted to be very shallow subtidal where marine cementation and early compaction combined to form the nodular fabric (Jones et al, 1979; Flugel, 1982; Coniglio, 1985; Stenzel, in prep.).

(2) Burrowed Lime mudstones - Massive, thoroughly burrowed lime mudstone beds are 1 to 2 m thick. Light-coloured calcite cements highlight subvertical tubular trace fossils. These beds are similar to the shallow subtidal Thalassinoides lithology of the Aguathuna Formation.

(3) Fenestral lime mudstone - Massive, stylolitic lime mudstones

and peloidal packstones have abundant fenestrae filled with clear calcite. The abundance of fenestrae increases towards bed tops where laminar fenestra are locally common. Desiccation cracks occur locally on upper surfaces. Fenestrae are generally attributed to shrinkage or gas and water bubbles in muds (Flugel, 1982). Collectively the lack of burrowing and megafossils, concentration of fenestrae at bed tops, and desiccation cracks imply a restricted origin in the intertidal to supratidal zones. Fenestrae imply early lithification (Grover and Read, 1978). This is verified by the presence of fenestral clasts in karst-related breccias.

4.6.4 Distribution of Lithologies

The 3 main lithologies are distributed in shallowing upward sequences. Thin 30 cm nodular beds form the basal units and grade upward into parted wackestones and/or burrowed beds and then into fenestral beds. Three or four sequences comprise the lower 25 metres of the Table Point Formation below a thick nodular unit. Above the nodular limestone, fenestral limestones are common from 30 m to their last occurrence 50 m above the base of the Table Point Formation.

Regionally, these peritidal facies dominate stratigraphic intervals 0 to 25 m and 30 to 50 m above the base of the Table Point Formation. In the mine area facies vary laterally from fenestral dominated to cyclic to nodular dominated. Drill hole data indicate that the fenestral and cyclic facies can be traced laterally for only a kilometre or two, where they grade into nodular facies.

4.6.5 Depositional Environment

The Spring Inlet Member accumulated on a shallow subtidal to peritidal platform inhabited by a low diversity, restricted water fauna. Drill hole information suggests that early broad, peritidal flats evolved into isolated peritidal islands a kilometre or more in width. This microtopography of broad tidal flats and intervening subtidal lagoons was probably controlled by growth faults (Stenzel, in prep.). The tidal flats accreted in shallowing upward sequences from subtidal nodular wackestones to burrowed mudstones and peritidal fenestral mudstones and wackestones. Desiccation cracks and thin dololaminites in the latter facies formed during intermittent exposure. The lack of pervasive dolomitization and evidence of evaporites plus the abundance of fenestrae suggests that these tidal flats were probably humid and not as arid or restricted as in the Aguathuna Formation (Grover and Read, 1978; S. Stenzel, pers. comm. 1988; Knight, in press). The flats were eventually drowned as platform subsidence exceeded the rate of sedimentation, so that the Spring Inlet Member was overlain by subtidal, fossiliferous shelf limestone of the upper Table Point Formation.

4.7 Summary of the Sedimentary and Stratigraphic Evolution of the Upper St. George Group and Lower Table Point Formation

During deposition of the upper St. George Group the Lower Paleozoic platform in Newfoundland shallowed upwards from an open subtidal shelf (Catoche Formation) to expansive peritidal flats (the Aguathuna Formation) as sedimentation outpaced a slowed rate of subsidence. Eustatic

sea level fall and/or regional uplift then dramatically left an emergent platform (St. George Unconformity) for as much as 1 to 3 ma. Prior to and during emergence surface and subsurface karst and block faulting formed an irregular, locally collapsed topography. Increased subsidence and eustatic rise combined to gradually submerge the platform at the end of this time. During this marine onlap peritidal dolomitized muds of the upper member of the Aguathuna Formation were blanketed by the peritidal to shallow subtidal Table Point Formation.

The gradual shallowing of the platform in the late Early Ordovician is described in four stages.

(1) Muddy, nodular limestones of the middle Catoche Formation accumulated on a low energy, open shelf during maximum marine submergence. Deep and shallow water fauna intermingled to form a diverse community around thriving algal-sponge bioherms, while intermittent storm waves entrained thin beds of intraclasts and skeletal debris. Periods of turbidity interrupted the activity of organisms.

(2) The transition from the middle to upper Catoche Formation was abrupt as shoaling above a critical depth dissipated the energy of storm waves and currents. This change dramatically affected sediments and organisms. The end of deposition of skeletal, intraclastic rudstones resulted from diminished bioherms and storm wave erosion. A low diversity community of shallow water organisms thoroughly reworked the fossiliferous muds as the rate of sedimentation slowed and waters remained relatively clear.

(3) Grainy peloidal sediments and shallow water mudstones became intercalated with the burrowed skeletal muds (Costa Bay Member, Catoche

Formation). The sediments were deposited in distinctive upward deepening sequences: a possible response to high frequency sea level oscillations of increasing amplitude. Large planispiral gastropods and large soft-bodied deposit feeders characterized a restricted shallow water fauna. Abundant peloids accumulated in the very shallow subtidal to intertidal zones where algae, burrowers and early diagenesis produced numerous grains.

(4) The platform shallowed upwards abruptly from the shallow-water, burrowed flats of the Catoche Formation to vast peritidal flats of the lower member of the Aguathuna Formation. These flats passed through recurring eustatic and/or tectonic-controlled cycles. The cycles began with emergence; followed by supratidal sedimentation during a static sea level; continued with upward deepening and low intertidal to subtidal onlap during a phase of sea level rise; succeeded by repeated emergence of subtidal flats during moderate to high amplitude sea level oscillations; and concluded with a return to emergence.

The sediments of the Aguathuna Formation reflect a restricted to arid environment. The firm, muddy subtidal substrates, unlike ones in the Catoche Formation, were deeply excavated by networks of Thalassinoides-type burrows. Wind-blown silts and evaporites covered intermittently flooded subaerial surfaces. Contemporary silica replaced evaporites and precipitated nodules, and was eroded to form pebble conglomerates. Dolomitized laminites and muds with desiccation cracks covered the supratidal flats.

At the close of the Early Ordovician major eustatic regression and/or tectonic uplift left a gently folded, faulted and karsted

surface, the St. George Unconformity. Tectonic loading during plate convergence flexed the lithosphere and fragmented and locally uplifted the platform (James et al., 1988). Prior to the marine regression, tectonism and subsurface karst formed gradually subsiding structural depressions, which were filled by peritidal deposits of the middle member of the Aguathuna Formation. During a hiatus of up to 3 ma., tectonism warped, tilted and faulted the platform, then erosion bevelled the stratigraphy and left a surface of relatively low relief covered by chert pebble conglomerates. The surface locally collapsed above fault-controlled subsurface caves to form sinkholes as much as 50 m deep.

Near the beginning of the Middle Ordovician, regional subsidence and possible eustatic sea level rise combined to produce gradual marine onlap. A uniform, 7 to 15 m thick, veneer of very shallow subtidal to peritidal muds (the upper member of the Aguathuna Formation) incorporated quartz clasts from the erosional surface. A mosaic of mud flats diachronously covered the unconformity, locally highlighted by thick fillings of sinkholes by subtidal rhythmites.

The conformably overlying Spring Inlet Member of the Table Point Formation composed of shallow subtidal to peritidal sediments, covered a fault-controlled microtopography of broad tidal flats and subtidal lagoons and onlapped remaining highs of the St. George Unconformity (Knight, 1986, 1987). Shallowing upward packages of nodular to burrowed and fenestral wackestones and mudstones lacked the pervasive dolomitization and evaporites of the arid, high peritidal flats of the Aguathuna Formation. The entire platform submerged at the top of the Spring Inlet Member as increasing rates of subsidence preceded later foundering of

the platform into a foredeep (Stenzel and James, 1987, 1988).

In conclusion, the sedimentary history of the St. George Group laid the framework for post-depositional events. Alternating mudstone and grainstone beds in the upper Catoche Formation established an anisotropic rock mass that strongly influenced selective dolomitization, deformation and fluid movement. The Aguathuna Formation formed a finely crystalline caprock over the Catoche Formation. Northeast-trending faults which were to become long-lived, influential structures began to alter the platform with the formation of local karst features, erosional horsts and sedimentary grabens.

PART III

MINERAL PARAGENESIS

INTRODUCTION TO PART III

In Part III the petrographic and geochemical attributes of dolomites, sulphides and sulphates are described. Petrographic, stratigraphic and structural relationships are utilized to define a clear paragenetic sequence of diagenetic events. The dolomitization history can be separated into a near-surface phase preceding karst formation, an early burial stage contemporaneous with the development of stylolites, a deep and late burial phase characterized by hydrothermal dolomites and late fault-related dolomitization. Sulphide precipitation is intimately related with the hydrothermal dolomites. The sulphide history includes an early and late ore stage and post-ore precipitation of galena and euhedral sphalerite. White, hydrothermal dolomites and sulphates precipitated in the post-ore stage.

CHAPTER 5 - DOLOMITE PARAGENESIS

5.1 Introduction

This chapter describes the petrographic character and geochemistry of the dolomite crystal types, evidence for their relative age, their position in the sequence of events and interpretations of the environments in which they crystallized. This description forms the basis for later discussion of the evolution of dolostones, breccias and sulphide bodies.

The upper St. George Group is extensively dolomitized at Daniel's Harbour from the base of the peloidal member of the Catoche Formation up through the entire Aguathuna Formation (Fig. 1.4). The variety of dolostone bodies which comprise the upper St. George Group include stratigraphic dolostones of the Aguathuna Formation, rock-matrix breccias, dolostone mottles and beds in limestone, stratabound coarse dolostones (pseudobreccia and coarse sparry dolostone) and discordant dolostones (Fig. 1.4). More than one type of dolomite constitutes most dolostones. Variable crystal textures, zoned crystals, ghost fabrics, veins and cemented dolostone breccias collectively record these multiple types of dolomite.

The constituent dolomite crystals are examined to establish constraints on the relative age and sequence of crystallization. The term **dolomite**, in this study, refers to crystals and **dolostone** to composites of the mineral. Seven dolomite types are recognized based on

on standard petrographic and cathodoluminescent observations. A **crystal type** is defined here as one or more crystal forms, e.g. microcrystalline, medium-sized rhombs or saddle dolomite, unified by specific cathodoluminescent (CL) properties, distinctive isotopic values and, in some cases, a characteristic trace element chemistry (Table 5.1). Relationships between the types indicate that each represents a distinct generation. The distribution of the seven dolomite types in the various dolostone bodies is shown in Fig. 5.1. The dolostone are described and interpreted in Parts 4 and 5.

Petrographic descriptions commonly use qualitative terms to refer to specific sizes of crystals and pores. Crystal sizes are defined as follows: microcrystalline (to small to measure), very fine (2 to 50 μm), fine (50 to 200 μm), medium (200 to 500 μm), coarse (500 μm to 1 mm) and megacrystalline (greater than 1 mm). The classification of pore types and sizes is based on Choquette and Pray (1970). Cavities, caves and caverns commonly can fit a human, but can be as small as 25 cm-high openings. Large megapores range from 3 to 25 cm in diameter. Small megapores vary in size from 0.4 to 3 cm. Mesopores measure between 50 μm and 4 mm, and micropores are the finest holes.

5.2 Analytical Methods

Crystal types were identified by transmitted light petrography, cathodoluminescence and staining for ferroan dolomites with potassium ferricyanide. Dolomite stoichiometry (mole percent $CaCO_3$) was measured on a Phillips x-ray diffractometer with Cu-K radiation at a scanning speed of one half degree/minute. The position of d(104) peaks of

dolomite powders were determined relative to the d(200) peaks of included powders of an NaCl standard. The position of the d(104) peak measured the amount of $MgCO_3$ substitution into the carbonate lattice with a precision of 0.02 mol % magnesium (Goldsmith and Graf, 1958; Blatt, Middleton and Murray, 1972).

Chemical composition of the dolostones was surveyed either in this study or previously by neutron activation analyses for 22 major and trace elements (Dillon, 1978); multielement ICP analyses for 33 elements (by Chemex Ltd.); non-quantitative analyses from the EDAX back scatter electron image on the SEM; and atomic absorption analyses of major elements. Individual crystal types were analyzed for nine elements (Ca, Mg, Fe, Mn, Na, Sr, Si, Al, P) by a focused electron beam of 2 μm on a JEOL JXA50 electron microprobe. A carbonate standard was calibrated relative to known values from crystals of dolomite, garnet, rhodonite, celestite and apatite. The equipment operated with a 15 KV beam, specimen current of 22 nannoamperes and a counting time of 30 seconds or 30,000 counts. The MAGIC program corrected the data. Carbon and oxygen isotopes of 49 samples were analyzed by Teledyne Isotopes (New Jersey) and reported in conventional delta notation in parts per mil (o/oo) versus the PDB-1 standard. Precision for both $\delta^{13}C$ and $\delta^{18}O$ is 0.1 o/oo. An engravers tool was utilized to sample millimetre-sized areas on dolostones and megacrystals. Homogeneous areas of similar crystal types were selected in fine to medium crystalline dolostones.

The composition and homogenization temperatures of fluid inclusions were measured by freezing and heating them on a Fluid Inc. digital unit. The calibration of the unit was tested on known synthetic and natural

TABLE 5.1

CHARACTERISTICS OF DOLOMITE TYPES

DOLOMITE TYPE	GENERAL PETROGRAPHIC FEATURES	CATHODO-LUMINESCENCE	ISOTOPES (o/oo PDB)	TRACE ELEMENTS (ppm)	FLUID INCLUSIONS (T = mode)	RELATIVE TIMING
I	Microcrystalline; fine crystals; euhedral; turbid;	Non-luminescent to purple	Enriched $\delta^{18}O$ -4 to -6 $\delta^{18}O$ Invariant -1 $\delta^{13}C$	85 to 240 Sr	no data	Clasts in conglomerates and karst replacive breccias
II	Fine to medium crystals; turbid; calcite inclusions; replacive; displacive	Purple to pink; zoned to patchy replacement by pink	Wide ranging $\delta^{18}O$ -6 to -10 $\delta^{18}O$ invariant - $\delta^{13}C$	70 TO 200 Sr locally ferroan 1000 to 4000	Inclusions in calcite: T_h = 115° 20%NaCl	Long ranging; early burro: replacement to growth along stylolites
III	Very fine to medium crystals; clear rim overgrowths on II; clear blocky isopachous cement	Finely zoned; bright yellow; orange red	-6 to -7 $\delta^{18}O$; variable -1 to -3 $\delta^{13}C$	50 to 90 Sr 100 to 1000 Fe <100 to 1500 Mn	Clear crystals; halite inclusions	Overgrowths on II; cements pores; growth along stylolites
IV	Fine to medium xenotopic crystals; cements between II and III crystals	Bright red overprints II and III	-7 to -8 $\delta^{18}O$ invariant -1 $\delta^{13}C$	<100 to 2500 Fe <100 to 2500 Mn Sr - no data	no data	Pre-ore veins; overprints II and III
V	Fine to mega-crystalline; xeno-topic replacive normal and saddle dolomite; idiotopic displacive and cement saddle dolomites	Uniform dull red; zoned cement crystals; overprints II, III & IV	Variable $\delta^{18}O$ -7 to -12 °/oo $\delta^{18}O$, invariant -1 $\delta^{13}C$ except late stage -2 $\delta^{13}C$	15 to 35 Sr 900 to 3500 Fe 250 to 300 Mn	T_h = 115° 24%NaCl	Post-ore; overprints II, III & IV; cements late veins
VI	Thin overgrowths on V and megacrystalline cements of saddle dolomite	Bright red	-7 to -9°/oo $\delta^{18}O$, depleted $\delta^{13}C$ -2 to -4°/oo $\delta^{13}C$	3000 to 5000 Fe 300 to 700 Mn Sr - no data	T_h = 110° Late calcite: T_h = 55° >24%NaCl	Overgrowths on V
VII	Very fine to medium crystals; replacive; idiotopic to xenotopic	Bright red	variable $\delta^{18}O$, $\delta^{13}C$ -5 to -14°/oo $\delta^{18}O$ 0 to -2°/oo $\delta^{13}C$	100 to 800 Fe <100 to 1500 Mn Sr - no data	T_h = 70° 24%NaCl	Replaces lime-stones around latest faults

Figure 5.1 Distribution of Dolomite Types

The seven designated dolomite types are variously distributed in the upper St. George Group. Dolomite I is abundant in the Aguathuna Formation and rock-matrix breccias and is commonly intermixed with and overprinted by Dolomites II and III. Dolomites II and III comprise dolostone mottles in limestones and form abundant zoned crystals in rock-matrix breccias. Dolomites IV, V and VI make up coarse stratabound dolostones in the upper Catoche Formation. These dolomites commonly overprint mottles of Dolomites II and III. Dolomite VII comprises late fault-related dolostones.

DISTRIBUTION OF DOLOMITE TYPES

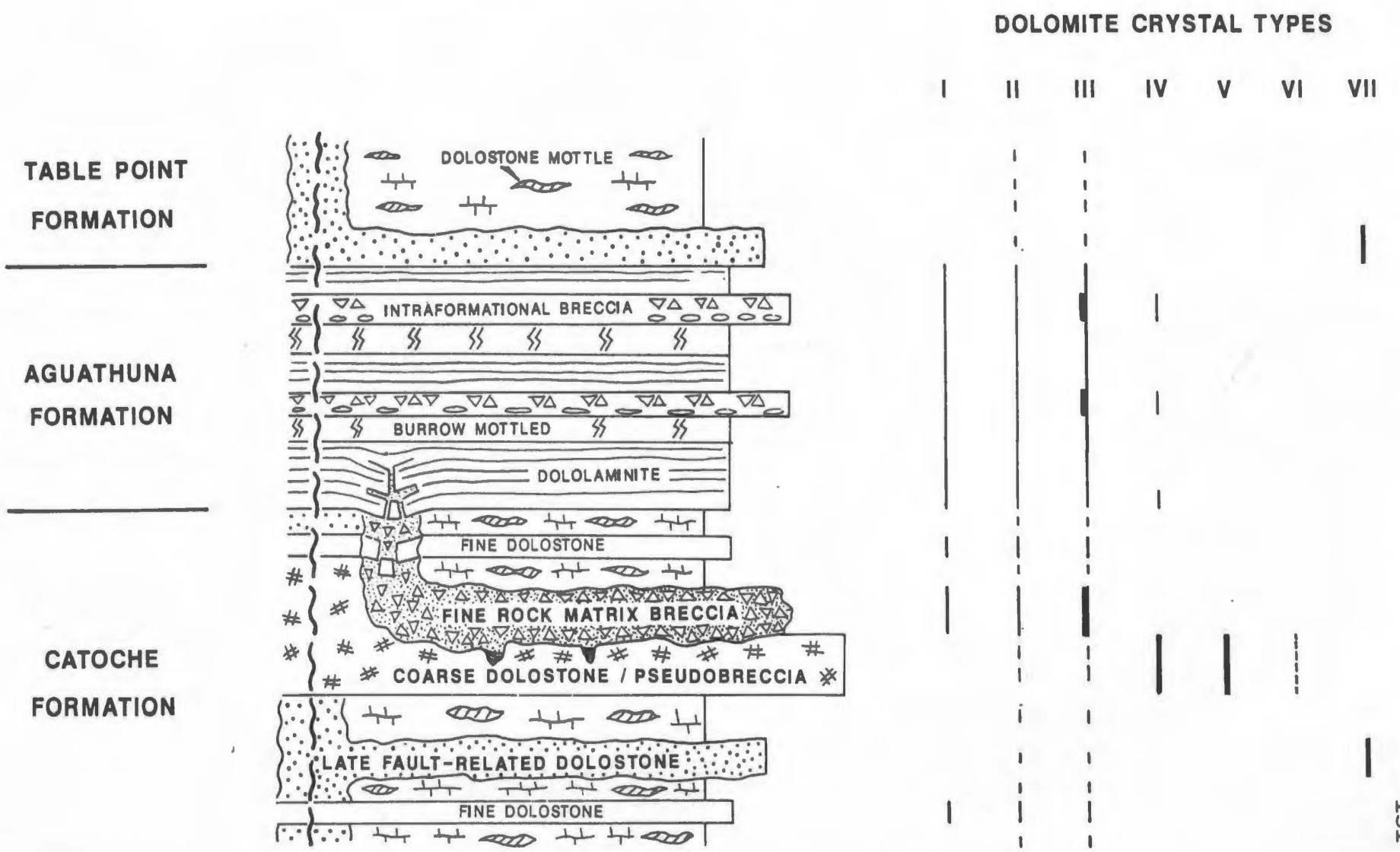

samples with varying NaCl + H_2O compositions. Homogenization temperatures were not corrected for pressure.

5.3 Dolomite Type I - Non-luminescent microcrystalline dolomite

Petrography and Distribution - Very fine to fine, dusky, euhedral crystals grow close together and are thinnly parted by brown to black interstitial material (Pl. 5.3b). All together the crystals constitute a gray-brown microcrystalline rock. This significant dolostone comprises most of the Aguathuna Formation, scattered beds of the Catoche Formation and portions of rock-matrix breccias. Crystal sizes vary according to the lithology: 10 to 20 μm in dololaminites; 20 to 30 μm in burrowed beds of the Aguathuna Formation (Pl. 5.1a,d); 20 to 100 μm in mudstone lithologies of the Catoche Formation (Pl. 5.1e); and 20 to 50 μm in matrix patches of rock-matrix breccias.

Cathodoluminescence - Microcrystalline dolomites are weak to non-luminescent (Pl. 5.1a,d). Fine crystals which replace Catoche mudstones, however, exhibit purple CL (Pl. 5.1e).

Geochemistry - These dolomites have distinctively heavy $\delta^{18}O$ PDB values of around -4.5 o/oo compared to other crystal types (Fig. 5.2, Appendix A). These values are 3 to 4 per mil heavier than St. George limestones $\delta^{13}C$ values of -0.5 to -1.5 o/oo PDB are similar to these limestones (Fig. 5.2, Appendix A).

The stoichiometric dolomites have a d_{104} peak at 2.885 nm which

Plate 5.1 Cathodoluminescent Petrography

a. A burrowed dolostone from the Aguathuna Formation with very fine crystals of dull CL Dolomite I (a) and patches of fine-sized, bluish to pink rhombs of Dolomite II (b). Extremely fine-sized crystals of orange CL Dolomite III are disseminated throughout. 1 mm scale.

b. Medium-sized crystals of Dolomite II comprise dolostone mottles in an upper Catoche limestone, 20 m below the top of the formation in DDH 1254. They have purple CL cores and overgrowths of pink CL dolomite which also partially replaces the cores. Calcite in the upper portion of the photomicrograph is non-luminescent. 1 mm scale.

c. Zoned rhombs of Dolomite II occur within stylomottles in the middle Catoche Formation, 70 m below the top of the formation in DDH 631. These crystals, unlike those in 5.1b, have bright cores and dark ferroan midsections. Abundant detrital feldspars (blue CL) are concentrated in the dolostone mottle and along the stylolite. 1 mm scale.

d. Medium-sized zoned crystals of Dolomite III replace the matrix of breccia beds in the Aguathuna Formation (DDH 626, 84 m). Later mega-quartz (black) partially replaces these crystals. Weakly luminescent Dolomite I on the left contains intercrystalline with pore cements of Dolomite III. 1 mm scale.

PLATE 5.1

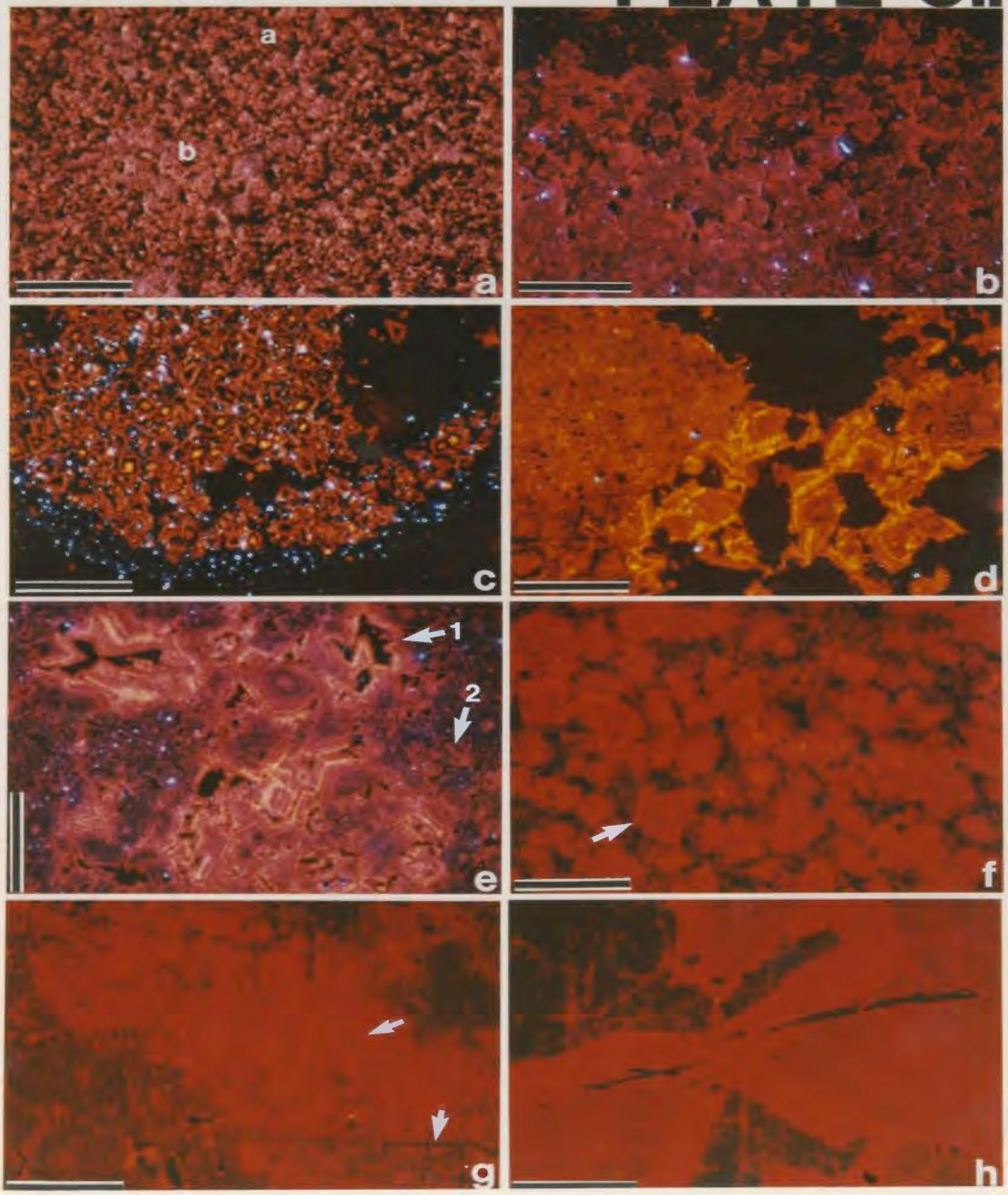

e. Purple CL crystals of Dolomite I or II are cut by pores filled with zoned cements of Dolomite III. Isopachous cements (1) line pores. Pink CL dolomite (2) which rims crystals of Dolomite II in 5.1b forms initial cements after dissolution. These dolomites replace a mudstone bed in the upper Catoche Formation (DDH 1254, 20 m b.w.m. 1 mm scale.

f. Red CL Dolomite IV overprints zoned rhombs with cores of Dolomite II and rims of Dolomite III (arrow). Dull red CL Dolomite V cements intercrystalline pores. These CL relics are preserved in a discordant dolostone beneath the east L Zone ore body in the middle Catoche Formation (DDH 1134, 55 m b.w.m. 1 mm scale.

g. Red CL Dolomite IV is preserved in a patch where it overprints zoned rhombs (arrow) similar to those in Pl. 5.1f. Coarse crystals of dull red CL Dolomite V surround the patch and also cement a late veinlet (arrow). Bright red CL Dolomite VI rims pores. Sample from upper Catoche Formation at Table Point. 1 mm scale

h. Saddle Dolomite B (bright red CL) overgrows and cements cleavage of curved crystals of Saddle Dolomite A (dull red CL). Non-luminescent calcite cements late pores between crystals. Underground sample from the K Zone. 1 mm scale.

Plate 5.2 Diagenetic Calcites and Early Dolomites

a. Peloidal packstone, upper Catoche Formation (DDH 1254, 22 m b.w.m.). Microspar replaces the matrix. Pseudospar replaces a burrow in the upper left. Turbid dolomites (II) replace another burrow in the lower right. 1 cm scale.

b. Burrows and a veinlet occur in a micrite and are filled with pseudospar and equant calcite cement. Sample from DDH 1254, 29 m b.w.m. 1 mm scale.

c. Burrowed wackestone, upper Catoche Formation (DDH 66, 128 m). Early dolostone mottles form after brecciation of pseudospar (1). Later veinlets cut the mottles (2), are cemented by calcite, compacted (3) and truncated by stylolites. Dolomite III replaces calcite in veinlets and cements vertical pores along stylolites (4). 1 cm scale.

d. Fluid inclusions (arrows) in early calcite cement in a veinlet vary in size from 1 to 10 μm. Sample from DDH 1254, 20 m b.w.m. 25 μm scale.

PLATE 5.2

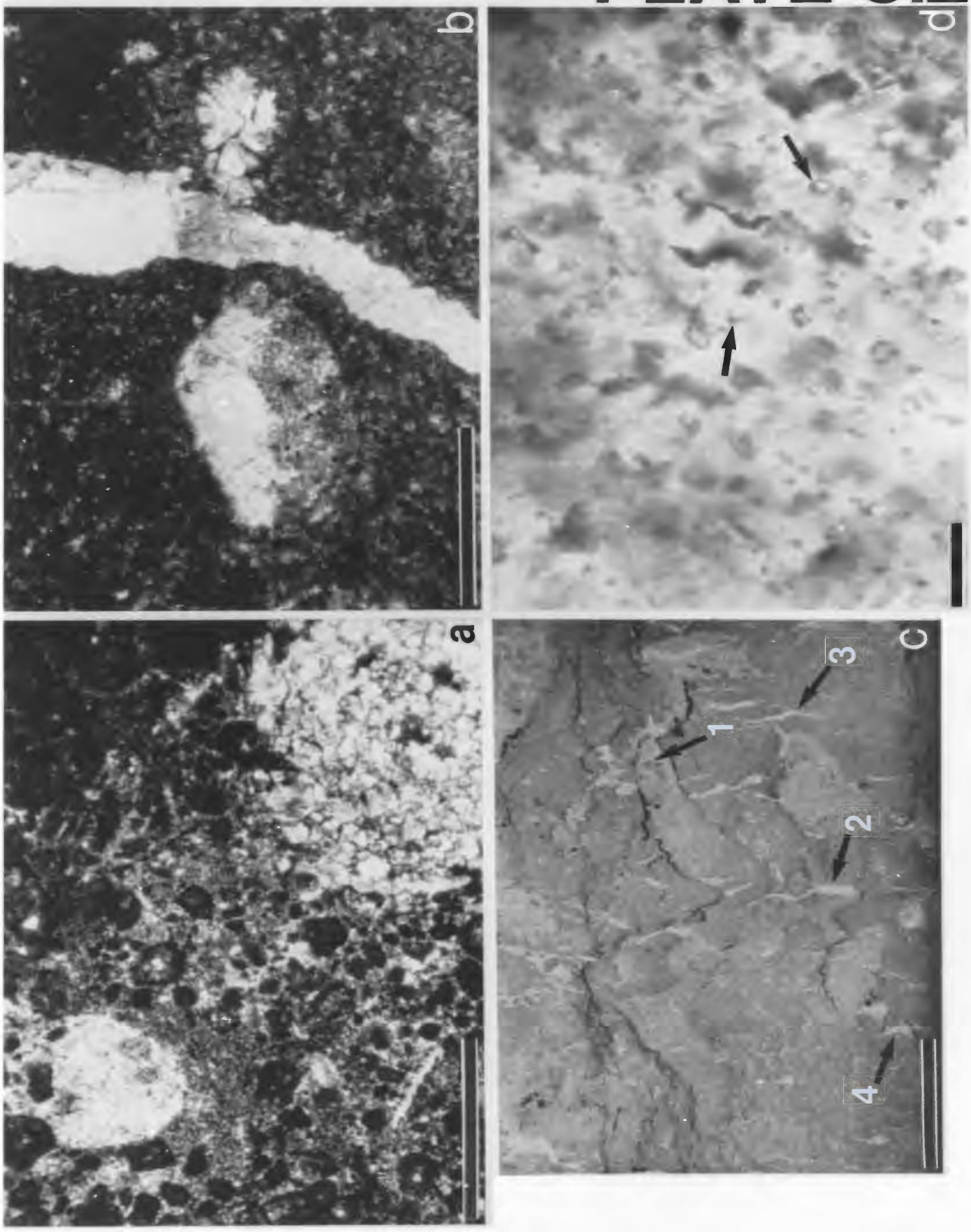

Plate 5.3 Dolomites I and II

a. Dolomite II occurs in stylomottles (1) and burrows not associated with stylolites (2). Dolomite III locally replaces veinlets of calcite cement (3) which cut dolostone mottles. Upper Catoche Formation, DDH 1254, 10 m b.w.m. 1 cm scale.

b. Fine crystals of Dolomite I are associated with planar micro-stylolites (arrows) in an early dolostone bed in the upper Catoche Formation (DDH, 29 m b.w.m.). 1 mm scale.

c. Turbid dolomites (II) occur clustered within a stylomottle on the right and as individual crystals along stylolites (1) and within peloids (arrow). These dolomites occur within a peloidal packstone of the upper Catoche Formation (DDH 1254, 20 m b.w.m.). 1 mm scale.

d. Fine crystals of Dolomite II (arrow) replace the matrix that surrounds brecciated pseudospar, attesting to the later origin of these crystals. The brecciation is related to karst from adjacent rock-matrix breccias. Upper Catoche Formation, DDH 66, 127 m. 1 mm scale.

e. Styloresidues displaced by Dolomite II crystals, generally euhedral rhombs (Pl. 5.1c, same under cathodoluminescence) which are partially corroded by pressure solution (arrow). Crystals cores preserve calcite (dark stains). Middle Catoche Formation, DDH 631, 49 m. 100 μm scale.

PLATE 5.3

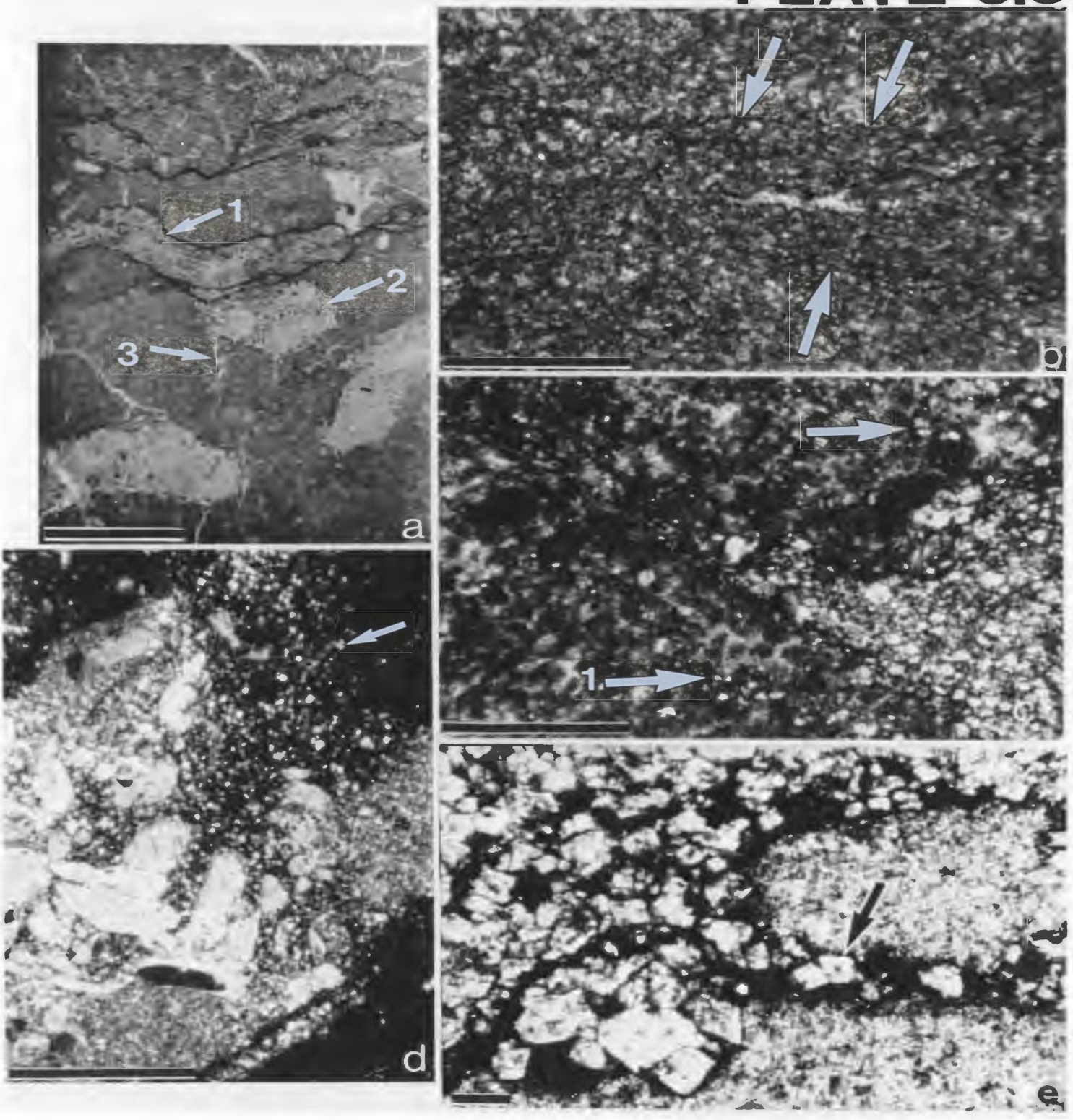

implies 50 mole % $CaCO_3$ (Appendix C). With the exception of Sr^{++}, trace elements of iron, manganese and sodium are minor (Appendix B). Sr^{++} content is highly variable between 85 and 240 ppm (Haywick, 1984). Interstitial quartz and clay make up 3 to 5 weight % of the dolostone (Appendix B).

Evidence of Timing - Microcrystalline dolomites pre-date erosion as intraclasts in the Aguathuna Formation and fragments within karst-related rock-matrix breccias in both the Aguathuna and Catoche Formations. This early age is confirmed by pre-compaction chert nodules which preserve dolomite inclusions. All other dolomite types cross-cut, overgrow or replace Dolomite I (Pl. 5.1a,d,e).

Interpretation - Microcrystalline dolomites replaced mudstones at or near the original depositional surface. Dololaminites within metres of the St. George Unconformity were dolomitized prior to incorporation into intraformational conglomerates and subsurface solution breccias. $\delta^{18}O$ values, enriched 3 to 4 o/oo relative to limestones, probably resulted from fractionation in the same near surface environment (Clayton et al., 1968). The texture-specific dolomitization extensively affected shallow subtidal stratigraphic units as well as peritidal ones. It was, therefore, not simply the result of evaporative reflux processes on the tidal flat (cf. Patterson and Kinsman, 1982). Alternative models suggest dolomitization within mixing zones of saline and meteoric waters (Hanshaw et al., 1971; Land et al., 1975) or from sea water in ground waters in the shallow subsurface (Sass and Katz, 1982; Simms, 1984;

Figure 5.2 Isotope and Fluid Inclusion Data for Early Dolomites and Calcites

Plot of $\delta^{18}O$ vs. $\delta^{13}C$ for primary limestones and early dolomites. Limestones contain -8 to -9 o/oo $\delta^{18}O$ PDB and -1 to -1.5 o/oo $\delta^{13}C$ (defined by 7 samples, Coron, 1982; Haywick, 1984; this study). Dolomite I is enriched in $\delta^{18}O$ (-4.5 to -6) relative to the limestones (defined by 8 samples, Coron, 1982; Haywick, 1984; this study). Dolomite II has a broad field of $\delta^{18}O$ values (-5.5 to -10)(defined by 15 samples, Haywick, 1984). Limited data on Dolomite III suggests limited variation of $\delta^{18}O$ values (-6 to -7), but considerable range in $\delta^{13}C$ values (-0.5 to -3)(Haywick, 1984). Dashed lines represent probable variations in water-rock ratios between initial dolomites with $\delta^{18}O$ values of -4.5 o/oo and fluids with initial $\delta^{18}O$ values of SMOW and +4 o/oo SMOW. In addition to data in Appendix A, Haywick (1984) analysed 24 samples of dololaminites (mostly Dolomite I) and mottle dolomites and beds of pervasive (A) dolomite composed mostly of Dolomite II.

Fluid inclusion data from equant calcite cements in veinlets indicates that fluids contemporaneous with Dolomite II were hypersaline (melting temperatures of -18°C)(Appendix F). Modal homogenization temperatures of 85°C were probably readjusted during later burial.

EARLY DOLOMITES

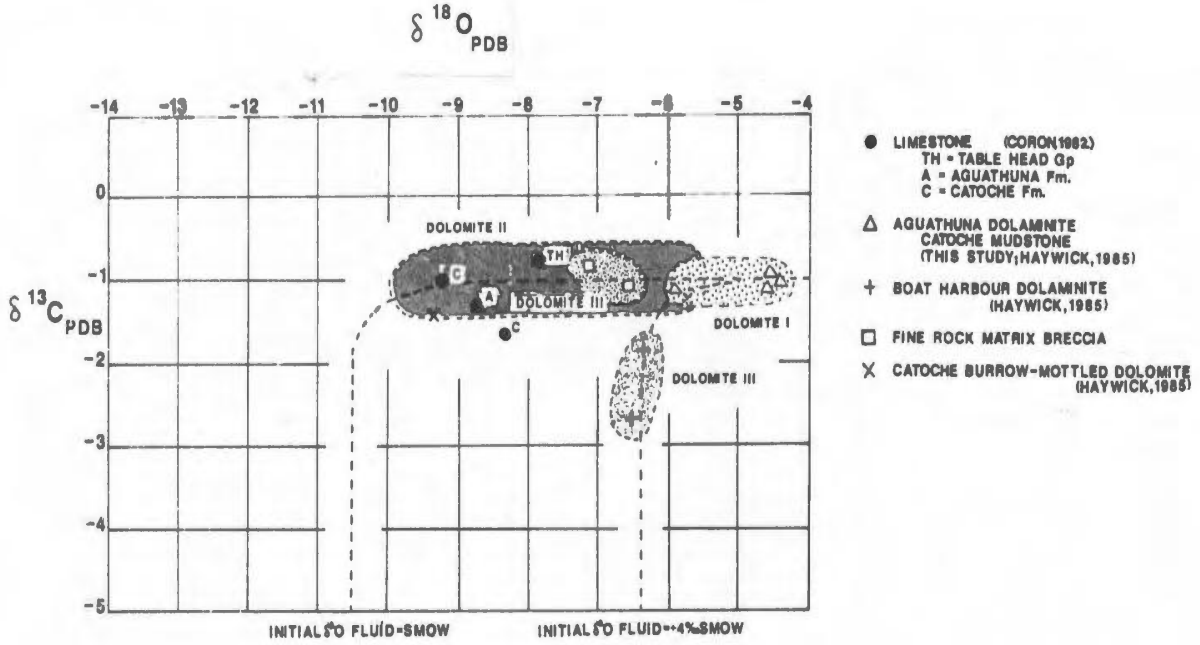

FLUID INCLUSION TEMPERATURES IN EARLY CALCITES

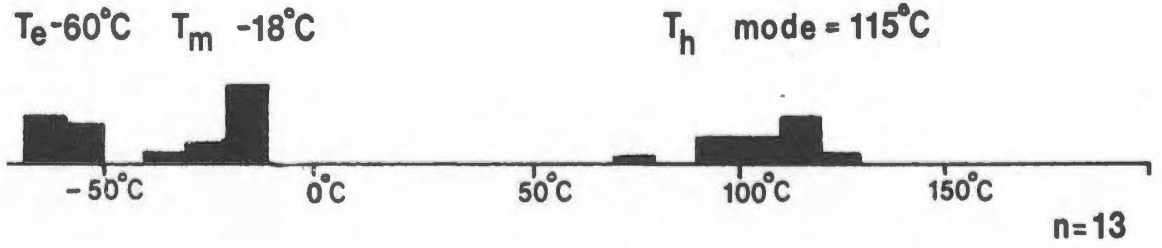

Hardie, 1987). The origin of the microcrystalline dolomites is considered again in Chapter 7.

5.4 Dolomite Type II - Very fine to medium crystalline, turbid dolomite with blue to pink CL

Petrography and Distribution - Ubiquitous rhombic, turbid crystals occur in Catoche and Table Point limestones as centimetre-sized mottles of fine to medium crystals, 50 to 300 μm in size, and in massive dolostones of the Aguathuna and Catoche Formations as very fine to fine crystals, 5 to 200 μm in size. Fine to medium crystals also pervade rock-matrix breccias. Most crystals in all occurrences have turbid cores with local calcite inclusions and clear rims (Pls.5.2a; 5.3e; 5.4a,b).

The most conspicuous dolomites of this type comprise dolostone mottles of the limestones (Haywick, 1984). Clusters of interlocking crystals replace burrows, the micritized rims of fossils and micritic seams of insoluble residues along stylolites (Pls. 5.1b,c; 5.2a,c; 5.3a,c,e). Individual crystals occur along seams of insoluble material and stylolites (Pl. 5.3c,e); replace micritic peloids (Pl. 5.3c); and are disseminated in micrite and microspar. The latter crystals commonly contain calcite inclusions and have irregular embayed boundaries with microspar and pseudospar. These crystals are associated with calcium-poor (dolomitic?) amorphous patches which overprint microspar. Disseminated crystals and patches and some mottles are separate from stylolites, which are associated with many of the mottle dolomites

(Pl. 5.3a,c,e).

Dolostone-mottled limestones grade vertically into pervasive dolostones (Haywick, 1984) near the contacts of dolomitized mudstones and intercalations of burrowed wackestone (Fig. 3.1). In these pervasive dolostone beds fine, 100 μm, crystals commonly replace burrows; very fine, 10 to 50 μm, crystals replace micrite matrix; and medium, 200 to 300 μm, rhombs replace interburrow spar. Abundant microstylolites commonly truncate and brecciate crystals (Pl. 5.3b).

In the Aguathuna Formation very fine to fine crystals of Dolomite II replace individual laminations in dololaminites and the matrix or burrows of burrow-mottled beds. Euhedral to subhedral crystals typically form intergrown clusters (Pl. 5.1a) and nucleate around 1 to 5 μm peloids.

Cathodoluminescence - Most crystals luminesce purple and pink (Pl. 5.1a,b). Fine growth zones in crystals with purple CL are commonly destroyed by dissolution, and irregular replacement and overgrowth by pink CL dolomite (Pl. 5.1a,b). These overgrowths are well developed in large individual crystals and along the edges of dolostone mottles.

Ferroan crystals are common in the middle Catoche Formation and in the lower portions of rock-matrix breccias. These zoned crystals have bright yellow CL cores containing common calcite inclusions. These cores are overgrown by non-luminescent ferroan dolomite and clear rims with bright orange CL (Pl. 5.1c). Crystals in dolostone mottles in the upper Catoche Formation exhibit ferroan inclusions but no CL zonation.

Geochemistry -Haywick (1984) regionally surveyed oxygen and carbon isotopes of six samples of dolostone mottles in St. George limestones, and $\delta^{18}O$ values span a wide range from -5.7 to -10.3 o/oo PDB (Fig. 5.2, Appendix A). The dolomites vary from 3.0 per mil enrichment to 1.2 per mil depletion in $\delta^{18}O$ relative to values of host limestones. Seven regional samples of pervasive dolostone have a similar broad range of $\delta^{18}O$ values between -4.7 o/oo PDB and -10.0 o/oo PDB (Haywick, 1984). Some of these dolostones have early dolomitized mottles with enriched $\delta^{18}O$ (-4.7 o/oo to -5.2 o/oo) similar to Dolomite I, and others are pervasively altered by dolomites with moderate $\delta^{18}O$ (-7 o/oo to -10 o/oo). Carbon isotope values do not vary from those of the original limestone (-0.5 0/00 to -1.5 0/00).

The dolomites are stoichiometric (50 mole % $CaCO_3$) with a d_{104} peak spacing of about 2.888 nm (Appendix C). The trace elements Fe, Mn, and Na are present in minor amounts (Appendix B). Iron locally reaches 1000 to 4000 ppm in the ferroan dolomites. Moderate 70 to 200 ppm concentrations of strontium are reported by Haywick (1984) for mottle dolostones.

Evidence of Timing - Crystallization of Dolomite II spans early diagenesis and the initial phases of pressure solution. Cathodoluminescence exhibits this history as zoned purple CL crystals overprinted by later pink CL dolomite (Pl. 5.1b). The wide-ranging isotopic values also reflect changing fluid chemistry.

Dolomite II replaces microspar and seams of insoluble material, and locally surrounds microbreccias of pseudospar (Pl. 5.3d). These features indicate that the dolomitization post-dates early compaction

and limestone diagenesis. Calcite veinlets which cut dolostone mottles (Pl. 5.2c; 5.3a) and stylolites which truncate brecciated rhombs (Pl. 5.3e), together demonstrate that some dolomites pre-date pressure solution. Pervasive dolostones also pre-date stylolites (Haywick, 1984). The many euhedral crystals which occur along stylolites in limestones, however, imply that dolomite growth continued during pressure solution (Pl. 5.1c). The crystals commonly displace stylocumulates of insoluble material (Pl. 5.3e) and others are surrounded by bifurcating stylolites (Pl. 5.3a,c).

Interpretation - Composite crystals of Dolomite II formed over a long period from shallow burial to pressure solution at depths greater than 300 m (Neugebauer, 1973). Purple CL dolomites in burrow mottles and pervasive dolostones were probably contemporary with Dolomite I, but most crystals nucleated in the shallow subsurface after the formation of microspar and compaction seams. Typical turbid dolomites incompletely replaced microspar, a characteristic of early dolomitization from fluids saturated with respect to calcite (Sibley, 1982). Brightly zoned, ferroan dolomites probably crystallized in areas of slow-moving reduced waters (cf. Frank et al., 1982; Grover and Read, 1983).

Pink CL dolomite developed euhedral rims during deeper burial and pressure solution. The early purple CL cores which formed in equilibrium with calcium-rich fluids became unstable and were partially replaced.

Although dolomitization occurred during pressure solution many crystal nucleii, some mottles and most pervasive dolostones had already

formed. The commonly dolomitized seams of insoluble material largely originated during early compaction (Shinn et al., 1983). Dolomites in burrows and many disseminated crystals nucleated separately from any seams or stylolites. These relationships support arguments of Pratt (1982) and Haywick (1984) against pressure solution as the major mechanism for dolomitization (Wanless, 1979) in these rocks. The abundance of detrital feldspars in dolostone mottles, highlighted in CL (Pl. 5.1b,c,e), suggests, however, that solution and displacement during dolomitization concentrated these grains.

5.5 Dolomite Type III - Very fine to medium crystalline, clear crystals with bright, zoned CL

Petrography and Distribution - Dolomite III constitutes only a minor portion of dolostones in the area, but it marks a significant change from turbid, replacement crystals to brightly luminescent zoned cements in secondary micropores and fractures. Dolomite III distinctively forms isopachous cements in former pores (Pl. 5.1e) and clear syntaxial rims on turbid Dolomite II crystals (Pls. 5.1c,d; 5.4a,b). The dolomite pervades precursor dolostones: rock-matrix breccias, Aguathuna dolostones and dolostone beds within the limestones. The dolomite is prominent in rock-matrix breccias where it overgrows fine 30 μm crystals in some fragments; forms thick rims on 100 to 500 μm rhombs which replace matrix (Pls. 5.1d; 5.4a); and cements fractures and solution pores. In fine crystalline dolostones of the Catoche Formation 50 to 200 μm rhombs and isopachous layers cement solution pores (Pl. 5.1e);

Plate 5.4 Dolomite III

a. Composite "CCCR" crystals with cloudy cores (Type II) and clear rims (Type III) replace rock-matrix breccia. Fine crystals overprint fragments whereas medium-sized ones occur in the matrix. Sample from DDH 66, 132 m, in the Mike Lake rock-matrix breccia (location, Fig. 1.4). 1 mm scale.

b. A combination of CCCR crystals and clear Dolomite III cements replace former mottles of coarse calcite in Catoche dolostone beds. Plate 5.1f is a similar example. Upper Catoche Formation, DDH 1254, 18 m b.w.m. 1 mm scale.

c. Clear crystals with minute fluid inclusions and halite inclusions (?) (arrow) characterize Dolomite III. Alternatively, the arrow points to a negative crystal two phase fluid-vapor inclusion. This inclusion morphology suggests formation at a significant burial depth (J. Reynolds, Fluid Inc. Course Notes). 75 μm scale.

PLATE 5.4

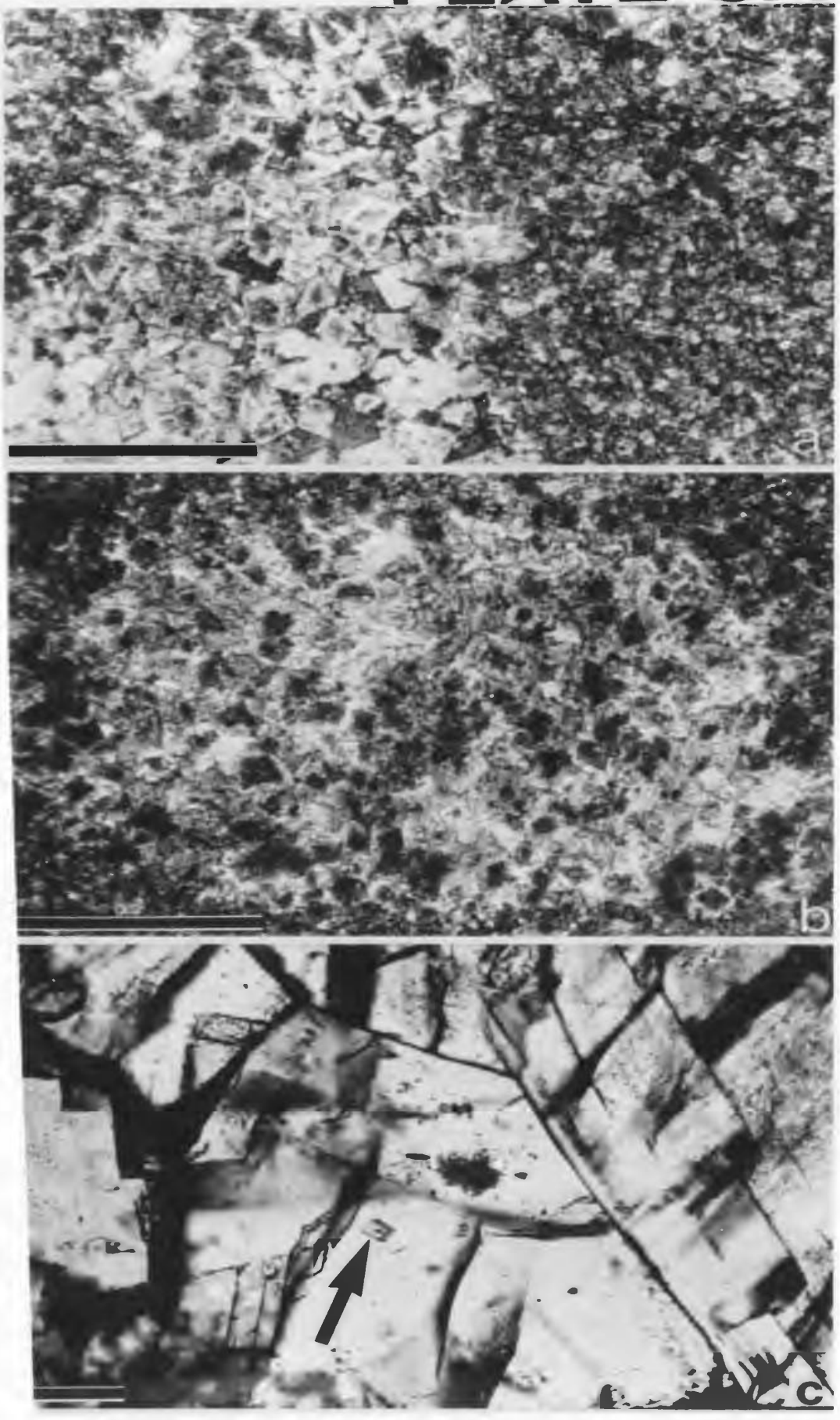

replace calcite-filled burrows (Pl. 5.4b); and form intercrystalline cements (Pl. 5.1e). In microcrystalline dololaminites only minute 5 to 20 μm rhombs occur in intercrystalline pores (Pl. 5.1a).

Occurrences of Dolomite III in limestones is scattered. It appears prominently in veinlets where medium 100 to 300 μm crystals commonly replace equant calcite cements (Pls. 5.2c; 5.3a). Isopachous cements of medium-sized crystals also fill solution pores around dolostone mottles (Pl. 5.3a) and along vertical sutures of stylolites. Within dolostone mottles very fine crystalline dolomite forms thin intercrystalline cements and overgrowths of Dolomite II crystals (Pl. 5.1b,e).

Cathodoluminescence - Dolomite III is distinctively zoned with 1 to 20 μm wide bands of alternating yellow-orange, red and pink CL (Pl. 5.1d,e). A stratigraphy of 5 to 12 zones in blocky pore cements correlates more than 5 km. Two bright yellow zones form the ubiquitous clear crystal rims. The distinction between pink CL Dolomite II and Dolomite III is arbitrary. Plate 5.1e clearly illustrates that the late pink CL phase of Dolomite II follows extensive dissolution of the carbonates and it forms the first isopachous cements. Zoned Dolomite III continues the growth of these cements.

Geochemistry - Dolomite III-rich dolostones from rock-matrix breccias (this study) and pervasive dolostone beds (Haywick, 1984) have moderate $\delta^{18}O$ values between -6.5 and -8.0 o/oo PDB (Fig. 5.2, Appendix A). $\delta^{13}C$ values are normal, -0.5 to -2.0 o/oo PDB, and depleted to -4.0 o/oo PDB.

The stoichiometric (51 mole % $CaCO_3$) dolomites have a d_{104} spacing around 2.888 nm (Appendix C). The dolomites are generally sodium-rich and vary in iron and manganese composition (Appendix B). Anomalous, 1000 to 30,000 ppm, sodium from microprobe point analyses is related to common halite crystal inclusions (Pl. 5.4c). Strontium is depleted, 50 to 90 ppm, relative to Dolomites I and II (Haywick, 1984).

Variations in manganese content and Fe''/Mn'' ratios correlate with luminescent zoning (Fig. 5.3). Manganese ranges from less than 100 to 500 ppm. Although highest concentrations are near the detection limits of the microprobe, highest values repeatedly correlate with luminescent zones. Bright zones have Fe''/Mn'' ratios of 0.08 to 0.05 compared to values of 2 to 5 for weakly luminescent bands.

Fluid Inclusions - Only scattered minute fluid inclusions and halite crystals occur in the clear crystals (Pl. 5.4c). What are identified as halite crystals may in fact be negative crystal inclusion morphology. Such negative crystals are characteristic of deep burial cements (J. Reynolds, Fluid Inc. course notes, 1990). Fluid inclusions in precursor calcite cements have salinities of 20 equiv-alent weight % NaCl and a modal homogenization temperature of 115°C (Fig. 5.2).

Evidence of Timing - Dolomite III clearly follows Dolomite II as overgrowths (Pl. 5.1e) and is overprinted by later Dolomites IV and V (Pl. 5.1f,g). Euhedral overgrowths within stylomottles (Pl. 5.1c) and cements along stylolite sutures indicate that the dolomites crystallized after formation of the stylolites at burial depths greater than 300

Figure 5.3 Variation in Iron and Manganese Abundances in Zoned Dolomite III

Microprobe traverses of iron and manganese abundance in zoned crystal layers of Dolomite III. Elevated Mn values (900 to 1700 ppm) with brightly luminescent (white) crystal layers. Moderately luminescent crystal layers (stippled) have Mn abundances of 400 ppm. This zoned Dolomite III crystal occludes a pore within a partially dolomitized limestone in the upper Catoche Formation (DDH 1254, 19 m b.w.m.).

Fe AND Mn IN ZONED DOLOMITE III

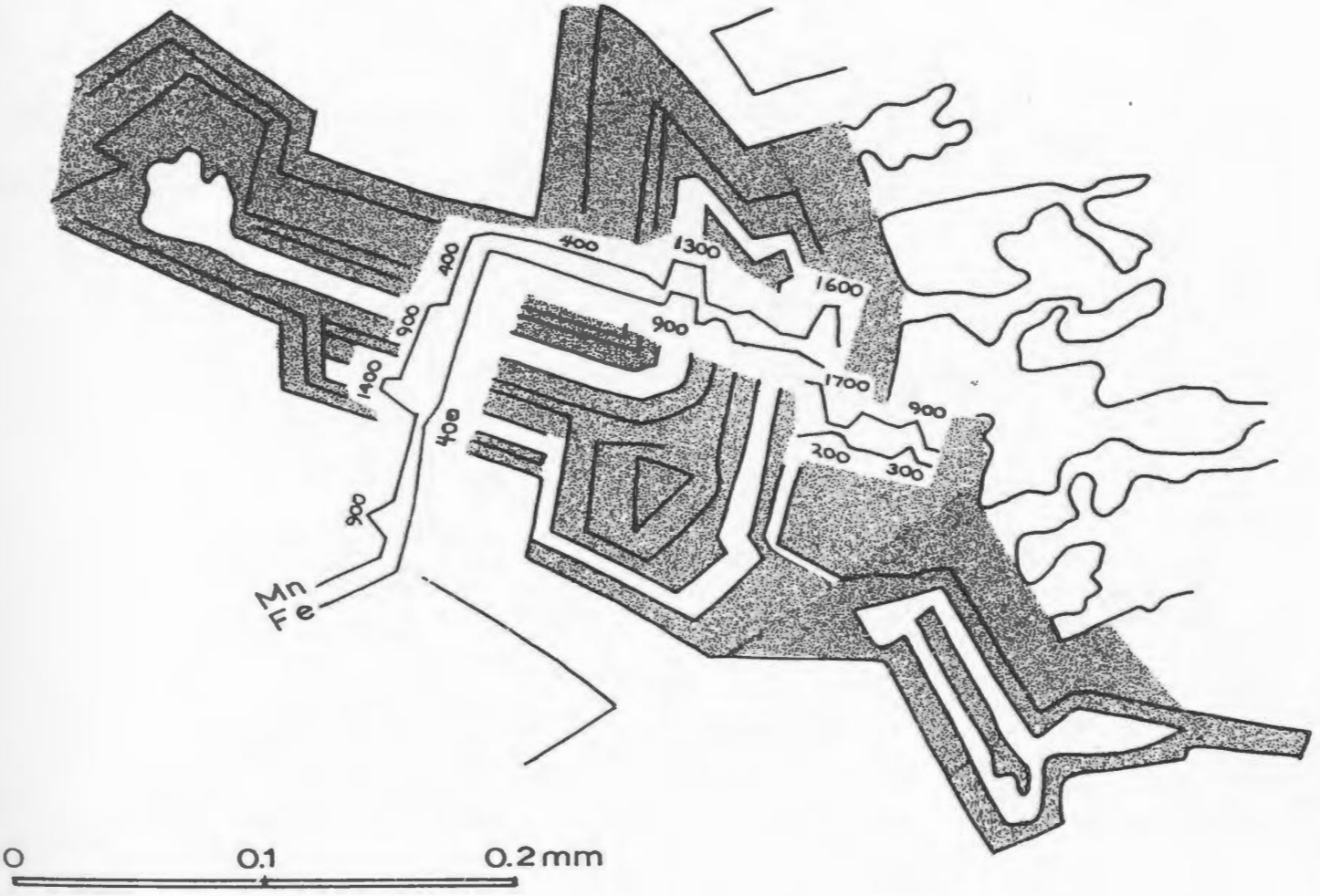

m (Neugebauer, 1973). Possible negative crystal inclusions support a deep burial origin.

Interpretation - The transition from weakly luminescent Dolomite II to zoned Dolomite III is characteristic of carbonate cementation at increasing burial depths (Frank et al., 1982; Grover and Read, 1983). Halite inclusions imply that the dolomites precipitated from hypersaline formational brines. The luminescent crystal layers probably incorporated Mn under reducing conditions (cf. Frank et al., 1982). Their association with stylolites implies that they precipitated at depths greater than 300 m.

Dolomitizing brines passed through permeable, precursor dolostones, but also along fractures and stylolites in limestones. The unstable early dolomites and some calcites partially dissolved; an event which was followed by the precipitation of the pink CL phase of Dolomite II and Dolomite III as crystal overgrowths and isopachous cements. Important geometric aspects of this dolomitization are considered in Chapter 8.

5.6 Dolomite Type IV - Fine to medium crystalline, replacement dolomite with red CL

Petrography and Distribution - Rare fine to medium crystalline mosaics of xenotopic dolomites (IV) occur instratigraphic gray dolostones within the uppermost Catoche Formation and discordant bodies

along faults in lower parts of the Formation (Pl. 5.5a). Coarse dolostone beds in the Catoche Formation locally preserve patches or mottles of these dolomites (Pl. 5.1g). Abundant gray dolostones predate Dolomite V because they are cross-cut by sulphide-cemented veins and solution pores. Other than the few remnant patches of Dolomite IV these gray dolostones are recrystallized to Dolomite V. Geometric relationships between these dolostones, sulphides and coarse dolostone beds are examined in Chapters 11 and 13.

Cathodoluminescence - Cathodoluminescence demonstrates that the medium to coarse-sized, 300 to 700 μm, crystals are poikilotopic ones which include and replace earlier rhombs of Dolomites II and III (Pl. 5.1f). The crystals luminesce bright red and the replaced rhombs have dull red cores and the orange-red signature of rims of Dolomite III (Pl. 5.1f,g).

Geochemistry - Oxygen isotopes of Dolomite IV samples have a moderate $\delta^{18}O$ of -6.88 to -8.30 o/oo PDB (Appendix A). $\delta^{13}C$ content varies from -0.9 to -1.48 o/oo PDB. This isotopic composition is similar or slightly depleted relative to Dolomite III and enriched relative to most samples of Dolomite V (Fig. 5.4).

Stoichiometric dolomites with 50 to 51 mole % $CaCO_3$ produce a d_{104} peak at 2.88 to 2.89 nm. Trace element content is variable:Fe'' at <100 to 2500 ppm with a 1300 ppm mean; Mn'' at <100 to 2500 ppm with a 600 ppm mean; and erratic amounts of sodium. Fe''/Mn'' ratios as low as 2 to 0.5 may partially account for the bright luminescence. Organic or

Plate 5.5 Epigenetic Dolomites IV and V

a. Xenotopic crystals of Dolomite IV form the coarse matrix of this discordant dolostone. Middle Catoche Formation, DDH 1134, 50 m. Polarized light. 1 mm scale.

b. Geopetal dolomites fill the base and saddle dolomite cements the upper portion of fractures which cut a precursor dolostone. Crystal textures of the inset are illustrated below in Pl. 5.5d. Underground sample from the west L Zone (Location, Fig. 1.4). 1 cm scale.

c. Pseudobreccia. Patches of gray dolomites comprise (A) gray matrix dolostone, (B) burrows and (C) coarse crystals with black intercrystalline material. White saddle dolomite occurs as replacement crystals (E) around gray dolomites and as a cement (D) around pores (p). From the G Zone open pit (Location, Fig. 1.4). 1 mm scale.

d. Equant rhombs (A) of Dolomite V with black intercrystalline material replace geopetal sediments and are overlain by megacrystalline cements (B) of Saddle Dolomite A with planar crystal boundaries. 1 mm.

e. Pseudobreccia. Turbid, xenotopic replacement dolomites (a) form gray patches. Replacement saddle dolomites (b) adjacent to patches grade outwards into large cement crystals (c) with planar boundaries. Polarized light. Sample same as 5.5c. 1 mm scale.

PLATE 5.5

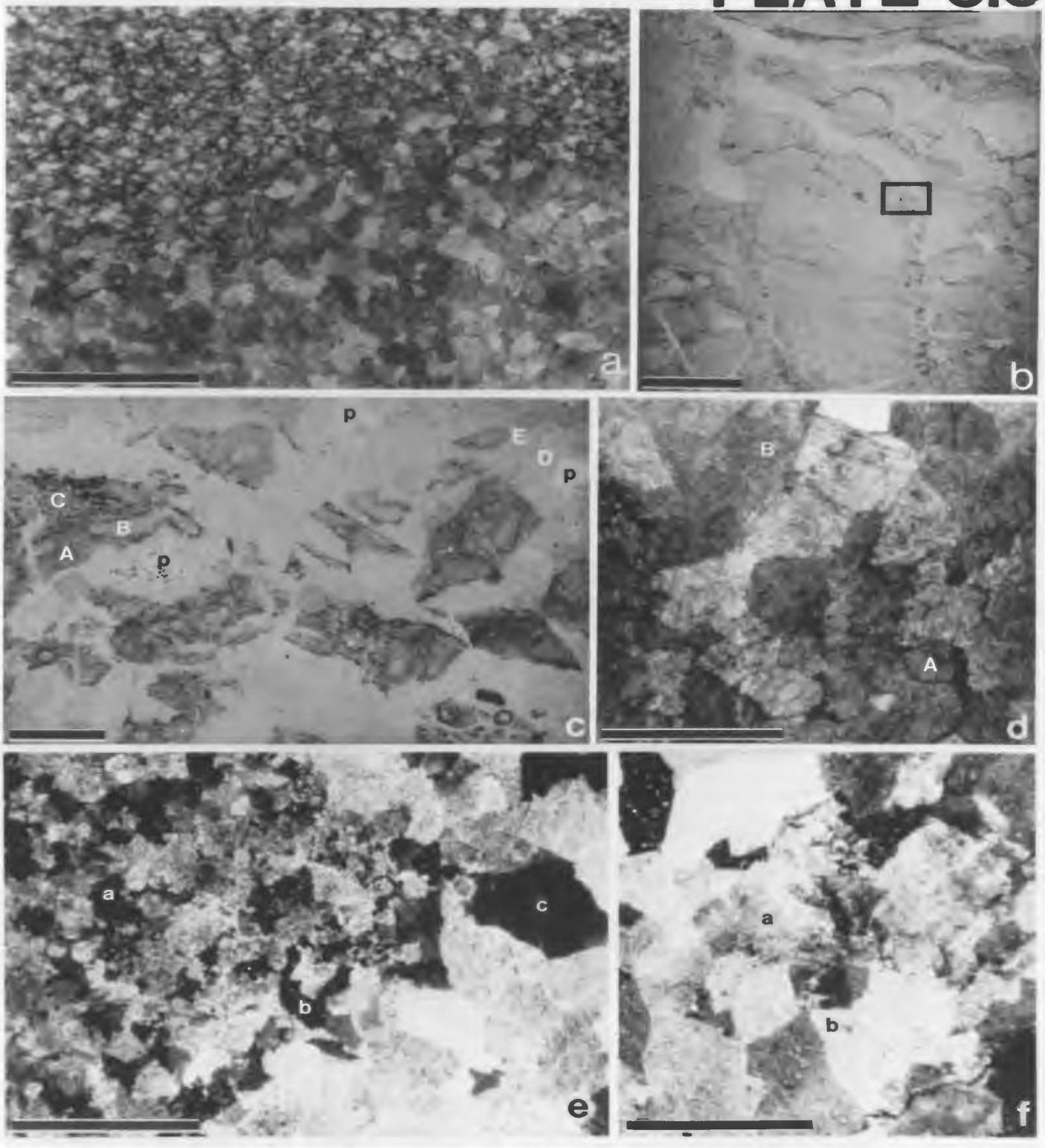

f. Xenotopic, replacement saddle dolomites (a) locally preserve brown to gray residues of precursor carbonates. Cement crystals (b), by comparison are white and planar-edged. Polarized light. Same sample as 5.5c. 1 mm scale.

Figure 5.4 Isotope and Fluid Inclusion Data for Epigenetic Dolomites and Calcites

Plot of $\delta^{18}O$ vs. $\delta^{13}C$ values for epigenetic dolomites (IV, V, VI) and late calcites (data in Appendix A and Coron, 1982).. Dolomite V is separated into 5 groups: (1) overall field of Saddle Dolomite A, (2) ore-stage Saddle Dolomite A, (3) late stage Saddle Dolomite A, (4) Saddle Dolomite A outlying ore zones and (5) coarse sparry dolostones adjacent to unaltered limestones. Dolomite VI is represented by Saddle Dolomite B which overgrows Saddle Dolomite A. Late calcite occludes former cavities lined by the saddle dolomites. The plot shows a depletion in $\delta^{18}O$ values of ore stage dolomites relative to other ones. Serial samples of cavity cements from ore-stage to late stage Saddle Dolomite A to Saddle Dolomite B demonstrates a progressive depletion of $\delta^{13}C$ and enrichment of $\delta^{18}O$ (open circles and arrows). Occluding late calcites indicate a depletion of $\delta^{18}O$ by fractionation relative to dolomite and further $\delta^{13}C$ depletion. The distinct fields for Saddle Dolomites A and B and late calcite suggest that they precipitated during three separate events from fluids with different chemistry.

Fluid inclusion data for Saddle Dolomite A and late calcites supports this conclusion. Late calcites have distinctly lower melting temperatures (-36°C) and homogenization temperatures (50°C) relative to Saddle Dolomite A (T_m = -25°C; T_h = 112°C).

EPIGENETIC DOLOMITE/ CALCITE

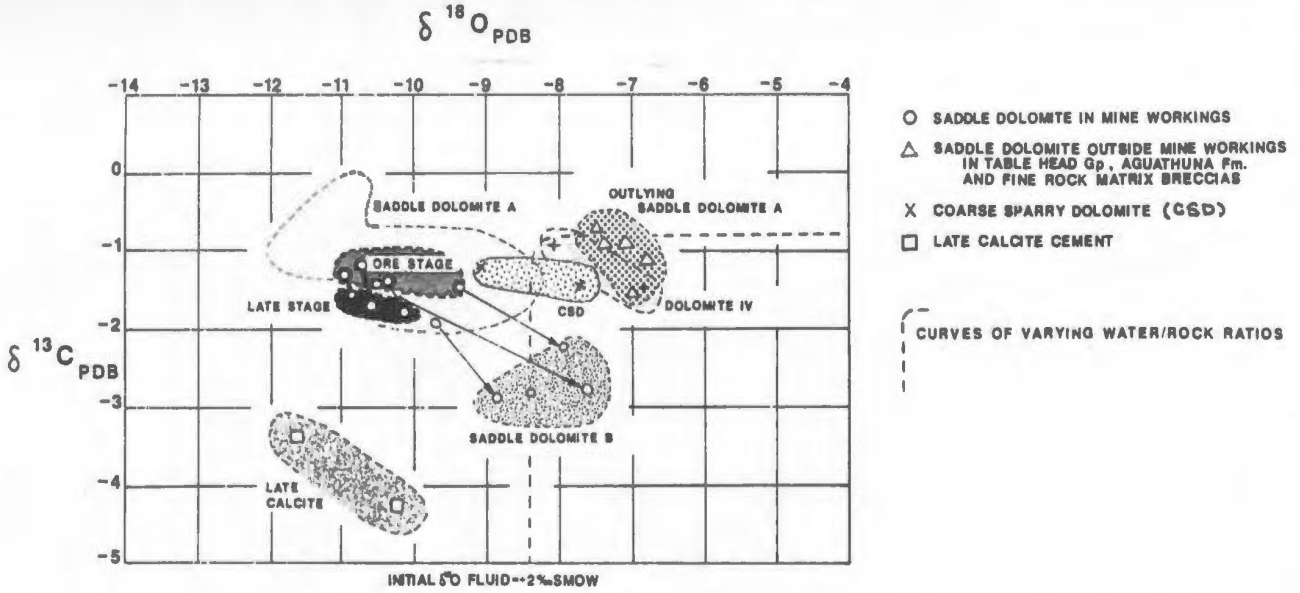

FLUID INCLUSION TEMPERATURES

SADDLE DOLOMITE A

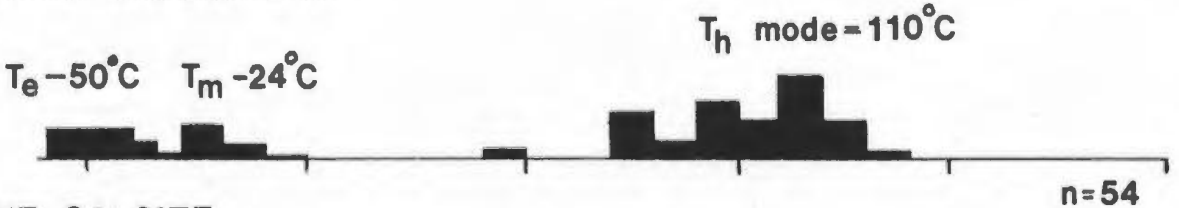

LATE CALCITE

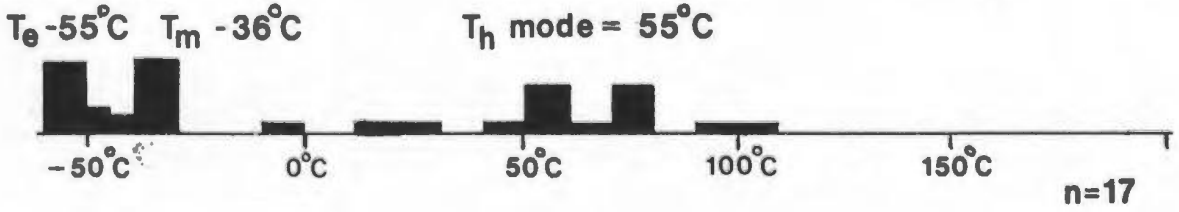

other trace matter in brown residue patches could also generate luminescence.

Evidence of Timing - Cathodoluminescence clearly shows that Dolomite IV overprints rhombs of Dolomite II and III and is crosscut by veinlets cemented by Dolomite V with its distinctive dull red CL (Pl. 5.1g). Sulphide-cemented veins indicate the pre-ore origin of these dolomites.

Interpretation - Dolomite IV pervasively replaced medium crystalline rhombs of earlier dolomites. Its position between Dolomite III and vein cements of Dolomite V implies that the dolomitization occurred during deep burial. The xenotopic crystal textures suggest hydrothermal origins (cf. Gregg and Sibley, 1984). The crystals probably incorporated the significant amounts of Fe and Mn under reducing conditions. Oxygen and carbon isotopic values similar to the precursor carbonates suggest that the fluids reached equilibrium with the host during the replacement dolomitization.

5.7 Dolomite Type V - Fine to megacrystalline dolomites with dull red CL

Petrography and Distribution - Important Type V dolomites with variable textures comprise most of the coarse dolostone complexes in the upper Catoche Formation and include the white, saddle dolomite cements which immediately follow sulphide precipitates. These dolomites comprise most of the dolostones in and around mine workings. The dolomites selectively replace former peloidal grainstones and wackestones and fill cross- cutting veins and megapores. The dolostone lithologies vary from uniform gray, medium to coarse dolostones to mottled gray and white pseudobreccias with megacrystalline saddle dolomite (Pl. 5.5; Chapter 13). Crystals can be categorized into three types: (1) fine to medium-sized xenotopic replacement crystals with plane extinction; (2) medium to coarse-sized, xenotopic to idiotopic, replacement crystals of equant saddle dolomite; and (3) prismatic and blocky, coarse to megacrystalline saddle dolomites which cement mesopores and megapores. Saddle or "baroque" dolomites are recognized by their sweeping undulatory extinction, cleavage and curved, deformed crystal structure (Folk and Asserto, 1974; Radke and Mathis, 1980). Saddle dolomites of generations V and VI are referred to as Saddle Dolomites A and B respectively.

(1) Fine to medium-sized, 20 to 200 μm, replacement crystals with plane extinction are largely xenotopic and equant. The turbid crystals contain residues and numerous micrometre-sized fluid inclusions (Pl. 5.5e). Neomorphism has enlarged earlier generations of crystals. The

replacement crystals within mottles or beds of gray dolostone grade into medium to coarse gray crystals of saddle dolomite with mild undulatory extinction (Pl. 5.5e).

(2) Medium to coarse-sized, 100 to 500 μm, replacement crystals of saddle dolomite with undulatory extinction are xenotopic and vary from gray to white in colour. The equant replacement crystals include a variety of crystal textures. Gray xenotopic crystals partially replace gray mottles (Pls. 5.5c,e; 5.7 a,b). Medium-sized, white crystals with irregular intergrown boundaries are transitional between gray mottles and void-filling saddle dolomite (Pl. 5.5c,e,f). Brown residues are commonly preserved in these crystals (Pl. 5.5f). These white replacement saddle dolomites are common in pseudobreccias with more than one-third white dolostone (Pl. 5.5c).

Euhedral equant rhombs of light gray dolomite replace geopetal sediments (Pl. 5.5b,d) and the tops of gray dolostone mottles in pseudobreccia (Pl. 5.5c). The crystals displace and concentrate black insoluble material between the euhedral rhombs. This material gives the dolostone a black colour.

Replacement saddle dolomites form coarse "sparry" dolostones in areas of transition between pseudobreccia and limestone (Fig. 1.5). The crystals are medium to coarse, equant, idiotopic rhombs with a light gray colour. Characteristically they overprint burrow-mottled and stylolitic fabrics (Pl. 5.7a,b). Crystals commonly nucleate around primary peloidal or inclusion-rich cores and are surrounded by uncemented intercrystalline pores (Pl. 5.7a,c). Intergrown xenotopic dolomites occur locally in gray mottles (Pl. 5.7c).

Plate 5.6 Fluid Inclusions in Saddle Dolomite and Late Calcite

a. Fluid inclusions in saddle dolomites vary from sparse occurrence in late Saddle Dolomite A in the lower left to great abundance in Saddle Dolomite B in the upper right. Underground sample from the K Zone (Location, Fig. 1.4). 100 μm scale.

b. Fluid inclusions in Saddle Dolomite A range in size from 1 to 10 μm. Same sample as 5.6a. 25 μm scale.

c. Millimetre-sized fluid inclusions in late calcite vary in shape from equant to tabular to necked forms. Underground sample from the K Zone (Location, Fig. 1.4). 75 μm scale.

PLATE 5.6

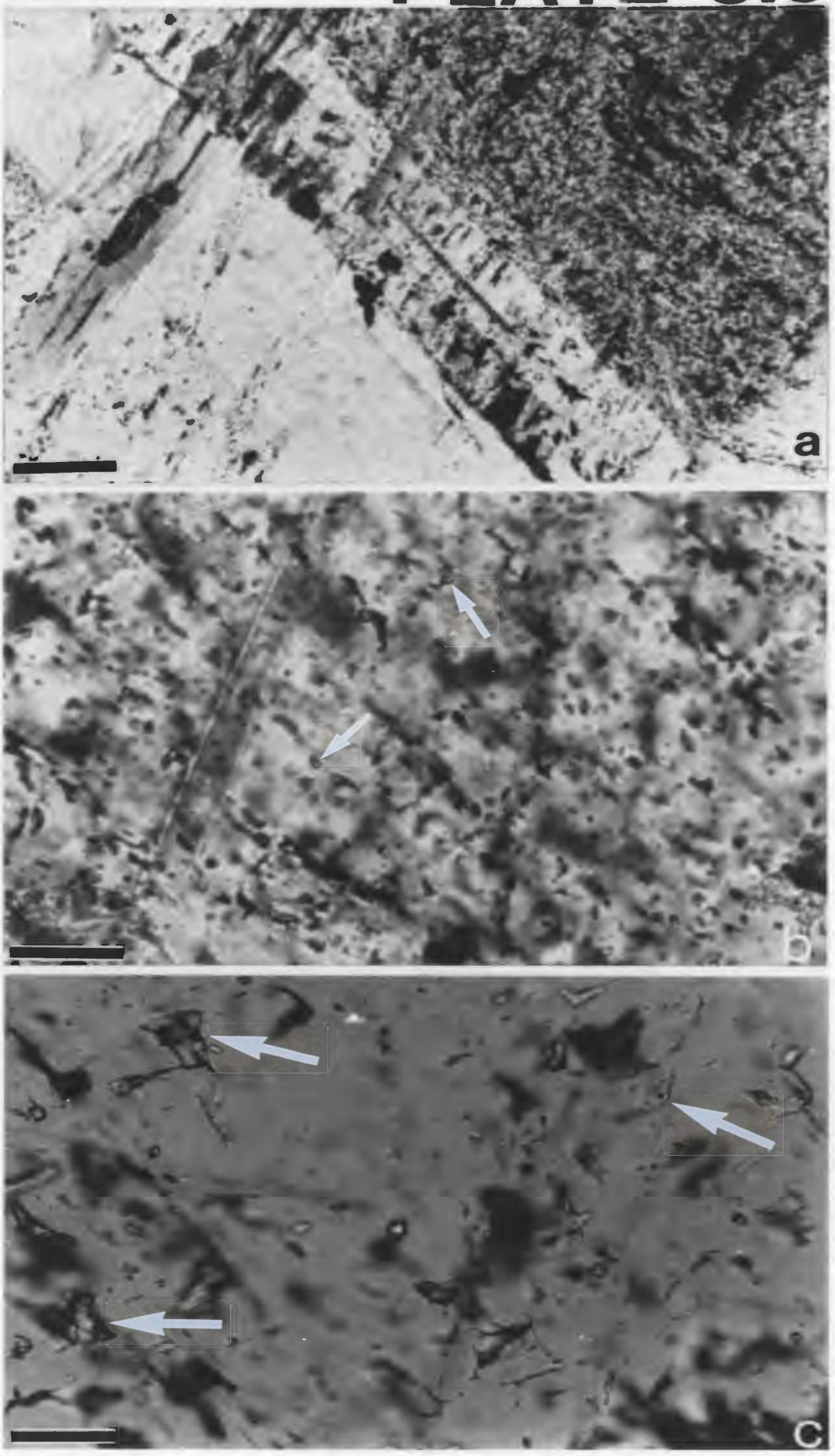

Plate 5.7 Dolomites V and VII in Coarse Sparry Dolostones

a. Coarse sparry dolostone. Equant, hypidiotopic saddle dolomites (V) replace and nucleate on precursor peloids (arrow). Sample from the L Zone area. 1 mm scale.

b. Coarse sparry dolostones replace the matrix surrounding early dolostone mottles, which they also overprint. Sample from the L Zone area. 1 cm scale.

c. One to two millimetre-sized pores characterize coarse sparry dolostones. Lack of a pore-filling geometry of surrounding rhombic crystals suggests that pores formed during late dissolution of unreplaced limestone patches (Murray, 1960). Polarized light. Sample from the L Zone, DDH 626, 155 m. 1 mm scale.

d. Late Dolomite VII uniformly overprints burrow fabrics (arrow). Solution pores along stylolites suggest that dissolution post-dated uplift. Sample from north of the L Zone, DDH 961, 165 m. 1 cm scale.

e. Similar solution pores along stylolites occur in finely crystalline dolomites in the Table Head Group. Many crystals are nucleated on dusky peloidal cores (arrow). Sample from the L Zone area. 1 mm scale.

f. Dolomites (VII) from Pl. 5.7d are finely crystalline, equigranular, euhedral and nucleated on primary peloids (arrow). 1 mm scale.

PLATE 5.7

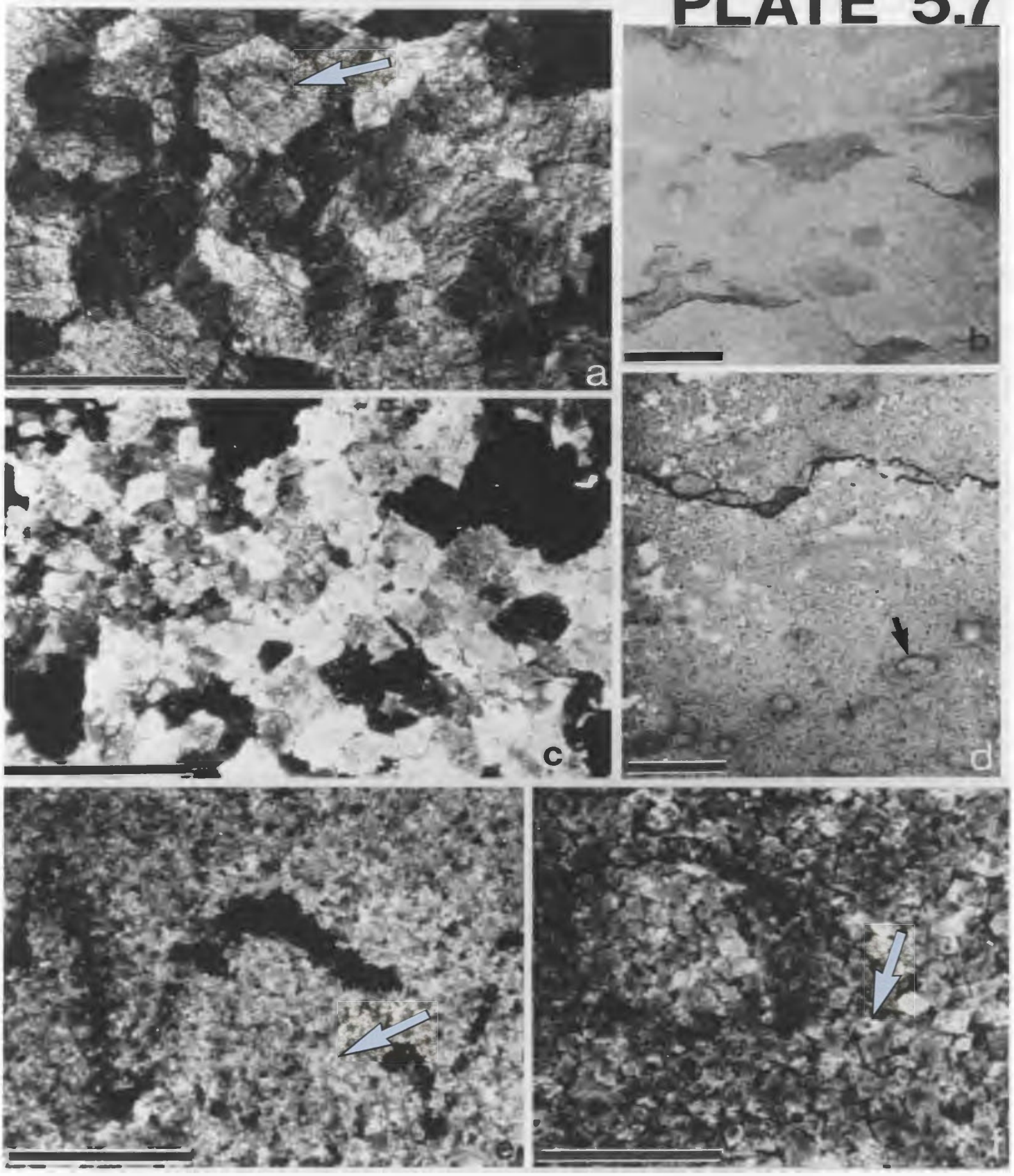

(3) White, translucent void-filling saddle dolomites contain abundant micrometre-sized fluid inclusions, minor residues and sweeping undulatory extinction (Pls. 5.5; 5.6b). Open space-filling dolomites distinctively have straight edges (Pl. 5.5e,f). Crystals at the edges of pores penetrate and replace 100 to 1000 μm into precursor dolomites (Pl. 5.5e,f). Crystals coarsen toward central pores from 100 to 500 μm long crystals along walls to 2 to 4 mm long prismatic forms to 4 to 10 mm diameter blocky crystals in centres. A 100 to 300 μm wide outer edge of these crystals has minor fluid inclusions (Pl. 5.6a).

Cathodoluminescence - Dolomite V crystal types uniformly luminesce dull red (Pl. 5.1g,h). Replacement crystals tend to luminesce darker red than the saddle dolomite cements. Local ferroan dolomites luminesce dark red. Faint zoning in the saddle dolomite cement, seen in plane light and hand specimen, appears as up to 12 zones under CL.

Coarse replacement crystals erase evidence of earlier dolomite CL where primary structures and fractures imply earlier dolomitization. Medium to coarse, 200 to 1000 μm, crystals commonly preserve evidence of neomorphic origin as dusky residues of peloids and burrow walls, but prior CL phases are lost (Pls. 5.5f; 5.7a). In fine crystals, less than 200 μm in diameter, bright orange CL rims of earlier zoned Dolomite III remain under a mask of dull red luminescence (similar to Pl. 5.1f).

Geochemistry - Forty-five oxygen isotope samples (this study and Coron, 1982) of Dolomite V define a broad field from normal to depleted values of -7 to -12 o/oo $\delta^{18}O$ PDB (Fig. 5.4, Appendix A). Carbon

isotopes values, which range from 0 to -2.0 o/oo $\delta^{13}C$ PDB, do not differ significantly from precursor limestones and dolostones. These results correspond to data for saddle dolomites throughout northwest Newfoundland (Haywick, 1984).

Detailed sample traverses across saddle dolomite cement sequences of the F, K, L and T ore zones reproduce significant parallel variations in both $\delta^{18}O$ and $\delta^{13}C$ (Fig. 5.4). Observations are summarized as follows: (1) Saddle dolomite cement in veins is depleted 0.5 to 2.0 per mil $\delta^{18}O$ relative to replacement crystals. (2) Dolomites precipitated directly after sphalerite crystallization form a tight group between -9 to -11 o/oo $\delta^{18}O$ and -1 to -1.5 o/oo $\delta^{13}C$. (3) Progressively younger dolomites are depleted in $\delta^{13}C$ 0.22 to 0.53 o/oo and enriched in $\delta^{18}O$ 0.10 to 0.23 o/oo PDB relative to initial cements. (4) Saddle dolomites and coarse sparry dolostones peripheral to ore zones are either depleted, -10.5 to -12 o/oo, or enriched, -6.5 to -9 o/oo, in $\delta^{18}O$ relative to ore zone dolomites.

These dolomites are stoichiometric (50 mole % $CaCO_3$) with a d_{104} peak spacing around 2.885 nm (Appendix C). Saddle dolomites from elsewhere on the Northern Peninsula tend to be enriched in $CaCO_3$ (Haywick, 1984). Most dolomites around the ore zones are slightly ferroan, 900 to 3500 ppm (Appendix B). Only the outer edges of ore zone crystals are ferroan. Ferroan dolomites occur locally outside the ore zones. Fe^{++}/Mn^{++} ratios of 14:1 are based upon Mn contents of 250 to 300 ppm. Strontium concentrations of 15 to 135 ppm with a mean of 67 ppm are depleted relative to Dolomite II (Haywick, 1984).

Fluid Inclusions - Typical, low relief fluid inclusions vary from one to several micrometres in size. Pink fluids contain small vapor bubbles, equal to 1 to 2% of the total volume (Pl. 5.6b). Sixty-three measured inclusions heat to modal homogenization temperatures of 112°C with a range from 92° to 133°C (Fig. 5.4). Anomalous inclusions homogenize at 48°, 65° and 164°C. Inclusions from earliest dolomites have the highest mean homogenization temperatures of 130°C. Eight of the studied inclusions are large enough to observe freezing and melting of fluids. Typical inclusions are $CaCl_2$-bearing and thus have initial melting, or eutectic, temperatures around -50°C. Salinities of 23 to 25 equivalent weight % NaCl (final melting temperatures of -24 to -28°C) are similar to those of sphalerite inclusions. A few lower salinity inclusions of 16 to 18 equivalent weight % NaCl have anomalously high and low homogenization temperatures of 48° and 130°C.

Evidence of Timing - Saddle Dolomite A which cements veins and macropores follows sphalerite precipitation and precedes occlusion of those pores by Saddle Dolomite B and late calcite (Pl. 5.1h). Saddle dolomite veins cut earlier dolostones and sphalerites. The similar CL and geochemical properties of and gradational relationships between all dolomite textures imply that replacement and cement dolomites are the same generation. Therefore Saddle Dolomite A has been grouped with the geochemically similar replacement dolomites under Type V. Stylolites along gray dolostone mottles imply that the dolomites crystallized during burial (Pl. 5.5b,c).

Interpretation - Dolomite V is a characteristic hydrothermal and deep burial dolomite. Fluid inclusions with elevated hypersalinities and homogenization temperatures indicate their origin from hydrothermal subsurface brines. Saddle dolomites and xenotopic textures are characteristic of hydrothermal dolomites (Radke and Mathis, 1980; Gregg and Sibley, 1984). Their association with sphalerite supports this conclusion. Depleted $\delta^{18}O$ values of saddle dolomites associated with sulphides probably record hydrothermal effects.

Replacement by both normal and saddle dolomites is pervasive and extensive. This observation is significant because most saddle dolomites are reported as pore-filling cements (Radke and Mathis, 1980). Similar pervasive dolostones with uniform luminescence are, however, recognized elsewhere as characteristic of deep burial dolomitization (Radke, 1978; Morrow et al., 1986; Lee and Friedman, 1987; Aulstead and Spencer, 1987; Freeman and Medary, 1987).

5.8 Dolomite Type VI - Megacrystalline Dolomites with Red CL

Petrography and Distribution - Poikilotopic, inclusion-rich saddle dolomites cement megapores after precipitation of Saddle Dolomite A (Pls. 5.1g; 5.6a). Although they constitute only a minor portion of the total saddle dolomite in the area, these crystals signify a distinct precipitation event. The translucent white to pink dolomites vary from thin mm-thick overgrowths to 15 cm-diameter megacrystals. Saddle Dolomite B syntaxially overgrows Saddle Dolomite A, but it also cements fractures and breccias of sphalerite and Saddle Dolomite A (Pl. 5.1h).

Cathodoluminescence - Dolomite VI is distinguished from preceding crystals by its bright red CL in which coincident crystal and CL zone boundaries are abrupt (Pl. 5.1h). Cathodoluminescence highlights cements in μm-thin fractures which cross-cut Saddle Dolomite A and sphalerites, and thin cements of solution rims around sulphides. Relic intercrystalline pores are also cemented (Pl. 5.1g). In places, these fine cements give the composite medium crystalline dolostones a brighter red luminescence than the coarse saddle dolomites of Dolomite V.

Geochemistry - Saddle Dolomite B is enriched 1 to 3 per mil in $\delta^{18}O$ and depleted 1 to 1.5 per mil in $\delta^{13}C$ relative to Saddle Dolomite A. Five samples of Saddle Dolomite B from centres of three ore zones define a field between -7.5 to -8.84 o/oo PDB $\delta^{18}O$ and -2.24 to -2.87 o/oo PDB $\delta^{13}C$ (Fig. 5.4, Appendix A). The isotopic trend of Saddle Dolomite A crystallization thus extends to Saddle Dolomite B crystals. Two samples reported by Coron (1982) from the outskirts of the L Zone continue the trend even further to -6.4 to -7.0 o/oo PDB $\delta^{18}O$ and -4.1 o/oo $\delta^{13}C$.

Late megacrystalline calcites which occlude megapores have depleted isotope values of both $\delta^{18}O$ (-10.19 to -11.60 o/oo PDB) and $\delta^{13}C$ (-3.35 to -4.21 o/oo PDB) (Fig. 5.4, Appendix A).

These dolomites are stoichometric (50 mole % $CaCO_3$), similar to Saddle Dolomite A, with spacing of the d_{104} peak around 2.885 nm (Appendix C). Saddle Dolomite B is slightly more ferroan than Saddle Dolomite A, 5000 ppm compared to 3500 ppm, and the crystals respond to potassium ferricyanide solution with a light blue stain (Appendix B). The manganese content is twice that of Saddle Dolomite A, 600 ppm

compared to 250 ppm. Fe/Mn ratios of 5 to 6 may account for the red luminescence.

Fluid Inclusions - Two fluid inclusions homogenized at temperatures of 107° and 110°C. No freezing measurements could be conducted. In general, the rock is too gray and inclusions are too small and closely spaced to be clearly visible (Pl. 5.6a). Salinities are above 24 equivalent weight % NaCl (T_m = -36°, Fig. 5.4), comparable to hypersaline inclusions in Saddle Dolomite A and late calcites.

Large fluid inclusions preserved in subsequent late calcites indicate progressive increase in salinity and decrease in fluid temperatures during pore filling relative to the saddle dolomites. The millimetre-sized fluid inclusions are hypersaline with low final melting temperatures of -34° to -38°C (Pl. 5.6c; Fig. 5.4). The inclusions also homogenize at relatively cool modal temperatures of 62°C.

Evidence of Timing - Dolomite VI (Saddle Dolomite B) follows Saddle Dolomite A as a cement in megapores and fractures. Megacrystalline late calcite locally occludes megapores. Euhedral crystal faces in open pores are overgrown by a variety of crystals of calcite, sulphates, marcasite, sphalerite and galena, and coatings of pyrobitumen and hematite.

Interpretation - After brecciation and fracturing of previous sulphide and Dolomite V cements Saddle Dolomite B precipitated as a poikilotopic cement from a hypersaline fluid. The crystals were

enriched in $\delta^{18}O$ and depleted in $\delta^{13}C$ relative to Saddle Dolomite A in response to cooler, reduced fluids and decreased fluid interaction with the host rocks. The depleted $\delta^{13}C$ values might be interpreted as introduction of organic hydrocarbons in the fluid and/or an increasing fluid vs. rock signature with decreasing wall rock interaction. These changes also led to increased Mn and Fe concentration and precipitation of calcites at low temperatures.

5.9 Dolomite Type VII - Fine to coarse crystalline dolomite with red CL distributed along late faults

Petrography and Distribution - Porous, pervasive dolostones replace Catoche and Table Point limestones along late faults which displace bodies of earlier dolomites. Fine to coarse-sized, equigranular and equant crystals replace the limestones and overprint primary mottling and stylolites (Pl. 5.7b,d). The idiotopic to slightly intergrown crystals are surrounded by abundant pores between crystals, along stylolites and in former calcite-filled fenestrae (Pl. 5.7c,d,e,f). Individual rhombs commonly nucleate around peloids (Pl. 5.7f). Dolostones which replace massive to fenestral mudstones of the Table Point Formation are distinctively fine crystalline and buff-coloured compared to fine to coarse dolostones which replace Catoche limestones (Pl. 5.7c,e,f). Nucleation around fine grains in mudstones as opposed to coarse peloids probably accounts for this difference. Solution pores in the Table Point Formation are partially cemented by coarse saddle dolomite and late luminescent yellow calcite.

Cathodoluminescence - Crystals luminesce a uniform bright red with no zonation. Residue-rich, irregular brown patches and peloid nucleii contribute significantly to this luminescence.

Geochemistry - Coron (1982) reported isotope analyses for a variety of these dolomite types. Dolomites in the Table Point Formation contain relatively undepleted $\delta^{18}O$ and $\delta^{13}C$, -6.7 to -7.6 o/oo PDB $\delta^{18}O$ and --0.6 to -0.7 o/oo PDB $\delta^{13}C$. One Catoche sample falls in the same field, -7.3 o/oo PDB $\delta^{18}O$ and -1.1 o/oo PDB $\delta^{13}C$ (Fig. 5.5). East of the mine area other Catoche dolostones of possible Dolomite VII origin have widely divergent depleted and enriched $\delta^{18}O$, e.g. -13.7 o/oo PDB $\delta^{18}O$ and -4.9 o/oo PDB $\delta^{18}O$ (Coron, 1982).

Stoichometric (50 mole % Ca) dolomites are iron-poor, <1000 ppm or below the limit of microprobe detection (Appendices B and C). Sporadic Mn-rich crystals, 1500 ppm, and Fe/Mn ratios less than 1 probably account for the moderate to bright luminescence.

Fluid Inclusions - Fluid inclusions are very small, micrometre-sized and most crystals are too gray and dusky for clear observation. Three inclusions along rims of the latest dolomite homogenized at 75° to 77°C. A final melting temperature of -25°C from one of the inclusions measures a salinity of 24 equivalent weight % NaCl.

Evidence of Timing - These dolomites are related to late faults around which they occur. These faults post-date and displace bodies of coarse dolostone (V and VI) and sphalerite. Solution along stylolites

Figure 5.5 Isotopic Data for Late Fault-Related Dolomites (VII)

Plot of $\delta^{18}O$ vs. $\delta^{13}C$ values for Dolomite VII (Coron, 1982). Isotopic values for Dolomite VII plot in three fields. Calculated water-rock ratios from variable water compositions (dashed lines) suggest that isotopic differences reflect the role of meteoric water in dolomitization.

FAULT-RELATED , POST-UPLIFT DOLOMITES

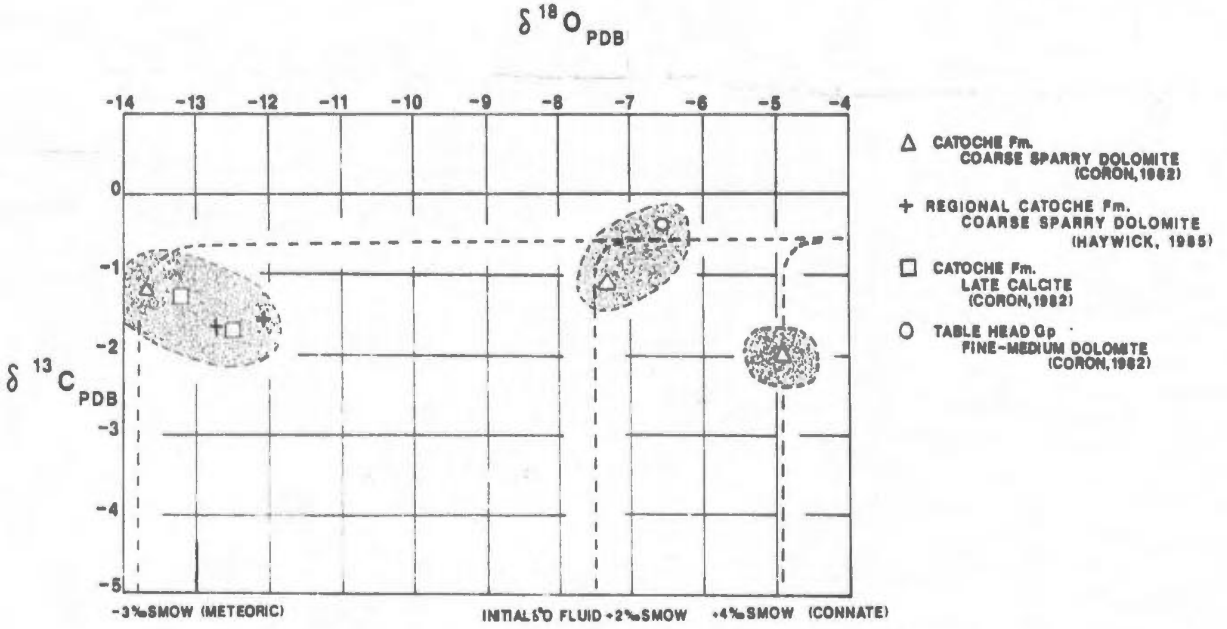

suggests that the dolomites crystallized at shallow depths after uplift and the cessation of pressure solution (Pl. 5.7e).

Interpretation - Late stage dolomitization replaced limestones along most faults. Fluid inclusions indicate that dolomitizing fluids were probably hypersaline, but variable isotopic values imply a variety of fluid sources and compositions. Crystals nucleated on fine mud and peloid grains. Limestone replacement left between crystals a combination of displaced insoluble material, intercrystalline mesopores and selective solution pores along stylolites and fenestrae. Late solution probably removed dolomites or limestone patches to form the intercrystalline mesopores (Pl. 5.7c). Selective solution along stylolites suggests that dolomitization occurred after uplift.

5.10 Diagenetic Stages of Dolomites

The seven dolomite types are grouped under four diagenetic environments which are loosely termed (1) syngenetic, (2) diagenetic, (3) epigenetic and (4) late fault-related settings (Fig. 5.6; also refer to Fig. 1.6).

Syngenetic or primary dolomites (Freeman, 1972) are identified as crystals which formed from solutions generated at the surface. Dolomite I and the nucleii of Dolomite II are included in this group. Dolostone fragments of I and II in intraformational conglomerates and karst breccias indicate their origin at or near the surface. The dolomitized matrix of subsurface karst breccias implies that syngenetic dolomitiza-

Figure 5.6 Paragenetic Sequence

Chart of paragenetic crystal stages and their relationship to geologic events and the presumed depth of burial and geological time scale.

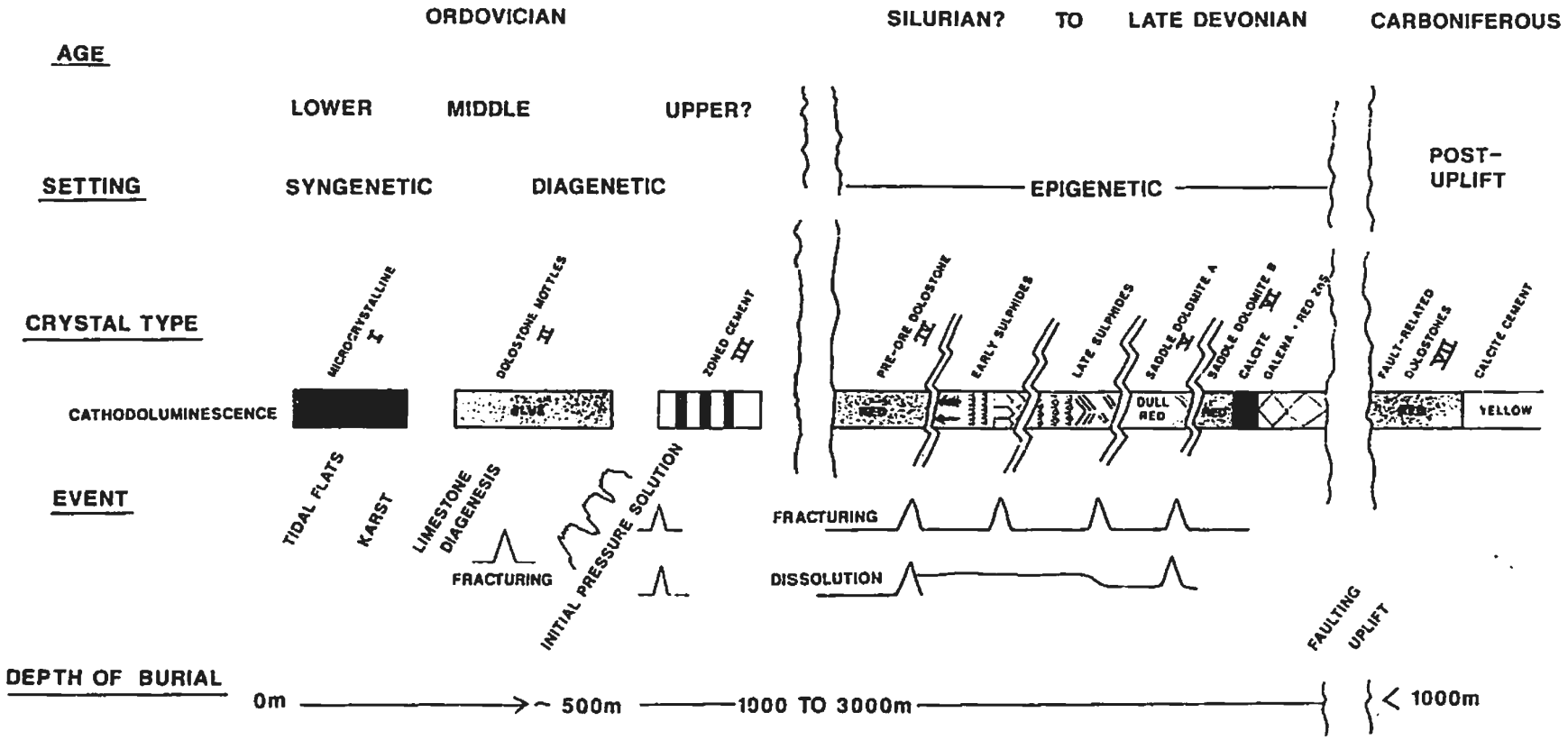

PARAGENESIS

tion penetrated tens of metres below the surface.

Diagenetic dolomites specify crystals which formed during burial and the change from near surface to subsurface pore fluids. This definition differs from others which encompass dolomitization after lithification or all early dolomites (Chilinger et al., 1979). Diagenetic dolomitization formed ubiquitous and stratigraphic dolomites as carbonates reacted to compaction, pressure solution and fluid migration through early dolostone beds. Typical composite crystals of Dolomite II experienced partial solution, replacement and overgrowth during progressive burial to depths of pressure solution. Zoned precipitates of Dolomite III marked the final phase of diagenetic crystallization from deep formational fluids.

Epigenetic dolomites, types IV, V and VI, crystallized in the deep subsurface where they were localized along structures (comparable to the definition of Friedman and Sanders, 1967). Although these dolomites occurred along faults and fractures they also extensively replaced stratigraphic units such as the upper Catoche Formation. This dolomitization was distinctively hydrothermal.

Late fault-related dolomites, type VII, were also structurally controlled. These dolomites, however, distinctively lacked abundant saddle dolomites and xenotopic textures that were typical of the hydrothermal epigenetic dolomites. They crystallized along faults that formed or reactivated during regional uplift. The dolomitization occurred during and after uplift when subsurface brines and meteoric waters migrated along the faults.

Figure 5.6 graphically displays the relationship between these

diagenetic stages and other events (see also Fig. 1.6). Most syngenetic dolomites crystallized prior to karstification. Dolomite II replaced diagenetic calcites (micrite, microspar and pseudospar) at this time and during burial. Calcite-cemented veinlets, however, cut early mottles of Dolomite II and were truncated, in turn, by pressure solution (Pls. 5.2; 5.3). Compacted layers of insoluble material along stylolites provided sites for growth of Dolomites II and III throughout burial.

Epigenetic dolomites preceded and followed sulphide mineralization as part of a tectono-hydrothermal event. These dolomites cemented fractures and replaced surrounding carbonates following several fracturing events. Extensive secondary solution preceded sulphide mineralization and, to a lesser degree, post-ore Dolomites V and VI.
After pervasive Dolomite V a wide variety of minerals precipitated in pores. The sequence of this mineralization is estimated as follows: (1) Saddle Dolomite B; (2) megacrystalline calcite; (3) gypsum, barite, celestite and fluorite; (4) marcasite during and after scalenohedral calcite; (5) galena; (6) red euhedral sphalerite; (7) pyrobitumen; and (8) hematite. These crystals probably precipitated from hydrothermal fluids at depth as pyrobitumen formed from thermal cracking of hydrocarbons (Evans et al., 1971). Late fault-related dolomites (VII) occurred during or after regional uplift. Late calcites with yellow CL, the last vug cements, probably were coeval with similar Carboniferous cements (Saunders and Strong, 1986).

5.11 Summary and Discussion of Fluid Inclusion Data

Microthermometric measurements of fluid inclusions sample a spectrum of paragenetic stages from early calcite cements to sphalerites, saddle dolomites and late non-luminescent calcites (Appendix F). All carbonates and sphalerites crystallized from hypersaline brines. Depression of ice melting temperatures to -10°C to -36°C imply the presence of 180 to 220 ppm total dissolved salts. Fluid inclusions homogenize at low to moderate temperatures of 60° to 180°C. Estimated burial depths of 2 to 3 km for epigenetic minerals implies that corrected homogenization temperatures should be 20° to 30°C lower (Potter, 1977).

A thermal high of 160° to 180°C during early sphalerite crystallization was preceded by cooler, but moderate, formation temperatures with a mode of 115°C during late limestone diagenesis and followed by a cooling trend to a mode of 115°C T_h for late sphalerites and most saddle dolomites to a mode of 55°C for late calcites and late fault-related dolostones (Fig. 5.7). The homogenization temperatures of early calcites were probably reset during maximum burial (Prezbindowski and Larese, 1987).

Salinity generally varies inversely with T_h (Fig. 5.7). Ore stage inclusions with high T_h's have lower salinities than late stage inclusions with low T_h's. Most saddle dolomite and sphalerite inclusions, however, have similar salinities around 25 equivalent weight % NaCl and homogenize over a broad temperature range from 95° to 170°C. Anomalous low salinity inclusions with high and low T_h probably sample

Figure 5.7 Fluid Inclusion Salinities vs. Homogenization Temperatures

Plot of homogenization temperatures of fluid inclusions versus their final melting temperatures, a measure of their salinity. Separate or overlapping fields of data can be drawn for each crystal stage. Early calcite inclusions are less saline than other populations. Their high T_h's were probably reset during burial. Salinities of saddle dolomites and sulphides are generally similar and their T_h's overlap. Inclusions in late calcites are distinctively different with high salinities and low T_h's. Suggested isochores are from Konnerup-Madsen (1979) and Lindblom (1986). They suggest that early ore brines were light compared to those found in late sulphides and saddle dolomites. More data is needed to evaluate the importance of low salinity inclusions.

FLUID INCLUSIONS: SALINITY VS. HOMOGENIZATION TEMPERATURE

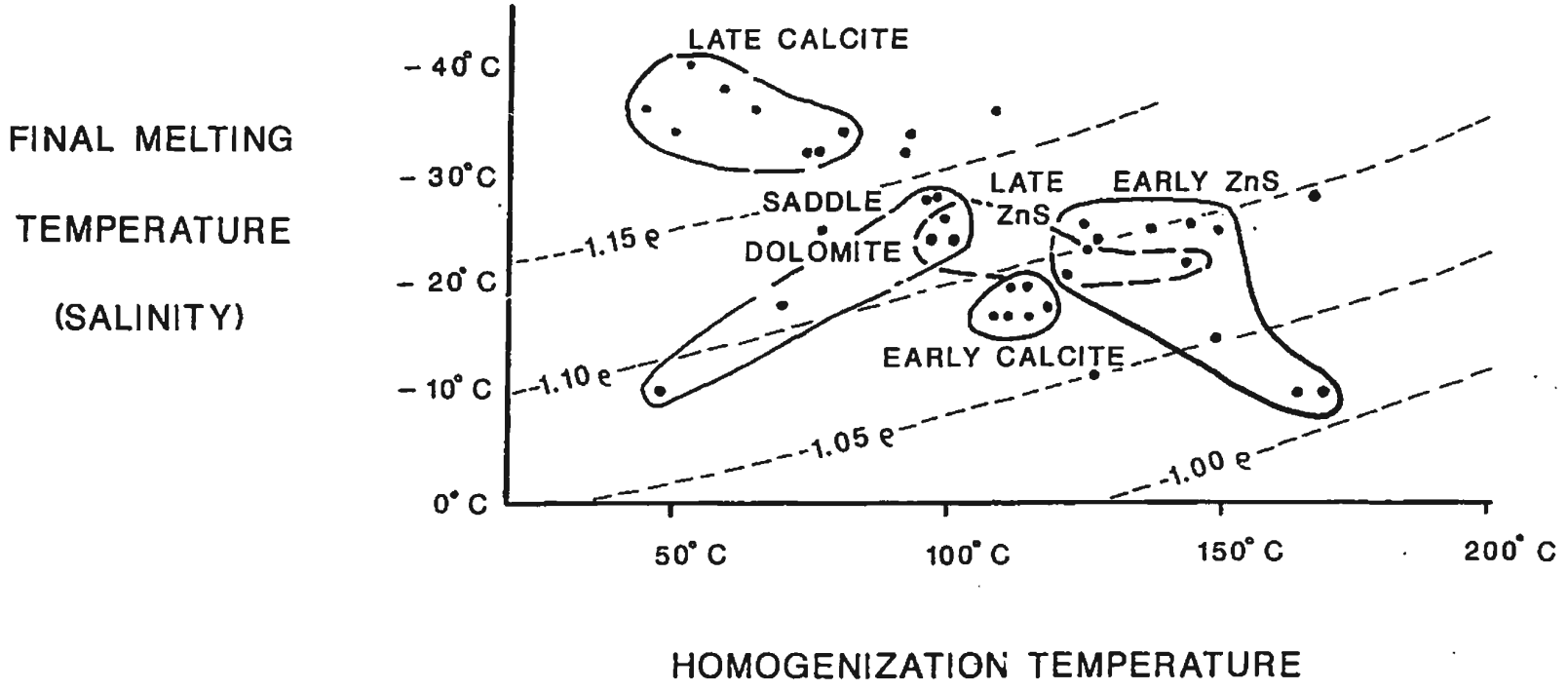

two or more separate fluids as suggested by some workers (e.g. Taylor et al., 1983; Lindblom, 1986). Populations of inclusions with low salinities and high T_h's occur in some localities elsewhere on the Northern Peninsula (C. Saunders, pers. comm. 1988)

Fluid inclusions from other MVT sphalerites and gangue carbonates outside Newfoundland also homogenize at temperatures of 90 to 120°C and are hypersaline (20 to 25 equivalent weight % NaCl) (Roedder, 1968, 1977; Leach, 1979; Taylor et al., 1983; Richardson and Pinckney, 1984; Lindblom, 1986; McNaughton and Smith, 1986; Gratz and Misra, 1987). Inverse relationships between inclusion salinities and homogenization temperatures are interpreted as mixing of two solutions; one hot and saline, the other cool with low salinity (Taylor et al., 1983; Lindblom, 1986). Conversely, invariant salinities of inclusions are interpreted as evidence of precipitation from a single fluid (Richardson and Pinckney, 1984; Gratz and Misra, 1987). Wide ranges in temperature, salinity and density of fluid inclusions at Daniel's Harbour, more than anything, displays variation of fluid composition through crystallization history rather than concrete evidence of fluid mixing.

5.12 Summary and Discussion of Oxygen and Carbon Isotope Data

Introduction - Oxygen and carbon isotopic data for all the dolomites exhibit a progressive depletion of $\delta^{18}O$ in most younger crystals and depletion of $\delta^{13}C$ in late Dolomite VI and late non-luminescent calcites (Fig. 5.8, Appendix A). This simple overall trend is complicated in detail. (1) Some mottle dolomites of Dolomite II type are depleted in

Figure 5.8 Relative $\delta^{18}O$ and $\delta^{13}C$ Compositions of the Dolomites

Comparative plots of $\delta^{18}O$ vs. $\delta^{13}C$ values for all the dolomite types and calcites (data listed in Appendix A; also fro Coron, 1982; Haywick, 1984). In Figure 5.8A primary limestones cluster between -8 and -9 o/oo $\delta^{18}O$ and -1 o/oo $\delta^{13}C$. $\delta^{13}C$ values in most dolomites are similar. Dolomite I has high $\delta^{18}O$ values (-4 to -6 o/oo). Dolomite II and III range between -6 and -10 o/oo.

In Figure 5.8B of epigenetic dolomites values, ore-stage Saddle Dolomite A has depleted $\delta^{18}O$ values (-9 to -11 o/oo) compared to Dolomite IV and other crystals of Dolomite V (-7 to -9 o/oo). Serial samples of cavity cements in ore zones (arrows) change progressively in isotopic composition from ore stage Saddle Dolomite A (-10 to -11 o/oo $\delta^{18}O$, -1 o/oo $\delta^{13}C$) to late stage Saddle Dolomite A (-10 to -11 o/oo $\delta^{18}O$, -2 o/oo $\delta^{13}C$) to Saddle Dolomite B (-7.5 to -9 o/oo $\delta^{18}O$, -2 to -3 o/oo $\delta^{13}C$) to late calcite (-10 to -11 $\delta^{18}O$, -3 to -4 $\delta^{13}C$).

In Figure 5.9C isotopic values of late fault-related dolomites (VII) vary widely.

A. EARLY DOLOMITES

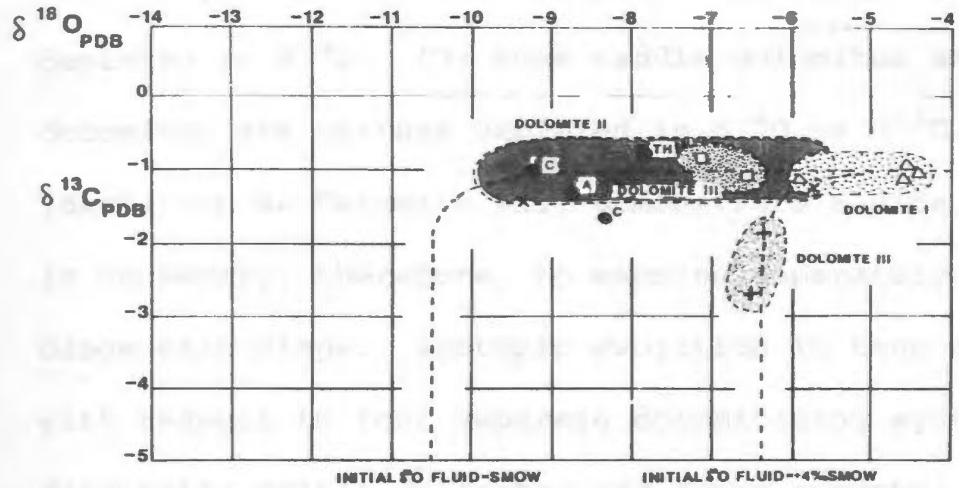

- ● LIMESTONE (CORON,1982) TH - TABLE HEAD Gp A - AGUATHUNA Fm. C - CATOCHE Fm.
- △ AGUATHUNA DOLAMINITE CATOCHE MUDSTONE (THIS STUDY; HAYWICK, 1985)
- \+ BOAT HARBOUR DOLAMINITE (HAYWICK, 1985)
- □ FINE ROCK MATRIX BRECCIA
- X CATOCHE BURROW-MOTTLED DOLOMITE (HAYWICK, 1985)

B. EPIGENETIC DOLOMITE/ CALCITE

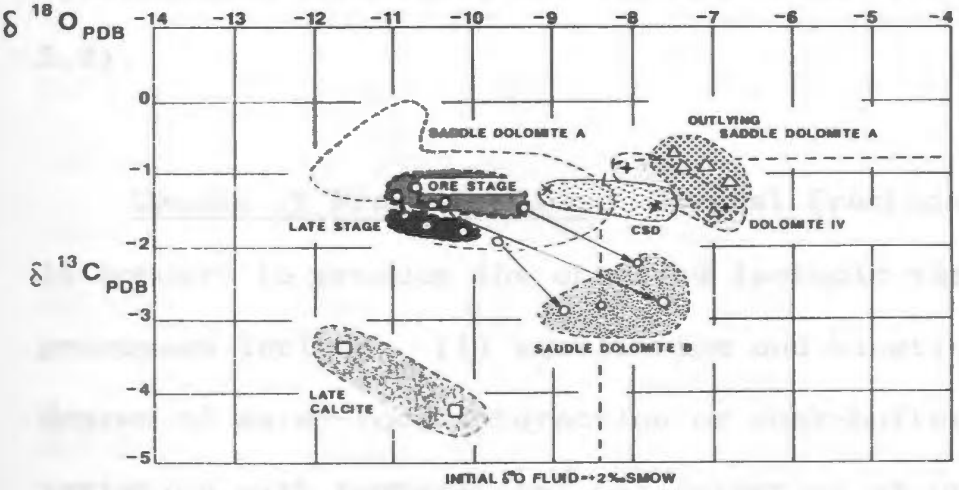

- ○ SADDLE DOLOMITE IN MINE WORKINGS
- △ SADDLE DOLOMITE OUTSIDE MINE WORKINGS IN TABLE HEAD Gp, AGUATHUNA Fm. AND FINE ROCK MATRIX BRECCIAS
- X COARSE SPARRY DOLOMITE = CSD
- □ LATE CALCITE CEMENT

CURVES OF VARYING WATER/ROCK RATIOS

C. FAULT-RELATED, POST-UPLIFT DOLOMITES

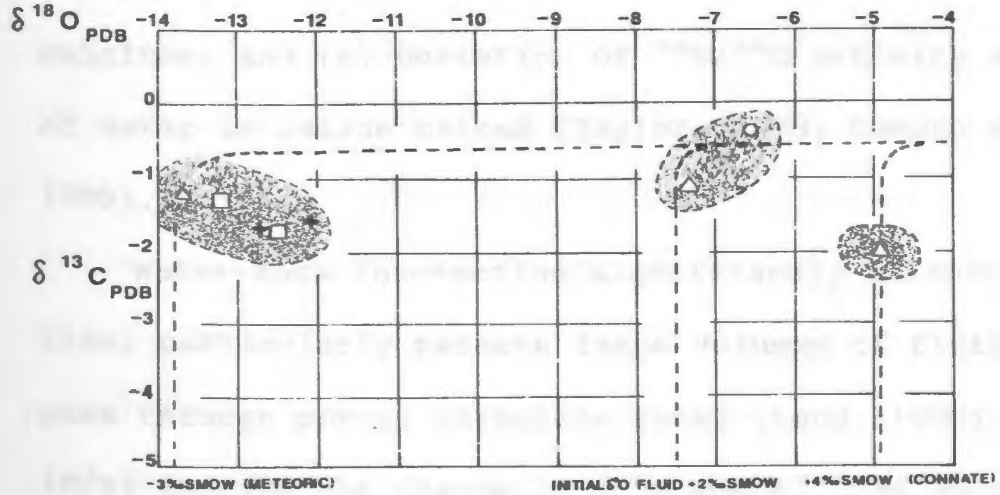

- △ CATOCHE Fm. COARSE SPARRY DOLOMITE (CORON, 1982)
- \+ REGIONAL CATOCHE Fm. COARSE SPARRY DOLOMITE (HAYWICK, 1985)
- □ CATOCHE Fm. LATE CALCITE (CORON, 1982)
- ○ TABLE HEAD Gp FINE-MEDIUM DOLOMITE (CORON, 1982)

$\delta^{18}O$ similar to late saddle dolomites, whereas Dolomites III and IV are not. (2) Samples of Dolomite III in the Boat Harbour Formation are depleted in $\delta^{13}C$. (3) Some saddle dolomites and late fault-related dolomites are neither depleted in $\delta^{18}O$ or $\delta^{13}C$. Other dolostones, identified as Dolomite VII, demonstrate a wide range of $\delta^{18}O$ values. It is necessary, therefore, to examine separately the data of each diagenetic stage. Isotopic evolution is thus described and analyzed with respect to four separate dolomitizing systems: (1) syngenetic; (2) diagenetic mottle dolomites and zoned cements; (3) epigenetic tectono-hydrothermal dolomites; and (4) late fault-related dolomitization (Fig. 5.8).

Causes of Fractionation - Several fractionation mechanisms operated in concert to produce the observed isotopic variations. Possible processes include: (1) equilibrium and kinetic fractionation; (2) degree of water-rock interaction or rock-buffering of fluids; (3) variation with temperature; (4) oxidation of organic or inorganic carbon; (5) difference of $\delta^{18}O$ fractionation in dolomites compared to calcites; and (6) deviation of $^{18}O/^{16}O$ activity ratio from atomic ratio of water in saline brines (Taylor, 1979; Ohmoto and Rye, 1979; Hoefs, 1980).

Water-rock interaction significantly affects isotopic fractionation, particularly because large volumes of fluid characteristically pass through porous carbonate rocks (Land, 1980). Water-rock ratios (W/R) express the change in $\delta^{18}O$ and $\delta^{13}C$ as increments of water in an ideal closed system pass through an aquifer and are represented by the

equation:
$$W/R = \log_{\Delta} \frac{(\delta^{initial}_{fluid} + \Delta - \delta^{initial}_{rock})}{(\delta^{initial}_{fluid} - \delta^{final}_{rock} + \Delta)}$$

where the temperature dependent equilibrium constant (Δ)

$$= \delta^{final}_{rock} - \delta^{final}_{fluid} \quad \text{and } \delta^{final}_{fluid}$$

is determined by isotopic equilibration with the rocks at a given temperature (Taylor, 1977). Due to the abundance of oxygen in water compared to carbon (89% to 0.0019%), carbonate rock $\delta^{18}O$ equilibrates rapidly with water, but large amounts of water need to react with rock to effect a change in $\delta^{13}C$. In terms of rock/water ratios, the molar abundance of oxygen in $CaCO_3$ is 1.474 times that of water and carbon in $CaCO_3$ is 1.7×10^7 greater than carbon in water. Rock carbon, thus, dominates equilibrated fluid carbon, and rock oxygen is important but not dominant (Meyers and Lohmann, 1985).

Water-rock ratio calculations plotted on $\delta^{18}O$ vs. $\delta^{13}C$ graphs describe inverted L-shaped curves. A series of model curves have been calculated for constant $\delta^{initial}_{rock}$ (-4.5 o/oo PDB $\delta^{18}O$, -1 o/oo $\delta^{13}C$) and temperature (100°C) and variable $\delta^{18}O^{initial}_{fluid}$ (Fig. 5.9). Fluids with an initial $\delta^{18}O$ of 2 to 3 o/oo SMOW would equilibrate with dolostones at values comparable to St. George rocks. Other curves have been calculated for variable temperature and constant initial fluid isotope values (Fig. 5.9). Water-rock ratios are employed to explain similar inverted L-shaped curves for data sets of carbonate rock $\delta^{18}O$, $\delta^{13}C$ in the Upper Mississippi Valley Lead-Zinc District (Sverjensky, 1981).

Progressive depletion of $\delta^{13}C$ can be explained in other ways. In

Figure 5.9 Calculated curves for varying water/rock ratios according to (A) variable $\delta^{18}O$ of the initial fluid and (B) variable fluid temperature

(A) Curves of $\delta^{13}C$ vs. $\delta^{18}O$ for varying water-rock ratios are plotted for interaction between an initial dolomite of -4.5 o/oo $\delta^{18}O$ and various fluids of initial isotopic compositions ranging from -2 o/oo to 4 o/oo $\delta^{18}O$. In all cases the fluid temperature is 100°C. Note that hypersaline brines (3 o/oo $\delta^{18}O$) equilibrate with the rocks at -7.5 o/oo, similar to the standard composition of St. George dolostones.

(B) Curves of $\delta^{13}C$ vs. $\delta^{18}O$ for varying water-rock ratios are plotted for interaction between an initial dolomite of -4.5 o/oo $\delta^{18}O$ and an initial fluid at SMOW. The two scenarios are different temperatures of 75°C and 100°C. Note that a 25°C change in fluid temperature causes a 3 o/oo shift in $\delta^{18}O$ values, similar to the difference between ore-stage dolomites and others.

WATER/ROCK RATIO CURVES

FOR VARIABLE INITIAL FLUID $\delta^{18}O$ AND FLUID TEMPERATURE

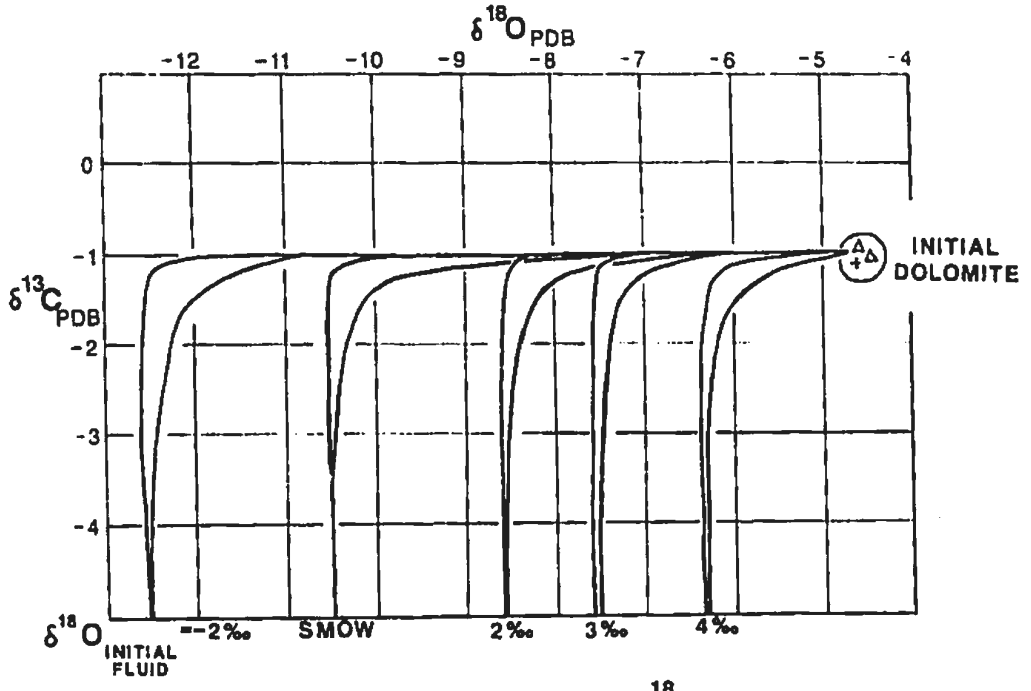

A. VARIABLE INITIAL FLUID $\delta^{18}O$

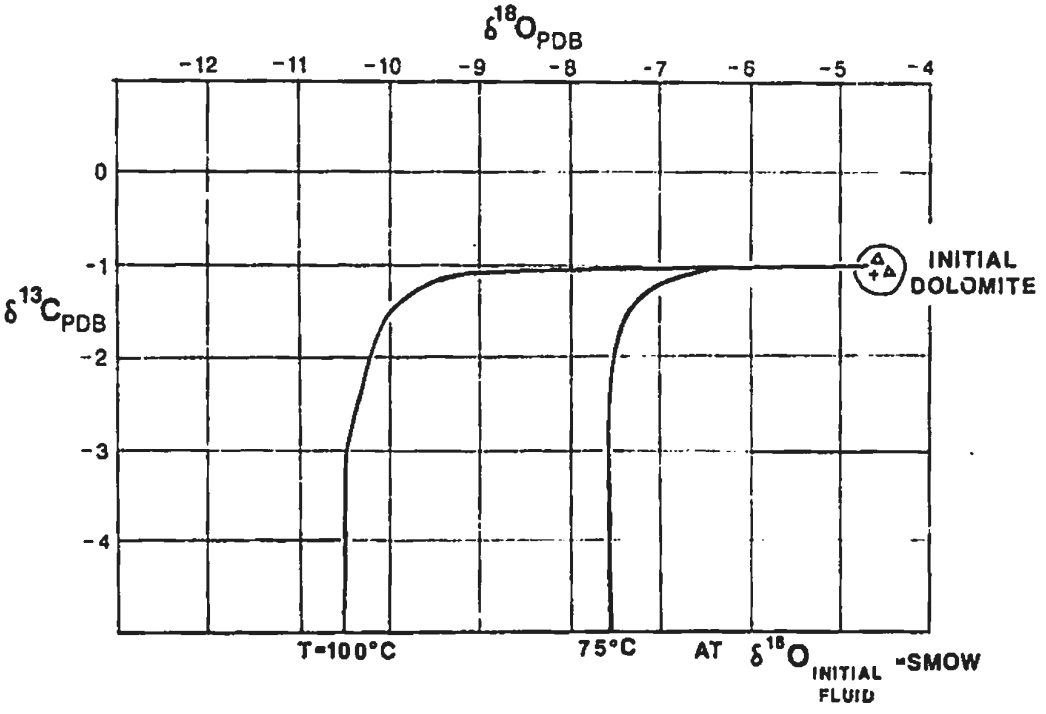

B. VARIABLE FLUID TEMPERATURE

an open, fluid-dominated system progressive cementation of pores leads to decreased wall rock interaction and increasing fluid signature in the $\delta^{13}C$ of the cement (cf. Meyers and Lohmann, 1985). The $\delta^{13}C$ of the the fluid, also, can be progressively depleted as CO_2/CH_4 ratios increase during oxidation of inorganic or organic carbons in either meteoric waters or subsurface hydrocarbons (Ohmoto and Rye, 1979).

Syngenetic Dolomitization - Both microcrystalline dolostones of the Aguathuna and Catoche Formations contain enriched -4.5 o/oo $\delta^{18}O$ PDB relative to contemporaneous lime mudstone and wackestone (-8 o/oo $\delta^{18}O$ PDB). The $\delta^{18}O$ enrichment can be attributed to two among several possible mechanisms: (1) 3 to 4 o/oo fractionation in contemporary dolomites; or (2) enrichment of $\delta^{18}O$ in near surface pore fluids through evaporation.

Diagenetic Dolomitization - Dolomite II varies broadly from moderate to depleted $\delta^{18}O$ and has invariant $\delta^{13}C$ (Haywick, 1984). Mottles of crystals with undepleted $\delta^{18}O$ probably originated early in comparison to typical composite crystals. Depletion of $\delta^{18}O$ values in composite crystals possibly reflects the equilibration between subsurface fluids and the host carbonates. The variable $\delta^{18}O$ values can be explained several ways: (1) by the amount of water-rock reaction or (2) by changing fluid composition via meteoric mixing or increasing salinity with depth. Fluid inclusions from equant calcite cements imply that pore fluids during early burial became saline (20 equivalent weight % NaCl) and warm (100°C). According to water-rock ratio calculations,

saline pore fluids at 100°C and initial $\delta^{18}O$ of SMOW to +2 o/oo SMOW could react with dolomites of initial $\delta^{18}O$ of -4.5 o/oo PDB to form crystals composed of $\delta^{18}O$ -8 to -10 o/oo PDB (Fig.5.8).

The few known $\delta^{18}O$ isotopic values of brightly zoned crystals of Dolomite III cement are not depleted (-6.5 to -7 o/oo PDB). Halite inclusions imply that saline fluids were supersaturated with respect to NaCl. Water-rock ratio calculations for equilibration with saline fluids with initial $\delta^{18}O$ of +4 SMOW and 75°C to 100°C reproduce a similar range of $\delta^{18}O$ values for cement crystals. Cements with depleted $\delta^{13}C$ (-2.7 to -4 o/oo) probably precipitated from extraformational fluids which possessed high water-rock ratios and experienced minor wall rock interaction.

Epigenetic "Tectono-Hydrothermal" Dolomites - Replacement Dolomite V and early Saddle Dolomite A cement display $\delta^{18}O$ depletion and late Saddle Dolomites A and B are progressively enriched in $\delta^{18}O$ and depleted in $\delta^{13}C$. Populations of early saddle dolomite have widely variable $\delta^{18}O$, e.g. -7 o/oo, -8.5 o/oo, -9 to -10 o/oo and -11 o/oo PDB. Ambient fluids, as preserved in fluid inclusions, homogenize at 90°C to 140°C and are hypersaline (25 equivalent weight % NaCl). Late non-luminescent calcites, depleted in both $\delta^{18}O$ and $\delta^{13}C$, are precipitates of different highly saline (greater than 25 equivalent weight % NaCl), "cool" (50° to 70°C) fluids. Sverjensky (1981) has explained a similar isotopic trend and paragenetic sequence from the Upper Mississippi Valley District by increased water-rock ratios.

Water-rock ratio calculations for initial water $\delta^{18}O$ of SMOW or +2

o/oo SMOW and an initial dolomite $\delta^{18}O$ of -4.5 o/oo PDB generates final rock $\delta^{18}O$ between -9 and -11 o/oo PDB. The isotopic data for epigenetic dolomites suggest that this model is too simple for several reasons. (1) Detailed paragenetic sample suites of saddle dolomite cements demonstrate progressive enrichment of $\delta^{18}O$ and depletion of $\delta^{13}C$ (Fig. 5.9). This trend is not predicted by W/R calculations for a single fluid in a closed system. Cooling or different fluid types could have generated these changes. Calculations show that a 25°C fluid temperature variation can effect a 3 per mil change in $\delta^{18}O$. Existence of several $\delta^{18}O$ populations of Dolomite V and varied fluid inclusion compositions of Dolomite V support the probability of several fluid types. Thermal changes are supported by fluid inclusion data.

(2) Water-rock ratio relationships assume change in rock isotopic composition according to the volume of fluid with which it has interacted. Although the wall rock was exposed to greater fluid volume through time, saddle dolomite and calcite cements rather represent incremental samples of changing pore fluids which probably experienced decreasing interaction with the host rocks. Fluid inclusions and trace elements demonstrate the dynamic change in fluid chemistry.

(3) The depletion of $\delta^{13}C$ correlates with the saddle dolomite cement sequence. Progressive cementation probably restricted interaction between the fluid and the original dolostone. The cement as a result crystallized in equilibrium with a light carbon fluid and not the original dolostone. The light carbon is attributed to the production of CO_2 either by oxidation of hydrocarbons or reduction of sulphates, both known to exist.

Post-tectonic fault-related dolomitization - Fault-related dolomites which replaced limestones have varied $\delta^{18}O$ isotopic compositions between -4 and -11 o/oo PDB and minor $\delta^{13}C$ depletion (data from Coron, 1982). The limited data on these dolomites suggests that different fluids with varying proportions of meteoric water and connate brine could have mixed along fault aquifers and crystallized dolomites with different $\delta^{18}O$ compositions. Models of water-rock reaction between a constant carbonate rock type and varible initial fluid $\delta^{18}O$ demonstrate that meteoric type fluids depleted in $\delta^{18}O$ (-2 o/oo SMOW) generate depleted $\delta^{18}O$ (-11 o/oo PDB) in dolomite crystals at equilibrium. In contrast, an initial formational or oil field brine enriched in $\delta^{18}O$ (+4 o/oo SMOW) would have dolomitized carbonates at an equilibrium of -6 to -7 o/oo PDB $\delta^{18}O$. Alternatively, the data set can be viewed as a broad field between -4 and -11 o/oo PDB $\delta^{18}O$ rather than separate populations. In a singular environment undepleted values would represent dolomitization from limited water-rock interaction with meteoric enriched waters. Depleted dolostones crystallized along major faults which were conduits for large volumes of water over an extended time period. Lack of $\delta^{13}C$ depletion and the replacement nature of crystallization implies that fluids completely interacted with the precursor carbonate and equilibrated with the rock carbon.

5.13 Implications of Trace Element Geochemistry and Cathodoluminescence

Introduction - Concentrations of minor and trace elements in the upper St. George Group at Daniel's Harbour are very low. This improverishment relates to the consistently good stoichiometric structure with 49 to 51 mole % $CaCO_3$. Trace element concentrations in crystals are commonly at or below the detection limits of the microprobe. Locally, FeO and Na_2O abundance rises to 0.20 to 0.55%. Sr is undetected. Variations in FeO and MnO from 0.04% to 0.15% are considered significant on the basis of correlation with luminescent zones. Whole rock atomic absorption analyses of total FeO, which range from 0.20 to 0.93%, include matrix plus crystal iron.

Strontium Depletion - Variation in strontium concentration is a potentially useful indicator of changes in fluid chemistry and the crystallization process (e.g. Land, 1980; Veizer, 1983). Characteristically, late dolomites are depleted relative to early dolostones (e.g. Veizer and Demovic, 1978; Veizer, 1978). In the St. George Group dololaminites and mottle dolostones containing Dolomites I, II and III have moderate 135 ±60 ppm abundances of Sr^{++} compared to saddle dolomites and coarse sparry dolomites of Dolomite V with 66 ppm ±35 ppm Sr (Haywick, 1984).

Several processes or environmental changes have been proposed to account for this depletion. (1) Early dissolution of aragonite could increase Sr^{++} in initial dolomitizing fluids. Many mottle dolomites,

however, crystallized at depth long after near surface aragonite dissolution (Haywick, 1984). (2) Pure meteoric fluids have small Sr/Ca ratios relative to early fluids with >5% sea water. Reaction with meteoric water, thus, could reduce Sr content. Most connate fluids and oil field brines, however, have elevated Sr/Ca (e.g. White, 1963). Hypersaline fluid inclusions with $CaCl_2$ suggest that Sr'' probably was abundant in dolomitizing waters. (3) Perfect stoichiometry could have prevented trace element substitution. Sr-depleted saddle dolomites in most of the St. George Group in other regions are, however, non-stoichiometric (55 mole % Ca) (Haywick, 1984). (4) Depletion of both near surface and deep subsurface limestones and dolostones by recrystallization in Sr-rich waters requires very low distribution coefficients for Sr (D^{Sr}) on the order of 10^{-4} (Land, 1980). Differences in rate and/or style of dolomitization may have controlled D^{Sr}. Mottle dolomites (II) and zoned dolomites (III) crystallized slowly and replaced limestone along stylolites with moderate D^{Sr}. Late pervasive and rapid (?) dolomitization of precursor dolomites and limestones occurred at a possible low D^{Sr}. (5) Mattes and Mountjoy (1980) calculated that dolomites incorporate low Sr concentrations when they replace limestones under equilibrium conditions. Replacement does not, however, explain the composition of saddle dolomite cements.

Fe/Mn Ratios and Cathodoluminescence - Elevated concentrations of manganese and low Fe''/Mn'' ratios correlate with luminescent zones and phases. Other minor elements (e.g. Pb'', REE's, Zn'', Ni'') of unknown concentration could contribute as activators, sensitizers or quenchers

(Machel, 1986). In multiple zoned dolomites 1100 to 1700 ppm Mn and Fe''/Mn'' ratios of 0.05 to 0.8 (from microprobe data) correlate with bright CL bands (Fig. 5.4). Bright red CL Saddle Dolomite B similarly contains twice the Mn of Saddle Dolomite A (600 ppm compared with 250 ppm) and possess lower Fe''/Mn'' ratios, 0.75 compared to 1.5. Correlations and assumptions about physical-chemical conditions on the basis of luminescence and limited geochemistry must be made with caution (Machel, 1986). Machel has emphasized that besides standard Eh and pH interpretations, luminescence is affected by trace element partitioning, organic and clay diagenesis and variations in trace element supply in dolomitizing fluids.

The dolomite stratigraphy at Daniel's Harbour is characterized by four CL crystal types: (1) fine dull CL (I); (2) blue-zoned and replaced rhombs (II); (3) bright multiple zoned cement (III); and (4) uniform bright to dull red replacement dolomite and cement (IV through VII). The transition from dull to bright zoned cements is comparable to burial trends elsewhere (cf. Frank et al., 1982; Grover and Read, 1983). A change from oxidized to reduced waters would allow incorporation of the reduced divalent species of Mn into dolomite (Frank et al., 1982). Multiple zones and coarse pore-filling crystals suggest slow crystallization from a long resident fluid which underwent fluctuations in Eh. Earlier dull CL dolomites (I and II) may have crystallized from oxidized waters. Dolomite II replaced limestones and nucleated on layers of insoluble material in contrast to cements of later Dolomite III. Pores, which Dolomite III slowly cemented, may have been a reduced setting. Uniformly bright to dull red luminescence characterizes both fine to

medium neomorphic crystals and coarse cement crystals of the epigenetic dolomites. Rapid, pervasive crystallization, similar to early dolomites, could account for uniform luminescence. Manganese activation and moderate iron quenching produce the prominent red spectrum. Both elements are present and manganese enrichment is identified in Saddle Dolomite B. Dull red CL Dolomite V, pervasive after sulphides, may be environmentally significant. Slightly oxidized fluids could have limited manganese substitution.

Ferroan Dolomite - Ferroan dolomites, revealed by potassium ferricyanide stain, are distributed locally within several dolomite phases. Among Dolomite III types ferroan dolomite (2000 to 5000 ppm Fe) cements intercrystalline areas of Aguathuna dololaminites, and syntaxial overgrowths of luminescent calcareous nuclei in fine rock matrix breccias and stylo-mottles of the lower Catoche Formation. The cause of the cement in the Aguathuna Formation is unknown. Dolomitization around calcite nuclei appears to have created a microenvironment for Fe'' substitution in the crystallization of the rim dolomites. If precipitation were governed by bulk solution disequilibrium (Veizer, 1983), the chemical composition would be controlled by thin reaction rims around crystals. Changes in concentration of Fe'' could have been affected by rapid precipitation around nuclei (e.g. Lorens, 1981) or elevated oxidation potential around crystallization centres. The iron-rich residues of the breccias and stylolites provided local surplus of Fe''.

In epigenetic dolostones, especially Dolomite V, deep discordant dolostones and outer coarse sparry dolostones are anomalously ferroan

(1000 to 5000 ppm). Both Saddle Dolomites A and B contain above average concentrations of Fe^{++} (600 to 3000 ppm). The increase in iron concentration away from centres of dolostone bodies could be related to several variables: (1) decrease in temperature; (2) oxidation; (3) change in water chemistry; and (4) rate of precipitation and diffusion across crystal surfaces (Veizer, 1983).

5.14 Summary of Dolomite Crystal Types and their Evolution

Seven generations of dolomites are distinguished from differences in crystal texture and chemistry. Varieties of crystal textures include: (1) microcrystalline texture; (2) very fine to medium euhedral rhombs which replace limestones and nucleate around peloids; (3) neomorphic dolomites with syntaxial overgrowths and intergrown, xenotopic contacts; (4) blocky cements; and (5) saddle dolomites. Important geochemical variables include: (1) Fe^{++} and Mn^{++} concentration which respectively quench and activate cathodoluminescence; (2) crystal $\delta^{18}O$ which traces the fluid source, water/rock equilibrium and temperature of crystallization; and (3) Sr^{++} concentration which is progressively depleted in late dolomites.

Dolomite I - Microcrystalline Aguathuna dololaminites and very fine crystalline Catoche dolostones are distinctively enriched in $\delta^{18}O$, -4 to -7 o/oo PDB, and Sr, 85 to 240 ppm. Microcrystals which originated from microdolomite or fine mud nucleii compare with "syngenetic" types described elsewhere (Matter, 1967; Behrens and Land, 1972). Fine

equigranular crystals, which replace Catoche mudstones, are texturally indistinguishable from Dolomite II crystals. Field and petrographic relationships imply early dolomitization prior to the formation of the St. George unconformity and contemporaneous fine rock matrix breccias.

Dolomite II - Very fine to fine crystals pervasively alter former burrowed mudstones and wackestones to fine sucrosic dolostones and medium rhombs replace micrite-microspar mottles in limestone. Ubiquitous dolostone mottles and some extensive dolostone beds resulted. The purplish to blue cathodoluminescence is slightly brighter than non-luminescent Dolomite I crystals. Most dolomites post-date Dolomite I because: (1) crystals replace diagenetic microspar calcite, and (2) many crystals have grown near or within stylolites. Pressure solution features developed at a minimum depth of 300 to 1000 metres. Stylolite-related dolomites imply dolomitization by one or more processes: (1) crystallization during chemical compaction; (2) fluid movement along stylolites; and (3) preferred crystallization around organic carbon and other stylolite residues. Common replacement and corrosion textures signify that crystals nucleated in the shallow subsurface and became metastable at depth. Differences between Daniel's Harbour blue CL dolomites and Port au Port finely zoned bright CL crystals implies local variations in water chemistry or time of crystallization.

Isotopic signature differs from Dolomite I and III. Widely variant $\delta^{18}O$ between -5 and -10 o/oo PDB probably relates to long term crystallization from fluids of different $\delta^{18}O$ composition and equilibration of original sea water pore fluids with the rock. Samples with enriched

$\delta^{18}O$ and Sr are comparable to Dolomite I and probably crystallized early during diagenesis. Rare petrographic features support this conclusion. For example, calcite cements which pre-date pressure solution truncate some early Dolomite II crystals (Haywick, 1984).

Dolomite III - Fracturing and solution produced a permeable network of fractures and solution and intercrystalline pores which was cemented by minor amounts Dolomite III. In particular, fracturing along the faulted margins of fine rock matrix breccias generated local concentrations of fracture pores. Dolomite III pervasively crystallized in the porous breccias surrounding these fractures. These zoned dolomites also precipitated ubiquitously in stratigraphic dolostones and along stylolites in limestones where very fine to medium-sized, blocky, finely zoned crystals cemented pores, and thin syntaxial overgrowths partially replaced Dolomite II rhombs. Medium-sized crystals selectively replaced equant calcites in burrow cores and fractures. Dolomite III was subsequently stable and resistent to dissolution during stages of late dolomitization. Although a minor constituent, Dolomite III cements are a paragenetic marker of subsurface dissolution, fracturing and change in pore fluid chemistry.

The numerous thin cement layers precipitated over a long period of fluctuating pore fluid chemistry. Reducing pore waters contributed to Mn^{++} concentration in bright cements. Formational brines saturated with salt and enriched $\delta^{18}O$ (+4 o/oo SMOW) probably account for the undepleted crystal $\delta^{18}O$ (-6 to -7 o/oo PDB). Light carbon cements precipitated in equilibrium with the fluid.

Dolomite IV - Upper Catoche coarse dolostone complexes crystallized during several successive generations of tectonic fracture and fluid migration (Chapter 9). In the first of three phases of dolomitization, medium neomorphic crystals and intercrystalline cements of red CL Dolomite IV crystallized locally in grainstones, burrowed wackestones, some Aguathuna breccia horizons, and extensive portions of deep discordant dolostones. Crystals commonly replaced earlier dolomites. Although only relict patches of Dolomite IV remain in pseudobreccias, Dolomite IV's ubiquitous distribution in gray dolostones suggests that most of the coarse dolostone complexes were dolomitized during this phase and later were extensively replaced by Dolomite V. Intermediate crystal $\delta^{18}O$ of -7.5 to -8.5 o/oo PDB implies that Dolomite IV crystallized from formational brines in equilibrium with the host carbonate rock. Xenotopic textures suggest that these were hydrothermal dolomites.

Dolomite V - Faults, fractures and solution by fluids along these fractured paths collectively created extensive porosity in the Upper Catoche Formation subsequent to crystallization of Dolomite IV. Multiple layers of sulphides partially cement these secondary pores and replace dolostones. Several generations of fractures interrupt and post-date sulphide precipitation. (Details of this geology are described in Part V.) Dolomite V, the dominant epigenetic dolomite, extensively cements mesopores and replaces precursor dolostones and limestones. Coarse to megacrystalline idiotopic saddle dolomites cement pores. Xenotopic replacement crystals grade between fine to medium dolomites

with plane extinction to medium and coarse saddle dolomites with undulose extinction. Euhedral rhombs of replacement saddle dolomite embedded in residues replace geopetal muds at the base of former pores. Coarse sparry dolostones replace limestones at the periphery of coarse dolostone complexes. Within these latter dolostones fine mottle dolomite crystals are neomorphosed and intermottle limestones are replaced by equigranular fine to coarse saddle dolomites which have nucleated around very fine peloids. In replacement dolostones uniform luminescence and masses of fine nucleated crystals imply relatively rapid dolomitization. Coarse zoned pore cements on the other hand, appear to have crystallized gradually.

Fluid-rock equilibrium at elevated temperatures produced depleted crystal $\delta^{18}O$ of -9 to -11 o/oo PDB. Variable temperatures and fluid compositions may have generated crystals of varying $\delta^{18}O$ composition, between -6.5 and -11 o/oo PDB. Late cements were enriched one per mil during late stage cooling. Cements isolated the fluid from interaction with the precursor dolostone such that latest crystals with depleted $\delta^{13}C$ were in equilibrium with light fluid carbon. Sr, 40 to 70 ppm, was depleted by (1) partitioning during neomorphism of dolomite and (2) cycling and equilibration of fluids within the sedimentary pile. Low Sr content may have resulted from a low D^{Sr} during pervasive and rapid crystallization.

Dolomite VI - Megacrystalline Dolomite VI locally cemented meso- and megapores and formed ubiquitous thin overgrowths after late fracturing and brecciation of veins and dolostones. The combined influence of

increased fluid-rock reaction, cooling, long fluid residence in pores, progressive cementation and change in fluid source, helped to enrich crystal $\delta^{18}O$ and deplete crystal $\delta^{13}C$. In particular, the cooling of formational fluids was a major contributor to $\delta^{18}O$ enrichment and, as cementation limited host rock-fluid interaction late crystals took on the light carbon signature of the fluids. Reducing conditions, which developed during isolation and decreased rates of water flow, led to Mn^{++} substitution in the bright CL dolomites. Further fluid cooling, salinity increase and oxidation led to the crystallization of late calcites and sulphates.

Dolomite VII - During and subsequent to late regional faulting and displacement, fine to medium crystalline Dolomite VII replaced limestones peripheral to late regional faults. Euhedral crystals nucleated on fine peloids and left intercrystalline porosity. Solution along stylolites and calcite spar left distinctive mesopores which were partially cemented by saddle dolomite and late luminescent calcite. Variable sources of pore fluids from connate brines to meteoric waters produced widely variant crystal $\delta^{18}O$ of -4 to -13 o/oo PDB.

CHAPTER 6 SULPHIDE AND LATE SULPHATE PARAGENESIS

6.1 Introduction

Sulphides were precipitated with epigenetic dolomites. Ore stage sulphides partially cement veins and pores which cut dolostones of Dolomite IV and they predate Saddle Dolomite A (Pl. 6.1a,g). The ore stage thus represents only a small portion of the paragenetic sequence dicussed in Chapter 5. Six discernible crystal types are stratified as multilayered millimetre thick cements and composite crystal clusters in a variety of pore types, e.g. veins, cavities and vugs. Veins and former large pores preserve the most complete stratigraphy of these crystal types. Two groups of early and late sulphides are separated by a significant phase of fracturing and brecciation. Two younger crystal types, galena and euhedral red sphalerite crystals post-date saddle dolomite cements (Table 6.1, Fig. 6.1).

Crystal types are distinguished by colours: red, tan, brown, yellow, yellow-brown to ochre, and yellow crystals with black patches. Each crystal type possesses a distinctive combination of crystal habit, trace element and sulphur isotope composition and fluid inclusion homogenization temperatures (Fig. 6.1). Table 6.1 outlines these aspects for nine crystal types. Discussion of each crystal type in the following sections is divided into petrography and distribution, geochemistry, fluid inclusions, evidence of timing and interpretation. General discussions at the end of the chapter cover topics of fluid

Plate 6.1 Colour Phases of Sphalerite

a. Colloform early sphalerites line the walls of a vein form the L Zone which is occluded by Saddle Dolomites A (gray) and B (white). The earliest sulphides are layers of pyrite and yellow sphalerite followed by red-brown to tan-brown fibrous sphalerite and prismatic, yellow crystals with layers of brown crystallites. Saddle Dolomite B cements a breccia of earlier dolomites and sphalerites. Scale in millimetres.

b. The core of a crystal rosette contains pleochroic brown sector zones typical of tan-brown sphalerite. Pl. 6.2a presents a larger scale perspective. Sample from the K Zone. 1 mm scale.

c. Pleochroic sector zones commonly occur in layers, relics of early crystallites that are now incorporated by coarse, elongate crystals. A close-up of thin bands in yellow sphalerite in Pl. 6.1a. 1 mm scale.

d. Cross-hatched twinning (gray) in early fibrous sphalerites (under polarized transmitted light) overprints fibrous pleochroic inclusions (red-brown). Quartz (white) occurs between dendrites. 100 μm scale.

e. Late yellow-brown sphalerites replace dolostones (brown) and are overgrown by coarse, prismatic cements of yellow-black sphalerites with black sector zones. Zoned Saddle Dolomite A cements over the sphalerite and is followed by Saddle Dolomite B which cements a breccia of yellow-

PLATE 6.1

black sphalerite and Saddle Dolomite A. Sample from DDH 640 of the Long Hole Stope of the central L Zone (Location in Figs. 1.4, 10.2 and 12.5). Scale in millimetres.

f. Breccia blocks of early massive, tan-brown sphalerite (1) are rimmed by late yellow-brown sphalerite (2), all of which is fractured, dilated and cemented by saddle dolomite. An underground wall in the east end of the T Zone (location in Figs. 1.4 and 10.1). Scale in tenths of feet.

g. Late sphalerites form "snow-on-the-roof" deposits on the bases of subhorizontal veins. Crystal rosettes at the top are probably breccia fragments with overgrowths (similar to Pl. 6.1e,h). An underground wall from the southern drift of the west L Zone. Red knife measures 8 cm.

h. Faceted, blue-white CL and bold, non-luminescent sphalerite overgrows a sphalerite fragment surrounded by Saddle Dolomite B cement which luminesces red. This dolomite fills small solution pores in the older generation of sphalerite. Cathodoluminescence photomicrograph of a sphalerite fragment in Pl. 6.1a. 250 μm scale.

TABLE 6.1 SULPHIDE CRYSTAL TYPES

SUBSTAGE	CRYSTAL TYPE OR EVENTS	CRYSTAL HABIT	TRACE ELEMENT (minimum to maximum)	$\delta^{34}S$ (minimum to maximum)	TH OF TPFI
PRE SADDLE DOLOMITE					
EARLY SULPHIDES					
1.	Early Pyrite	Fine Framboidal	—	23.4, 23.7o/oo	—
2.	Early Red ZnS	Microcrystalline, Dendritic, Fibrous	Fe (1-5%) TrCu, Ag	25, 27.4o/oo	—
3.	Early Tan-brown ZnS	Fine Fibrous, Rosettes	Fe (0.5-2%)	27, 28o/oo	125° to 155°C 144° C mode
4.	Dissolution				
5.	Early Yellow ZnS	Medium-Coarse Prismatic	Fe (0.2-1.5%) Cd	20.5, 25o/oo	95° to 185°C 175°C mode
6.	Major Fracturing		(0.2-0.35%)		
LATE SULPHIDES					
7.	Late Yellow-brown ZnS ZnS	Medium-Coarse Equant	Fe (0.5-2.5%) (0.5-2.5%) Cd (0.2-0.6%)	19.9, 14.5o/oo	125° to 170°C 135°C mode
8.	Late Yellow-black ZnS	Medium-Coarse Prismatic	Fe (0.15-0.6%) Cd (0.4-0.6%) Cu (0.1-0.3%)	18.4,22.4o/oo	90° to 168°C 115°C mode
9.	Luminescent Zns Overgrowths				
POST-SADDLE DOLOMITE					
10.	Galena	Coarse Equant	—	15,22o/oo	—
11.	Late Red Zns	Euhedral Crystals in vugs	Cd (0.4-0.6%) Cu (0.1-0.3%)	10.8,20.5o/oo	—
12.	Pyrite Marcasite	Cubes in vugs Coarse Needles in vugs			

Figure 6.1 Paragenesis of Epigenetic Sulphides, Dolomites and Calcite

A complete epigenetic sequence of pore cements is illustrated on the left. The cement stratigraphy of early and late sphalerites and Saddle Dolomites A and B correlates throughout the mine area. Important implications of this correlation are discussed in Chapters 12 and 14. Early and Late Sphalerites commonly occupy separate vein systems, however, and only locally overlap (illustrated in Fig.12.5).. Pl. 6.1a shows Early Sphalerites followed by Saddle Dolomites A and B. In Pls. 6.1e and 6.1g Late Sphalerites are succeeded by both saddle dolomites. The two sphalerite stages overlap in Pl. 6.1f.

Variations in geochemistry and homogenization temperatures of fluid inclusions are displayed on the right. $\delta^{34}S$ values of sulphides generally decrease through the paragenetic sequence. Iron is abundant in early sulphides in contrast to cadmium content which increases in late sphalerites. Iron increases in late saddle dolomites. Homogenization temperatures progressively decrease through the paragenetic sequence. Note that T_h modes of late sulphides and Saddle Dolomite A are similar.

PARAGENESIS OF EPIGENETIC SULPHIDES AND DOLOMITES

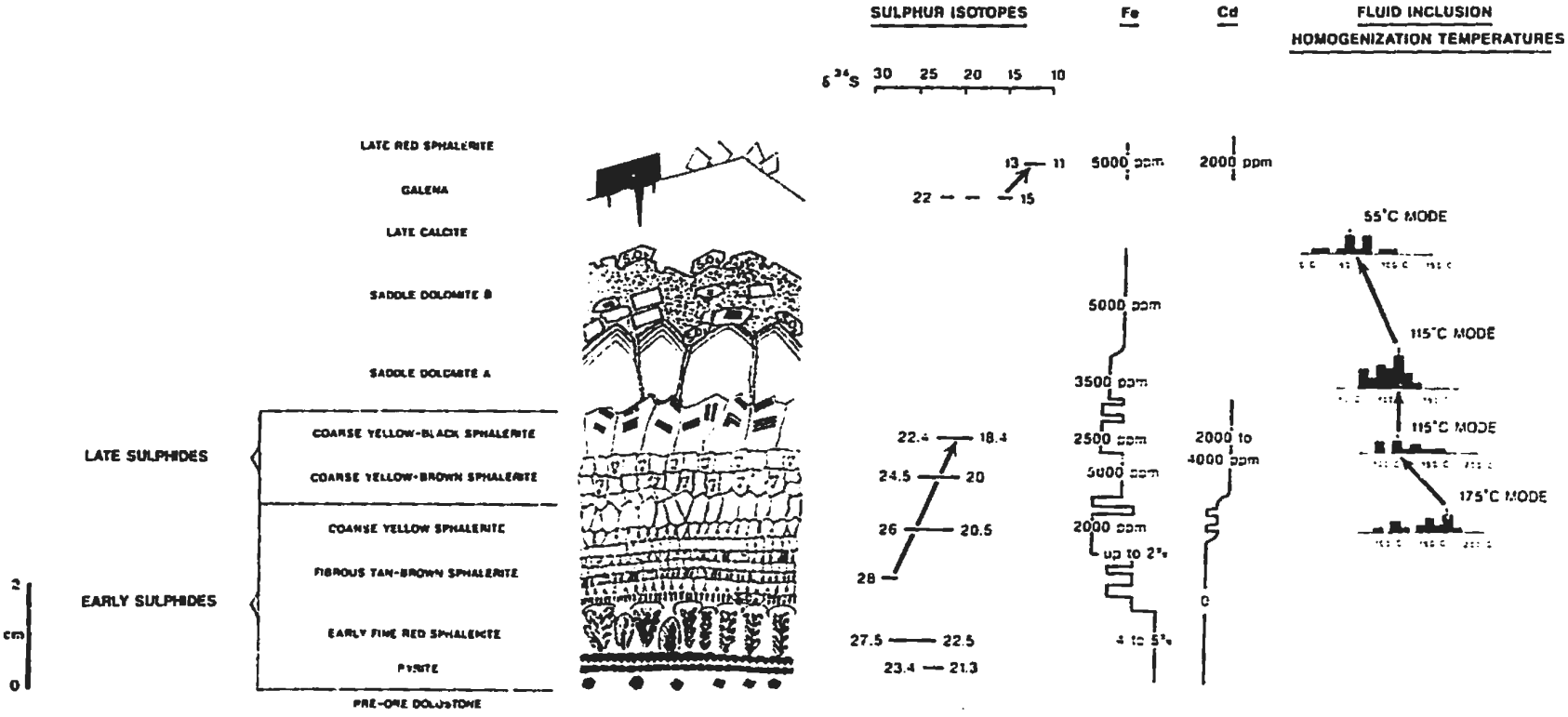

inclusions, sulphur and lead isotopes and an overview of the sulphide paragenesis. A description of the setting of the sulphides is developed in Part V and is based on the paragenetic relationships established in this and the previous chapter. Ore zones, referred to in the text, are located on the map of the mine area (Fig. 1.4).

6.2 Analytical Methods

Thin sections were finely and doubly polished with 0.001 mm grit to improve detail for examination under plane and polarized light. Abundance of Cd, Fe, Cu, Ag, Zn and S were examined on detailed traverses on the JEOL electron probe microanalyzer using the Magic Program for sulphide standards. No other significant elements were identified by multi-element ICP geochemical analyses and back-scatter EDAX on the scanning electron microscope. Twenty-two analyses of sulphur isotopes (Geochron Laboratories) checked eight sulphide phases and several sulphates. Microthermometric measurements of 160 two phase fluid inclusions were carried out on a Fluid Inc. Digital freezing and heating stage.

6.3 Early Pyrite

Petrography and Distribution - Very fine framboidal, or hexagonal, crystals of pyrite are disseminated in gray dolostone beds or mottles within pseudobreccia (Pl. 6.2c). Crystals commonly coalesce in mm-thick rims around pseudobreccia mottles (Pl. 6.2f). Outer crystals of these

Plate 6.2 Early Pyrite, Red and Tan-brown Sphalerites

a. Crystal rosettes of tan-brown sphalerite possess replacive cores with fibrous, pleochroic brown sector zones and outer rims of prismatic to equant yellow sphalerite. Sample from the K Zone. 5 mm scale.

b. Dendritic growths of early red sphalerite are overgrown by colloform fibrous tan-brown to prismatic yellow sphalerite. Sample from the H Zone. 5 mm scale.

c. Very fine, framboidal pyrites (gray) are disseminated in dolomite (black) and interlayered with sphalerite (white). This is a back scatter electron image from the SEM. Sample from the L Zone, same as Pl. 6.1a. 1 mm scale.

d. Fibrous crystals of tan-brown sphalerite. A reflected light view of an acid-etched polished surface. Sample from the L Zone, same as Pl. 6.1a. 250 μm scale.

e. A probable dissolution surface (arrow) between fibrous crystals in the lower right and later prismatic ones in the upper left. Sample from the L Zone, same image as in Pl. 6.2d. A reflected light view of an acid-etched surface. 1 mm scale.

f. Pyrite (black) occurs as thick layers on top of gray dolostone mottles (gray) and as disseminated crystals around the remaining edges. Saddle dolomite (white) occludes the pores. L Zone. 1 cm scale.

PLATE 6.2

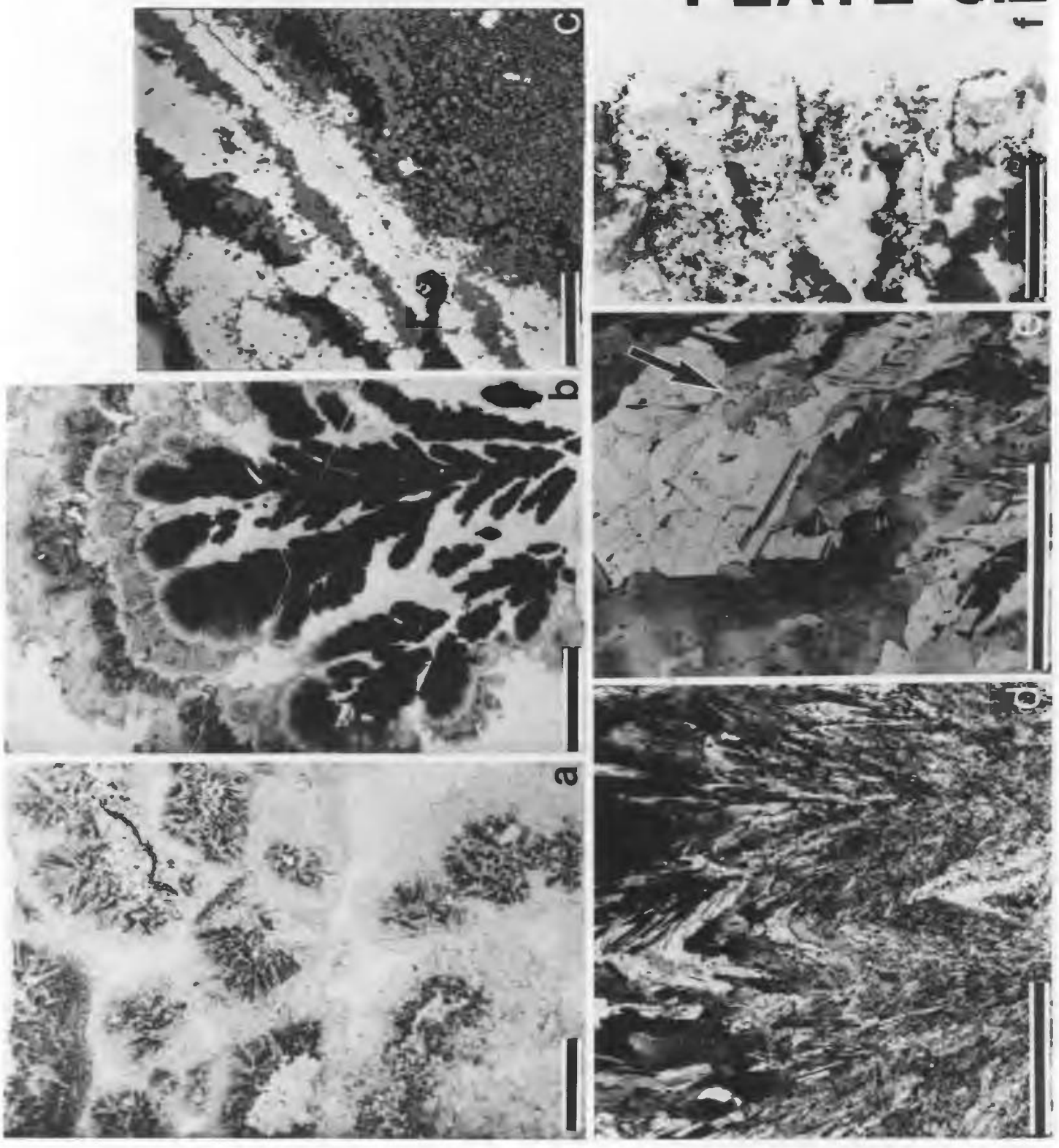

rims cement surfaces of vugs; the inner ones precipitate along intercrystalline pores and also replace dolomite. Pyrite and early sphalerites on top of dolostone fragments, mottles and the bases of horizontal veins grow in a pattern referred to as "snow-on-the-roof: (Oder and Hook, 1950) (Pl. 6.2f). Common disseminated crystals within dolostones fill intercrystalline pores and form poikilotopic inclusions within younger dolomite (V) (Pl. 6.2c).

Geochemistry - Positive $\delta^{34}S$ values of 23.4 to 23.7 o/oo are comparable to cogenetic early sphalerites with values ranging from 22 to 27.5 o/oo (Fig. 6.1, Appendix D). No other geochemical data have been collected from pyrites.

Evidence of Timing - Pyrite forms the first sulphide crystals along the edges of mesopores and is succeeded by a cement sequence of pale yellow, red, tan-brown and yellow sphalerite (Pl. 6.1a). Pale yellow sphalerite is commonly associated and intercalated with pyrite (Pl. 6.2c).

Interpretation - Very fine crystalline pyrite precipitated before most sphalerite. Pale yellow iron-poor sphalerites with similar $\delta^{34}S$ values (23 o/oo) precipitated after pyrite. Association of pyrite with gray dolostone mottles and beds implies that residues within the dolostones could have provided iron, sulphide nucleii or H_2S in reduction of sulphates by organic material.

6.4 Early Red Sphalerite

Petrography and Distribution - Microcrystalline to very fine fibrous red to black to gray-brown crystals occur in three habits: (1) nucleii of rosettes 1 cm in diameter; (2) linked crystals encircling dolostone mottles; and (3) inclusions and interstitial crystals within dolostones (Pls. 6.1b; 6.2a). Early red sphalerites typically surround dolostone mottles, partially replace dolomites and coalesce to form rosettes. Very fine fibrous crystals radiate 5 to 20 mm from cores of crystal rosettes as dendritic growths and are concentrically overgrown by mm to cm thick bands of fibrous tan-brown and prismatic yellow sphalerites (Pl. 6.2b). Under polarized light in doubly polished thin sections lamellar twinning is visible parallel to long crystal axes of the fibrous forms (Pl. 6.1d). This microstructure overprints fibrous to dendritic red brown to black pleochroic colouration, part of which comprises very fine micrometre-sized dark inclusions. Fine euhedral quartz crystals are included within and between sphalerites. Coarse galena commonly is associated with red sphalerite which it partially replaces. Red sphalerite forms massive beds in narrow erratic lenses in the upper parts of ore zones and nucleii of composite sphalerites elsewhere. Massive beds contain pyrite and minor galena, and generally are cemented and replaced by only minor saddle dolomite.

Geochemistry - Iron enriched (1 to 5% FeO) early sphalerites lack detectable cadium and contain minor traces of 0.1% copper and 0.1% silver (Fig. 6.1, Appendix D). Positive $\delta^{34}S$ values from two samples of

25 o/oo and 27.4 o/oo are comparable to later tan-brown sphalerites (Fig. 6.1, Appendix D). Associated galenas have lighter $\delta^{34}S$ values (23 o/oo to 15 o/oo).

Evidence of Timing - Fibrous red crystals are the earliest sphalerites. Locally red sphalerites cement over or are interlayered with earlier pyrite (Pls. 6.1a and 6.2c) and fibrous tan-brown and prismatic yellow crystals form younger, outer rims on common rosettes (Pls. 6.1a and 6.2b).

Interpretation - Iron-rich, fine, red sphalerite nucleated on many points in medium to coarse gray dolostones and rapidly accreted radiating and branching fibrous and dendritic growths and microcrystalline layers. These crystal forms with abundant impurities are characteristic of rapid crystallization (e.g., Buckley, 1951). Massive beds replaced gray dolostone and were subject to minor subsequent solution and cementation by later sphalerites and saddle dolomite. Disseminated crystals grew on mesopores in surrounding beds and formed nucleii for rosettes of later tan-brown and yellow sphalerites.

6.5 Early Tan-brown Sphalerite

Petrography and Distribution - Tan/brown sphalerites occur as disseminated individual fine crystals, composite rosettes and discontinuous millimetre-thick laminations (Pls. 6.1a,b; 6.2a). Individual crystals are dispersed among intercrystalline pores of gray dolostones.

Crystal rosettes, 5 to 20 mm in diameter, vary from dispersed clusters around mesopores to coalesced spheres in beds of massive, brown sphalerite. Laminated sphalerites cement horizontal veins and sheet cavities (Pl. 6.1a). Coarse crystals, 0.5 mm wide by 1 to 2 mm long, which radiate outwards from dolostone mottles, are stubby, triangular forms with narrow bases and broad outer ends (Pl. 6.1b,c). A fibrous texture is macroscopically visible as alternating pleochroic brown and tan crystals (Pl. 6.2b, c). Similar to the red crystals, the brown colour is acquired from inclusions of iron-rich impurities. The brown crystals are concentrated at the base of rosettes and along separate multiple growth bands (Pls. 6.1a,b; 6.2a,b). All crystals have a fibrous to cross-hatched lamellar twinning which overprints the colour fabric (Pl. 6.1d).

Fibrous tan/brown crystals are ubiquitous throughout ore lenses of early sphalerite. They locally form massive, brown sphalerite beds along fracture zones where crystal rosettes replace up to two-thirds of coarse gray dolostone beds.

Geochemistry - These relatively pure sphalerites contain FeO ranging between 0.5 and 2.0%, but no other measureable traces (Fig. 6.1, Appendix E). Sulphur isotope ratios of 27 to 28 o/oo $\delta^{34}S$ are heavier than later sphalerites by 2 to 10 per mil (Fig. 6.1, Appendix D). Tested samples come from deep stratigraphic ore in the western C and eastern T zones (location, Fig. 1.4).

Fluid Inclusions - Five fluid inclusions homogenize at mean temperatures (T_h) of 144°C with a range from 124°C to 155°C and salinity of 24 equivalent weight % NaCl (Figs. 6.1, 6.2, Appendix F). Irregular shaped dark inclusions are associated with pleochroic zones in these and younger sphalerite crystals.

Evidence of Timing - Fibrous tan/brown sphalerites lie sequentially between early red and prismatic yellow crystals (Pls. 6.1a; 6.2b). Tan-brown crystals form the cores of rosettes outside the range of early red crystals (Pl. 6.2a).

Interpretation - Tan-brown sphalerite precipitated rapidly and extensively in porous dolostones, veins and large solution pores. Both the fibrous crystal form and layers of pleochroic brown sphalerite imply rapid growth rates (e.g., Buckley, 1951). Centimetre-scale crystal rosettes coalesced from numerous nucleation sites on surfaces of dolostone mottles. Elsewhere, fine crystals precipitated as multiple mm-thin laminations in extensive horizontal cavities.

6.6 Early Yellow Sphalerite

Petrography and Distribution - Yellow sphalerites are ubiquitous throughout the mine area in early sulphide bodies. They occur in four different habits: (1) disseminated 1 to 3 mm thick crystal clusters surrounding gray dolostone mottles in pseudobreccia; (2) 2 to 5 cm thick multilayered colloform growth bands along vein walls and former cavities

Figure 6.2 Fluid Inclusion Data from Sphalerites

The histograms display eutectic, melting and homogenization temperatures for fluid inclusions in sphalerites. Data is listed in Appendix F.

PLATE 6.3

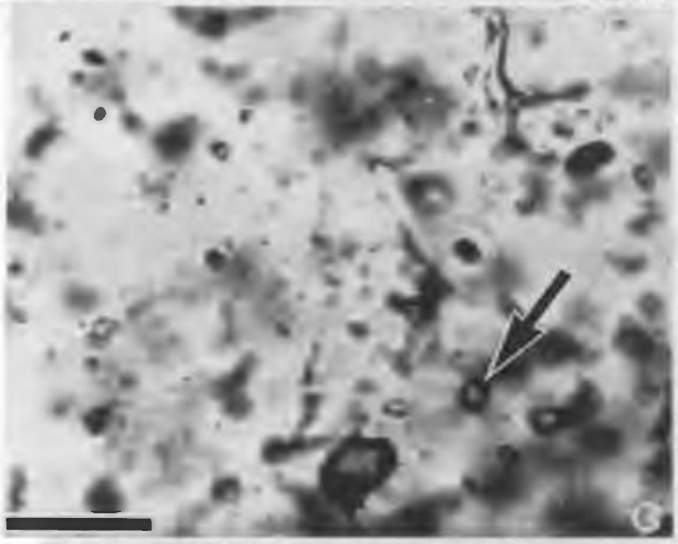

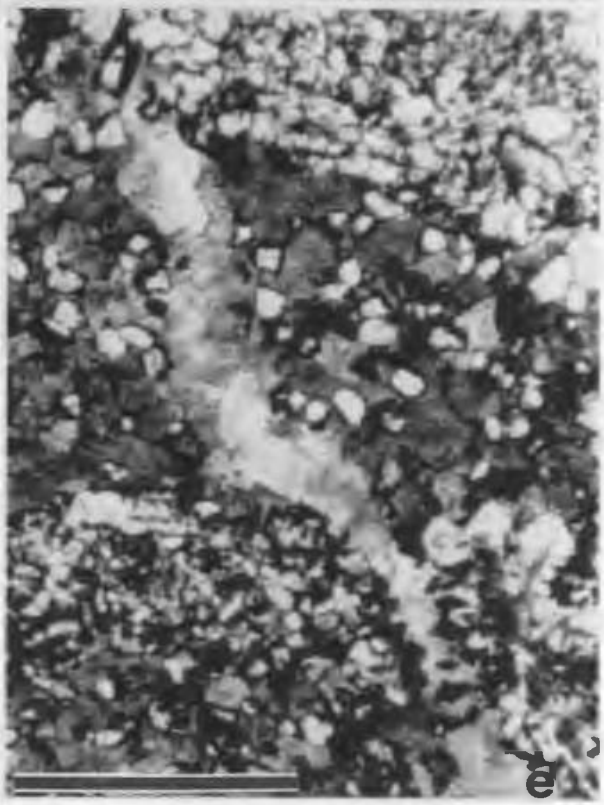

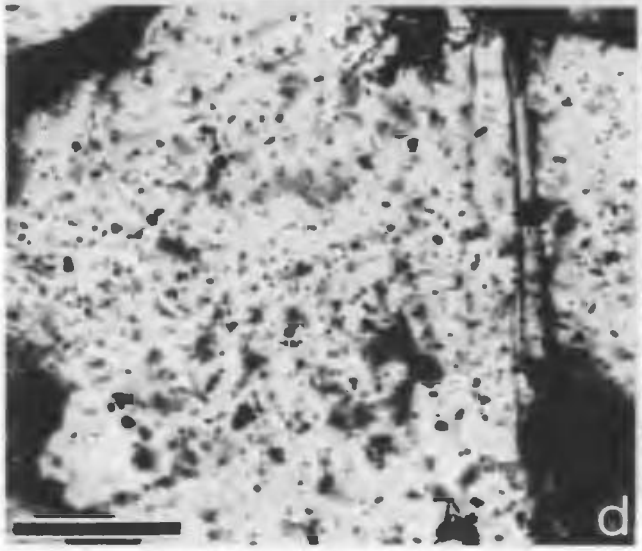

(Pl. 6.1a); (3) massive crystallization of up to two-thirds of coarse dolostone beds by 5 to 10 mm thick crystal composites and rosettes which cement microcavities and partially replace dolostones (Pl. 6.2a); and (4) disseminated fine to medium euhedral crystals within gray mottled and laminated geopetal dolostone (Pl. 6.3a).

The coarse pale yellow crystals, in contrast to earlier fine fibrous sphalerites, have grown in extensive open vugs and veins (Pls. 6.1a; 6.2a). C-axes of elongate prismatic crystals are oriented normal to void walls (Pl. 6.3a,b). A microstructure of radial and inverted twin fabrics of millimetre long lamellae contrast with the short fibrous and cross-hatched lamellae of earlier sulphides. Post-crystallization features around the outer edge of crystals include (1) cross-cutting isotropic twin lamellae; (2) fractures cemented by saddle dolomite and late luminescent sphalerites; and (3) corrosion of crystal surfaces prior to saddle dolomite cementation.

Both fibrous tan/brown and pale yellow sphalerites contain millimetre-thick growth bands of alternating in colour from mixed tan and brown to homogeneous brown to yellow crystals (Pl. 6.1a). A microstratigraphy of multiple paired bands and microcrystalline layers traced along ore zones and throughout the mine area imply that precipitation of millimetre-thin deposits is regional. This microstratigraphy is illustrated schematically in Fig. 6.1. Stratigraphy observed in the T and L Zones (Pl. 6.1a) can be correlated up to 7 km away in the other zones (Pl. 6.2a, K Zone; Pl. 6.2b, H Zone) (locations on Fig. 1.4). Similar phenomena are observed in the Upper Mississippi Valley District of Wisconsin (McClimans et al., 1980).

Plate 6.3 Early Yellow Sphalerites

a. Growth layers of prismatic crystals are seen on acid etched polished surfaces in oblique reflected light (Nomarski Interference). Sample from the L Zone (Pl. 6.1a; Fig. 1.4). 1 mm scale.

b. Typical prismatic yellow crystals in contact with saddle dolomite cement in the upper left. Sample from the F Zone (Fig. 1.4). 1 mm scale.

c. Spherical fluid inclusions, 2 to 15 μm in diameter, from the B Zone (Fig. 1.4) have high homogenization temperatures (160°C to 185°C). 25 μm scale.

d. Fluid inclusions in Pl. 6.3d are evenly distributed through patches like this one. 100 μm scale.

e. Disseminated, equant yellow crystals occur at dolomite crystal boundaries. Saddle dolomite cements a late dilatent fracture. Sample from the F Zone (Fig. 1.4). 1 mm scale.

PLATE 6.3

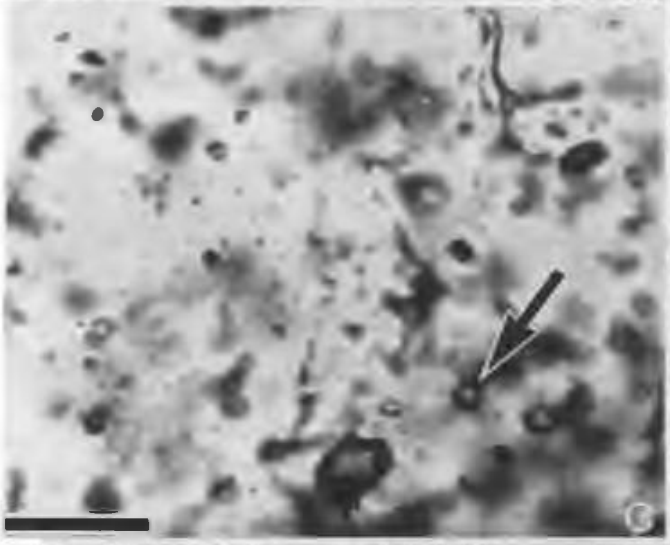

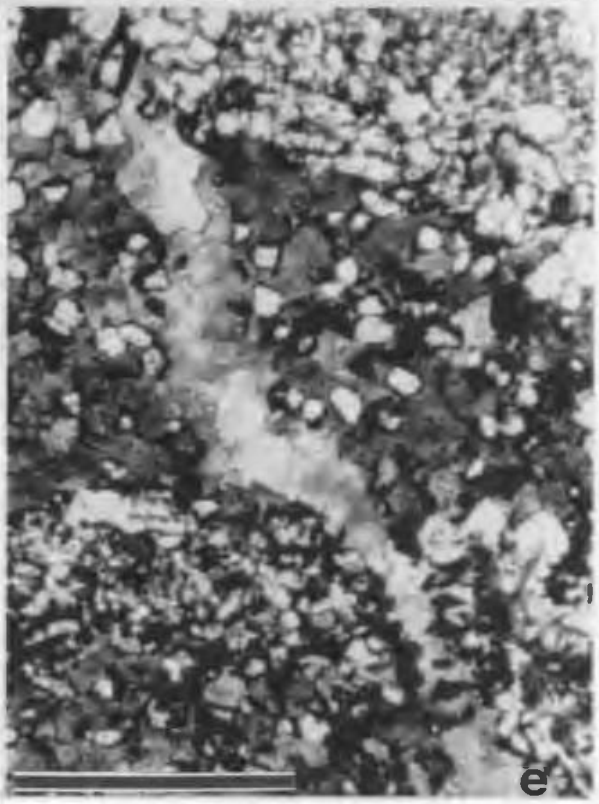

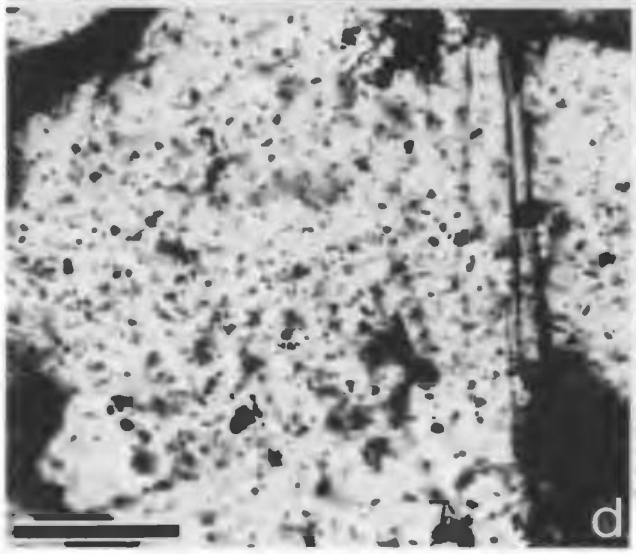

Geochemistry - The yellow sphalerites characteristically contain minor iron (0.20% FeO) and moderate cadmium (0.20 to 0.35% CdO)(Table 6.1; Fig. 6.1, Appendix E). Intercalated brown sphalerites are relatively iron-rich (0.8 to 1.5% FeO) and cadmium poor (0.05% CdO).

Sulphur isotope data for yellow sphalerites from this study and Coron (1982) range widely between 25 o/oo and 20.5 o/oo $\delta^{34}S$ and have a mean value of 22.4 o/oo $\delta^{34}S$ (Fig. 6.1, Appendix D). Test samples suggest that crystals in peripheral areas are depleted in ^{34}S relative to overgrowths of early sphalerite rosettes. Late brown sphalerites from the K Zone (Fig. 1.4) possess heavier $\delta^{34}S$ values (23 o/oo) than earlier, underlying yellow crystals with 21 o/oo $\delta^{34}S$.

Fluid Inclusions - Abundant two phase fluid inclusions, 1 to 10 μm in size, occur in yellow sphalerites of the B and H Zones (Fig. 1.4). They are hypersaline and homogenize at a high mean and mode of 175°C (Pl. 6.3c,d). Homogenization temperatures range from 150°C to 185°C (Figs. 6.1, 6.2, Appendix F). Salinities range from 20 to 27 equivalent wgt. % NaCl (Fig. 6.2). Anomalous lower temperature inclusions, 110°C T_{h}, have relatively low salinities of 20 equiv. wgt. % NaCl. In contrast to inclusions from the B and H Zones, those from an F Zone sample (Fig. 1.4) have lower homogenization temperatures of 92° to 115°C and comparable high salinities (Fig. 6.3).

Evidence of Timing - Yellow sphalerite commonly forms overgrowths on tan-brown sphalerites (Pls. 6.1a; 6.2a,b). Solution contacts occur between these sphalerites (Pl. 6.2e). Yellow sphalerites also occur in

Figure 6.3 Distribution of Fluid Inclusion Homogenization Temperatures in the Mine Area

Highest homogenization temperatures (170° to 175°) occur locally in early yellow sphalerites in the B and H Zones. Similar sphalerites have lower T_h's elsewhere: 92° to 115° in the F Zone and 138° to 145° in the L Zone. Late yellow-black shalerites in the L Zone, noted by brackets, vary from 100° to 130° in modal T_h. The ore zones are identified in Fig. 1.4.

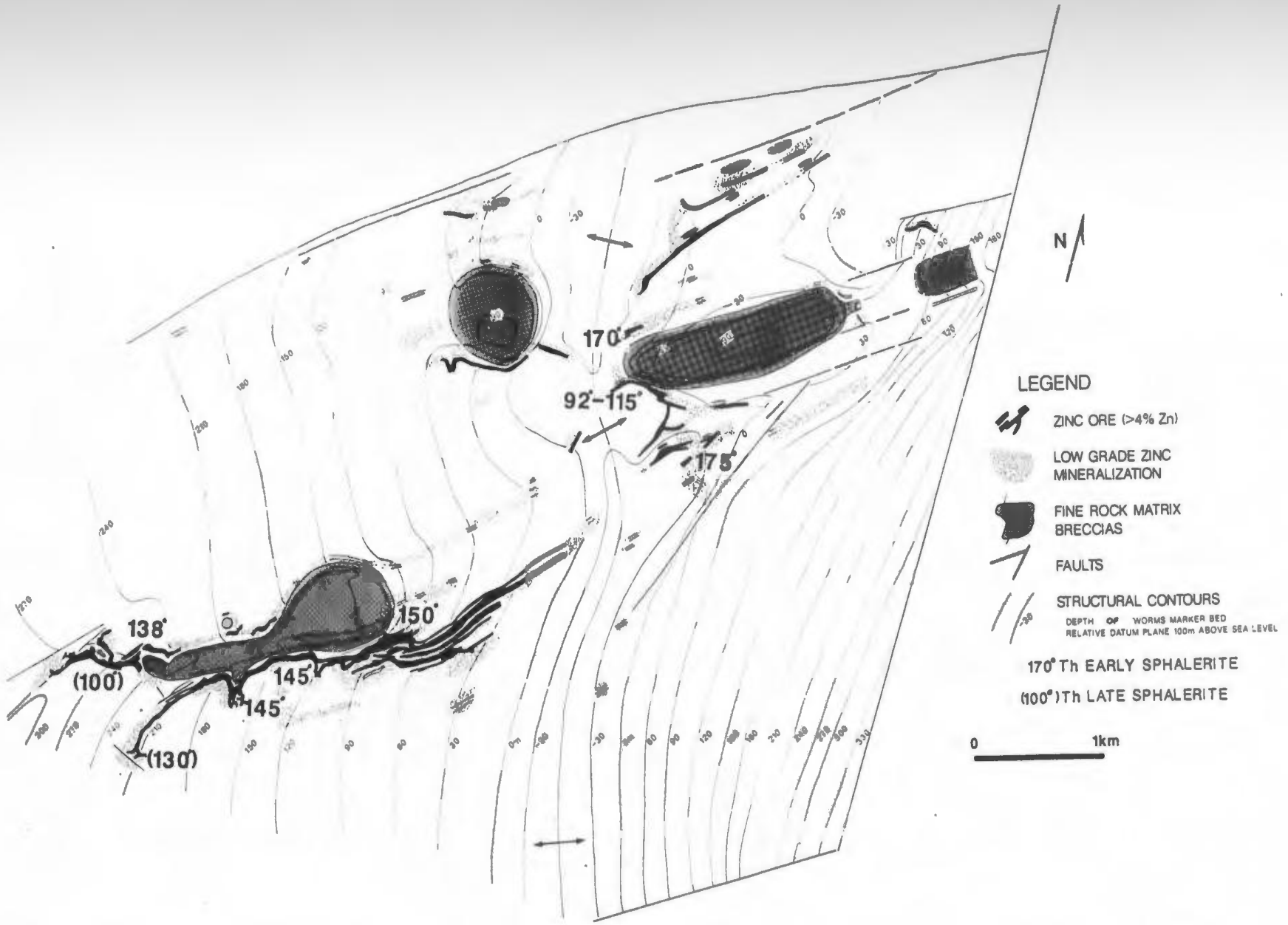

DISTRIBUTION OF SPHALERITE HOMOGENIZATION TEMPERATURES OF FLUID INCLUSIONS

NEWFOUNDLAND ZINC MINES

Figure 6.4 Field Relationships Between Early Sphalerites and Saddle Dolomite

Present beds of early sphalerite developed in three phases.

(1) Massive tan-brown sphalerite crystallized in porous dolostones.

(2) Yellow sphalerite precipitated in solution megapores which formed around the margins of the earlier sulphide bodies.

(3) Late veins and solution cavities dissected the sphalerite body prior to extensive saddle dolomite cementation and replacement. This view is the present day appearance of a wall in the G Zone (location of the zone indicated in Fig. 1.4).

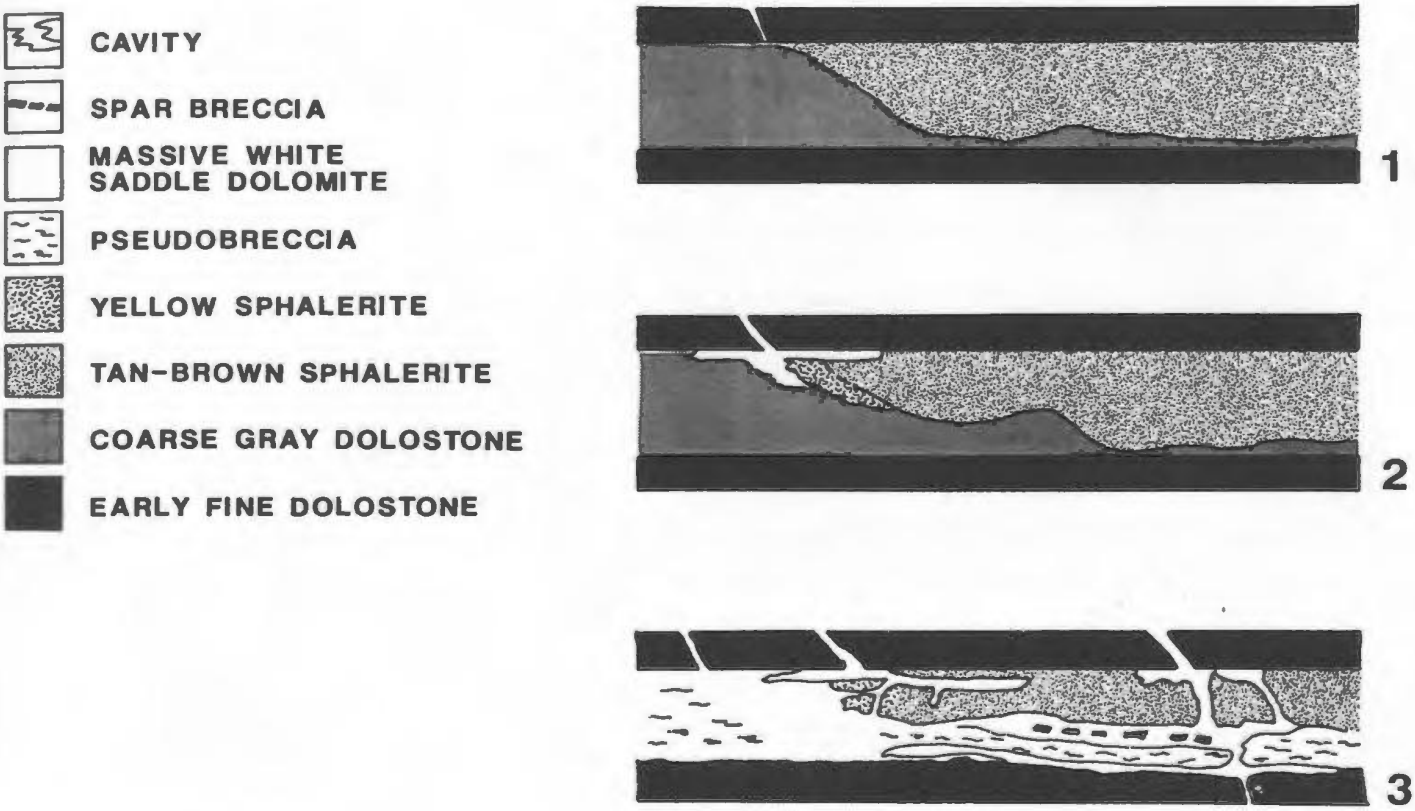

EVOLUTION OF AN ORE BED

large solution pores outside bodies of tan-brown sphalerite (Fig. 6.4). The prismatic yellow crystals generally cement the edges of former vugs that were subsequently filled by saddle dolomite. An early brown, late yellow-brown and late yellow-black sphalerites locally overgrow yellow crystals.

Interpretation - Yellow sphalerites precipitated on rosettes of early sphalerites in porous dolostones. Crystals in large pores coarsened as rates of crystallization and, possibly, fluid flow slowed. Pleochroic brown crystals, in contrast, crystallized rapidly before diffusion of impurities (e.g., Buckley, 1951; Hollister, 1970). A millimetre-scale stratigraphy of brown and yellow sphalerite layers precipitated throughout the region. Each layer, with variable iron and $\delta^{34}S$, regionally precipitated from separate "pulses" of metal-bearing fluids.

6.7 Late Yellow-brown Sphalerite

Petrography and Distribution - Medium to coarse, 0.5 to 10 mm, equant crystals are either disseminated through pseudobreccias or massively replace medium crystalline dolostones in a similar fashion to early sphalerites (Pl. 6.4a). Fine, fibrous crystal forms, however, are absent or minor. Crystal habits may be categorized into two groups: (1) pore cements of linked coarse prismatic crystals which sit on top of and around dolostone mottles and fragments, and on walls of veins (Pl. 6.1e,f,g); and (2) medium to coarse disseminated crystals, linked dendritic chains and composite rosettes which interstitially cement and

Plate 6.4 Late Sphalerites

a. Medium to coarse (200 to 500 μm) yellow-brown sphalerites coalesce in massive ore beds. Example from the eastern L Zone (Fig. 1.4). 1 mm scale.

b. Irregular patches of fluid inclusions in yellow-black sphalerites are associated with large opaque inclusions up to 40 μm in diameter. The irregular, opaque inclusions possibly represent inclusions destroyed during recrystallization. Sample from the L Zone. 100 μm scale.

c. Micrometre-sized inclusions comprise black pleochroic, sector zones in yellow-black sphalerites. Sample from the L Zone. 100 μm scale.

d. Two phase fluid inclusions in yellow-black sphalerite range in size from 1 to 10 μm. Sample from the L Zone. 25 μm scale.

e. Banded, black sector zones outline crystal forms and tend to occur at the base and outer portions of crystals. Sample from the L Zone. 500 μm scale.

f. Long lamellar growth twins, visible in polarized light, overprint black sector zones. Sample from the L Zone. 200 μm scale.

PLATE 6.4

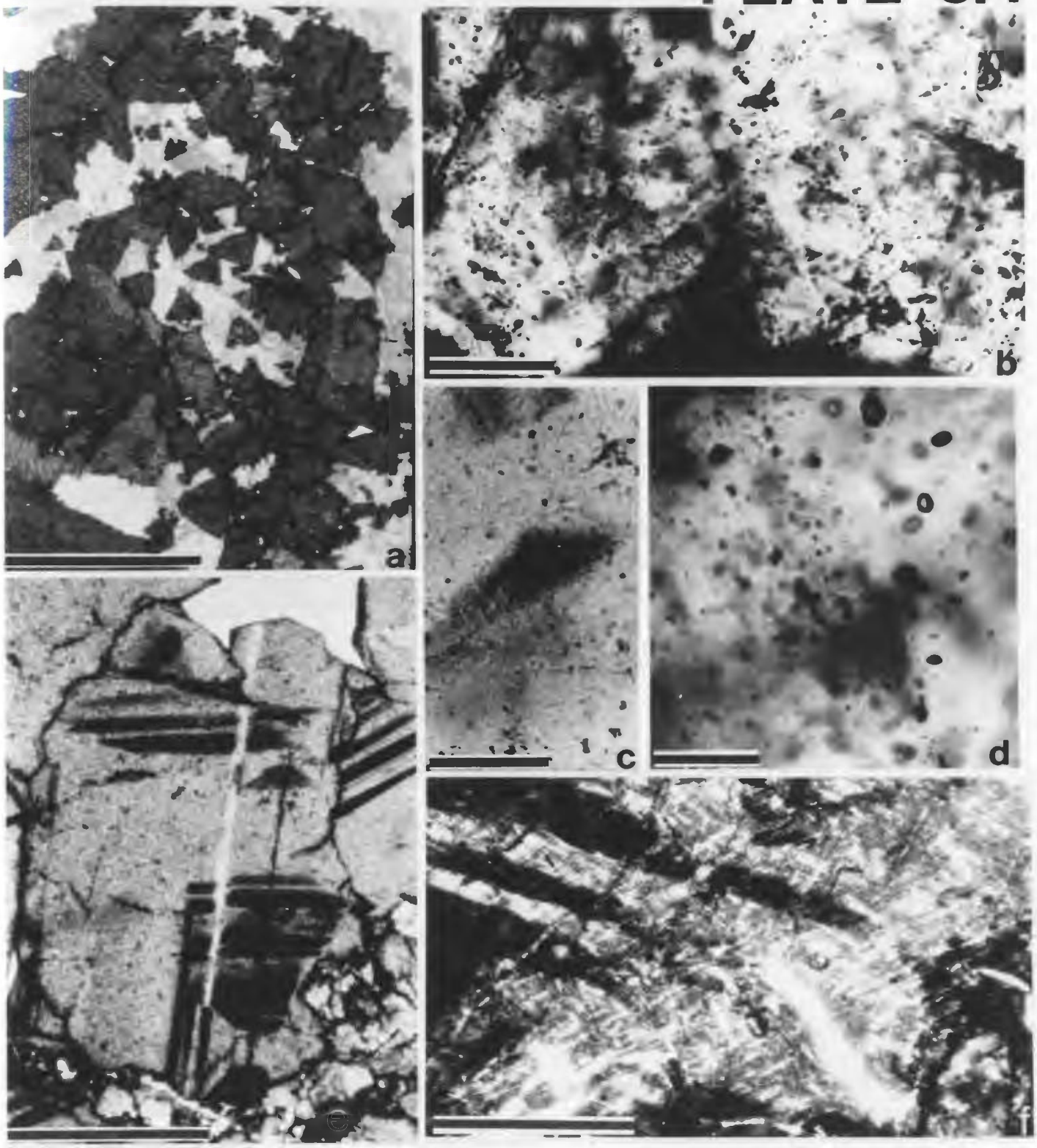

replace medium crystalline gray dolostones (Pl. 6.4a). Group 1 cements are commonly associated with veins and pseudobreccia that contain greater than one third white saddle dolomite cement in veins and pseudobreccia, in contrast to group 2 beds which contain only minor spar.

These sphalerites are coloured an overall light brown to yellow-brown to orangish ochre. Elongate, 1 to 2 mm, rectangular to triangular brown pleochroic patches are scattered throughout the crystals, similar to tan/brown sphalerites. A microstructure of cross-hatched lamellar twinning overprints this fabric. Minor pyrite is locally disseminated at the base of crystals at gray dolostone contacts.

Geochemistry - FeO content varies from 0.5 to 2.5%. Cadmium abundances of 0.2 to 0.6% are distinctively higher than those of earlier sphalerites (Fig. 6.1, Appendix E). Sulphur isotopes ratios of two samples, in addition to four samples from Coron's (1982) study, range from 18.5 o/oo to 19.9 o/oo $\delta^{34}S$ with a mean at 21.9 o/oo. This range is comparable to that of pale yellow sphalerites (Fig. 6.1, Appendix D). The most positive values occur in the centre of the L Zone and decrease toward the edge of the ore body (Fig. 6.5).

Fluid Inclusions - Fluid inclusions have been measured in only one sample from the T-Zone. Homogenization temperatures of six inclusions range from 125°C to 170°C with the mode at 135°C. One inclusion with high T_h of 170°C is a low salinity inclusion (-10°C T_m and -30°C T_e). Lower temperature inclusions with a T_h mode of 138°C have more typical high salinity, $CaCl_2$-bearing fluids (-25°C T_m and -60°C T_e) (Fig. 6.1,

Figure 6.5 Variation of Late Sphalerite $\delta^{34}S$ Across The L Zone

$\delta^{34}S$ values for late yellow-brown sphalerite vary across the L Zone (location, Fig. 1.4). Highest values occur in the ore body's central core to the northwest and the lowest values are found on the outer flank to the southeast. Three closely spaced samples constitute a detailed profile across the Long Hole Stope, the thickest portion of the L Zone. These samples also suggest that $\delta^{34}S$ values decrease away from the centre of ore zones. Data in Appendix D and in Coron (1982).

VARIATION OF LATE SPHALERITE $\delta^{34}S$ ACROSS THE L ZONE

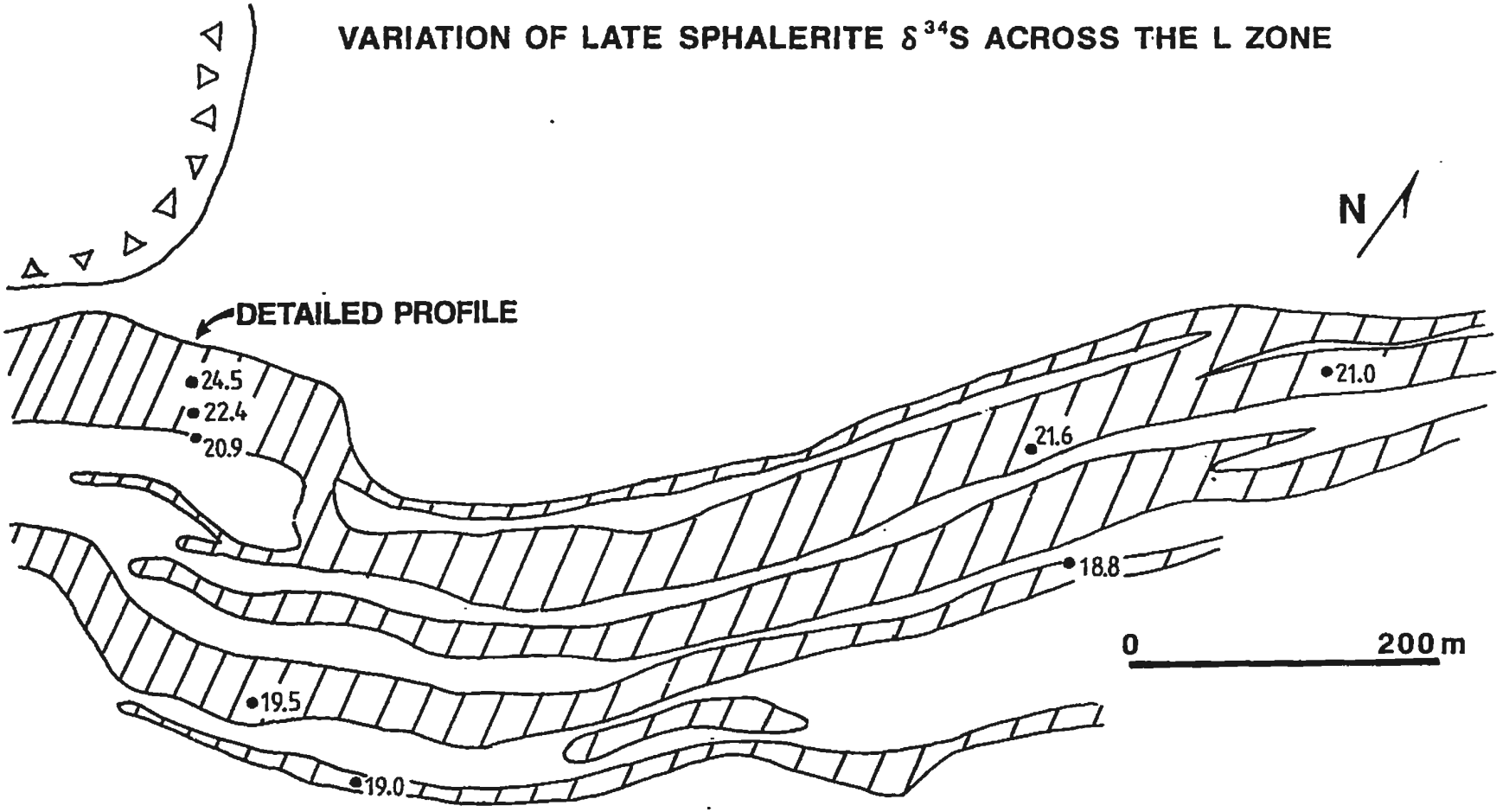

Appendix F).

Evidence of Timing - Yellow-brown sphalerite occurs with yellow-black crystals in separate ore lenses in the L and T Zones where it forms the earliest cements along veins and vugs (Pl. 6.1e,g) or replacement crystals in massive ore beds. These late sulphides also occupy veins and pores which locally cut bodies of early sphalerite. In these areas yellow-brown sphalerite overgrows early yellow crystals and precipitates around fragments of massive tan-brown ore (Pl. 6.1f).

Interpretation - Medium to coarse yellow-brown crystals nucleated on fracture and solution pores generated after early sulphides. The style of mineralization varied from massive crystallization of coarse dolostones peripheral to fractures to coarse crystal growth along abundant veins and cavities. The coarse crystals grew more slowly than the early fine, fibrous sulphides; but, more rapidly than late, very coarse yellow-black crystals.

6.8 Late Yellow-black Sphalerite

Petrography and Distribution - Yellow-black sphalerite occurs in late sulphides and also as ubiquitous, disseminated crystalswith early sulphides and outside ore zones. Fine to megacrystalline, 0.2 to 8 mm, crystals of pale to bright yellow and black sphalerite vary in habit from disseminated individual crystals to linked prismatic vein and vug cements (Pl. 6.1g) to massive clusters of crystals which replace medium

crystalline dolostones (as in Pl. 6.4a). These textures are comparable to those of yellow-brown crystals (same plates). Coarse crystalline open space cements are typical (Pls. 6.1e,g; 6.4e). In these cements palisades of coarse prismatic crystals nucleate on yellow-brown or fine yellow black crystals (Pls. 6.1e; 6.4e).

Black, pleochroic sector zones form central inclusions in yellow crystals and give the crystals their distinctive yellow-black colouration (Pls. 6.1e; 6.4c,e). The sector zones vary from cubic to rectangular, millimetre-scale patches to very thin laminations which outline internal crystal faces (Pl. 6.4e). Black residues along crystal cleavage are outlined by bright yellow sphalerite. The black zones comprise laminations of bluish-black pleochroic stain and very fine bead-like inclusions (Pl. 6.4c). Millimetre-long growth twins overprint the sector zones (Pl. 6.4f).

Geochemistry - FeO content ranges from 0.15 to 0.25% in pale yellow crystals to 0.4 to 0.6% in black patches. Abundances of 0.4 to 0.6% cadmium and 0.1 to 0.3% copper are higher than earlier crystals (Fig. 6.1, Appendix E).

Sulphur isotope ratios, which range between 18.4 o/oo and 22.4 o/oo, have a lower mean value of 19.6 o/oo than earlier sulphides (Fig. 6.1, Appendix D). The most positive isotopes are associated with crystals in the core of fracture zones, such as the Long Hole Stope of the L Zone. The $\delta^{34}S$ of yellow-black crystals are one to three per mil lighter than $\delta^{34}S$ of associated, precursor yellow-brown sphalerites in sampled cement sequences (this study; Coron, 1982).

Fluid Inclusions - One to twenty μm, two phase fluid inclusions are $CaCl_2$-bearing (T_m = -55°C) with high salinities of 20 to 24 equivalent weight % NaCl and variable homogenization temperatures between 90°C and 168°C with a mean of 123°C and a mode of 105°C (Pl. 6.4d; Figs. 6.1, 6.2, Appendix F). Irregular black 10 to 50 μm inclusions, possible significant hydrocarbons, are abundant (Pl. 6.4b).

Evidence of Timing - Yellow-black crystals are the last of the paragenetic sequence of ore-forming sphalerites. They clearly follow yellow-brown crystals in an apparent continuous and gradational precipitation sequence (Pl. 6.1e). The faces of yellow-black crystals are slightly corroded and overgrown by Saddle Dolomite A. Minor μm-sized bead-like sphalerite inclusions occur locally in Saddle Dolomite A. Saddle Dolomite B cements fragments of yellow-black sphalerite which were broken during post-ore fracturing (Pl. 6.1e, g).

Interpretation - Late cooling ore fluids pervaded extensive secondary porosity, which developed during earlier fracturing and sulphide precipitation. Late precipitation in widespread veins and porous dolostones occurred as slow growth of coarse crystals with depleted iron and ^{34}S punctuated by periodic rapid accumulation of inclusion-rich sector zones (Dowty, 1976; Lindblom, 1986). Cadmium enrichment and depleted ^{34}S characterized late ore fluids in general.

6.9 Luminescent Sphalerite Overgrowths

Thin faceted overgrowths or fine euhedral crystals of light blue to yellow luminescent to non-CL sphalerite coat brecciated crystals within Saddle Dolomite B cement (Pl. 6.1h). The bright luminescence compared to the non-luminescent character of most of the sphalerite, may be attributed to trace variations in minor elements. Microprobe and EDAX analyses around rims of crystals did not detect any element differences.

Interpretation - Sphalerite fragments within Saddle Dolomite B continued to grow as luminescent and non-CL overgrowths. The faceted crystal structure suggests crystallization in fluids generally undersaturated with respect to sphalerite. Gregg and Hagni (1987) demonstrated this faceted crystal structure in ore zone dolomites.

6.10 Galena

Petrography and Distribution - Minor galena occurs with early sphalerites in local areas several metres in diameter. Fine to coarse, 1 to 5 mm diameter crystals cement vugs and intercrystalline pores, and partially replace both sphalerite and saddle dolomite. The anhedral crystals have embayed to irregular "fuzzy" edges, where they replace dolomite and sphalerite and penetrate crystal cleavage (Pl. 6.5a,e).

Geochemistry - The galena is a pure lead sulphide with no sig-

Plate 6.5 Post-Ore Sulphates, Sulphides and Pyrobitumen

a. Earliest sphalerite (gray) is left with ragged edges after replacement by dolomite (black) and galena (white). Latest galena also partially corrodes euhedral dolomites. Sample from south of the K Zone (Fig. 1.4). 1 mm scale.

b. Flakes of pyrobitumen cover the surface of a vug (arrow), partially forming a black film on saddle dolomite crystal faces. Colloform sphalerite and megacrystalline white saddle dolomite surrounds the vug. Sample from the L Zone (Fig. 1.4). Scale in centimetres.

c. Fine marcasite needles (dark overgrowths) have grown on the surfaces of saddle dolomites. Sample from the L Zone (Fig. 1.4). Scale in millimetres.

d. Euhedral selenites (large crystals) and celestites (small crystals at bottom) are precipitated on saddle dolomite and locally include marcasite. Samples from the L and T Zones (Fig. 1.4). 3 cm scale.

e. Vug-filling galena cement (black) post-dates saddle dolomite. The crystals fill cleavage in the saddle dolomite. Sample from lead showing south of the H Zone (Fig. 1.4). 1 cm scale.

PLATE 6.5

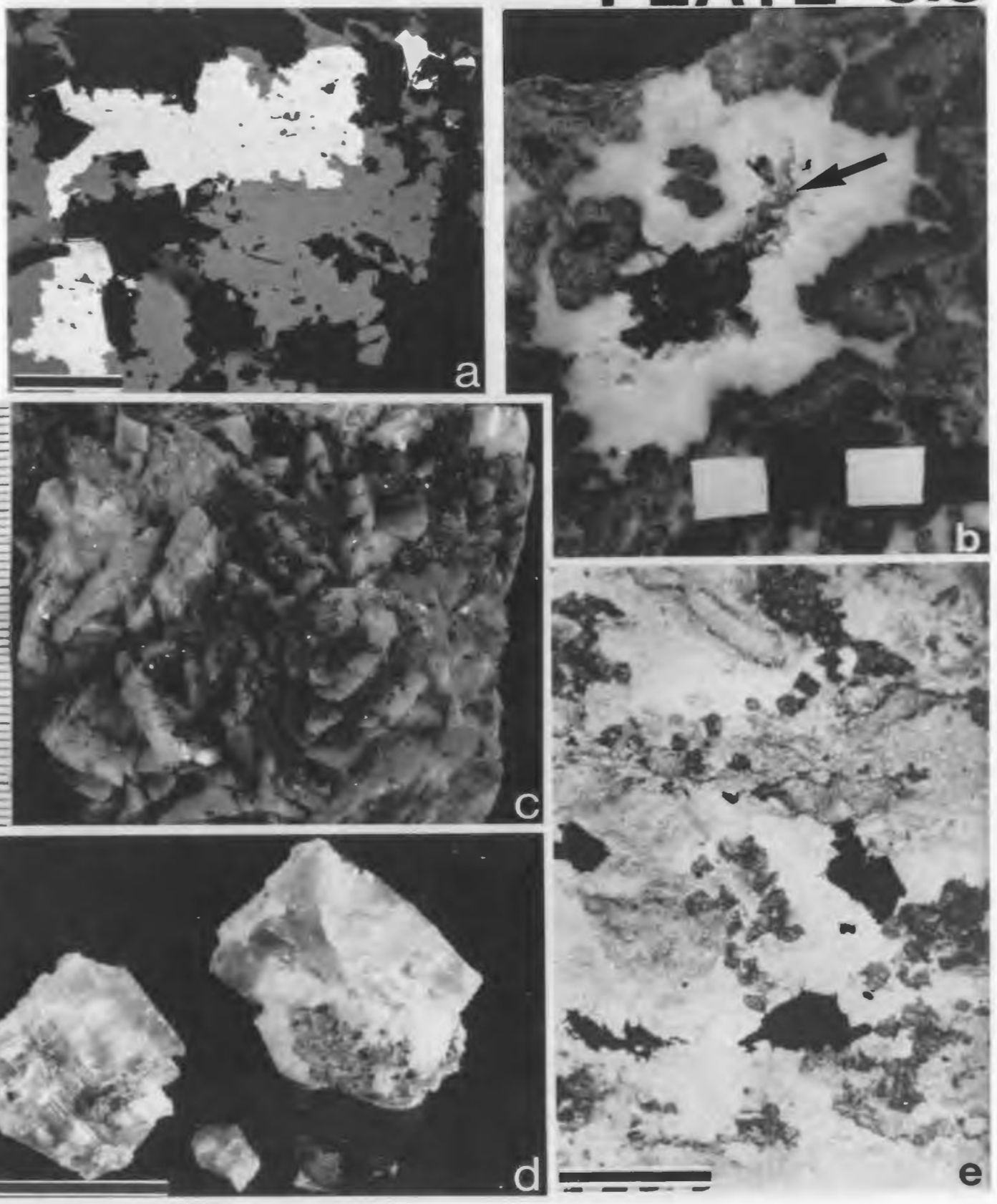

nificant trace element abundances. $\delta^{34}S$ values range from 15 o/oo to 22 o/oo and are 1 to 12 per mil lighter than associated sulphides (Fig. 6.1, Appendix D).

Lead isotope analyses reported from four samples by Swinden et al. (1988)(Appendix G) and five samples by Coron (1982) have low uranogenic lead (206_{Pb} and 207_{Pb}) and relatively high thorogenic lead (208_{Pb}). $206_{Pb}/204_{Pb}$ ratios range between 17.8 and 18.2, $207_{Pb}/204_{Pb}$ around 15.5 and $208_{Pb}/204_{Pb}$ between 38.4 and 38.7 (Fig. 6.6a,b). Daniel's Harbour data cluster in a tight group and, along with other Catoche Formation data, forms the intermediate portion of a positive linear trend for galenas hosted by all Cambro-Ordovician formations. Galena hosted by Cambrian strata is the least radiogenic; whereas, crystals in the Table Head Group have the highest uranogenic lead (Fig. 6.6a,b).

$206_{Pb}/204_{Pb}$ ratios are plotted vs. $\delta^{34}S$ data for five samples from Coron (1982) and this study (Fig. 6.7). Samples with 19 to 22 o/oo $\delta^{34}S$ tend to be more radiogenic. These galenas are associated with early red sphalerites in upper and central portions of the ore zones. Less radiogenic samples with 15 to 16 o/oo $\delta^{34}S$ are associated with yellow sphalerites where they fill pores within saddle dolomites (Pl. 6.5e).

Evidence of Timing - Galena fills late pores in saddle dolomite (Pl. 6.5e) and partially replaces sphalerite and saddle dolomite (Pl. 6.5a). The relationship between galena and other late minerals is unknown.

Figure 6.6 Lead-isotope compositions of Zn-Pb deposits in Cambro-Ordovician carbonates of the Northern Peninsula. Zartman and Doe (1981) model growth curves are shown for reference. Abbreviations: UC, upper crust; O, orogene; M, mantle; and LC, lower crust. Daniel's Harbour samples plot in the shaded area. Data are from Swinden et al. (1988).

a. $^{207}Pb/^{204}Pb$ vs. $^{206}/^{204}Pb$

b. $^{208}Pb/^{204}Pb$ vs. $^{206}Pb/^{204}Pb$

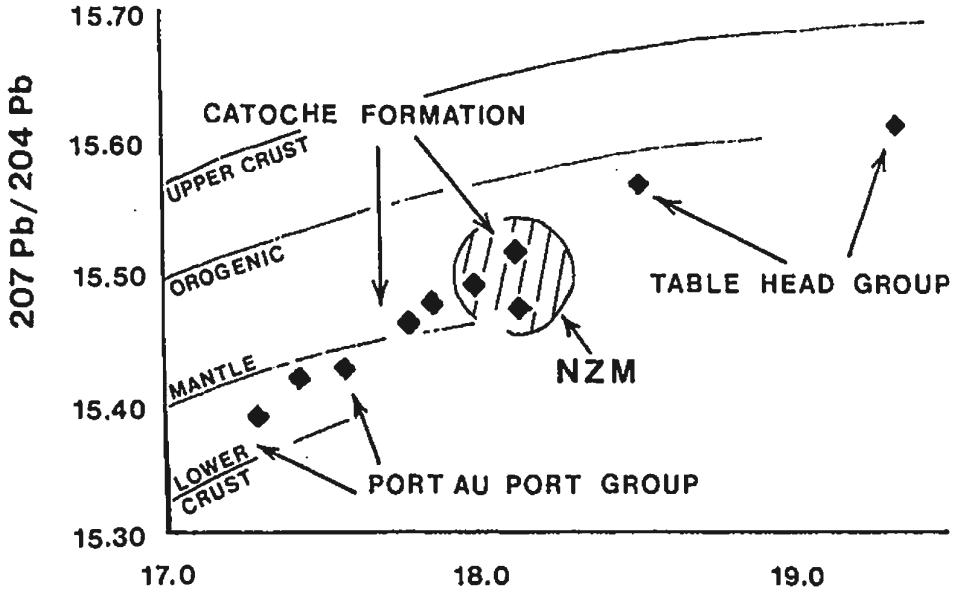
15.70
15.60
15.50
15.40
15.30
207 Pb/ 204 Pb
CATOCHE FORMATION
UPPER CRUST
OROGENIC
MANTLE
LOWER CRUST
TABLE HEAD GROUP
NZM
PORT AU PORT GROUP
17.0
18.0
19.0

a.

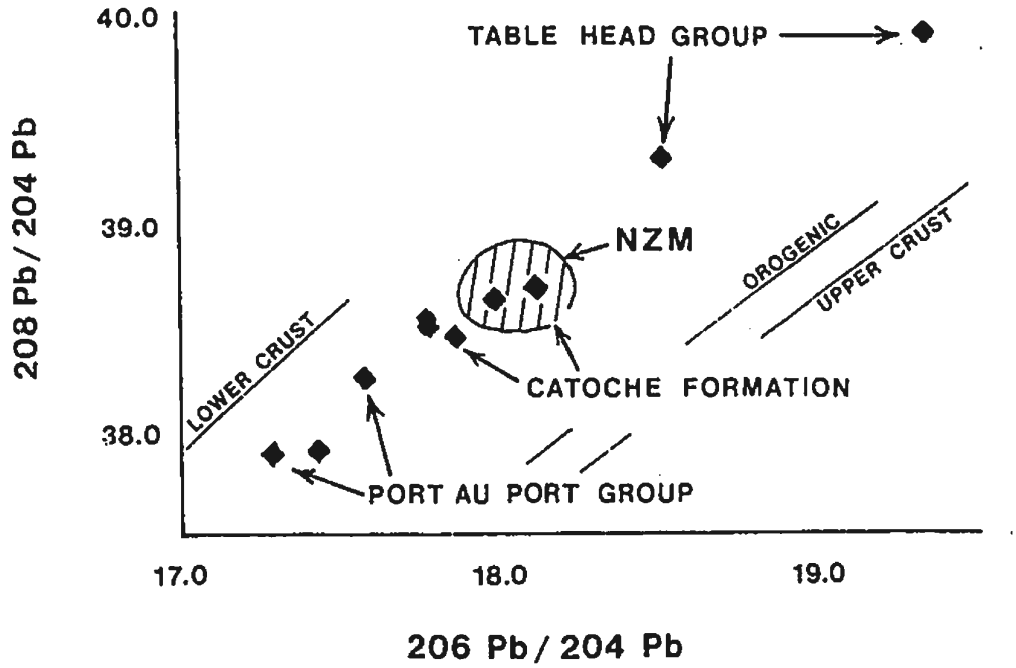
40.0
39.0
38.0
208 Pb/ 204 Pb
TABLE HEAD GROUP
NZM
OROGENIC
UPPER CRUST
LOWER CRUST
CATOCHE FORMATION
PORT AU PORT GROUP
17.0
18.0
19.0
206 Pb/ 204 Pb

b.

Figure 6.7 $^{206}Pb/^{204}Pb$ of Galenas at the Mine plotted versus $\delta^{34}S$

Galenas at the mine segregate into two groups on the basis of occurrence, $\delta^{34}S$ composition and lead composition. Galenas which replace early red sphalerites contain heavy $\delta^{34}S$ values and are slightly more radiogenic than crystals that cement pores in saddle dolomites. Data are form this study, Coron (1982) and Swinden et al (1988).

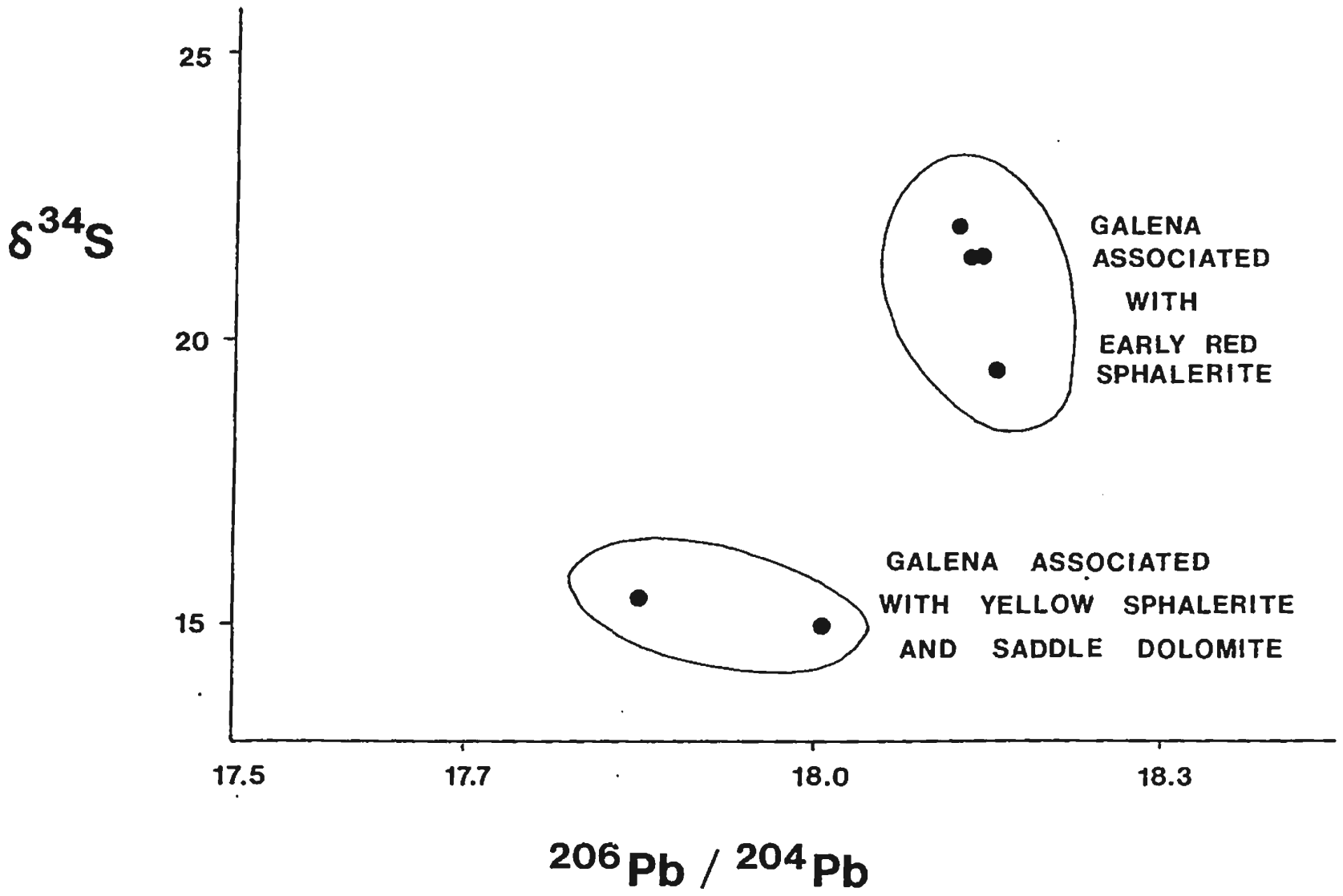
25
20
15
$\delta^{34}S$
GALENA ASSOCIATED WITH EARLY RED SPHALERITE
GALENA ASSOCIATED WITH YELLOW SPHALERITE AND SADDLE DOLOMITE
17.5
17.7
18.0
18.3
^{206}Pb / ^{204}Pb

Interpretation - Galena crystallized after ore stage sphalerite and saddle dolomites and partially replaced both these predecessors. The ordinary or non-radiogenic nature of lead at Daniel's Harbour is similar to numerous MVT deposits (Gulson et al., 1983; Sangster, in prep.) with the exception of radiogenic, crustally derived MVT leads of midcontinent North America (Heyl et al., 1974).

Relatively high thorogenic 208_{Pb} and low uranogenic 206_{Pb} and 207_{Pb} fingerprints the galena's principal source as the evolved high grade metamorphic terrane of the Grenville basement (Coron, 1982; Swinden, et. al., 1988). High Th/Pb is not characteristic of other potential source areas, e.g., mantle, oceanic crust and sedimentary basins (Doe and Zartman, 1979). Increase in radiogenic lead with stratigraphic height implies that as the lead-bearing fluids rose they assimilated increasing quantities of radiogenic lead from the sedimentary pile. Variable lead compositions at stratigraphic horizons are products of uneven mixing of the two end members (Swinden et al., 1988). The two separate groups of galenas at the mine are interpreted to contain different proportions of these end members. Galenas with more radiogenic (formational?) Pb and positive $\delta^{34}S$ values probably precipitated from from fluids dominated by "basinal" brines. Replacement of sphalerite alternatively accounted for the sulphur composition. The light $\delta^{34}S$ values of galenas with less radiogenic (basement) Pb suggest crystallization from fluids more typical of the basement source. The sulphur derived from this deep source was probably light compared to that of formational waters. Alternatively the light sulphur of late galenas, sphalerites and sulphates may be attributed to fractionation

during oxidation of formational fluids.

Alternative interpretations of the lead composition such as a lead growth curve or secondary isochron are rejected for several reasons. (1) Linear regression analysis of $207_{Pb}/204_{Pb}$ vs. $206_{Pb}/204_{Pb}$ data gives a steeper slope (0.1113) than Phanerozoic lead growth curves. (2) Projection of secondary isochrons require a source area of 1500 Ma age, greater than that of the radiometric 1250 Ma age of the basement. (3) Compositional variation of heterogeneous leads transported and deposited in the sedimentary succession should be independent of stratigraphic position (Swinden et al., 1988).

6.11 Late Red Sphalerite

Petrography - Euhedral coarse to megacrystalline deep red to orange sphalerite is scattered on open vug surfaces. The crystals sit on euhedral saddle dolomites and share vug surfaces with late pyrite, marcasite, calcite, barite and gypsum.

Geochemistry - Abundances of 0.4 to 0.6% cadmium and 0.1 to 0.3% copper compare with the yellow-black sphalerites (Appendix E). Variable sulphur isotope compositions are light relative to other sphalerites. An analysis of $\delta^{34}S$ by Coron (1982) from an A Zone sample at 10.8 o/oo $\delta^{34}S$, is lighter than a K Zone sample at 20.5 o/oo (this study). No fluid inclusions were found.

Evidence of Timing - These latest sphalerites form euhedral crystals in vugs on the surfaces of saddle dolomites which they post-date. Their age relationship to other vug crystals is unknown.

Interpretation - Late red sphalerites crystallized in open vugs after both ore stage sulphides and post-ore saddle dolomite. Although the trace element composition is similar to yellow-black sphalerites, $\delta^{34}S$ isotopes lighter by up to 8 o/oo imply a different, fluid chemistry.

6.12 Late Pyrite, Marcasite and Hematite

Similar to late red sphalerite, euhedral cubes and needles of fine to coarse pyrite and marcasite form a glittery "dust" over saddle dolomite surfaces in open vugs (Pl. 6.5c). No geochemical data have been gathered on these sulphides. Although widespread throughout the mine area, these iron sulphides are particularly common along late faults over stratigraphic thicknesses of 5 to 40 metres. This distribution implies that the crystals precipitated from fluids migrating along late faults or relate to redox fronts along faults.

Hematite has a similar distribution. It commonly stains dolostone beds underneath and outside sulphides east of the B and F Zones (Fig. 1.4). It also occurs along late faults in all areas.

6.13 Late Sulphates

Petrography and Distribution - Euhedral megacrystals of selenite gypsum, barite and celestite overgrow saddle dolomites in large vugs. Gypsum locally cements pores in pseudobreccia and rock-matrix breccia. These sulphates are common along northeast-trending faults and the intersection of ore zones with north-trending cross-faults.

Geochemistry - Sulphates have both heavy and light $\delta^{34}S$ values (Appendix D; Coron, 1982). Barite, celestite and some gypsum have highly positive values, 26 to 30.6 o/oo, which approximate those of Ordovician sea water sulphate (Claypool et al., 1980). Other cements and euhedral crystals of selenite gypsum have low positive values of 9.8 to 10.5 o/oo.

Evidence of Timing - Selenite overgrows saddle dolomite and marcasite. Relationships to late sulphides are unknown. Occurrences along faults suggest that the crystals precipitated from fluids migrating along these structures.

Interpretation - Sulphates crystallized in vugs peripheral to faults after precipitation of saddle dolomite and late marcasite. Heavy $\delta^{34}S$ values imply that most crystals formed from saturated formational brines which experienced minor fractionation. Some gypsum, however, precipitated from sulphur sources that experienced significant fractionation by, for example, oxidation of sulphides or oxidation of H_2S

along faults by meteoric waters.

6.14 Discussion of Fluid Inclusion Data

General conclusions concerning fluid inclusion data from both carbonates and sulphides are reported in section 5.11. Five specific characteristics of sphalerite inclusions are discussed here.

(1) Fluids contain an mixture of unknown proportions of $CaCl_2$, NaCl and probably $MgCl_2$ and KCl. Most fluid eutectic temperatures range from -60°C to -47°C and a few lower salinity inclusions in saddle dolomite have a T_e of -33°C to -36°C. Lack of halite daughter minerals in the fluids imply that they are undersaturated in NaCl.

(2) Final melting temperatures of sphalerite and ore stage dolomite range between -22°C and -28°C which connote salinities of 22 to 25 equivalent weight % NaCl. A few inclusions melt at -30 to -33°C and -12 to -15°C.

(3) Homogenization temperatures of sphalerites range widely between 90°C and 180°C. The mode of T_h measurements for all sulphide inclusions is indefinite, but the mean is 140°C. The limited survey of the paragenetic sequence shows an extreme variation in modal T_h from 175°C in early yellow crystals to 115°C in late yellow-black sphalerite.

(4) Among early yellow sphalerites, samples with high homogenization temperatures of 170°C come from possible "hot spots" in the B and H Zones where stratigraphically deep ore is associated with deep fracture systems (Chapter 12). In contrast, samples from the K and L Zones have homogenization temperature modes of 140°C. More extensive

sampling across the mine area is needed to test for thermal anomalies and "hot spot" potential.

(5) Two possible types of hydrocarbon inclusions are (1) interconnected networks of secondary black to dark brown single phase inclusions (Pl. 6.3c), and (2) light brown, two phase inclusions in which dark vapor bubbles with a high refractive index do not homogenize when heated above 300°C. Although methane inclusions are common in MVT deposits (Roedder, 1984), the composition of the ones here are unknown. Recent studies have found abundant CO_2 inclusions in other MVT deposits (Rod Randell, 1987, personal communication; unpublished USGS studies).

Interpretation - Fluids trapped by inclusions at Newfoundland Zinc Mines are typical of other MVT deposits. $CaCl_2$-bearing brines with a relatively high salinity of greater than 24 equivalent weight % NaCl were trapped at a moderately hot temperature range of 90°C to 185°C and at T_h modes of 115°C to 140°C for the various crystal stages. Burial to depths of 2 to 4 km, as suggested by conodont alteration indices of 2 to 2.5, would require pressure correction to even higher homogenization temperatures. Some hydrocarbons such as CH_4 and possible CO_2 were probably contained. Fluid densities were greater than one, mostly around 1.10e.

Relative variation of homogenization temperatures and salinities may lend insight into the composition and variety of fluids in the subsurface (Fig. 5.8). In systems of two or more mixed fluids many inclusions are considered hybrid mixtures of several original brines (e.g. Lindblom, 1986). The majority of contemporary sphalerites and saddle dolomite inclusions which have similar salinities (23 to 25 wgt %

NaCl) and a broad T_h range (75°C to 185°C), probably crystallized from one hybrid or single fluid. The total array of data from calcites, saddle dolomites and sphalerites display a wide variation along an inverse trend of high T_h/moderate salinity to low T_h/high salinity inclusions and a few dolomite inclusions which represent a third mode low T_h/moderate salinity. These variable compositions sample either an evolving fluid through time and/or two or more fluids before mixing, each of which had variable salinities and densities. These variations are not adequately explained by single fluid models. Similar conclusions were made from much larger data sets by Taylor et al., (1983) and Lindblom (1986) in similar settings.

Some mixed fluid models propose combination highly saline metal-rich fluids with low salinity "meteoric" waters (e.g., Hall and Friedman, 1963; Taylor et al., 1983; Lindblom, 1986). Salinities of inclusions at Newfoundland Zinc Mines, particularly of pre-ore and post-ore calcites, are greater than 20 equivalent weight % NaCl. These hypersaline brines suggest no meteoric dilution. Plots of D/H and $\delta^{18}O$ isotopic composition of inclusions could better evaluate meteoric influence.

6.15 Discussion of Sulphur Isotopes

Introduction - Similar to other MVT deposits, sulphur isotope ratios are positive and slightly depleted (1 to 18 o/oo) relative to sea water sulphate of the host rocks (28 o/oo $\delta^{34}S$) (Claypool et al., 1980). Main ore stage sphalerites vary from 27.5 o/oo to 18 o/oo (Fig. 6.1).

Late red sphalerite is relatively depleted at 10.8 o/oo (Coron, 1982). Late galenas form two groups at 19 to 22 o/oo and 15 o/oo. Late sulphates separate into three groups: (1) enriched gypsum with 29.9 o/oo and 30.6 o/oo (Coron, 1982); (2) barite and celestite with respective 26.2 o/oo and 28.2 o/oo close to Ordovician sea water sulphate; and (3) depleted gypsum with 9.8 o/oo to 10.5 o/oo.

Ore Stage Sphalerite - Ore stage sphalerite $\delta^{34}S$ values progressively decrease through the paragenetic sequence, but individual substages have broad ranges of 3 to 6 o/oo and successive crystal layers fluctuate in composition (Fig. 6.1). Early tan brown and red sphalerites are only slightly depleted relative to the 27 to 28 o/oo of Ordovician sea water sulphate. Both red and yellow sphalerites range widely over 3 to 6 per mil, 22 to 19 o/oo and 25.9 to 20.4 o/oo respectively. From one example, a brown sphalerite band with 25.9 o/oo is enriched 5 per mil relative to preceding yellow crystals with 21 o/oo.

Sulphur isotopes of late sulphides are, likewise, variable. Isotope ratios of yellow-brown and yellow-black crystals range from 24.5 o/oo to 19.9 o/oo, and 22.4 o/oo to 18.4 o/oo respectively. Late crystals of individual sequences are depleted 1 to 2 per mil relative to earlier ones. In both crystal stages, $\delta^{34}S$ values tend to be depleted 4 to 5 per mil laterally away from fracture zones.

Post-Ore Sulphides - Galenas and late red sphalerites, which postdate saddle dolomite, fall into three isotopic groups: (1) galenas with early red sphalerite with 22 o/oo to 19 o/oo are only 1 to 3 per mil lighter than the sphalerites; (2) galenas with a separate signature of 15.5 o/oo to 14 o/oo with 8 to 12 per mil depletion relative to as-

sociated sulphides; and (3) late red sphalerite at 10.8 o/oo. The source(s) of sulphur were depleted relative to the ore stage, except where galenas replaced sphalerites and incorporated their sulphur.

Sulphide Pairs- The only possible cogenetic sulphide pairs from petrographic evidence are early pyrite and sphalerite. Pyrite is 3.5 to 4.2 per mil lighter than cogenetic sphalerite pairs. Cogenetic pyrite, however, should be heavier than its sphalerite pair according to the relative strength of the metal-sulphur bonds (Bachinski, 1969). Thus the early pyrite and sphalerite are either (1)not cogenetic and precipitated in two different stages or (2) cogenetic but not in equilibrium. The occurrence of interlayered sulphides supports the later hypothesis.

Galenas 1 to 3 per mil lighter than early red sphalerite pairs are determined to be much younger on petrographic evidence (Section 6.10). If a cogenetic origin or similarity of conditions of precipitation is assumed, calculations from equations for equilibrium fractionation (Ohmoto and Rye, 1979) imply high temperatures of crystallization around 216°C or greater. Such a temperature is 30°C warmer than known T_h's of fluid inclusions.

Interpretation- The sulphur of Newfoundland Zinc sulphides and sulphates, similar to other MVT deposits, is derived from basinal, in this case, Cambro-Ordovician sea water sulphate with 31 o/oo to 27 o/oo $\delta^{34}S$ (e.g. Claypool et. al., 1980). The positive $\delta^{34}S$ values of the sulphides range from 27.5 o/oo to 10.8 o/oo, or 0 o/oo to 17 o/oo less than Ordovician sea water sulphate. Both early tan-brown sphalerite and barite preserve unfractionated sulphur. In the formation of H_2S and

crystallization of sulphides sulphur fractionated by one or more of several processes: (1) by depletion of $\delta^{34}S$ according to the increasing ratio of SO_4^{-2}/H_2S of a hydrothermal fluid; (2) by kinetic effects, ie., more rapid reaction rates for light isotope species; (3) by inorganic sulphate reduction to "light" H_2S which is enhanced in the presence of H_2S and organic compounds; (4) by bacterial reduction of sulphate below 50°C; and (5) by concentration of ^{34}S in fluids as clay-rich sediments absorb ^{32}S (Ohmoto and Rye, 1979). Fractionation was most likely affected by inorganic sulphate reduction and kinetics because known homogenization temperatures place reactions in the 90°C to 180°C range (Ohmoto and Rye, 1979; Robinson, 1980). These reactions generated sulphides enriched in ^{32}S and depleted in ^{34}S relative to sea water sulphate.

Post-ore sulphates fractionated according to relative insolubility of minerals and by the reduction and oxidation of fluids. Barite is relatively insoluble in water and tends to precipitate rapidly prior to significant fractionation (Sangster, 1976). Barite should provide a true sample of the isotopic composition of the formational fluids. In contrast, the more soluble, isotopically heavy, gypsum is a later precipitate from waters which were enriched in ^{34}S as kinetics of sulfate reduction concentrated ^{32}S in H_2S, sulphides and clay residues. Such changes occur within closed fluid systems where crystallization selectively and rapidly removes ^{32}S. (Thode and Monster, 1965; Ohmoto and Rye, 1979).

Isotopically light gypsum from pseudobreccia vugs and cement of rock-matrix breccia probably acquired its sulphur by oxidation of H_2S or

predominance of SO_4 over H_2S. Near surface oxidation of H_2S forms an isotopically light "fresh water" sulphate (Robinson, 1980). This crystallization may have been contemporary with hematite oxidation and migration of fresh oxidized waters along late faults. Light and heavy gypsum is indistinguishable in the field and petrographically. The two types may have been contemporary and oxidizing waters along faults caused local oxidation.

6.16 Significance of Lead Isotopes

Lead isotope data and their interpretation have been presented in section 6.11. In general, the lead isotopes give essential information on potential sources of metals and configurations of fluid transport systems, which may be summarized in three points.

(1) The pronounced non-radiogenic, thorogenic composition of the galena implies major contribution of lead from the high grade metamorphic basement, where fluids resided, leached metals, and subsequently circulated through the sedimentary pile. Fluids and their cements in basins elsewhere contain geochemical signatures, e.g., isotopes of D/H, Sr and Pb, which suggest or demonstrate that basinal brines circulated through the basement and equilibrated with it (Heyl et al., 1974; Foley et al., 1981; Kelly et al., 1986; Morrow et al., 1986).

(2) The linear array of lead isotope data on compositional plots (Fig. 6.6) shows that deposits at various stratigraphic levels were interrelated by one hydrologic system in which fluids with "basement lead" accumulated increasing quantitites of radiogenic lead as they rose

through the sedimentary pile (Swinden et al., 1988). This fluid could have leached lead from the sedimentary pile and/or mixed with formational fluids bearing radiogenic lead.

(3) Variable mixing of non-radiogenic "basement" and radiogenic "sedimentary" lead generated a range of compositions at each stratigraphic level. A heterogeneous network of vertical and horizontal fractured aquifers probably accounted for inhomogeneous mixing of leads.

6.17 Summary of the Paragenesis of the Sulphides and Sulphates

Sphalerites crystallized in two general sequences identified as Early and Late Sulphides. Major fracturing preceded both sequences. Dissolution, which generated extensive porosity prior to sulphide deposition, continued throughout the process. As early sulphide bodies precipitated, resulting acids or undersaturated fluids partly dissolved surrounding dolostones. Later sphalerites precipitated in these secondary pores.

Early sulphides crystallized in four distinctive phases: (1) initial crystallization of fine pyrite in gray dolostones; (2) rapid precipitation of $\delta^{34}S$ heavy and iron-rich red sphalerite and rosettes of fibrous tan brown crystals; (3) precipitation at varying rates of millimetre-thick fibrous crystal layers from repeated fluid pulses; and lastly (4) slow cementation in voids of palisades of coarse prismatic yellow crystals. Throughout the sequence $\delta^{34}S$ values decreased. In detail, however, $\delta^{34}S$ fluctuated in successive crystal laminations as degrees of sulphur fractionation in the source (?) varied with each

influx of metal-bearing fluid. Variations in homogenization temperatures of yellow sphalerites across the mine area suggest that certain zones, such as the B and H, reached higher temperatures of 165° to 185°C (Fig. 6.3).

In certain respects, the transition between early and late ore-stage sphalerites was a continuum. Yellow and yellow-brown sphalerites precipitated from fluids of similar temperature and salinity. Early and late sulphides contained a continuous array of sulphur isotope compositions between 28 o/oo and 18.4 o/oo and ranges of $\delta^{34}S$ of crystal stages overlapped significantly. Only the mean value of $\delta^{34}S$ of each crystal stage was depleted progressively. Fractures and breccias, however, cut early sulphides and were cemented by late ones (Pl.6.1f) (see Chapter 12).

Late ore-stage sphalerites differed from their predecessors in several ways: (1) a general lack of fibrous crystals and millimetre laminations in cements; (2) enrichment in cadmium; and (3) 6 to 10 per mil depletion of $\delta^{34}S$ relative to tan-brown sphalerites. The crystallization of late sphalerites occured in two phases: (1) Yellow-brown sphalerite nucleated at a moderate rate as fine to coarse crystals within dolostones and along vein and pore walls. (2) Yellow-black sphalerite then precipitated slowly as coarse, prismatic crystals from cooling fluids (decrease in the T_h from 135°C to 115°C) as ^{34}S was depleted in the source. The crystallization of the generally yellow crystals was punctuated by growth zones with dark (hydrocarbon-rich?) impurities. These sector zones accumulated during temporary periods of rapid crystal growth (Hollister, 1970; Dowty, 1976). In general, the

end of mineralization in both early and late sulphide sequences was marked by crystallization of coarse prismatic cements in pores.

Marcasite, coarse galena and euhedral red sphalerites crystallized in vugs and cavities along with sulphates after post-ore saddle dolomites. These late crystals with depleted $\delta^{34}S$ precipitated from H_2S with a high $^{32}S/^{34}S$ ratio, which could have resulted from (1) long term accumulation of $H_2{}^{32}S$ relative to $H_2{}^{34}S$ due to reaction kinetics, and/or (2) depletion of fluid ^{34}S during oxidation and sulphate crystallization.

Lead isotopes give some clues to the source of metals and configuration of pathways of metal-bearing fluids. Fluids with the $\delta^{34}S$ seawater signature of the Lower Paleozoic sediments migrated into the basement or overlying arkoses where they leached high thorogenic, low uranogenic lead from feldspars of the high grade metamorphic terrane. These fluids recirculated up section and in the process acquired radiogenic lead from leached sediments and/or formation fluids. The rising fluids deposited leads which linearly increase in radiogenic content with greater stratigraphic height (Swinden et al., 1988).

VOLUME II

PART IV

EARLY DOLOSTONES AND BRECCIAS

INTRODUCTION TO PART IV

Part IV describes the composition, geometry, origin and relative time of formation of the various dolostones and breccias that pre-date the epigenetic dolomites and sulphides. The rock bodies that characterize the early dolostones and breccias are separated into three main groups: (1) microcrystalline "syngenetic" dolostones; (2) rock-matrix breccias; and (3) early burial dolostones (Fig. 7.1). Figure 1.6 displays their relative timing. Microcrystalline dolostones form the extensive, stratabound peritidal beds typical of the Aguathuna Formation. They developed near the surface prior to incorporation into conglomerates and karst breccias. Rock-matrix breccias originated during subsurface karstification when caves formed along growth faults metres to more than 200 m below the surface. The crystallization of early burial dolostones spanned the time of progressive burial and initiation of pressure solution when dolomite nucleii accreted zoned rims. This process completed dolomitization of microcrystalline beds, converted rock-matrix breccias into dolostone bodies and formed mottles and beds in limestone formations (Catoche and Table Point). This framework of sealed, brittle dolostone bodies constrained the later position and development of epigenetic dolostones and sulphides. The terminology used in this description is compared and related to the classification of Haywick (1984) in Table 7.1.

Figure 7.1 Cross-section of Dolostone Bodies

A cross-section across the L Zone ore body and the Trout Lake rock-matrix breccia illustrates the configuration of the various dolostone bodies that comprise the dolostone complexes of the upper St. George Group. (1) Early fine dolostones are stratigraphic bodies forming most of the Aguathuna Formation. (2) Fine rock-matrix breccias are both localized stratabound and discordant forms. Early burial dolostones consist of (a) a medium crystalline overprint of the fine dolostones and breccias, (b) ubiquitous mottles and beds in the limestone formations and (c) bodies of discordant dolostones (3) along fracture zones and margins of rock-matrix breccias. Epigenetic dolostone bodies include stratabound pseudobreccias (4) and coarse sparry dolostones (5) and discordant, late fault-related dolostones (6).

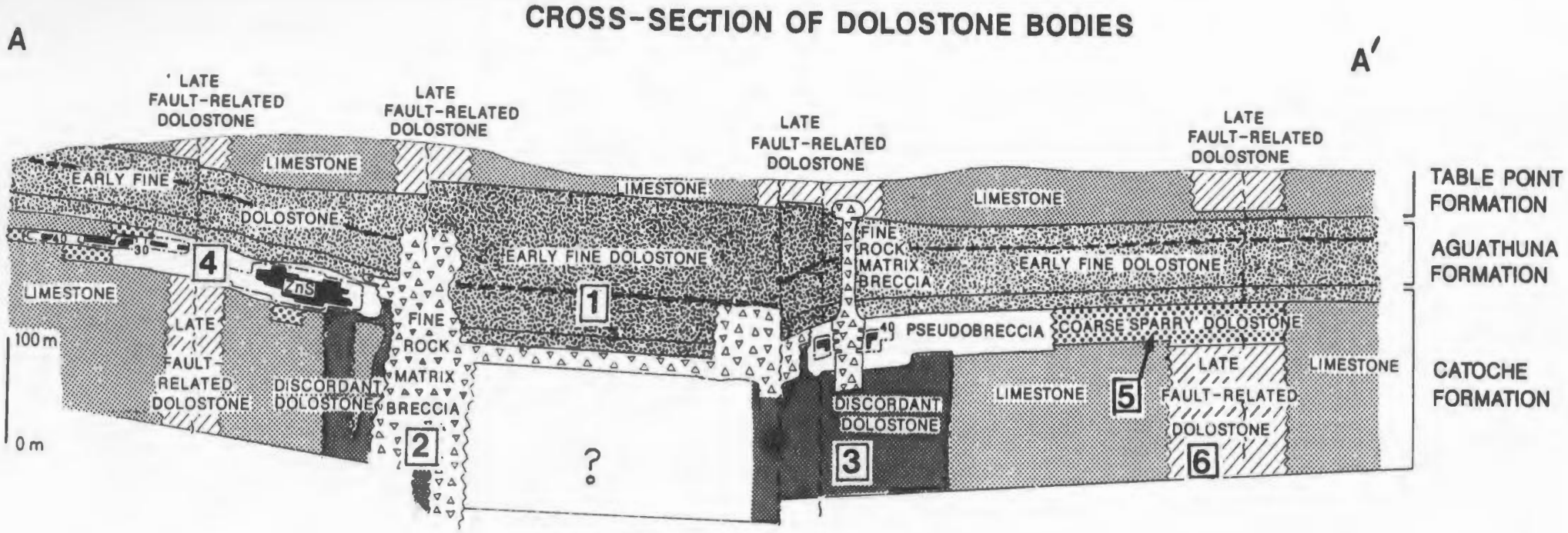
CROSS-SECTION OF DOLOSTONE BODIES
A
A′
LATE FAULT-RELATED DOLOSTONE
LATE FAULT-RELATED DOLOSTONE
LATE FAULT-RELATED DOLOSTONE
LATE FAULT-RELATED DOLOSTONE
LIMESTONE
LIMESTONE
LIMESTONE
EARLY FINE DOLOSTONE
EARLY FINE DOLOSTONE
FINE ROCK MATRIX BRECCIA
PSEUDOBRECCIA
COARSE SPARRY DOLOSTONE
LIMESTONE
LIMESTONE
LATE FAULT-RELATED DOLOSTONE
DISCORDANT DOLOSTONE
DISCORDANT DOLOSTONE
FINE ROCK MATRIX BRECCIA
LATE FAULT-RELATED DOLOSTONE
LIMESTONE
40
30
40
ns
100 m
0 m
?
1
2
3
4
5
6
TABLE POINT FORMATION
AGUATHUNA FORMATION
CATOCHE FORMATION

TABLE 7.1

COMPARISON OF DOLOMITE AND DOLOSTONE TYPES WITH CLASSIFICATION OF HAYWICK (1984)

DOLOSTONE CLASSIFICATION HAYWICK, 1984	DISTRIBUTION	DOLOMITE TYPE, THIS STUDY	DOLOSTONE TYPES, THIS STUDY
1. DOLOLAMINITES	VERY FINE CRYSTALLINE; AGUATHUNA FORMATION	I AND MINOR II, III	EARLY FINE DOLOSTONE
2. MATRIX DOLOMITE	DISSEMINATED TO CLUSTERED CRYSTALS IN LIMESTONES	II	EARLY BURIAL DOLOSTONE - ONLY DOLOMITE NUCLEII IN LIMESTONE
3. MOTTLE DOLOMITE	MOTTLES IN LIMESTONES	II AND III	EARLY BURIAL DOLOSTONE - SELECTIVE REPLACEMENT OF BURROWS, MICRITIC MOTTLES
4. PERVASIVE A DOLOSTONE	FINE CRYSTALLINE DOLOSTONE SELECTIVELY REPLACES MUDSTONE AND WACKESTONE BEDS	I, II, III or II, III	EARLY FINE DOLOSTONE OR LATER BURIAL DOLOSTONE BEDS IN LIMESTONES OR COARSE DOLOSTONES
5. PERVASIVE B DOLOSTONE	COARSE MATRIX DOLOSTONE OR COARSE SPARRY DOLOSTONE	IV V	PRE-ORE AND POST-ORE EPIGENETIC DOLOSTONES REPLACE LIME GRAINSTONE/ WACKESTONE MATRIX
6. CAVITY-FILLING	VERY FINE DOLOSTONE IN CAVITIES IN A AND B DOLOSTONES (RARE)	II/III – V	EQUIVALENT TO EPIGENETIC GEOPETAL DOLOMITES (GENERALLY COARSE CRYSTALLINE)
7. SADDLE DOLOMITE	PSEUDOBRECCIA, SPAR BRECCIA VEINS	VI, VII	POST-ORE EPIGENETIC DOLOSTONE FILLS PORES AND REPLACES PRECURSOR DOLOSTONES

CHAPTER 7 EARLY FINE DOLOSTONES AND ROCK-MATRIX BRECCIAS

7.1 Introduction

This chapter describes and interprets dolostone bodies formed at or near the surface (Fig. 1.6). These include (1) the microcrystalline dolostones characteristic of hypersaline lagoon and tidal flat settings and (2) dolomitized rock-matrix breccias associated with subsurface karst.

7.2 Early Fine Dolostone

Early fine or syngenetic dolostones, comprised of microcrystalline Dolomite I with enriched $\delta^{18}O$, selectively replace mudstone beds in the Aguathuna and upper Catoche Formations. The crystal characteristics are described in Chapter 5, section 5.3. The euhedral crystals replace and overprint peloids and other primary textures and structures. These dolomitized mudstones include beds of supratidal dololaminite to subtidal, massive or burrowed mudstones and comprise the mud matrix of some subsurface rock-matrix breccias. This type of dolostone makes up most of the Aguathuna Formation, and occurs as distinct 0.5 to 1 m thick beds between otherwise grainy limestones in the upper Catoche Formation. These stratigraphic dolostones are more pervasive along the northwest coast of Newfoundland than to the south and east (Haywick, 1984).

A variety of features, discussed in Chapter 5, demonstrate that the dolostones formed at or near the surface. The most important criteria are the occurrence of the dolostones as intraclasts directly

above the St. George Unconformity and their incorporation in rock-matrix breccias.

Interpretation - Syngenetic dolomites generally crystallized at or just beneath the surface as indicated by fragments incorporated in intraformational conglomerates and rock-matrix breccias. The dolomitization extensively affected supratidal Aguathuna lithologies similar to sabkhas (cf. Patterson, 1972), but also extended into subtidal mudstones, subsurface rock-matrix breccias and along faults to depths of 200m. The replacement nature of the syngenetic dolostones is unlike dolostones beneath Neogene sabkhas which are composed of precipitated microdolomites (Von der Borch and Jones, 1976; Patterson and Kinsman, 1982). Present models for similar replacement dolostones suggest long term alteration ($\geq 10^4$ yr?) in the near-surface platform under the influence of stable ground water-flow systems (Sass and Katz, 1982; Simms, 1984; Machel and Mountjoy, 1986; Hardie, 1987). Northeast-trending fracture systems and a regionally elevated platform probably controlled the distribution and movement of these dolomitizing fluids.

Evaporation on the elevated platform probably accounted for the extensive supratidal dolostones and the enriched $\delta^{18}O$ values of the dolomites. Alternatively, kinetic and equilibrium effects caused ^{18}O concentration in dolomites (Clayton et al., 1968). The general absence of dolomites in peritidal deposits of the Spring Inlet Member suggests that evaporation on Aguathuna flats played an important role in dolomitization by increasing Mg/Ca and CO_3/Ca ratios in hypersaline ground waters. Sea water (and meteoric water?) circulating beneath the

platform along regional fractures probably caused replacement dolomitization over extended time periods (Sass and Katz, 1982; Bein and Land, 1983; Simms, 1984; Hardie, 1987). At the time of the unconformity fresh water dilution of sea water also could have caused dolomitization as it increased Mg/Ca and CO_3 ratios (Land, 1983).

7.3 Fine Rock-Matrix Breccias

7.3.1 Definition

The term "fine rock-matrix breccia" is defined and applied to breccias of the Lower Ordovician Knox Group of East and Central Tennessee, which possess fragments of angular, microcrystalline dolostone and chert in a matrix of finely crystalline, gray to green to red dolomite and minor silica and clay minerals (Kendall, 1960; Hoagland et al., 1965; Kyle, 1976, 1983). Mussman and Read (1986) refer to these bodies as intraformational breccias. At Daniel's Harbour, similar breccias with angular fragments of early fine dolostone have an altered matrix of euhedral, very fine- to medium-sized crystals of Dolomites I, II and III. The breccias (Figs. 4.6, 7.1, 7.2) occur locally in the St. George Group and lowermost Table Point Formation in bodies of varying shapes: (1) large stratabound complexes within the upper Catoche Formation which are circular to oval in outline and extend up to 400 m in width by 1000 m in length (Fig. 1.4); (2) discordant, linear bodies which occur within the stratabound complexes and penetrate vertically more than 200 m (Figs. 4.6, 7.1, 7.2); (3) small stratabound bodies, tens of metres in diameter that occur outside the large complexes; and

Figure 7.2 Distribution of the five breccia types across an ore zone, a large composite rock-matrix breccia and a chimney breccia.

Intrastratal rock-matrix breccias (Bx 1) occur extensively in the Aguathuna Formation.

Local composite bodies of rock-matrix breccia include stratabound oligomict bodies (Bx 2) in the upper Catoche Formation and discordant polymict bodies (Bx 3) along faults. These complexes are characterized by stratigraphic collapse of the upper St. George Group and sediment-filled dolines described in Chapter 4.

Chimney breccias outside major bodies exhibit minor collapse and affect the lower Table Point Formation.

Spar breccias (Bx 4) and pseudobreccias (Bx 5) with saddle dolomite occur in the upper Catoche Formation peripheral to the rock-matrix breccias.

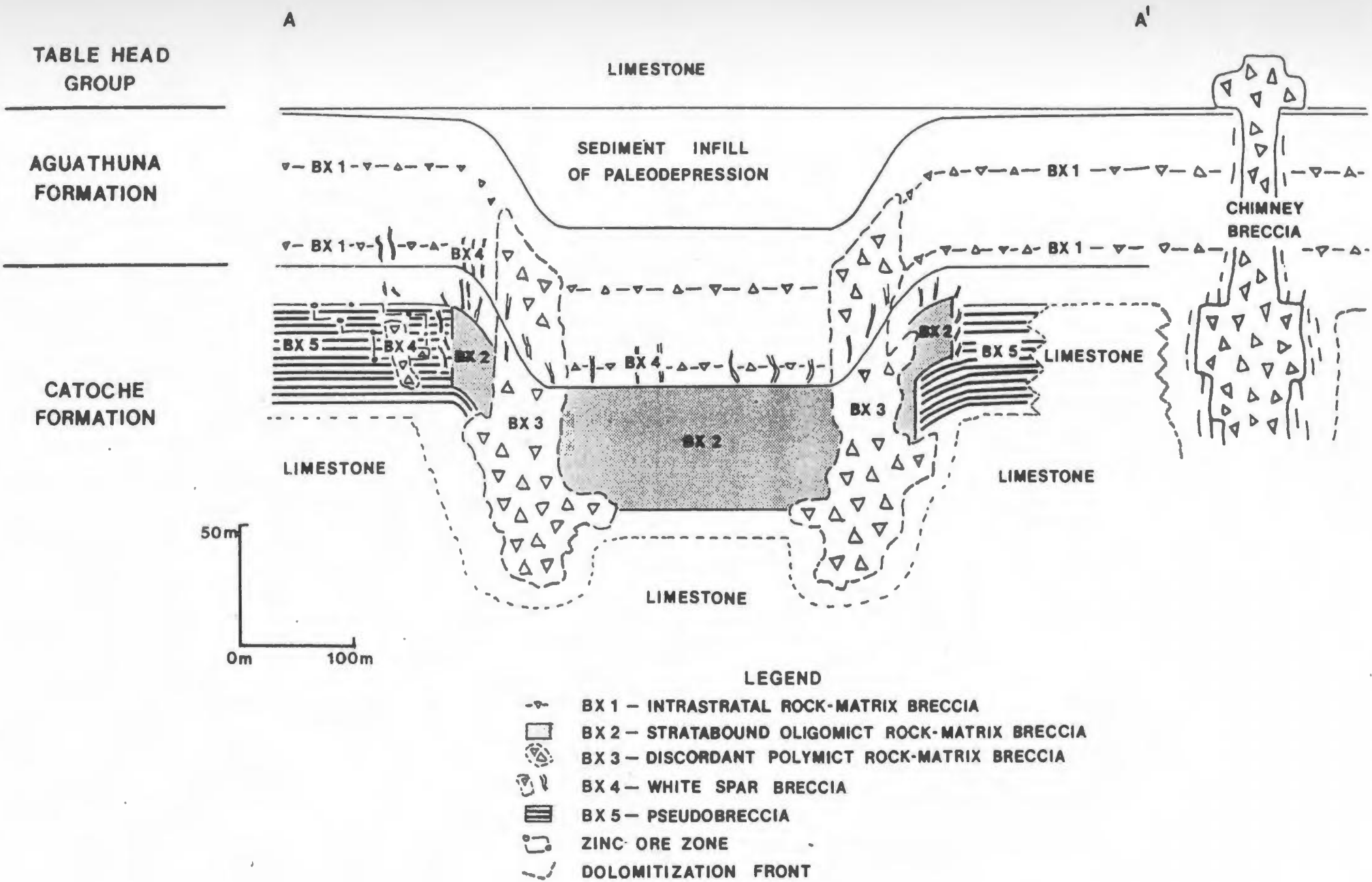
A
A'
TABLE HEAD GROUP
AGUATHUNA FORMATION
CATOCHE FORMATION
LIMESTONE
SEDIMENT INFILL OF PALEODEPRESSION
BX 1
BX 2
BX 3
BX 4
BX 5
CHIMNEY BRECCIA
LIMESTONE
LIMESTONE
LIMESTONE
LIMESTONE
50m
0m
100m
LEGEND
BX 1 — INTRASTRATAL ROCK-MATRIX BRECCIA
BX 2 — STRATABOUND OLIGOMICT ROCK-MATRIX BRECCIA
BX 3 — DISCORDANT POLYMICT ROCK-MATRIX BRECCIA
BX 4 — WHITE SPAR BRECCIA
BX 5 — PSEUDOBRECCIA
ZINC ORE ZONE
DOLOMITIZATION FRONT

(4) distinctive chimney breccias that cut both the upper St. George Group and the lower Table Point Formation (Figs. 7.1, 7.2).

Several lines of evidence suggest that most of the fine rock-matrix breccias at Daniel's Harbour are related to dissolution and deformation of strata below the contemporaneous St. George Unconformity. (1) The breccia bodies are situated below faulted depressions and dolines (sinkholes) which have been filled and levelled by the middle and upper members of the Aguathuna Formation as described in Chapter 4 (Figs. 4.1, 4.6). The recognition of the stratigraphy constrains the development of the breccias.(2) Measurements of stratigraphic thickness between the "worms" and chert marker beds in the Catoche Formation indicate that brecciated strata have been thinned to one-third of original thickness (Fig. 7.3). (3) This stratigraphic thinning is restricted to limestone beds in the upper Catoche Formation. Thin argillaceous residues and concentrated silica nodules are the remnants of these partially or totally dissolved beds (Fig. 7.3; Pl. 7.1). (4) Fragments of the Aguathuna Formation are displaced up to 120 m below normal stratigraphic position (Fig. 7.3). (5) Mud-supported rubble breccias fill former dissolution cavities in the Catoche Formation. One exposure of the wall of one paleocave reveals that corrosive dissolution produced an irregular, scalloped surface (Pl. 7.1b,d). The lack of dripstone or flowstones suggest that the cave was never part of an open, vadose network. (7) The interplay of normal faulting, fracturing and dissolution is apparent from their spatial relationship, displaced breccia stratigraphy, linear and graben geometry of structural depressions and abundant collapse-breccia infilling of cavern systems along

Figure 7.3 A profile of fine rock-matrix breccias that shows the geometry of the various types of rock-matrix breccia bodies reconstructed from drill core. The cross-section between drill holes is schematic. The location of the drill holes is shown on the map on the lower right.

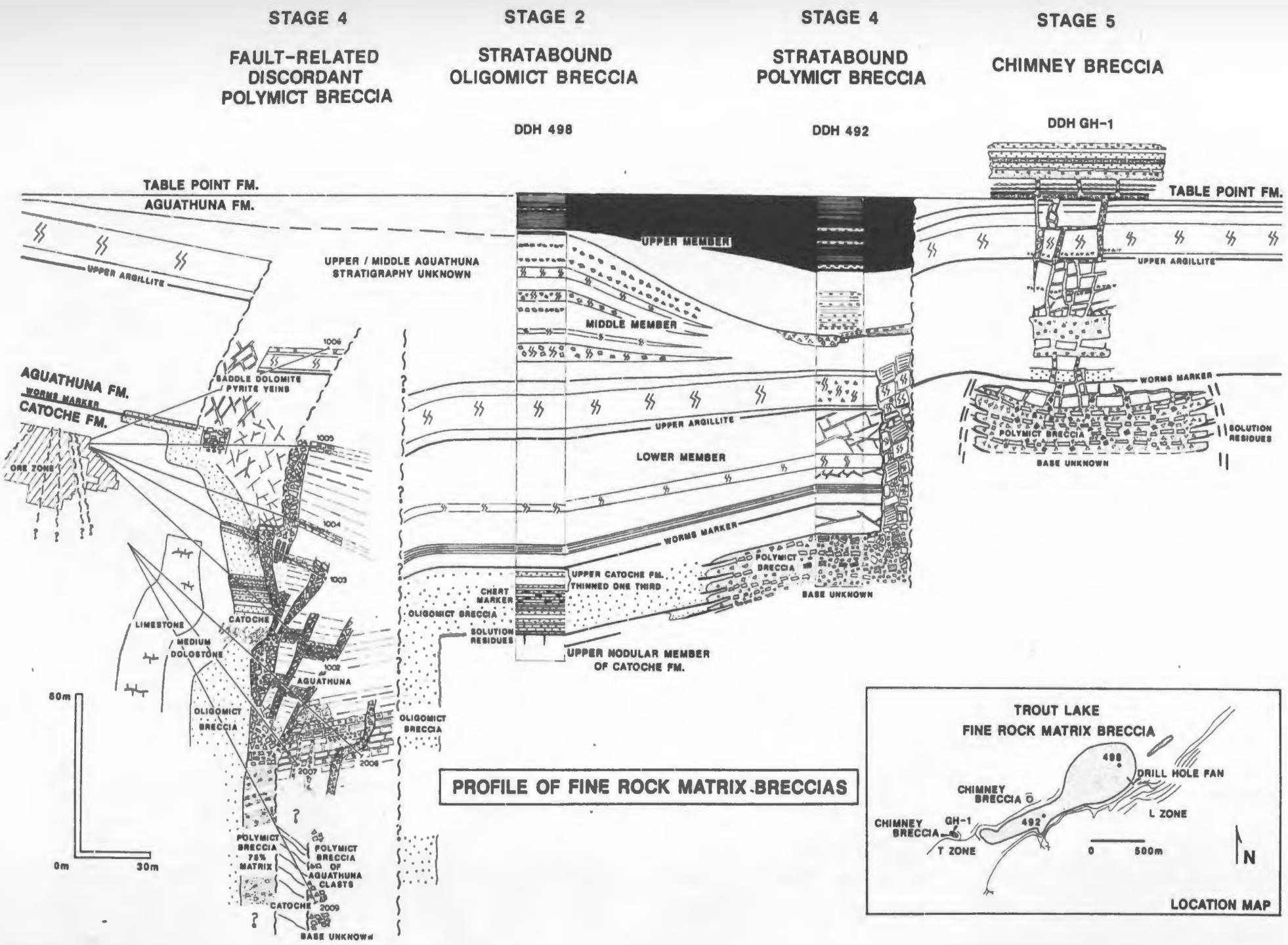
STAGE 4
FAULT-RELATED DISCORDANT POLYMICT BRECCIA
STAGE 2
STRATABOUND OLIGOMICT BRECCIA
STAGE 4
STRATABOUND POLYMICT BRECCIA
STAGE 5
CHIMNEY BRECCIA
DDH 498
DDH 492
DDH GH-1
TABLE POINT FM.
AGUATHUNA FM.
UPPER ARGILLITE
UPPER / MIDDLE AGUATHUNA STRATIGRAPHY UNKNOWN
UPPER MEMBER
MIDDLE MEMBER
LOWER MEMBER
WORMS MARKER
CATOCHE FM.
ORE ZONE
SADDLE DOLOMITE PYRITE VEINS
1006
1005
1004
1003
1002
1001
LIMESTONE / MEDIUM DOLOSTONE
CATOCHE
AGUATHUNA
OLIGOMICT BRECCIA
2007
2008
2009
POLYMICT BRECCIA 75% MATRIX
POLYMICT BRECCIA OF AGUATHUNA CLASTS
BASE UNKNOWN
UPPER CATOCHE FM. THINNED ONE THIRD
CHERT MARKER
SOLUTION RESIDUES
POLYMICT BRECCIA
UPPER NODULAR MEMBER OF CATOCHE FM.
SOLUTION RESIDUES
60m
0m
30m
PROFILE OF FINE ROCK MATRIX BRECCIAS
TROUT LAKE
FINE ROCK MATRIX BRECCIA
498
DRILL HOLE FAN
CHIMNEY BRECCIA
GH-1
492
L ZONE
T ZONE
0
500m
N
LOCATION MAP

Plate 7.1 Underground Exposures of a Polymict Rock-Matrix Breccia

The lower portion of a chimney breccia was cross-cut by an underground drift in the T Zone (Fig. 1.4). The geometry of this breccia body is reconstructed in Figure 7.3 from a central drill hole and horizontal underground workings.

a,c. A polymict breccia in the centre of the body fills a former cavity where Catoche limestone was removed. Light gray fragments (5 to 20 cm in diameter) of the Aguathuna Formation and medium-gray blocks (20 to 100 cm in diameter) of early fine Catoche dolostone, are surrounded by gray rock matrix and by gypsum-cemented fractures. The field book is 20 cm long.

b,d. Pseudobreccia beds on the right in abrupt contact with a rock-matrix breccia on the left. An early fine dolostone bed collapses in the breccia where dissolution of former limestone beds has left only thin, laminated beds of shale. These shales also fill steep extensional fractures which dip outward from the breccia. The field book is 20 cm long.

PLATE 7.1

a
EARLY FINE DOLOSTONE
b
SOLUTION RESIDUES
PSEUDOBRECCIA
EARLY FINE DOLOSTONE BED
PSEUDOBRECCIA
c
d

fault zones (Figs. 4.6, 4.7, 7.3).

7.3.2. Petrography of Fine Rock-Matrix Breccias

Fine rock matrix breccias are complexes of multiple dolomite generations: (1) Dolomite I occurs in clasts of pre-karst, fine dolostone; (2) Dolomites II and III occur in early dolomitized matrix and clasts; and (3) clear Dolomite III is ubiquitous as secondary overgrowths, replacement crystals and pore cements (Pls. 5.4a, 7.2d). In addition, epigenetic dolomites IV and V partly replace the fringes of breccia bodies. The breccia complexes can be subdivided into several generations based on the following characteristics: (1) the oligomictic or polymictic composition of clast lithologies; (2) crystal size and type of dolomite(s) that replace matrix and clasts; (3) the abundance of intercrystalline, insoluble residues and stylolites; and (4) the relationships of breccia bodies to stratigraphy and structure.

The fine rock-matrix breccias can be classified into two general lithological types, fine-crystalline polymict breccias and medium-crystalline oligomict breccias (Fig. 7.2, Pl. 7.2).

Typical **polymict breccias** contain angular fragments of four to five lithologies of very finely crystalline, pre-karst dolostone, finely crystalline secondary dolostone and chert. Where the rock is a breccia of Aguathuna fragments assembled in a mosaic of clasts that show *in situ* disruption, its composition may be oligomict or monomict. Fragment size varies from 1 mm to 1 m diameter, but is commonly bimodal with 1 cm to 1 m diameter fragments surrounded by 1 to 5 mm clasts and matrix (Pl. 7.2b,c,g,h). The abundance of matrix varies within and between breccia

Plate 7.2 Petrography of Rock-Matrix Breccias

a. Oligomict breccia, Catoche Formation. Medium-crystalline clasts and matrix that are cut by fractures filled with clear Dolomite III and gypsum cement (G). Stylolites (S) and black solution residues (R) are abundant. Mike Lake Breccia, DDH 66, 132 m (Fig. 1.4). Scale is 1 cm.

b. Polymict breccia, Catoche Formation. Light-gray fragments from the Aguathuna Formation (A) are supported by a matrix of medium-crystalline (100 μm) dolomite and millimetre-sized dolostone fragments. Mike Lake Breccia, DDH 66, 90 m (Fig. 1.4). Scale is 1 cm.

c. Polymict breccia, Aguathuna Formation. A light gray, very finely crystalline (Dolomite I) matrix surrounds dark and light fragments of the Aguathuna Formation. From discordant breccia north of the L Zone, underground angle hole, DDH 1003, 120 m (Fig. 7.3). Scale is 1 cm.

d. Oligomict breccia, Catoche Formation. Zoned dolomite (II and III) crystals which overprint the breccia vary in size from 100 μm in fragments (F) to 300 μm rhombs with thick, clear rims (III) that replace matrix (M). Mike Lake Breccia, same sample as Pl. 7.2a. Scale is 100 μm.

PLATE 7.2

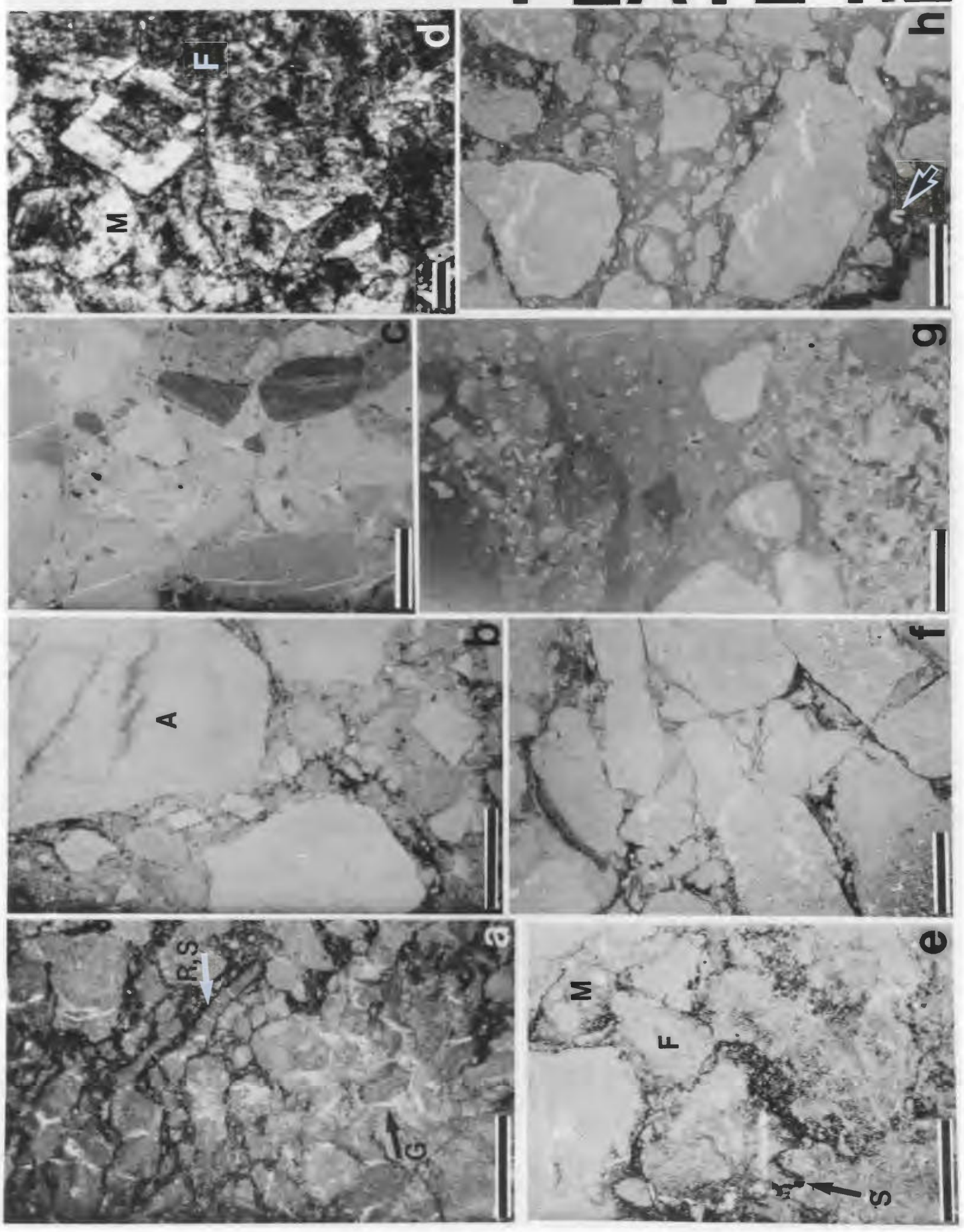

e. Oligomict breccia, Catoche Formation. Mostly of fragments (F) that are indistinguishable from matrix (M) after pervasive dolomitization (Dolomites II and III). Stylolites (S) are common. South margin of the Trout Lake Breccia, DDH 1236, 188m (sout of DDH 492 in Fig. 7.3). Scale = 1 cm.

f. Monomict breccia, Table Point Formation. Lithified parts of former nodular limestone beds which are dolomitized, broken and rotated. Chimney breccia adjacent to the North L Zone(Fig. 1.4), DDH 2377, 112 m. Scale is 1 cm.

g. A matrix-supported polymict breccia which contains rafts of clasts within a debris flow fabric. Table Point Formation. T Zone chimney breccia, DDH GH-1, 100 m (Fig. 7.3). Scale is 1 cm.

h. Oligomict breccia, Table Point Formation. Solution-scalloped clasts are supported by a very fine dolomite matrix with some skeletal fragments (arrow). Cemented dilatant fractures in fragments. T Zone chimney breccia, DDH GH-1, 150 m (Fig. 7.3). Scale is 1 cm.

bodies, but breccias commonly are matrix-supported. The matrix is composed of microcrystalline to very fine (10 to 50 μm) rhombs of non-luminescent Dolomite I, blue CL Dolomite II and zoned CL Dolomite III with minor intercrystalline residues. In places, medium (50 to 200 μm) crystals with turbid Dolomite II cores and clear Dolomite III rims comprise the entire matrix. In most cases, however, vug and fracture fillings of Dolomite III cross-cut a finely crystalline, Dolomite I-II type matrix (Pl. 7.2c).

Medium-crystalline **oligomict breccias**, in contrast, contain small 1 to 12 mm-sized, subrounded fragments which are altered, like the matrix, by fine- to medium-sized composite crystals of Dolomites II and III (Pl. 7.2a,e). These breccias occur in only the Catoche and Table Point Formations. The fragments include one to four locally-derived lithologies: (1) dolomitized limestone clasts; (2) dolostone mottles; (3) clasts of early fine dolostone; and (4) chert. Foreign fragments from the Aguathuna Formation are generally absent. Zoned, euhedral, dolomite rhombs overprint most clasts and matrix and overlap their boundaries (Pl. 7.2 d,e). Dolomites II and III form medium (100 to 300 μm) crystals with turbid cores (II) and thick clear rims (III) in matrix, fractures and pores. Fine (50 to 100 μm) crystals which replace fragments have only thin clear rims (III) developed on ferroan to bright CL calcic cores (II). The calcic cores suggest an original limestone precursor. Abundant dark intercrystalline material in the matrix gives the breccia a dark gray to black colour. Quartz silt content increases to 6 to 10 weight % toward the base of breccia bodies, where 1 to 3 cm-thick shale layers of black residuals are common (Fig. 7.3). Abundant

stylolites separate fragments and patches of medium-crystalline matrix. Stylolites are also common in clast-supported, polymict breccias.

The petrographic differences between the two breccia types indicate distinct origins. The medium-crystalline, oligomict breccia originated by partial dissolution of limestone and condensation of the stratigraphy with minor cave development. This process left only small rounded fragments in a residue-rich matrix, all of which was dolomitized during burial. In contrast, the polymict breccia formed from fragments of early fine dolostone which collapsed into caves in the Catoche Formation. A gravelly mud either filtered down between collapsed fragments or accumulated with clasts as mud-supported debris (Pl. 7.2g). During burial only the matrix was altered to fine- and medium- crystalline dolomite. Some of the original matrix may have been a dolomite silt and mud which filtered down from the surface (Knight, 1986).

7.3.3. Comparison With Other Breccia Types

Fine rock-matrix breccias (Pl. 7.2) differ from "tectonic" fault zone breccias and saddle dolomite-cemented "spar" breccias (Pl. 7.3; Table 7.1) (Lane, 1984). Fault zone or "tectonic" breccias are confined to narrow zones (1 to 10 cm wide) that occur at steep angles to bedding. They are composed of multiply-fractured fragments and very fine "granulated" fragments in a very finely crystalline matrix of white dolomite "rock flour" (Pl. 7.3b). Several generations of fractures and veinlets crosscut both matrix and fragments. Spar breccias which cross-cut stratigraphy are commonly arranged in mosaics of partly collapsed to

Plate 7.3 Other Breccia Types

a. Fault breccia (F) showing subvertical planes, several centimetres wide, offsets bedding. Numerous saddle dolomite veins cross-cut the surrounding rocks. West end of the T Zone (Figs. 1.4, 10.1). The length of the field book is 20 cm.

b. Microbreccia from a fault zone. Fragments are outlined by black ink lines. Typical of all fault zones. Scale is 1 cm.

c. Late spar breccias consisting of broken dark gray dolostone beds and saddle dolomite cement. Breccia fabrics include <u>in situ</u> mosaic brecciation (M) and collapsed fragments (C). Adjacent to cross-fault in the west L Zone. The scale is 2 m.

d. Early rock-matrix breccia showing its matrix (M) locally replaced by saddle dolomite. Some of the saddle dolomite fills late veins (V) and megapores (P). Where L Zone intersects Trout Lake rock-matrix breccia at a cross-fault in the west L Zone (Figs. 1.4, 7.3). The scale is 1 m.

PLATE 7.3

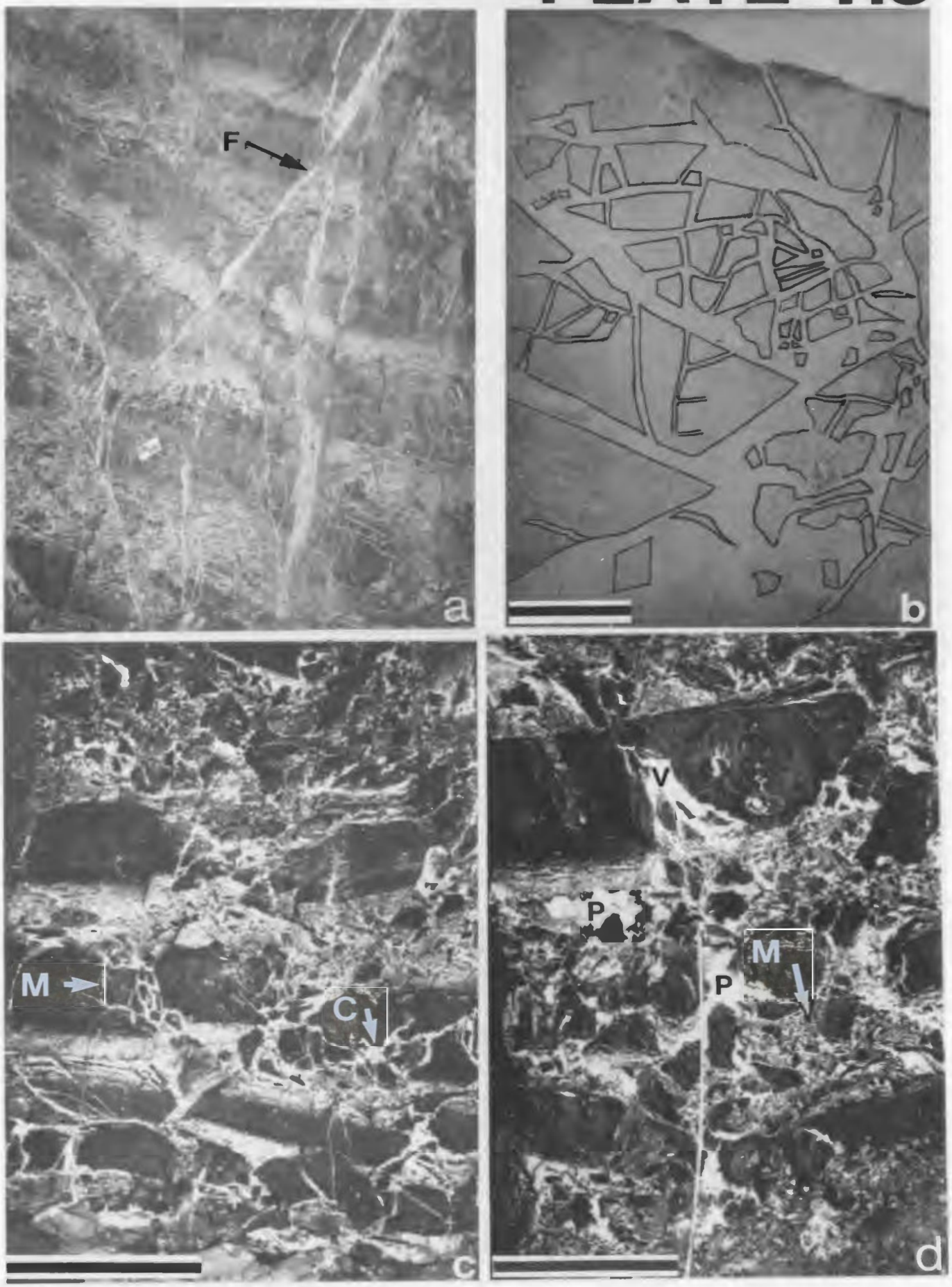

TABLE 7.2

BRECCIA TYPES

TYPE	VARIETY OF FRAGMENTS	FRAGMENT SIZE	SHAPE AND CRYSTAL SIZE	MATRIX	DISTRIBUTION
Fine Rock-Matrix					
Oligomict	2-3	1-3 cm	Rounded, medium crystalline (II,III)	Medium crystalline (II,III)	Stratabound in limestones
Polymict	4-7	1 cm - 1 m	Angular, very fine crystalline (I)	Fine (I) to medium crystalline (II, III)	Discordant, "Cave Filling"
Fault Zone	1-2	1 mm-1 cm	Angular	White rock flour	1 to 10 cm wide along faults
Spar Breccia	1-2	up to 1 m	Angular	Megacrystalline saddle dolomite	Discordant, along veins and faults
Pseudobreccia	1	mm - cm	Irregular, aggradational replacement	Medium to mega-crystalline saddle dolomite	Stratabound over 1000's of metres

uncollapsed, angular fragments "supported" by white saddle dolomite (Pl. 7.3c,d). The saddle dolomite in these breccias occurs as a pore-filling cement between fragments. In contrast, stratabound pseudobreccias contain abundant white saddle dolomite which both cements networks of solution pores and partially replaces gray dolostone. The remaining patches of gray dolostone leave a breccia-like fabric (Pl. 5.5a). The saddle and "white rock flour" dolomites are younger "deep" burial dolomites (V and VI) compared to Dolomites I,II and III which comprise the rock-matrix breccias. The relative timing of the dolomites is analyzed in Chapter 5 and the temporal relationships of dolomites and breccia types is graphically presented in Figure 1.6.

7.3.4 Types of Breccia Bodies

Four types of fine rock-matrix breccia bodies occur in the mine area (Table 7.2). A complex history of several events of brecciation and faulting during near-surface karstification generated overlapping relationships between these various types (Figs. 1.6, 7.2).

1) Intrastratal Breccias - Intrastratal breccias, 10 to 30 cm thick, occur as regionally extensive stratabound layers that represent disconformities in the Aguathuna Formation (see Chapter 4 for details). By coincidence, however, they may form part of breccia complexes. In addition, they are also locally overprinted by collapsed dolostones associated with sagging of overlying beds above the disconformity surface (Fig. 4.4).

The breccia matrix has undergone several episodes of dolomitiza-

TABLE 7.3

BODY TYPES OF ROCK-MATRIX BRECCIA

BODY TYPE	GEOMETRY	COMPOSITION	STRATIGRAPHY	INTERPRETATION
Intrastratal	Extensive intraformational bed (10-50 cm thick)	monomict to oligomict	Aguathuna Formation; shale-conglomerate evaporite-horizons	widespread dissolution of conglomerate-evaporite beds; unrelated to other bodies
Stratabound Oligomict	Stratabound, 1-30 m thick; 10 to 1000 m^2; elliptical area	oligomict with local polymict bodies	upper Catoche Formation; geometrically related to sedimentation of the middle Aguathuna member	subsidence doline caused by early widespread and incomplete dissolution of the upper Catoche Formation
Discordant Polymict	Narrow (3-40 m wide); up to 200 m deep; elongate along faults	polymict including large blocks; halo of oligomict	along faults; related to sinkholes filled with the Upper Aguathuna Formation	collapse doline indicated by cave formation along faults beneath the St. George Unconformity, followed by collapse
Chimney Breccia	Cylindrical; 50-80 m diameter up to 200 m deep	generally polymict to locally oligomict	cuts upper St. George Group and the lower Table Point Formation	dissolution along fractures formed local deep caves beneath Table Point platform

tion. Dolomite I commonly forms the matrix which is locally cut by veinlets and pores cemented by medium-sized, composite crystals of Dolomites II and III (Pl. 5.1d). In some places these early burial dolomites replace all of the matrix. Late megaquartz locally replaces these dolomites and minor saddle dolomite mainly fills late veins (Pl. 5.1d).

Interpretation - Intrastratal breccias are the remains of beds of shale, quartz conglomerate and evaporite which accumulated at regional inter-Aguathuna disconformities. The beds originated initially as conglomerates and breccias at erosion surfaces (Chapter 4), but later shallow subsurface waters are interpreted to have dissolved evaporites, limestones and/or carbonate mud matrix causing overlying dolostones to founder and partially collapse into solution cavities. The presence of Dolomite I matrix in these breccias suggests that collapse was early, occurring only metres below the depositional surface. This more permeable matrix was then subject to dolomitization and silicification several times during burial.

2) Stratabound Oligomict Breccias - Broad, oligomict breccias, up to 1 km^2 in areal extent, occur in the upper 10 to 60 m of the Catoche Formation (Figs. 1.4, 4.6, 7.2, 7.3). The bodies are oval to circular in plan and elongated along northeast-trending faults (Fig. 1.4). The breccias coincide with structural depressions, but extend over 100 m beyond the margins, where they are displaced along faults that bound the depressions (Fig. 4.6, 7.2). Brecciation, in these marginal areas, is commonly restricted to the upper 10 to 15 m of the Catoche Formation.

The lower member of the Aguathuna Formation above the breccias is fractured in its lower 10 to 20 m but is otherwise relatively undisturbed even though it settled or sagged to form structural depressions which were filled by the middle member of the Aguathuna Formation. The middle member gradually thickens from 5 to 25 m over the margins and reaches a maximum thickness of 70 m over the centres of breccias (Figs. 4.6, 4.7). The marginal faults also offset the middle member. Small (20 to 30 m wide) oligomict breccias also occur along northeast-trending faults and are associated with minor or no structural collapse (Fig. 1.4).

Oligomict breccia is distributed through vertical sections of the upper Catoche Formation either as 10 m thick uninterrupted breccia sections or intercalated with 20 to 50 cm thick early fine dolostone beds (Fig. 7.3). In these sections the upper Catoche Formation between the "worms" marker and chert markers has commonly been thinned up to 30 % and argillaceous residues are the only remainder of limestone beds. This argillaceous material occurs in a matrix of Dolomites II and III between dolostone fragments, forms prominent layers at the base of breccia "beds" and fills fractures in underlying limestones (Pl. 7.1; Fig. 7.3).

Locally these oligomict breccias are cross-cut by polymict breccias, 4 to 10 m thick of unknown geometry (Fig. 7.3). Compositionally they range from matrix-supported breccias to upward-coarsening, clast-supported breccias.

Interpretation - The stratabound oligomict breccias formed during the deposition of the middle member of the Aguathuna Formation when

faulting, local subsidence and uplift began to affect the platform. During this time, subsurface groundwater flowed through the phreatic zone along northeast-trending fractures and into permeable, early fine dolostones. These fluids probably travelled in the subsurface from distant recharge areas in uplifted and exposed portions of the platform (cf. deep ground-water models for the Florida Peninsula, Back and Hanshaw, 1970; Kohout et al., 1977). These ground waters extensively affected the upper Catoche Formation in closed, circular to elliptical areas (up to 1 km^2) along the fracture zones. The waters probably migrated throughout these areas along networks of small fractures, pores and intercalated dolostone beds. Partially dissolved and "condensed" limestone beds collapsed into oligomict breccias of local dolostone and limestone fragments and insoluble residues. This phase of subsurface karst probably resembled the immature stage of diffuse fluid movement described by White (1969) and Ford (1988). The fluids eventually focussed along fractures, where they excavated local caves which filled with collapsed, polymict debris (cf. mature stages of White, 1969; Parizek, 1976).

One or more reasons account for the dissolution in the upper portion of the limestone Catoche Formation. Waters probably travelled through dolostone beds that were abundant within and above the upper Catoche Formation. These fluids were most corrosive where they contacted and mixed with near surface waters and mixing of the fluids caused them to become undersaturated with respect to calcium carbonate (Bogli, 1980; Ford, 1988).

The broad and gradual dissolution of the upper Catoche Formation

caused subsidence of the lower member of the Aguathuna Formation. The resulting subsidence dolines (Jennings, 1971) allowed local flooding and the deposition of the middle member of the Aguathuna Formation. The elliptical geometry of the dolines and their marginal sag imply a karst rather than structural origin.

(3) Discordant Polymict Breccias - Elongate vertical bodies of polymict breccia penetrate over 400 metres of section from the top of the Aguathuna to at least the base of the Catoche Formation (Figs. 4.6, 7.2, 7.3). They form along faults which cut earlier bodies of oligomict breccia and also displace the middle member of the Aguathuna Formation up to 50 m. The width of the bodies varies from 10 to 100 metres along strike and they can be traced laterally 500 to 2000 m. The breccias are steepsided and composed entirely of fragments of Aguathuna Formation and rock matrix. They cut surrounding 30 m-wide haloes of oligomict breccia which replace Catoche limestones (Fig. 7.3). The breccias are overlain unconformably by argillaceous limestones of the upper member of the Aguathuna Formation (Fig. 4.6).

Large breccia bodies, 50 to 100 m in width, include large blocks of the Aguathuna Formation tens of metres in diameter, but narrower, vein-like bodies, 50 to 300 cm wide, are filled with polymict clast-supported breccias (Fig. 7.3). Breccia with abundant matrix occurs in the sheltered margins of bodies (Fig. 7.3).

Interpretation - Stratigraphic and structural relationships demonstrate that these breccias post-date the stratabound oligomict types and the deposition of the middle member and were controlled by faults that

displaced both the middle member and the oligomict bodies. Initial faulting and incipient breccias may have been coeval with stratabound types,however. Where breccias stoped upwards to the surface of the St. George Unconformity they floored collapse dolines which were later filled by sediment of the upper Aguathuna Formation (refer to section 4.5). Slumped beds within these deposits suggest that collapse continued during the deposition of the upper member.

The faults which displaced the middle member facilitated ground water movement. Increasing volumes of ground water excavated narrow cavities along the faults deep into the Catoche limestones as fluid mixing and turbulence enhanced dissolution (Thraillkill, 1968; White, 1969; Bogli, 1980; Ford, 1988). Ground waters also pervaded 30 m laterally into surrounding limestones to partially disintegrate the wall rock and form haloes of oligomict breccia.

The Aguathuna Formation collapsed and filled the cavities either as large fractured and tilted blocks or as a polymict debris of small fragments. The matrix-supported polymict breccias and lack of vadose dripstones suggest subaqueous deposition in the phreatic zone. Final collapse of the Aguathuna Formation into the caves may have occurred during the St. George Unconformity when supportive ground water drained from the cavities (Knight et al., in press). This collapse along fault lines created linear sinkholes up to 50 m deep on the unconformity. These collapse dolines were filled by terrestrial muds and subtidal rhythmites of the upper member of the Aguathuna Formation as subsurface karst and faulting probably continued.

4) Chimney Breccias - Chimney-shaped breccias occur along fractures and faults outside the large breccia complexes described above. They are narrow and circular in plan with an approximate diameter of 80 m and penetrate more than 150 m of section from within or below the Catoche Formation to 20 m above the base of the Table Point Formation. The chimney breccias cut through normal Aguathuna stratigraphy that has only thin middle and upper members. These relationships suggest that the development of these breccias had no affect on Aguathuna Formation and probably post-dated deposition of the St. George Group.

The breccias possess an hourglass geometry which reflects vertical changes in their structure and composition (Fig. 7.3). In the Table Point Formation, the breccias are up to 80 m wide and include oligomict breccias (Pl. 7.2f,h), local polymict cavity fills (Pl. 7.2g) and intercalated unbroken beds. The breccias narrow to a 30 m width in the Aguathuna Formation where the stratigraphy is broken and partially collapsed, but exhibits only minor evidence of dissolution. Fragments of the Table Point Formation occur locally within this part of the section. In the Catoche Formation where the bodies broaden out again they consist of polymict breccias including large fragments of the Aguathuna Formation and broken dolostone beds of the Catoche Formation (Pl. 7.1a,c; Fig. 7.3). Limestone beds are completely removed except for abundant accumulations of black, insoluble residues in fractures and stratified layers (Pl. 7.1b,d; Fig. 7.3). The composition of these breccias is indistiguishable from earlier ones, but the abrupt cave walls suggest that a lithified and cemented wall rock resisted disintegration to oligomict breccia.

Interpretation - The chimney breccias are interpreted to have formed during deposition of the Table Point Formation when ground waters migrated through the subsurface along vertical fractures. This event may have occurred during an interval of regional exposure and deformation of the platform that occurs 20 m above the base of the Spring Inlet Member (S. Stenzel, pers. comm. 1988). Dissolution at intersections of vertical fractures removed limestones of the Catoche Formation to form cylindrical caves. The Aguathuna Formation fractured and partially collapsed to form polymict, rock-matrix breccias that filled the underlying phreatic caves. Subsurface waters entered the basal 20 m of the Table Point Formation where they locally dissolved limestone beds.

7.3.5. The History of Fine Rock-Matrix Breccias

The rock-matrix breccias in the mine area have a complex but well documented history that suggests they formed by dissolution in the phreatic mixing zone generally close to northeast-trending faults and fractures. Concurrent with tidal flat deposition of the middle member of the Aguathuna Formation the platform was dissected by northeast-trending fracture zones. Meteoric fluids (and/or other subsurface saline waters) infiltrated and migrated along these fractures, became undersaturated where they mixed with near surface waters and dissolved limestone beds in the upper Catoche Formation. This resulted in the local development of subsidence and collapse dolines along northeast-trending fracture zones.

Fracturing and subsurface karst occurred in five stages (Fig.7.4):

Stage 1 - Fracturing of the platform probably initiated during the deposition of the lower member of the Aguathuna Formation as localsubsidence and flooding of the tidal flats occurred above fracture zones (Fig. 4.1).

Stage 2 - Fractures became well developed during deposition of the middle member of the Aguathuna Formation. At this time meteoric waters migrated along fractures, pervaded the upper Catoche Formation along networks of small fractures and partially dissolved and transformed limestone beds into stratabound oligomict breccias. Progressive dissolution localized fluid movement through fractures and large pores where local stratabound caves were formed and filled with polymict breccia. Dissolution of the upper Catoche Formation in concert with growth faults caused gradual subsidence of the Aguathuna Formation and local flooding of contemporaneous tidal flats of the middle member. Tidal flat sedimentation kept pace with subsidence creating an anomalous 60 to 70 m thickness of the middle member over the subsurface breccias.

Stage 3 - During subaerial exposure of the Ordovician platform, regional faults displaced the middle member and the stratabound oligomict breccias and facilitated migration of increased volumes of meteoric water.

Stage 4 - Dissolution of limestones along faults to depths as great as 200 m excavated cavities in the Catoche Formation. Large blocks and polymict fragments from the Aguathuna Formation collapsed into these caves and left 50 m deep, linear sinkholes on the subaerial surface of the unconformity. A succession of terrestrial and subtidal

Figure 7.4 Possible chronology of events during the formation of fine rock-matrix breccias. Subsurface fracturing and karst occurred in five stages which are correlated with the deposition of coeval sedimentary formations.

Stage 1 - Increased rates of subsidence of the platform along fracture zones resulted in a thicker, more subtidal lower member of the Aguathuna Formation relative to adjacent areas.

Stage 2 - Stratabound dissolution of the upper Catoche Formation and initial faulting resulted in the formation of oligomict breccias and subsidence dolines which were gradually filled and levelled by the middle member of the Aguathuna Formation.

Stage 3 - As tectonism continued faults displaced stratabound oligomict breccias and the middle member of the Aguathuna Formation.

Stage 4 - At the time of the St. George Unconformity dissolution of limestones along faults produced deep discordant caves which filled with polymict breccias. Abrupt collapse of the Aguathuna Formation produced collapse dolines (sinkhole troughs) which were filled by shales and rhythmites of the upper member.

Stage 5 - Late narrow chimney breccias which penetrate from the lower Table Point Formation to the Catoche Formation did not affect Aguathuna sedimentation and probably developed later.

EVOLUTION OF KARST BRECCIAS

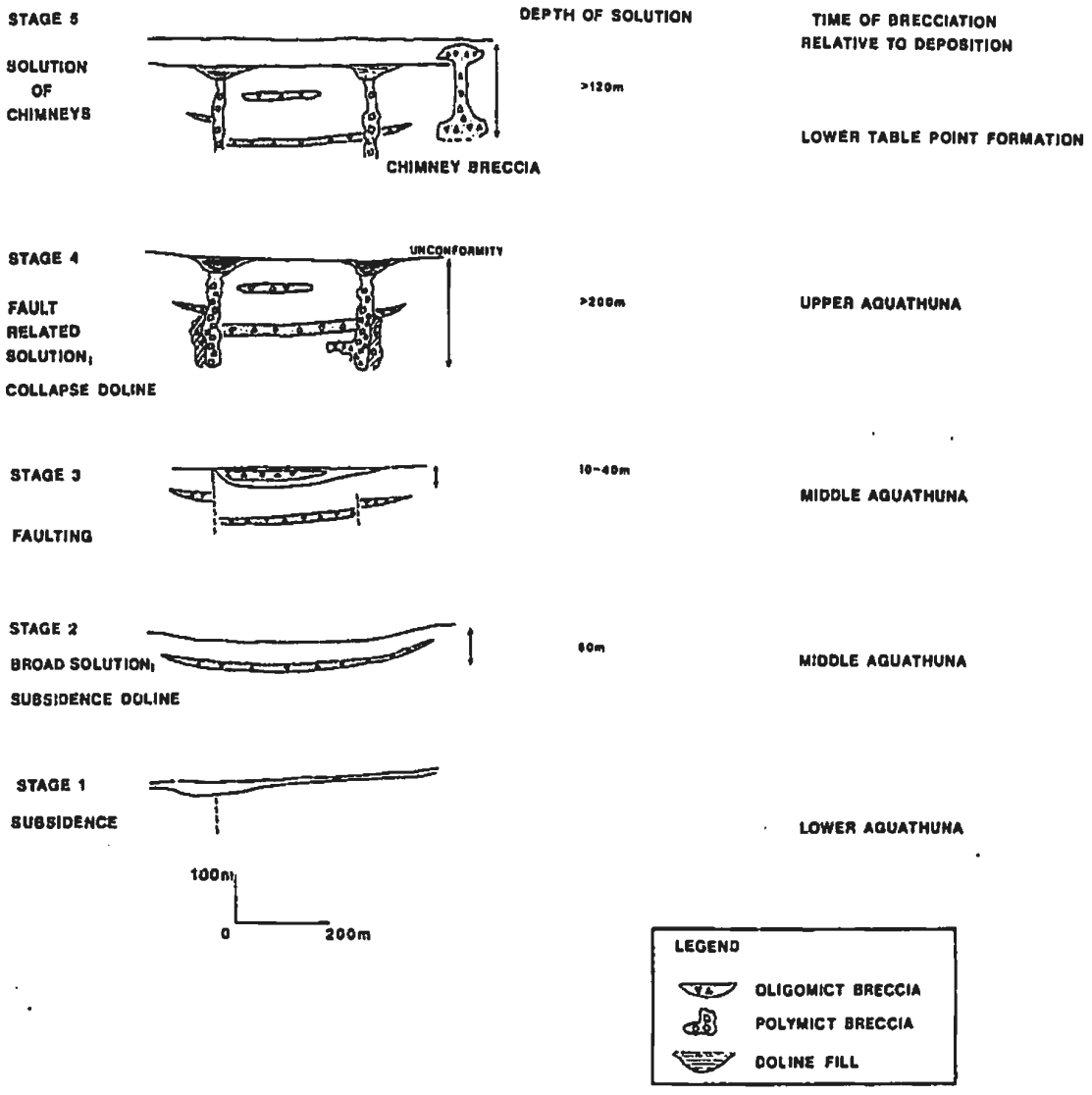

muds of the upper member of the Aguathuna Formation filled the sinkholes during late stages of faulting and solution collapse.

Stage 5 - During deposition of the Spring Inlet Member regional faulting and marine regression renewed meteoric circulation through the Catoche Formation. Chimney caves formed along the intersections of steep fractures separate from earlier breccias. Subsequently, Aguathuna dolostones fractured and partially collapsed to fill the caves with polymict rock-matrix breccia. This probably facilitated upward movement of ground waters into the lower Spring Inlet Member where furthur dissolution and brecciation took place.

In conclusion, the regional distribution of rock-matrix breccias and early fine dolostones along northeast-trending faults of northwest Newfoundland implies that a complex system of subsurface ground water movement strongly influenced karstification and dolomitization. Regional fractures served as conduits for the flow of meteoric waters which dissolved Catoche limestones adjacent to faults and more than 200 m below the surface. These meteoric (and/or formational brines) waters probably became undersaturated and particularly corrosive at mixing zones along faults and stratigraphic dolostones. Fracture conduits also may have enabled warm saline waters to circulate through the subsurface and cause early dolomitization of the matrix of discordant breccias and portions of limestone formations (cf. Florida Peninsula, Kohout et al., 1977; and the East Texas Basin, Abbot, 1975).

CHAPTER 8 - EARLY BURIAL DOLOSTONES

8.1 Introduction

The formation of early dolostone bodies was completed during initial burial to depths greater than 300m with the development of crystals of Dolomite II and III, the ubiquitous cloudy-core, clear-rim crystals which are interpreted to have grown during burial (sections 5.4, 5.5) (Fig. 1.6). This phase of dolomitization established the dolostone framework which constrained deformation and fluid movement during epigenetic events. Although many crystals nucleated early during diagenesis, their final development occurred concurrently with pressure solution at burial depths greater than 300 m. The detailed crystal petrography described in Chapter 5 demonstrates a multistage history of crystal growth. Corroded, dull CL cores of Dolomite II are partially replaced and overgrown by pink CL dolomite (Pl. 5.1b). Dolomite III forms clear-rim overgrowths on some of these crystals and pore cements with multiple layers (Pls. 5.1e; 5.4a,b).

8.2 Distribution

Evidence of early burial dolomitization is widespread in all formations. The widespread nature of these dolostones contrasts to the fault/fracture-controlled distribution of later epigenetic dolostones. The dolostones composed of these dolomites vary from massive dolostone beds to disseminated crystals in limestones (Fig. 8.1). In the Aguathuna Formation Dolomite II replaces some laminations and portions of burrowed beds (Pl. 5.1a). Ubiquitous cements of Dolomite III fill

Figure 8.1 Dolostone Evolution from
Near-surface to Burial Dolomitization

The illustration depicts the dolomitization history of lithologies of the upper St. George Group from early on the left to late on the right. Five centimetre-scale magnifications illustrate the overprinting effects of burial dolomitization. Finely crystalline dolostones, fine rock-matrix breccias and dolostone mottles within lime wackestones and packstones formed in the near-surface with the crystallization of Dolomite I and nucleii of Dolomite II. During early burial the long term growth of Dolomites II and III resulted in composite crystals, and beds and patches of medium crystalline dolostone. The crystallization history of finely crystalline beds and rock-matrix breccias virtually ended after closing of pores by Dolomite III. Epigenetic dolomitization (Dolomites IV, V, VI and VII) selectively altered limestone beds adjacent to fracture systems and cemented fractures cutting earlier dolostone bodies. During the first epigenetic event coarse matrix dolostone replaced limestones and early dolostone mottles. Ore-stage and post-ore veins and solution pores then cut pre-ore, coarse matrix dolostones (IV). After sulphide deposition, mega-crystalline saddle dolomites (V) filled pores and pervasively replaced pre-ore dolostones to form pseudobreccias. Late fault-related dolomites (VII) replaced limestones along the latest faults. Subsequent dissolution of incompletely replaced limestone left ubiquitous porosity.

DOLOSTONE EVOLUTION

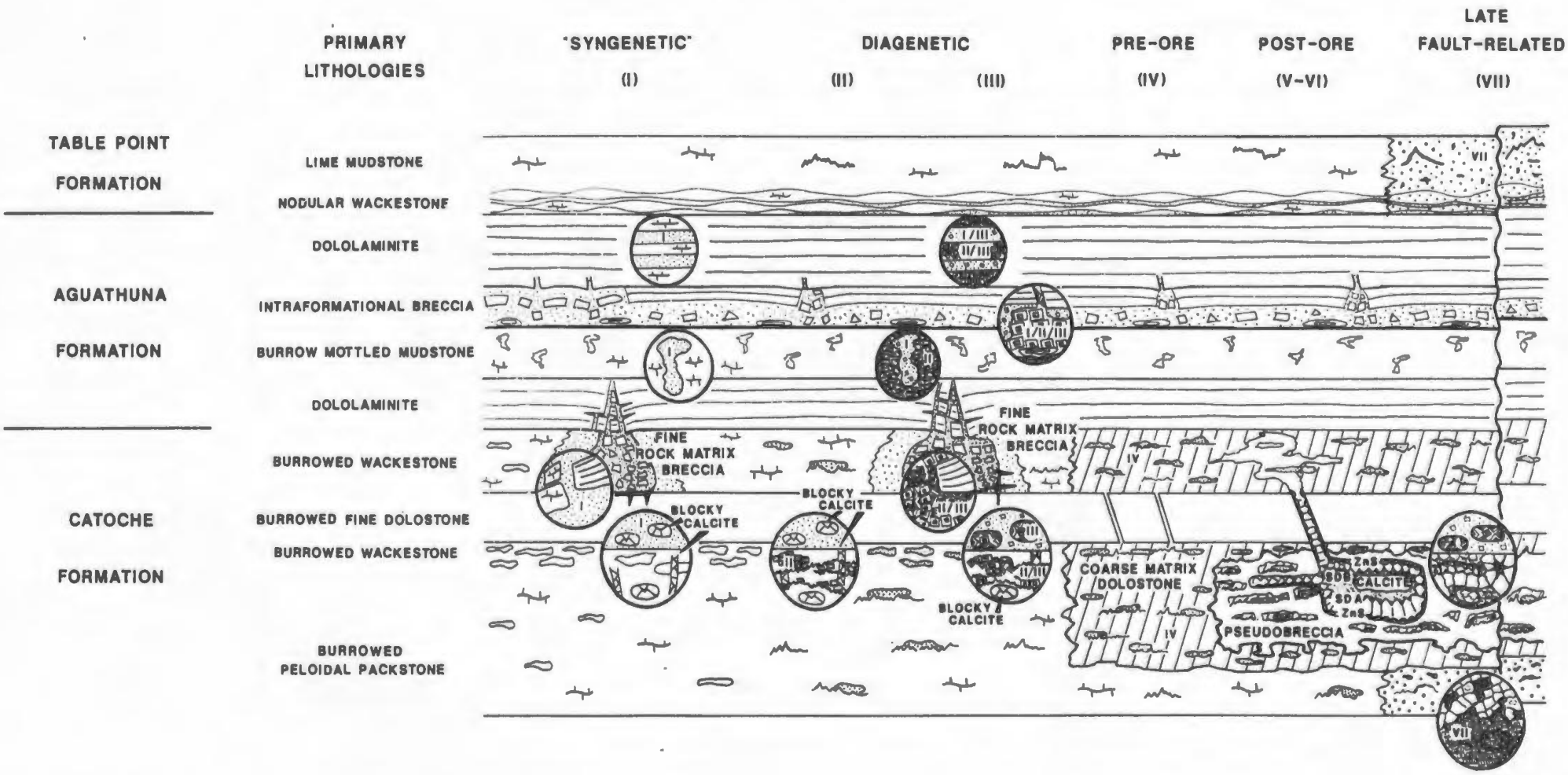

secondary pores in these dolostones (Pl. 5.1a,d,e). Composite crystals of Dolomite II and III pervasively replace rock-matrix breccias in both the Aguathuna and Catoche Formations (Pls. 5.1d; 5.4a; 12.2d). Dolomite III also cements numerous fractures which cut the breccias (Pl. 12.2a). The lack of later dolomites in these dolostone bodies indicates that Dolomite III ultimately sealed the rocks.

In the Catoche Formation Dolomites II and III occur as pore cements (mostly III) in finely crystalline dolostones (former mudstone beds) (Pl. 5.1e) and (mostly II) replace varying portions of other lithologies from entire beds of burrowed wackestone to small patches or mottles and disseminated crystals in grainstones as discussed in sections 5.4 and 5.4 (Fig. 8.1; Pl. 5.3a). Dolomite II replacement of burrows and compacted mud layers pre-dates calcite veinlets (Pls. 5.2c; 5.3a). Dolomite II also occurs along later stylolites. Cements of Dolomite III along the vertical sutures of stylolites suggest that these crystals precipitated contemporaneously with pressure solution. Dolomite III is common in dolostone beds where it cements intercrystalline pores and replaces burrow molds of coarse calcite. In the limestones it does not replace these calcite molds and its distribution is sporadic as pore-fillings in veinlets and around the margins of patches of Dolomite II.

Early burial dolomites (II and III) also form pervasive dolostone bodies in the Catoche Formation. Stratabound dolostones occur extensively in the upper 10 m of the Catoche Formation and are recognized in the mine stratigraphy as the Dark Gray Dolomites (section 3.2). Discordant bodies of dolostone locally penetrate the entire Catoche

Formation. They occur in several forms: as cylindrical or tabular bodies along faults or fracture zones or as envelopes around rock-matrix breccias (Fig. 8.2).

The distribution of Dolomites II and III imply that fluids primarily migrated along stratigraphic dolostones and vertical fracture systems. At increasing depths of burial subsurface fluids reacted with Dolomite II crystals and remnant limestone patches, causing dissolution and secondary porosity. Dolomite III cements subsequently filled these pores and significantly reduced the permeability.

8.3 Interpretation

The widespread distribution of these dolostones as mottles and beds in all limestone formations and composite additions to earlier dolostones imply that limestone formations partially or completely dolomitized during burial as a result of pressure solution, change in pore fluid chemistry with burial and/or long term exposure to formational waters. Much of the dolomitization was probably generated by waters which circulated along the same northeast-trending fractures that influenced karstification. Dolomite III-cemented fractures within the rock-matrix breccias and elongate bodies of discordant dolostone are evidence of this later fracture-controlled fluid movement (Fig. 8.2). Abundant solution features and Dolomite III cements within stratabound, fine crystalline dolostones also indicate that fluids migrated laterally through these beds.

Early burial dolomitization can be summarized in four stages separated by two events of fracturing and dissolution. This history is

Figure 8.2 Distribution of Deep Discordant Dolostones

Elongate patches of medium crystalline dolostone (black) penetrate the middle Catoche Formation along northeast-trending fracture zones and form continuous bodies peripheral to rock-matrix breccias. Linear bodies of late epigenetic, coarse sparry dolostones also reflect dolomitization along steep fault/fracture zones.

The map was produced from a pattern of more than 500 drill holes which penetrate the middle Catoche Formation.

DISTRIBUTION OF DEEP DISCORDANT DOLOSTONES

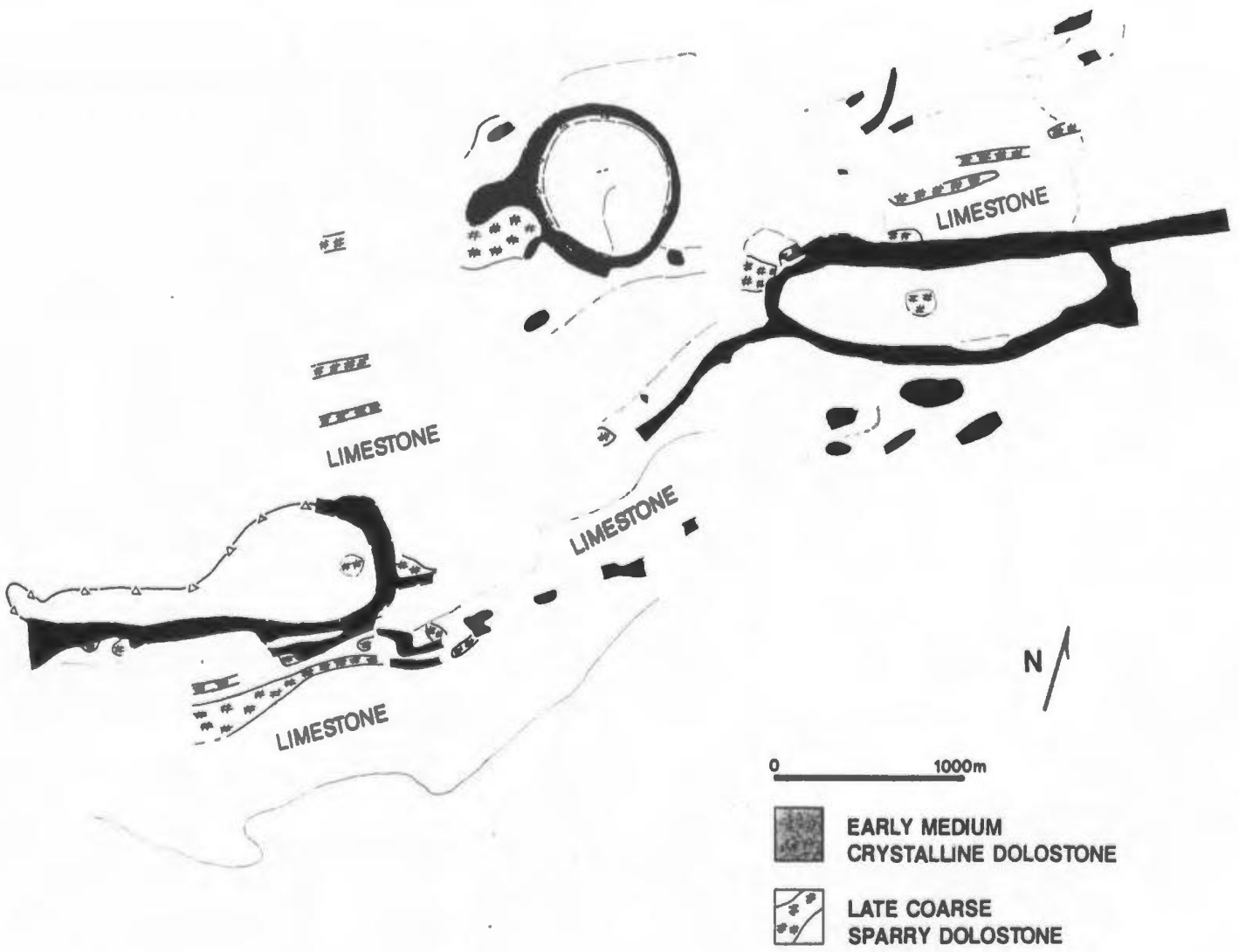

based on detailed petrographic relationships described in sections 5.4, 5.5 and 5.10.

Stage I - Dolomite II replaced compacted muds and burrows prior to pressure solution. These early replacement dolomites (II) crystallized from fluids in equilibrium with calcite and gained their turbid texture from numerous inclusions and incomplete calcite replacement. Generally these crystals first appeared as disseminated nucleii in limestones.

Stage II - The preceding replacive dolomitization continued during initial development of stylolites, but an event of fracturing and calcite cementation separated Stages I and II. Final stylo-mottle textures of euhedral dolomites displacing insoluble residues suggests that the crystals were stylo-reactates or stylo-cumulates (Pl. 5.1c) (Logan and Seminiuk, 1976).

Stage III - Dolomite II crystals became unstable during continued burial as fluids corroded rims and later pink CL phase dolomite partially replaced cores and overgrew rims (Pl. 5.1b,e). This resulted from the changes in the fluid chemistry either (1) as progressive burial encountered more saline fluids at depth (Bonham, 1980) or (2) as renewed fracturing facilitated the introductiion of allochthonous fluids. The evidence of fractures and discordant dolomitization support this later scenario. The emplacement of the Taconic Allochthon, which abruptly buried the St. George Group, probably generated the fracturing.

Stage IV - Zoned cements and overgrowths of Dolomite III closed pores in massive dolostone beds and rock-matrix breccias. A significant change occurred in the subsurface as dolomites began to mainly form cements rather than replacement crystals. Dolomite III gradually

cemented pores as variations in the regional fluid flow and the rate of precipitation created fluctuating redox conditions resulting in a zoned crystal chemistry. Fluid inclusions with negative crystal morphology suggest that Stage III followed significant burial of the St. George Group beneath the Taconic Allochthon. The absence of later dolomite overprints in most finely crystalline dolostones imply that cements of Dolomite III made these dolostones impervious to later fluids.

PART V

EPIGENETIC COARSE DOLOSTONE/SPHALERITE COMPLEXES

CHAPTER 9 INTRODUCTION TO EPIGENETIC COARSE DOLOSTONE/ SPHALERITE COMPLEXES

Stratabound complexes of epigenetic, coarse crystalline dolostones and sphalerites comprise approximately 75 % of the upper 50 m of the Catoche Formation. They locally penetrate the entire formation as narrow, discordant, tabular and chimney-shaped dolostones. The dolostone/sphalerite (D/S) complexes range from 300 to 1000 m wide and surround early subvertical faults and linear systems of stratabound veins. These vein systems encircle early, karst-related rock-matrix breccia bodies, parallel faults and occur on the flanks of gentle folds. These dolostone/sphalerite complexes are offset by late faults related to the Long Range Uplift. Late stage dolostones replace limestones adjacent to these structures, forming narrow, tabular bodies that cross-cut the entire Catoche and Table Head section (Fig. 7.1).

In Part V coarse dolostone / sphalerite complexes constitute the entire epigenetic bodies of rock. The rock bodies consist of several main components. Vein systems (described in Chapter 10), composed of several generations of fractures, characterize the cores of complexes. Sulphide bodies (described in Chapter 12) generally overprint portions of the vein systems. Coarse dolostones envelope all these components and extend well beyond the vein systems. The coarse dolostones are made up of pre-ore dolostones (described in Chapter 11) and post-ore dolostones (described in Chapter 13), which overprint and generally replace the earlier carbonates. A series of figures illustrate these relationships. Figure 7.1 is a typical cross-section of the dolostones and ore

zones. A map of the same area (Fig. 9.1) shows the distribution of dolostone facies in the upper Catoche Formation. Abundant saddle dolomite (>40% in coarse dolostone beds) occurs locally along ore zones and vein systems. A map of the mine area (Fig. 9.2) exhibits the intimate relationship between linear ore zones and rock-matrix breccias. The structural contours demonstrate folding around these bodies. All generations of faults and veins closely conform to the distribution of ore zones (Fig. 9.3). Discordant dolostones are distributed along these structures and the boundaries of rock-matrix breccias (Figs. 8.2, 9.4).

Petrographic and field relationships constrain the origin of D/S complexes to a period of tectonic fracturing after early burial dolomitization (Dolomites II and III) and preceding folding and faulting associated with the uplift of the Long Range Inlier (petrographic evidence discussed in sections 5.6 through 5.10). The thermal maturation of conodonts (CAI 2 - 2 1/2) probably occurred at a burial depth between 1000 and 3000 m, a thermal maximum which corresponds to the 140°C T_h mode of fluid inclusions in the sphalerites. Some regional uplift probably occurred between maximum burial and sphalerite deposition (Sangster et al., 1989). The age of initial uplift of the Long Range, determined from metamorphic cooling ages east of the Long Range, was Middle Silurian to Devonian (375 - 430 $\pm$ 10 ma.) (Dallmeyer, 1977; Hibbard, 1983). The youngest date for the uplift, determined from Carboniferous sediments that onlap the Long Range Inlier, is earliest Carboniferous (Tournaisian 345 - 340 ma.) (Hyde, 1983). Authigenic potassium feldspars in carbonate veins suggest that earlier sulphide mineralization was Devonian or older (Ar^{39}/Ar^{40} ages, Hall et al.,

Figure 9.1 Upper Catoche Dolostone Facies at the Ore Horizons

A map of the upper 50 m of the Catoche Formation in the vicinity of the L Zone and Trout Lake Rock-Matrix Breccia (location map, Fig. 1.4) demonstrates that areas of abundant saddle dolomite occur locally within and around fracture zones and they are surrounded by broad areas of gray dolostone with less than 20 % patches of white saddle dolomite. Zones of coarse sparry dolostone are a light gray, medium crystalline rock without patches of white saddle dolomite. This lithology is commonly transitional with limestone at the margins of coarse dolostone complexes. Limestone remains in local patches distant from fracture zones and rock-matrix breccias.

UPPER CATOCHE DOLOSTONE FACIES AT THE ORE HORIZONS

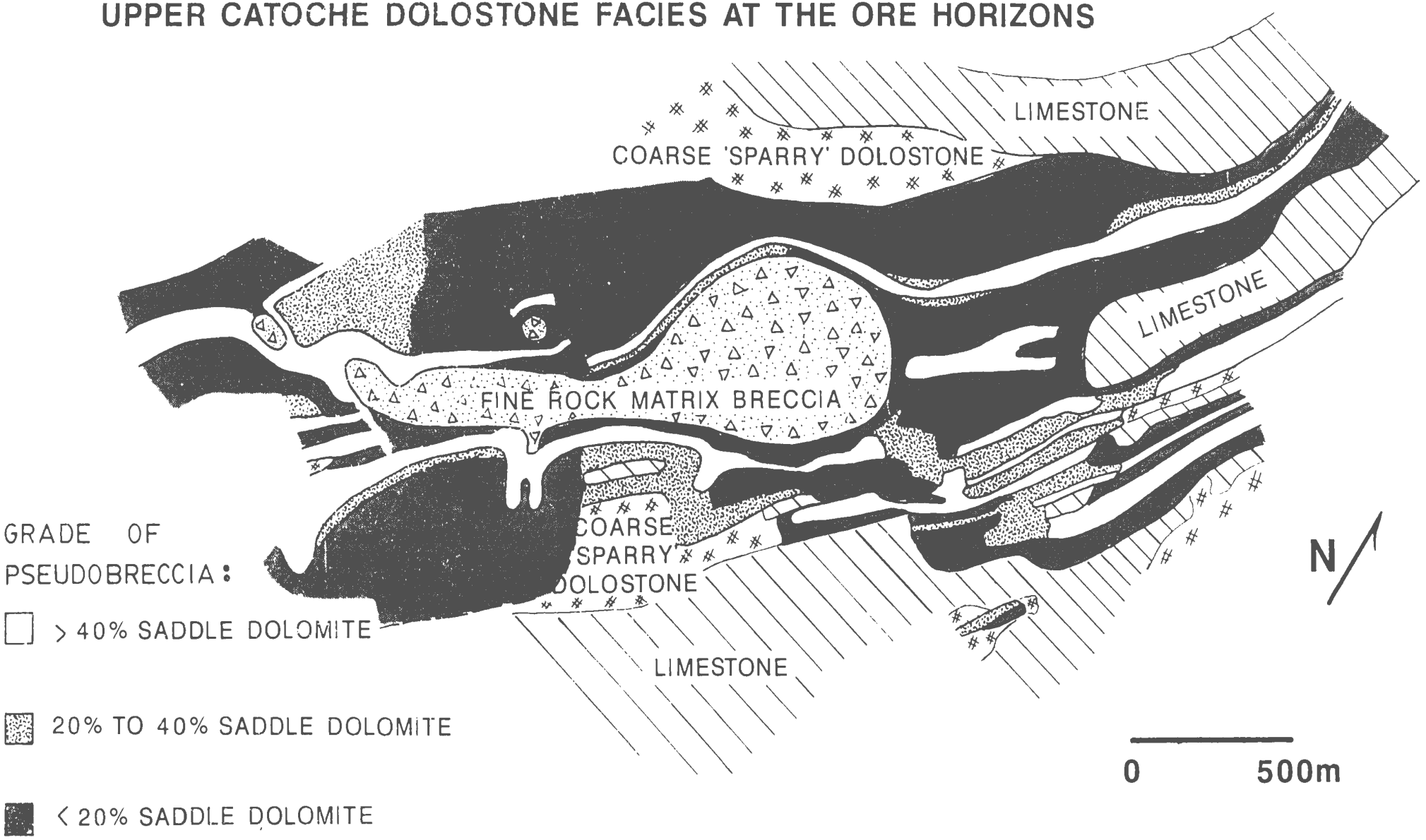

Figure 9.2 Relationship between Sphalerite Bodies, Structural Contours and Rock-Matrix Breccias

Linear ore zones in the upper Catoche Formation occur along inflections in structural contours which represent deformation along fracture zones, faults or margins of fine rock-matrix breccias. Major ore zones occur along the southern margins of rock-matrix breccias. Although the L Zone in the southwest extends for a length of 4 km, all ore bodies are discontinuous. Names of ore zones and rock-matrix breccias are identified on the location map, Fig. 1.4).

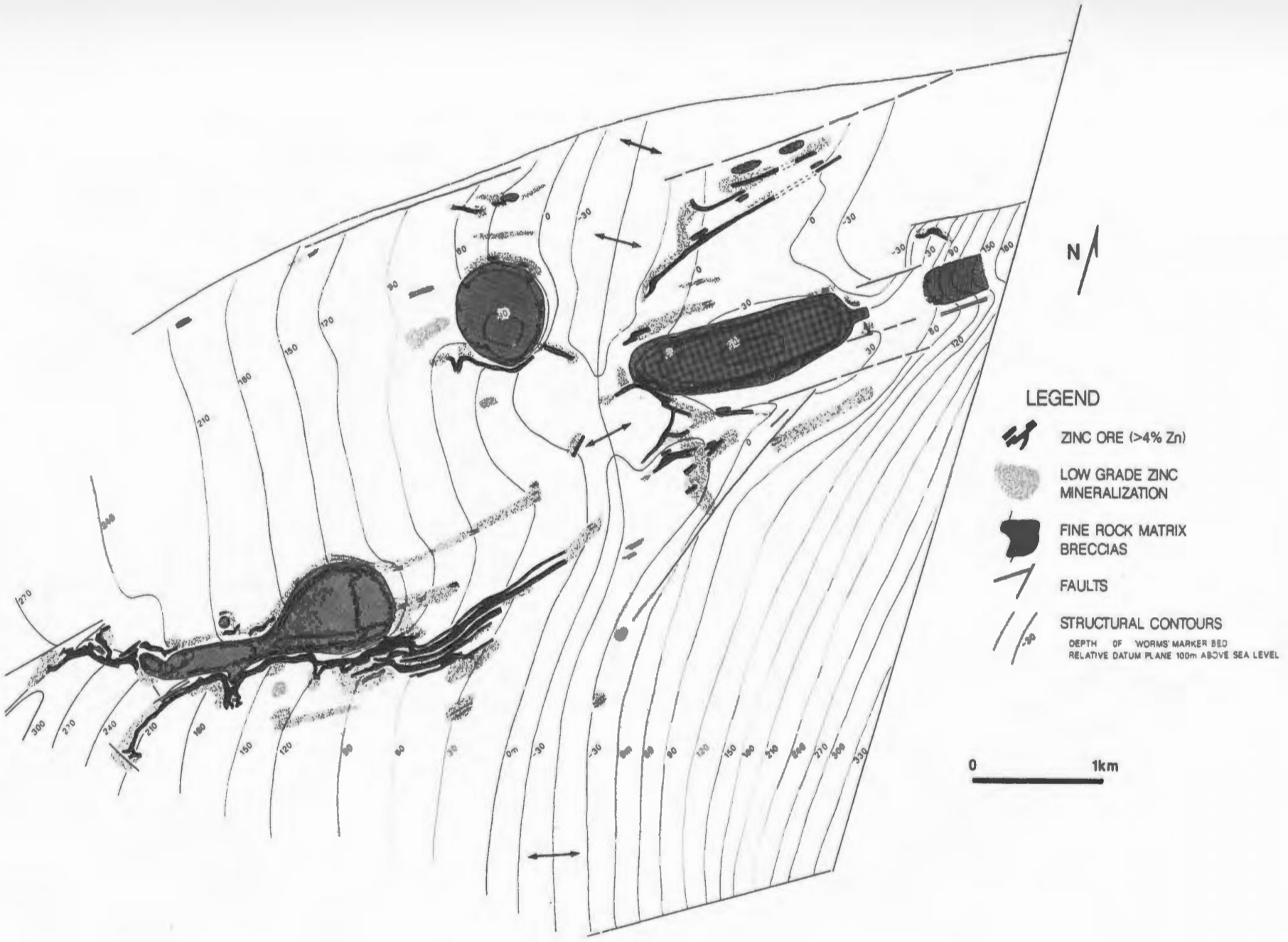
N
LEGEND
ZINC ORE (>4% Zn)
LOW GRADE ZINC MINERALIZATION
FINE ROCK MATRIX BRECCIAS
FAULTS
STRUCTURAL CONTOURS
DEPTH OF 'WORMS' MARKER BED
RELATIVE DATUM PLANE 100m ABOVE SEA LEVEL
0
1km

Figure 9.3 Generations and Distribution of Faults and Vein Systems

A minimum of three generations of faults occur along fault zones. Synsedimentary faults control the boundaries of rock-matrix breccias and influence changes in thickness of the upper Aguathuna Formation. Ore-stage faults constrain the position of ore lenses and coarse dolostone facies. Vein systems surround these fault zones. Post-ore faults displace coarse dolostone/sphalerite complexes.

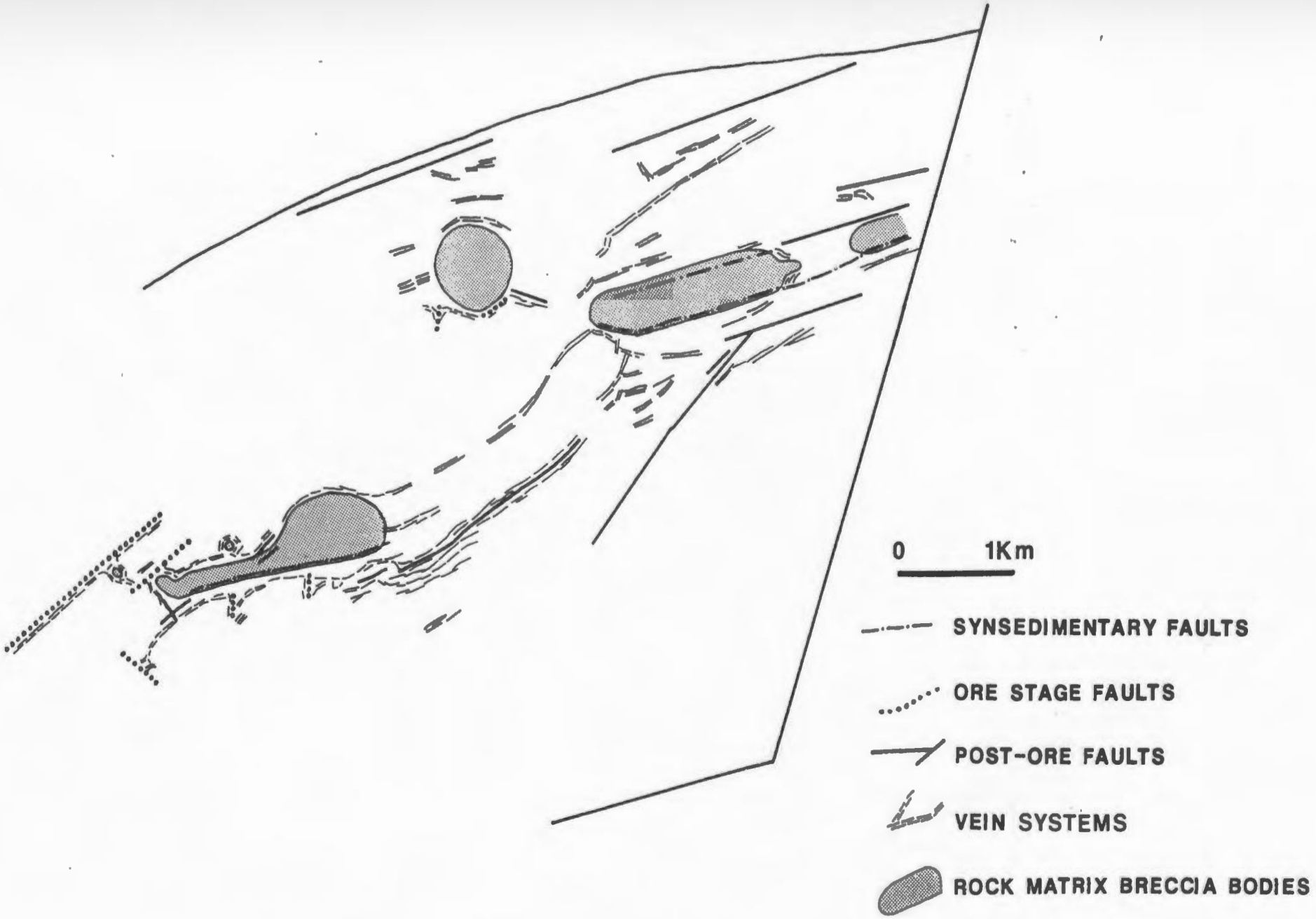

DISTRIBUTION OF FAULTS AND VEIN COMPLEXES

Figure 9.4 Distribution of Late Fault-Related Dolostones in the Table Head Group

Discordant bodies of finely crystalline dolostone composed of Dolomite VII replace the Table Point Formation along late steep faults which displace coarse dolostone/sphalerite complexes of the upper Catoche Formation. The pattern of these dolostones in otherwise undolomitized Table Point Formation defines the areas of influence of late fluids which migrated along the faults. The distribution of discordant coarse sparry dolo-stones which replace Catoche limestones along late faults is illustrated in Fig. 8.2.

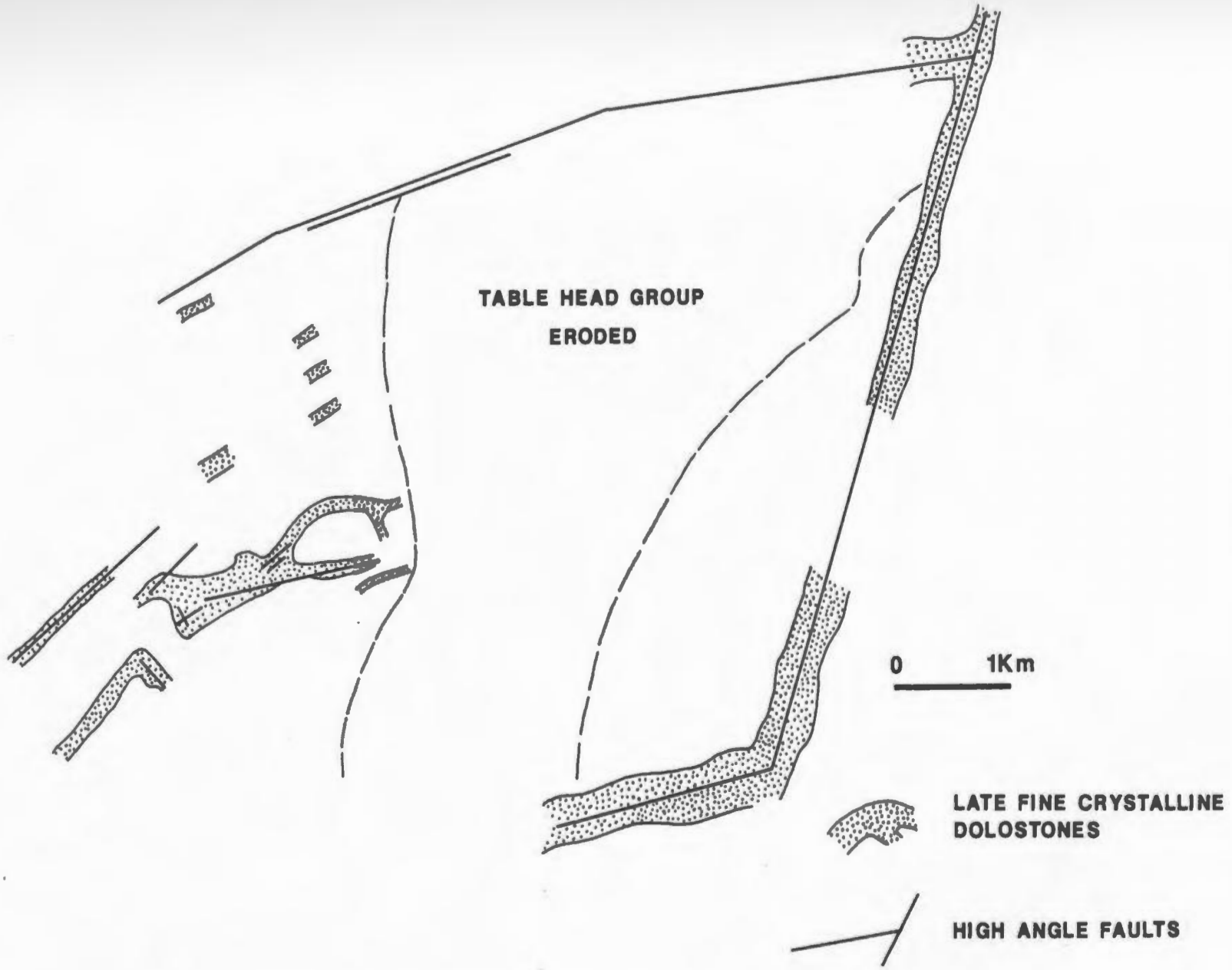

DISTRIBUTION OF LATE FAULT-RELATED DOLOSTONES

IN THE TABLE HEAD GROUP

1989).

The epigenetic history of the D/S complexes post-dates early burial dolomitization (Dolomites II and III) and pre-dates uplift (after Dolomite VII). This history is divided into seven events: (1) Regional deformation faulted and fractured the area. (2) Pervasive dolomitization (Dolomite IV) around these fractures converted dolostone-mottled limestones (Dolomites II and III) to coarse matrix dolostone. (3) A second episode of faulting and folding facilitated extensive dissolution of the carbonates by "pre-ore" fluids. (4) Two main stages of sulphides (early and late) crystallized concurrently with fracturing and carbonate dissolution. (5) Extensive replacement and cementation by saddle dolomite and calcite occurred after post-ore fracturing. (6) During the uplift of the Long Range Inlier regional folds and faults tilted and offset D/S complexes. This rotation is recorded in post-ore geopetal sediments. (7) Late dolomitization (Dolomite VII) of limestones along the faults occurred during or after uplift.

Epigenetic D/S complexes are described in detail and interpreted in the next five chapters. The nature and evolution of the structural framework is established in Chapter 10. The description of the dolostone/sphalerite bodies is divided into three chronologic chapters: Chapter 11 on the pre-ore dolostones, Chapter 12 on the sphalerite bodies and Chapter 13 on the post-ore dolostones. The history and genesis of the D/S complexes is synthesized in Chapter 14.

CHAPTER 10 STRUCTURAL FRAMEWORK OF COARSE DOLOSTONE/ SPHALERITE COMPLEXES

10.1 Relative Age Relationships of Structures in the St. George Group

Faults, folds and veins in the mine area range from faults active during deposition to structures formed during regional uplift. Late structures commonly overprint earlier ones along the same trends (Fig. 9.3). The various structures are separated into four different age groups based on their relationships to both large scale stratigraphy and to cement stratigraphy (Fig. 9.3).

(1) **Synsedimentary Faults** - The sedimentary thickness of the Aguathuna Formation and Table Head Group varies abruptly across structural lineaments such as the Torrent River Fault (Fig. 1.3) (Knight, 1986; Knight et al., in press). The middle and upper members of the Aguathuna Formation reach their maximum thickness over rock-matrix breccias developed along early northeast and north-trending faults and fractures (sections 4.3 to 4.5; Figs. 4.1, 4.6, 4.7). Variable regional thicknesses of these units imply differential subsidence rates in fault blocks which segmented the platform at the end of the Lower Ordovician and during the early Middle Ordovician (Klappa et al., 1980; James et al., 1989; Stenzel and James, 1988; Stenzel et al., 1990).

(2) **Early Burial Fractures and Faults** - Dolostone bodies composed of Dolomites II and III and fracture cements of blocky calcite and

Dolomites III formed along vertical fracture systems during early burial (refer to Chapters 5 and 8). Some of these dolomitized fracture systems cut the previously faulted margins of rock-matrix breccias.

(3) **Epigenetic Veins and Faults** - Linear vein systems contemporary with D/S complexes fracture the upper Catoche Formation over widths of 50 to 500 m along the margins of late faults and around rock-matrix breccias (Fig. 9.3). Locally these veins deeply penetrate the Catoche Formation. Associated faults oriented northeast-southwest, east-west and northwest-southeast exhibit small-scale (1 - 10m) vertical displacements. Northeast-trending fold axes and southeasterly dipping reverse faults imply northwest-directed regional compression. The differing generations of vein cements from early sphalerite to saddle dolomite demonstrate that fracturing occurred throughout the crystallization of D/S complexes, from fractures controlling distribution of Dolomite IV to veins cemented by Saddle Dolomite B (see graphic illustrations, Figs. 1.6, 5.7, 6.1 and 8.2).

The association of tectonism, dilatant fracturing, dolomitization and sphalerite precipitation is based on several observations: (1) Faults locally control dolostone facies (Fig. 9.1). (2) Sulphides and saddle dolomites terminate at faults (observed in the K, L and T Zones, Figs. 10.1 through 10.5). (3) Some sulphide mineralization post-dates faults and overprints them (observed in the F, east L and T Zones). (4) Sulphide and saddle dolomite-cemented veins are localized along flexures and faults (Figs. 9.1 to 9.3).

(4) **Late Cross-cutting Faults** - Three generations of faults displace dolostone/sphalerite complexes up to 500 m. Early northeast-

trending reverse and thrust faults (eg. Kill Devil Fault, Fig. 1.3) and later north-trending normal to steep reverse faults (eg. Brian's Fault, Figs. 1.3, 1.4) displace west-dipping flanks of asymmetrical anticlines such as the Mike Lake Anticline. Late right lateral strike-slip occurs on some of these faults, such as Torrent River Fault (Fig. 1.3).

10.2 Epigenetic Vein Systems and their Relationship to Other Structures

Narrow, linear vein systems vary in width from 20 to 70 m, are stratabound over thicknesses of 3 to 40 m, and strike hundreds to thousands of metres along the gently folded margins of rock-matrix breccias and faults (Figs. 9.3, 10.1). The veins are distributed over thick stratigraphic intervals (10 to 30 m) adjacent to faults and breccia margins, but occur in progressively higher stratigraphic levels and in thinner stratigraphic intervals away from these structures (Fig. 10.2). This pattern is also repeated along the strike of vein systems (Figs. 10.2, 10.3).

Fracture zones parallel not only the boundaries of main trend faults (IB, Fig. 10.4) and rock-matrix breccias (IA, Fig. 10.4), but also loop around 100 to 300 m-long northwest-trending cross-faults (IIA, Fig. 10.4) and follow the axial traces of folds between these cross-faults (III, Fig. 10.4; Fig. 10.5). Vein systems also reflect the discontinuous and en echelon nature of main trend hinge and scissor faults (Fig. 10.2). Inflections in trends of vein systems cross-over from the end of one fault to another en echelon fault (Fig. 10.2; IIB, Fig. 10.4). Fractures in these areas deeply penetrate the Catoche

Figure 10.1 Structure of the T Zone

Relationship between Sulphides, Veins, Faults and Rock-Matrix Breccias

A. The T Zone ore body (loacation, Fig. 1.4) flanks faults and the margins of rock-matrix breccias. Sleeves of pyrite occur between these structures and the ore. The base of sphalerite ore in the T Zone varies systematically from local deep areas (120 feet below the Worms Marker) along northeast-trending faults to 95 feet (b.w.m.) between faults and 85 to 75 feet (b.w.m.) in parallel ore lenses away from main structures.

B. In cross-section A-A' stratabound veins in the upper Catoche Formation occur along major structures.

C. Vein systems are shaped asymmetrically. Cross-hatching indicates zinc mineralization.

D. Sphalerite occupies inclined veins in finely crystalline dolostones (black) and sheet megapores in pseudobreccia beds (white). Post-ore veins are steep and cemented only by saddle dolomite.

E. Veins in the T Zone area preferentially dip to the southwest.

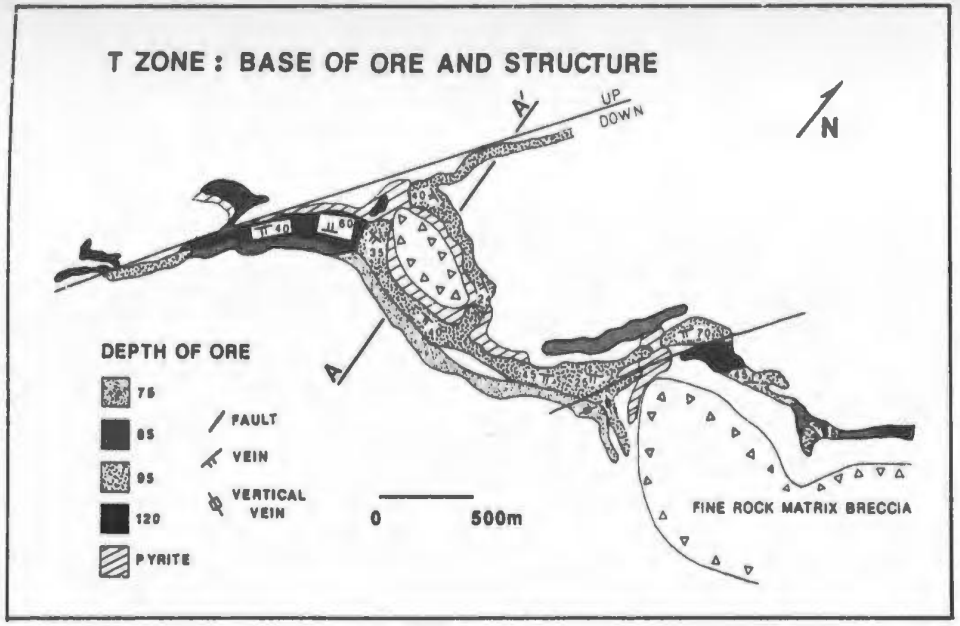
T ZONE : BASE OF ORE AND STRUCTURE
A'
UP
DOWN
N
A
DEPTH OF ORE
75
85
95
120
PYRITE
FAULT
VEIN
VERTICAL VEIN
0
500m
FINE ROCK MATRIX BRECCIA

A

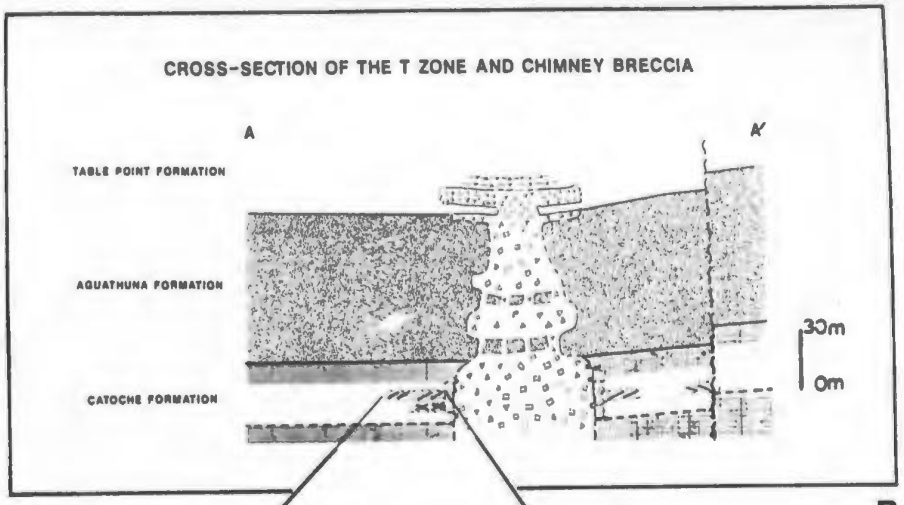
CROSS-SECTION OF THE T ZONE AND CHIMNEY BRECCIA
A
A'
TABLE POINT FORMATION
AQUATHUNA FORMATION
CATOCHE FORMATION
30m
0m

B

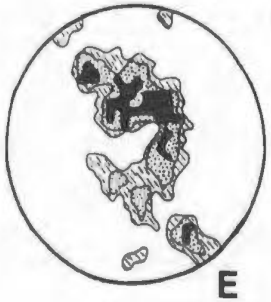

E

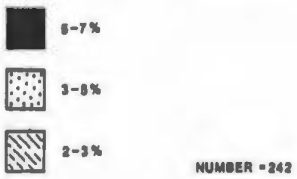
π DIAGRAM OF POLES TO VEINS
5-7%
3-5%
2-3%
NUMBER = 242

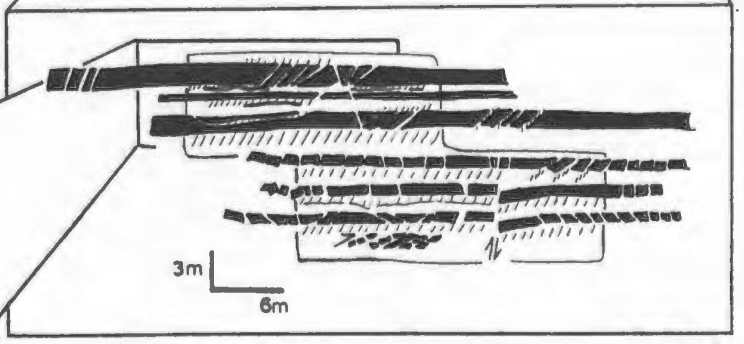
3m
6m

C

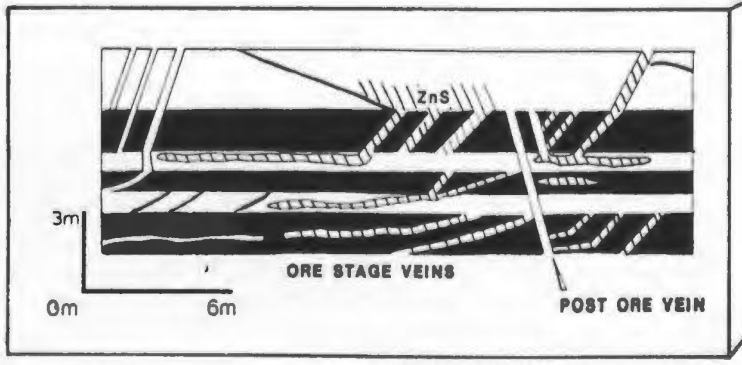
ZnS
3m
ORE STAGE VEINS
0m
6m
POST ORE VEIN

D

Figure 10.2 Structure of the East L Zone

Relationship between Ore Body Isopachs, Hinge Faults

and Structural Contours

Ore lenses and coincident vein systems occur along the folded flanks of faults and rock-matrix breccias and cross-over between en echelon fault zones and along cross-faults. The ore occupies a body of fractured strata in section A-A'. Thick, deep ore occurs along faults, whereas, thin, late ore occupies upper beds along the southern flank of the L Zone (section B-B'). Section A - A' is illustrated in larger scale in Fig. 12.6 and section B - B' is shown again in Fig. 12.4. The L Zone is located on Figure 1.4

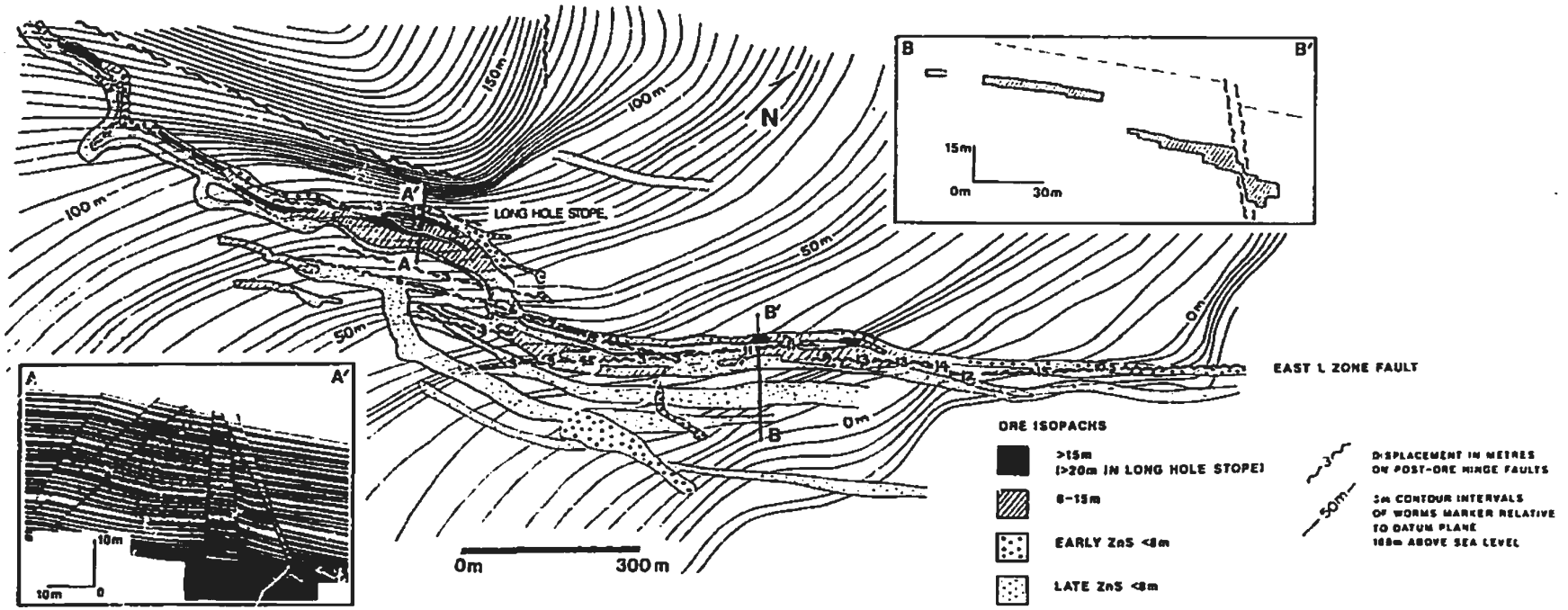

RELATIONSHIP BETWEEN ORE ISOPACHS, HINGE FAULTS AND STRUCTURAL CONTOURS, EAST L ZONE

Figure 10.3 Southwest L Zone

Detailed Cross-sections of an Upward Migrating Vein System

The southwest L Zone (location, Fig. 1.4) terminates along a cross-fault. At this position the ore occupies a 13 m thickness of fractured dolostones. The vein system becomes narrow and linear in a northeasterly direction where fracturing is restricted to 3 to 6 m of strata at increasingly higher stratigraphic levels. Section A-A' illustrates the localization of ore/fracture zones along faults and flexures. Dolostone zebra bands are inclined toward faults (section A-A'). Finely crystalline dolostone beds (black) are segmented and displaced along reverse faults (sections A-A', B-B'). Fracturing and mineralization is confined below and/or between 1.5 to 3 m-thick finely crystalline beds (section C-C').

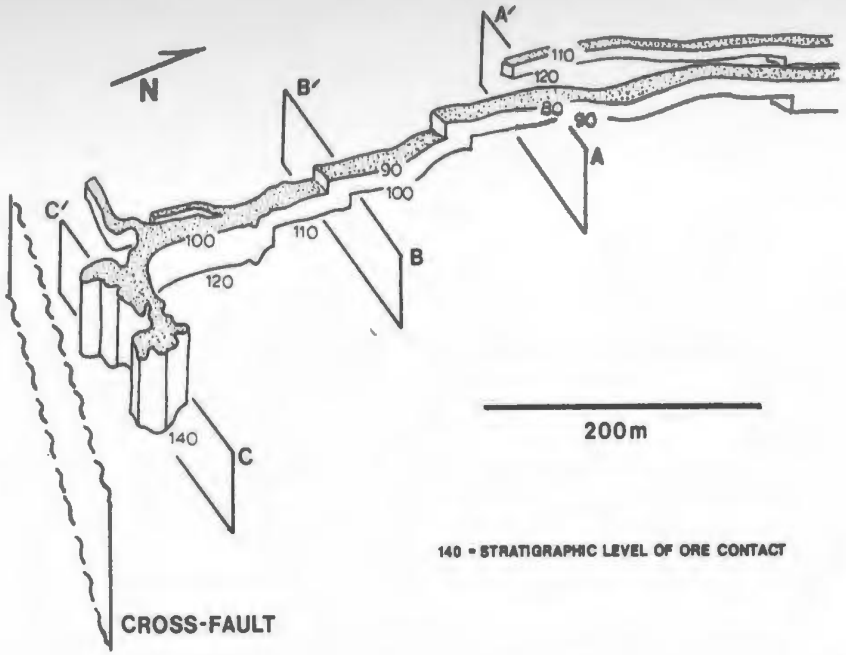

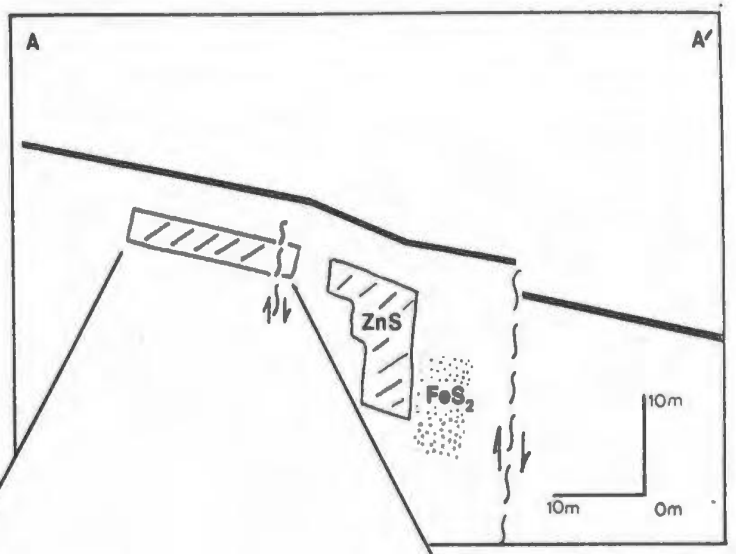

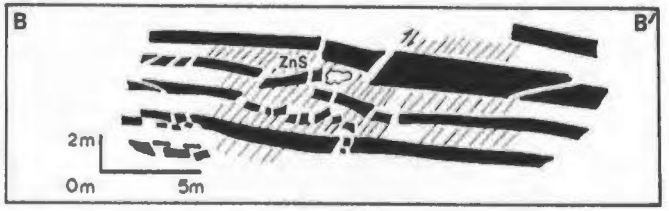

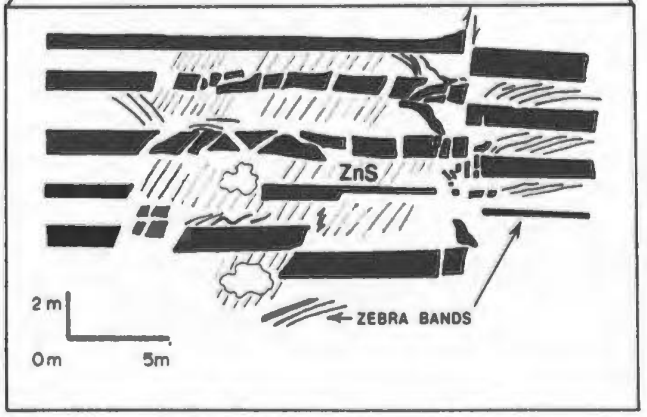

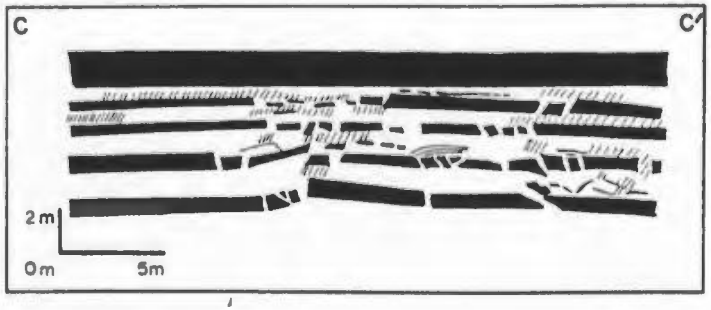

STRUCTURE OF THE SOUTHWEST L ZONE

Figure 10.4 Distribution of Types of Vein Systems

A map of ore distribution demonstrates the varied relationship of vein systems to rock-matrix breccias (shaded), faults and structural contours. The position of vein systemscan be categorized into five types.

I Along Major Structures	IA Breccia Margin
	IB Fault Margin
II Deflections	IIA Cross Fault
	IIB Between Hinge Faults
III Between Major Structures on the limbs of monoclines	

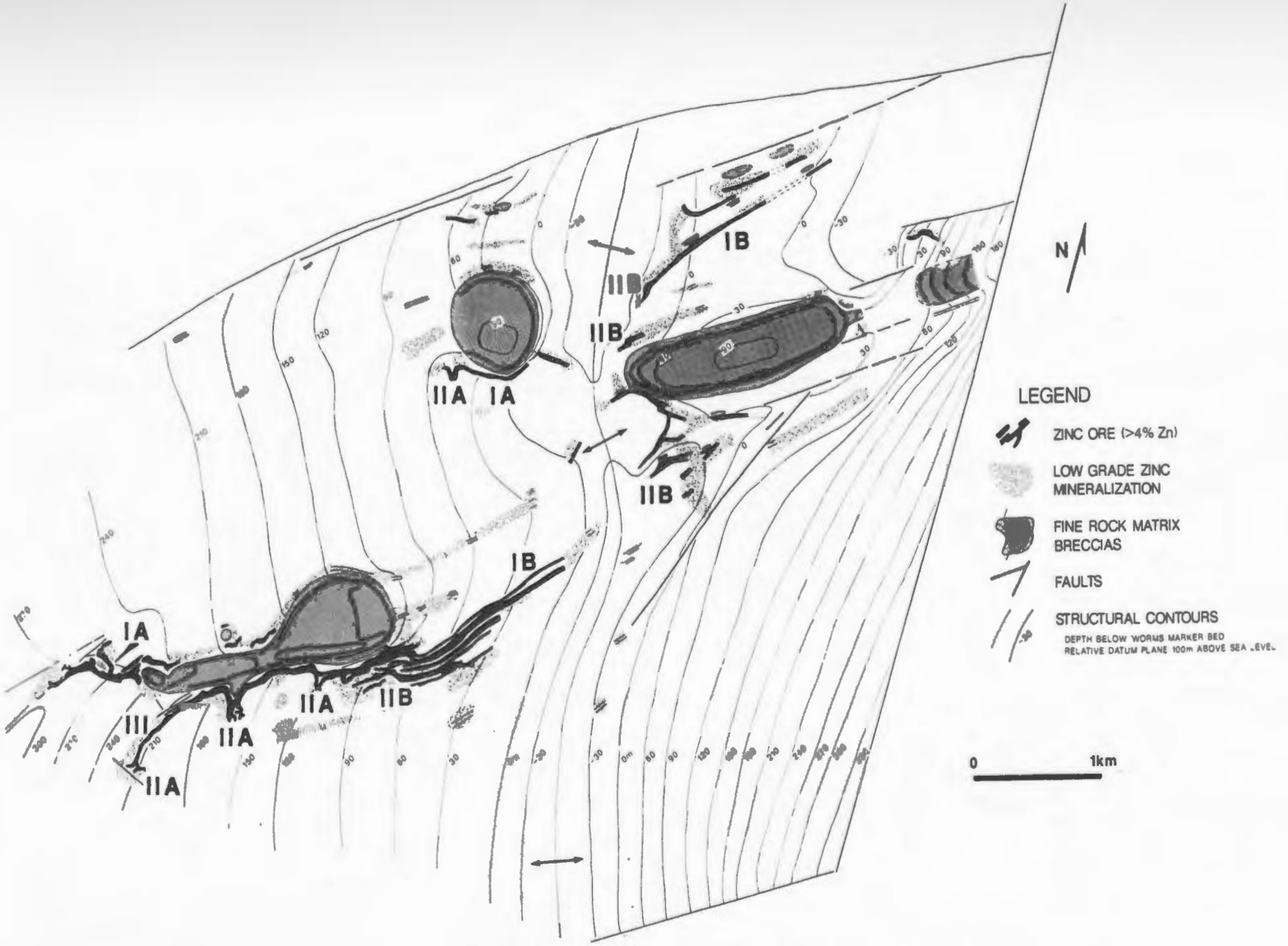

DISTRIBUTION OF TYPES OF VEIN COMPLEXES

Figure 10.5 Structural Control by a Cross Fault at the K Zone

A northwest-trending cross-fault alters the northeast trend of a vein system which hosts the southwest K Zone (location, Fig. 1.4). The trend of veins and the strike of bedding is rotated parallel to the cross-fault. The ore occupies fractured dolostones in the vicinity of the cross-fault and along fracture zones (section A-A'). Along the fault (inset) mineralization replaces the upper portion of beds and cements eastward dipping and horizontal veins. Post-ore veins, cemented only by saddle dolomite, are both vertical and west-dipping (π diagram). The change in fracture orientation over time indicates a change in the direction of extension as displacement occurred along the cross-fault.

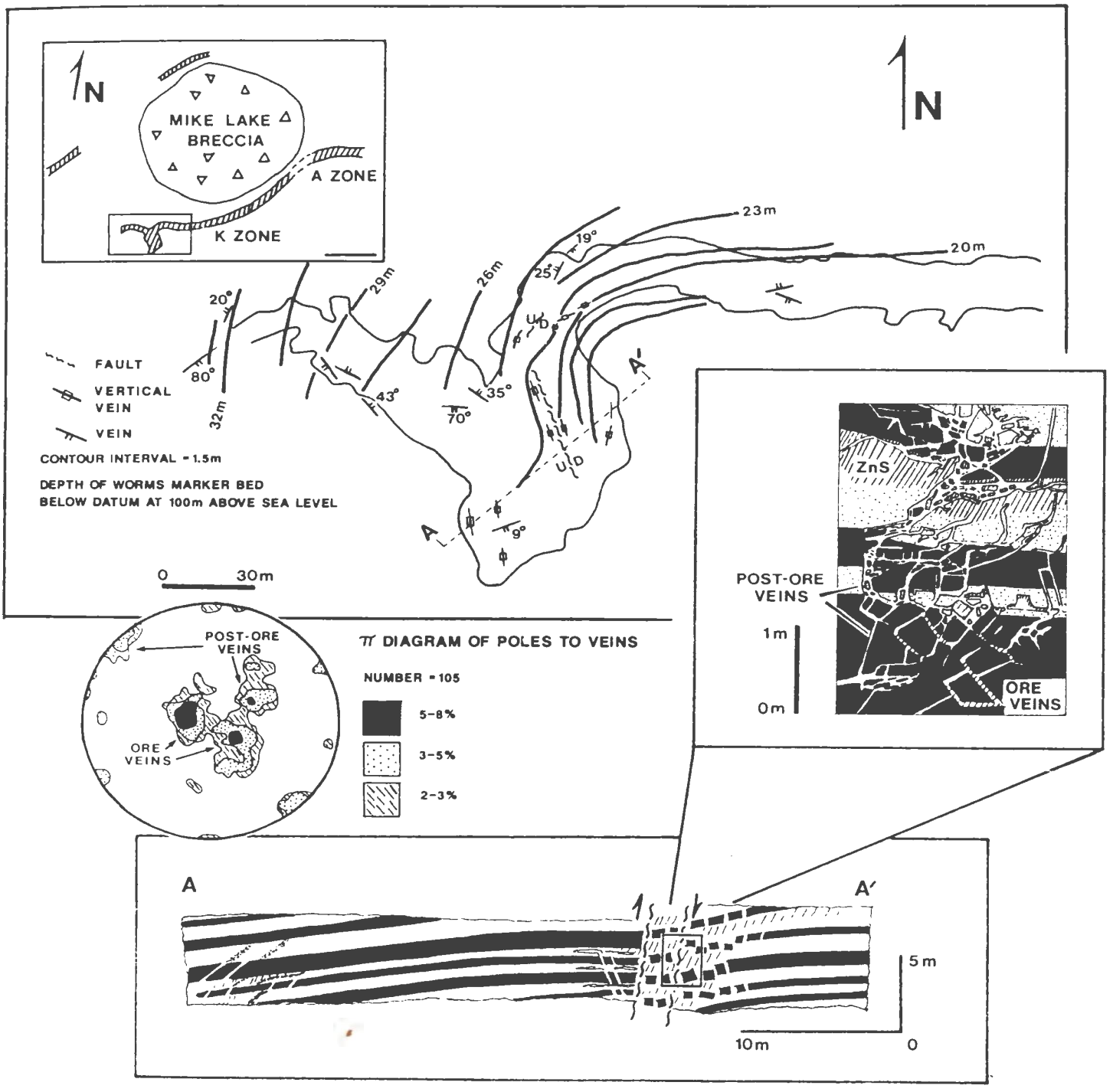

STRUCTURE AT K ZONE CROSS-FAULT

Formation. Mineralized veins are related to early deformation along these structures, prior to significant fault displacement. The discontinuous, en echelon faults resemble fault bridges and the corresponding inflections in vein systems are comparable to transfer zones between the faults (Ramsey and Huber, 1987).

10.3 Internal Structure of Vein Complexes

10.3.1 Introduction

Vein systems are composites of several generations of structures from initial compressional fractures to late dilatent ones. A gently folded stratigraphy is extensively fractured and brecciated around steep reverse and normal faults (Figs. 10.1, 10.3, 10.5, 10.6). The fracturing is confined to thin, gray dolostone beds, 10 to 50 cm thick, over vertical sections of a limited 5 to 30 m thickness. One to two metre thick beds of gray dolostone commonly impede the vertical penetration of veins, and thus, they commonly form hanging and footwalls of vein systems (Fig. 10.3, section C-C').

In detail, vertical and low angle veins segment the thin, gray dolostone beds into 0.5 to 6.0 m lengths which commonly display a reverse sense of displacement (Fig. 10.6; Pl. 10.1). Horizontal veins part the tops and bottoms of these beds and inclined veins flatten toward the bases (Pl. 10.1a; Figs. 10.1, 10.6). Most veins do not cross-cut coarse dolostone beds, but instead merge with sheet megapores and irregular solution cavities (Figs. 10.1, 10 .6).

Figure 10.6 Structure of the F Zone

Detailed Map and Cross-section of a Vein Complex

The F Zone (location, Fig. 1.4) parallels the faulted margin of a rock-matrix breccia and makes a right angle bend along a cross-fault. Fracturing occurs around reverse faults in the centre of the ore zone (section A-A'). Most of these fractures are inclined to the south (π diagram). Sphalerite mineralization occurs along reverse faults and is confined above bands of zebra dolostone, convex upward features which merge with veins in overlying beds (sections A-A', B-B'). Mineralized thrust faults displace finely crystalline dolostone beds at the bend in the ore zone. Plates 10.1a, 13.1c and 13.1e illustrate portions of wall section B - B'.

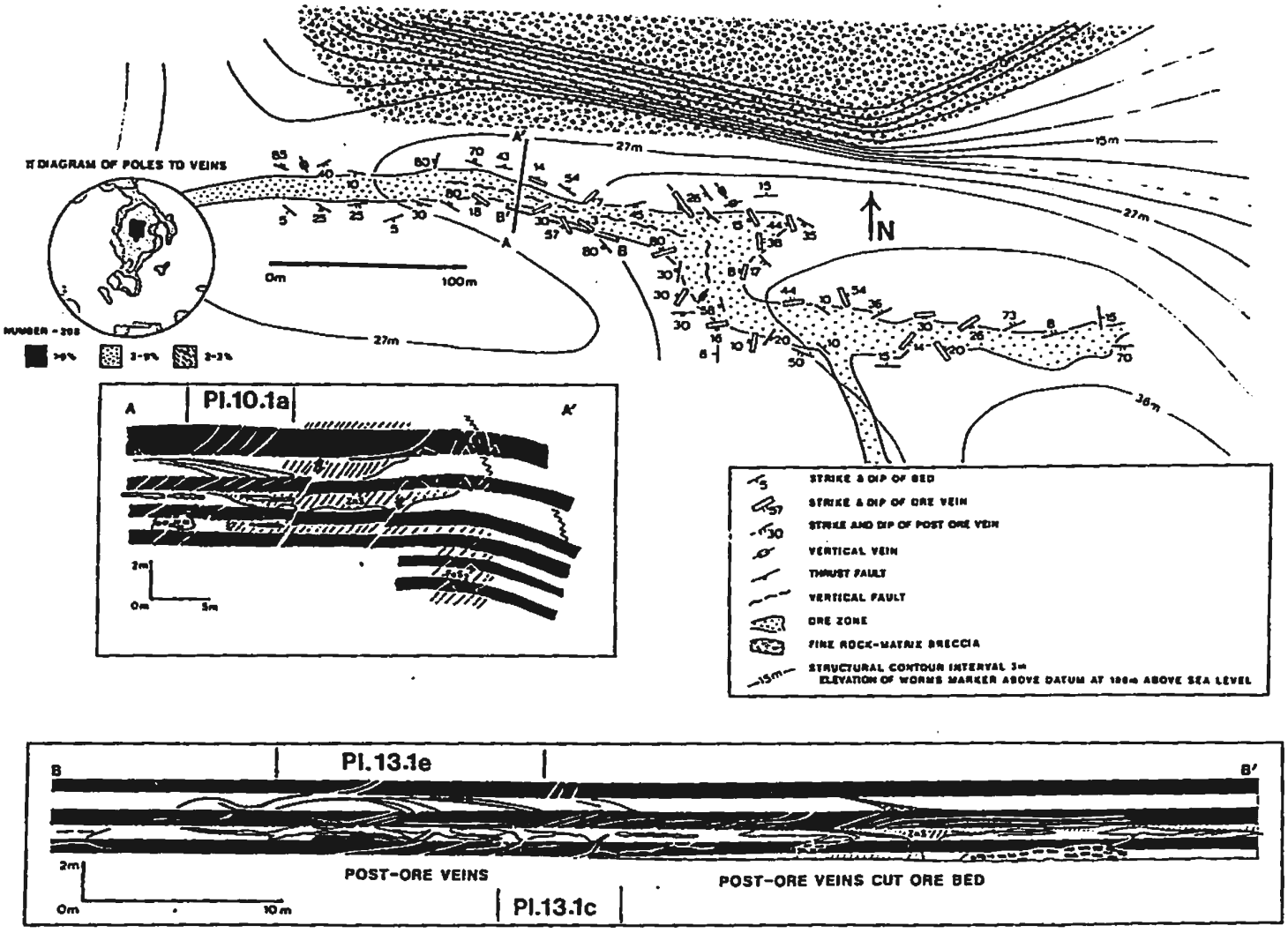

STRUCTURE OF F ZONE

Plate 10.1 Veins and Vein-Breccias

a. Low angle veins in a finely crystalline dolostone flatten towards the base of the bed where they merge with a sheet cavity in the underlying pseudobreccia bed. Reverse view of the left side of section A-A' in Fig. 10.6. F Zone. 1 m scale.

b. A reverse fault offsets dolostone beds which locally form dilatent vein-breccias. A view of part of section A-A' in Fig. 10.7. North L Zone. 1 m scale.

c. Finely crystalline dolostones and sphalerites are brecciated along dilatent veins adjacent to a fault (same as inset in Fig.10.5). Splinter breccias in the upper middle suggest hydraulic fracturing. Adjacent to the cross-fault in the southwest K Zone. Pen measures 15 cm.

PLATE 10.1

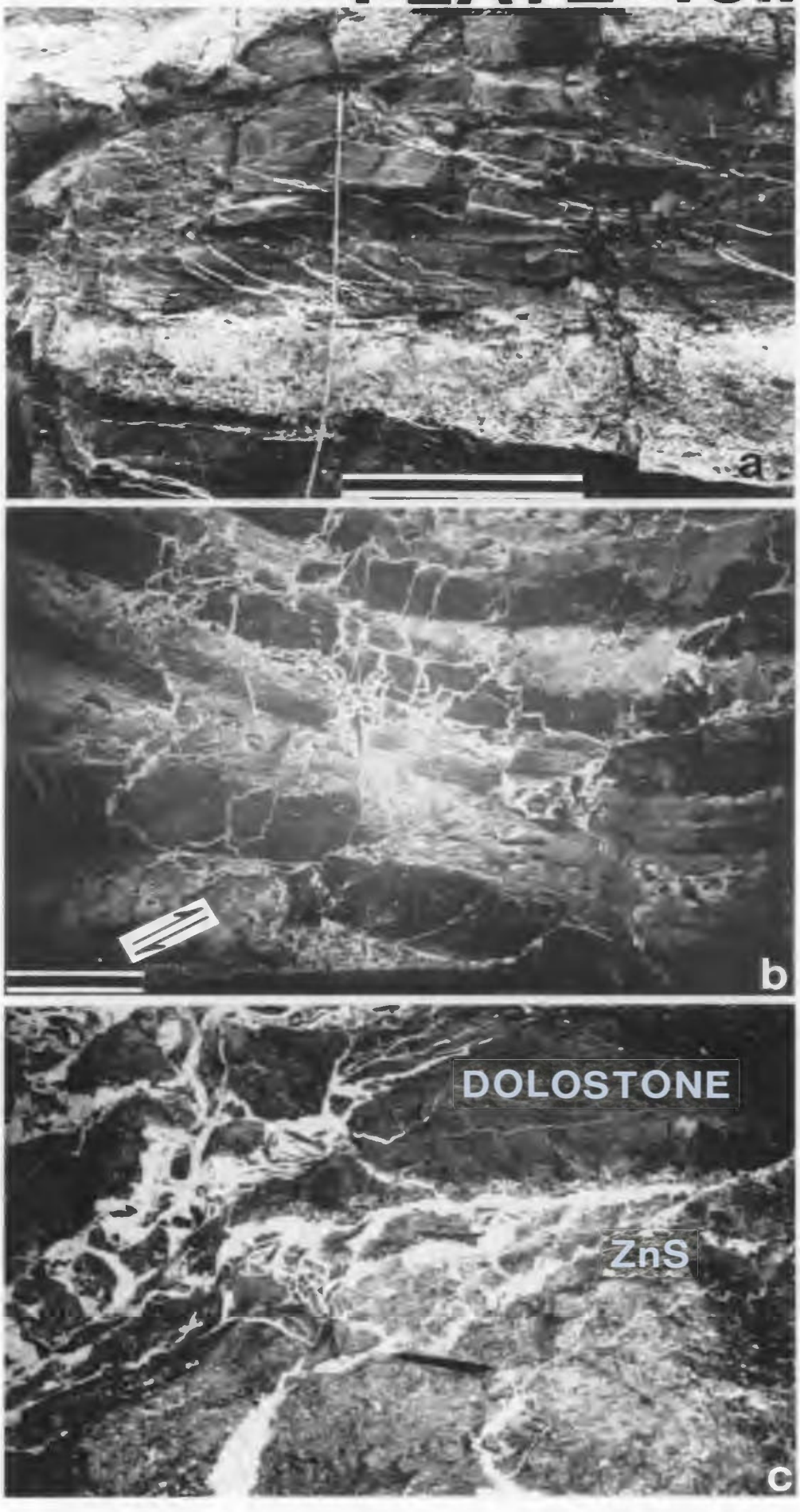

Figure 10.7 Cross-section of Reverse Fault - Spar Breccia Structures

Two underground drifts north of the L Zone exposed rare northwest-southeast cross-sections of fracture zones. Beds are gently folded and displaced along reverse faults. Finely crystalline dolostone beds are fractured and brecciated over 20 m widths along synclines bounded by low angle reverse faults. Reverse displacement of dolostone beds (section B-B') implies that these are not solution collapse breccias.

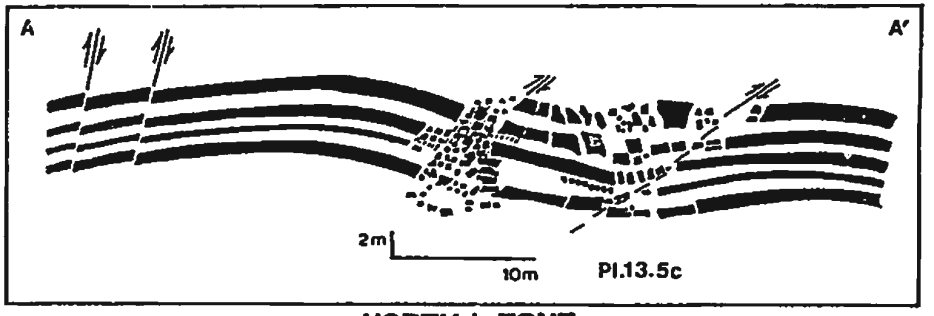

NORTH L ZONE

T ZONE ACCESS DRIFT

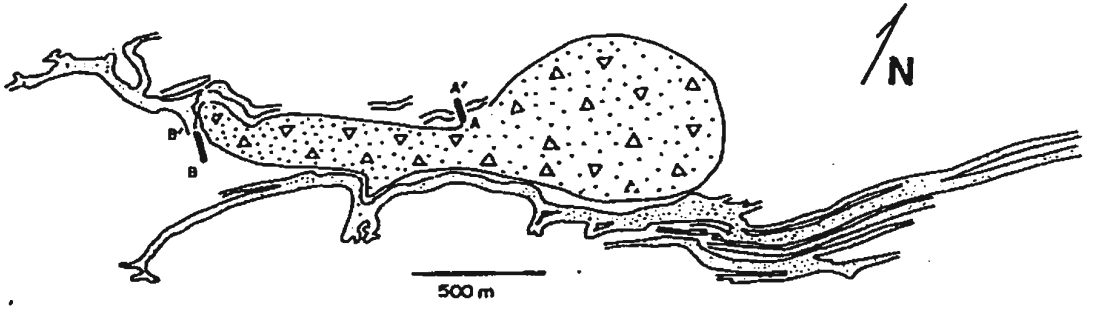

CROSS-SECTION OF REVERSE FAULT-SPAR BRECCIA STRUCTURES

Three generations of structures, which comprise the vein systems include early compressional structures and ore stage and post-ore dilatent fractures. The nature of each of these generations is described and interpreted in the following three sections.

10.3.2 Early Compressional Structures

Reverse faults, the central structures of most vein systems, occur within open upright fold structures (Fig. 10.7; Pl. 10.1b). These structures are generally northeast-trending and dip to the southeast, they locally diverge around rock-matrix breccias and other faults (Fig. 10.1). Many low angle fractures in gray dolostone beds are probably related to the reverse faults (Fig. 10.6). Gray dolostone beds are locally buckled and displaced in a reverse sense along these fractures (Fig. 10.3). Mineralized bedding plane thrusts also cut these beds (Fig. 10.6).

Interpretation - Northwest-directed regional compression gently folded and displaced beds of the upper Catoche Formation along reverse faults. Deformation propagated outward from these faults by fracturing thin, brittle beds of finely crystalline dolostone and was confined between thick beds. The fracture systems conformed to the geometry of thick dolostone bodies (eg. rock-matrix breccias) and to large faults which both caused local rearrangement of compressional and extensional features.

10.3.3 Dilatant Ore Stage Fractures

Networks of sphalerite veins vary from horizontal to subvertical ($\leq$60°) and are generally discontinuously clustered (Fig. 10.6; Pl. 10.1a). Inclined veins generally exhibit preferred orientations, dipping the same direction as reverse faults and opposite to the general inclination of bedding (Figs. 10.1, 10.5, 10.6). π-diagrams of over 1000 measurements from 8 areas emphasize the importance of low angle veins with preferred orientations which tend to dominate populations of conjugate fractures (Fig. 10.8).

Evidence of small-scale solution collapse occurs locally through out vein complexes. Most fractured and brecciated dolostones, however, remain as <u>in situ</u> mosaic breccias (Figs. 10.1, 10.3, 10.7). Solution collapse features include: (1) local thinning of coarse dolostone beds (Fig. 10.3); (2) local sagging of overlying beds several metres in areas 5 to 20 m wide (Fig. 10.7; Pl. 10.1b); and (3) displacement of gray dolostone fragments several metres down into solution cavities (Pls. 7.3d, 10.1b). Large -scale, ore-stage solution breccias comparable to MVT deposits in East Tennessee and Poland (McCormick et al., 1971; Dzulynski and Sass-Gustkiewicz, 1986) are not observed. The largest breccia bodies, 10 to 40 m wide and up to 100 m long, occur in the Long Hole Stope (Fig. 10.2), along cross-faults (Fig. 10.3) and in the North L Zone (Fig. 10.7). Although these bodies are highly fractured, they display only minor collapse. Spar breccias are discussed further in Chapter 13.

<u>Interpretation</u> - Steep reverse faults displaced beds and low angle to horizontal tension fractures opened as extension occurred in subhor-

Figure 10.8 Orientation of Veins in the Mine Area

Over 1000 veins were measured in eight localities across the mine area. Stereoplots record the density of intersection points of poles to veins with 1% of the area of a lower hemisphere projection.Conjugate sets of veins are present most places, but these populations are dominated by groups of low angle veins dipping either to the southeast or northwest. The inclined, listric veins imply extension along subhorizontal planes relative to maximum shortening in a horizontal direction.

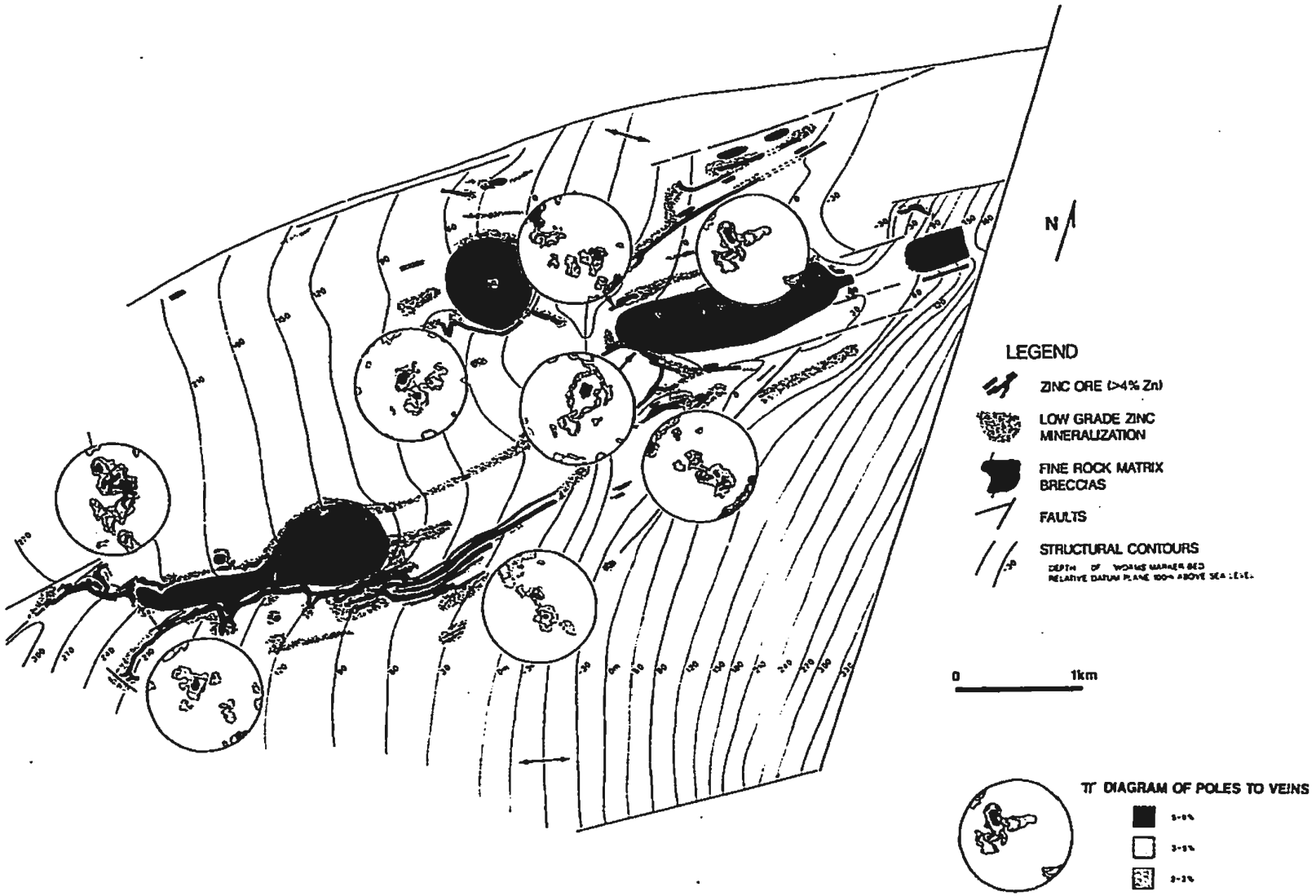

ORIENTATION OF VEINS IN THE MINE AREA

izontal planes. Maximum shortening was directed horizontally from the southeast. These veins, with consistent orientations, opened in relationship to deformation along reverse faults and probably in response to flexural slip on the limbs of monoclines (Bles and Feuga, 1986). Fracturing and dilation intensified around faults where abundant veins penetrated maximum thicknesses of stratigraphy.

Solution collapse played an important, but subordinate role in the formation of vein complexes. Sagging or collapse of beds generated a variety of structures: (1) vertical veins in gray dolostone beds above sheet cavities (Figs. 10.1, 10.3; Pl. 10.1b); (2) local collapse of fragments of these beds into megacavities 1 to 2 m in diameter (Pls. 7.3c, 10.1b,c); and (3) downdropped segments of beds or blocks of stratigraphy bounded by outward dipping faults (Fig. 10.2, section A - A'). In the Long Hole Stope cumulative dissolution over 30 m of stratigraphy caused large-scale faulting and collapse (Fig. 10.2).

10.3.4 Post-Ore Dilatant Fracturing

The orientation of post-ore veins generally differs from ore-stage ones. Steep, post-ore veins cut earlier low angle ones and locally exhibit opposite inclinations (Figs. 10.1, 10.5). Post-ore sets of low angle veins also occur ,however (Pl. 10.1a). Myriads of late ore-stage and post-ore veins and megabreccias surround cross-faults which generally post-date early ore (Fig. 10.5; Pl. 10.1c). These late veins significantly enlarge vein systems from their earlier extent (Fig. 10.9).

Post-ore saddle dolomites cement all ore-stage veins, post-ore

Figure 10.9 Cross-section of a Vein System North of the L Zone

A vein system northeast of the L Zone and Trout Lake Breccia (Fig. 1.4) developed along an inherited synsedimentary fault. During earlier history this fault was the locus of karst brecciation and deep discordant dolomitization. Limestone solution resulted in rock-matrix breccias and solution residue layers. Stratabound sphalerite mineralization occurred in the middle of the vein complex alongside and beneath pyrite mineralization. Post-ore veins significantly increased the size of the vein system both laterally and vertically.

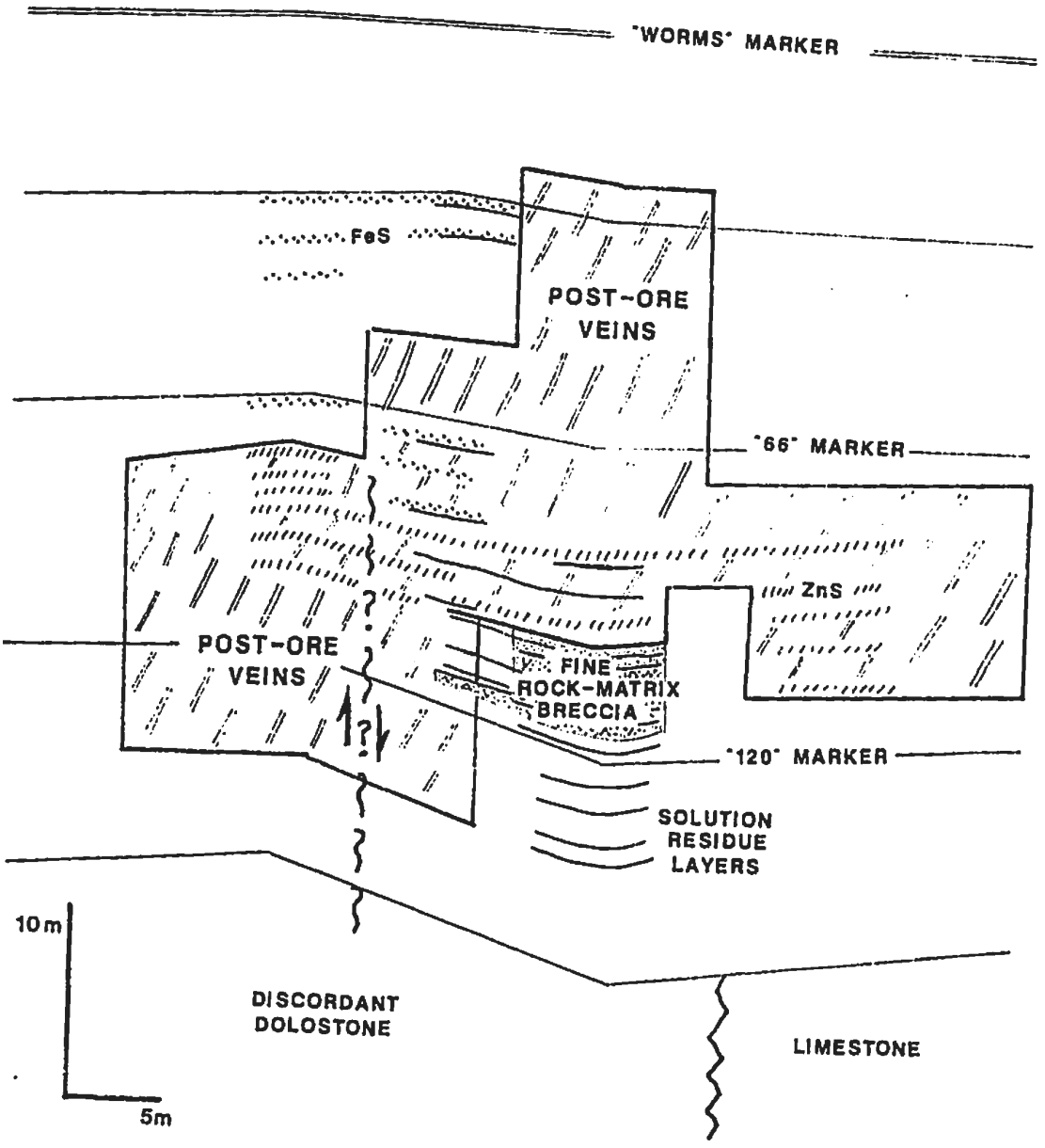

CROSS SECTION OF VEIN SYSTEM

fractures and breccias. Both Saddle Dolomites A and B cement splinter-like vein-breccias of dolostone and sphalerite wall rock (Pls. 6.1a, 10.1c). These late cements signify that post-ore deformation reopened ore-stage fractures as well as creating new ones.

Interpretation - The upper Catoche Formation fractured extensively and all veins dilated prior to cementation by saddle dolomite. Extension also reopened previous sulphide-cemented veins as saddle dolomite subsequently filled them. Lateral extension related to late vertical fault movement opened new, steep fractures which cut low angle ore-stage veins (Figs. 10.1, 10.5). Deformation along faults produced abundant fractures, vein-breccias and megabreccias (Figs. 10.3, 10.7; Pl. 10.1b,c). Fluids dissolved carbonates along the veins to form metre-wide cavities which filled with collapsed fragments (Pl. 10.1b).

Elevated pore fluid pressures probably combined with tectonically-controlled extension to fracture the dolostones and to maintain open pores. The linear vein systems became river-like conduits or sills in which strata and fractures expanded under elevated pore fluid\ pressure (Fyfe et al., 1979). Cemented veins and finely crystalline dolostone beds formed temporary aquicludes and allowed pore fluid pressures to periodically exceed the tensile strength of the rock, causing hydraulic fracturing (eg. Phillips, 1972; Price, 1975). Wall rocks splintered into numerous fragments during at least three phases of fracturing (Pl. 10.1c).

Typical mosaic breccias remained in situ as sphalerite and saddle dolomite gradually cemented veins and solution pores.. This relationship suggests that initial fracturing and rotation of fragments created pore

space and lack of large cavities prevented collapse. If pore fluid pressure exceeded lithostatic pressure for extended periods of time, however, the fluids alone could have maintained the pore space (Fyfe et al., 1979). A prolonged period of extensional stress during cementation also could have contributed to dilatancy.

10.4 Summary

Regional compression reactivated northeast-trending faults and secondary fracture systems that affected the St. George Group during deposition, subsurface karst and early burial. Most fracturing occurred in linear, stratabound areas of extension along four types of structures: (1) main trend faults, (2) rock-matrix breccias and other large dolostone bodies, (3) short cross-faults and (4) transfer zones between discontinuous faults. On a large scale entire vein systems (eg. L and T Zones, Fig. 10.3) can be considered zones of extension between major northeast-trending faults and around rigid dolostone bodies (mainly rock-matrix breccias)..

Fracturing and extension occurred throughout epigenetic dolomitization and sulphide mineralization. The entire mine area was fractured during early compression. Ore-stage fracturing and dilation formed low angle veins as northwest-directed regional compression warped beds around reverse faults and rock-matrix breccia bodies. Significant vertical displacement took place along cross-faults during late ore to post-ore stages. This vertical movement generated steep veins and extensive fracturing as most early fractures were reopened.

Solution collapse and hydraulic fracturing probably played impor-

tant but subordinate roles. Dolostones locally collapsed above metre-scale solution cavities. Significant fracturing and solution along faults formed narrow, breccia bodies, 5 to 30 m thick. Elevated pore fluid pressures combined with tectonic-controlled extension to maintain dilatent conditions during the cementation by sphalerites and saddle dolomites, and at least three times caused "splinter" brecciation during hydraulic fracturing.

CHAPTER 11 PRE-ORE EPIGENETIC DOLOSTONES

Gray, medium to coarse crystalline Dolomite IV with its characteristic xenotopic textures (Pl. 5.5a) overprints early burial dolostones (Dolomites II and III) (Pl. 5.1 f,g) forming pervasive dolomitized bodies in the Catoche Formation (Fig. 8.2, discussion in section 5.6). In coarse dolostone/pseudobreccia beds uniformly coarse, gray pre-ore dolomites are referred to as **coarse matrix dolostones** (Fig. 8.1). In contrast to earlier stratigraphic dolostones which generally are not related to faults these bodies occur locally around fractures. Cross-cutting veins and pores filled with sphalerite and post-ore dolomite indicate the pre-ore age of the dolostones (Fig. 8.1). Post-ore Dolomite V in turn overprints and effectively destroys these pre-ore dolostones where they form coarsely crystalline beds (Chapter 5, Pl. 5.1g).

Pre-ore, red CL Dolomite IV occurs in three forms:

(1) Most important, it locally replaces mottles, beds and fault-enveloping bodies of medium crystalline type Dolomites II and III (Chapter 5, Pl. 5.1f). These gray dolostones occur and are preserved outside areas of pseudobreccia, in the upper 10 to 20 m of the Catoche Formation and within deep discordant dolostones (Fig. 7.1). A few interbeds of this form occur between pseudobreccia beds. Such interbeds are only dolomitized around fracture zones in D/S complexes in contrast to extensive early fine dolostones. In Figure 3.1 gray dolostone bed "55" is only partially dolomitized in the limestone section in contrast to extensive

dolostone beds at "30" and "66".

(2) Dolomite IV also appears as minor intercrystalline cements in early fine dolostones.

(3) Small patches of Dolomite IV occur in pseudobreccia beds (Pl.5.1g). These relics within beds of later replacement dolostone (V) suggest that Dolomite IV was once much more extensive.

In the coarse dolostone-pseudobreccia beds patches and bands of gray to black, medium crystalline dolostone (V) replace precursor limestones and form a **coarse matrix dolostone** around finely crystalline mottles of former early dolostone (II and III) (Pl. 5.5c; Fig. 8.1). The gray dolomites which comprise this coarse matrix dolostone possess the dull red CL signature of post-ore Dolomite V and are partially replaced by Saddle Dolomite A (Pl. 5.5c). Although the replacement crystals are post-ore, cross-cutting sphalerite and saddle dolomite-filled pores and veins imply that the gray dolomites replace a pre-ore dolostone. The preservation of relic patches of Dolomite IV (Pl. 5.1g) supports this conclusion.

Interpretation - During the early stages of regional deformation linear fracture systems developed; warm, formational brines then migrated along them, permeated the surrounding limestones and dolostones and, in time, altered them. Increased temperature and salinity of formation waters promoted conversion to dolomite (Gaines, 1974) with xenotopic textures (Gregg and Sibley, 1984). Abnormal Mg abundances, CO_3/Ca ratios and/or elevated temperatures in these early, allochthonous

brines could have generated the presumed dolomitization of limestone matrix. (Low Mg/Ca ratios in most formation waters inhibit dolomitization of limestones in the deep subsurface (Morrow, 1982; Land, 1987)). Alternatively, pervasive dolomitization of the upper Catoche Formation occurred during early burial (II and III) and Dolomite IV largely replaced these dolostones. The common appearance of Dolomite IV as a replacement mineral supports this latter hypothesis. The destructive recrystallization (V) of coarse matrix dolostones, however, erased the petrographic evidence of their prehistory.

It is presumed here that epigenetic fracturing of the upper Catoche Formation led to extensive dolomitization of the limestones. The nature of the dolomitization (IV) varied from replacement of beds, discordant bodies and mottles of early burial dolomites (II and III), to conversion of burrowed lime wackestones to finely crystalline dolostones and alteration of lime grainstone matrix to coarse matrix dolostones (Fig. 11.1). These dolostones did not extend laterally beyond fracture zones as earlier, ubiquitous dolomitization (I,II and III) had done. During later epigenetic events finely crystalline beds fractured and coarse dolostone lithologies suffered extensive dissolution and recrystallization by post-ore Dolomite V.

Figure 11.1 Evolution of Coarse Matrix Dolostone

a. Early burial dolomites (II and III) formed dolostone mottles within limestone beds and discordant dolostones along steep fracture zones and margins of rock-matrix breccias.

b. Coarse matrix dolostone (IV) recrystallized some of these precursor dolostones and replaced beds of peloidal limestone in the vicinity of epigenetic fractures. Two types of fine to medium crystalline gray dolostone are shown: (1) extensive early fine dolostones (white, 2 m beds) and (2) pre-ore, epigenetic beds of local extent (stippled, 2 m beds between mottled dolostones).

EARLY BURIAL DOLOSTONE

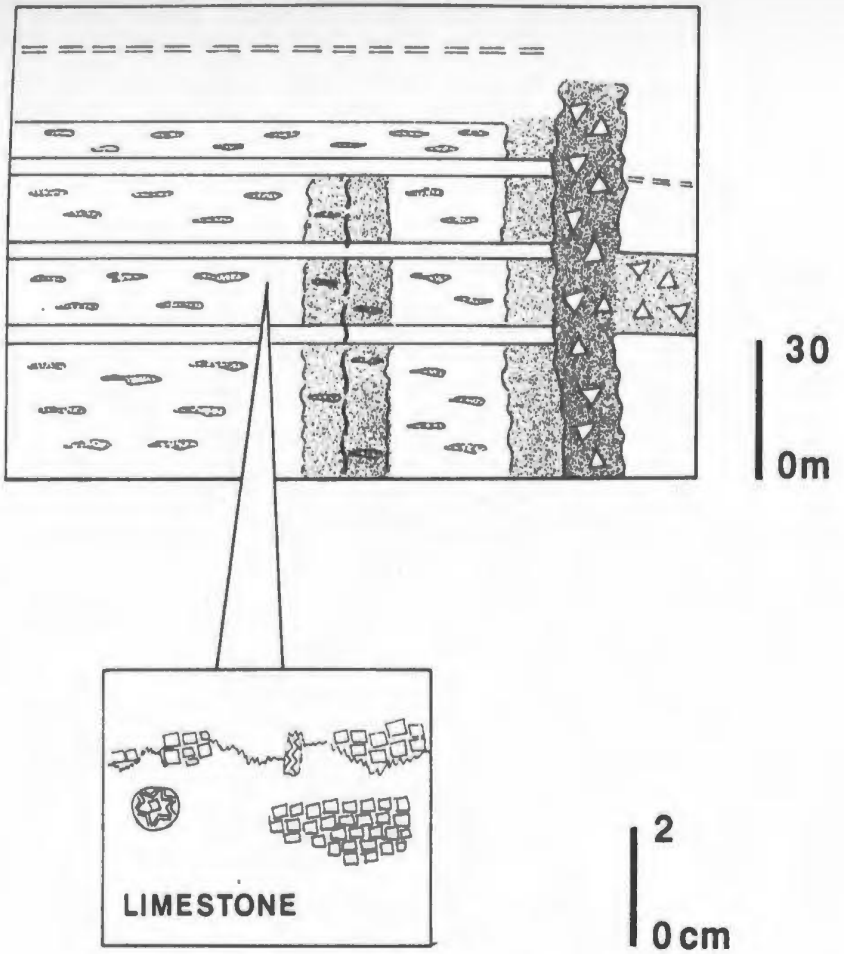

PERVASIVE PRE-ORE DOLOSTONE

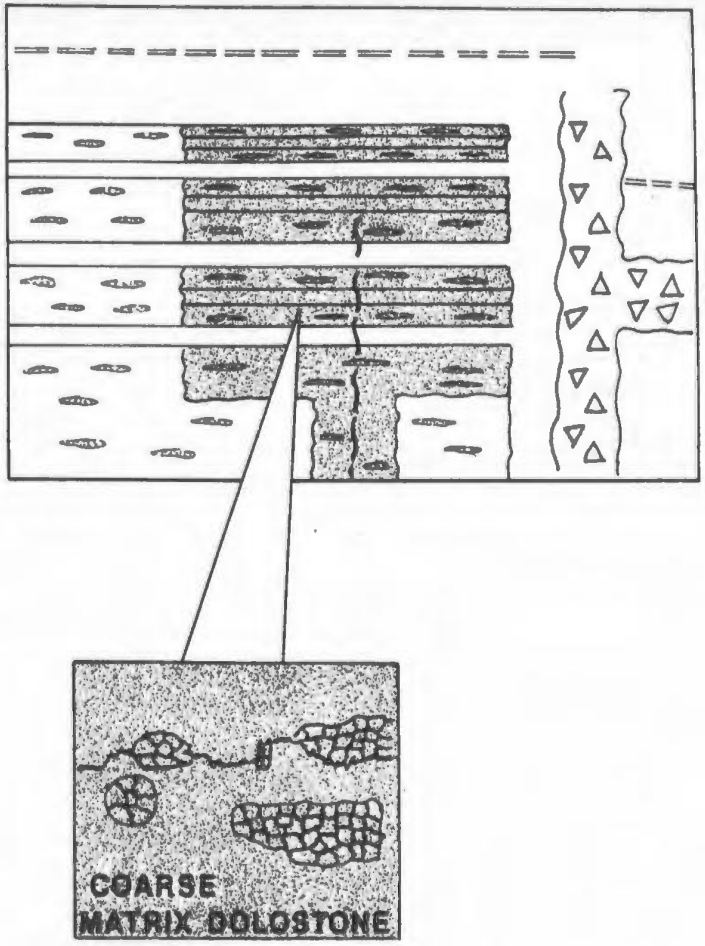

ROCK MATRIX BRECCIA

DOLOSTONE MOTTLES
IN LIMESTONE

EARLY DISCORDANT DOLOSTONE

COARSE MATRIX DOLOSTONE

CHAPTER 12 SPHALERITE ORE BODIES

12.1 Introduction - Relationship between Sphalerite Bodies, Vein Systems and Coarse Dolostones

Stratabound and discontinuous sphalerite ore bodies and low grade mineralized zones are curvilinear, shoestring shapes, 10 to 60 m wide by 3 to 30 m thick and 1000 to 5000 m long. They occur within vein systems that encircle rock-matrix breccias or follow nearby faults (Fig. 9.2). They are also enveloped by even larger bodies of coarse dolostone, 30 to 300 m wide by 50 m or more thick (Figs. 7.1, 9.1). Limestone is present 6 m or more below mineralization and only rarely are lateral remnants found in the proximity of sphalerite (Fig. 7.1).

The sphalerite bodies are composites of the two major generations of sulphides which crystallized during regional events of fracturing and faulting (described in Chapter 6). Early sphalerites occupy early, narrow vein systems which surround most faults and rock-matrix breccias. Late sphalerites overprint sets of veins which cut earlier sulphides and surround late, ore-stage faults along the L and T Zones (location map, Fig. 1.4). Acadian faults and folds deform the sphalerite bodies and, thus, constrain the timing of sulphide deposition to a pre-Devonian age.

12.2 Sphalerite Bodies: Their Internal Framework and Zinc Grade Distribution

12.2.1 Description

An ore lens comprises 3 to 30 mineralized coarse dolostone/pseudobreccia beds, each with 10 to 40% zinc in 15 to 60% sphalerite. These beds are interconnected by sulphide-cemented veins, the "conduits of mineralizing fluids", which cut barren gray dolostone interbeds. The intervening gray dolostone beds dilute the ore grade of lenses down to an average of 8% zinc (Fig. 12.1; Pl. 12.1b).

Ore zones and vein systems are nearly coincident. Beds within ore zones are intensively broken compared to outlying areas. Gray dolostone interbeds in the central and lower portions of ore zones are highly segmented by conjugate vein sets, normal and reverse faults and spar-cemented, mosaic breccias described in Chapter 10. These interbeds are progressively less disrupted toward the tops and sides of ore bodies (Figs. 10.1, 10.2, 12.1). Abundant megapores in coarse dolostone beds of highly veined areas give way to uniform fabrics of mesopores and replacement dolostone in less fractured portions of ore bodies.

Mineralization is usually concentrated in the upper half to upper third of pseudobreccia beds, where it partially fills ubiquitous mesopores, precipitates around the rims of megapores and replaces gray matrix and mottle dolostone (Figs. 12.1, 12.2; Pl. 12.1c,e). In many cases sphalerite is confined between an overlying gray dolostone interbed and an underlying discordant, 1 to 10 cm-thick band of gray/black dolostone in the middle of the pseudobreccia bed (Fig. 12.1, 12.2; Pl. 12.1d). Elsewhere, massive sphalerite is distributed uniformly

Figure 12.1 Cross-section of an Ore Body, the K Zone

Lenses of 5 to 45 % zinc occupy the upper portions of up to 10 pseudobreccia beds along a steep reverse fault. The lenses are bounded above by finely crystalline dolostone beds and below by curved, discordant gray dolostone bands (illustrated in Pls. 12.1d 13.2a). These bands also form inclined upper contacts on the north side of some ore lenses. Mineralization along the fault and veins interconnects the lenses. Pyrite occurs above and along the north side of the zinc ore.

The K Zone (location on Fig. 1.4) is situated on the gently folded flank of a rock-matrix breccia. It is surrounded by pseudobreccias which contain abundant saddle dolomite to the south and are transitional into gray dolostones and rock-matrix breccias 50 m to the north.

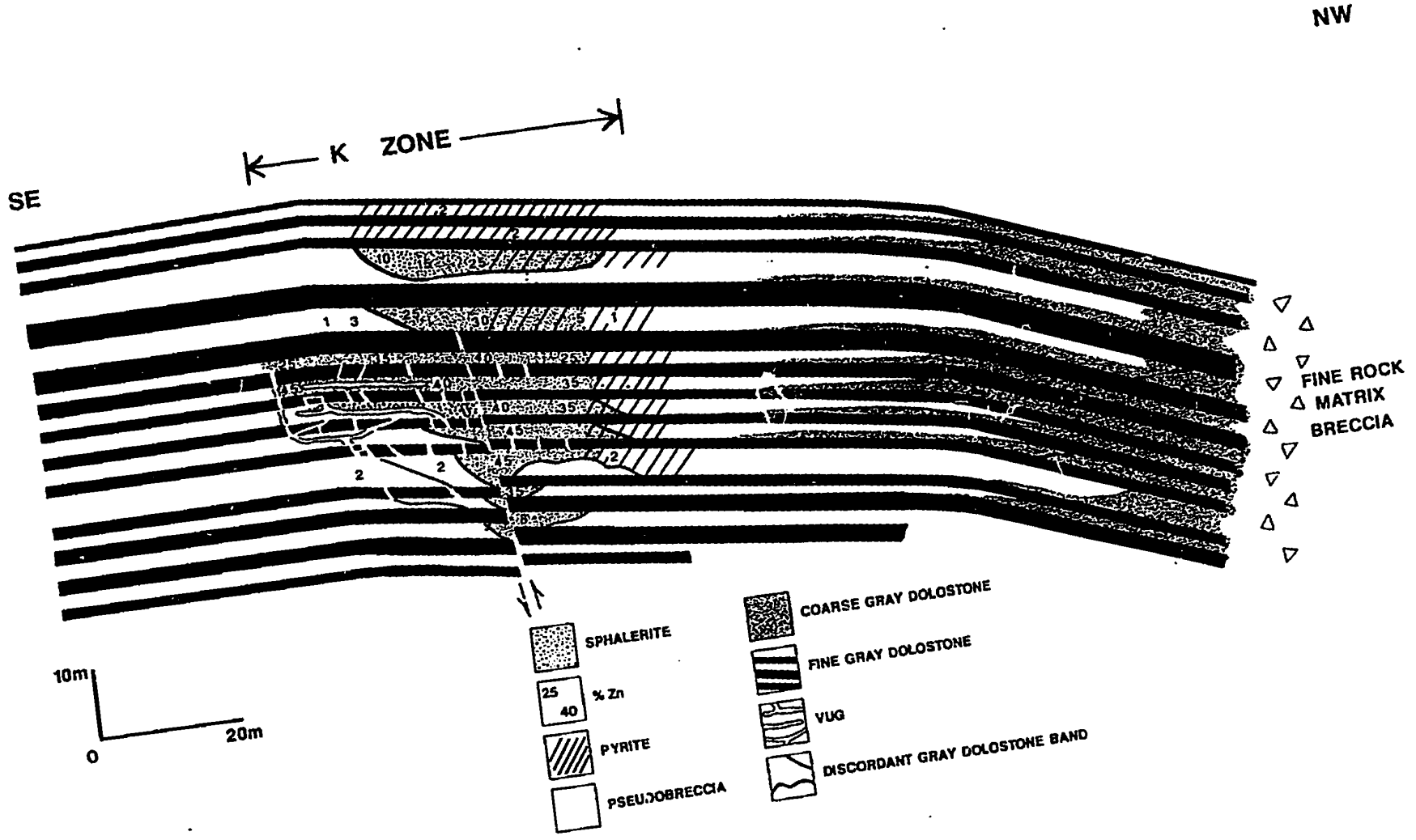
NW
SE
K ZONE
FINE ROCK
MATRIX
BRECCIA
10m
0
20m
SPHALERITE
25
40
% Zn
PYRITE
PSEUDOBRECCIA
COARSE GRAY DOLOSTONE
FINE GRAY DOLOSTONE
VUG
DISCORDANT GRAY DOLOSTONE BAND

Figure 12.2 Longitudinal Profile of the Lower K Zone

A longitudinal cross-section of the lower ore beds of the K Zone (location map, Fig. 1.4) is sketched from an underground rib pillar just below the portal. Early yellow sphalerite generally occurs in the upper portions of pseudo-breccia beds above discontinuous, cuspate bands of black dolostone (illustrated in Pls. 12a,d; 13.2a). These black bands probably acted as impervious boundaries, but also could have provided a source for sulphide reduction. (Any organic or H_2S content was removed during later events.) Megapores within ore beds, shown on the inset, are cemented in sequence by sphalerite, black geopetal dolomite, saddle dolomite and calcite (illustrated in Pl. 12.2f). The important geopetal dolomites are tilted and parallel the dip of bedding, indicating that the beds were flat-lying during ore deposition. Early yellow sphalerite mineralizes beds to the right. Later brown sphalerite occurs after yellow crystals in megapores (Pl. 12.2f) and forms ore beds at the left and bottom of the pillar.

LONGITUDINAL PROFILE OF THE LOWER K ZONE

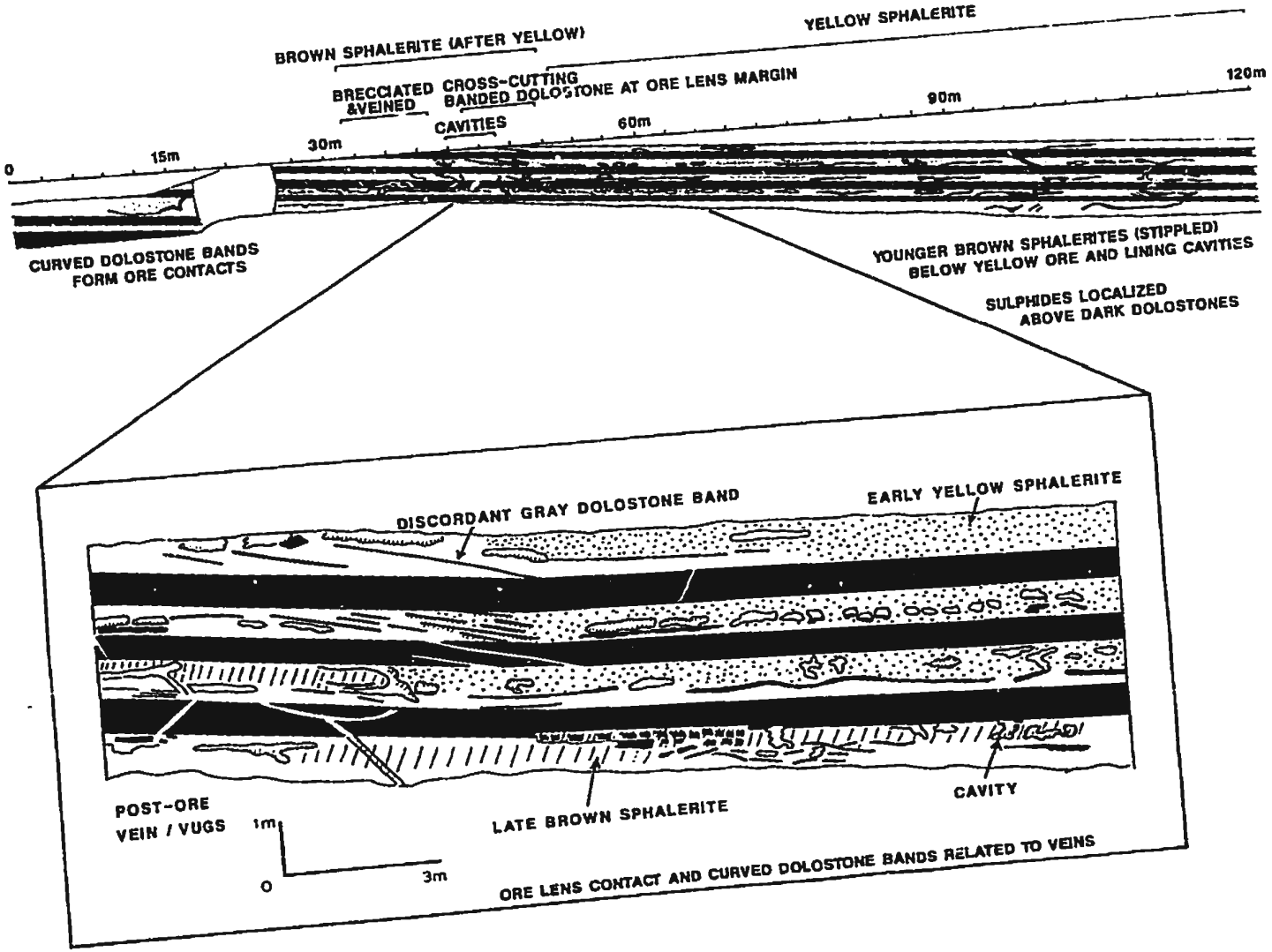

Plate 12.1 Distribution of Sphalerite in Coarse Dolostone Beds

a. Massive sphalerite (ZnS) occurs along the base of former sheet cavities and the margins of veins occluded with saddle dolomite. Zebra fabric on the lower left is curved downward toward the vein. East K Zone (Fig. 1.4), underground rib pillar. 1 m scale.

b. Contact of a sphalerite body. On the right sphalerite occurs along veins and horizontal cavities (arrows at right) and replaces surrounding dolostones (R). The sulphides end at an abrupt contact with a saddle dolomite-rich bed (arrow at left) associated with post-ore veins (all white veins inclined to the left). Saddle dolomites partially replace sulphides along the 'ragged' contact. Southwest end of the L Zone (location, Fig. 1.4). 1 m scale.

c. Massive sphalerite (ZnS) occurs in the upper portion of a coarse dolostone bed beneath an impervious, finely crystalline dolostone. Southwest L Zone (location, Fig. 1.4). 1 m scale.

d. Massive yellow sphalerite (ZnS) mineralizes the porous mid-portion of a pseudobreccia bed. Discontinuous black dolostone bands occur just below the sphalerite. East K Zone (location, Fig. 1.4). 1 m scale.

e. Sphalerite breccias (S) and megacrystalline saddle dolomites occupy the former site of sheet cavities just beneath a finely crystalline dolostone bed. Tabular layers of colloform sphalerite that once coated the cavity roof have collapsed (arrow). T Zone. 50 cm scale.

PLATE 12.1

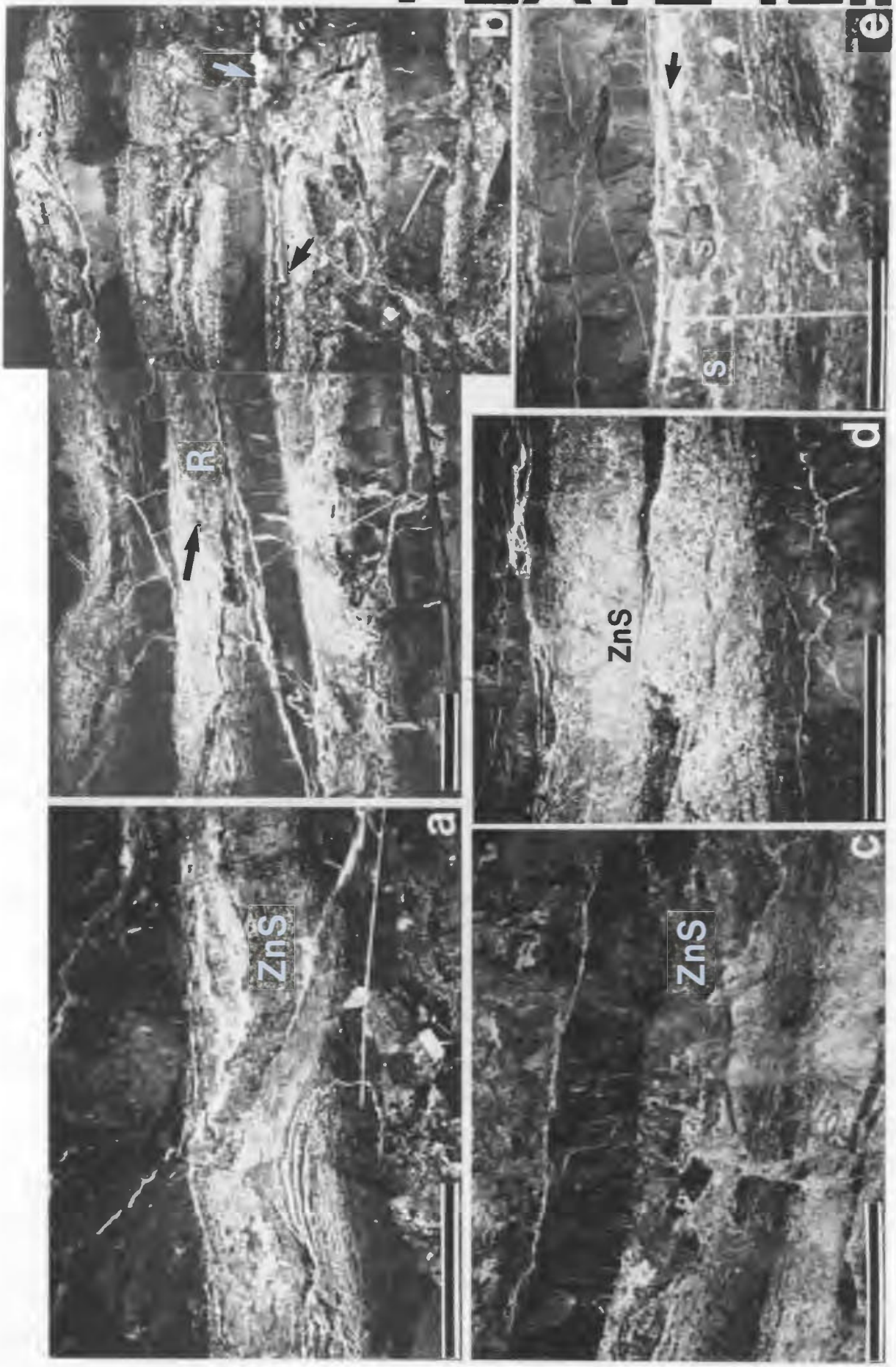

throughout pseudobreccia beds or decreases in abundance to trace amounts toward bases. Mineralization ends laterally either over narrow gradational zones or at abrupt contacts (Fig. 12.1). If abrupt, 8 to 45% ore grade zinc abuts against barren pseudobreccia either at a discordant gray dolostone band or a zone of abundant, 60 to 80%, white saddle dolomite (Fig. 12.1, Pl. 12.1b). Zinc abundances at gradational contacts diminish gradually to less than 3% over 1 to 5 m widths and locally over 30 m (Fig. 12.3). Disseminated mineralization broadens out over 100 to 300 m at the ends of ore bodies (Figs. 9.2, 12.3).

12.2.2 Interpretation

Fluids migrated horizontally through vein systems and sulphides precipitated in veins and pores of surrounding coarse dolostone beds. High grade concentrations of sulphides crystallized within narrow, highly permeable zones of abundant veins and large cavities and massively replaced adjacent coarse dolostone beds. Fluids diffused broadly along strike into porous dolostones and disseminated sulphides precipitated where veins and cavities were not abundant.

In individual coarse dolostone beds, metal-bearing fluids flowed through the upper parts of beds and particularly along cavities. Sulphides precipitated along the rims of cavities and in pores of surrounding dolostones. High grade mineralization commonly stopped at underlying gray-black dolostone bands, probable aquicludes which also could have caused local sulphur reduction. The bed-top ore lenses imply that the sulphides precipitated from a buoyant fluid that migrated to the upper parts of beds below impervious fine dolostones beds. Post-ore

Figure 12.3 Detailed Zinc Grade Distribution, F Zone

Zinc mineralization in the F Zone (location map, Fig. 1.4) occurs over widths of 10 to 50 m. Ore grade concentrations of zinc abruptly contact barren dolostone to the south. To the north and east zinc abundance diminishes to trace amounts over widths of 10 m. Closely spaced test holes for open pit development provided exceptional control on zinc grade variation in the F Zone. Zinc grades of 5 to 7 % in the F Zone were lower than most other zones which averaged 8 % zinc.

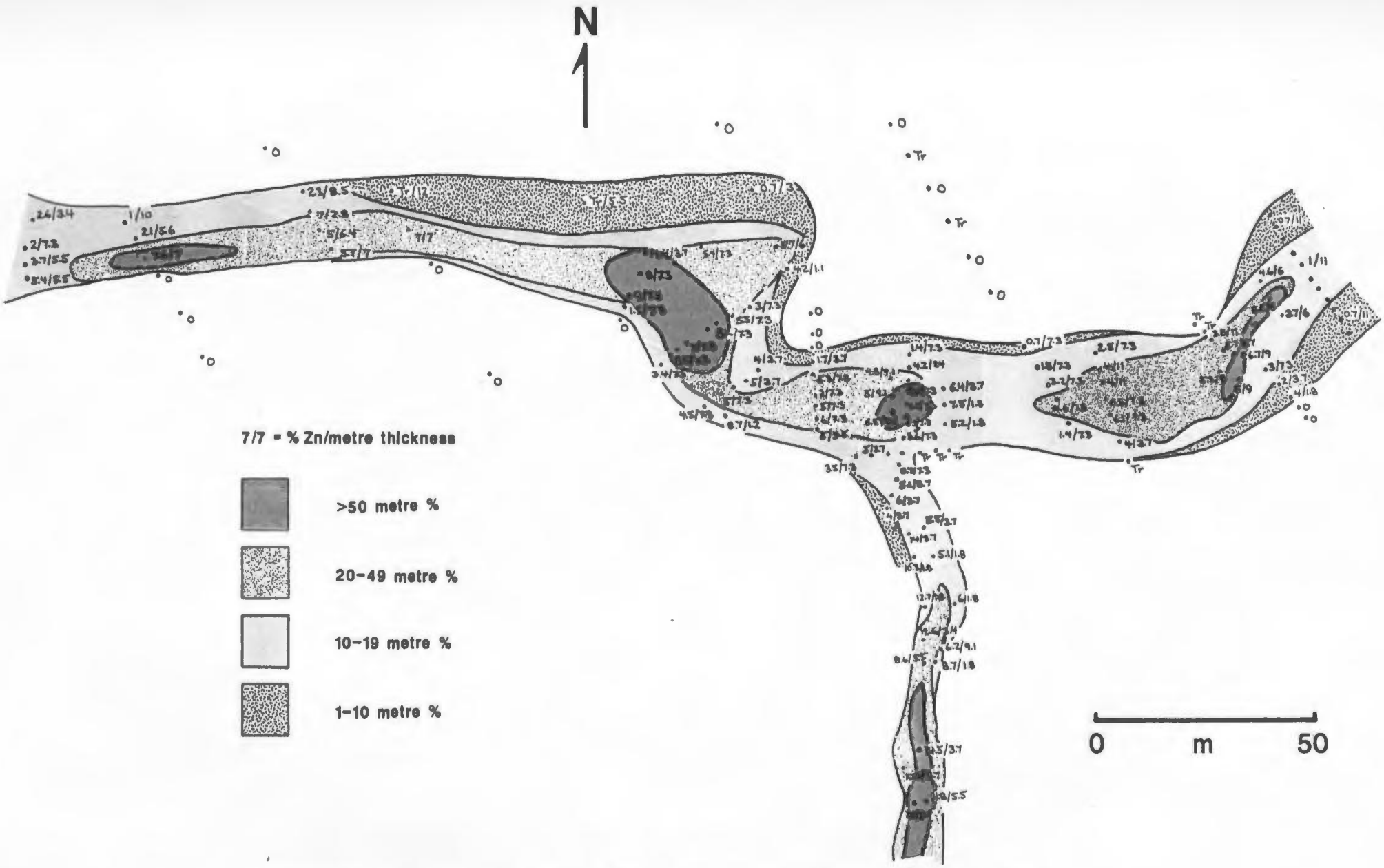

DETAILED ZINC GRADE DISTRIBUTION, F ZONE

saddle dolomites partially replaced sphalerite and, in particular, produced sharp boundaries at the edges of lenses.

12.3 The Habit of Mineralization

12.3.1 Description

Sphalerite cements pores and replaces dolomites. As a cement it lines and fills veins and solution pores and isopachously coats breccia fragments (Pls. 6.1a,g; 12.1b; 12.2c,f). Replacement modes range from wholesale replacement of portions of dolostone beds (Pls. 12.1a,b,c; 12.2a,b,d) to homogeneous dissemination of individual or groups of crystals in coarse dolostones (Pls. 6.3e; 12.2b).

(1) **Vein and cavity mineralization** forms centimetre-scale layers around fracture and solution megapores (Pls. 6.1a; 12.1b). Most mineralized veins occur in gray dolostone interbeds, whereas former solution cavities appear as sheet megapores in pseudobreccia beds. Pore cements coarsen outwards in colloform bands from very finely crystalline to fibrous to coarse, prismatic sphalerite (Fig. 6.1a). Later saddle dolomite and calcite occlude centres of pores. Sulphides also penetrate the wall rock in pseudobreccias as 10 to 15 cm-wide haloes of disseminated to massive sphalerite (Pls. 6.1e; 12.2d).

Sphalerite is commonly thickest on cavity floors and locally absent on roofs (Pls. 6.1a,g; 12.1b; 12.2c,d,e). Sphalerite also occurs on the tops of gray dolostone fragments and isolated dolostone mottles. This pattern of mineralization, characteristic of MVT deposits, is colloquially called "snow-on-roof" texture (Oder and Hook, 1950).

Plate 12.2 Sphalerite Ore Habits

a. Coalesced rosettes (medium gray) typical of massive early tan-brown ore. Laminated finely crystalline sphalerite, black geopetal sediments and white saddle dolomite fill pores between rosettes. Sample from massive ore beds adjacent to the cross-fault in the southwest K Zone (location, Figs. 1.4, 10.5). Scale in centimetres.

b. Rosettes of early red sphalerite replace gray coarse matrix dolostones and are partially replaced by saddle dolomite (arrows). Sample from massive red ore in the G Zone (location, Fig. 1.4; section, Fig. 6.4). 1 cm scale.

c. Disseminated sphalerite crystals occur on the tops of gray dolostone mottles (snow-on-roof texture) and nucleate on residues along stylolites. Sample from the L Zone (location map, Fig.1.4). 1 cm scale.

d. Rosettes of sphalerite replace dolostone nucleii. Saddle dolomite cements surrounding solution pores. Sample from the F Zone (location map, Fig. 1.4). Scale in centimetres.

e. Cavity mineralization. Sphalerite (medium gray) precipitates the base of a former sheet pore and as disseminated mineralization around dolostone mottles (black). Post-ore veins cut and brecciate sulphides. Saddle dolomite cements veins and sheet pores. Sample from the L Zone (location map, Fig. 1.4). Scale in centimetres.

PLATE 12.2

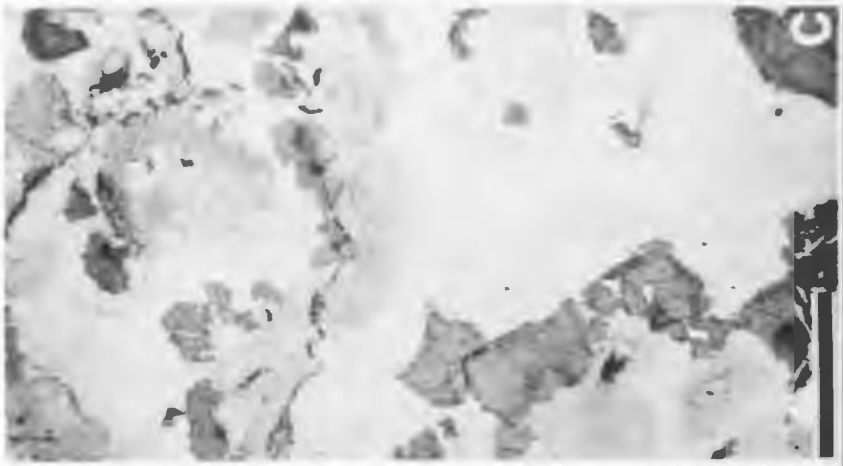

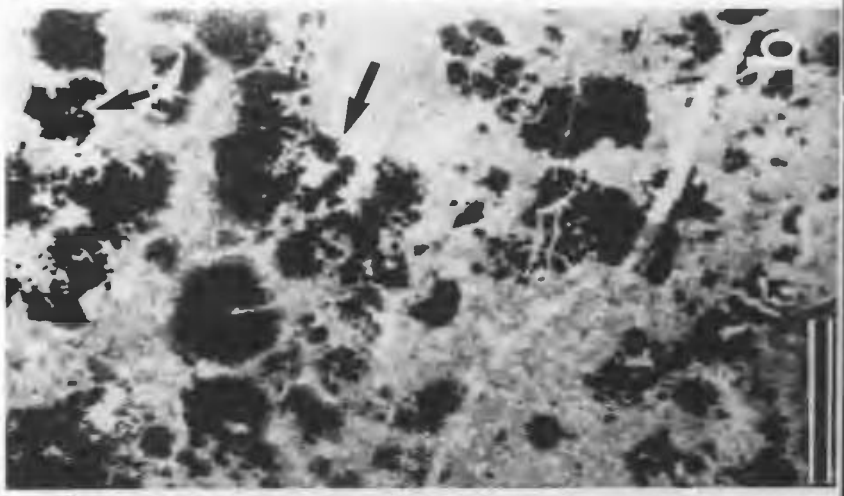

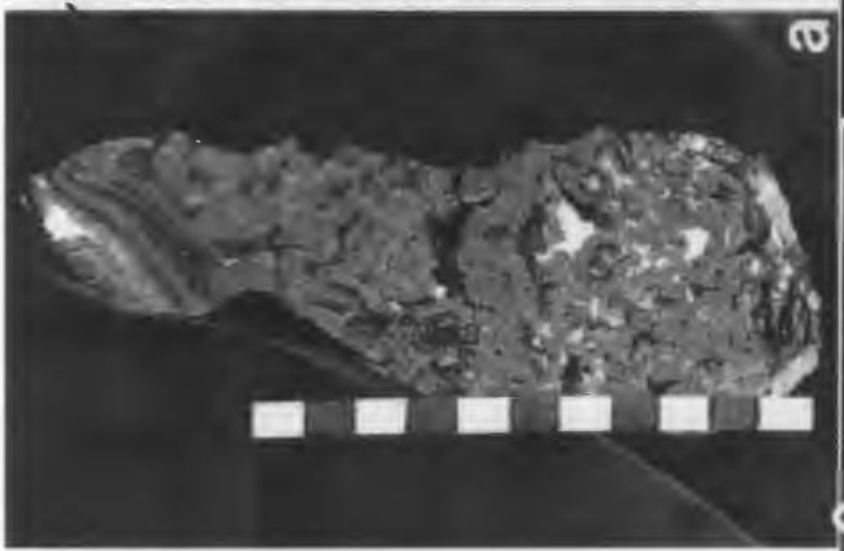

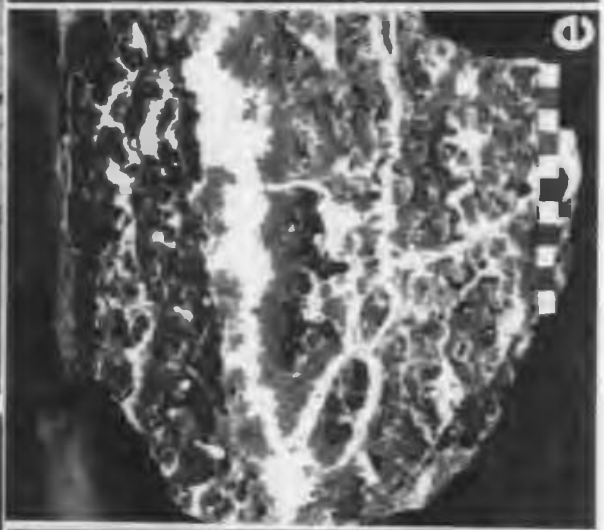

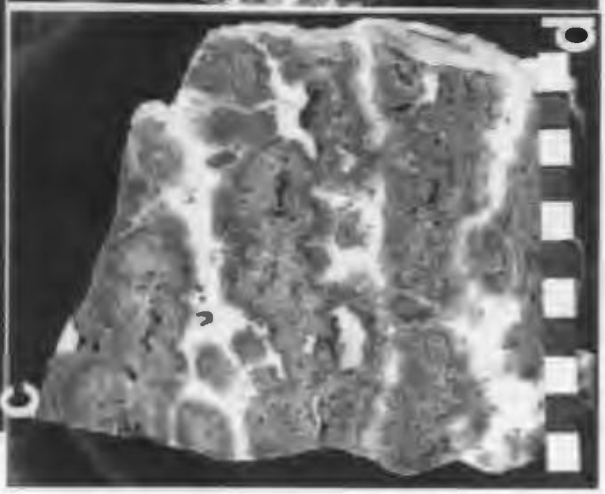

f. Massive sphalerite consists of rosettes of yellow sphalerite (pale gray) with brown sphalerite rims developed on resistent cores of early dolomitized burrows. A honey-comb network of solution pores between rosettes are filled with geopetal black dolomite and white saddle dolomite. Typical of massive early yellow ore in the lower K Zone (location map, Fig. 1.4; Figs. 12.1, 12,2; Pl. 12.1d). Scale in centimetres.

Cavity-base precipitates are also termed "mud in the cellar". These textures can be used as geopetal indicators.

Spar breccias with saddle dolomite cement also contain some sphalerite, generally disposed as a thin rim cement around fragments. Zinc grade in breccias is generally low (1 to 3%) compared to that around pseudobreccia cavities (10 to 25%). This style is common along highly brecciated cross-faults and in the North L Zone.

(2) **Massive sphalerite** locally replaces up to 75% of coarse dolostone beds (Fig. 12.1; Pl. 12.1a,b,c). Massive mineralized beds commonly contain 40 to 60% sphalerite (25 to 45% zinc). Sphalerite typically occurs as clusters of crystals and rosettes which either coalesce or are separated by dolomite. These crystals form both precipitates around dolostone (Pl. 12.2f) and partially or completely replace those cores (Pl. 12.2b,d). Surrounding geopetal sediments and saddle dolomite cements indicate the pore-filling origin of some sphalerites (Pl. 12.2d,f). Elsewhere, however, massive beds of 50 to 70 % sphalerite replace significant amounts of dolostone (Pl. 12.2a,b).

(3) **Disseminated mineralization** in pseudobreccia is widespread and characteristic of beds with partial mineralization around cavities and in the transitional boundaries of ore bodies. Typically individual and coalesced sphalerite crystals in pseudobreccia beds sit on the tops of gray dolostone mottles at the base of mesopores (Pl. 12.2c). Sphalerite is also disseminated within the intercrystalline pores of matrix dolostone and decorates residue-rich stylolites, like "pearls on a necklace" (Pls. 6.3e; 12.2c). The one to three sphalerite generations at each precipitation site only represent part of the sulphide cementa-

tion history in contrast to the multilayered cavity cements (compare Pls. 12.2c and 6.1a). Zinc grades in beds of disseminated sphalerite vary from trace quantities up to 25%.

In summary, ore bodies exhibit all three habits of sulphides. Most ore bodies contain 2 to 4 heavily mineralized to massive ore beds which assay between 25% to 45% zinc (Fig. 12.1). In veined and faulted areas, vein and cavity mineralization rims and surrounds sheet cavities in the upper half of pseudobreccia beds (Pl. 12.1b). Massive sphalerite "replaces" coarse dolostones adjacent to veins and cavities (Pl. 12.1a,b,c). Crystal rosettes in these beds nearly coalesce, occlude mesopores and partially replace dolostone mottles that they envelope (Pl. 12a,d,f). Disseminated sphalerite is distributed in lower halves of ore beds, the margins of ore bodies and throughout low grade mineralized zones (Pl. 12.2c, Fig. 12.1).

12.3.2 Interpretation

The different habit types reflect differences in focused vs. diffuse flow of ore fluids and in rates of nucleation and precipitation of crystals. In veins and cavities fluid flow was focused along large pores and fluids only pervaded 10 to 30 cm into the surrounding dolostone. In massive sphalerite beds, fluids diffused through the entire beds along a network of intercrystalline micropores and mesopores. Fibrous rosettes of sphalerite crystallized rapidly on numerous nucleation sites as zinc was rapidly "dumped". Solution pores enlarged during mineralization and coarse crystals precipitated the last cements. Disseminated sphalerite, in contrast, crystallized from fluids which

pervaded uniformly porous dolostones a metre to hundreds of metres away from open conduits. Sphalerite in these areas precipitated as coarse crystals at local sites such as residue-rich stylolites as a result of a dilute supply of zinc and sulphur..

12.4 The Geometry and Development of Composite Sphalerite Bodies

12.4.1 Introduction

Ore is commonly located 19 to 30 m below the top of the Catoche Formation (Worms Marker). Equivalent mine level numbers of 66 to 100 refer to feet below the Worms Marker (See Chapter 3, Fig. 3.1). The 80-90 level is the most common ore bed. "55, 60 and 66" gray dolostone interbeds commonly form hanging walls or backs of mine workings. Mineralization between "30 and 50" levels is rarely ore grade. Ore locally reaches deep levels between "100 and 165" (ie. 30 to 52 m below the top of the Catoche Formation) (Figs. 10.1, 10.3).

Typical 10 to 15 m-thick ore zones are asymmetric in cross-section similar to the geometry of vein systems which they overprint (Figs. 10.1, 12.1, 12.4). Relationships were well documented by the author and mine staff through serial sections of mapped faces and drill hole sections of all mined zones. Representative sections are illustrated in Chapters 10 and 12. A narrow (3 to 10 m-wide) area of stratigraphically deep ore, here called the "keel", commonly occurs on one side of the ore body. The "keel" surrounds high angle fault(s) and fractured rocks and is commonly situated adjacent to a fault or fine rock-matrix breccia body. Examples of well documented faults can be seen in Pls. 7.3a and

Figure 12.4 Cross-section through the east end of the L Zone

A cross-section through the east L Zone (section B - B' from Fig. 10.2; L Zone location in Fig. 1.4) illustrates the asymmetric geometry and composite nature of the ore body. Thick and stratigraphically deep ore is situated along a fault/fracture zone. A narrow lens of early ore occurs north of the fault. Several broad lenses of late sphalerite to the south step up the stratigraphy from a deep "keel" adjacent to the fault. In both early and late sulphide lenses progressively younger sphalerite precipitates occupy lower and outer edges of the bodies. Massive sphalerite beds in the L Zone have ore grades (10 to 20 %) compared to the F Zone (3 to 9 %, see Fig. 12.3) where mineralization was more patchy and disseminated.

CROSS SECTION THROUGH THE EAST END OF THE L ZONE

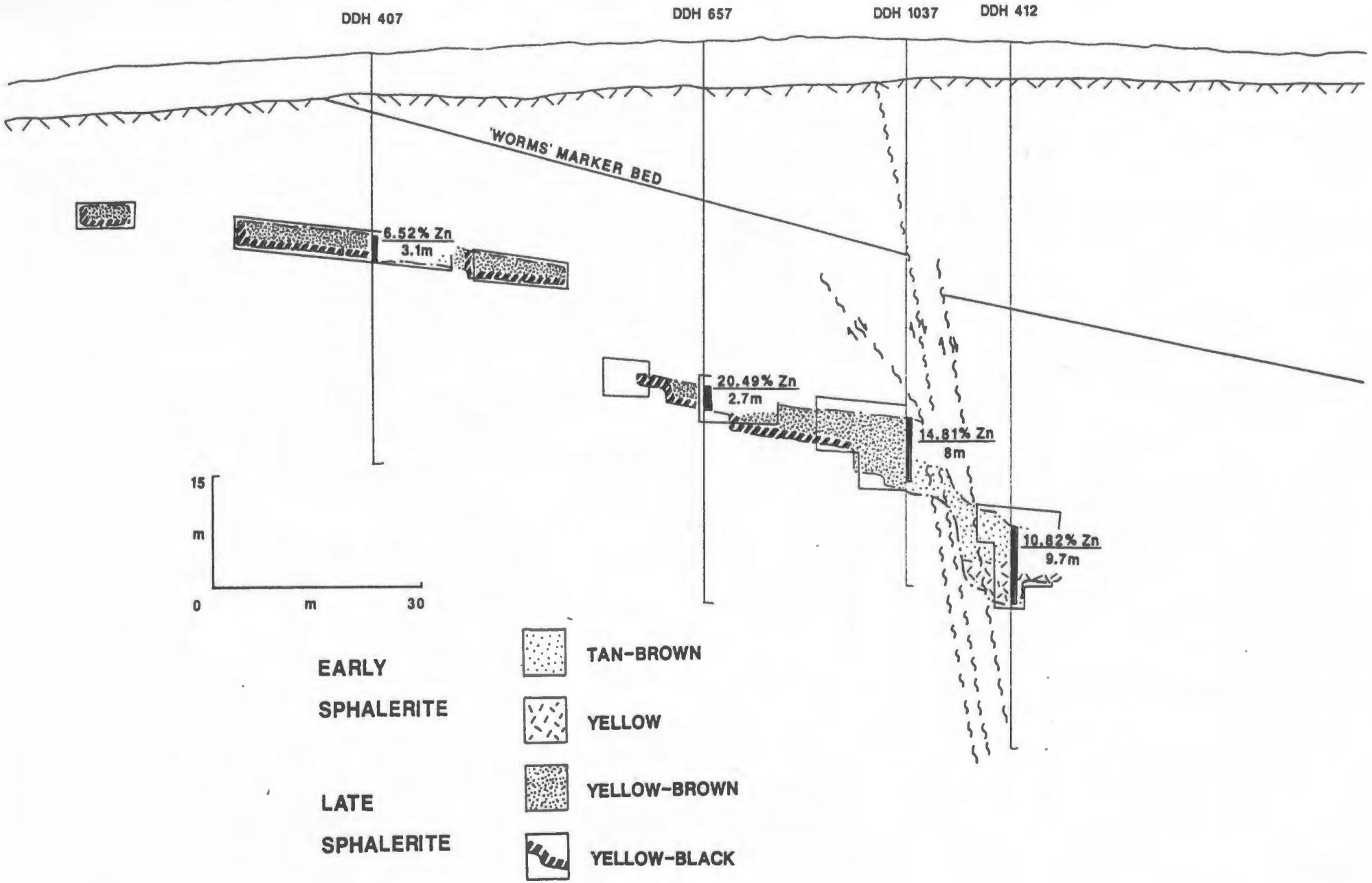

13.2c. The footwall and, in places, the hanging wall of the ore body climbs up-section in 3 to 10 m wide steps away from the keel to the outer edge of the ore body (Fig. 12.4). The up-section climb is accompanied by vertical thinning and lateral spreading of the ore body, decreasing in thickness from 10 to 30 m at the "keel" to 3 to 15 m at the outer edge and increasing in width from 15 to 70 to 200 m in the same direction. In places the keel is situated above deep fractures and discordant dolostones (Figs. 8.2, 12.1). The vertical continuity of these narrow, deep structures is unknown. Rare occurrences of pyrite and sphalerite are scattered in the underlying deep, discordant dolostones. Deep drilling beneath the east L Zone and the A Zone traced pyrite 50 m below ore horizons along fractured fault zones which penetrate below the Boat Harbour Formation.

The stratigraphic position of ore varies along as well as across strike. Hanging walls and footwalls abruptly rise and fall 3 to 10 m every 100 to 500 m along strike (Figs. 10.2, 10.3). The stratigraphic position and total thickness of veined and mineralized beds is controlled by major structures (Figs. 10.2, 10.3). Sphalerite penetrates deep strata (33 to 50 m below the top of the Catoche Formation) at cross fractures, breccia corners and along some faults. The Long Hole Stope of the L Zone at a breccia corner is an extreme example of anomalously thick ore with a deep footwall and high hanging wall (Fig. 10.2). Ore bodies commonly terminate laterally at these areas of deep mineralization (Fig. 10.1, 10.3).

Early and late sphalerites, described in Chapter 6, occur in separate or composite bodies in the mine area (Fig. 12.4, 12.5, 12.6).

Figure 12.5 Distribution of Early and Late Sulphides in the central L Zone

In the central L Zone sulphide bodies decrease in age with distance south from the Trout Lake fine rock-matrix breccia and the east L Zone fault (location map, Fig. 1.4). A zone of pyrite occurs between the breccia and a narrow body of early sphalerites. Broad lenses of late sphalerite partially overlap earlier ones and form several separate bodies. Bends in ore bodies are related to fracturing along cross-faults which acquired pronounced offsets during late ore stages.

DISTRIBUTION OF EARLY AND LATE SULPHIDES IN THE CENTRAL L ZONE

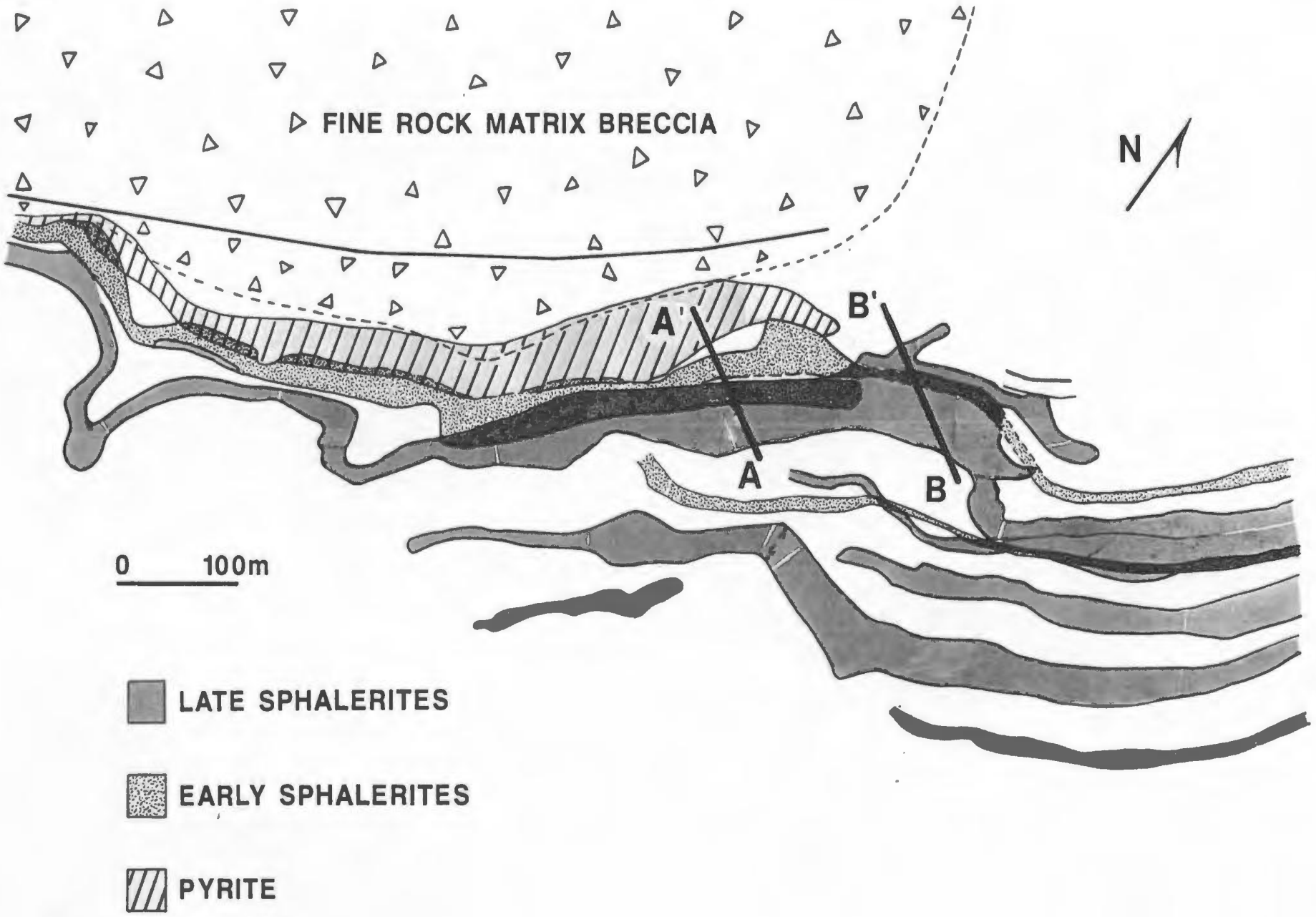

Figure 12.6 Sulphide Zonation, Long Hole Stope of the L Zone

Cross-sections of the Long Hole Stope of the L Zone illustrate structural controls on the distribution of sulphides (location on Figs. 1.4, 10.2, 12.5).

Geological cross-section A - A' is an interpretative compilation of drifts mapped across the top by R. Crossley, cross-sections constructed from drill core and observation of pillars 10 m wide by 30 m high. Outward-dipping faults flank vertical faults which control deep mineralization. Dolostone beds in the area are broken and sag.

Sphalerite zonation. Early sulphides form a narrow, vertical body. Pyrite occurs along the top and north flank. The earliest sphalerites appear only in the upper portion. Later yellow sphalerite forms cement rinds after earlier crystals at high levels and the only ore towards the base of the body.

Late, predominantly yellow-brown, sphalerites occupy the main faulted and brecciated body. Latest yellow-black sphalerite precipitates the lower and outer portions of the ore body, in a similar fashion to earlier mineralization.

The distribution of early and late sphalerites suggests that prior to early mineralization local fracturing occurred along the north side of the L Zone. Widespread fracturing, brecciation and displacement along outward-dipping faults did not occur, however, until the beginning of late mineralization.

SULPHIDE ZONATION, LONG HOLE STOPE, L ZONE

GEOLOGICAL CROSS-SECTION A-A'

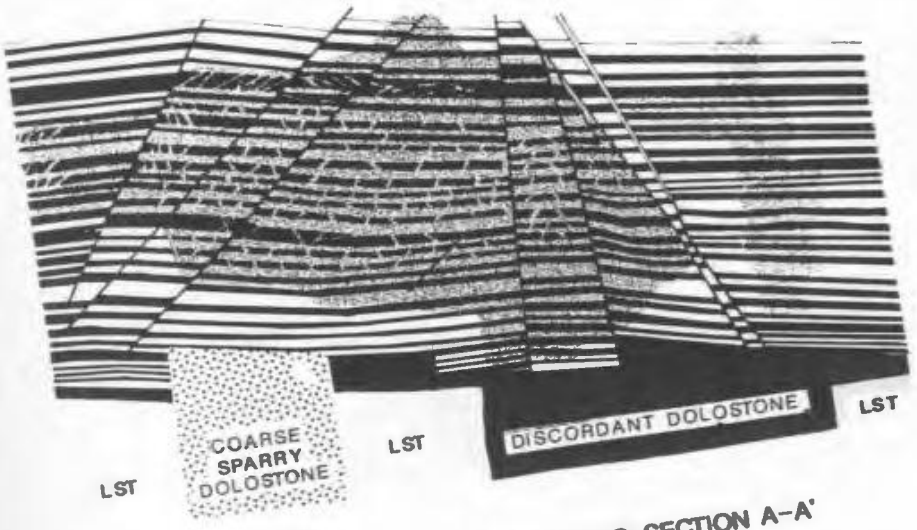

SPHALERITE ZONATION OF CROSS-SECTION A-A'

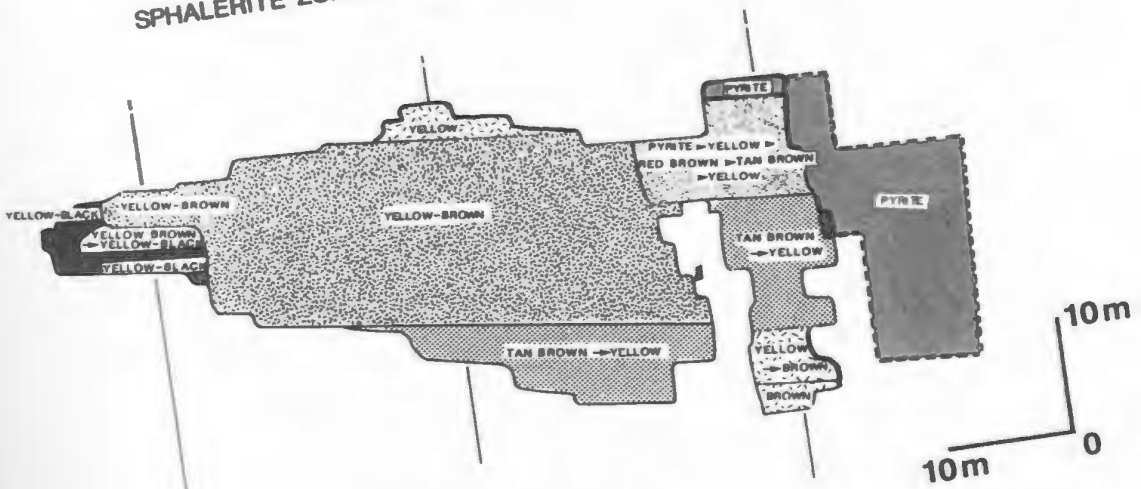

CROSS-SECTION B-B'

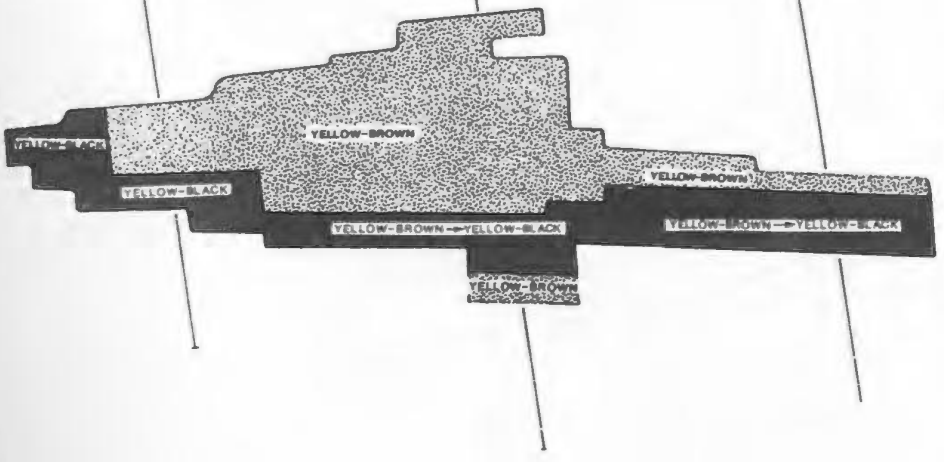

Widespread, early sphalerites constitute approximately 4 million short tons in the mine area. Late sphalerite ore only occurs along the linear trend of the L and T Zones where it adds 3 million tons to form the largest ore bodies in the mine area. The following description of the development of the sphalerite bodies is divided into a discussion of the early and late sulphides.

12.4.2 Early Sphalerite Bodies

Early sphalerites are distributed throughout the mine area as narrow, 10 to 35 m-wide lenses with a vertical to horizontal ratio of 2:1 to 1:1. Both ore and low-grade mineralization lie within 50 m of breccia margins and faults compared to late sphalerites which occur further from these structures (Fig. 12.6).

A typical ore body is characterized by precipitation of successively younger sphalerites down through the ore body: Early red sphalerite and pyrite occur in the top 1 to 5 m. Tan-brown sphalerites dominate the middle 5 to 10 m. Yellow sphalerite is disposed in the basal 5 to 20 m (Figs. 12.4, 12.6). Pyrite is also only concentrated in a narrow zone along the vertical contact between the ore body and gray, medium crystalline dolostones. The development of early sphalerite is separated and described in four stages of mineral paragenesis. Chapter 6 describes petrographic and geochemical details.

<u>Stage 1, Pyrite Haloes</u> - The pyrite generally occurs as very fine to fine-sized framboidal crystals disseminated through gray dolostone. Locally it is a first stage cement along pores within pseudobreccia beds, appearing before or interlayered with the earliest sphalerites.

Stage 2, Red Sphalerite - Early red sphalerites at the top of ore bodies are disposed in narrow, anastomosing stringers that also contain minor pyrite and galena. They are finely crystalline, commonly displaying fibrous to dendritic habits. They form only a minor portion of the ore bodies.

Stage 3, Tan-brown Sphalerite - Fibrous, tan-brown sphalerites precipitate in the middle to upper parts of most early ore lenses as rosettes and banded, colloform cements around cavity rims (Pl. 12.2d). This sphalerite also occurs in cross-fractures as massive, 8 to 13 m-thick bodies, 40 to 55 m below the top of the Catoche Formation (the 120 to 165 foot mine levels). Crystal rosettes in these massive beds coalesce, replace precursor dolostones and occlude most secondary pores (Pl. 12.2a,b). These massive sphalerite beds constitute some of the highest grades and tonnages per area at the mine.

Stage 4, Yellow Sphalerite - Coarse, prismatic yellow sphalerites which occur in the bottom half to two-thirds and outer extensions of ore lenses generally cement the edges of mesopores and cavities (Pls. 6.1a, 12.2f). Abundant rosettes of yellow sphalerite also make up massive ore beds, 3 to 15 m thick and 15 to 30 m wide, which constitute nearly two-thirds of the early ore lenses within the A, K and L Zones (Fig. 12.2; Pl. 12.2f).

Homogenization temperatures of fluid inclusions from yellow sphalerite vary throughout the mine area. Anomalously high T_h's (160 to 185°C) occur in stratigraphically deep sphalerites in the B and H Zones. Inclusions from the L and T Zones have T_h modes of 140°C, whereas ones from the F Zone range from 95°C to 115°C (Fig. 6.3).

12.4.3 Late Sphalerite Bodies

Late yellow-brown to yellow-black sphalerites occur as ore bodies in the L and T Zones where they constitute nearly two-thirds of the total ore tonnage and as areas of low grade mineralization to the southwest and northeast of the L Zone (U, V, M and Black Duck Zones) (locations on Figs. 1.3, 1.4). The latest yellow-black sphalerite is widely disseminated throughout the region.

Late sphalerite ore bodies are generally tabular in cross-section with a vertical to horizontal ratio of 3:4 to 1:5 (Fig. 12.4). They are situated as far as 200 m from faults or rock-matrix breccias where they constitute separate ore lenses or the up-dip and upper stratigraphic portions of composite bodies (Fig. 12.4). Mineralization and veining in these areas is commonly restricted to a few beds in intervals only 3 to 10 m thick (Fig. 12.4). Anomalous thicknesses of late sphalerite (up to 30 m) occur locally along cross-faults and in the Long Hole Stope (Figs. 12.5, 12.6)

Late sphalerite bodies locally diverge from northeasterly trends where they loop around cross-faults in what are colloquially termed "whoop-de-doos" (R. Crossley, pers. comm. 1980)(Figs. 9.3, 12.5). They also occur as multiple, parallel lenses in the east L Zone (Figs. 9.3, 10.2, 12.5).

These ore bodies, similarly to the early ones, are characterized by the occurrence of successively younger sphalerites down section and toward the up-dip, outer edge: Yellow-brown sphalerite occurs in the upper 5 to 15 m. Latest yellow-black sphalerites are disposed in the basal 2 to 5 m and over widths of 2 to 10 m on the outer edge (Figs.

12.4, 12.6). A two stage development of late sphalerites is described below.

Stage 1, Yellow-brown Sphalerite - Coarse crystals of yellow-brown sphalerite occur in the middle to upper portions of late ore bodies both as vein and cavity cements and as massive beds. They isopachously cement breccias of early sphalerites where early and late bodies overlap (Pl. 6.1f). In contrast to early tan-brown sphalerites with fine, fibrous crystals in colloform and rosette habits, these crystals are disposed in patches of coalesced coarse crystals which partially replace dolostones (Pl. 6.4a).

Stage 2, Yellow-black - Yellow-black crystals, the latest ore-stage sphalerites, are disposed in the bottom third and the edges of late ore bodies, but also occur throughout the area as minor ore concentrations in early ore bodies and as widespread disseminated crystals. The typical coarse, prismatic crystals commonly occur as vein and vug cements, but locally they form massive ore beds. Their widespread distribution is related to regional networks of late veins and mesopores in coarse dolostones. The range and distribution of $\delta^{34}S$ values of late sphalerites exhibit a decrease from 24 o/oo in the centres of ore bodies to 18.8 o/oo in outlying areas (Coron, 1982; this study) (refer to discussion in Chapter 6).

12.4.4 Interpretation of Mineral Zonation

The geometries of bodies of early and late sphalerite conformed to the changing dimensions of fracture systems as deformation continued throughout the ore stage. Early sphalerites mineralized narrow fracture

zones within tens of metres of faults (Fig. 12.4, 12.6). The position of sulphides at tops of fractured aquifers suggests that warm, metal-bearing fluids were buoyant, rose upwards within the Catoche Formation and probably displaced denser local formation waters. Fibrous to dendritic red sphalerite rapidly precipitated from initial iron-rich fluids. Fine pyrite precipitated where the fluids encountered and permeated fine gray dolostones above, beside and below vein systems. Fluids progressively migrated through lower stratigraphic levels as sphalerites cemented upper beds and as carbonate dissolution increased permeability in underlying dolostones. The acidic products of sulphide precipitation and carbonate undersaturation from fluid mixing probably caused this dissolution. Finely crystalline, fibrous rosettes and colloform deposits of tan-brown sphalerite rapidly and extensively precipitated in the upper to middle portions of the aquifer. Finally, coarse yellow sphalerites mineralized the lower portions of vein systems as they grew slowly on extensive veins and solution pores that had formed during the first influxes of metal-bearing fluids.

A separate phase of regional compression and displacement along faults followed the deposition of early sphalerites and propagated folds and fractures up to 200 m from these faults. This fracturing affected thin packages of beds up dip from faults and produced looping paths of fractures around cross-faults. Late sphalerites precipitated within these late fracture systems in downward and outward younging sequences, similar to early bodies. Comparatively coarse yellow-black crystals precipitated extensively in pores as they formed the lower and outer portions of late ore bodies and widely disseminated crystals throughout

the area.

The discontinuous nature of both early and late ore bodies was related to one or more reasons. Firstly, local abundances of H_2S in rock-matrix breccias and other early dolostone bodies could have catalysed sulphide precipitation, as in the organic brown dolostones in the southeast Missouri Viburnum district (J. Viets, pers. comm. 1988). Extension around rock-matrix breccias and between northeast-trending faults, a second possible reason, provided local areas of permeability into which ore fluids migrated. Faults beneath deep fracture zones served as vertical conduits for the migration of ore fluids. Various features support the latter hypothesis. Deep discordant dolostones around these faults contain scattered sulphides. Thick deposits of massive, tan-brown sphalerite crystallized where fluids entered deep fracture zones in the upper Catoche Formation. The positive $\delta^{34}S$ values (24 to 28 o/oo) and high T_h's (165 to 185°C) of these deposits probably represent the composition of relatively warm ore fluids with unfractionated sulphur as they emanated from deep faults.

12.5 Constraints on the Interpretation of Ore Genesis

12.5.1 Introduction

Features of the Daniel's Harbour deposit narrow the possible interpretation of the subsurface environment of ore deposition. The important constraints are discussed in terms of how they affect interpretation of the setting, timing, nature and source of ore fluids and, lastly, the pathways of these fluids.

12.5.2 Setting

Ore deposition was an epigenetic, deep, burial event. This is implied by elevated fluid inclusion temperatures, pressure solution features in ore-stage dolostones and suggestion of lithostatic fluid pressures. A minimum estimated depth of 700 to 1000 m accounts for known cover rocks of the Table Head and Goose Tickle Groups and the Humber Arm Allochthon. Thermal maturation of conodonts (CAI of 2 to 2 1/2; Nowlan and Barnes, 1987) suggests further burial to 2000 to 3000 m (Harris, 1979). Near Cape Norman lack of correlation between elevated thermal maturation of conodonts (CAI of 4 to 5) and sphalerite fluid inclusion T_h's (140°C) implies, however, some regional uplift prior to sulphide deposition (Sangster et al., 1989).

Ore deposition is intrinsically related to regional tectonism which is interpreted to be the early stages of Acadian tectonism. The sphalerite bodies overprint fracture systems which developed before, during and after ore deposition. These fractures formed the conduits for lateral fluid movement. Deep fracture zones and discordant dolostones along northeast-trending faults also suggest that the fluids moved vertically along these fractures. These vertical conduits may have enabled buoyant ore fluids to transport Pb directly from basement sources.

12.5.3 Timing

Ore deposition occurred long after the onset of pressure solution and crystallization of early burial dolomites (I and II), followed epigenetic Dolomite IV and pre-dated basement uplift. Pre-ore dolomites

(IV) and sphalerite overprint stylolites and early burial dolomites (II and III) which formed during Middle Ordovician burial at the time of the Taconic Orogeny. Regional conodont alteration implies that maturation occurred after burial beneath the Humber Arm Allochthon. These relationships suggest a maximum age of ore deposition in the Upper Ordovician, after the Taconic Orogeny.

Coeval fracturing and displacement along steep faults is related to regional compression and fragmentation of the autochthon during the early stages of the Acadian Orogeny. The Taconic deformation does not have such a penetrative effect on the autochthon (Cawood and Williams, 1988). The earliest "Acadian" tectonism in central Newfoundland and the White Bay area is dated as Silurian (423 to 428 ma., Dunning et al., 1988).

Laser $^{40}Ar/^{39}Ar$ dating of K-feldspars cemented with sphalerite in the region indicates an age of 350 to 370 ma. (Hall et al., 1989).

Numerous faults which displace the ore zones are related to broad folding and fragmentation of the autochthon coeval with the uplift of the Long Range Inlier. The age of the uplift is no older than Silurian and no younger than early Carboniferous (Visean) (Hyde et al., 1983; Cawood, pers. comm., 1988).

In conclusion, these various constraints suggest that sphalerite deposition occurred during the early stages of the Acadian Orogeny, possibly during the Silurian. It post-dated the Middle Ordovician Taconic Orogeny and happened before the uplift of the Long Range Inlier, an event with broad age constraints. The apparent pre-Carboniferous and possible Silurian age of this uplift, however, precludes that the

mineralization was a Late Paleozoic event.

12.5.4 Nature and Source of the Ore Fluids

Fluids preserved in the sphalerite inclusions are hypersaline brines with 24 weight % NaCl and a combination of Ca, K and Mg chlorides. Such brines are typical of formational fluids of sedimentary basins (White, 1968; Sverjensky, 1983) and basinal fluids which have passed through, resided in and interacted with metamorphosed basement rocks (Kelly et al., 1986). This origin is confirmed by the positive $\delta^{34}S$ values (18 to 28 o/oo) of the sphalerites, which imply derivation of sulphur from Lower Paleozoic sea water sulphate (Claypool et al., 1980).

Pb isotope data and homogenization temperatures of fluid inclusions suggest that the fluids travelled from deeper source areas. The non-radiogenic Pb was probably leached from feldspars in the Grenvillian basement or arkoses at the base of the sedimentary pile (Coron, 1982; Swinden et al., 1988). Fluid inclusion T_h's (mode=140°C, maximum=185°C) are higher than the expected thermal maximum caused by burial (120°C at 3000 m depth) and, thus, suggest heating of fluids in a deeper source area.

Much of the chemistry of the ore fluids remains unknown, however. The ore fluids were probably one of two main types: (1) acidic fluids which carried both metal-chloride complexes and reduced sulphur (Sverjensky, 1986) or (2) neutral to alkaline brines that transported metal-complexes, but no reduced sulphur (Anderson, 1973, 1983). A single fluid with metals and reduced sulphur can repeatedly generate

sulphide precipitation as regionally extensive layers and produce reversible dissolution/precipitation reactions (McClimans et al., 1980; Sverjensky, 1986). These features are characteristic of the Daniel's Harbour deposit (Chapter 6, Fig. 6.1). Local epigenetic silicification in the vicinity of faults may also reflect the acidic nature of fluids. The survival of acidic fluids travelling through carbonates is questionable, however. The fluids must maintain high partial pressures of CO_2 and an abundance of Ca to prevent carbonate dissolution and buffering of the acidic brines (Anderson, 1983).

Oxidized brines with a neutral to high pH could maintain metals in solution as they pass through carbonates (Anderson, 1973, 1983). Sulphides would precipitate either where SO_4 in the ore fluid is reduced to H_2S or where metal-complexes mix with another fluid containing reduced sulphur (Anderson, 1983).

12.5.5 Pathways of the Fluids

Metal-bearing fluids in other MVT districts are commonly interpreted to have migrated up dip from shale basins into shallow subsurface carbonates (eg. Jackson and Beales, 1967; Leach and Rowan, 1986). Brines dewatered from basinal shales migrate under the force of compaction, tectonic compression or gravity-driven meteoric fluids recharging from tectonic uplands (Garven, 1985). These models generally presume that the basin - platform transition is relatively undisturbed. (These models are discussed in Chapter 14).

In western Newfoundland the basinal sediments were tectonically emplaced on top of the platform during the Taconic Orogeny. Fluid

migration prior to and during early phases of the Acadian Orogeny was constrained by this complex tectono-stratigraphic framework. Regional compression continued to dewater shales with the formation of slatey cleavage during the Acadian Orogeny. Deep crustal anatexis to the east probably caused thermal convection of fluids and release of water, metals and sulphur during mineral transformations.

Stratabound patterns of mineralization and dolomitization imply that fluids migrated laterally along linear fracture systems for thousands of metres. The discontinuous and local nature of ore bodies, deep discordant dolostones and the Grenvillian signature of Pb isotopes suggest, however, that ore fluids may have migrated vertically from basement depths along steep faults. The sphalerite stratigraphy shows that warm metal-bearing fluids were buoyant and migrated to the top of the fractured aquifers in the upper Catoche Formation, where the sulphides precipitated.

12.6 Interpretation: Formation of the Ore Bodies

Sphalerites crystallized in and around vein systems in the upper Catoche Formation. The geometry and extent of early and late sulphide bodies varied according to the style of coeval deformation and porosity development. Early sulphides crystallized in narrow, ubiquitous vein systems which bordered fracture lineaments and rock-matrix breccia bodies throughout the mine area. Late sulphide bodies formed only along the L Zone trend, the main area of late fracturing. These volumetrically significant late sphalerite deposits of the L Zone replaced extensive

porous dolostones along multiple fracture zones.

In all ore bodies, sphalerites crystallized from fluids which migrated through veins, cavities and coarse dolostones. Sphalerites massively replaced up to 60% of dolostones proximal to veins and diminished distally to disseminated crystals. Ore grade sphalerite crystallization commonly ended at abrupt or narrow gradational contacts with barren dolostone.

Metal-bearing fluids migrated up cross-faults and locally up "main trend" faults; passing through deep discordant dolostones on their way into vein systems (Fig. 12.7). The buoyant warm fluids rose to the top of vein systems, spread out along the upper halves of coarse dolostone beds and migrated laterally along the strike of vein trends. As early sulphides filled pores and reduced permeability in upper levels of the aquifer, succeeding sphalerites crystallized at progressively lower stratigraphic levels. At the same time thick massive deposits of early sulphides were rapidly "dumped" around cross-fractures, where fluids may have emanated from depth. Early tan-brown sphalerites accumulated as correlative millimetre-sized multiple layers in most megapores in the mine area. In both early and late sulphide crystallization sequences, early rapid precipitation slowed in late stages as coarse crystals grew in pores and veins.

Sulphide precipitation may be attributed to several reasons. The entrance and expansion of ore fluids into the fractured aquifer of the upper Catoche Formation resulted in significant decreases in temperature, fluid pressure and partial pressure of CO_2, and an increase in pH with carbonate dissolution. These physio-chemical changes would have

Figure 12.7 Model for Ground Preparation and Ore Deposition

Schematic diagrams interpret ground preparation and ore deposition. Prior to and during sulphide deposition regional compression directed towards the northwest and local deformation along reverse faults formed linear, stratabound fracture systems in the anisotropic dolostone stratigraphy of the upper Catoche Formation. Warm, metal-bearing fluids may have risen from depth at local, deeply penetrating tensional zones along steep, main-trend faults and cross-faults. Features of the feeder zones of this hydrogeologic system include: (1) deep discordant dolostones which penetrate the entire Catoche Formation, (2) pyrite and rare sphalerite at deep stratigraphic levels, and (3) thick, deep stratigraphic bodies of rapidly precipitated early sphalerite characterized by elevated fluid inclusion T_h's and positive $\delta^{34}S$ values, indicative of an uncooled ore fluid with undifferentiated sulphur. Ore fluids travelled outward from these feeder zones, rising to the top of the aquifer and migrating laterally 1000 m or more along the fracture systems. Distal precipitates along the stratabound aquifer have lower T_h's and $\delta^{34}S$ values, indicative of fluid cooling and sulphur differentiation.

MODEL FOR GROUND PREPARATION AND ORE DEPOSITION

DEFORMATION

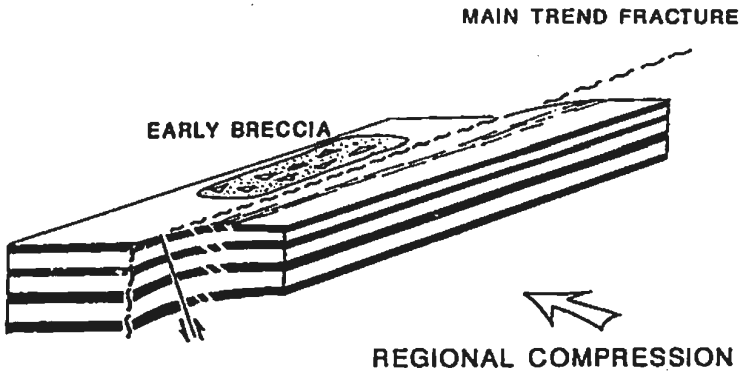

ORE DEPOSITION

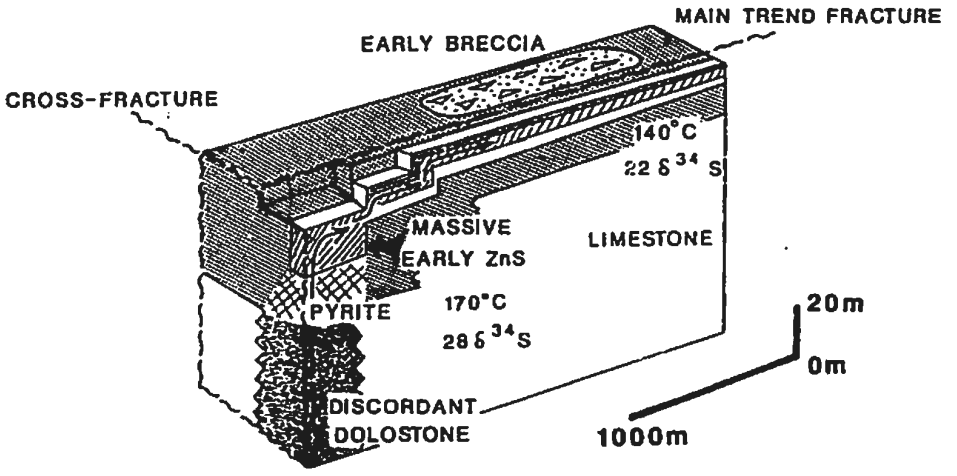

caused rapid precipitation of sulphides where the fluid entered the aquifer. In addition, common gray to black dolostones within and flanking ore bodies may have provided in situ H_2S for sulphide precipitation.

The density difference between invading buoyant metal-rich fluids and denser formational fluids could be attributed to three or more physio-chemical properties: (1) salinity; (2) temperature; or (3) total gas dissolved in fluid. Density differences between a halite-saturated solution (1.15 gm/cc) and one with 20% per volume NaCl (1.10 gm/cc) is only 0.05 gm/cc (Haas, 1976). Fluid inclusion compositions between 20 and 24 equivalent wgt. % NaCl indicate only minor density differences. Since sphalerite fluid inclusions are only the end product of ore fluids, the formational fluid is an unknown. A stagnant in situ formational fluid at 1000 m depth could have been near halite saturation (Hanor, 1979). Temperature differences of 100°C to 150°C in fluids of the same salinity generate a 0.10 gm/cc density difference. If the fluid salinity varies 10 to 15% the density contrast at these temperatures could be 0.15 gm/cc (Schlumberger, 1969). Warm fluids, 140°C to 200°C under hydrostatic pressure in excess of 100 bars also could dissolve significant amounts of H_2S and CO_2 gas. Although quantities of 0.5 ppm H_2S are commonly reported from oil field brines, and a maximum of 43 ppm H_2S occurs in Alberta oil fields at 1800 m depth (White, 1965), the precise effect on fluid density of this amount of dissolved H_2S is unknown. In conclusion, in the absence of a salinity contrast, temperature would have the most apparent effect on density. Abundant dissolved H_2S and CO_2 gases could also have decreased the density.

Thus, warm to hot ore fluids possibly with abundant dissolved H_2S and/or CO_2 rose through cooler and possibly 10% more saline formational fluids and displaced them at the top of the aquifer.

Evidence of a warm, possibly H_2S, CO_2-bearing, ore fluid lighter than dense, cooler, saline formational waters relates to other observations:

(1) A fluid carrying zinc-chloride complexes and H_2S would have less than neutral pH (reduced sulphur model of Sverjensky, 1981, 1984). As the fluid enters and expands into the fractured Catoche aquifer the acidic fluid would in succession: cool, dissolve carbonate, increase in pH and precipitate sulphides via the following reactions.

$$2H_2S + CaCO_3 \rightarrow 2HS^- + Ca^{++} + H_2CO_3$$

$$CaCO_3 + H_2CO_3 \rightarrow Ca^{++} + 2HCO_3^-$$

$$CaCO_3 + Zn^{++} + HS^- \rightarrow ZnS + Ca^{++} + HCO_3^-$$

Variation in concentration of carbonate and sulphur species relative to pH is expressed in Fig. 12.8. Saturation of zinc would rise as solution of carbonates exposed residues of detrital silicates and sulphides (Sverjensky, 1984, 1986). Field evidence shows that porosity increased throughout crystallization of sulphides as carbonates and some sulphides dissolved (eg. Pls. 6.1f, 12.1b; Fig. 6.4).

(2) Decrease of fluid inclusion homogenization temperatures away from cross-fractures (Fig. 6.3) correlates with cooling of fluids in the aquifer with increasing distance from vertical feeders.

(3) The decreasing $\delta^{34}S$ values away from fracture zones (Fig. 6.5) suggest fractionation by cooling of fluid as it progressed through the aquifer. Such an interpretation implies that the sulphur was carried in

Figure 12.8 Variation in Concentration of Sulphide and Carbonate Species with change in pH and fO_2

a. Log of the concentration of carbonat species with respect to variation in pH (from Krauskopf, 1967). Progressive dissolution of carbonate rocks by sulphuric and carbonic acids increases pH by increasing concentrations of bicarbonate.

b. Log of the concentration of sulphur species with respect to the variation in pH (from Krauskopf, 1967). Hydrogen sulphide is unstable in solutions above a pH of 7 and the precipitation of sulphide minerals results. Such a pH change would result from progressive dissolution of carbonate rocks.

c. The distribution of sulphur species and solubility of Pb and Zn with respect to variations in the fugacity of oxygen and pH (from Anderson 1973, 1975, 1983). Pb and Zn are soluble in solutions with reduced sulphur only at low pH's. At higher pH's metals can travel with oxidised sulphur species.

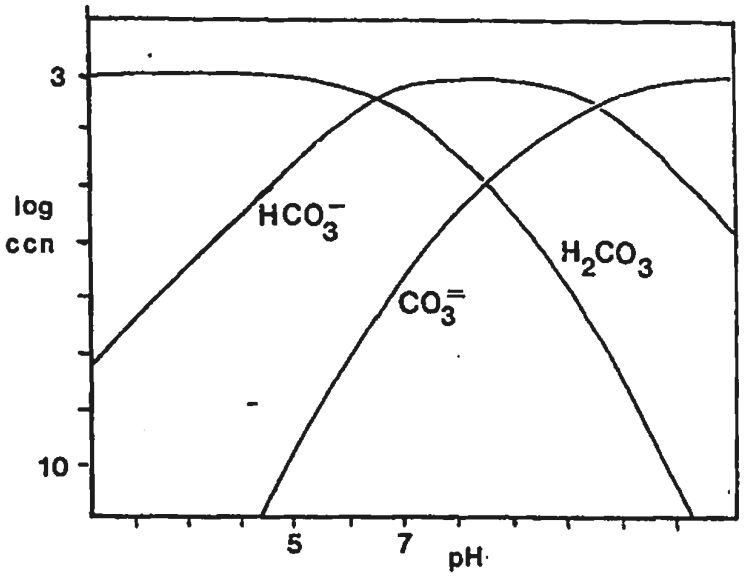
3
log
ccn
10
HCO_3^-
H_2CO_3
$CO_3^=$
5
7
pH

a

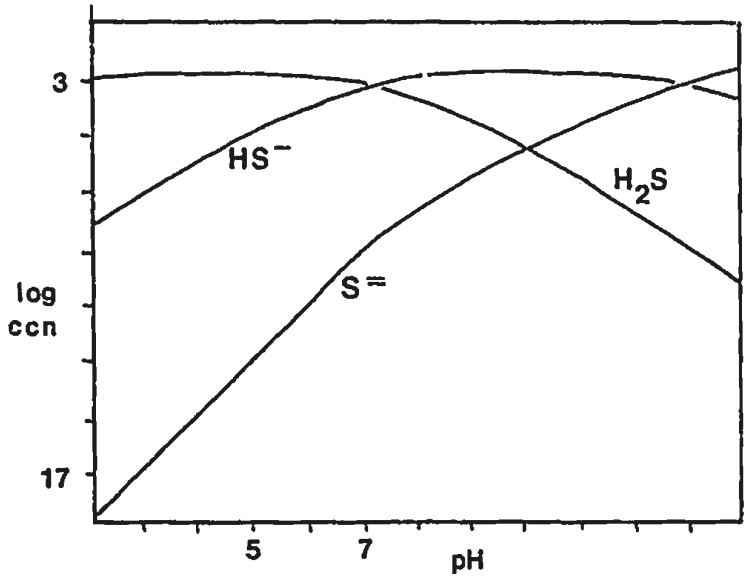
3
log
ccn
17
HS^-
H_2S
$S^=$
5
7
pH

b

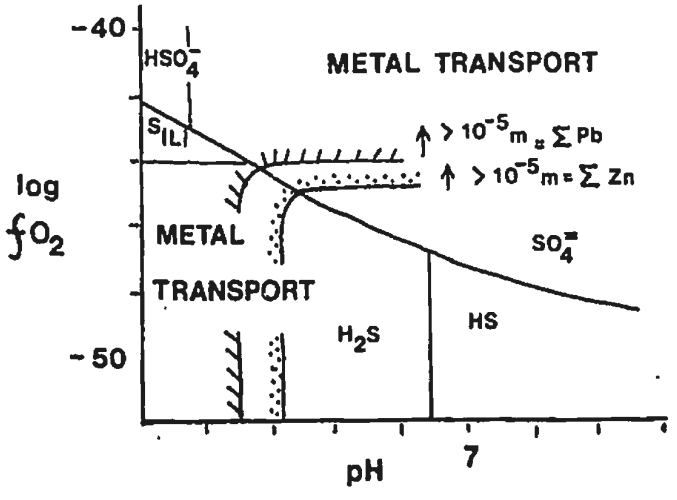
-40
-50
log
fO_2
HSO_4^-
$S_{(L)}$
METAL TRANSPORT
$\uparrow > 10^{-5} m \Sigma Pb$
$\uparrow > 10^{-5} m = \Sigma Zn$
METAL
TRANSPORT
$SO_4^=$
HS
H_2S
pH
7

c

the ore fluid as H_2S.

(4) The five major sphalerite generations and, in particular, the correlative millimetre-scale bands of tan-brown and yellow sphalerites represent repeated depositional events. $\delta^{34}S$ values vary up to 5 per mil in successive crystal layers. Similar stratigraphies in the Upper Mississippi Valley (McClimans et al., 1980) and Southeast Missouri (Sverjensky, 1981) have multiple sulphide stages with variable sulphur and lead isotopic compositions punctuated by dissolution surfaces. Mixed fluid models can not produce on a regional scale consistency of sulphide deposition, reversible dissolution/precipitation and slow coarse crystal growth (McClimans et al., 1980; Hanor, 1979; Ohle, 1980).

(5) Abrupt underlying and lateral ore contacts with barren pseudobreccia suggest that ore fluids displaced formational fluids and mixed only over very narrow transitional zones. This relationship implies that sulphides would have precipitated out of the ore fluids, rather than by mixing with a sulphur-bearing fluid.

(6) The dense saline formational fluids were probably not diluted by meteoric water. Hypersaline inclusion fluids in post-ore carbonates, late Saddle Dolomite B and late non-luminescent calcite (Fig. 5.5, 5.8), support this conclusion. Only late fault-related dolostones, hematite and sulphates may have crystallized from fluids influenced by oxidized meteoric waters. Fluid inclusion studies in other districts (e.g., East Tennessee, Taylor, et. al. 1984; Laisvall, Lindblom, 1986) have interpretated similar data as mixing of meteoric and saline fluids.

12.7 Summary

Deformational events created fracture permeability and predetermined pathways of early and late sulphides. Periods of faulting and fracturing punctuated the history of mineralization and dolomitization and, in particular, separated early and late sulphides. Deep faults tapped deep basinal waters, particularly at the intersections of cross-faults and northeast-trending ones. Narrow zones of deep dilatent fractures around faults expanded into zones of stratabound veins in the heterogeneous dolostones of the upper Catoche Formation. These curvilinear vein systems conformed to the gently folded margins of rock-matrix breccias, faults and cross-faults.

Metal-bearing fluids emanated from depth. Lead isotopes indicate that some or all metals migrated from basement depths. Fluids probably passed through vertical fractures which cut narrow bodies of deep discordant dolostone. Fluids dumped early tan-brown sphalerites at cross-fractures as thick, stratigraphically deep, massive precipitates of fine, fibrous crystals with unfractionated $\delta^{34}S$ and high fluid inclusion homogenization temperatures around 170°C.

The sphalerite ore precipitated in asymmetric bodies which conformed to the geometry of vein systems. Successive sphalerite stages crystallized in a top to bottom sequence. Early metal-bearing fluids rose to the tops of vein systems and individual coarse dolostone beds and migrated along the strike of veins. These initial fluids permeated surrounding gray dolostones and left fine crystalline pyrite. Later fluids migrated along lower strata as permeability in upper beds was

reduced. Progressive solution throughout sulphide crystallization created porous dolostones beneath and along side early sphalerites. These pores were partially cemented by coarse later stage sphalerites. A period of faulting and fracturing after early sphalerite deposition opened a new system of veins along the L Zone trend which was mineralized by late sphalerites.

Sulphide habit in all ore bodies varied from precipitation around veins and cavities to massive crystallization of adjacent coarse dolostones to disseminated mineralization in dolostones distant from megapores. Central megapores preserved the sulphide history as thin multiple crystal layers which can be traced throughout the mine area. Preferred precipitation at the base of pores occurred by gravitational settling of zinc, possibly as a colloid, prior to crystallization.

Transport of metals by a single acidic fluid with reduced sulphur could have accounted for the collective features of the Daniel's Harbour deposit. Warm to hot (100°C to 180°C) and hypersaline (22 to 25 equivalent weight % NaCl) metal-bearing fluids were buoyant relative to local formational fluids. High temperature and dissolved H_2S and CO_2 gases propelled the fluid to the top of aquifers where it displaced the formational brines. Metals and reduced sulphur could only be carried in the same fluid at acidic pH (Sverjensky, 1981, 1986). This combination facilitated the observed corrosion of carbonates and sulphides before and during the ore precipitation. The rise in pH induced by carbonate solution caused simultaneous sulphide precipitation. The reduced sulphur model is the simplest interpretation of several features: (1) multiple sulphide precipitation layers with variable $\delta^{34}S$; (2) coeval

solution of carbonates; (3) apparent minimal mixing at abrupt boundaries of ore lenses; and (4) decrease of $\delta^{34}S$ values presumeably by cooling away from the centre of fluid flow.

Alternatively, metal-bearing fluids were buffered by carbonate rocks during transport and, as a result, were incapable of carrying reduced sulphur. In this scenario cooling and undersaturated fluids generated carbonate solution and in situ H_2S in gray to black dolostones caused local reduction and sulphide precipitation.

CHAPTER 13 POST-ORE COARSE DOLOSTONES

13.1 Introduction

Coarse dolostones of Dolomite V (section 5.7) that form the ore gangue and dominate the surrounding carbonates are a post-ore phenomenon which overprints pre-ore dolostones and sulphides. White sparry (saddle) dolomites, the most striking component of these coarse dolostones, clearly post-date the ore-stage sulphides as late cements in veins and pores. Not only do these dolostones extensively cement pores, but they pervasively recrystallize and destroy earlier dolomites and replace limestones. The pervasive, uniformly luminescent character of Dolomite V is comparable to deep burial dolostones (Lee and Friedman, 1987). Abundant stylolites along saddle dolomites is direct evidence of burial below depths of 300 m.

These late dolostones occur as widespread stratabound lithologies (in contrast to the local sphalerite bodies) in the upper Catoche Formation and other stratigraphic units such as the lower Boat Harbour Formation. They extend throughout northwest Newfoundland where they are associated with regional northeast-trending faults (Fig. 13.1). Discordant dolomitization along these faults further affects the entire Catoche and Table Point Formations.

In the mine area stratabound, saddle dolomite-rich pseudobreccias (Dolomites V and VI; see sections 5.7, 7.3.3) overprint ore bodies and extend 5 to 30 m below and laterally 10 to 300 m beyond them (Figs. 7.1, 9.1). Pseudobreccias replace beds tens of metres beyond fractures, in

Figure 13.1 Regional Distribution of Epigenetic Coarse Dolostone in the Lower Ordovician of Northwest Newfoundland

Coarse epigenetic dolostones in the Lower Ordovician St. George Group are widely distributed in northwest Newfoundland along northeast-trending fault systems. In contrast, the St. George Group is largely limestone east of these faults on the northeastern portion of the Great Northern Peninsula. This distribution of dolostone suggests that the faults were important conduits for dolomitizing fluids.

REGIONAL DISTRIBUTION OF EPIGENETIC COARSE DOLOSTONE IN THE LOWER ORDOVICIAN OF NORTHWEST NEWFOUNDLAND

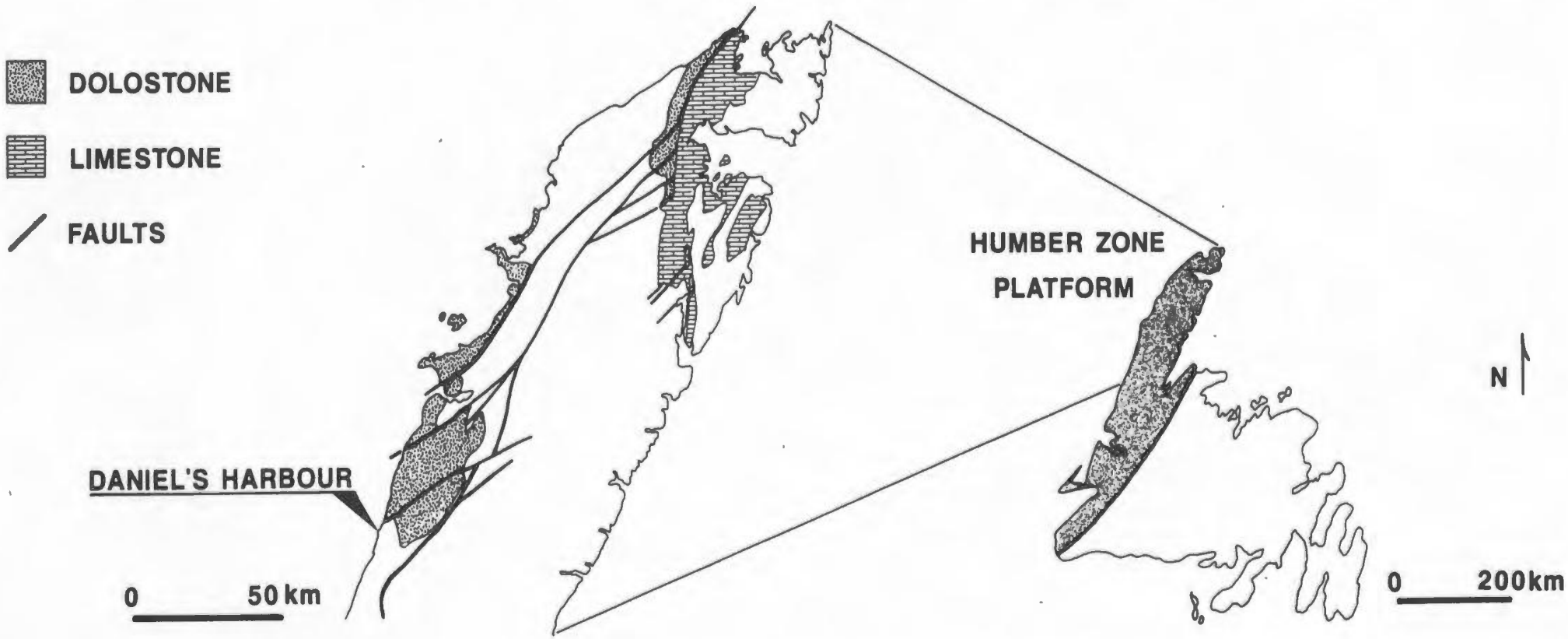

contrast to the local occurrence of sphalerite bodies along vein systems. Broad, up to 1000 m wide, zones of coarse sparry dolostone (section 5.7; Pl. 5.7) commonly separate pseudobreccia facies from areas of unaltered limestone (Fig. 9.1). At depth, coarse dolostones end 45 to 65 m below the top of the Catoche Formation where a 1 to 10 m thick gray, medium crystalline dolostone is transitional with underlying limestones. Outside of these stratabound bodies saddle dolomite occurs locally as veins and patches in fine rock- matrix breccias, in the Aguathuna Formation and where faults intersect the lower Catoche and lower Table Point Formations.

In addition, post-ore dolomites (V,VI,VII) comprise narrow (20 to 30 m-wide) discordant bodies that differ in relative age, origin and crystal texture. Early vertically oriented, tabular to pipe-like bodies are composed of medium crystals of Dolomites II, III, IV and V. They encircle rock-matrix breccias and underlie faulted and fractured portions of ore zones (Fig. 8.2). Late linear bodies of Dolomite VII are, in contrast, variably fine to coarse crystalline and vuggy. They comprise envelopes around late faults that cross-cut both the Catoche and Table Point Formations (Figs. 8.2, 9.4).

13.2 Lithologies

Post-ore dolostones within coarse dolostone/sphalerite complexes (Fig. 7.1) are separated into five types:

(1) **Pseudobreccia** - Former limestone beds of peloidal grainstone and successor gray, coarse matrix dolostones composed of Dolomite IV (Chapter 11) are pervasively recrystallized to gray coarse matrix

dolostones composed of Dolomite V with 5 to 80% white saddle dolomite (Dolomites V and VI). Saddle dolomite occurs both as a pore-filling cement and a replacement mineral of precursor type IV dolomite.

(2) **Spar Breccia** - In vein systems pseudobreccias and finely crystalline interbeds are commonly broken, brecciated and cemented by megacrystalline saddle dolomite (V and VI).

(3) **Coarse Sparry Dolostone** - Equigranular mosaics of coarse crystalline dolomite and saddle dolomite replace limestones and overprint early dolostone (II and III) mottles in the limestone. These dolostones are situated outside pre-ore dolostone complexes.

(4) **Discordant Bodies of Gray Dolostone** - Discordant bodies which penetrate the entire Catoche Formation beneath vein systems are composed of pervasive early burial dolomites (II and III), replacement crystals of pre-ore Dolomite IV and vug fillings and local replacement by post-ore Dolomite V. Veins and thin beds of saddle dolomite (V) occur locally.

(5) **Late Fault-related Discordant Dolostones** - Equigranular mosaics of fine to medium crystalline dolostones replace limestones and envelope late faults which displace the coarse dolostone/sphalerite complexes.

These various lithologies are described in detail and interpreted in the following sections.

13.3 Coarse Dolostones - Pseudobreccia

13.3.1 Definition

The rock named pseudobreccia at Daniel's Harbour (Watson, 1964; Cumming, 1968; Collins and Smith, 1975) consists of irregular mottles of fine to medium crystalline gray dolostone surrounded by coarse to megacrystalline white saddle dolomite. Pseudobreccia was originally defined as a neomorphic fabric in lime wackestones or packstones. The fragments were identified as "islands" of either coarse neomorphic calcite in otherwise fine crystalline limestone (Dinantian limestones, Dixon and Vaughn, 1911; Bathurst, 1958) or remnants of fine crystalline limestone in a coarsely crystalline lithology (e.g. Blount and Moore, 1969). The fragments of pseudobreccia were distinguished by their irregular shape, indistinct gradational boundaries and that they partially enclose the "groundmass" (Dixon and Vaughn, 1911).

The pseudobreccia at Daniel's Harbour, in contrast, is a secondary dolostone fabric. Here saddle dolomite both replaces dolomite and fills secondary pores. The gray dolostone mottles or "fragments" are patches of equant medium to coarse dolomite with the same dull red CL, and hence generation (V) as the saddle dolomite (section 5.7). The mottles, however, retain residues and local chemical imprints of precursor carbonates. Replacement crystals grade in size across irregular boundaries between gray mottles and saddle dolomite (Pls. 5.5e,f; 13.3b,e). Coron (1982) refers to these lithologies with undisturbed primary fabrics as c-type pseudobreccias.

Plate 13.1 Pseudobreccia

a. Alternating beds of pseudobreccia (white) and finely crystalline dolostone (black). Low angle veins cut the fine dolostones. Horizontal gray dolostone bands occur in the lower half of the lower pseudobreccia bed. Breccias in upper beds are interpreted to be broken bands associated with megapores. The lower third of pseudobreccia beds contains minor amounts of white dolomite. K Zone (Fig. 1.4). Scale is 3 m.

b. Pseudobreccia bed and gray dolostone interbed. The finely crystalline dolostone has abrupt contacts (arrows) with typical pseudobreccia beds with uniformly distributed vugs and mottled fabrics which become planar toward the top of the bed. White dolomite decreases toward bed contacts. H Zone (Fig. 1.4). Scale intervals are 20 cm.

c. Irregular pseudobreccia fabrics around veins and megapores. Low angle veins cut finely crystalline dolostone beds. Gray dolostone bands which cut across the pseudobreccia bed are spatially related to the veins. Former solution pores filled with breccia and saddle dolomite occur along veins and the base of dolostone bands. F Zone (location, Fig. 1.4; part of wall section B-B', Fig.10.6). Scale is 50 cm.

d. A former solution cavity in the middle of a pseudobreccia bed is lined by colloform sphalerite (arrow) and occluded by saddle dolomite. A patch of black dolomite occurs beneath the megapore. K Zone (location, Fig. 1.4; cavity-fill, inset in Fig. 12.2). Book is 20 cm. long.

PLATE 13.1

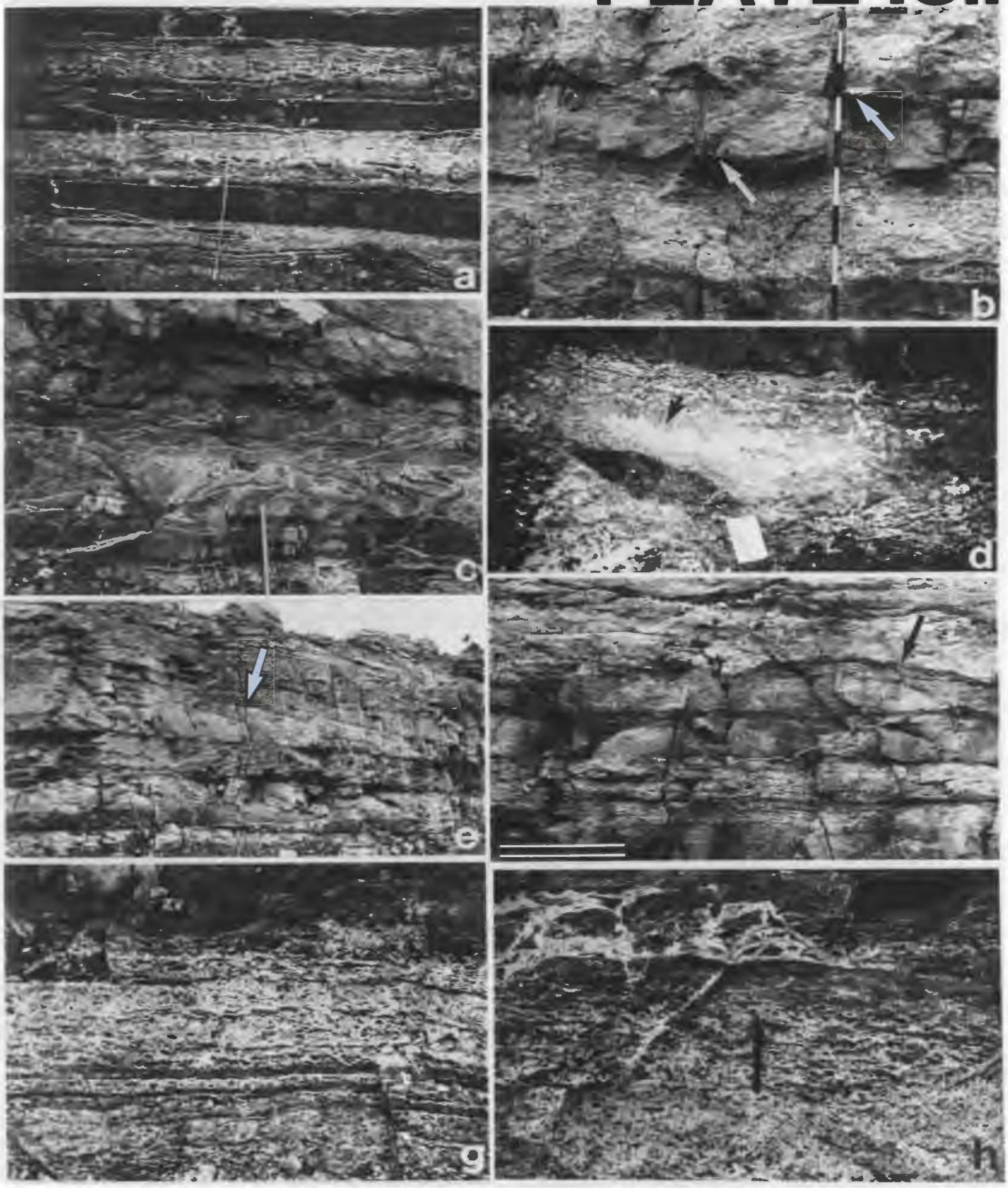

e. Curved planar boundaries (arrow) control the abundance of saddle dolomite in a pseudobreccia bed. The upper right hand portion of the bed has minor white saddle dolomite. The underlying finely crystalline dolostone bed is cut by low angle veins and vein-breccias. F Zone (Fig. 1.4; part of the wall section B-B', Fig. 10.6). Scale intervals = 20 cm.

f. Abrupt, undulating boundary (arrow) separates abundant saddle dolomite from moderate development in the lower portion of a pseudobreccia bed. A fine crystalline dolostone lies between this bed and one below which contains zebra banding. H Zone (Fig. 1.4). Scale is 50 cm.

g. Horizontal fabric of gray dolostone mottles in a pseudobreccia bed varies form thin, irregular and discontinuous stylomottles to continuous horizontal bands with abrupt, planar bases and irregular tops. Close-up of bottom of Pl. 13.1f. H Zone (Fig. 1.4). Pen in upper left is 14 cm.

h. Saddle dolomite at the top of a pseudobreccia bed cements a breccia, veinlet, replaces a horizontal mottle fabric and leaves only disseminated mottles in the middle of the bed at the base of the photograph. G Zone (Fig. 1.4). Pen is 14 cm long.

Plate 13.2 Gray Dolostone Bands and Zebra Fabrics

a. Cuspate gray dolostone band in the middle of a pseudobreccia bed resembles a boundary between two fluids. K Zone (location, Fig. 1.4; opposite cuspate bands mapped in Fig. 12.2). Scale is 1 m.

b. Three bands of dark gray dolostone alternate with gray dolostone partially replaced by white saddle dolomite. Light gray dolostone burrows are preserved throughout the rock. Saddle dolomite-cemented veinlets cross-cut all fabrics. C Zone (Fig. 1.4). Scale in centimetres.

c. Zebra fabrics within pseudobreccias abutting a fault. Fractured gray dolostones are offset along a fault at the left side of the photograph. The inclination of the bands is opposite that of the fractures and towards the fault. T Zone (location, Fig. 1.4; southern fault in Fig. 10.1A). Scale is 2 m.

d. Typical zebra fabric in pseudobreccia. Dolostone bands have near planar bases and irregular tops. Early dolostone burrow mottles (arrows) are preserved in gray bands and pseudobreccia. A former sheet cavity beneath the upper band is partially cemented by saddle dolomite. F Zone (Fig. 1.4; zebra bands in section B-B', Fig. 10.6). Scale in centimetres.

PLATE 13.2

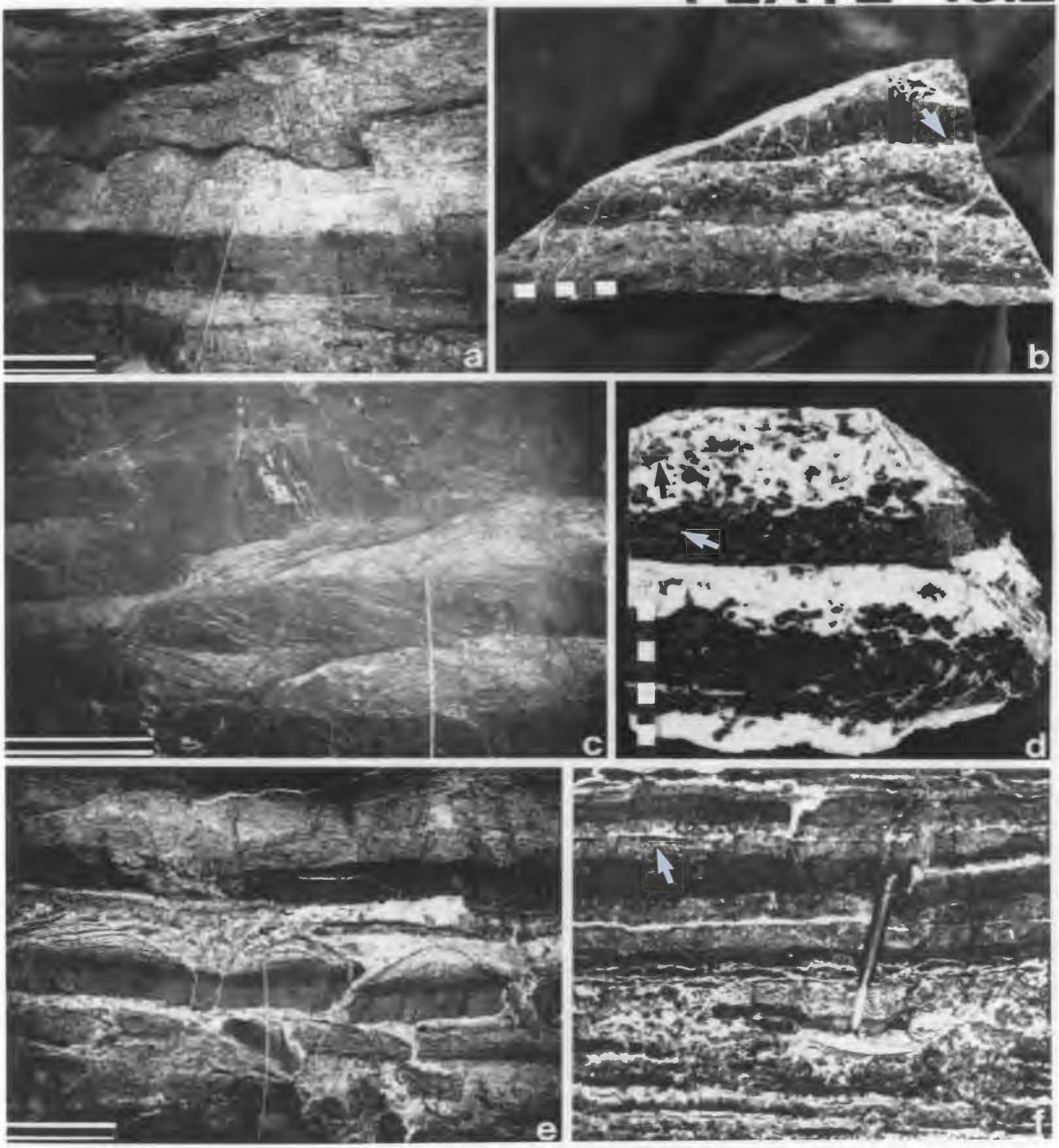

e. Domal zebra fabrics associated with fragmented gray dolostone beds. Bands are inclined towards vertical fractures. In the white areas saddle dolomite cements megapores associated with veins and sheet cavities beneath dolostone interbeds. L Zone, at cross-fault, Fig. 1.4. Scale is 1 m.

f. Former sheet pores between zebra bands are filled in sequence by sphalerite, black geopetal dolomite and white saddle dolomite (arrow). At the top of the photo saddle dolomite cements a fracture that cuts a zebra band and sphalerite cement. L Zone (location, Fig. 1.4). Hammer handle is 40 cm long.

Plate 13.3 Pseudobreccia Textures

a. Pseudobreccia (white saddle dolomite, black matrix dolostone and gray early burrow mottles) abruptly underlain by a burrow-mottled, finely crystalline dolostone. Saddle dolomite selectively replaces the black matrix dolostone. A Zone (Fig. 1.4). Scale in centimetres.

b. Stylolites form boundaries between the bases of gray dolostone mottles and underlying replacive saddle dolomites. Drill hole south of L Zone (Fig. 1.4). Scale is 1 cm.

c. Pseudobreccia with abundant saddle dolomite. Saddle dolomite forms cements peripheral to vugs (v). Extensive replacement leaves disseminated gray dolostone mottles, silica nodules (SiO_2), and residual dolostone along stylolites. F Zone (location, Fig. 1.4). Scale in centimetres.

d. Pseudobreccia with less than 25% saddle dolomite exhibits several types of gray dolostone: (1) resistant light gray burrow mottles (1,4), (2) gray matrix dolostone and (3) black matrix dolostone which may largely be geopetal. White saddle dolomite cements subhorizontal pores and veinlets and selectively replaces matrix dolostones. C Zone (Fig. 1.4). Scale in centimetres.

PLATE 13.3

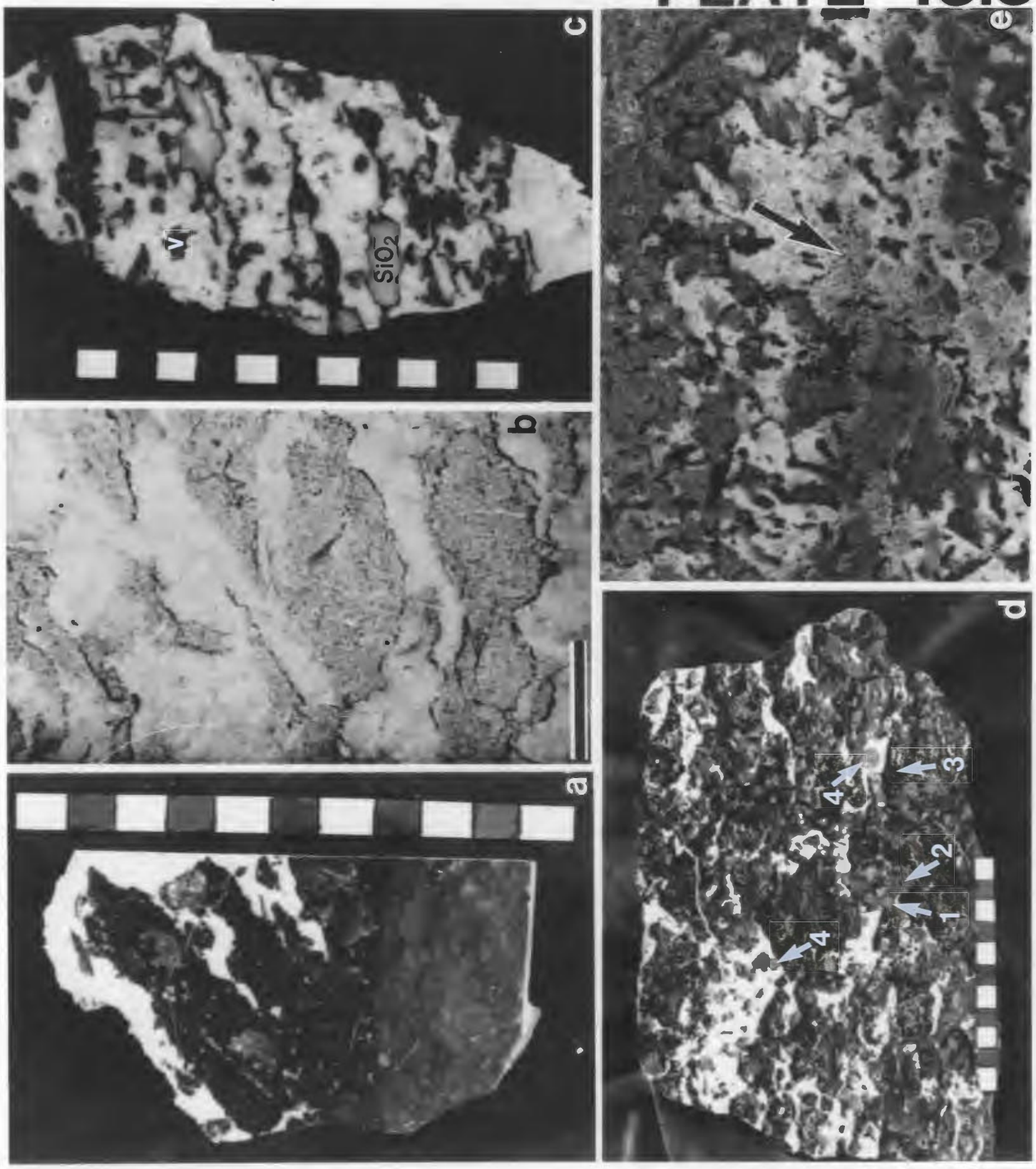

e. Coarse sparry dolostone matrix (gray) aggrades into megacrystalline, white saddle dolomite (arrow). Early dolomitized burrows (black) are relatively unaffected. Bedding plane, Table Point coastal section. Quarter is 2.3 cm in diameter.

Plate 13.4 Replacement by Pseudobreccia

a. Saddle dolomite replaces molds of gastropods (1,2). White saddle dolomite locally forms aggrading fronts with gray, coarse sparry dolostone (2). Bedding plane, Table Point coastal section. Pen is 13 cm.

b. Saddle dolomite replaces a gastropod mold (1). Resistant silica nodules (other arrows) dominate mottles. Bedding plane, Table Point coastal section. Pen is 13 cm.

PLATE 13.4

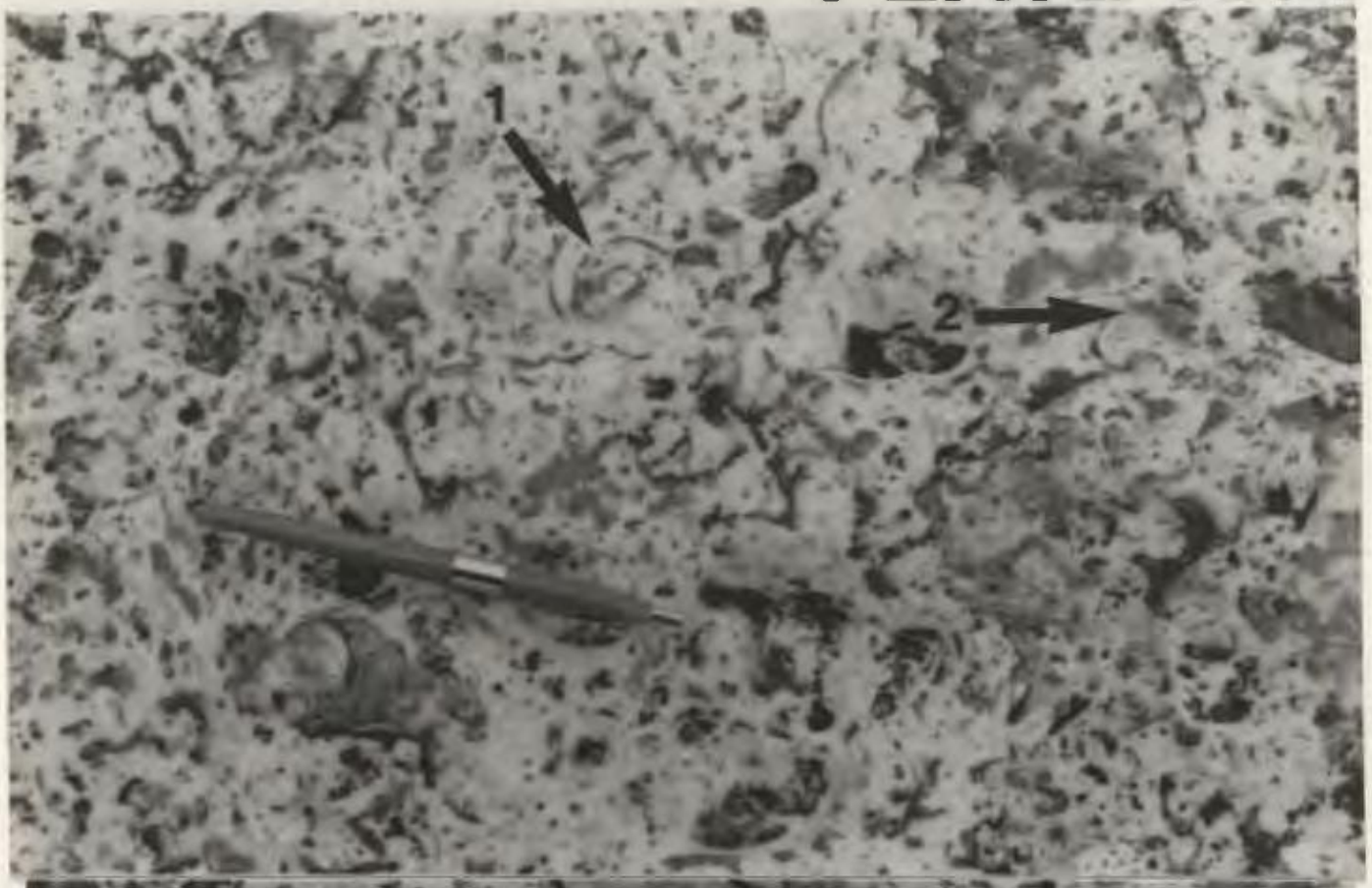

13.3.2 Crystal Textures of Pseudobreccia

In general pseudobreccia consists of gray, fine to medium crystalline, residue-rich dolostone and white, coarse, to megacrystalline saddle dolomite. The gray dolostones are comprised of three texturally different components. Dolomite V overprints finely crystalline dolostone (II, III, IV) mottles which originated during early burial. The result appears as xenotopic, medium (100 to 200 μm) crystals with dull red CL of Dolomite V (Pl. 5.5e). Other cylindrical burrows, once filled with coarse calcite, are replaced by clear, medium-sized (200 μm) crystals of Dolomite V (Pl. 13.3a). The remaining gray to black dolostones between these early burrows and dolostone mottles originated as coarse matrix dolostones (IV) and geopetal sediments deposited in ore-stage pores (Pls. 5.5b,c; 12.2f; 13.3a,d). Medium to coarse (100 to 500 μm) equant crystals of Dolomite V replace these carbonates. Black insoluble residues characteristically occur between the xenotopic to idiotopic crystals (Pl. 5.5d).

White saddle dolomites around the gray dolostones include both cement and replacement crystals (Pls. 5.5f; 13.3b,c,e). Saddle dolomite cements (A and B) display an increase in crystal size (200 μm to 1 mm) as they progressively fill centimetre-sized pores. The increase in crystal size is accompanied by a change in crystal habit from prismatic to equant (Pl. 5.5e). Crystal contacts are generally planar. In contrast, where Saddle Dolomite A replaces a precursor dolomite it forms a mosaic of (100 to 500 μm) irregular, xenotopic crystals (Pl. 5.5e,f). Boundaries between cement and replacement crystals are vague because plane-edged, prismatic crystals penetrate 100 to 200 μm inside residual

margins of gray mottles (Pl. 5.5f). Assuming that all euhedral crystals filled open pores, many pseudobreccias contained 40 to 60% porosity prior to saddle dolomite precipitation (Pl. 12.2f).

13.3.3 General Fabric and Geometry of Pseudobreccia Bodies

Saddle dolomite selectively replaces bodies of coarse matrix dolostone (Dolomite IV) that originally were peloidal packstones and grainstones (Fig. 3.1). In the upper 40 to 60 metres of the Catoche Formation approximately 30 beds of pseudobreccia, each 50 to 100 cm thick, are interbedded with finely crystalline, gray dolostone beds varying in thickness form 20 to 100 cm (Fig. 3.1; 13.2). The gray dolostone beds crystallized either near surface as early fine dolostones (Dolomite I) or during pre-ore epigenetic dolomitization (as Dolomite IV).

Bodies of pseudobreccia envelope the length of fracture systems and extend 10's to 1000's of metres away from fracture zones into structurally undisturbed stratigraphy. The fabric and geometry of pseudobreccia change outwards from vein systems and bodies of early dolostone (such as rock-matrix breccia) (Fig. 13.2). In the vicinity of early dolostone bodies pseudobreccia occurs as sparse patches and veinlets of saddle dolomite (termed patchy pseudobreccia by exploration geologists at the mine). Within and around vein complexes abundant veins and spar breccias are associated with large solution pores. Here the characteristic even bedded, mottled fabric of pseudobreccia (c-type of Coron, 1982) becomes an irregular fabric of cross-cutting veins, saddle dolomite-filled cavities, breccias and patches and curved bands of

Figure 13.2 Distribution of Pseudobreccia Fabrics

Pseudobreccia is widespread in the upper 50 m of the Catoche Formation. Three main facies of pseudobreccia include (1) veined pseudobreccia with irregular fabrics which occurs along fracture zones, (2) bedded pseudobreccia which replaces surrounding areas without structural disruption and (3) patches of pseudobreccia which partially replace margins of bodies of early dolostone. Coarse sparry dolostones occur at the lateral transition intc limestones and at depth beneath stratabound pseudobreccias. The profile is compiled from a cross-section of the Long Hole Stope area of the L Zone (Figs. 10.2, 12.5), but it applies to most coarse dolostone/ sphalerite bodies in the mine area.

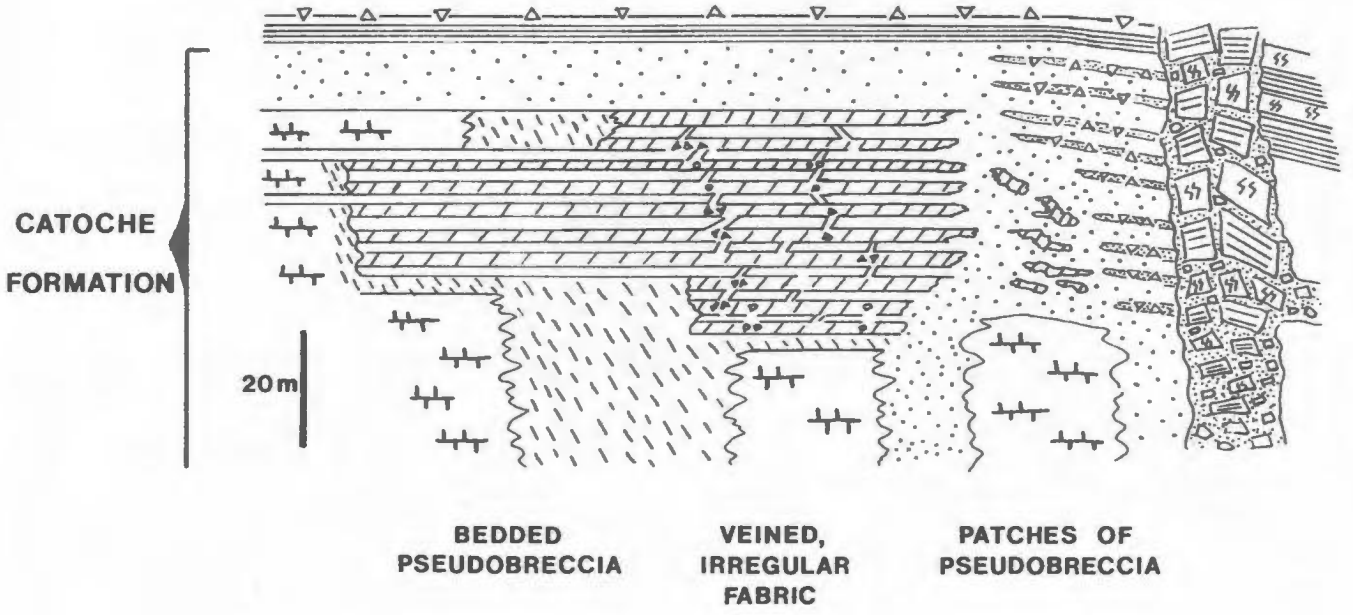

VARIATION OF PSEUDOBRECCIA GEOMETRY

medium crystalline gray dolostone. The bands and patches of precursor gray dolostone are the result of dolomitization along pre-ore fractures and solution pores. This distinctive form of pseudobreccia is termed disrupted or d-type by Coron (1982) (Fig. 13.2; Pl. 13.1c). Only metres away from fractures evenly bedded pseudobreccias have the typical uniform mottled fabric of the c-type (Plate 13.1b). Toward limestone contacts decreasing amounts of saddle dolomite are irregularly distributed between "layers" of coarse sparry dolostone (V) (Pl. 13.3b,e).

13.3.4 Fabric Elements of Pseudobreccia Beds

Coarse crystalline gray dolostones become pseudobreccias where they consist of more than 10 per cent white saddle dolomite. Pseudobreccias, thus, range in appearance from beds with millimetre-scale wisps of saddle dolomite to those dominated by white dolomite with isolated gray dolostone mottles. Commonly the percentage of saddle dolomite in a given pseudobreccia bed decreases away from the middle of the bed (Pl. 13.1a,b,f,h). Pseudobreccias exhibit four different fabric elements: (1) normal (c-type) pseudobreccia; (2) veins and megapores; (3) rhythmic gray bands; and (4) breccias (Fig. 13.3; Pl. 13.1).

(1) Normal Pseudobreccia Fabric - The most common and typical pseudobreccia fabric is composed of *in situ* relics of gray dolostone surrounded by white saddle dolomite which cements former mesopores and megapores and replaces gray dolostone along the interface with the cements. The relic gray dolostone "mottles" exhibit two different geometries: (a) horizontal and (b) disseminated, irregular shapes with no orientation (Fig. 13.3, Pl. 13.1b).

Figure 13.3 Fabric Elements of Pseudobreccia

Pseudobreccia beds contain five main fabric elements. (illustrated examples in Pls. 12.1a,d; 13.1b,c,d,g,h)

(1) Horizontal mottles occur in the upper portions of most beds.

(2) Mottles commonly are disseminated and irregular shapes in the middle of beds.

(3) Veins cut gray dolostone interbeds and merge with macropores and sheet cavities which commonly occur in the middle to upper portions of pseudobreccia beds.

(4) Single dolostone bands are found beneath former cavities. Rhythmic dolostone bands are found in the lower portion of pseudobreccia beds.

(5) Fragments of interbeds, pseudobreccia and gray bands locally form breccias within megapores and along veins.

FABRIC ELEMENTS OF PSEUDOBRECCIA BEDS

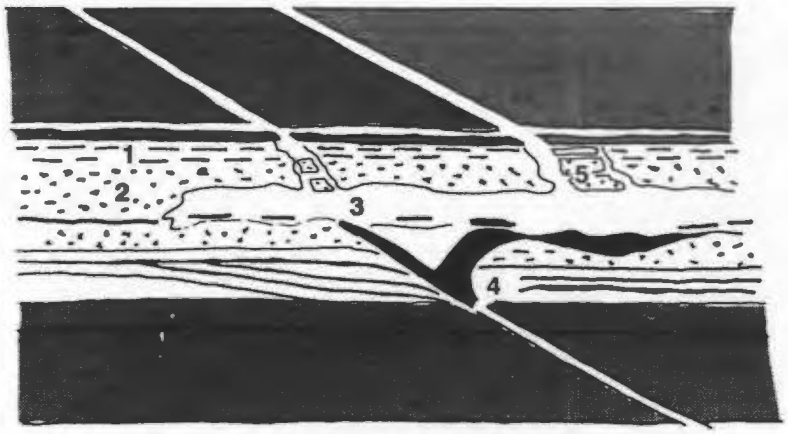

FINE/MEDIUM GRAY DOLOSTONE

PSEUDOBRECCIA

FINE/MEDIUM GRAY DOLOSTONE

1 HORIZONTAL MOTTLES

2 DISSEMINATED MOTTLES

3 VEINS AND MACROPORES

4 RHYTHMIC AND SINGLE GRAY DOLOSTONE BANDS

5 BRECCIAS

(1a) **Horizontal Gray Dolostone Mottles** - Discontinuous, horizontal mottles, 1 to 2 cm thick, characterize the upper portions of pseudobreccia beds (Pl. 13.1h). The preferred orientation reflects earlier bedding, horizontal burrows and stylofabric (Chapters 4,8)(Pl. 13.3e). The original styloresidues commonly persist and form stylolitic mottle/saddle dolomite contacts (Pl. 13.3b,c). The regular, vertical spacing of horizontal mottles and gray dolostone layers is a secondary, epigenetic phenomena, however, which bears no relation to depositional fabrics (Pl. 13.1f,g; 13.3b).

(1b) **Disseminated Gray Dolostone Mottles** - Equidimensional, evenly distributed mottles surrounded by white saddle dolomite generally characterize the middle of pseudobreccia beds with more than 40% saddle dolomite (Pl. 13.1g,h). At least half of the saddle dolomite is cement. The remaining spar is neomorphic, replacing margins of gray dolostone mottles (Pl. 5.5c). This fabric also reflects the irregular distribution of minor amounts of early dolostone in the original peloidal grainstones, compared to the abundant horizontal burrows in the upper parts of beds.

(2) **Veins and Macropores** - Finely crystalline gray dolostone strata intercalated with pseudobreccia beds are commonly broken and cross-cut by saddle dolomite veins. These veins merge with the upper parts of pseudobreccia beds and effectively connect irregular, subhorizontal networks of macropores (Fig 13.3, Pls. 10.1a; 13.1a; 13.1c,d). The resulting channel and sheet pores extend laterally along horizons in the middle or upper third of pseudobreccia beds (Pl. 10.1).

These veins and megapores, previously excavated by ore-stage

fluids, are reduced in size from original openings of 5 to 50 cm wide to present vugs of 1 to 20 cm diameter by cement sequences of sphalerite, saddle dolomite (A and B) and calcite (Pls. 6.1a; 13.1d). Megacrystals of Saddle Dolomite B and calcite up to 20 cm in diameter occlude some pores. Pores that remain are commonly "peppered" with fine marcasite crystals which are overgrown by euhedral calcites and sulphates. The saddle dolomites also locally bear thin coatings of hematite and pyrobitumen.

(3) Gray Dolostone Bands - On the walls of mine workings the lower third of pseudobreccia beds typically contain multiple or individual gray dolostone bands cross-cutting primary depositional fabrics (Pls. 13.1a,c,e,f,g; 13.2). These bands or patches comprise areas without saddle dolomite or solution pores (Pl. 13.2b,d). Individual bands commonly occur below megapores and adjacent to veins and faults (Pl. 13.1c,d). The discontinuous bands pinch and swell in actual thickness from 1 to 30 cm and exhibit cuspate, lobate or v-shaped morphologies (Fig. 12.2; Pls. 13.1c; 13.2a). The convex downwards or undulating bands commonly separate pseudobreccia with sulphides in the upper portions of beds from underlying coarse dolostones containing only minor sphalerite (Figs. 12.1, 12.2; Pl. 13.2a) and, in places, minor saddle dolomite (Pl. 13.1f). Sulphides above gray dolostone bands "pinch-out" where bands rise to meet overlying finely crystalline dolostones. These "pinch-outs" are commonly repeated in 3 or 4 successive pseudobreccia beds (Fig. 12.1; Pl. 13.2c). These relationships suggest that the dolostone bands impeded fluid movement during sulphide deposition and saddle dolomite crystallization.

Multiple gray dolostone bands occur as evenly spaced rhythmic layers (2 to 5 cm thick) (Pls. 13.1g; 13.2b,e,f). They are separated by 3 to 6 cm-thick layers of saddle dolomite and/or sulphides (Pl. 13.2 d,f). The resulting striped appearance is variously described as "zebra rock" or "coontail rock" (e.g. Grogan, 1949; Beales and Hardy, 1980; Devoto, 1985; Cowan et al., 1985) and diagenetic crystallization rhythmites (DCR's of Fontebote and Amstutz, 1983). At Daniel's Harbour 4 to 7 repeated gray dolostone bands are common (Pl. 13.2), and rarely exposed "cross-layering" contains up to 25 rhythmic layers (Fig. 10.3). This fabric mimics primary horizontal stratification, cross-bedding and stromatolites (Pls. 13.1g; 13.2c,e). Three-dimensional exposures, however, reveal that undulating bands cross-cut primary fabric and commonly steepen past the angle of repose. Individual bands are discontinuous, and they either end abruptly, bifurcate, or merge with other bands. They are commonly truncated by overlying gray dolostone bands (Fig. 13.2). Most rhythmic layers are associated with cross-cutting veins and faults. They commonly are inclined down toward veins, where they merge with steeply inclined bands of thick gray dolostone (Fig. 13.2; Pl. 13.1c). Rhythmic layering is also well developed in pseudobreccias along faults where the beds abut finely crystalline dolostone strata (Pl. 13.2c). These features imply that the bands developed on a fractured and faulted framework.

In detail the gray dolostone layers with the primary mottled fabric of pre-ore dolostones have planar bases and irregular tops deeply indented by replacive saddle dolomite (Pl. 13.2d). Planar bases which are nearly coincident with stylolites are mildly indented and replaced

by saddle dolomite. The gray dolostone bands are commonly black to dark gray. These black dolostones (V) includes precursor early mottles (II,III) and matrix dolostone (IV) (Pl. 13.2d). Abundant black intercrystalline material and vague fragments suggest some dissolution in these layers. The intercrystalline material is composed mostly of clay minerals; organic matter constitutes only 0.30% to 0.90% of the rock (Appendix B).

Cemented sheet cavities commonly occur between gray dolostone layers. Sequences of sphalerite, geopetal sediment and saddle dolomite (A and B) locally fill these cavities (Pl. 13.2f). In most places, however, saddle dolomite is the only cement and grades into replacement spar in the upper portions of the gray layers (Pl. 13.2d). Where cemented sheet cavities are absent saddle dolomite selectively replaces light gray layers of precursor dolostone between the darker bands (Pl. 13.2b). In all examples Saddle Dolomite A cements veins which cut all features.

This collective evidence indicates that rhythmic layering formed in association with fractures during a pre-ore event, probably at the time of type IV dolomitization. Selective dissolution of intercalated carbonates formed sheet cavities prior to sulphide deposition. During post-ore dolomitization (V) gray dolostones recrystallized as Saddle Dolomite A occluded late veins and sheet cavities, and partially replaced and obliterated the earlier fabrics.

(4) Breccias - Displaced and rotated fragments are locally incorporated into pseudobreccia beds (Pls. 7.3, 10.1, 13.1a). These breccias are associated with cross-cutting veins and fractures and cement-reduced

megapores. Varieties of breccia, in order of abundance, include: (1) disrupted gray dolostone bands (Pl. 13.1a); (2) fragmented gray dolostone along veins (Pls. 10.1, 13.1h); (3) collapsed fragments of overlying fine dolostone beds (Pls. 7.3, 10.1b); and (4) wholesale microfractured and fragmented precursor dolostone, usually along faults (Pl. 7.3a). As noted in the description of spar breccias (Section 13.4) most fragments remain nearly in place as mosaic breccias separated by saddle dolomite cement.

13.3.5 Interpretation of Pseudobreccia

The composite fabrics and textures of pseudobreccia formed through six or more episodes (summarized in four stages in Fig. 13.4): (1) early burial dolomitization (II,III) of stylo-mottles (described in Chapter 8); (2) pervasive pre-ore epigenetic dolomitization (IV) of limestone matrix to coarse matrix dolostone (Chapter 11); (3) fracturing and selective solution of this matrix dolostone immediately preceding ore deposition; (4) cementation in pores and partial replacement by sphalerite (Chapter 12); (5) fracturing and solution of sphalerites and dolostones (clearly seen in Pls. 10.1c, 12.2e); and (6) cementation of pores and partial replacement by Saddle Dolomite A while pervasive dolomitization (V) recrystallized the remnant gray dolostone (Pls. 5.5c; 13.3c,d,e).

During post-ore dolomitization hydrothermal fluids migrated along vein systems just as previous ore fluids had done. Fluid flow, solution and cementation focused around veins and macropores and was confined between gray dolostone bands. Fluids diffused outwards tens to hundreds

Figure 13.4 Evolution of Pseudobreccia

a. **Early Burial Dolostone** - Early dolomitization (I, II, III) replaced peritidal mudstones with stratigraphic dolostones, formed ubiquitous dolostone mottles in limestones and converted early fault zones and rock-matrix breccias into discordant dolostone bodies.

b. **Pervasive Pre-ore Dolostone** - Dolomitization (IV) replaced limestones with coarse matrix dolostone adjacent to early epigenetic fractures. These dolostones overprinted early dolostone mottles.

c. **Fracturing, Dissolution and Sulphide Deposition** - Ore-stage fractures cut both early burial and pre-ore dolostones. Selective dissolution of coarse matrix dolostone / limestone beds produced sheet cavities and honeycomb networks of mesopores. Sphalerite cemented the rims of these pores and partially replaced the dolostone. Geopetal sediments covered the sulphide crystals.

d. **Pervasive Post-ore Dolostone** - Extensive dolomitization followed post-ore fracturing. Saddle dolomite cemented and closed much of the pore space. Saddle dolomites also replaced coarse matrix dolostones to form pseudobreccia fabric with relic islands of gray dolostone and as much as 80 % saddle dolomite.

EVOLUTION OF PSEUDOBRECCIA

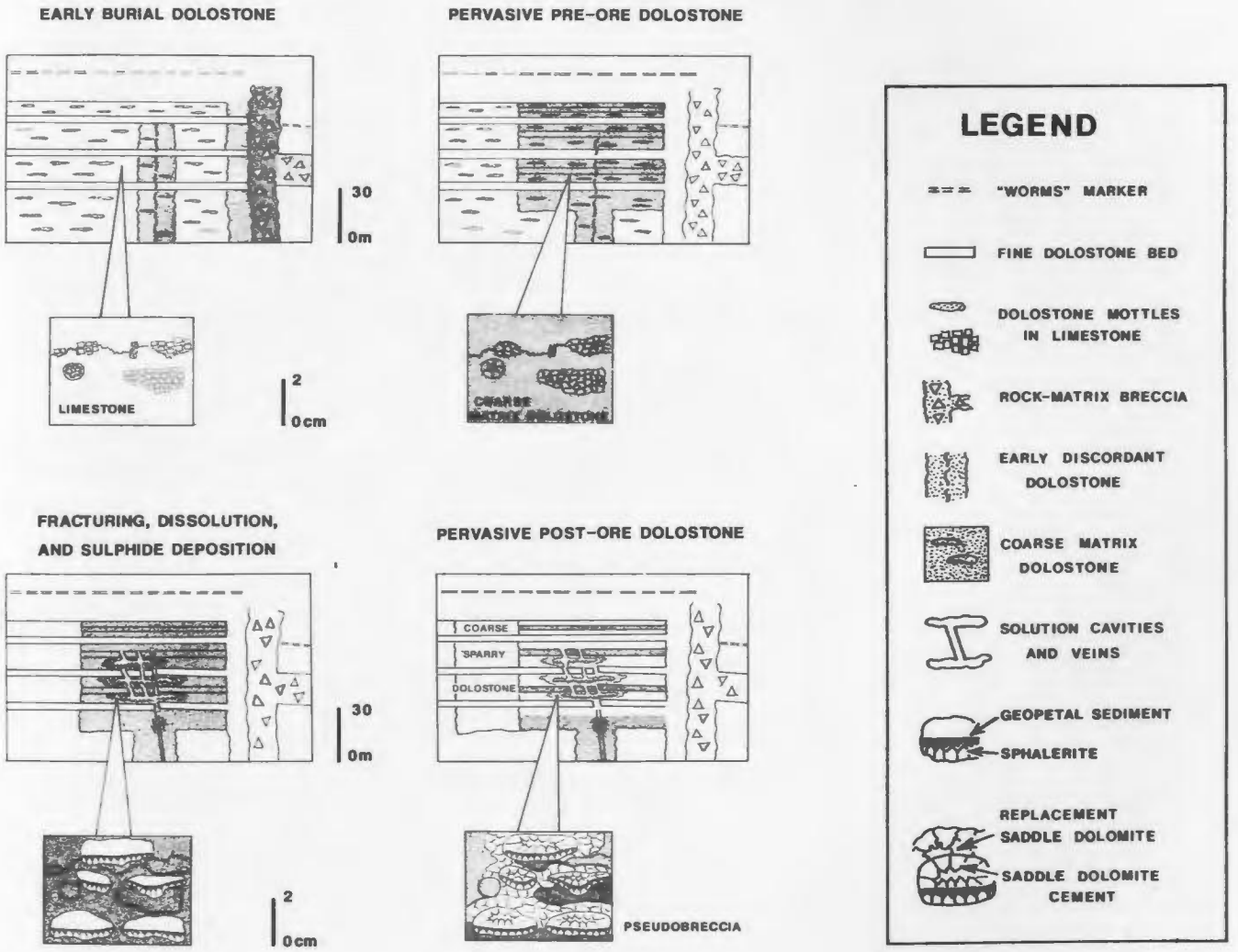

of metres through coarse gray dolostone beds and transformed them to the characteristic mottled pseudobreccia fabric. Euhedral prismatic megacrystalline saddle dolomites cemented mesopores whereas neomorphic crystals developed intergrown xenotopic boundaries. Elevated pore fluid pressures (>hydrostatic pressure) probably supported beds with abundant open pores while coarse crystals slowly precipitated. Abundant stylolites at gray dolostone/saddle dolomite contacts attest to the burial nature of this dolomitization. Minor variation in Eh and fluid chemistry left uniformly luminescent dolostones, characteristic of deep burial dolomitization (Lee and Friedman, 1987).

13.3.6 Interpretation of Gray Dolostone Bands/Zebra Fabric

Theories of Origin - "Diagenetic rhythmites" or zebra rocks are puzzling features and so have been the subject of seven or more interpretations.

(1) Layering in some instances follows sedimentary stratification of primary bedding (Samaniego, 1982) or secondary cavity fills (Cowan et al., 1985). Similar fabrics occur in layered Stromatactis, also called zebra limestones. In Stromatactis, calcite cements and geopetal sediment fill cavities that develop by erosion or solution of "unconsolidated" lime muds between early cemented crusts or organically bound layers (Bathurst, 1980, 1982; Pratt, 1982).

(2) Intercalated sulphates and carbonates typical of supratidal and other hypersaline sequences also evolve into rhythmic layers. Expansion of layers and nodules of anhydrite during the mineral trans-

formation to gypsum further separates carbonate beds. Deformation during this transformation produces chicken-wire fabrics and fragmentation of surrounding carbonates (Bosellini and Hardie, 1973). Pseudobreccia fabrics suggest these features (Beales and Hardy, 1980; Coron, 1982). Selective dissolution of sulphates by waters undersaturated in SO_4^{-2} generates sheet cavities. Sulphates tend to be dissolved by fresh water either (1) in early stages of sedimentation (e.g. Lucia, 1972) or (2) in later history, in near surface portions of basins (e.g. Sando, 1967).

(3) Dilation of brittle rock commonly opens families of subparallel fractures. The most familiar of such fractures are en echelon tension gashes which form at an angle in zones of simple shear (Ramsey, 1967). Typical inclined rhythmic layering mimics this fracture pattern.

(4) Selective dolomitization along fractures and stylolites may form local dolostones resistant to later dissolution and replacement by saddle dolomite. Although stylolites are plentiful in limestones, a regular distribution of stylolites and stylomottles characteristic of rhythmites is not present.

(5) Fontbote and Amstutz (1983) identified these features as "diagenetic crystallization rhythmites", recognizing that most aspects of the dolostone layers are diagenetic and display features similar to those thought to form by diagenetic crystallization (Fontbote and Amstutz, 1983). Their periodicity is considered too regular to be sedimentary. In theory, during a process of fractional crystallization minerals were segregated into three generations: (1) starting sheets of gray dolostones; (2) bipolar subhedral pore-rim cements; and (3)

occluding pore-centre cements.

(6) Dolostone bands may also form at the boundary of two fluids in a porous medium. Single- and multiple-precipitate bands of organic matter in uranium-roll front deposits have a comparable morphology to cuspate, lobate thick dolomite bands. Residue-rich organic layers would be potential sites of selective dolomitization. In laboratory experiments Ethridge et al. (1980) modelled the development of organic bands at the interface of two fluids in a porous sandy media in the laboratory. Organic matter precipitates during a drop in pH at the boundary of two fluids. As rates of fluid flow change, a rising fluid boundary leaves below multiple bands of organic precipitate. Descending fluids dissolve or flush out the organics. This process has the capability of producing single or multiple bands which cross-cut sedimentary fabric and which can be "dissolved" by subsequent fluid fronts and truncated by their respective deposits. The lobate and cuspate forms of fluid boundaries can be produced by irregular displacement between two immiscible fluids, flow eddies, gravitational descent of a heavier upper fluid into a lighter underlying one and deflection of the boundary across primary mudstone lenses.

(7) Double diffusion convection between two fluids of different temperature and salinity is employed to explain layering of fluids in ocean water, magma chambers and porous media (Turner and Chen, 1974; Turner 1974, 1985; Griffiths, 1979). Turner (1974, 1985), Griffiths (1979) and others demonstrate that multiple subhorizontal diffusion boundary layers develop in a fluid when a warm brine is placed underneath or alongside a cooler brine with different salinity. The layer

boundaries, or density steps, are static interfaces of rapid heat and slow chemical/salinity diffusion. Since MVT deposits are considered sites of mixing fluids of variable temperature, salinity, sulphur and metal content (e.g. Anderson, 1973; Lindblom, 1986) double diffusion convection could produce the boundaries for secondary rhythmite layering.

Constraints - Five or more constraints at Daniel's Harbour limit possible origins and timing of development of gray dolostone bands:

(1) The fabric is secondary and epigenetic and it cross-cuts primary burrow-mottles and horizontal stylo-mottles.

(2) Bands are preferentially developed in the vicinity of fractures and faults. Bands surround fractures and demonstrate progressive evolution with them (Pls. 13.1c, 13.2c,e). Inclined multiple layers are localized along faults where they either descend toward a vertical dilatent vein or rise to a confining reverse fault where pseudobreccias abut fine dolostone beds (Pl. 13.2c).

(3) The form and orientation of bands vary from thick, cuspate to singular lobate to multiple, rhythmic layers. Any process must thus account for a variety of features: commonly curved layers steeper than 45°; convex downward bases with lobate to cuspate form; bifurcation; and truncation by overlying bands (Plate 13.2).

(4) The characteristic features of zebra fabrics developed in at least 6 paragenetic stages. Bands formed and dolomitized along or relative to initial fractures. Bands then were fractured; the dolostone between layers was selectively dissolved; and these sheet pores remained

open during the four stage precipitation of sphalerite, geopetal sediment and Saddle Dolomites A and B.

(5) Evidence presented in Chapter 12 suggests allochthonous, metal-bearing, hydrothermal fluids rose from deep in the sedimentary pile and probably displaced formational waters in the upper Catoche Formation.

Genesis - Based on the foregoing constraints, the following hypothesis is suggested for the origin of the dolostone bands. The bands were pre-ore epigenetic dolostones which formed subsequent to fracturing and during continued deformation. Warm fluids rising from deep in the sedimentary pile traveled along veins and faults, and encountered cooler brines in adjacent beds. The more buoyant warm fluids displaced the local, formational brines in the upper, permeable portions of beds. Multiple density layers developed at the fluid boundaries as the brine cooled and mixed with the resident fluid by double diffusion. The static density layers became sites of residue concentration. Fluctuations in relative supply and volume of the two fluids altered their boundaries. The shifting fluids dissolved or flushed some residue layers and truncated others with new deposits of residue.

Major fracturing and dissolution arrested this process as the ubiquitous mesopores and cavities of pseudobreccias formed. The framework of dolostone bands resisted dissolution and formed dividing boundaries of low permeability between sheet pores and coarse dolostone bodies of variable porosity. Subsequent metal-bearing brines and later dolomitizing fluids were funnelled between dolostone bands, with the ore

fluid usually confined to the upper portions of beds. It is unknown whether gray bands developed further during mineralization. The dolostone bands were neomorphosed during post-ore dolomitization but resisted saddle dolomite replacement. The sheet pores gradually filled with precipitates of sphalerite, geopetal sediments and saddle dolomite. Maintenance of multiple sheet pores over the duration of sulphide and dolomite precipitation required support by pore fluids near lithostatic pressure.

13.4 Coarse Dolostones - Spar Breccias

13.4.1 Distribution

The term spar breccia is assigned to fragmented dolostones cemented by white saddle dolomite. Such spar breccias are common in the coarse dolostone complexes of the upper Catoche Formation, and are also scattered throughout the Aguathuna Formation, the upper portions of rock-matrix breccias and, locally, in the lower Table Point Formation.

The style and distribution of spar breccia can be resolved into five types:

(1) Linear Fracture Zones - The most common and important spar breccias are the ore-bearing stratabound vein systems 10 to 30 m thick by 20 to 60 m wide by 1000's of metres long. Veins fracture brittle finely crystalline gray dolostones in these systems. Dolostones between veins are broken into mosaic "fitted" fabrics and cemented by saddle dolomite (Pl. 10.1). Most of these veins do not penetrate intercalated

pseudobreccia beds, which also contain minor breccia fragments. The few veins which cross-cut pseudobreccia beds are enlarged by dissolution and merge with subhorizontal cement-filled cavities (Pl. 10.1a). Fragments of overlying gray dolostones commonly fill these veins and cavities (Pl. 10.1b). These vein-breccias are common in densely fractured zones. Spar breccias locally incorporate rotated blocks of pseudobreccia along north-south cross-fractures, the south sides of main trend fracture zones and in the North L Zone (Pls. 7.3b, 13.5c).

(2) **Breccia Associated with Widespread Pseudobreccia** - Brittle finely crystalline gray dolostone beds between pseudobreccia beds are mildly fractured and brecciated away from fracture zones. Pseudobreccia beds are locally internally brecciated as described in the previous section.

(3) **Domal Spar Breccia Bodies** - Large domal spar breccias are rare at Daniel's Harbour. The Long Hole Stope of the L Zone is a breccia body 30 m high by 60 m wide by 300 m long. Outward dipping veins at the top of the breccia suggest domal collapse (Fig. 12.6). Several domal breccias with spar matrix are also well exposed along the coast 1 to 5 km north of Table Point in the Deer Cove-Bateau Cove area. Breccias in this area were described by Coron (1982) and Knight (1986). These 50 m wide by 30 m high breccias are distributed along a linear zone of vertical spar veins which parallel a fault zone. Saddle dolomite partially replaces fine rock matrix in some of the breccias.

Domal spar breccias, or collapse breccias with coarse rock-matrix, are common in east and central Tennessee. They vary in size from small linear V-shaped structures, 5 m by 5 m, to large domes 30 to

Plate 13.5 Spar Breccias

a. Splinter-type spar breccia in a finely crystalline dolostone bed. The brittle dolostone has broken into a series of splinters and angular fragments. Palisades of white saddle dolomite cement an expanded volume of rock leaving scattered vugs. Sample from fractured gray dolostone interbed in the F Zone (location map, Fig. 1.4). Similar breccias seen in Pl. 10.1. Scale in centimetres.

b. Saddle dolomite (at the left) replaces matrix of a rock-matrix breccia which is preserved at the right. Cathodoluminescent petrography indicates that the matrix was neomorphosed by post-ore (V) dolomitization. A coarse dolostone/sphalerite complex intersects a rock-matrix breccia at a cross-fault in the L Zone (locaton map, Fig. 1.4). Scale is 10 cm.

c. A 10 m by 10 m breccia body from the North L Zone. Finely crystalline dolostone beds are cleaved into 10 to 100 cm-wide fragments along the same synclinal fold and reverse fault indicated in Fig. 10.7 and Pl. 10.1b. Fragments at the top of the structure remain in situ, others are displaced up and down relative to each other and some are collapsed into a rubble breccia in the centre. North L Zone (location map, Figs. 1.4, 10.7). Scale is 2 m.

PLATE 13.5

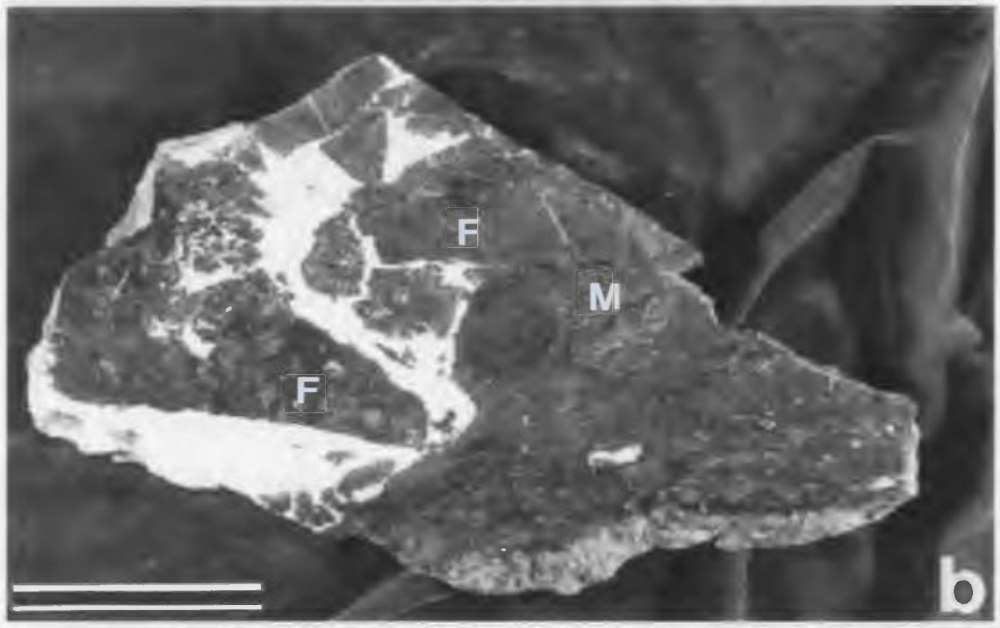

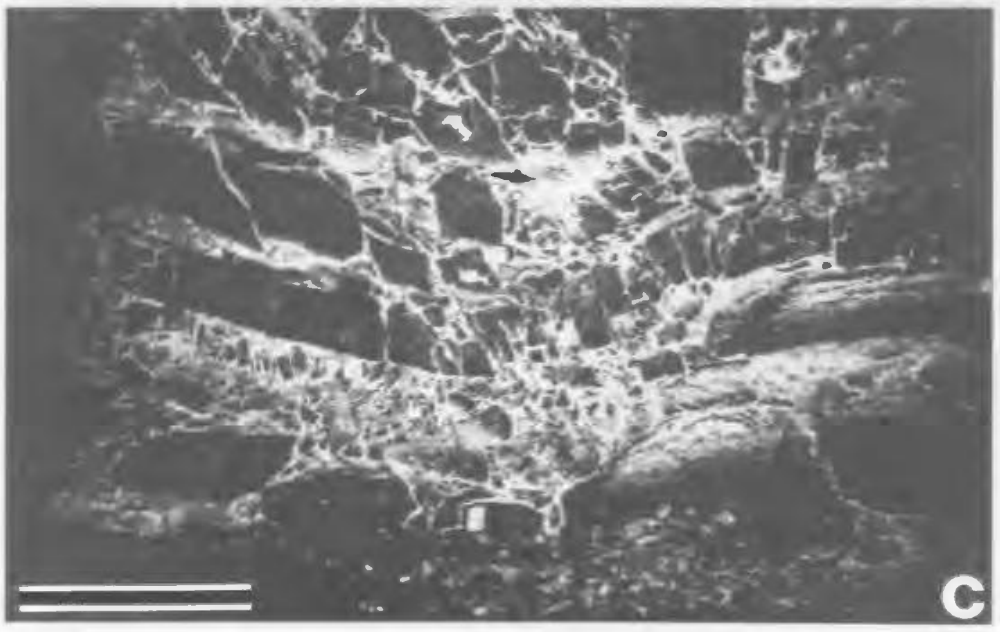

100 metres in diameter by 20 to 50 m in height (McCormick et al., 1971; Gaylord and Briskey, 1983). It is unclear what percentage of the structures is early karst breccia, but late saddle dolomite matrix is widespread. These domal structures characteristically have internally broken and collapsed stratigraphy. Mosaic and crackle breccias, fractures and veins cut peripheral strata. Veins and faults surrounding the breccias tend to dip outward.

(4) **Altered Margins of Rock-Matrix Breccias** - Saddle dolomite selectively replaces the matrix of rock-matrix breccias around margins of these older bodies. Replaced breccias occur at Deer Cove, the large cross-fracture of the west L Zone and in the North L Zone. The fragments are distinctly oligomictic to polymictic and non-fitted. Highly variable sizes and shapes include abundant centimetre-sized clasts (Pl. 7.3d). Most replaced breccias contain relict patches fine rock-matrix (Pl. 13.5b).

(5) **Veined Tops of Rock-Matrix Breccias** - Saddle dolomite cements networks of veins and mosaic breccias in the Aguathuna Formation above dolomitized mud-filled rock-matrix breccias in the Catoche Formation.

13.4.2 Interpretation

The characteristics of spar breccias are key to their interpretation. (1) The breccias are chiefly mosaics of the original rock with gaps (one-fifth to one-quarter volume) cemented by saddle dolomite (Pl. 10.1b). The fragments are not in clast support. (2) Crystals have grown into central voids from fracture walls. (3) Gravity collapsed fragments do not accumulate in rubble heaps but instead, appear suspend-

ed in saddle dolomite near the original site of formation and are only slightly displaced (Pl. 10.1b,c). (4) Finely crystalline dolostones are brittlely fractured into small elongate clasts (Pls. 10.1c, 13.5a). These spalled slivers are commonly incorporated into the saddle dolomite cement.

At least 6 models potentially explain the brecciation:

(1) Collapse and fracture related to intrastratal solution;

(2) Deformation during anhydrite-gypsum transformation and later evaporite replacement by saddle dolomite;

(3) Replacement of matrix of earlier rock-matrix breccia;

(4) Tectonic fracturing;

(5) Fracturing and vein crystallization under elevated fluid pressure and hydraulic fracturing; and

(6) Fragmentation from temperature and chemical changes - "chemical brecciation".

Evidence for most of these processes is present. Evaporite replacement is considered unlikely, however, because precursor sedimentary lithologies of the upper Catoche Formation lack evidence of depositional evaporites (see Chapter 3). The problem here is to find a unifying process which explains the combination of features. The breccia fabric and vein geometry is interpreted to be the result of tectonically directed compression at elevated fluid pressures. The distinctive separation of mosaic fragments by pore-filling saddle dolomite indicates that breccia fragments were suspended and cemented in a fluid-filled pores. These conditions could have been satisfied only if pore fluid pressure equalled or exceeded lithostatic pressure (e.g. Fyfe et al.,

1979). Fluid pressure could have built up beneath low permeability barriers, such as the Aguathuna Formation and fine dolostone beds of the Catoche Formation.

Brecciation and cementation occurred in more than five discrete stages: two episodes of brecciation followed by precipitation of multiple layers of sphalerite (PL. 6.1f); brecciation of sphalerite and gray dolostone prior to cementation by Saddle Dolomite A (Pls. 10.1c; 12.2e); and rupture of veins and rehealing by Saddle Dolomite B around fragments of sphalerite and Saddle Dolomite A (Pl. 6.1a,e). These repeated cycles of cementation and rupture characterize the evolution of pore fluids in some sedimentary basins (e.g. Fyfe et al., 1979). The crack-seal mechanism of hydraulic fracturing occurs when impervious strata cause a build-up of pore fluid pressure, brecciation releases the pressure and cementation of veins leads to another cycle of increased pressure and rupture (Hubbert and Willis, 1957; Phillips, 1972). Splintering of wall rock can be explained by brittle failure associated with hydraulic fracturing along multiple fractures on the margins of veins, rather than by simple gravitational collapse.

A drawback of the hydraulic fracturing model is the observed separation of splinter breccias by saddle dolomite cements (Pls. 10.1c; 13.5a). This pattern suggests that fragments remained suspended after fracturing and does not exhibit evidence of pressure release and collapse after hydraulic fracturing.

Fluid pressure-induced breccias, however, were probably part of a larger system of oriented veins and fracture zones related to regional tectonics (Chapter 10). The tectonically generated system of fractures

became the conduit within which elevated fluid pressures produced the expansional breccias. Although tectonic compression produced consistent vein orientations the sporadic distribution of veins in clusters probably formed during local upward propagation of pressurized fluids (Fig. 10.6; Pl. 10.1a).

The curious stratabound nature of veins and breccias implies one or several styles of deformation. (1) Dissolution within pseudobreccia strata could have generated gravitational collapse. This hypothesis is supported by local thinning of pseudobreccias beds and disruption of gray dolostone strata over areas of maximum dissolution in zones of mineralization and abundant saddle dolomite. (2) Fluid "sills" localized along fracture zones and porous beds and confined by impervious finely crystalline gray dolostones could have expanded volumetrically as fluid pressure increased (Fyfe et al., 1979). The dolostones would have ruptured both by hydraulic fracturing and by subsequent collapse as fluids were released. (3) The principal control on stratabound veins was probably tectonic deformation, however. The oriented geometry of veins and their spatial association with faults and competent dolostone bodies (described in Chapter 10; Fig. 10.8) reflects regional deformation as the causal mechanism. Dissolution and pore fluid pressure are considered to have been important, but secondary.

13.5 Coarse Sparry Dolostones

13.5.1 Description and Distribution

Coarse sparry dolostones (V) occur at the lateral transition

between pseudobreccia and limestone and as separate bodies surrounded by limestone (Figs. 7.1, 9.1). Their geometry varies significantly from stratabound beds 5 to 250 m wide to discordant bodies which penetrate the entire Catoche Formation. They are equigranular mosaics of medium to coarse-sized, euhedral to subhedral rhombs that have replaced original limestones and retained residues of primary burrow-mottled and peloidal textures (Pls. 5.7a,b; 13.3e). Extensive intercrystalline porosity is commonly uncemented, but in some places crystals are intergrown (Pl. 5.7c,d). Coarse crystals define areas of "matrix" between fine to medium crystalline dolostone mottles (Pls. 5.7b; 13.3b,e). Dolomite V overprints precursor dolostones (II,III) in the mottles. In some cases an equigranular mosaic of medium to coarse crystals overprints all primary fabrics (Pl. 5.7f). This is the same lithology described as Pervasive B dolostone by Haywick (1984). Although coarse sparry dolostones can be defined as a distinctive mappable facies, their distinction from coarse matrix dolostones of pseudobreccia facies is not clear (eg. Pl. 13.3e).

13.5.2 Interpretation

The laterally extensive coarse sparry dolostones originated during pervasive post-ore dolomitization (V) when fluids emanating from vein complexes passed through porous pre-ore dolostone bodies into limestones. Coarse dolomites (V) overprinted early dolostone (II,III) mottles and incompletely replaced the limestone matrix. Later dissolution of the remaining limestone produced the ubiquitous centimetre-sized pores.

13.6 Discordant Gray Dolostones

13.6.1 Description and Distribution

Discordant bodies beneath vein complexes are narrow, 10 to 30 m wide, laterally discontinuous along the strike of main trend faults, and underlie most cross-faults. Limited drill hole information suggests the geometry of vertical bodies is cylindrical and/or elongate and tabular (Fig. 8.2).

The fine to medium crystalline gray dolostones possess only minor white saddle dolomite. Early burial Dolomites II and III occur pervasively in these dolostones (Chapter 8). Among the bodies of discordant early dolostone, those beneath vein complexes are affected by up to 4 epigenetic events: (1) pervasive neomorphism by pre-ore Dolomite IV; (2) minor fracturing and dissolution; (3) scattered precipitation of minor pyrite and sphalerite in intercrystalline pores; and (4) varying styles of post-ore dolomitization (V) from (a) cementation of pores between earlier crystals (Pl. 5.1f) to (b) precipitation of coarse crystals in veinlets and mesopores to (c) local pervasive replacement. Thin beds of pseudobreccia and veinlets of white saddle dolomite are minor. Deep dolostone bodies along the margins of rock- matrix breccia bodies are not altered by these epigenetic phases.

13.6.2 Interpretation

Deep fractures and faults served as vertical fluid conduits for early burial and epigenetic dolomitization (Dolomites II through VI). Fluids migrated up localized chimney to tabular-shaped dolostone or

fracture conduits adjacent to reactivated faults. Partially to completely dolomitized early bodies were pervasively recrystallized by pre-ore Dolomite IV. Subsequent fracturing and dissolution created pores which were cemented by medium to coarse, post-ore dolomites (V,VI). Pseudobreccia and pervasive gray dolostone locally formed within porous horizons and along highly fractured zones. Occlusion of the previously ubiquitous porosity by Dolomites V and VI effectively sealed the dolostones.

13.7 Late Fault-related Dolostones

13.7.1 Description and Distribution

Bodies of fine to coarse crystalline dolostone replace limestones of the Catoche and Table Point Formations peripheral to most of the major faults related to the uplift of the Long Range Inlier (Figs. 8.2, 9.4). These dolostone bodies range in width from 30 m up to a kilometre at intersections of major faults. The timing of dolomitization is considered to be coeval with or following regional uplift because the dolostones are developed along the latest faults and they overprint stylolites. Wide ranging $\delta^{18}O$ values of the dolostones suggest that they formed during several events. Local distribution of some dolostones above thrust faults imply that some dolomitization occurred during syntectonic fluid migration along those faults (Fig. 13.5).

In typical dolostones in the Catoche Formation mosaics of euhedral to subhedral rhombs with intercrystalline porosity and uniform red-orange CL overprint depositional fabrics (Pl. 5.7d,f). The fine to

medium crystalline dolostones are difficult to distinguish from older coarse sparry dolostones (V) which have dull red CL and intercrystalline Dolomite VI cement (Pl. 6.1g). Late saddle dolomite (VII) and luminescent calcite cement veins along faults.

Late fault-related dolostones in the Table Head Group are distinctively very fine to fine crystalline and weather buff to tan colours. This appearance has lead to the supposition that these lithologies might be facies-specific, early supratidal dolostones Coron, 1982). This dolostone, however, overprints all sedimentary facies identified in limestone sections. Bright red CL overprints stylolites and secondary pores occur selectively along former stylolites and coarse calcite cements. This secondary porosity is partially cemented by saddle dolomite (VII) and late luminescent calcite.

13.7.2 Interpretation

Middle Paleozoic uplift of the Long Range Inlier fractured and faulted the platform and displaced coarse dolostone/sphalerite complexes. Over a protracted history fluids migrated along faults and dolomitized tens of metres into Catoche and Table Point limestones. Inter- crystalline pores and solution mesopores were subsequently cemented by saddle dolomite and late luminescent calcite.

Figure 13.5 Late Dolomitization (VII) Along a Thrust Fault

Pervasive late dolostones (VII) in the Table Point Formation 3 km southwest of the T Zone are distributed throughout the hanging wall of a thrust fault zone (cross-section constructed from a detailed fence of drill holes). The fault steepens as it passes through the St. George Group where it displaces a coarse dolostone complex. Localization of dolomite veins along the fault indicates that the structure affected earlier fracturing and dolomitization.

These relationships suggest that dolomitization was syntectonic. The fault may have acted as an impervious barrier and/or provided a pathway for upward migration of fluids.

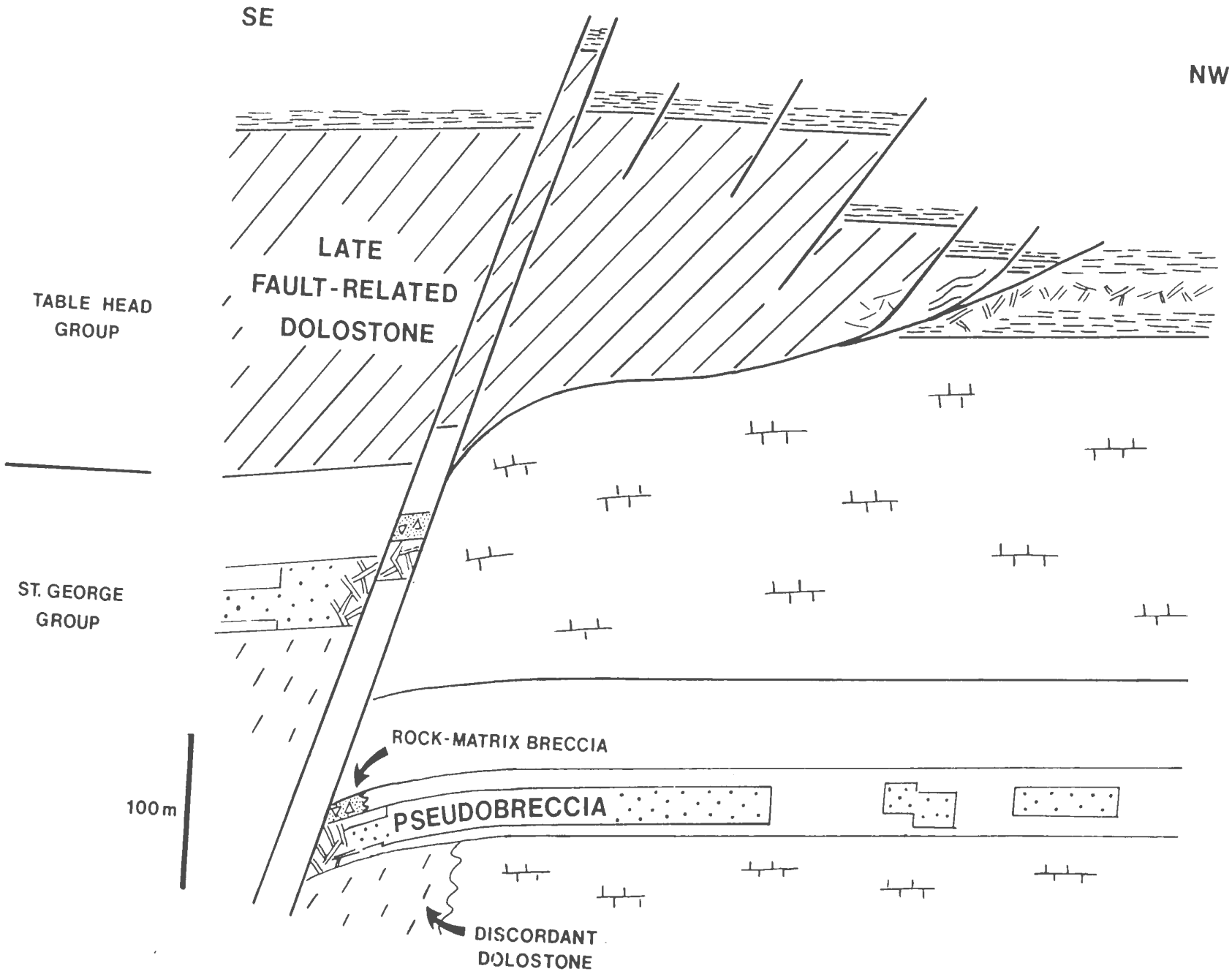
SE
NW
LATE
FAULT-RELATED
DOLOSTONE
TABLE HEAD
GROUP
ST. GEORGE
GROUP
ROCK-MATRIX BRECCIA
PSEUDOBRECCIA
100 m
DISCORDANT
DOLOSTONE

13.8 Geochemical Zonation in Dolostone Bodies

13.8.1 Description

Potassium ferrocyanide staining for iron, together with trace element and oxygen isotope analyses, differentiate otherwise homogenous dolostone bodies or facies. Saddle dolomites with 2000 to 6000 ppm total Fe are localized to lower parts of coarse dolostone bodies, deep discordant dolostones and some coarse sparry dolostones on the outer edges of complexes. Late dolomite cements, the latest zones of Dolomite V and Dolomite VI, are also ferroan. Some saddle dolomite veins along faults in rock-matrix breccias are surrounded by oxidation rims.

Oxygen isotopes distinguish different dolomite stages as documented in Chapter 5. Ore-stage saddle dolomite is tightly constrained with $\delta^{18}O$ values which range between -9.3 and -10.8 o/oo. Pure cements in veins and mesopores are confined to a small field between -10 and -10.8 o/oo (Fig. 5.6, Appendix A). This data corresponds to the field for saddle dolomites elsewhere in the Northern Peninsula saddle dolomites (Haywick, 1984). Saddle dolomite outside ore zones have both heavier, -9.3 to 6.7 o/oo, and lighter, -11 to -12 o/oo, $\delta^{18}O$ values (Fig. 5.6; Appendix A). One coarse sparry dolostone of Dolomite V stage has -7.7 o/oo $\delta^{18}O$. Saddle dolomite veins within rock-matrix breccias and the Table Point Formation are particularly enriched, -6.8 to -7.0 o/oo. In contrast to the limited range of values for most saddle dolomites, samples from late fault-related dolostones have a wide ranging iso- topic composition -5 to -13 o/oo $\delta^{18}O$ PDB (Coron, 1982) (Fig. 5.6).

13.8.2 Interpretation

Saddle dolomites in vein complexes precipitated from hydrothermal hypersaline fluids. The light isotopic signature of hydrothermal dolomite is best represented by cement crystals in veins. As fluids migrated laterally away from vein complexes, crystals precipitating from cooler fluids contained enriched $\delta^{18}O$. This same cooling trend occurred in the transition of crystallization of Saddle Dolomites A and B (Chapter 5). Alternatively, hydrothermal fluids could have gained increased ^{18}O by (1) mixing with saline formational fluids with high initial ^{18}O or by (2) reacting with dolostones with heavy $\delta^{18}O$ values.

Iron-enriched saddle dolomites probably precipitated from reduced (?) pore waters on the lower and outer extremities of complexes and throughout the complexes during late crystallization. Waters which reached these areas had been depleted in dissolved oxygen by several possible processes: (1) organic or hydrocarbon oxidation; (2) bacterial respiration; (3) sulphate reduction; and (4) iron oxidation to form hematite. Oxidation rims on veins along faults suggest that relatively oxidized fluids migrated along these structures.

Late fault-related dolostones crystallized from fluids with various compositions of meteoric water and formational brine. These fluid sources communicated along the faults. The wide range of crystal $\delta^{18}O$ reflects the varying influence of these sources.

13.9 Interpretation/Summary

Post-ore dolomitization occurred in two separate events: (1) Post-Ore Stage I, closely related to sphalerite deposition, when fluid temperatures were over 100°C; and (2) Post-Ore Stage II during and after regional uplift.

Post-Ore Stage I- Following extensive regional fracturing at the end of sulphide deposition, fluids initially dissolved sulphide crystal faces, then Saddle Dolomite A precipitated. The fluids followed vertical and subhorizontal pathways: migrating up local porous discordant dolostones; flowing horizontally along vein complexes; and pervading coarse dolostone beds as far as 1000 m from vein complexes. Saddle dolomite crystallized locally within and around veins and cavities. In bedded sections of pseudobreccia, saddle dolomite uniformly cemented mesopores and replaced coarse gray matrix dolostone. Beyond complexes of pre-ore dolostone, coarse sparry dolostone replaced limestone. Ferroan dolomites with heavy $\delta^{18}O$ values in the lower and outer extremities of coarse dolostone complexes crystallized from cooler and more reduced fluids than in veined centres.

Pore fluid pressure approached lithostatic pressure, and in combination with tectonic dilation, maintained extensive openings in veins, breccias and solution pores. Mosaic spar breccias and coarse dolostones with more than 40% porosity did not collapse. Hydraulic fracturing occurred immediately prior to the precipitation of both Saddle Dolomite A and B. The sudden release of pore pressure and spread of fluid into new fractures may have partially caused precipitation of

saddle dolomite.

Discordant gray dolostone bands and zebra fabrics developed near fractures in coarse dolostones during pre-ore dolomitization. The distinctive zebra fabrics probably formed by double diffusion at mixing boundaries between hydrothermal fluids and cooler formational brines. The position of these residue-rich layers constrained later events as dissolution occurred between layers and sulphides and saddle dolomite precipitated in singular and multiple sheet cavities. During ore-stage and post-ore cementation, the thinly layered framework of gray dolostone bands and sheet cavities required fluid support under elevated fluid pressures.

Post-Ore Stage II - During uplift of the Long Range, most regional faults displaced coarse dolostone/sphalerite complexes. Dolomitization within 10 to 300 m of these faults altered Catoche and Table Point limestones to equigranular fine to medium crystalline dolostones with ubiquitous intercrystalline pores. Both saline formational fluids and meteoric waters migrated along the faults and left a varied $\delta^{18}O$ isotopic imprint on the dolostones. Hematite deposits and sulphate crystals attest to the oxidizing effects of some of these fluids.

CHAPTER 14 SYNTHESIS OF COARSE DOLOSTONE/SPHALERITE COMPLEXES

14.1 Introduction

The development of epigenetic complexes can be separated into seven stages (listed at the end of Chapter 9): (1) initial tectonic development of a fractured framework; (2) crystallization of pervasive pre-ore dolostones; (3) major fracturing and partial dissolution of coarse dolostone beds; (4) deposition of sulphides; (5) crystallization of post-ore dolostones and calcite; (6) regional faulting and uplift; and (7) crystallization of late fault-related dolostones. Certain processes were continuously or intermittently active throughout the history of the complexes. Significant episodes of fracturing separate early and late sulphide deposition and predate the precipitation of both Saddle Dolomites A and B. Dissolution appears to have continued throughout sulphide deposition and sulphides were partially dissolved prior to the two phases of saddle dolomite precipitation.

14.2 Development of the Initial Structural Framework

Stratabound vein systems occurred in the upper Catoche Formation where thin, brittle dolostone beds fractured between coarse dolostones in response to deformation along steep faults and around massive bodies of rock-matrix breccia. Fracture systems developed in curvilinear zones that spanned 3 to 30 m thick stratigraphic intervals. Early fractures deeply penetrated stratigraphy along faults. Deformation then propagated fractures outward from faults into progressively higher stratigraphic levels and thinner packages of beds. Solution collapse and hydraulic

fracturing during fluid migration through the fracture systems increased the amount of fracturing and brecciation.

14.3 Crystallization of Pre-Ore Dolostones

Bodies of pre-ore medium to coarse matrix dolostone (IV) overprinted carbonates in vein systems. Fine to medium gray dolostones selectively replaced lime wackestones and overprinted medium crystalline early burial dolostones (II,III). Coarse matrix dolostone preferentially replaced peloidal grainstones. The dolomitizing hydrothermal fluids migrated along faults and fractures and formed zebra bands along double diffusion fronts where the fluids encountered formational waters in coarse dolostone beds.

14.4 Major Fracturing and Dissolution

Continued deformation fractured pre-ore dolostones (IV) and dilated earlier fractures. This increased permeability and focused fluid flow. Fluids entering the upper Catoche Formation extensively dissolved the carbonates, creating many megapores and mesopores in the coarse dolostones, including sheet pores in zebra rocks. Corrosive fluids could have been generated in a number of ways: (1) by production of CO_2, hydrocarbon gas and carboxylic acids during thermal maturation of kerogen between 80° and 200°C (Schmidt and McDonald, 1979; Kharaka et al., 1983, 1985; Franks and Forester, 1984), (2) by simple recharge of CO_2- enriched meteoric waters into basin sediments (Back and Hanshaw, 1971; Hitchon et al., 1971), (3) by the release of CO_2 during metamorphism of carbonate rocks at 500° to 600°C, (4) by the release of CO_2

during reactions between carbonates and clay minerals at 180° to 225°C (Hutcheon et al., 1980), (5) by acids of H_2CO_3, H_2S and H_4SiO_4 possibly carried within metal-bearing solutions (Sverjensky, 1981, 1986), (6) by undersaturation of waters at the deposition site during mixing of two fluids (Moore and Sullivan, 1977), or (7) by production of acids (H_2S, H_2CO_3 and HCl) during sulphide precipitation or sulphate reduction at the site of deposition (Anderson, 1983). The presence of hydrocarbons in the region suggests that organics could have been the source of acids. The most probable sources of corrosive components, however, were the accumulation of CO_2 and acids in fluids at depth, production of acids during sulphide deposition and mixing of two fluids at the ore site. Petrographic and field observations suggest that all three processes could have operated. Significant dissolution happened in ore zones prior to sulphide deposition, but corrosion also occurred synchronously with precipitation. Widespread dissolution well beyond the areas of sulphide deposition probably resulted from undersaturation with respect to calcite/dolomite during fluid mixing.

14.5 Deposition of Sulphides

Sphalerites precipitated in two main stages, the resulting cement stratigraphy of which can be traced laterally throughout the mine area. Early sphalerite crystals were fine-grained to fibrous in habit. They precipitated rapidly in disseminated pores and fractures and locally massively replaced gray dolostones. Contemporaneous fluids aided by acid products of sulphide precipitation dissolved surrounding dolostones and enlarged pores, which were subsequently filled by slowly precipitat-

ing coarse crystalline sphalerite at the end of the first stage. A period of fracturing accompanied faulting between early and late stages of mineralization. Late mineralizing fluids shifted to these highly permeable new fracture zones where late sphalerites precipitated as massive deposits of coarse pore-filling crystals. Regional fracturing and dissolution of carbonates preceded extensive crystallization of the latest yellow-black sphalerite. These important relationships demonstrate that many veins, solution pores and breccias formed in the midst of ore deposition.

In a suggested model for ore deposition, it is hypothesized that buoyant, warm, metal-bearing fluids rose through fractures, possibly directly from basement depths. Dissolved gases of CO_2 and H_2S may have enhanced the buoyancy. Upon entering the fractured aquifer of the upper Catoche Formation, the fluids rose to the top and flowed laterally along porous beds and linear fractures beneath impervious beds of finely crystalline dolostone. Metal-bearing fluids probably sat above cooler formational fluids within porous coarse dolostone beds. Abrupt ore contacts along impervious black dolostone bands marked boundaries of minor mixing. Contemporaneous dissolution and fracturing increased porosity and permeability which redirected fluid flow to areas beneath and outside of older deposits and created pores throughout the deposits for late coarse sulphide cements. The nature of the ore fluids are considered in section 14.9.

14.6 Crystallization of Post-Ore Dolostones and Calcite

Throughout northwest Newfoundland pseudobreccia and associated

coarse dolostones (V,VI) crystallized after the sulphides, filled ubiquitous pores and overprinted most pre-ore dolostones (IV). Cementation and selective replacement by Saddle Dolomite A completed the development of zebra dolostones.

In the chain of post-ore events regional deformation extensively fractured sphalerites and dolostones, then allochthonous brines migrated through the fracture systems and pervaded regionally porous dolostones. The fluids were undersaturated with respect to sphalerite and partially dissolved the sulphides. Post-ore dolostones (V) crystallized following the release of CO_2 during fracturing and while fluid temperatures still exceeded 100°C. Saddle Dolomite B and calcite with distinctive isotopic signatures precipitated after later fracturing during progressive cooling and decreasing rock-water interaction as fluid flow slowed in cemented and diminished pores. Late pyrobitumen covered vug surfaces during a late hydrothermal event when hydrocarbons cracked.

A zonation of dolostone facies developed across the dolostone/sphalerite complexes. In the fractured centres of d/s complexes Saddle Dolomites A and B cemented abundant veins, solution megapores and spar breccias, and outside of deformed zones Saddle Dolomite A cemented mesopores and replaced coarse matrix dolostones (IV) to form bedded pseudobreccias. Coarse sparry dolostones (V) replaced limestones where dolomitization extended beyond the earlier limits of pre-ore dolostone (IV).

Elevated fluid pressures were probably instrumental in the precipitation and textural development of late dolostones. Dolomite precipitation occurred after extensive tectonic and probable hydraulic

fracturing as the sudden decrease in pore fluid pressure and pCO_2 dropped dolomite solubility (Sippel and Glover, 1964; Fyfe et al., 1979). Low angle ore stage veins imply that any hydraulic fracturing propagated under a tectonic regime with a near-horizontal direction of regional compression.

Throughout the crystallization of sphalerite and coarse dolostones the combination of elevated pore fluid pressure near lithostatic pressure and tectonic extension maintained extensive porosity that locally totalled up to 40% of the rock volume in the form of networks of mesopores, multiple sheet cavities and open work breccias.

14.7 Siluro-Devonian Faulting and Uplift

Regional faults associated with the Long Range uplift vertically displaced earlier coarse dolostone/sphalerite complexes. Associated folds tilted ore-stage geopetal sediments in former cavities. Sulphates and hematites precipitated along faults from late stage oxygenated waters. Hematite also precipitated extensively below present near-surface sulphide bodies which possibly lay immediately beneath a regional unconformity of Late Paleozoic or Early Mesozoic age (Hyde, 1983; Tuach, 1987). Euhedral pyrite crystals with a similar fault-related distribution precipitated during slightly reducing conditions at moderate pH.

14.8 Crystallization of Late Fault-related Dolostones

Fine to medium crystalline dolostones replaced St. George and Table Head limestones along the late faults. Fractures and solution

pores were cemented with minor saddle dolomite and bright luminescent calcites which may correlate with Late Paleozoic to early Mesozoic calcites in Carboniferous strata of the Port-au-Port Peninsula (Saunders and Strong, 1986).

14.9 Nature of the Basinal Fluids and Their Transport

The fluid inclusions preserve remnants of the original hydrothermal (85°C to 185°C) brines from which sulphides and epigenetic dolomites precipitated. These highly saline fluids with $CaCl_2$ and 20 to greater than 24 equivalent weight % NaCl compare with deep basinal brines found below 2km in present day basins (e.g. White, 1964; Hanor, 1979; Sverjensky, 1984). The positive $\delta^{34}S$ values of sulphides and sulphates confirm that the brines were largely derived from sedimentary sulphides or sulphates or connate sea water trapped within Lower Paleozoic rocks of the sedimentary basin. Many MVT deposits, however, have never been buried to the depths at which fluids of such salinity and temperature reside, thus most ore deposition models presume that fluids migrated to most deposits from the deeper parts of basins (Ohle, 1980).

The basinal brine hypothesis, the popular theory for fluid transport (e.g. Jackson and Beales, 1967; White, 1967; Ohle, 1980), suggests that brines are flushed out of the deep basin along stratigraphic aquifers to shallow marginal platforms. Recent studies of stratigraphic dolostones document dolomitization from fluids which migrated along regional aquifers (Gregg, 1985; Rowan, 1986; Voss and Hagni, 1986; Morrow et al., 1986; Freeman and Medary, 1987). Mechanisms of fluid

migration and nature of the fluids have not, however, been clearly established.

Several models exist for fluid transport in sedimentary basins. Compaction dewatering of basinal shales are envisaged by Jackson and Beales (1967) as a means of deriving metals and large volumes of saline water. In young basins, such as the Gulf of Mexico, compaction driven and geopressured fluids migrate both up stratigraphic dip and up along faults (e.g. Galloway, 1984). Hydrological models (Back and Hanshaw, 1970; Garvin and Freeze, 1984; Garvin, 1985; Bethke, 1986) emphasize the importance of topographic or gravity-driven flow to flush the basin at rates of flow great enough to maintain elevated fluid temperatures. This model particularly applies to mature basins rimmed by topographic highs. Orogenic events involving major thrusting such as the Alleghenian orogeny are identified as periods of major gravity driven flow (e.g. Leach and Rowan, 1986). Some workers suggest that tectonic "pumping" of pulses of fluids are necessary to maintain anomalous temperatures (Sibson et al., 1975; Cathles and Smith, 1983). Deep hydrothermal fluids driven by thermal convection without the aid of gravity-driven flow rise through cooler overlying waters along permeable pathways such as growth faults or porous aquifers (Hanor, 1979; Wood and Hewett, 1982; Simms, 1984; Kreitler, 1987). In any of these models maintenance of hydrothermal temperatures at high rates of fluid flow requires conduits, such as faults and cavity-riddled formations, with permeabilities around one darcy (Kreitler, 1987).

Any hydrogeological models for the Daniel's Harbour deposit must account for the complex tectono-stratigraphy of the Humber Zone and that

the deposit pre-dates basement uplift. As a result the Daniel's Harbour setting differs significantly from the Pine Point models of Jackson and Beales (1967) and Garven (1985). The mineralization post-dated Middle Ordovician deformation and tectonic displacement of basinal shales to a position above the platformal sequence. The resulting Taconic thrusts probably constrained later lateral transport of fluids. The sulphide deposition was probably coeval with early Acadian crustal heating, deformation and fracturing. The crustal heating probably drove fluid convection and caused metal and sulphur release through mineral transformations and hydrothermal leaching. The fractures provided fluid conduits. The occurrence of mineralization on major lineaments emphasizes the importance of fracture-controlled fluid flow. The importance of gravity-driven flow is unknown. Stratabound coarse dolostones and sphalerite bodies imply lateral fluid flow. A lowland terrestrial to shallow marine geography prior to uplift of the Long Range, however, probably lacked a mountainous upland recharge area capable of generating significant hydraulic head.

Two different models for ore deposition propose that either one or two fluids carry metals and sulphur (Sverjensky, 1986). A single hydrothermal metal-bearing fluid with reduced sulphur (H_2S) would retain soluble metals only at an acid pH less than 4 (Anderson, 1973). If such a fluid travelled any distance through carbonates it would be buffered to alkaline pH and precipitate sulphides, unless original concentrations of Ca and partial pressures of total dissolved CO_2 were high (Anderson, 1983). As a result of this solubility problem, Anderson (1975) and others hypothesize that metals are transported in an oxidized solution

free of H_2S and precipitate sulphide when they meet reduced sulphur in another fluid at the ore site. Other workers suggest that SO_4 or partly oxidized sulphur species are carried with the metals and precipitate sulphides during organic or inorganic reduction of sulphur (Barton, 1967; Anderson, 1983; Spirakis, 1983). H_2S-bearing lithologies, such as some rock-matrix breccias, could provide a local source of sulphur and/or a reducing environment for sulphide precipitation.

Certain features of Daniel's Harbour and other MVT deposits favor precipitation from a single fluid. Firstly, the narrow ore lenses with their abrupt contacts surrounded by barren dolostones suggest that ore fluids only travelled locally in the upper Catoche Formation and experienced minor mixing with formational fluids. Secondly, the regional multilayered sphalerite stratigraphy has several implications. Disequilibrium between fluids, sulphides and carbonates is indicated by pre-ore solution pores in dolostones, by sulphide replacement of dolostone and by solution-etched surfaces on successive crystal layers. This repeated dissolution/precipitation differs from the assumed irreversibility of sulphide precipitation during mixing of fluids (Anderson, 1975, 1983). The extensive nature of the sphalerite stratigraphy also requires uniform conditions for precipitation over a broad area which is difficult to achieve along fluid mixing fronts (McClimans et al., 1980). The variation between early stage rapid precipitation and late stage slow growth of coarse crystals also contrasts with rapid "dumping" expected upon mixing of fluids. Lastly, the apparent decrease of $\delta^{34}S$ values away from fracture zones or centres of fluid flow suggests that sulphur was carried in the metal-bearing fluid.

Low to moderate pH brines carrying reduced sulphur species (Sverjensky, 1981, 1986) is an attractive model for metal transport in this setting for several reasons. In basement and basinal source areas such fluids would effectively leach metals. During transport dissolved H_2S gases would enhance buoyancy and abundant $CaCl_2$ and CO_2 would retard carbonate buffering. At the deposit site fluid temperature and CO_2 partial pressure would decrease with fluid expansion in the interval of stratabound fractures. Simultaneous dissolution of carbonates by acidic solutions would combine with the changes to buffer the fluids and result in extensive sulphide precipitation. Successive generations of acidic fluid would repeat this process leaving a stratigraphy of dissolution surfaces between crystal layers.

In a suggested model epigenetic fluid migration occurred in the early stages of the Acadian Orogeny when crustal thickening and anatexis heated the sedimentary pile and generated thermal convection (Fig. 14.1). At the same time steep fractures, including reactivated Ordovician structures, created fluid conduits (Fig. 14.2). Deep basinal fluids, from more than 2 km depth, circulated through the basement and up along faults. Lateral fluid movement may have occurred as well along faults by gravity-driven flow. The hydrothermal fluids were buoyant relative to other formational waters which they displaced at the top of aquifers in the upper Catoche Formation.

At the deposit site fluids entered the upper Catoche Formation in five main stages following repeated fracturing events. The first hydrothermal fluids caused pervasive dolomitization along fractures. Subsequent fractures tapped metal-bearing brines in the deep portions of

Figure 14.1 Schematic Cross-section of the Northern Appalachians in the Late Silurian: the Framework for Fluid Flow

The regional setting of mineralization is reconstructed for the late Silurian - early Devonian prior to uplift of the Long Range. Basinal waters could have been recharged in terrestrial regions to the southeast and hydraulic head caused gravity-driven fluid flow. Structural boundaries and metamorphosed terranes may, however, have hindered fluid flow. Thermal convection above an elevated geothermal gradient was an alternative cause of fluid movement. This process could have generated vertical movement of heated, therefore less dense, fluids up steep basement-related fracture systems.

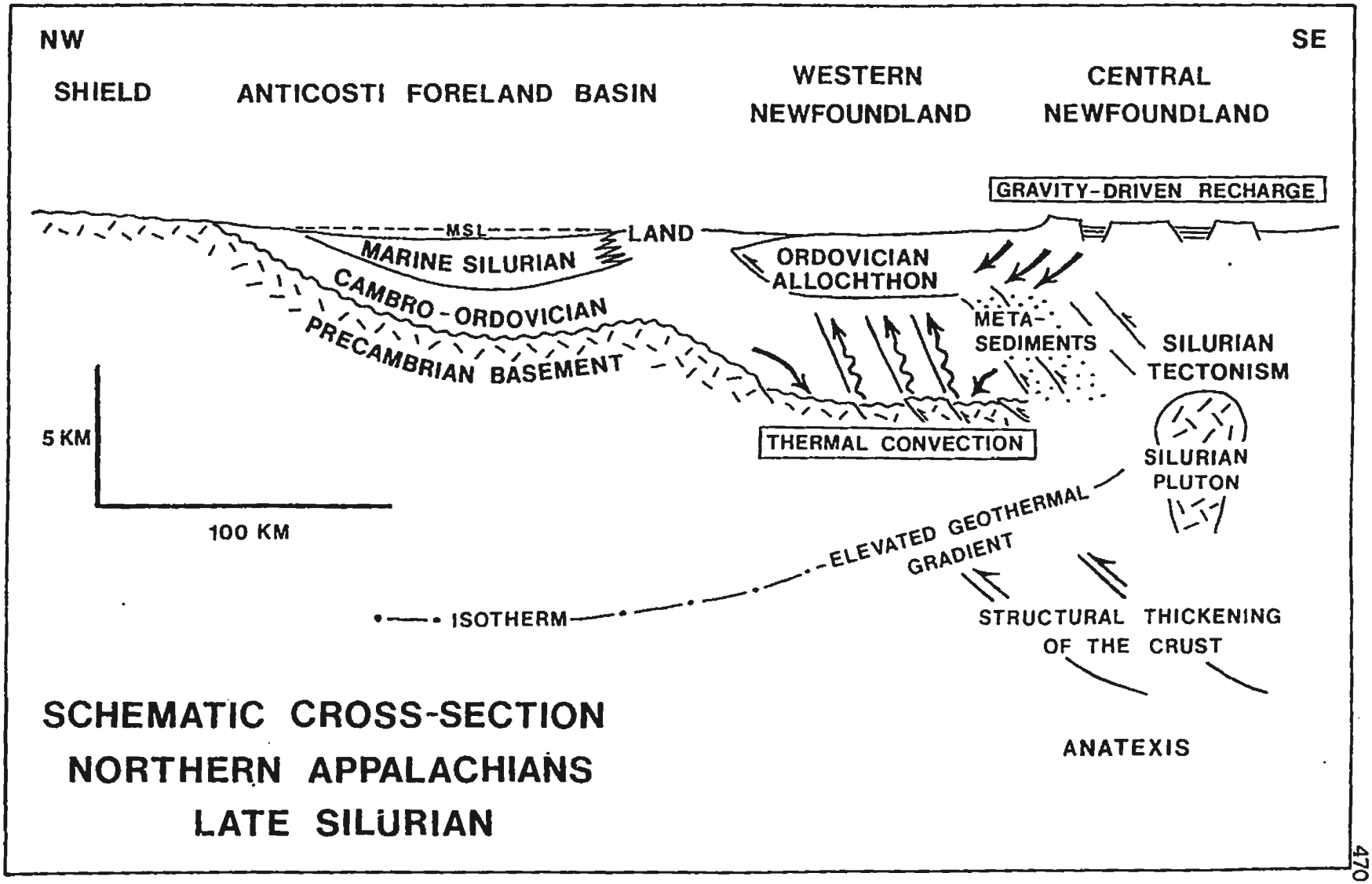

SCHEMATIC CROSS-SECTION
NORTHERN APPALACHIANS
LATE SILURIAN

Figure 14.2 Fault and Stratigraphic-Controlled Routes of Fluid Migration

A reconstruction of the platform stratigraphy at the end of the Silurian indicates the distribution of coarse dolostones (cross-hatched) as stratigraphic units and discordant bodies (cross-hatched) enveloping faults. Suggested routes of fluid migration (arrows) are vertically up along faults and laterally outwards along stratigraphic horizons.

ROUTES OF FLUID MIGRATION IN THE NORTHWEST NEWFOUNDLAND PLATFORM

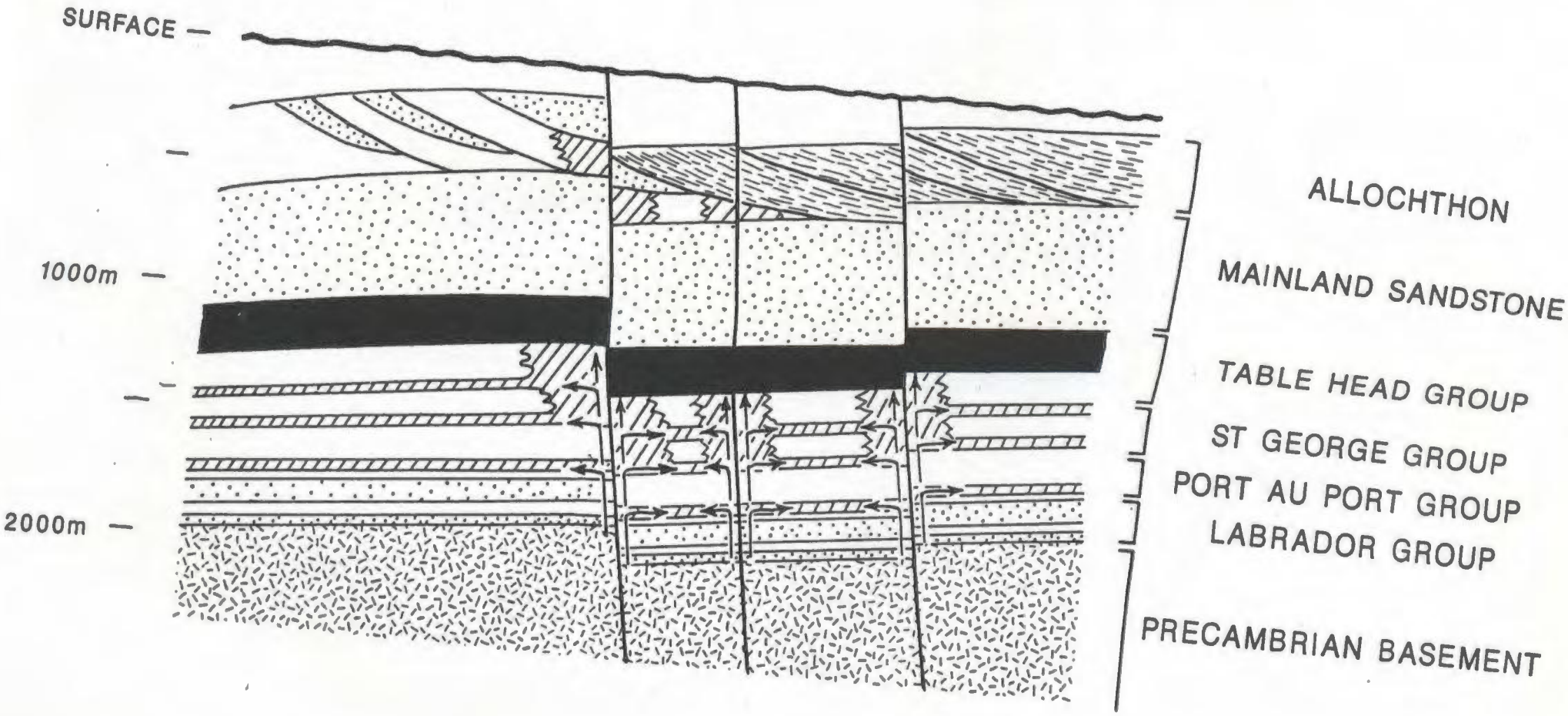

the basin during a thermal peak. Initial ore fluids rose up deep fracture zones, entered the upper Catoche Formation where they dissolved carbonates to form abundant megapores and sheet cavities prior to the rapid crystallization of early sulphides. The pre-ore dissolution and extensive sphalerite stratigraphy probably resulted from acidic ore fluids of largely unknown composition which probably carried both metals and reduced sulphur. Late stage ore fluids flowed only along one fracture zone, the L and T Zone trend. Progressive faulting and fracturing throughout northwest Newfoundland opened the region to extensive fluid migration and post-ore dolomitization. During this fourth stage late yellow-black sphalerite widely precipitated and Saddle Dolomite A closed much of the ubiquitous porosity. After a late fracturing event in the fifth and final stage megacrystals of Saddle Dolomite B and calcite occluded pores as fluids progressively cooled and increased in salinity. Later episodic invasions of hydrothermal fluids probably resulted in the precipitation in vugs of marcasite, galena, late red sphalerite and pyrobitumen. Further dolomitization (VII) occurred along faults during and after regional uplift (Stages 6 and 7 at the beginning of the chapter).

PART VI

SUMMARY AND CONCLUSIONS

CHAPTER 15 SUMMARY OF THE SEDIMENTARY AND BURIAL HISTORY

15.1 Sedimentary History

During the deposition of the upper St. George Group in the Early Ordovician, the carbonate platform progressively shallowed upwards from (1) an open marine, subtidal, muddy shelf (Catoche Formation) to (2) shallow subtidal flats covered by peloidal grainstones and mud beds (upper Catoche Formation) to (3) arid peritidal flats (Aguathuna Formation) (Fig. 15.1a-c). Many laterally extensive beds accumulated on a nearly level platform as moderate amplitude cycles of marine flooding and regression inhibited normal processes of tidal flat progradation.

Toward the end of Early Ordovician time the platform fragmented along northeast-trending faults and was extensively exposed during regional uplift and/or eustatic regression. Initially sedimentation continued as the middle member of the Aguathuna Formation filled grabens and subsidence dolines along faults and above stratabound oligomict breccias. Faulting continued and differential uplift occurred as the entire platform became exposed. At this time erosional beveling of exposed St. George carbonates created the St. George Unconformity. At the same time subsurface waters generated collapse dolines along faults characterized by solution cavities, discordant polymict breccias and surface sinkholes.

Subsequent marine onlap over the St. George Unconformity in Early Middle Ordovician time locally resulted in deposition of carbonate muds and reworked residual chert sands which comprise the upper member of the

Figure 15.1 Sedimentary Evolution of the Platform at the end of the Early Ordovician and during the early Middle Ordovician at the mine

a. Middle Catoche Formation - Scattered thrombolite mounds characterized an open marine muddy shelf with intraclastic, skeletal storm beds and mudstones.

b. Upper Catoche Formation - Peloidal grainstones dominated very shallow water subtidal flats.

c. Lower Aguathuna Formation - Supratidal flats of dololaminites alternated and interfingered with burrowed mudstones of intertidal to subtidal flats. Subaerial regions along fault blocks to the north were prominent by the time of the middle member.

d. Upper Aguathuna Formation - A veneer of peritidal dolomudstones covered an irregular topography of sinkholes and shallow flats.

e. Lower Table Point Formation - An irregular topography of peritidal flats and subtidal areas were covered respectively by fenestral mudstones and nodular bioclastic wackestones.

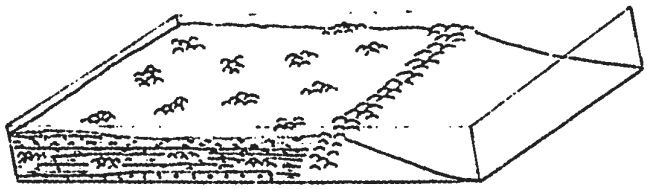

a. MIDDLE CATOCHE FORMATION

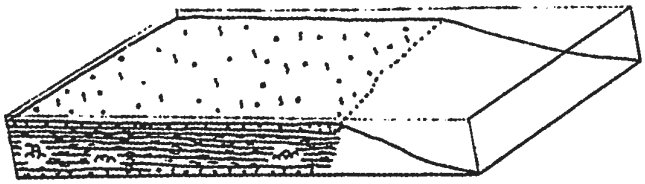

b. UPPER CATOCHE FORMATION

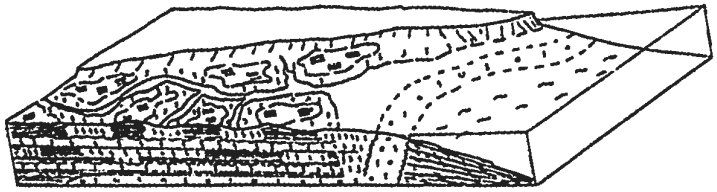

c. LOWER AGUATHUNA FORMATION

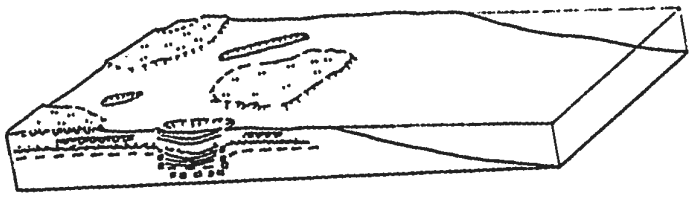

d. UPPER AGUATHUNA FORMATION

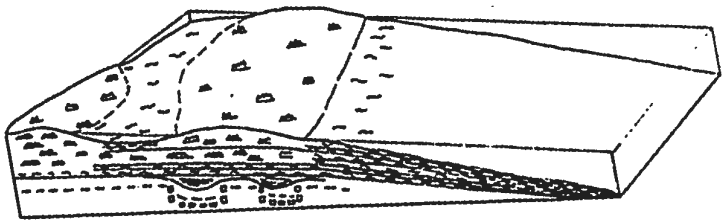

e. LOWER TABLE POINT FORMATION

SEDIMENTARY EVOLUTION

Aguathuna Formation. Initially argillaceous lime muds accumulated in sinkholes and valleys on the Unconformity surface; but lime muds blanketed much of the the platform (Fig. 15.1d).

Low relief topography persisted as Table Point peritidal sediments (Spring Inlet Member) accumulated on broad islands (Fig. 15.1e). Subsurface karst reoccurred as deep-seated meteoric aquifers generated local chimney pipe breccias.

Increased subsidence eventually produced shallow subtidal conditions across the platform. Sedimentation, however, kept pace with subsidence until the platform abruptly foundered and a siliciclastic foreland basin was generated prior to the emplacement of Taconic allochthons (Stenzel and James, 1987, 1988).

15.2 Dolomitization and Brecciation During Early Burial

Dolomitization of the upper St.George Group carbonates began at or just below the sediment surface. Early ^{18}O-enriched, finely crystalline dolomite (I) selectively replaced peritidal mudstone beds. Clasts of these dolostones were incorporated in pebble beds on erosional surfaces, in other intraformational conglomerates and in subsurface karst breccias.

Brecciation caused by subsurface karst spanned the time from deposition of the middle member of the Aguathuna Formation through deposition of the lower Table Point peritidal limestone. Ground waters attacked the upper Catoche Formation as they migrated along northeast-trending faults. Three stages of subsurface karst are recognized: (1)

extensive stratabound dissolution of limestones in the Catoche Formation leading to subsidence, (2) deep, local dissolution of limestones along contemporaneous faults followed by collapse and cave filling with polymict breccia, (3) late formation of chimney caves beneath the Table Point platform. Contemporaneous fluids circulated along faults and dolomitized (I, II) the breccia matrix.

Middle Ordovician sediments (700+ m thick) and allochthons (500+ m thick) buried the upper St. George Group to depths between 700 and 1500+ m. During the burial Catoche limestones were progressively recrystallized and dolomitized. The relationship between burial, age and dolomitization is presented graphically in Figure 15.2. Composite dolomite crystals (II) with turbid cores and clear rims nucleated near the surface and completed their growth along stylolites. After initiation of stylolites and a fracturing event, allochthonous brines migrated along fractures, through dolostones and locally dissolved limestones to form secondary pores. Clear, zoned Dolomite III cemented these pores and sealed early dolostone beds.

15.3 Epigenetic Dolomitization and Sulphide Mineralization

The St. George Group was buried to a maximum of 2 to 3 km (based on the thermal maturation of conodonts to CAI of 2 to 2.5, Nowlan and Barnes, 1987). This occurred between the Late Ordovician and Late Silurian (Fig. 15.2). In the Siluro-Devonian the platform was deformed along reactivated northeast-trending faults in response to regional compression at the beginning of the Acadian Orogeny. Linear, strata

Figure 15.2 Relationship of Dolomitization Events and Sulphide Mineralization to Burial of the Upper St. George Group at Daniel's Harbour.

Timing of dolomitization events is related to depth of burial. Dolomite I formed near surface and mostly pre-dates karstification. The prolonged growth of Dolomites II and III occurred after karstification and during burial beneath Middle Ordovician sediments and the Taconic Allochthon. Maximum depth of burial is unknown. The upper St. George Group was buried beneath a minimum of 1000 m of known cover rocks. If conodont alteration indices of 2 to 2.5 directly reflect burial, however, the overburden was greater than 2500 m. Epigenetic dolomitization (IV, V and VI), sulphide, sulphate and hydrocarbon deposition occurred in association with regional fracturing during the initial stages of Acadian uplift. Late fault-related dolomitization (VII) occurred along late steep faults associated with basement uplift during the climax of the Acadian Orogeny. Subsequent dissolution of intercrystalline limestone created secondary porosity which partially filled with calcite, saddle dolomite and hydrocarbons.

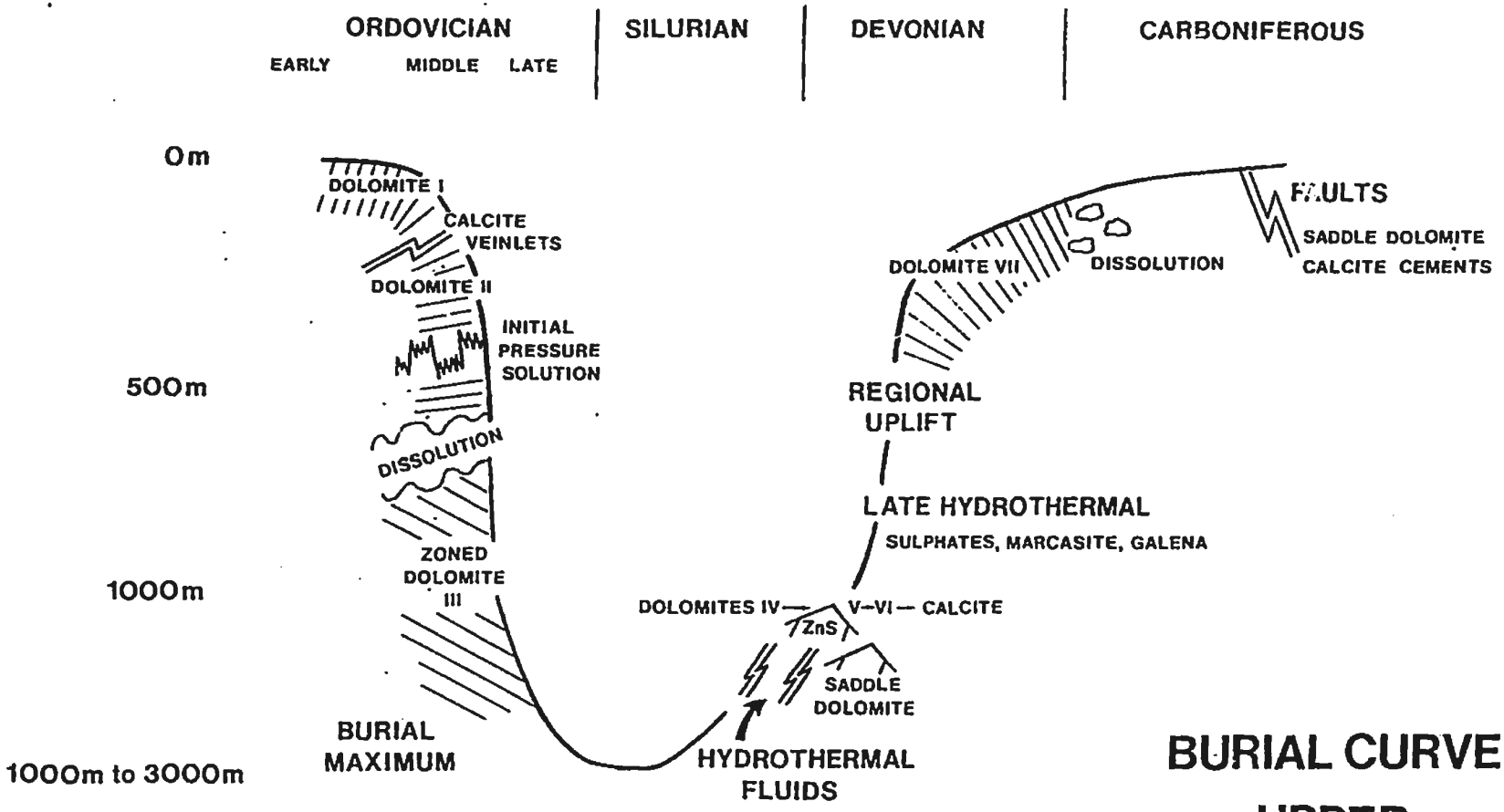

BURIAL CURVE
UPPER
ST. GEORGE GROUP

bound fracture systems formed as another product of the deformation event and served as conduits for the migration of hydrothermal brines which generated coarse dolostone/sphalerite bodies. The first fluids locally dolomitized upper Catoche limestones and overprinted earlier dolostones (II,III) along fractures. Subsequent higher temperature ore fluids partially dissolved carbonates prior to the precipitation of the first sulphides. Multiple layers of sphalerite precipitated throughout the mine area as fracturing and carbonate dissolution continued and fluid temperatures decreased. Vertical fault displacement and broad fracturing along the L and T Zones localized the flow of late ore fluids.

Extensive fracturing and dilation of earlier fractures preceded widespread post-ore dolomitization (V) which overprinted earlier medium to coarse crystalline dolostones (II, III, IV) and replaced limestones. Saddle Dolomite A filled ubiquitous veins and solution pores and partially replaced dolostones. Late Saddle Dolomite B, calcite and sulphates precipitated in pores as late fluids progressively cooled (to 50°C) and increased in salinity. Late sulphides and pyrobitumen precipitated during intermittent late invasions of hydrothermal fluid.

15.4 Dolomitization Related to Regional Uplift

During late stages of the Acadian Orogeny regional uplift fragmented and displaced the platform stratigraphy, including D/S complexes. Discordant dolostones (VII) replaced limestones surrounding most of these faults. Dolostones above thrust faults probably developed during

syntectonic fluid migration. Other dolostones with variable isotopic signatures crystallized during post-tectonic, meteoric fluid movement. These fluids also generated a ubiquitous vuggy porosity which late saddle dolomites and calcites partially cemented in the Late Paleozoic.

CHAPTER 16 CONCLUSIONS

16.1 Major Controls on Dolomitization and Fluid Movement

Primary lithology and fracture lineaments constitute the two major controls on processes throughout the burial history of the upper St. George Group. Mudstones were selectively converted to dolostone (I) beds near the surface. In early burial these beds became aquifers and later, after being sealed by Dolomite III, acted as stratigraphic aquicludes. During deep burial they behaved brittlely when deformed, thus generating the stratabound, fracture aquifers which carried the ore fluids. Peloidal grainstones of the upper Catoche Formation, in contrast, remained limestones during early dolomitization (I). As a result they were locally subjected to meteoric dissolution and only later altered to coarse, permeable dolostone during deep burial.

Synsedimentary faulting along northeast and northwest-trending lineaments controlled deposition of the middle member of the Aguathuna Formation and later sediments and also provided conduits for local subsurface karst. Reactivation of these same lineaments during early burial dolomitization (II, III) and late epigenetic dolomitization (IV, V) renewed fracture-controlled fluid movement. During regional uplift high angle reverse faults formed along northeast trends and controlled late fault-related dolomitization (VII). Further vertical and strike-slip displacement occurred along many of these structures in the Carboniferous.

16.2 Nature of the St. George Unconformity

The stratigraphy of the upper St. George Group reflects the progressive shallowing and subsurface karstification of the platform in five stages during the late Canadian and early Whiterockian. During extensive sedimentation of the lower Aguathuna Formation (Stage 1), peritidal sediments rhythmically "deepened" upwards into regional intertidal beds with erosional caps, interpreted as a response to moderate amplitude sea level oscillations prior to marine regression. Extensive sedimentation ended as the platform fragmented along northeast-oriented fractures. The middle member of the Aguathuna Formation accumulated over subsiding fault blocks and subsidence dolines related to subsurface ground water dissolution of limestone in the upper Catoche Formation (Stage 2). Continued faulting displaced these strata and subsurface collapse breccias during regional deformation, marine regression and exposure of the entire platform (Stage 3). During this hiatus meteoric waters excavated the Catoche limestones along these faults. The Aguathuna Formation then collapsed over these caves as they filled with polymict rock-matrix breccias causing collapse dolines to form on the surface. Erosion left a low-relief topography (the unconformity surface) as it bevelled a gently folded and faulted stratigraphy and locally removed up to 80 m of section. During marine onlap a veneer of peritidal dolostones filled sinkholes and covered this topography. Subsurface karst occurred again beneath peritidal limestones near the base of the Table Point Formation as beds collapsed during the development of chimney breccias.

16.3 Multi-stage Dolomitization

Most dolostone beds in the mine area record two to six episodes of dolomitization (Fig. 8.1) which occurred in four main environments: syngenetic (I), diagenetic (II, III), epigenetic (IV, V, VI) and post-uplift (VII). Syngenetic dolomitization (I) replaced subtidal to supratidal mudstones and breccia matrix in the subsurface. These microcrystalline, ^{18}O-enriched dolomites formed at or near the surface as implied by dolostone (I) fragments in conglomerates and karst breccias. Evaporative processes on the arid/resricted platform probably generated this dolomitization. The extensive, replacive dolostones, locally penetrating stratigraphy along faults, suggest, however, that dolomitization extended beyond the zone of evaporative reflux-sabkha processes.

Turbid to clear crystals (II and III) are defined as diagenetic and interpreted to have started growth near surface and completed at burial depths of more than 300 m. Early turbid, replacive blue-CL crystals (II) capture insoluble residues and calcite inclusions and are partially replaced and overgrown by clear, pink-CL dolomites. These crystals occur in limestones as individual crystals and patches replacing burrows and stylomottles. They also form pervasive dolostones in wackestone beds, replacing rock-matrix breccias and surrounding vertical fractures. Their nucleation and early growth happened near the surface in equilibrium with the calcites that were incompletely replaced. The crystals became metastable with increasing burial and were overprinted by pink-CL dolomite in response to changing pore water chemistry.

Clear, zoned Dolomite III with bright yellow to red CL occurs as isopachous cements in solution pores and as syntaxial overgrowths on Dolomite II crystals. These dolomites are particularly common in early dolostone beds and rock-matrix breccias, both of which were permeable units at the time. Their occurrence along dilatent, vertical planes of stylolite sutures implies their coeval origin with pressure solution. The precipitation of Dolomite III is interpreted to have occurred after deep, probably allochthonous, fluids migrated vertically along fractures and laterally along dolostones, caused partial solution of calcites and dolomites and became saturated with respect to dolomite. Warm fluid temperatures, hypersalinity, alkalinity and reducing conditions probably caused the precipitation of the luminescent dolomites.

Epigenetic dolomitization (IV, V, VI) occurred during deep burial (1000 - 3000 m) around tectonic fractures, which acted as conduits for allochthonous hydrothermal fluids derived from a deep source. Xenotopic pre-ore dolomitization (IV) replaced limestone beds and recrystallized early dolostone mottles (II, III), forming coarse matrix dolostones. Post-ore dolostones (V) overprinted the earlier dolostones (IV) as Saddle Dolomite A cemented pores and extensively replaced gray dolostones. Replacive saddle dolomite was a common component of post-ore epigenetic dolomitization (V). Megacrystals of Saddle Dolomite B (VI) and late calcite occluded pores as fluids became progressively cooler and more saline than ore-stage ones.

Post-uplift dolostones (VII) replaced limestones surrounding late faults. Field relationships and variable isotope geochemistry suggest that dolomitization occurred during and after uplift from formational

brines and meteoric waters that migrated along the faults.

16.4 Timing and Nature of Sulphide Deposition

16.4.1 Timing of Sulphide Deposition

Several lines of evidence indicate that sulphide deposition occurred prior to regional uplift in the early stages of the Siluro-Devonian Acadian Orogeny. (1) Ore stage dolomites (IV and V) overprint diagenetic dolomites (II, III) which probably crystallized during burial beneath the Taconic Allochthon. (2) The sulphides fill extensive subhorizontal fractures that formed from northwest-directed regional compression during the early stages of the Acadian Orogeny. By comparison, the Taconic Orogeny caused only minor deformation of the autochthon (Cawood et al., 1988). (3) Tilting of post-ore geopetal sediments indicates that sulphide deposition pre-dated regional folding associated with uplift. (4) Stylolites associated with post-ore dolomites also indicate that these processes occurred at depth. (5) Regional uplift, and associated faults which displace dolostone/ sulphide complexes, probably occurred during the late Silurian and happened no later than the early Carboniferous (Cawood et al., 1988).

16.4.2 Nature of Sulphide Deposition

Sulphide deposition occurred in two main stages as buoyant, warm ore fluids migrated laterally along stratabound fracture systems and probably displaced denser, formational fluids at the top of aquifers beneath finely crystalline dolostone aquicludes. Separate generations

of fractures created two different pathways for ore fluids and different depositional sites for early and late sphalerites. During the two ore stages discrete generations of sphalerite precipitated as extensive crystal layers throughout the mine area. Successive layers changed abruptly in colour, crystal habit and sulphur and iron chemistry. During each stage the crystal habit of the sphalerite changed from microcrystalline, fine or fibrous crystals to coarse, prismatic ones. Contemporaneous dissolution affected previous sulphides and created porosity in adjacent dolostones. The final sphalerites of each stage precipitated in these more permeable carbonates.

16.4.3 Interpretation of Genesis

A variety of data suggest that ore fluids were derived from sedimentary basin waters that travelled from depth up along deep fracture systems largely because of thermal convection and the buoyancy of the fluid. Sphalerite sulphur with positive $\delta^{34}S$ values originated from Lower Paleozoic sea water sulphate that had been stored in pore waters, evaporites and/or sedimentary pyrite. The hypersaline and $CaCl_2$-rich inclusion fluids are typical of brines from the lower sedimentary pile (Hanor, 1979). The high homogenization temperatures of these fluids (mode 140°C, maximum 185°C) suggest a source at greater burial depths than the deposit site. The basement source of Pb also supports this origin (Swinden et al., 1988).

The hydrological driving force is unknown. Gravity-driven flow from topographic ground water recharge probably was insignificant prior to regional uplift. Thermal heating of the crust accompanying regional

deformation generated regional metamorphism and anatexis in the Siluro-Devonian and probably caused fluid convection within the platform. Thermally controlled mineral transformations, also, probably released sulphur and zinc from sediments (eg. Spirakis and Heyl, 1988). Deep fracturing, also, provided permeable pathways (approaching 1 darcy) for the vertical movement of fluids. Once the hydrothermal fluids entered vertical conduits their buoyancy carried them upwards.

Chemistry of the ore fluids, in particular pH and sulphur content, is unknown. Indirect evidence, however, supports the theory that metals and sulphur travelled together in an acidic fluid (Sverjensky 1981, 1986). Significant pre-ore dissolution of carbonates suggests that the fluids were acidic. Dissolution of carbonates and sulphides and sulphide replacement of dolomites throughout ore deposition indicates general disequilibrium between fluid and minerals. Widespread crystal layers imply that Zn and reduced sulphur precipitated sulphides from a common fluid, rather than at a front of fluid mixing or sulphur reduction (cf. McClimans et al., 1980). Suggested fractionation of sulphur away from fluids conduits, also, intimates that the fluids contained sulphur.

Acidic fluids, however, cannot travel long distances through carbonates and remain unbuffered unless they carry abundant amounts of CO_2 and $CaCl_2$ (Anderson, 1983). An alternative model proposes that oxidized sulphur species travelled in a neutral ore fluid (Spirakis, 1983). These sulphur species are then reduced at the ore site along fracture-related bodies of early dolostones which contain H_2S and organics. Rock-matrix breccias at the mine contain H_2S and disseminated

pyrite in unaltered early dolostones (II, III). Black dolostones and rock-matrix breccias within or adjacent to ore zones are altered by epigenetic, dolomitization (IV, V) and lack or have lost H_2S or organics.

16.5 Nature and Origin of Epigenetic Dolostone Fabrics

Pseudobreccia, the ore gangue, is a post-ore dolostone fabric which overprints several generations of pre-ore dolostone in the upper Catoche Formation. A typical pseudobreccia fabric consists of in situ patches of gray dolostone surrounded by both replacement and pore-filling crystals of white, saddle dolomite.

Zebra dolostone, a form of pseudobreccia, has a distinctive fabric of multiple, rhythmic gray dolostone bands separating "bands" of saddle dolomite. The zebra fabric is localized along faults and fractures where it commonly dips into these structures. Cross-cutting sheet cavities and veins filled with sphalerite and saddle dolomite indicate that the origin of the fabric pre-dates ore deposition.

Pseudobreccia fabrics vary systematically across the linear, stratabound fracture systems in the upper Catoche Formation. Saddle dolomite occurs only in veins and patches of pseudobreccia in early dolostone bodies adjacent to vein systems. Megapores and zebra fabrics are abundant around the fracture systems. Regular pseudobreccia and coarse sparry dolostone occur outside of fractures.

These dolostones acquired their fabrics over a minimum of 4 events (Fig. 13.3) when fracturing preceded the migration of allochthonous,

hydrothermal fluids into the upper Catoche Formation. Initial hydrothermal fluids migrated up along early fractures and laterally through fractures and limestone beds. They probably encountered formational fluids at fracture/bed intersections and mixed with them along double diffusion fronts. Dolostone bands (zebra fabric) developed along diffusion layers where they collected an abundance of insoluble material. At the same time xenotopic dolostone (IV) replaced early dolostone stylomottles (II, III) and surrounding limestone matrix.

A second generation of fractures tapped anomalously hydrothermal fluids which carried metals. The undersaturated, possibly acidic, brines entered the upper Catoche Formation where they preferentially dissolved matrix dolostone and remnant patches of limestone, but not zebra bands. The dissolution of dolostones continued throughout periods of sulphide deposition. Sulphides precipitated around the margins of these secondary pores and locally replaced dolostones. Subsequently, geopetal carbonates settled on top of sphalerites at the bottom of pores.

Following ore deposition, late hydrothermal fluids, saturated with carbonate, pervaded the entire region along an extensive network of fractures, causing pervasive dolomitization (V). Saddle Dolomite A cemented most pores and extensively replaced matrix dolostone (IV). Xenotopic gray dolostones (V) recrystallized the remaining dolostones (IV) and geopetal sediments.

Saddle Dolomite B, calcites and sulphates precipitated when cooler and more hypersaline brines migrated up along late fractures. The precipitation of these and all post-ore carbonates probably occurred

when fracturing caused the partial pressure of CO_2 to decrease and incoming hydrothermal brines increased pore water temperatures.

16.6 Nature and Significance of the Various Breccias

True breccias within the upper Catoche Formation are classified into three types: (1) rock-matrix breccia, (2) fault or tectonic breccia and (3) spar breccia (Table 7.2). Rock-matrix breccias all formed by subsurface dissolution between the time of deposition of the middle member of the Aguathuna Formation and that of the lower Table Point Formation. They are composed of early dolostone (I) fragments within a distinctive gray dolostone matrix of early dolomites I, II and III. Three geometric types of bodies are recognized (Table 7.3). Intrastratal breccias are regionally extensive beds associated with conglomerate-evaporite horizons in the Aguathuna Formation. Stratabound oligomict breccias represent local and partial solution of upper Catoche limestones below subsidence dolines. Discordant polymict breccias crosscut the stratigraphy as vertical, tabular bodies along faults or chimneys. These latter breccias are the products of wholesale collapse of the Aguathuna Formation into phreatic caves in the Catoche Formation.

Fault breccias occur only within centimetres of faults. Small, centimetre to millimetre-sized, fragments are cemented by white, very fine crystalline dolomite (or rock flour). Both fragments and matrix are cut by several generations of rock flour-filled veinlets related to numerous episodes of deformation along faults.

Spar breccias are typical of fracture zones in coarse dolostone/

sphalerite complexes. These "open work" breccias are cemented by sphalerite and saddle dolomite. Apparent cement support and only partial collapse of typical mosaic breccias suggests that cementation occurred under elevated pore fluid pressures and tectonically induced extension. "Splinter" breccias and fragmentation of blocks intimate that pore fluid pressure and tectonism combined to cause hydraulic fracturing and shattering.

REFERENCES

ABBOTT, D.L., 1975, On the hydrology of the Edwards Limestone, south-central Texas. Jour. of Hydrology, v. 24, p. 251-269.

ANDERSON, G.M., 1973, The hydrothermal transport and deposition of galena and sphalerite near 100°C. Econ. Geology, v. 68, p. 480-492.

ANDERSON, G.M., 1975, Precipitation of Mississippi Valley-type ores. v. 70, p. 937-942.

ANDERSON, G.M., 1983, Some geochemical aspects of sulfide precipitation in carbonate rocks. In: Kisvarsanyi, G.; Grant, S.K.; Pratt, W.P; and Koenig, J.W. (eds.) International Conference on Mississippi Valley type lead-zinc deposits. Proceedings volume: Rolla, Univ. Missouri-Rolla Press, p. 61-76.

ANDERSON, G.M., 1989, Organic maturation and the origin of MVT deposits, (abstr.), Geological Society of America Absracts with Programs, p.A4.

ANDERSON, G.M. and GARVEN, G., 1987, Sulfate-sulfide-carbonate associ ations in Mississippi Valley-type lead-zinc deposits. Econ. Geology, v. 82, p. 482-488.

ANDERSON, G.M. and MACQUEEN, R.W., 1982, Ore Deposit Models - 6. Mississippi Valley-Type Lead-Zinc Deposits. Geoscience Canada, v. 9, p. 108-117.

ASSERTO, R. and FOLK, R.L., 1980, Diagenetic fabrics of aragonite, calcite, and dolomite in an ancient peritidal-spelean environment: Triassic calcare Rosso, Lamardia, Italy. Jour. of Sed. Petrology,

v. 50, p. 371-394.

AULSTEAD, K.L. and SPENCER, R.J., 1985, Diagenesis of the Keg River Formation, northwestern Alberta: Fluid inclusion evidence. Bull. Can. Petrol. Geology, v. 33, p. 167-183.

AULSTEAD, K.L. and SPENCER, R.J., 1987, Diagenesis of the Manetoe facies, Yukon and Northwest Territories, Canada (abstr.). In: Soc. Econ. Paleont. Mineral. Annual Midyear Meeting Abstracts, p. 5.

BACHINSKI, D.J., 1969, Bond strength and sulfur isotopic fractionation in coexisting sulfides. Econ. Geology, v. 64, p. 56-65.

BACK, W. and HANSHAW, B.B., 1970, Comparison of chemical hydrogeology of the carbonate peninsulas of Florida and Yucatan peninsulas. Jour. of Hydrology, v. 10, p. 330-368.

BAKER, P.A. and KASTNER, M., 1981, Constraints on the formation of sedimentary dolomite. Science, v. 213, p. 214-216.

BANKS, N.G., 1970, Nature and origin of early and late cherts in the Leadville Limestone, Colorado. Bull. Geol. Soc. America, v. 81, p. 3033-3048.

BANNER, J.L. and HANSON, G.N., 1989, Simultaneous isotopic and trace element variations during water-rock interaction: quantitative models with applications to carbonate diagenesis, (abstr.), geological Society of America Abstracts with Programs, p. A221.

BARNES, H.L., 1979, Solubilities of Ore Minerals, In: Barnes, H.L. (eds.) Geochemistry of Hydrothermal Ore Deposits. 2nd Ed., New York, Wiley-Interscience, p. 404-460.

BARNES, H.L., 1983, Ore-depositing reactions in Mississippi Valley-type deposits. In: Kisvarsanyi, G.; Grant, S.K.; Pratt, W.P. and

Koenig, J.W. (eds.) Proceedings Volume, International Conference on Mississippi Valley Type Lead-Zinc Deposits, p. 77-85.

BARNES, H.L.; ADAMS, S.J. and ROSE, A.W., 1981, Ores formed by diagenetic and metamorphic processes. In: Studies in Geophysics: Mineral Resources: Genetic understanding for practical applications, Washington D.C. National Academy Press, p. 73-81.

BARTON, P. B. Jr., 1967, Possible role of organic matter in the precipitation of the Mississippi ores, in BROWN, J. S. (ed). Genesis of stratiform lead-zinc-barite-fluorite deposits, Econ. Geology Monograph No. 3, p. 371 - 378

BATHURST, R.G.C., 1958, Diagenetic fabrics in some British Dinantian limestones Liverpool and Manchester. Geol. Jour., v. 2, p. 11-36.

BATHURST, R.G.C., 1959, Diagenesis in Mississippian calcilutites and pseudobreccias. Jour. Sed. Petrol., v. 29, p. 365-376.

BATHURST, R.G.C., 1975, Carbonate sediments and their diagenesis. Developments in Sedimentology, v. 12, Amsterdam, Elsevier, 620p.

BATHURST, R.G.C, 1980, Stromatactis-origin related to submarine-cemented crusts in Paleozoic mud mounds. Geology, v. 8, p. 131-134.

BATHURST, R.G.C., 1982, Genesis of stromatactis cavities between submarine crusts in Paleozoic81. carbonate mud buildups. Jour. Geol. Soc. London, v. 139, p. 165-1.

BEALES, F.W., 1971, Cementation by white sparry dolomite. In: Bricker, O., carbonate cements The John's Hopkins University Studies in Geology No. 19, The John's Hopkins Press, Baltimore. p. 330-338.

BEALES, F.W. and JACKSON, S.A., 1966, Precipitation of Pb-Zn ores in

carbonate reservoirs as illustrated by Pine Point ore field, Canada. Canadian Inst. of Mining and Metall., Transactions, v. 79, p. B145-B154.

BEALES, F.W. and HARDY, J.L., 1980, Criteria for the recognition of diverse dolomite types with an emphasis on studies on host rocks for Mississippi Valley-type ore deposits. Soc. Econ. Paleon. Mineral. Spec. Publ. 28, p. 197-313.

BEHRENS, E.W. and LAND, L.S., 1972, Subtidal Holocene dolomite, Baffin Bay, Texas. Jour. Sed. Petrology, v. 42, p. 155-161.

BEIN, A. and LAND, L.S., 1983, Carbonate sedimentation and diagenesis associated with Mg-Ca-Chloride brines: the Permian San Andres Formation in the Texas panhandle. Jour. Sed. Petrology, v. 53, p. 243-260.

BENEDICT, G.L. III, 1977, Lenoir, Holston and Ottosee Formations: shallow shelf lagoon, deeper shelf and shelf marginal environments. In: S.C. Ruppel and K.R. Walker (eds.) The ecostratigraphy of the Middle Ordovician of the southern Appalachians, USA: field excursion, University of Tennessee, Dept. of Geological Sciences. Studies in Geology No. 77-1, p. 52-58.

BETHKE, C.M., 1986a, Hydrologic constraints on the genesis of the Upper Mississippi Valley mineral district from Illinois basin brines. Econ. Geology, v. 81, p. 233-249.

BETHKE, C.M., 1986b, Roles of sediment compaction, tectonic compression, and topographic relief in driving deep groundwater migration. Geol. Soc. Amer. Abstract with Programs, v. 18, p.

BLATT, H., MIDDLETON, G. and MURRAY, R., 1972, Origin of Sedimentary

Rocks. Prentice Hall Inc., New Jersey, 634p.

BLES, J-L. and FEUGA, B., 1986, The fracture of Rocks. Elsevier, Amsterdam, 131p.

BLOUNT, D.N. and MOORE, C.H. Jr., 1969, Depositional and non-depositional carbonate breccias, Chiantla Quadrangle, Guatemala. Geol. Soc. Amer. Bulletin, v. 80, p. 429-442.

BOGLI, A., 1980, Karst hydrology and physical speleology: New York. Springer Verlag, 284p.

BONHAM, L.C., 1980, Migration of hydrocarbons in compacting basins: Tulsa, Oklahoma. Amer. Assoc. Petrol. Geology, Studies in Geology, v. 10, p. 69-88.

BOSELLINI, A. and HARDIE, L.A., 1973, Depositional theme of a marginal marine evaporite. Sedimentology, v. 20, p. 5-27.

BOSTOCK, H.H., CUMMING, L.M., WILLIAMS, H. and SMYTH, W.R., 1983, Geology of the Strait of Belle Isle area, northwestern insular Newfoundland, southern Labrador, and adjacent Quebec. Geol. Surv. of Canada, Memoir 400, Map 1495A.

BOYCE, W.D., 1983, Preliminary Ordovician trilobite biostratigraphy of the Eddies Cove West-Port au Choix area, western Newfoundland. Mineral Develop. Division, Newfoundland Dept. Mines and Energy, Report 83-1, p. 11-15.

BOYCE, W.D., 1985, Cambrian-Ordovician biostratigraphic investigations, Great Northern Peninsula. Mineral Develop. Division, Newfoundland Dept. Mines and Energy, Report 85-1, p. 60-88.

BOYCE, W.D., 1986, Ordovician biostratigraphic investigations, Great Northern Peninsula. Mineral Develop. Division, Newfoundland Dept.

Mines and Energy, Report 86-1, p. 161-188.

BRACE, W., 1968, The mechanical effects of pore pressure on fracturing of rock, Proceedings, Conference on Research in Tectonics, Geol. Surv. of Canada, Paper 68-5, p. 113-123.

BRADLEY, D.C., 1982, Subsidence in late Paleozoic basins in the northern Appalachians. Tectonics, v. 1, p. 107-123.

BRADLEY, D.C., 1989, Mississippi Valley-type Pb-Zn mineralization during Ordovician arc-continent collision in the Appalachians, (abstr.), Geological Society of America Abstracts with Programs, p. A8.

BREDEHOEFT, J.D.; BACK, W. AND HANSHAW, B.B., 1982, Regional groundwater flow concepts in the United States: Historial perspective. In: Narasimhan, T.N. (ed.) recent Trends in Hydrogeology. Geol. Soc. Amer., Spec. Paper 189, p. 297-316.

BRIDGE, J., 1955, Disconformity between Lower and Middle Ordovician Series at Douglas Lake, Tennessee. Geol. Soc. Amer. Bulletin, v. 66, p. 725-730.

BRISKEY, J.A.; DINGESS, P.R.; SMITH, F.; GILBERT, R.C.; ARMSTRONG, A.K. and COLE, G.P., 1986, Localization and source of Mississippi Valley-type zinc deposits in Tennessee, USA and comparisons with Lower Carboniferous rocks of Ireland. In: Andrew, C.J. et. al., (eds.) Geology and Genesis of Mineral Deposits in Ireland. Irish Assoc. for Econ. Geology, p. 635-661.

BROWN, J.S. (ed.), 1967, Genesis of stratiform lead-zinc-barite-fluorite deposits. Econ. Geology, Monograph No. 3, 443p.

BUCKLEY, H.E., 1951, Crystal Growth. New York, John Wiley and Sons Inc.

571p.

CATHLES, L.M. and SMITH, A.T., 1983, Thermal constraints on the formation of the Mississippi Valley-type lead-zinc deposits and their implications for episodic basin dewatering and deposit genesis, Econ. Geology, v. 78, p. 983-1002.

CARPENTER, A.B.; TROUT, M.L. and PICKETT, E.E., 1974, Preliminary report on the origin and chemical evolution of lead- and zinc-rich brines in central Mississippi. Econ. Geology, v. 69, p. 1191-1206.

CAWOOD, P.A. and WILLIAMS, H., 1986, Northern extremity of the Humber Arm Allochthon in the Portland Creek area, western Newfoundland and relationships to nearby groups. In: Current Research Part A, Geol. Surv. of Canada, Paper 86-1A, p. 675-682.

CAWOOD, P.A.; WILLIAMS, H. and GRENIER, R., 1987, Geology of Portland Creek area (12 I/4), western Newfoundland. Geol. Surv. of Canada, Open File 1435, Scale 1:50,000.

CAWOOD, P.A. and WILLIAMS, H., 1988, Acadian basement thrusting, crustal delamination and structural styles in and around the Humber Arm Allochthon, western Newfoundland. Geology, v. 16, p. 370-373.

CAWOOD, P., WILLIAMS, H., O'BRIEN, S.J. and O'NEILL, P.P., 1988, Trip A1. A geologic cross-section of the Appalachian Orogen. Field Trip Guidebook. Geological Association of Canada Annual Meeting. St. John's, Nfld.

CHILINGAR, G.V.; ZENGER, D.H.; BISSELL, H.J. and WOLF, K.H., 1979, Dolomites and Dolomitization In: G. Larsen and G.V. Chilingar (eds.) Diagenesis in Sediments and Sedimentary Rocks. Elsevier, Amsterdam, p. 423-536.

CHOQUETTE, P.W., 1971, Late ferroan dolomite cement, Mississippian, carbonates, Illinois Basin, U.S.A. In: Bricker, O.P. (ed.) Carbonate Cements. The John's Hopkins University Studies in Geology, No. 19, The John's Hopkins Press, Baltimore, p. 339-346.

CHOQUETTE, P.W. and PRAY, L.C., 1970, Geologic nomenclature and classification of porosity in sedimentary carbonates, Bulletin of the American Assoc. of Petroleum Geol., Vol. 54, p.207 - 250.

CHOQUETTE, P.W. and JAMES, N.P., 1987, Diagenesis 12. Diagenesis in limestones -3. The deep burial environment. Geoscience Canada, v. 14, p. 3-35.

CHOW, N., 1986, Sedimentology and diagenesis of Middle and Upper Cambrian platform carbonates and siliciclastics, Port au Port Peninsula, western Newfoundland. Unpubl. Ph.D. thesis, Memorial University of Newfoundland, 458p.

CHOWNS, T.M. and ELKINS, J.E., 1974, The origin of quartz geodes and cauliflower cherts through silicification of anhydrite nodules. Jour. Sed. Petrology, v. 44, p. 885-903.

CISNE, J.L., 1985, Depth dependent sedimentation and the flexural edge effect in epeiric seas: measuring water depth relative to the lithosphere's flexural wavelength. Jour. Geology, v. 93, p. 567-576.

CISNE, J.L.; GILDNER, R.F.; and RABE, B.D., 1984, Epeiric sedimentation and sea level: Synthetic ecostratigraphy. Lethaia, v. 17, p. 267-288.

CLAYPOOL, G.E.; HOLSER, W.T.; KAPLAN, I.R.; SAKAI, H. and ZAK, I., 1980, The age curves of sulfur and oxygen isotopes in marine sulfate and

their mutual interpretation. Chemical Geology, v. 28, p. 199-260.

CLAYTON, R.N.; JONES, B.F. and BERNER, R.A., 1968, Isotope studies of dolomite formation under sedimentary conditions, Geochim. et Cosmochim. Acta, v. 32, p. 415-432.

COLLINS, J.A., 1971, Carbonate lithofacies and diagenesis related to sphalerite mineralization near Daniel's Harbour, western Newfoundland. Unpubl. M.Sc. thesis, Queen's University, 184p.

COLLINS, J.A., 1972, Sphalerite as related to the tectonic movements, deposition, diagenesis and karstification of a carbonate platform, Proceedings of the 24th International Geological Congress, Montreal, section 6, p. 208

COLLINS, J.A. and SMITH, L., 1972, Lithostratigraphic controls of some Ordovician sphalerite, in AMSTUTZ,G.C. and BERNARD, A.J., (eds.), Ores in Sediments, Springer Verlag, Heidelberg, p. 79 -91.

COLLINS, J.A. and SMITH, L., 1975, Zinc deposits related to diagenesis and intrakarstic sedimentation in the Lower Ordovician St. George Formation, western Newfoundland. Bull. Can. Petrol. Geology, v. 23, p. 393-427.

CONIGLIO, M., 1985, Origin and diagenesis of fine-grained slope sediments: Cow Head Group (Cambro-Ordovician), western Newfoundland. Unpubl. Ph.D. thesis, Memorial University of Newfoundland, 684p.

CONIGLIO, M. and JAMES, N.P., 1985, Calcified algae as sediment contributors to Early Paleozoic limestones: evidence from deep water sediments of the Cow Head Group, western Newfoundland. Jour. of Sed. Petrology, v. 55, p. 746-754.

COOKE, R.B., 1969, Report of work done by Cominco on Leitch Concessions

Daniel's Harbour, western Newfoundland. Unpubl. report.

CORON, C.R., 1982, Facies relations and ore genesis of the Newfoundland zinc mines deposit, Daniel's Harbour, western Newfoundland. Unpubl. Ph.D. thesis, University of Toronto, 164p.

COWAN, C.A., KELLY, W.C. and WILKINSON, B.H., 1985, "Coontail" fluorite rhythmites of southern Illinois: Evidence for episodic basin dewatering, Geological Society of America, Abstracts with Programs, v. 17, p. 554.

CRAIG, J.R. and VAUGHAN, D.J., 1981, Ore Mineralogy and Ore Petrography, Wiley Interscience, 409p.

CRAIG, J.R.; SOLBERT, T.N. and VAUGHAN, D.J., 1983a, Compositional variations in sphalerite ores of the East and Central Tennessee zinc districts. In: Craig J.R. (ed.) Tennesse zinc deposits field trip guidebook. Virginia Tech Dept. of Geological Sciences, Guidebook No. 9, p. 152-164.

CRAIG, J.R.; SOLBERG, T.N. and VAUGHAN, D.J., 1983b, Growth characteristics of sphalerites in Appalachian zinc deposits. In: Kisvarsanyi, G.; Grant, S.K.; Pratt, W.P. and Koenig, J.W. (eds.) Proceedings Volume, International Conference on Mississippi Valley-type lead-zinc deposits. Univ. Missouri-Rolla Press, Rolla Missouri, p. 317-327.

CUMMING, L.M., 1968, St. George-Table Head disconformity and zinc mineralization, western Newfoundland. Canadian Mining and Metallurgical Bulletin, v. 61, p. 721-725.

DALLMEYER, R.D., 1977, $^{40}Ar/^{39}Ar$ spectra of minerals from the Fleur de Lys terrane in northwest Newfoundland: their bearing on chronology

of metamorphism within the Appalachian orthotectonic zone. Jour. of Geology, v. 85, p. 89-103.

DALLMEYER, R.D. and HIBBARD, J., 1984, Geochronology of the Baie Verte Peninsula, Newfoundland, implications for the tectonic evolution of the Humber and Dunnage Zones of the Appalachian Orogen, Journal of Geology, v. 92, p. 489 - 512.

DALRYMPLE, R.W; NARBONNE, G.M. and SMITH, L., 1985, Eolian action and the distribution of Cambrian shales in North America, Geology, v. 13, p. 607-610.

DESROCHERS, A., 1985, The Lower and Middle Ordovician platform carbonates of the Mingan Islands, Quebec: stratigraphy paleokarst and limestone diagenesis. Unpubl. Ph.D. thesis, Memorial University of Newfound-land, 342p.

DEVOTO, R.H., 1985, Sedimentology, dolomitization and mineralization of the Leadville Limestone (Mississippian), central Colorado. Guidebook for Soc. Econ. Paleon. Mineral., Field Trip No. 6, SEPM Midyear Meeting Golden, Colorado.

DILLON, E.P., 1978, A multi-element geochemical study of the pseudobreccia host rock of the Newfoundland Zinc Mine. Unpubl. M.Sc. thesis, University of Toronto, 31p.

DISNAR, J.R.; GAUTHIER, B.; CHABIN, A. and TRICHET, J., 1986, Early biodegradation of ligneous organic materials and its relation to ore deposition in the Trèves Zn-Pb ore body (Gard, France). Organic Geochemistry, v. 10, p. 1005-1013.

DIXON, E.E.L. and VAUGHAN, A., 1911, The Carboniferous succession in Gower (Glamorganishire), with notes on its fauna and conditions of

deposition. Quart. Jour. Geol. Society, v. 67, p. 477-567.

DIXON, J., 1976, Patterned carbonate - a diagnetic feature. Bull. Can. Petrol. Geology, v. 24, p. 450-456.

DOE, R.B. and ZARTMAN, R.E., 1979, Plumbotectonics, the Phanerozoic. In: Barnes, H.L. (ed.) Geochemistry of hydrothermal ore deposits. John Wiley and Sons, p. 22-70.

DOWTY, E., 1976, Crystal structure and crystal growth: II. Sector zoning in minerals. Amer. Mineralogist, v. 61, p. 460-469.

DUNNING, R.G.; KROGH, T.E.; O'BRIEN, S.J.; COLMAN-SADD, S.P. and O'NEILL, P., 1988, Geochronologic framework for the central Mobile belt in southern Newfoundland and the importance of Silurian Orogeny (abstr.). In: Program with Abstracts, v. 13, Annual Meeting of Geol. Assoc. Canada, p. A34.

DUNNING, G.R.; O'BRIEN, S.J.; COLMAN-SADD, S.P.; O'NEILL, P.P. and KROGH, T.E., in press, Silurian orogeny in Newfoundland. Jour. of Geology.

DUNSMORE, H.E., 1973, Diagenetic processes of lead-zinc emplacement in carbonates. Inst. Mining Metall. Bulletin, v. 82, p. 9-13.

DZULYNSKI, S. and SASS-GUSTKIEWICZ, M., 1986, Hydrothermal karst phenomena as a factor in the formation of Mississippi Valley-type deposits. In: Wolf, K.H., (ed.) Handbook of Strata-bound and Stratiform Ore Deposits, v. 13, Elsevier Amsterdam, p. 391-439.

EBERS, M.L. and KOPP, O.C., 1979, Cathodoluminescent microstratigraphy in gangue dolomite, the Mascot-Jefferson City district, Tennessee. Econ. Geology, v. 74, p. 908-918.

EKDALE, A.A.; BROMELY, R.G. and PEMBERTON, S.G., 1984, Ichnology: the

use of trace fossils in sedimentology and stratigraphy. Soc. Econ. Paleon. Miner. Short Course No. 15.

ELLIOT, D., and JOHNSON, M.R.W., 1980, The structural evolution of the northern part of the Moine thrust zone. Royal Society Edinburgh Trans. Ear. Science, v. 71, p. 69-96.

ETHINGTON, R.L. and CLARK, D.L., 1971, Lower Ordovician conodonts in North America. Geol. Soc. Amer., Memoir 127, p. 63-82.

ETHINGTON, R.L. and CLARK, D.L., 1981, Lower and Middle Ordovician Conodonts from the Ibex area, western Millard County, Utah. Brigham Young University Geology Studies, v. 28, Part 2, 160p.

ETHRIDGE, F.G.; ORTIZ, N.V.; GRANGER, H.C.; FERENTCHAK, J.A. and SUNADA, D.K., 1980, Effects of ground-water flow on the origin of Colorado Plateau-type uranium deposits. In: New Mexico Bureau of Mines and Mineral Resources, Memoir 38, p. 98-106.

EVANS, C.R.; ROGERS, M.A. and BAILEY, N.J.L., 1971, Evolution and alteration of petroleum in western Canada. Chem. Geology, v. 8, p. 147-170.

FÅHRAEUS, L.E., 1970, Conodont-based correlations of Lower and Middle Ordovician strata in western Newfoundland. Geol. Soc. Amer. Bulletin, v. 81, p. 2061-2076.

FINNEY, S.C., and SKEVINGTON, D., 1979, A mixed Atlantic-Pacific province Middle Ordovician graptolite fauna in western Newfoundland. Can. Jour. Earth Sciencs, v. 16, p. 1899-1902.

FISCHER, A.G., 1964, The Lofer cyclothems of the Alpine Triassic. Bull. Geol. Soc. Kansas, v. 169, p. 107-149.

FLUGEL, E., 1982, Microfacies Analysis of Limestones. Springer-Verlag,

New York, 633p.

FOLEY, N.K., SINHA, A.K. and CRAIG, J.R., 1981, Isotopic composition of lead in the Austinville-Ivanhoe Pb-Zn district, Virginia. Econ. Geology, v. 76, p. 2012-2017.

FOLK, R.L. and ASSERTO, R., 1974, Giant aragonite rays and baroque white dolomite in tepee-fillings, Triassic of Lombardy, Italy (abstr.). Amer. Assoc. Petrol. Geologists. Abstracts with Program, Annual Meeting San Antonio, p. 34-35.

FOLK, R.L. and LAND, L.S., 1975, Mg/Ca ratio and salinity: two controls over crystallization of dolomite. Amer. Assoc. Petrol. Geol. Bulletin, v. 59, p. 60-68.

FONTBOTE, L. and AMSTUTZ, G.C., 1983, Diagenetic crystallization rhythmites in Mississippi Valley-type ore deposits. In: Kisvarsanyi, G.; Grant, S.K.; Pratt, W.P.; and Koenig, J.W. (eds.) Proceedings Volume-International Conference on Mississippi Valley-type lead-zinc deposits. Univ. Missouri-Rolla Press, Rolla Missouri, p. 328-337.

FORD, D., 1988, Characteristics of dissolutional cave systems in carbonate rocks. In: James, N.P. and Chouquette, P.W. (eds.) Paleokarst, New York, Springer Verlag, p. 25-57.

FORTEY, R.A., 1979, Early Ordovician trilobites from the Catoche Formation (St. George Group), western Newfoundland. Geol. Surv. of Canada. Bulletin 321, p. 61-114.

FORTEY, R.A., 1984, Global earlier Ordovician transgressions and regressions and their biological implications. In: D.L. Bruton (ed.) Aspects of the Ordovician System. Paleontological Contrib.

from the University of Oslo, Universitetsforlaget 295, p. 37-50.

FRANK, J.R.; CARPENTER, A.B. and OGLESBY, T.W., 1982, Cathodoluminescence and composition of calcite cement in the Taum Sauk Limestone (Upper Cambrian), southeast Missouri. Jour. of Sed. Petrology, v. 39, p. 1438-1454.

FRANKS, S. and FORESTER, R., 1984, Relationships among secondary porosity, pore-fluid chemistry, and CO_2, Texas, Gulf Coast. Amer. Assoc. Petrol. Geology, Memoir 37, p. 63-80.

FREEMAN, T., 1972, Sedimentology and dolomitization of Muschelkalk carbonates (Triassic), Iberian Range. Spain. Bull. Amer. Assoc. Petrol. Geology, v. 59, p. 60-68.

FREEMAN, T., and MEDARY, T., 1987, Modification of precursor dolostone by a later dolomitizing event: the Bonneterre Formation (Cambrian), southern Missouri (abstr.). In: Soc. Econ. Paleont. Mineral. Annual Midyear Meeting Abstracts, p. 28.

FRIEDMAN, G.M., 1965, Terminology of crystallization textures and fabrics in sedimentary rocks. Jour. Sed. Petrology, v. 35, p. 643-655.

FRIEDMAN, G.M. and SAUNDERS, J.E., 1967, Origin and occurrence of dolostones. In: Chilinger, G.V.; Bissell, H.J. and Fairbridge, R.W. (eds.) Carbonate Rocks. Origin, Occurrence and Classification, Elsevier, Amsterdam, p. 267-348.

FYFE, W.S.; PRICE, N.J. and THOMPSON, A.B., 1979, Fluids in the Earth's Crust, Developments in Geochemistry 1. Elsevier, 383p.

GAINES, A.M., 1974, Protodolomite synthesis at 100°C and atmospheric pressure. Science, v. 183, p. 518-520.

GAINES, A.M., 1980, Dolomitization Kinetics: recent experimental studies. In: Zenger, D.H.; Dunham, J.B. and Ethington, R.L. (eds.) Concepts and Models of Dolomitization. Soc. Econ. Paleon. Mineral. Spec. Publ. 28, p. 81-86.

GALLOWAY, W.E., 1984, Hydrogeologic regimes of sandstone diagenesis. In: McDonald, D.A. and Surdam, R.C. (eds.) Clastic Diagenesis. Amer. Assoc. Petrol. Geology, Memoir 37, p. 3-14.

GARVEN, G., 1985, The role of regional fluid flow in the genesis of the Pine Point deposit, Western Canada sedimentary basin. Econ. Geology, v. 80, p. 307-324.

GARVEN, G. and FREEZE, R.A., 1984a, Theoretical analysis of the role of groundwater flow in the genesis of stratabound ore deposits. 1. Mathematical and numerical models. Amer. Jour. of Science, v. 284, p. 1085-1124.

GARVEN, G. and FREEZE, R.A., 1984b, Theoretical analysis of the role of groundwater flow in the genesis of stratabound ore deposits. 2. Quantitative results. Amer. Jour. of Science, v. 284, p. 1125-1174.

GARVEN, G. and SVERJENSKY, D.A., 1989, Hydrogeology of regional flow systems associated with the formation of Mississippi Valley-type ore deposits in the mid-continent, (abstr.), Geological Society of America Abstracts with Programs, p.A9.

GAWTHORPE, R.L., 1987, Burial dolomitization and porosity development in a mixed carbonate-clastic sequence: an example from the Bowland Basin, northern England. Sedimentology, v. 34, no. 4, p. 533-558.

GAYLORD, W.B. and BRISKEY, J.A., 1983, Geology of the Elmwood and

Gordonsville mines, central Tennessee zinc district: Tennessee zinc deposit field trip guide book; Virginia Polytechnic Institute, Blacksburg, Va., Guidebook 9.

GOLDHAMMER, R.K.; DUNN, P.A. and HARDIE, L.A., 1987, High frequency glacio-eustatic seal level oscillations with Milankovitch characteristics recorded in Middle Triassic cyclic platform carbonates, northern Italy. Amer. Jour. Science, v. 287, p. 853 -892.

GOLDSMITH, J.D. and GRAF, D.L., 1958, Relation between lattice constants and composition of the Ca-Mg carbonates. Amer. Mineralogist, v. 43, p. 84-101.

GRATZ, J.F. and MISRA, K.C., 1987, Fluid inclusion study of the Gordonsville zinc deposit, central Tennessee. Econ. Geology, v. 82, p. 1790-1804.

GREGG, J.M., 1985, Regional epigenetic dolomitization in the Bonneterre Dolomite (Cambrian) Southeastern Missouri. Geology, v. 13, p. 503-506.

GREGG, J.M. and HAGNI, R.D., 1987, Irregular cathodoluminescent banding in late dolomite cements: Evidence for complex faceting and metalliferous brines, Geological Society of America Bulletin, v. 98, p.86-91.

GREGG, J.M. and SIBLEY, D.F., 1984, Epigenetic dolomitization and the origin of xenotopic dolomite texture. Jour. Sed. Petrology, v. 54, p. 908-931.

GRENIER, R., 1990, The Appalachian fold and thrust belt, northwest Newfoundland, unpublished M.Sc. thesis, Memorial University of Newfoundland, St.John's.

GRENIER, R. and CAWOOD, P., 1988, Variations in structural style along the Long Range Front, western Newfoundland. In: Current Research, Part B. Geol. Surv. of Canada, Paper 88-1B, p. 127-133.

GRETENER, P., 1969, Fluid pressure in porous media, its importance in geology: a review. Can. Petrol. Geol. Bulletin, v. 17, p. 255-295.

GRETENER, P.E., 1981, Pore pressure: Fundamentals, general ramifications, an implications for structural geology (revised). Amer. Assoc. Petrol. Geology, Education Course Note Series No. 4, 131p.

GRIFFITHS, R.W., 1981, Layered double-diffusive convection in porous media. Journal of Fluid Mechanics. v. 102, p. 221 -248.

GROGAN, R.M., 1949, Structures due to volume shrinkage in the bedding-replacement fluorspar deposits of Southern Illinois. Econ. Geology, v. 44, p. 606-616.

GROTZINGER, J.P., 1986, Upward shallowing platform cycles: a response to 2.2 billion years of low-amplitude, high-frequency (Milankovitch band) sea level oscillations. Paleoceanography, v. 1, p. 403-416.

GROTZINGER, J.P., 1986, Cyclicity and paleoenvironmental dynamics, Rocknest platform, northwest Canada. Geol. Soc. Amer. Bulletin, v. 97, p. 1208-1231.

GROVER, G. Jr. and READ, J.F., 1978, Fenestral and associated vadose diagenetic fabrics of tidal flat carbonates, Middle Ordovician New Market limestone, southwestern Virginia. Jour. Sed. Petrology, v. 48, p. 453-473.

GROVER, G. Jr. and READ, J.F., 1983, Paleoaquifer and deep-burial-related cements defined by regional cathodoluminescent patterns,

Middle Ordovician carbonates, Virginia. Bull. Amer. Assoc. Petrol. Geology, v. 67, p. 1275-1303.

GRUNDMANN, W.H. Jr., 1977, Geology of the Viburnum No. 27 Mine, Viburnum Trend, Southeast Missouri. Econ. Geology, v. 72, p. 349-364.

GULSON, B.L., 1985, Shale-hosted lead-zinc deposits in northern Australia: Lead isotope variations. Econ. Geology, v. 80, p. 2001-2012.

GULSON, B.L., PERKINS, W.G., and MIZON, K.J., 1983, Lead isotope studies bearing on the genesis of copper orebodies at Mount Isa, Queensland. Econ. Geology, v. 78, p. 1466 - 1504.

HAAS, J.L., 1976, Thermodynamic properties of the coexisting phases and thermochemical properties of the H_2O component in boiling NaCl solutions. U.S. Geol. Surv. Bulletin 1421-B, p. 1-71.

HAGNI, R.D., 1983, Ore microscopy, paragenetic sequence, trace element content and fluid inclusion studies of the copper-lead-zinc deposits. In: Kisvarsanyi, G.; Grant, S.K.; Pratt, W.P.; Koenig, J.W. (eds.) Proceedings Volume, International Conference on Mississippi Valley Type Lead-Zinc Deposits. Univ. Missouri-Rolla Press, Rolla Missouri, p. 243-256.

HALL, C.M., YORK, D., SAUNDERS, C.M. and STRONG, D.F., 1989, Laser $^{40}Ar/^{39}Ar$ dating of Mississippi Valley Type mineralization from western Newfoundland, (abstr.), Abstracts 28th International Geological Congress, v. 2, p.10.

HALL, W.E. and FRIEDMAN, I., 1963, Composition of fluid inclusions, Cave-in-Rock fluorite district, Illinois, and Upper Misissippi Valley zinc-lead district. Econ. Geology, v. 58, p. 886-911.

HALLEY, R.B., 1987, Burial diagenesis of carbonate rocks. Colorado

School of Mines Quarterly, v. 82, p. 1-15.

HANOR, J.S., 1979, The sedimentary genesis of hydrothermal fluids. In: Barnes, H.L. (ed.) Geochemistry of hydrothermal ore deposits, 2nd ed: New York, John Wiley and Sons, p. 137-172.

HANSHAW, B.C.; BACK, W. and DEIKE, R.G., 1971, A geochemical hypothesis for dolomitization by groundwater. Econ. Geology, v. 66, p. 710-724.

HARDIE, L.A., 1986, Stratigraphic models for carbonate tidal flat deposition. Colorado School of Mines Quarterly, v. 81, p. 59-74.

HARDIE, L.A., 1987, Dolomitization: a critical view of some current views. Jour. Sed. Petrology, v. 57, p. 185-202.

HARDIE, L.A.; BOSELLINI, A. and GOLDHAMMER, R.K., 1986, Repeated subaerial exposure of subtidal carbonate platforms, Triassic, northern Italy: evidence for high level frequency sea level oscillations on a 104 year scale. Paleoceanography, v. 1, p. 447-457.

HARRIS, A.G., 1979, Conodont color alteration and organo-mineral metamorphic index and its application to Appalachian Badsin geology. In: Scholle, P.A. and Schluger, P.R. (eds.) Aspects of Diagenesis. Soc. Econ. Paleon. Mineral. Spec. Publ., v. 26, p. 3-16.

HAYWICK, D.W., 1984, Dolomite within the St. George Group (Lower Ordovician), western Newfoundland. Unpubl. M.Sc. thesis, Memorial University of Newfoundland, p.

HAYWICK, D.W. and JAMES, N.P., 1984, Dolomites and dolomitization of the St. George Group (Lower Ordovician) of western Newfoundland. In:

Current Research, Part A, Geol. Surv. of Canada, Paper 84-1A, p. 531-536.

HECKEL, P.H., 1972, Possible inorganic origin for stromatactis in calcilutite mounds in the Tully Limestone, Devonian of New York. Jour. Sed. Petrology, v. 42, p. 7-18.

HELGESON, H.C., 1969, Thermodynamics of hydrothermal systems at elevated temperatures and pressures. Amer. Jour. of Science, v. 269, p. 729-804.

HEYL, A.V., 1983, Geologic characteristics of three major Mississippi Valley districts. In: Kisvarsanyi, G.; Grant, S.K.; Pratt, W.P. and Koenig, J.W. Proceedings Volume, International Conference on Mississippi Valley Type Lead-Zinc Deposits, Univ. Missouri-Rolla Press, Rolla Missouri, p. 27-59.

HEYL, A.V.; LANDIS, G.P. and ZARTMAN, R.E., 1974, Isotopic evidence for the origin of Mississippi Valley-type mineral deposits: a review. Econ. Geology, v. 69, p. 992-1006.

HIBBARD, J., 1983, Geology of the Baie Verte Peninsula, Newfoundland. Memoir 2, Newfoundland Dept. Mines and Energy, Mineral Devel. Division, Newfoundland, 279p.

HINTZE, L.F., 1952, Lower Ordovician trilobites from western Utah and eastern Nevada, Utah. Geological and Mineralogical Survey Bulletin, 48, 249p.

HISCOTT, R.N., JAMES, N.P. and PEMBERTON, S.G., 1984, Sedimentology and ichnology of the Lower Cambrian Bradore Formation: Fluvial to shallow marine transgressive sequence, coastal Labrador, Bulletin of Canadian Petroleum Geology, v. 32, p. 11 -26.

HTTCHON, B., 1969, Fluid flow in western Canada sedimentary basin. 1. Effect of topography. Water Resources Research, v. 5(1), p. 186-195.

HITCHON, B.; BILLINGS, G.K. and KLOVAN, J.E., 1971, Geochemistry and origin of formation waters in the Western Canadian sedimentary basin - III: Factors conrolling chemical composition. Geochim. et Cosmochim. Acta., v. 35, p. 567-598.

HOAGLAND, A.D., 1976, Appalachian zinc-lead deposits. In: K.H. Wolf (ed.) Handbook of stratabound and stratiform ore deposits, v. 6, Chapt. 11, New York, Elsevier, p. 495-534.

HOAGLAND, A.D.; HILL, W.T. and FULWEILER, R.E., 1965, Genesis of the Ordovician Zinc deposits in east Tennessee. Econ. Geology, v. 60, p. 693-714.

HOEFS, J., 1980, Stable Isotope Geochemistry. Berlin, Springer Verlag, 208p.

HOLLAND, H.D. and MALININ, S.D., 1979, The solubility and occurrence of non-ore minerals. In: Barnes, H.L. (ed.) Geochemistry of Hydrothermal Ore Deposits, 2nd ed. New York, Wiley-Interscience, p. 461-508.

HOLLISTER, L.S., 1970, Origin, mechanism and consequences of compositional sector-zoning in staurolite. Amer. Mineralogist, v. 55, p. 742-766.

HORTON, R.A. Jr., 1985, Dolomitization of the Leadville Limestone. In: DeVoto, R.H. (ed.) Sedimentology, Dolomitization, Karstification and Mineralization of the Leadville Limestone (Misissippian), central Colorado. SEPM Field Trip No. 6 Guidebook, SEPM Annual

Midyear Meeting, Golden Colorado, p. (6)57-(6)70.

HUBBERT, M.K. and WILLIS, D.G., 1957, Mechanics of hydraulic fracturing. Petroleum transactions, AIME, v. 210, p. 153-163.

HUTCHEON, I.; OLDERSHAW, A. and GHENT, E.D., 1980, Diagenesis of Cretaceous sandstones of the Kootenay Formation at Elk Valley (southeastern British Columbia) and Mt. Allan (southwestern Alberta). Geochim. et Cosmochim. Acta, v. 44, p. 1425-1435.

HYDE, R.S., 1979, Geology of Carboniferous strata in portions of the Deer Lake Basin, western Newfoundland, Newfoundland and Labrador Department of Mines and Energy, Mineral Development Division, Report 79-6, 43p.

HYDE, R.S., 1983, Geology of the Carboniferous Deer Lake basin. Newfoundland Dept. of Mines and Energy Mineral Devel. Division, Map 82-7.

HYDE, R.S., MILLER, H.G., HISCOTT, R.N. AND WRIGHT, J.A., 1988, Basin architecture and thermal maturation in the strike-slip Deer Lake Basin, Carboniferous of Newfoundland, Basin Research, v. 1,

ILLING, L.V., 1959, Deposition and diagenesis of some upper Paleozoic carbonate sediments in western Canada. In: Proceedings, World Petroleum Congress, 5th, New York, Secl., p. 23-52.

IMBRIE, J. and IMBRIE, J.Z., 1980 Modeling the climatic response to orbital variations. Science, v. 207, p. 943-952.

IRVINE, W.T., 1957, The Bluebell Mine. In: Structural Geology of Canadian Ore Deposits Vol II. 6th Commonwealth Mining and Metallurgical Congress, p. 95-104.

IRVINE, T.N., 1980, Magmatic infiltration metasomatism, double diffusive

fractional crystallization, adcumulus growth in the Musk Ox and other layered intrusions, in HARGRAVES, R.B., (ed.) Physics of Magmatic Processes, Princeton University Press, Princeton, N.J., p. 325 -383.

IRWIN, M.L., 1965, General theory of epeiric clear water sedimentation. Bull. Amer. Assoc. Petrol. Geology, v. 49, p. 445-459.

JACKSON, S.A. and BEALES, F.W., 1967, An aspect of sedimentary basin evolution: The concentration of Mississippi Valley-type ores during late stages of diagenesis. Canadian Petrol. Geol. Bulletin, v. 15, p. 383-433.

JACOBI, R.D., 1981, Peripheral bulge - a causal mechanism for the Lower/Middle Ordovician unconformity along the western margin of the Northern Appalachians. Earth and Planetary Science Letters, v. 56, p. 245-251.

JAMES, N.P., 1984, Shallowing-upward sequences in carbonates. In: R.G. Walker (ed.) Facies Models. Geoscience Canada Reprint Series, No. 1, p. 213-228.

JAMES, N.P. and KLAPPA, C.F., 1983, Petrogenesis of Early Cambrian reef limestones, Labrador, Canada, Journal of Sedimentary Petrology, v. 53, p. 1051 -1096.

JAMES, N.P. and STEVENS,R.K., 1986, Stratigraphy and correlation of the Cow Head Group (Cambro-Ordovician), western Newfoundland. Geol. Surv. of Canada Bulletin, v. 366, p.

JAMES, N.P.; KNIGHT, I.; STEVENS, R.K. and BARNES, C.R., 1988, Sedimentology and paleontology of an early Paleozoic continental margin, western Newfoundland, Trip B1, Field trip guidebook, Geol. Assoc.

Canada Annual Meeting, St. John's, Newfoundland, 121 p.

JAMES, N.P.; BARNES, C.R.; STEVENS, R.K. and KNIGHT, I., 1989, A Lower Paleozoic continental margin carbonate platform, northern Canadian Appalachians. In: T. Crevello, et. al., (eds.) Controls on Carbonate Platforms and Basin Development, SEPM Spec. Publ. 44, p. 123 - 146.

JENNINGS, J.N., 1971, Karst: An introduction to systematic geomorphology. Australian National Univ. Press, Canberra, 252p.

JI, Z., 1989, Lower Ordovician conodonts of the St. George Group of Port au Port Peninsula, western Newfoundland, unpublished Ph.D. thesis, Memorial University of Newfoundland.

JODRY, R.L., 1969, Growth and dolomitization of Silurian reefs, St. Clair County, Michigan. Amer. Assoc. Petrol. Geol. Bulletin, v. 53, p. 957-981.

JONES, B.; OLDERSHAW, A.E. and NARBONNE, G.M., 1979, Nature and origin of rubbly limestone in the upper Silurian Read Bay Formation of Arctic Canada. Sed. Geology, v. 24, p. 227-252.

KELLY, W.C.; RYE, R.O. and LIVNAT, A., 1986, Saline mine waters of the Keweenaw Peninsula, Northern Michigan: Their nature, origin and relation to similar deep waters in Precambrian crystalline rocks of the Canadian Shield. Amer. Jour. Science, v. 286, p. 281-308.

KESLER, S.E., 1989, Evolution of Mississippi Valley-type (MVT) brines in Lower Ordovician carbonate rocks of the Appalachian Orogen, (abstr.), Geological Society of America Abstracts with Programs, p. A8.

KENDALL, A.C., 1984, Evaporites. In: Walker, R.G., (ed.) Facies Models.

Geol. Assoc. of Canada. Geoscience Canada Reprint Series 1, p. 259-298.

KENDALL, C.G.St.C, and SKIPWITH, P.A.D'e, 1969, Holocene shallow-water carbonate and evaporite sediments of Khor als Bazam Abu Dhabi, southwest Persian Gulf. Bull. Amer. Assoc. Petrol. Geology, v. 53, p. 841-869.

KENDALL, D.L., 1960, Ore deposits and sedimentary features, Jefferson City Mine, Tennessee. Econ. Geology, v. 55, p. 985-1003.

KHARAKA, Y.K.; CAROTHERS, W.W. and ROSENBAUER, R.J., 1983, Thermal decarboxylation of acetic acid: implications for origin of natural gas: Geochim. et Cosmochim. Acta., v. 47, p. 397-402.

KHARAKA, Y.K.; HULL, R.W. and CAROTHERS, W.W., 1985, Water-rock interactions in sedimentary basins. In: Relationship of Organic Matter and Mineral Diagenesis, lecture notes for Short Course No. 17. Soc. Econ. Paleon. Mineral., pp. 79-176.

KLAPPA, C.F., OPALINSKI, P., and JAMES, N.P., 1980, Stratigraphy of the Table Head Group, Canadian Journal of Earth Sciences, v. 17, p. 1007 - 1019.

KLUYVER, H.M., 1975, Stratigraphy of the Ordovician St. George Group in the Port Au Choix area, western Newfoundland. Can. Jour. of Earth Sciences, v. 12, p. 589-594.

KNIGHT, I., 1977, The Cambrian-Ordovician platformal rocks of the Northern Peninsula, Newfoundland. Mineral Devel. Division, Newfoundland Dept. of Mines and Energy, Report 77-6.

KNIGHT, I., 1978, Platformal sediments on the Great Northern Peninsula: stratigraphic studies and geological mapping of the north St.

Barbe district. Mineral Devel. Division, Newfoundland Dept. of Mines and Energy, Report 78-1, p. 140-150.

KNIGHT, I., 1980, Cambro-Ordovician carbonate stratigraphy of western Newfoundland; sedimentation, diagenesis and zinc-lead mineralization. Mineral Devel. Division, Newfoundland Dept. of Mines and Energy, Open File Nfld. 1154.

KNIGHT, I., 1983, Geology of Cambro-Ordovician rocks in parts of the Castor River, St. John Island and Port Saunders map sheets. Mineral Devel. Division, Newfoundland Dept. of Mines and Energy, Report 83-1, p. 1-10.

KNIGHT, I., 1984, Mineralization in Cambro-Ordovician rocks, western Newfoundland, in SWINDEN H.S.(ed.), Mineral Deposits of Newfoundland: A 1984 Perspective, Newfoundland and Labrador Department of Mines and Energy, Mineral Development Division, p.37.

KNIGHT, I., 1985a, Geological mapping of Cambrian and Ordovician sedimentary rocks of the Bellburns (12 I/5,6), Portland Creek (12 I/4) and Indian Lookout (12 I/3) map areas, Great Northern Peninsula, Newfoundland. Mineral Devel. Division, Newfoundland Dept. of Mines and Energy, Report 85-1, p. 79-88.

KNIGHT, I., 1985b, Geology of the Bellburns map sheet (12 I/6 and 12 I/5), western Newfoundland. Mineral Devel. Division, Newfoundland Dept. of Mines and Energy, Provisional Map 85-63, scale 1:50,000.

KNIGHT, I., 1986a, Ordovician sedimentary strata of the Pistolet Bay and Hare Bay area. Mineral Devel. Division, Newfoundland Dept. of Mines and Energy, Report 86-1, p. 147-160.

KNIGHT, I., 1986b, Geology of the Port Saunders map sheet (12 I/11), western Newfoundland. Mineral Devel. Division, Newfoundland Dept. of Mines and Energy, Map 86-59, scale 1:50,000.

KNIGHT, I., 1987, Geology of the Roddickton map area (12 I/16). Mineral Devel. Division, Newfoundland Dept. of Mines and Energy, Report 87-1, p. 343-357.

KNIGHT, I. and, BOYCE, W.D., 1984, Geological mapping of the Port Saunders (12 I/11), St. John Island (12 I/14) and parts of the Torrent River (12 I/10) and Bellburns (12 I/6) map sheets, northwestern Newfoundland. In: Current Research. Mineral Devel. Division, Newfoundland Dept. of Mines and Energy, Report 84-1, p. 114-124.

KNIGHT, I. and JAMES, N.P., 1987, The stratigraphy of the Lower Ordovician St. George Group, western Newfoundland: the interaction between eustasy and tectonics. Can. Jour. of Earth Sciences, v. 24, p. 1927-1951.

KNIGHT, I.; JAMES, N.P. and LANE, T.E., in press, The St. George Unconformity, Ordovician, Northern Appalachians: effects of lithospheric dynamics on the Sauk-Tippecanoe sequence boundary. Bulletin of the Geological Society of America.

KOHOUT, F.A., 1967, Groundwater flow and the geothermal regime of the Floridian plateau. Gulf Coast Association of Geological Societies Transactions, v. 17, p. 339-354.

KOHOUT, F.A., HENRY, H.R. and BANKS, J.E., 1977, Hydrogeology related to geothermal conditions of the Floridan Plateau, in SMITH, D.L. and GRIFFIN, G.M. (eds.) The Geothermal Nature of the Floridian

Plateau. Special Publication. no. 21. Florida Bureau of Geology, p. 1 - 41.

KONNERUP-MADSEN, J., 1979, Fluid inclusions in quartz from deep-seated granitic intrusions, south Norway. Lithos, v. 12, p. 13-23.

KREITLER, C.W., 1987, Sedimentary basin hydrology and its relation to dolomitization, abstract. SEPM Annual Midyear Meeting Abstracts, p. 44.

KYLE, J.R., 1976, Brecciation, alteration, and mineralization in the Central Tennessee zinc district. Econ. Geology, v. 71, p. 892-903.

KYLE, J.R., 1981, Geology of the Pine Point lead-zinc district. In: Wolf, K.H., (ed.) Handbook of Strata-bound and Stratiform Ore Deposits, v. 9, p. 643-741.

KYLE, J.R., 1983, Economic aspects of subaerial carbonates. In: Scholle, P.A.; Bebout, D.G. and Moore, C.L. (eds.) Carbonate depositional environments. Amer. Assoc. Petrol. Geology, Tulsa Okla., p. 73-92.

LAND, L.S., 1973, Contemporaneous dolomitization of Middle Pleistocene reefs by meteoric water, North Jamaica. Bull. Marine Science, v. 23, p. 64-92.

LAND, L.S., 1980, The isotopic and trace element geochemistry of dolomite: the state of art. In: Zenger, D.H.; Dunham, J.B. and Ethington, R.L. (eds.) Concepts and Models of Dolomitization. Soc. Econ. Paleo. Mineral., Spec. Publ. No. 28, p. 87-110.

LAND, L.S., 1983, Dolomitization. Amer. Assoc. Petrol. Geol. Education Course Notes, Ser. No. 24.

LAND, L.S., 1985, The origin of massive dolomite. Jour. Geological Education, v. 33, p. 112-125.

LAND, L.S., 1987, Basinal dolomitization: constraints imposed by formation-water chemistry (abstr.). In: Abstracts Vol. IV, SEPM Annual Midyear Meeting, Austin, Texas, p. 46.

LAND, L.S., 1989, Dolomitization and dolomite recrystallization, Hope Gate Formation, North Jamaica: reassessment of mixing zone dolomite, (abstr.), Geological Society of America Absracts with Programs, p. A220.

LAND, L.S.; SALEM, M.R.I. and MORROW, D.W., 1975, Paleohydrology of ancient dolomites: geochemical evidence. Amer. Assoc. Petrol. Geol. Bulletin, v. 59, p. 1602-1625.

LANE, T.E., 1984, Preliminary classification of carbonate breccias, Newfoundland Zinc Mines, Daniel's Harbour, Newfoundland. In: Current Research Part A, Geol. Surv. of Canada, Paper 84-1A, p. 505-512.

LAURENCE, R.A., 1944, An early Orovician sinkhole deposit of volcanic ash and fossiliferous sediments in East Tennessee. Jour. Geology, v. 52, p. 235-249.

LEACH, D.L., 1979, Temperature and salinity of the fluids responsible for minor occurrences of sphalerite in the Ozark region of Missouri. Econ. Geology, v. 74, p. 931-937.

LEACH, D.L., and ROWAN. E.L., 1986, Genetic link between Ouachita foldbelt tectonism and the Mississippi Valley-type lead-zinc deposits of the Ozarks. Geology, v. 14, p. 931-935.

LEE, Y.I. and FRIEDMAN, G., 1987, Deep-burial dolomitization in the Ordovician Ellenburger Group Carbonates, western Texas and southwestern New Mexico. Jour. of Sed. Petrology, v. 57, No. 3, p. 544-

557.

LEVESQUE, R.J., 1977, Stratigraphy and sedimentology of Middle Cambrian to Lower Ordovician shallow water carbonate rocks, western Newfoundland, unpublished M. Sc. thesis, Memorial University of Newfoundland, 256p.

LINDBLOM, S., 1986, Textural and fluid inclusion evidence of ore deposition in the Pb-Zn deposit of Laisvall, Sweden. Econ. Geology, v. 81, p. 46-64.

LOGAN, B.W.; DAVIES, G.R.; READ, J.F.; CEBULSKI, D.E., 1970, Carbonate sedimentation and environments, Shark Bay, Western Australia. Amer. Assoc. Petrol. Geology, Memoir 13, Tulsa, Okla., 223p.

LOGAN, B.W., et. al., 1974, Evolution and diagenesis of Quaternary carbonate sequences, Shark Bay, Australia. Amer. Assoc. Petrol. Geology, Memoir 22, 358p.

LOGAN, B.W. and SEMENIUK, V., 1976, Dynamic metamorphism; processes and products in Devonian carbonate rocks, Canning Basin, Western Australia. Geol. Soc. Australia, Spec. Publ. 6, 138 p.

LOGAN, R.G. and WALKER, R.N., 1985, Lineament study, Great Northern Peninsula, Newfoundland. Image processing services, Brisbane, Australia, Unpubl. report.

LORENS, R.B., 1981, Sr, Cd, Mn and Co distribution coefficients in calcite as a function of calcite precipitation rate. Geochim. Cosmochim. Acta, v. 45, p. 553-561.

LOVERING, T.G. and PATTEN, L.E., 1962, The effect of CO_2 at low temperature and pressure on solutions supersaturated with silica in the presence of limestone and dolomite. Geochim. Cosmochim. Acta, v.

74, p. 787-796.

LOVERING, T.S., 1969, The origin of hydrothermal and low temperature dolomite. Econ. Geology, v. 64, p. 743-754.

LOVERING, T.S.; TWETO, O. and LOVERING, T.G., 1978, Ore deposits of the Gilman district, Eagle County, Colorado. U.S. Geol. Surv. Prof. Paper 1017, 90p.

LUCIA, F.J., 1972, Recognition of evaporite-carbonate shoreline sedi-- mentation. In: Rigby, J.K. and Hamblin, W.K. (eds.) Recognition of Ancient Sedimentary Environments, Soc. of Econ. Paleon. Mineral., Spec. Publ. 16, p. 160-191.

MACHEL, H.G., 1985, Cathodoluminescence in calcite and dolomite and its chemical interpretation. Geoscience Canada, v. 12, p. 139-148.

MACHEL, H.G., 1987, Some aspects of diagenetic sulphate-hydrocarbon redox-reactions. In: Marshall, J.D. (ed.) Diagenesis of sedimentary sequences. Geol. Soc. of London Spec. Publication.

MACHEL, H.-G., 1987, Saddle dolomite as a by-product of chemical compaction and thermochemical sulfate reduction. Geology, v. 15, No. 10, p. 936-940.

MACHEL, H.-G. and MOUNTJOY, E.W., 1986, Chemistry and environments of dolomitization - a reappraisal. Earth-Sci. Reviews, v. 23, p. 175-222.

MACHEL, H.-G. and MOUNTJOY, E.W., 1987, General constraints on extensive pervasive dolomitization and their application to the Devonian carbonates of western Canada. Bull of Can. Petrol. Geology, v. 35, p. 143-158.

MATTER, A., 1967, Tidal flat deposits in the Ordovician of western

Maryland. Jour. Sed. Petrology, v. 37, p. 601-609.

MATTES, B.W., and MOUNTJOY, E.W., 1980, Burial dolomitization of the Upper Devonian Miette buildup, Jasper National Park, Alberta. In: Zenger, D.H.; Dunham, J.B., and Ethington, R.L. (eds.) Concepts and Models of Dolomitization. Soc. Econ. Paleo. Mineral., Spec. Publ. No. 28, p. 259-297.

MAYNARD, J.B., 1983, Geochemistry of Sedimentary Ore Deposits, New York. Springer Verlag. 305p.

McCLIMANS, R.K., 1977, Geologic, fluid inclusion and stable isotope studies of the Upper Mississippi Valley zinc-lead district, southwestern Wisconsin. Unpubl. Ph.D. thesis, Pennsylvania State Univ., 175p.

McCLIMANS, R.K.; BARNES, H.L. and OHMOTO, H., 1980, Sphalerite stratigraphy of the Upper Mississippi Valley zinc-lead district, southwest Wisconsin. Econ. Geology, v. 75, p. 351-361.

McCORMICK, J.E.; EVANS, L.L.; PALMER, R.A. and RASNICK, F.D., 1971, Environment of the zinc deposits of the Mascot-Jefferson City district, Tennessee. Econ. Geology, v. 66, p. 757-762.

McNAUGHTON, K. and SMITH, T.E., 1986, A fluid inclusion study of sphalerite and dolomite from the Nanisivik lead-zinc deposit, Baffin Island, Northwest Territories, Canada. Econ. Geology, v. 81, p. 713-720.

MEYERS, W.J. and LOHMANN, K.C., 1985, Isotope geochemistry of regionally extensive calcite cement zones and marine components in Mississippian limestones, New Mexico. In: Schneidermann, N. and Harris, P.M. (eds.) Carbonate Sediments. Soc. Econ. Paleo. and Mineral.

Spec. Publ. 36, p. 223-240.

MOORE, G.W. and SULLIVAN, G.N., 1977, Speleology: Zephyrus Press, Teaneck, N.J., 151p.

MOORE, N.K., 1977, Distribution of the benthic algal flora in Middle Ordovician carbonate environmental units of the southern Appalachians. In: S.C. Ruppel and K.R. Walker (eds.) The ecostratigraphy of the Middle Ordovician of the southern Appalachians, USA: A field excursion, University of Tennessee, Dept. of Geological Sciences Studies in Geology. No. 77-1, p. 18-29.

MORROW, D.W., 1975, The Florida aquifer: a possible model for a Devonian paleoaquifer in northeastern British Columbia. Geol. Surv. of Canada, Paper 75-1, Part B, p. 261-266.

MORROW, D.W., 1982a, Diagenesis I., Dolomite - part 1: the chemistry of dolomitization and dolomite precipitation. Geoscience Canada, v. 9, p. 5-13.

MORROW, D.W., 1982b, Dolomite - part 2: dolomitization models and ancient dolostones. Geoscience Canada, v. 9, p. 95-107.

MORROW, D.W., 1982c, Descriptive field classification of sedimentary and diagenetic breccia fabrics in carbonate rocks. Bull. Can. Petrol. Geology, v. 30, p. 227-229.

MORROW, D.W.; CUMMING, G.L. and KOEPNICK, R.B., 1986, Manetoe facies - a gas bearing, megacrystalline, Devonian dolomite, Yukon and Northwest Territories, Canada. Amer. Assoc. Petrol. Geol. Bulletin, v. 70, p. 702-720.

MUIR, M.; LOCK, D. and VON DER BORCH, C., 1980, The Coorong Model for penecontemporaneous dolomite formation in the Middle Proterozoic

McArthur Group, Northern Territory, Australia. In: Zenger,D.H.; Dunham, J.B. and Ethington, R.L. (eds.) Concepts and Models of Dolomitization. Soc. Econ. Paleon. Mineral., Spec. Publ. No. 28, Tulsa, Okla., p. 51-68.

MURRAY, R.C., 1960, The origin of porosity in carbonate rocks. Jour. Sed. Petrology, v. 30, p. 1063-1077.

MURRAY, R.C. and LUCIA, F.J., 1967, Cause and control and dolomite distribution by rock selectivity. Geol. Soc. Amer. Bulletin, v. 78, p. 21-36.

MUSSMAN, W.J. and READ, J.F., 1986, Sedimentology and development of a passive to convergent margin unconformity: Middle Ordovician Knox unconformity Virginia Appalachians. Geol. Soc. Amer. Bulletin, v. 97, p. 292-295.

MUSSMAN, W.J.; MONTANEZ, I.P. and READ, J.F., 1988, Ordovician Knox paleokarst unconformity, Appalachians. In: James, N.P. and Chouquette, P.W. (eds.) Paleokarst, New York. Springer Verlag, p. 211-228.

NARBONNE, G.M., 1984, Trace fossils in Upper Silurian tidal flats to basin slope carbonates of Arctic Canada. Jour. of Paleontology, v. 58, p. 398-415.

NEUGEBAUER, J., 1973, The diagenetic problem of chalk - the role of pressure solution and pore fluid. Neves Jahrbuch fur Geol. Palaontol. Abh. 143, p. 223-245.

NOWLAN, G.S. and BARNES, C.R., 1987, Thermal maturation of Paleozoic strata in eastern Canada from conodont colour alteration index (CAI) data with implications for burial history, tectonic evolu-

tion, hotspot tracks and mineral and hydrocarbon potential. Geol. Surv. Canada Bulletin 369.

ODER, C.R.L. and HOOK, J.W., 1950, Zinc deposits in the southeastern states In: Snyder, F.G. (ed.) Symposium on mineral resources of the southeastern United States: Knoxville, Tennessee. University of Tennessee Press, p. 72-87.

OHLE, E.L., 1959, Some considerations in determining the origin of ores of the Mississippi Valley-type. Con. Geology, v. 54, p. 769-789.

OHLE, E.L., 1980, Some considerations in determining the origin of ore deposits of the Mississippi Valley type - Part II. Econ. Geol., v. 75, p. 161-172.

OHLE, E.L., 1985, Breccias in Mississippi Valley-type deposits. Econ. Geology, v. 80, p. 1736-1752.

OHMOTO, H. and RYE, R.O., 1979, Isotopes of sulfur and carbon. In: Barnes, H.L. (ed.) Geochemistry of Hydrothermal Ore Deposits, New York. John Wiley and Sons, p. 509-567.

OLIVER, J., 1986, Fluids expelled tectonically from orogenic belts: Their role in hydrocarbon migration and other geologic phenomena, Geology, v. 14, p. 99-102.

OLSON, R.A., 1984, Genesis of paleokarst and strata-bound zinc-lead sulfide deposits in a Proterozoic dolostone, northern Baffin Island, Canada. Econ. Geology, v. 79, p. 1056-1103.

PARK, D.G. and JONES, B., 1985, Nature and genesis of breccia bodies in Devonian strata, Peace point area. Wood Buffalo Park, northeast Alberta. Bull. Can. Petrol. Geology, v. 33, p. 275-294.

PARK, R.K., 1976, A note on the significance of lamination in stroma-

lites. Sedimentology, v. 23, p. 379-393.

PARIZEK, R.R., 1971, Hydrogeologic framework of folded and faulted carbonates - influence of structure, In: Parizek, R.R., White, W.B. and Langmuir, D., ed., Hydrology and geochemistry of folded and faulted carbonate rocks of the central Appalachian type and related land use problems, College of Earth and Mineral Science, Pennsylvania State University, Circular 82

PARIZEK, R.R., 1976, On the nature and significance of fracture traces and lineaments in carbonate and other terranes, in Yevjevich, V., ed., Karst Hydrology and Water Resources, p. 47 - 108.

PATTERSON, R.J., 1972, Hydrogeology and carbonate diagenesis of a coastal sabkha in the Persian Gulf, unpublished Ph. D., Princeton University, N.J., 472p.

PATTERSON, R.J. and KINSMAN, D.J., 1982, Formation of diagenetic dolomite in coastal sabkha along Arabian (Persian) Gulf. Amer. Assoc. Petrol. Geology, v. 66, p. 28-43.

PHILLIPS, W.J., 1972, Hydraulic fracturing and mineralization. Jour. Geol. Soc. London, v. 128, p. 337-359.

PIERSON, B.J., 1981, The control of cathodoluminescence in dolomite by iron and manganese. Sedimentology, v. 28, p. 601-610.

POTTER,R.W., 1977, Pressure corrections for fluid-inclusion homogenization temperatures bsed on the volumetric properties of the system NaCl-H_2O. Jour. Research U.S. Geol. Survey, v. 5, p. 603-607.

PRATT, B.R., 1979, Sedimentology, diagenesis and cryptalgal structures, the St. George Group (Lower Ordovician), western Newfoundland. Unpubl. M.Sc. thesis, Memorial University of Newfoundland.

PRATT, B.R., 1982, Limestone response to stress: pressure solution and dolomitization - discussion and examples of compaction in carbonate sediments. Jour. of Sed. Petrology, v. 52, p. 323-328.

PRATT, B.R. and JAMES, N.P., 1982, Cryptalgalmetazoan bioherms of Early Ordovician age in the St. George Group, western Newfoundland. Sedimentology, v. 29, p. 543-569.

PRATT, B.R. and JAMES, N.P., 1986, The St. George Group (Lower Ordovician) of western Newfoundland: tidal flat island model for carbonate sedimentation in shallow epeiric seas. Sedimentology, v. 33, p. 313-344.

PREZBINDOWSKI, D.R. and LARESE, R.E., 1987, Experimental stretching of fluid inclusions in calcite - Implications for diagenetic studies. Geology, v. 15, p. 333-336.

PRICE, N.J., 1975, Fluids in the crust of the earth, Scientific Progress, v. 62, p. 245

QUINLAN, G.M. and BEAUMONT, C., 1984, Appalachian thrusting, lithospheric flexure, and the Paleozoic stratigraphy of the eastern interior of North America. Can. Jour. Ear. Science, v. 21, p. 973-996.

RADABAUGH, R.E.; MERCHANT, J.S. and BROWN, J.M., 1968, Geology and ore deposits of the Gilman (Red Cliff, Battle Mountain) district, Eagle County, Colorado. In: Ridge, J.D. (ed.) Ore Deposits of the United States 1933-1967. Amer. Inst. Mining. Metal and Petrol. Engineers, v. 1, p. 641-664.

RADKE, B.M., 1978, Carbonate sedimentation in tidal and epeiric environments and diagenetic overprints: the Nimaroo Formation (Upper

Cambrian-Lower Ordovician), Central Australia. Unpubl. Ph.D. thesis, Troy, N.Y. Rensselaer Polytechnic Institute, 254p.

RADKE, B.M. and MATHIS, R.L., 1980, On the formation and occurrence of saddle dolomite. Jour. of Sed. Petrology, v. 50, p. 1149-1168.

RAMSEY, J.G., 1967, Folding and Fracturing of Rocks. McGraw-Hill, New York, 568p.

RAMSEY, J.G., 1980, The crack-seal mechanism of rock deformation. Nature, v. 284, p. 135-139.

RAMSEY, J.F. and HUBER, M.I., 1987, The Techniques of Modern Structural Geology Vol. 2: Folds and Fractures. Academic Press, New York, 700p.

READ, J.F.; GROTZINGER, J.P.; BOVA, J.A. and KOERSCHNER, W.F., 1986, Models for generation of carbonate cycles. Geology, v. 14, p. 107-110.

RHODES, D.; LANTOS, E.A.; LANTOS, J.A.; WEBB, R.J. and OWENS, D.C., 1984, Pine Point ore bodies and their relationship to the stratigraphy, structure, dolomitization, and karstification of the Middle Devonian barrier complex. Econ. Geology, v. 79, p. 991-1055.

RICHARDSON, C.K. and PINCKNEY, D.M., 1984, The chemical and thermal evolution of the fluids in the Cave-in-Rock fluorspar district, Illinois: Mineralogy, paragenesis and fluid inclusions. Econ. Geology, v. 79. p. 1833-1856.

ROBINSON, B.W., 1980, Isotopic evidence on the origin of sulfur in Mississippi Valley-type deposits, particularly in the British Isles, in Ridge, J. D., ed., Proceedings of the 5th Quadrennial

IAGOD Symposium, Snow Bird, Utah, p. 487-493.

ROEDDER, E., 1968a, Temperature, salinity, and origin of the ore-forming fluids at Pine Point, Northwest Territories, Canada, from fluid inclusion studies. Econ. Geology, v. 63, p. 439-450.

ROEDDER, E., 1968b, The non-colloidal origin of "colloform" textures in sphalerite ores. Econ. Geology, v. 63, p. 451-471.

ROEDDER, E., 1977, Fluid inclusion studies of ore deposits in the Viburnum Trend, southeast Missouri. Econ. Geology, v. 72, p. 474-479.

ROEDDER, E., 1984, Fluid Inclusions. Reviews in Mineralogy, v. 12, Washington, D.C., Mineral. Soc. America.

ROEDDER, E. and DWORNIK, E.J., 1968, Sphalerite color banding: lack of correlation with iron content, Pine Point, Northwest Territories, Canada. Amer. Mineral., v. 53, p. 1523-1529.

ROEHL, P.O., 1981, Dilation brecciation - a proposed mechanism of fracturing, petroleum expulsion, and dolomitization in the Monterey Formation, California. In: Garrison, R.E.; Douglas, R.G.; Pisciotto, K.E.; Isaacs, C.M. and Ingle, J.C. (eds.) The Monterey Formation and Related Siliceous Rocks of California. Soc. Econ. Paleo. Miner. Pacific Section, Symposium, p. 285-315.

ROSS, R.J. Jr., et. al., 1982, The Ordovician System in the United States of America. International Union of Geological Sciences Publication 12, 73p.

ROSS, R.J. Jr. and JAMES, N.P., 1987, Brachiopod biostratigraphy of the Middle Ordovician Cow Head and Table Head Groups, western Newfoundland. Can. Jour. Ear. Science, v. 24, p. 70-95.

ROWAN, E.L., 1986, Cathodoluminescent zonation in hydrothermal dolomite cements: relationship to Mississippi Valley-type Pb-Zn mineralization in southern Missouri and northern Arkansas. In: Hagni, R.D. (ed.) Process Mineralogy VI. The Metallurgical Society Inc. Publ., p. 69-87.

RUPPEL, S.C., 1977, The Chickamauga limestone - a complex mosaic of supratidal to subtidal carbonate shelf environments. In: S.C. Ruppel and K.R. Walker (eds.) The ecostratigraphy of the Middle Ordovician of the southern Appalachians; USA: A field excursion, University of Tennessee, Department of Geological Sciences Studies in Geology, No. 77-1, p. 39-48.

RYE, R.O. and OHMOTO, H., 1974, Sulfur and carbon isotopes and ore genesis: a review. Econ. Geology, v. 69, p. 826-842.

SAMANIEGO, A., 1982, Correlation of stratabound mineral deposits in the Early Cretaceous Santa Metallotect of North and Central Peru. In: Amstutz, G.C., et. al. (eds.) Ore Genesis. The State of the Art Heidelberg Springer Verlag, p. 508-527.

SANDO, W.J., 1967, Madison limestone (Mississippian), Wind River, Washakie, and Owl Creek Mountains, Wyoming. Amer. Assoc. Petrol. Geol. Bulletin, v. 51, p. 529-557.

SANGSTER, D.F., 1976, Sulphur and lead isotopes in strata-bound deposits. In: Wolf, K.H. (ed.) Handbook of Stratabound and Stratiform Ore Deposits. v. Elsevier, Amsterdam, p. 219-266.

SANGSTER, D.F., 1983, Mississippi Valley-type deposits: a geological mélange. In: Kisvarsanyi, G.; Grant, S.K.,; Pratt, W.P.; Koenig, J.W. (eds.) Proceedings Volume - International Conference on

Mississippi Valley-type zinc-lead deposits. Univ. Missouri-Rolla Press, Rolla, Missouri, p. 7-19.

SANGSTER, D.F., 1988, Breccia-hosted lead-zinc deposits in carbonate rocks. In: James, N.P. and Choquette, P.W., Paleokarst, New York, Springer Verlag.

SANGSTER, D.F., NOWLAN, G.S., BARNES, C.R., HITCH, M.W., STRONG, D.F. and SAUNDERS, C.M., 1989, Are Mississippi Valley Type (MVT) deposits thermal anomalies?, abstract, Abstracts 28th International Geological Congress, Washington, D.C., v.3, p.18.

SASS, E., and KATZ, A., 1982, The origin of platform dolomites: new evidence. Amer. Jour. Science, v. 282, p. 1184-1213.

SAUNDERS, C.M. and STRONG, D.F., 1986, Assessment of lead-zinc deposits of the western Newfoundland carbonate platform. In: Current Research, Part A, Geol. Surv. of Canada, Paper 86-1A, p. 229-237.

SCHLAGER, W., 1981, The paradox of drowned reefs and carbonate platforms. Geol. Soc. Amer. Bulletin, v. 92, p. 197-211.

SCHLUMBERGER, 1972, Log Interpretation, Vol. 1. Principles, New York, Schlumberger Limited, 113p.

SCHMIDT, V. and MacDONALD, D.A., 1979, The role of secondary porosity in the course of sandstone diagenesis. Soc. Econ. Paleo. Mineral., Spec. Publ. 26, p. 175-207.

SCHOLLE, P.A. and HALLEY, R.B., 1985, Burial diagenesis out of sight, out of mind! In: Schneidermann, N. and Harris, P.M. (eds.) Carbonate Cements. Soc. Econ. Paleo. Mineral., Spec. Publ. 36, p. 309-334.

SCHUCHERT, C. and DUNBAR, C.O., 1934, Stratigraphy of western New-

foundland. Geol. Soc. Amer., Memoir 1, 123p.

SCOTESE, C.R., et. al., 1979, Paleozoic base maps. Jour. of Geology, v. 87, p. 217-268.

SEARLE, M.P.; JAMES, N.P.; CALON,T.J.; and SMEWING, J.D., 1983, Sedimentological and structural evolution of the Arabian continental margin in the Musandam Mountains and Dibba Zone, United Arab Emirates. Geol. Soc. Amer. Bulletin, v. 94, p. 1381-1400.

SECOR, D.T. Jr., 1965, Role of fluid pressure in jointing. Amer. Jour. of Science, v. 263, p. 633-646.

SHEEHAN, P.M. and SCHIEFELBEIN, D.R.J., 1984, The trace fossil Thalassinoides from the Upper Ordovician of the eastern Great Basin: deep burrowing in the early Paleozoic. Jour. of Paleontology, v. 58, p. 440-447.

SHINN, E.A., 1968, Burrowing in recent lime sediments of Florida and the Bahamas. Jour. of Paleontology, v. 42, p. 879-894.

SHINN,E.A., 1986, Modern carbonate tidal flats: their diagnostic features. Colorado School of Mines Quarterly, v. 81, p. 7-35.

SHINN, E.A.; LLOYD, R.M. and GINSBURG, R.N., 1969, Anatomy of a modern carbonate tidal flat, Andros Island, Bahamas. Jour. Sed. Petrology, v. 39, p. 1202-1228.

SHINN, E.A. and ROBBIN, D.M., 1983, Mechanical and chemical compaction in fine-grained shallow-water limestones. Jour. of Sed. Petrology, v. 53, p. 595-618.

SIBLEY, D.F., 1982, The origin of common dolomite fabrics: clues from the Pliocene. Jour. Sed. Petrology, v. 52, p. 1087-1100.

SIBLEY, D.F., 1989, Dolomite stoichiometry, (abstr.), Geological Society of America Abstracts with Programs, p. A221.

SIBSON, R.H.; McMOORE, J. and RANKIN, R.H., 1975, Seismic pumping - a hydrothermal fluid transport mechanism. Jour. Geol. Soc. London, v. 131, p. 653-659.

SIMMS, M., 1984, Dolomitization by groundwater - flow systems in carbonate platforms. Transactions of the Gulf Coast Association of Geological Societies, v. 34, p. 411-420.

SIPPEL, R.F., and GLOVER, E.D., 1964, The solution alteration of carbonate rocks; the effects of temperature and pressure. Geochim. et Cosmochim. Acta, v. 28, p. 1401-1417.

SLOSS, L.L., 1963, Sequences in the cratonic interior of North America. Geol. Soc. Amer. Bulletin, v. 74, p. 93-114.

SPIRAKIS, C.S., 1983, A possible precipitation mechanism for sulfide minerals in Mississippi Valley-type lead-zinc deposits. In: G. Kisvarsanyi, et. al. (ed.) Proceedings Volume International Conference on Mississippi Valley-type Lead-Zinc Deposits. Univ. of Missouri-Rolla, Rolla Missouri, p. 211-215.

SPIRAKIS, C.S.,and HEYL, A.V., 1988, Preference of Mississippi Valley-type ores for Paleozoic rocks: A consequence of conditions for forming potential sulfur source sediments, (abstr.), Geological Society of America Abstracts with Programs, p. A39.

SPIRAKIS, C.S. and HEYL, A.V., 1989, Possible relationships among volcanic ash, pre-ore diagenetic pyrite, and Mississippi Valley-type deposits of southeast Missouri, (abstr.), Geological Society of America Abstracts with Programs, p. A130.

STAIT, K.A., 1988, Upper Canadian to Whiterockian (Ordovician) conodont biostratigraphy of the upper St. George Group, western Newfoundland, unpublished M.Sc. thesis, Memorial University of Newfoundland.

STENZEL, S.R. and JAMES, N.P., 1987, Death and destruction of an early Paleozoic carbonate platform, western Newfoundland (abstr.). In: Abstracts Vol. IV, SEPM Annual Midyear Meeting, Austin, Texas, p. 80.

STENZEL, S.R. and JAMES, N.P., 1988, Foundering and burial of an early Paleozoic carbonate platform, western Newfoundland (abstr.). In: Program with Abstracts, Vol. 13, Joint Annual Meeting, Geol. Assoc. Canada, p. A117.

STENZEL, S.R., KNIGHT, I. and JAMES, N.P., 1990, Carbonate platform to foreland basin; revised stratigraphy of the Table Head Group (Middle Ordovician), western Newfoundland, Canadian Journal of Earth Sciences, Vol. 27, p. 14 -26.

STEVENS, R.K., 1970, Cambro-Ordovician flysch sedimentation and tectonics in west Newfoundland and their possible bearing on a proto-Atlantic Ocean. Geol. Assoc. of Canada, Special Paper 7, p. 165-177.

STEVENS, R.K., and JAMES, N.P., 1976, Large sponge-like mounds from the Lower Ordovician of western Newfoundland (abstr.). Geol. Soc. Amer. Abstracts with Programs, v. 8, p. 1122.

STOUGE, S.S., 1980, Conodonts of the Table Head Formation (Middle Ordovician); western Newfoundland. unpublished Ph. D. thesis, Memorial University of Newfoundland, St. John's, 413p.

STOUGE, S.S., 1982, Preliminary conodont biostratigraphy and correlation of Lower and Middle Ordovician carbonates of the St. George Group, Great Northern Peninsula, Newfoundland. Mineral Develop. Division, Newfoundland Dept. of Mines and Energy, Report 82-3, 59p.

STOUGE, S.S., 1984, Conodonts of the Middle Ordovician Table Head Formation, western Newfoundland. Fossils and Strata, v. 16, 145p.

SVERJENSKY, D.A., 1981a, Isotopic alteration of carbonate host rocks as a function of water to rock ratio - an example from the Upper Mississippi Valley zinc-lead district. Econ. Geology, v. 76, p. 154-172.

SVERJENSKY, D.A, 1981b. The origin of Mississippi Valley-type deposits in the Viburnum Trend, Southeast Missouri. Econ. Geology, v. 76, p. 1848-1872.

SVERJENSKY, D., 1984, Oil field brines as ore-forming solutions. Econ. Geology, v. 79, p. 27-37.

SVERJENSKY, D.A., 1986, Genesis of Mississippi Valley-type lead-zinc deposits. Annual Review Earth Planet. Science, v. 14, p. 177-199.

SWEET, W.C.; ETHINGTON, R.L. and BARNES, C.R., 1971, North American Middle and Upper Ordovician Conodont faunas. Geol. Soc. Amer., Memoir 127, p. 163-193.

SWINDEN, H.S.; LANE, T.E. and THORPE, R.I., 1988, Lead-isotope compositions of galena in carbonate-hosted deposits of western New foundland: evidence for diverse lead sources. Can. Jour. Ear. Science, v. 25, p. 593-602.

TAYLOR, H.P. Jr., 1974, Oxygen and hydrogen isotope evidence for large-scale circulation and interaction between ground waters and

igneous intrusions, with particular reference to the San Juan volcanic field, Colorado. In: Hofmann, B.J., et. al. (eds.) Geochemical Transport and Kinetics. Carnegie Instit. Washington, D.C., p. 299-324.

TAYLOR, H.P., 1977, Water/rock interactions and the origin of H_2O in granitic batholiths. Jour. Geol. Soc. London, v. 133, p. 177.

TAYLOR, H.P. Jr., 1979, Oxygen and hydrogen isotope relationships in hydrothermal mineral deposits. In: Barnes, H.L. (ed.) Geochemistry of Hydrothermal Ore Deposits, New York, John Wiley and Sons, p. 236-277.

TAYLOR, M.; KELLY, W.C.; KESLER, S.E.; McCORMICK, J.E.; RASNICK, F.D. and MELLON, W.V., 1983, Relationship of zinc mineralization in East Tennessee to Appalachian orogenic events. In: G. Kisvarsanyi, et. al. (eds.) Proceedings, International Conference on Mississippi Valley-type lead-zinc Deposits, Rolla, Univ. of Missouri, p. 271-278.

TAYLOR, M.; KESLER, S.E.; CLOKE, P.L. and KELLY, W.C., 1983, Fluid inclusion evidence for fluid mixing. Mascot-Jefferson City Zinc District, Tennessee. Econ. Geology, v. 78, p. 1425-1439.

THODE, H.G. and MONSTER, J., 1965, Sulphur isotope geochemistry of petroleum evaporite and ancient seas. Amer. Assoc. Petrol. Geology, Memoir 4, p. 367-377.

THRAILKILL, J., 1968, Chemical and hydrologic factors in the excavation of limestone caves. Geol. Soc. Amer. Bulletin, v. 79, p. 19-45.

TUACH, J., 1987, Mineralized environments, metallogenesis and the Doucers Valley Fault Complex, western White Bay: A philosophy for

gold exploration in Newfoundland. In: Current Research, Newfoundland Dept. of Mines and Energy, Report 87-1, p. 129-144.

TURNER, J.S., 1974, Double-diffusive phenomena, Annual Review of Fluid Mechanics, v. 6, p.37-74.

TURNER, J.S., 1985, Multicomponent convection, Annual Review of Fluid Mechanics, v.17, p.11-44.

TURNER, J.S. and CAMPBELL, I.H., 1986, Convection and mixing in magma chambers, Earth Science Reviews, v.23, p.255-352.

TURNER, J.S. and CHEN, C.F., 1974, Two-dimensional effects in double-diffusive convection. Jour. Fluid. Mech., v. 63, p. 577-592.

TURNER, R.J.W. and EINAUDI, M.T. (eds.), 1986, The genesis of stratiform sediment-hosted lead and zinc deposits: conference proceedings. Stanford University Publications, Geological Sciences, Vol. XX.

VAIL, P.R.; MITHCUM, R.M. Jr. and THOMPSON, S. III, 1977, Seismic stratigraphy and global changes of sea level. Part 4. Global cycles of relative changes of sea level. In: C.E. Payton (ed.) Seismic stratigraphy applications to hydrocarbon exploration. Amer. Assoc. Petrol. Geology, Memoir 26, p. 83-97.

VAN DER PLUIM, B.A. and KESLER, S.E., 1989, Relationship between Appalachian orogenic events, MVT mineralization and remagnetization, (abstr.), Geological Society of America Abstracts with Programs, p. A226.

VEIZER, J., 1978, Simulation of limestone diagenesis - a model based on strontium depletion: discussions. Can. Jour. Ear. Science, v. 15, p. 1683-1685.

VEIZER, J., 1983, Chemical diagenesis of carbonates: theory and application of trace element technique. In: Arthur, M.A.; Anderson, T.F.; et. al., (eds.) Stable Isotopes in Sedimentary Geology. Soc. Econ. Paleon. Mineral., Short Course No. 10, p. 3-1 - 3-100.

VEIZER, J. and DEMOVIC, R., 1974, Strontium as a tool in facies analysis. Jour. of Sed. Petrology, v. 44, p. 93-115.

VON DER BORCH, C.C., 1977, Stratigraphy and formation of Holocene dolomitic carbonate deposits of the Coorong area, South Australia. Jour. of Sed. Petrology, v. 46, p. 952-966.

VON DER BORCH, C.C. and JONES, B., 1976, Spherular modern dolomite from the Coorong area, south Australia, Sedimentology, v. 23, p. 587 - 591.

VOSS, R.L. and HAGNI, R.D., 1986, The application of cathodoluminescence microscopy to the study of sparry dolomite from the Viburnum Trend, southeastern Missouri. In: Hausen, D.M. and Kopp, O. (eds.) Mineralogy - Applications to the Minerals Industry. Proceedings Paul F. Kerr Memorial Symposium, New York. AIME, p. 51-68.

WALKER, K.R. and LAPORTE, L.F., 1970, Congruent fossil communities from Ordovician and Devonian carbonates of New York. Jour. Paleon., v. 44, p.

WANLESS, H.R., 1979, Limestone response to stress - pressure solution and dolomitization - reply. Jour. of Sed. Petrology, v. 52, p.328-332.

WARD, W.C. and HALLEY, R.B., 1985, Dolomitization in a mixing zone of near-sea water composition, late Pleistocene, northeastern Yucaton Peninsula. Jour. of Sed. Petrology, v. 55, p. 407-420.

WATSON, I.M., 1964, Daniel's Harbour, Nfld. Mike Lake Property, Assessment Work Report. Unpubl. report, Newfoundland Zinc Mines.

WHITE, D.E., 1965, Saline waters of sedimentary rocks. In: Fluids in subsurface environments - a symposium. Amer. Assoc. Petrol. Geologists, Memoir 4, p. 342-366.

WHITE, D.E., 1968, Environments of generation of some base-metal ore deposits. Econ. Geology, v. 63, p. 301-335.

WHITE, D.E.; HEM, J. and WARING, C., 1963, Chemical composition of subsurface waters. U.S. Geol. Survey Prof. Paper 440-F, 67p.

WHITE, W.B., 1969, Conceptual models for carbonate aquifers. Groundwater, v. 7, p. 15-21.

WHITTINGTON, H.B. and KINDLE, C.H., 1963, Middle Ordovician Table Head Formation, western Newfoundland. Geol. Soc. Amer. Bulletin, v. 74, p. 745-758.

WILLIAMS, H., 1978, Tectonic lithofacies map of the Appalachian orogen. Memorial University of Newfoundland, Map 1.

WILLIAMS, H., 1978, Geological development of the northern Appalachians; it's bearing on the evolution of the British Isles. In: D.S. Bowes and B.E. Leake (eds.) Crustal evolution in northwestern Britain and adjacent regions. Seal House Press, Liverpool, England, p. 1-22.

WILLIAMS, H., 1984, Miogeoclines and suspect terranes of the Caledonian-Appalachian orogen: tectonic patterns in the North Atlantic region, Canadian Journal of Earth Sciences, v. 21, p. 887 -901.

WILLIAMS, H., and STEVENS, R.K., 1974, The ancient continental margin of eastern North America. In: C.A. Burk and C.L. Drake. The Geology

of Continental Margins. Springer Verlag, NY, NY, p. 781-796.

WILLIAMS, H.; JAMES, N.P. and STEVENS, R.K., 1986, Humber Arm Allochthon and nearby groups between Bonne Bay and Portland Creek, western Newfoundland. In: Current Research, Part A, Geol. Surv. of Canada, Paper 85-1A, p. 399-406.

WILLIAMS, S.H.; BOYCE, W.D. and JAMES, N.P., 1987, Graptolites from the Lower-Middle Ordovician St. George and Table Head Groups, western Newfoundland, and their correlation with trilobite, brachiopod and conodont zones. Can. Jour. Ear. Sciences, v. 24, p. 456-470.

WILSON, J.L., 1967, Carbonate-evaporite cycles in lower Duperow Formation of Williston basin. Can. Petrol. Geol. Bulletin, v. 15, p. 230-312.

WILSON, J.L., 1975, Carbonate Facies in Geologic History. Springer Verlag, New York, 471p.

WOOD, J.R. and HEWETT, T.A., 1982, Fluid convection and mass transfer in porous sandstones - a theoretical model: Geochim. et Cosmochim. Acta, v. 46, p. 1707-1713.

WOOD, J.R. and HEWETT, T.A., 1984, Reservoir diagenesis and convective fluid flow. In: McDonald, D.A. and Surdam, R.C. (eds.) Clastic Diagenesis. Amer. Assoc. Petrol. Geologists, Memoir 37, p. 99-110.

ZARTMAN, R.E. and DOE, B.R., 1981, Plumbotectonics - the model. Tectonophysics, v. 75, p. 135-162.

ZENGER, D.H., 1983, Burial dolomitization in the Lost Burro Formation (Devonian), east-central California and the significance of late diagenetic dolomitization. Geology, v. 11, p. 519-522.

ZENGER, D.H., 1988, Dolomitization: a critical view of some current

views - discussion. Jour. of Sed. Petrology, v. 58, p. 162-163.

APPENDIX A

Oxygen and Carbon Isotope Data for Dolomites

LITHOLOGY	SAMPLE, SOURCE	$\delta^{18}O$ PDB	$\delta^{18}O$ SMOW	$\delta^{13}C$ PDB
Aguathuna Dololaminite	Haywick, 1984	-5.17 ± .07		-1.38.02
	Haywick, 1984	-7.83 ± .05		-1.86 ± .05
	Haywick, 1984	-6.54 ± .08		-2.70 ± .04
	Coron, 1982	-5.9	+24.1	-1.1
Catoche Fine Dolostone	DH-1254-378.5	-4.48 ± .04		-1.05 ± .02
	DH-1254-342	-4.54 ± .05		-0.94 ± .02
Rock-matrix Breccia	66A	-7.04 ± .04		-0.88 ± .02
	626-629	-6.49 ± .03		-1.10 ± .03
Saddle Dolomite Table Head	DH-1927-TH	-6.81 ± .01		-1.10 ± .03
Saddle Dolomite in Rock-matrix Breccia	DH-66-C	-7.00 ± .03		-1.53 ± .03
Coarse Sparry Dolostone	626-507	-7.70 ± .07		-1.44 ± .04
Catoche Limestone	Coron, 1982	-8.3	+22.30	-1.57
	Coron, 1982	-9.2	+21.4	-1.0
Table Head Limestone	Coron, 1982	-7.8	+22.79	-.78
Aguathuna Limestone	Coron, 1982	-8.7	+21.9	-1.3
Saddle Dolomite A	L7500-5A	-10.51 ± .02		-1.44 ± .03
Saddle Dolomite B	L7500-5B	-7.63 ± .04		-2.77 ± .03
Black Dolomite	L7500-2B	-8.48 ± .07		0.60 ± .03
Gray Dolomite	L7500-4B	-9.01 ± .04		-1.57 ± .01
Pseudobreccia	L7500-4A	-8.41 ± .05		-2.80 ± .03
Pseudobreccia	F11B	-9.15 ± .03		-1.48 ± .04
Saddle Dolomite in vein	F11A	-10.12 ± .03		-1.40 ± .02
Saddle Dolomite A	K1060-9B	-9.38 ± .03		-1.44 ± .02
Saddle Dolomite B	K1060-9A	-7.92 ± .07		-2.24 ± .02
Saddle Dolomite A	T9180-2A	-9.68 ± .02		-1.90 ± .01
Saddle Dolomite B	T9180-1A	-8.84 ± .06		-2.87 ± .02
Late Calcite	L76805	-11.60 ± .07		-3.35 ± .02
Late Calcite	K1060-11	-10.19 ± .03		-4.21 ± .01

APPENDIX B

DOLOMITE GEOCHEMISTRY

SAMPLE	METHOD	% CaO	% MgO	% SiO_2	% Al_2O_3	% Fe_2O_3	% TOTAL Fe	% Na_2O	% K_2O	% MnO	TOTAL ORGANIC CARBON	LOI
PSEUDOBRECCIA	ICP	31.20	20.76	1.68	0.20	0.23		0.04	<0.01	0.03		
FINE DOLOSTONE (CATOCHE FM)	ICP	29.85	20.59	3.04	0.72	0.30		0.48	0.52	<0.02		
3.3M LENGTH OF CATOCHE DOLOSTONE	ICP	20.60 (% Ca)	12.20 (% Mg)		0.14 (%Al)		0.13 (% Fe)	0.05 (% Na)	0.09 (% K)	107 (Mn ppm)		
DOLOLAMINITE	AAS	29.8	18.9	4.0	0.4		0.37	0.02	0.27	0.017		44.13
ROCK-MATRIX BRECCIA	AAS	26.9	17.5	10.6	2.0		0.93	0.03	1.42	0.015		39.45
ROCK-MATRIX BRECCIA BLACK RESIDUE	AAS	16.0	15.5	32.3	4.7		0.91	0.04	2.72	0.18	0.93	27.05
FINE DOLOSTONE	AAS	30.5	20.7	1.7	0.4		0.30	0.03	0.15	0.02		45.64

SAMPLE	METHOD	% CaO	% MgO	% SiO_2	% Al_2O_3	% Fe_2O_3	% TOTAL Fe	% Na_2O	% K_2O	% MnO	TOTAL ORGANIC CARBON	LOI
BLACK COARSE DOLOSTONE	AAS	29.2	19.6	4.2	0.6		0.43	0.03	0.29	0.03	0.30	44.33
COARSE SPARRY DOLOSTONE	AAS	30.5	19.5	1.9	0.5		0.22	0.03	0.19	0.02		45.75
SADDLE DOLOMITE A	AAS	30.4	20.8	0.3	0.0		0.35	0.02	0.01	0.03		46.66
SADDLE DOLOMITE B	AAS	30.0	19.8	0.2	0.0		0.56	0.02	0.01	0.07		47.40
DOLOMITE II (IN LIMESTONE)	PROBE	33.51	18.32	0.39	2.05	0.03		0.11		0.09		
DOLOMITE III (IN LIMESTONE)	PROBE	36.80	19.87	0.00	0.04	0.03		0.36		0.13		
DOLOMITE IV	PROBE	32.13	22.02	0.28	0.34	0.13		0.16		0.06		
DOLOMITE III (IN ROCK-MATRIX BRECCIA)	PROBE	31.17	21.55	0.88	0.20	0.50		0.00		0.01		

SAMPLE	METHOD	% CaO	% MgO	% SiO_2	% Al_2O_3	% Fe_2O_3	% TOTAL Fe	% Na_2O	% K_2O	% MnO	TOTAL ORGANIC CARBON	LOI
SADDLE DOLOMITE A	PROBE	33.27	21.80	0.04	0.00	0.14		0.30		0.11		
SADDLE DOLOMITE A	PROBE	31.95	22.57	0.06	0.00	0.25		0.00		0.06		
SADDLE DOLOMITE A	PROBE	30.40	22.42	0.04	0.00	0.11		0.02		0.04		
SADDLE DOLOMITE B	PROBE	32.68	22.16	0.09	0.00	0.09		0.00		0.12		
SADDLE DOLOMITE B	PROBE	31.66	22.23	0.04	0.00	0.18		0.04		0.09		
DOLOMITE V (COARSE SPARRY DOLOSTONE)	PROBE	30.06	21.29	0.00	0.04	0.22		0.05		0.08		
DOLOMITE V (COARSE SPARRY DOLOSTONE)	PROBE	32.86	21.43	0.31	0.30	0.07		0.20		0.04		

SAMPLE	METHOD	% CaO	% MgO	% SiO_2	% Al_2O_3	% Fe_2O_3	% TOTAL Fe	% Na_2O	% K_2O	% MnO	TOTAL ORGANIC CARBON	LOI
DOLOMITE V (COARSE SPARRY DOLOSTONE)	PROBE	29.60	21.48	0.07	1.28	0.25		0.01		0.01		
DOLOMITE VII (TABLE HEAD)	PROBE	31.98	21.89	0.00	1.32	0.05		0.23		0.01		

APPENDIX C

X-RAY DIFFRACTION DATA FOR DOLOMITES

LITHOLOGY	CRYSTAL TYPE	d_{104} PEAK	ESTIMATED % $CaCO_3$
Dololaminite	I	2.8847	50%
Coarse Dolostone (Aguathuna)	II	2.8716	48-49%
Fine Dolostone (Catoche)	I, II	2.8801	49%
Rock-matrix Breccia	II, III	2.8883	51%
Medium Crystalline Dolostone (Catoche)	II, III, IV	2.8801	49%
Medium Crystalline Gray Dolostone (Catoche)	II, III, IV	2.8892	51%
Coarse Crystalline Black Dolostone (Catoche)	V	2.8847	50%
Saddle Dolomite A	V	2.8847	50%
Saddle Dolomite B	VI	2.8848	50%
Coarse Sparry Dolostone	V	2.8801	50%

APPENDIX D

SULPHUR ISOTOPE DATA

CRYSTAL TYPE (symbols=cement sequence)	LOCATION	SAMPLE NUMBER	$\delta^{34}S$	DUPLICATE
Early Pyrite	vein in Rock Matrix Breccia	DH PY 1	+21.3	
Early Pyrite	T Zone	PY 2	+23.4	
Early Pyrite	K Zone	PY 3	+23.7	
Galena	Lead Lake	Pb 1	+22.0	
Galena	T Zone	Pb 2	+15.0	
Early Red ZnS	Lead Lake	ZN 1	+25.0	
Early Red ZnS	F Zone	ZN 2	+27.4	
Early Brown ZnS	T Zone	ZN 3	+27.6	+28.2
Early Brown ZnS	K Zone	ZN 4	+27.2	
Early Yellow ZnS	F Zone	ZN 5	+24.9	
Early Yellow ZnS	K Zone	ZN 6	+21.0	
Brown after Yellow ZnS	K Zone	DH ZN 7	+25.9	
Late Yellow Brown ZnS	L Zone	ZN 8	+24.5	
Late Yellow Black ZnS	L Zone	ZN 9	+22.4	
Late Yellow Brown ZnS	L Zone	ZN 10	+22.4	
Late Yellow Black ZnS	L Zone	ZN 11	+21.3	+21.2
Late Red ZnS	K Zone	ZN 12	+20.5	
Late Yellow ZnS	Table Head	ZN 13	+21.2	
Gypsum	Rock Matrix Breccia	GYP 1	+ 9.8	
Gypsum	L Zone	GYP 2	+10.5	
Barite	L Zone	BA 1	+26.2	
Celestite	T Zone	CE 1	+28.2	

Unless otherwise noted, analyses are reported in o/oo notation and are computed as follows:

$$^{34}S \text{ sample o/oo} = \left(\frac{^{34}S/^{32}S \text{ sample}}{^{34}S/^{32}S \text{ standard}} - 1 \right) \times 1000$$

Where: $^{34}S/^{32}S$ standard is Canon Diablo troilite

And: $^{34}S/^{32}S = 0.0450045$

A P P E N D I X E

SPHALERITE GEOCHEMISTRY

1. MULTIELEMENT ANALYSES (ICP/INAA)

ELEMENT	ORE CONCENTRATE
Zn%	63.4%
S%	32.9%
Fe%	0.20 - 5.0
Cd ppm	200 - 4000
Pb ppm	650 - 4%
Cu ppm	650 - 3300
Ag ppm	7 - 1000
Ge ppm	80
Ga ppm	7
As ppm	8 - 80
Sn ppm	1 - 50
Sb ppm	0.6 - 60
Ni ppm	10-14
Cr ppm	14 - 18
Co ppm	9 - 10
Mo ppm	7
Hg ppb	20 - 2400
Bi ppm	12 - 23
Tl ppm	0.6

2. PROBE ANALYSES OF SPALERITE CRYSTAL TYPES

SAMPLE	Zn %	S %	Cd %	Fe %	Cu %	Ag %
Early Red (PbL)	61-63.3	37	0.02	3.9-7.0	0.03	0.04
Early Red (F8)	64-65.5	34	0.05	3.9-5.7	0.05	0-0.10
Early Red (DH-C-1)	68.6-70	34	0.09	1.0-2.0	0.11	0-0.10
Tan-Brown (KDC-1)	69	34	0.06	0.40		
Tan-Brown (L10 B)	67	35	0.07	0.43	0.08	0.02
Tan-Brown (UC)	65-67	34	0.07	0.39	0.05	0.08
Tan Brown	67	36	0.07	0.82	0.08	0.03
Yellow (H2)	67	35	0.11	0.17	0.00	0.05
Yellow (NL2)	67.5	35	0.19	0.17	0.02	0.00
Yellow (K 1060)	67	35	0.22	0.24	0.07	0.03
Brown After Yellow (K 1060)	66	35	0.13	1.14	0.04	0.02
Yellow-Brown (L 3700)	66	36	0.40	0.55	0.14	0.04

SAMPLE	Zn %	S %	Cd %	Fe %	Cu %	Ag %
Yellow-Black yellow	66.8	35.4	0.18	0.12	0.08	0.02
Yellow-Black black (3700)	66.4	35.7	0.62	0.36	0.17	0.00
Yellow-Black (L 3800)	68	34	0.37	0.50	0.09	0.03
Yellow-Black yellow (T 1100-2)	70	33.5	0.35	0.15	0.10	0.05
Yellow-Black black (T1100-2)	70	33.5	0.20	0.45	0.10	0.05
Yellow-Black yellow (C-2)	66	35	0.18	0.11	0.08	0.00
Yellow-Black black (C2)	66	34	0.50	0.45	0.13	0.00
Late Red (K 30)	66.6	35.7	0.15	0.27	0.20	0.02

APPENDIX F
FLUID INCLUSION DATA

Crystal Type	Sample No.	% Volume	Te	Tm	Th
Early Yellow ZnS	B-1	0.5	-56°	-32°	
		0.1			110°
		1.0		-34°	
		0.5			170°
		1.0			168°
		1.0			160°
		2.0			170°
		8.0	-53°	-25°	150°
		1.0			175°
		1.5			175°
		2.0			157°
Early Yellow ZnS	H-2	0.5			185°
		0.5			175°
		0.5	-46°	-19.5°	112°
		2.0	-46°	-20°	
Early Yellow ZnS	L6240-2C	1.0	-40°	-15°	150°
		5.0			155°
		2.0			145°
Early Yellow ZnS	L7500-2A	1.5	-45°	-25.5°	125°
		2.0	-45°	-25.5°	145°-150°
Early Yellow ZnS	F23	0.5	-50°	-32°	92°
		0.5	-55°	-30°	
		1.0			115°

Crystal Type	Sample No.	% Volume	Te	Tm	Th
Late Yellow-Brown ZnS	T9170-1A	1.0		141°	
		2.0			165°
		5.0	-30°	-10°	170°
		2.0	-60°	-25°	138°
		5.0			130°
		3.0			125°
Late Yellow-Black ZnS	LWD-3	5.0	-45°	-23°	
		5.0	-45°	-18°	
		5.0	-56°	-22°	144.5°
		5.0	-51°	-21°	120°
		2.0			136°
		1.0			105°
		2.0	-52°	-28°	168°
		2.0	-52°	-26°	
		2.0			130°
		3.0	-52°	-26°	99.5°
		2.0			90°
		2.0			164°
Late Yellow-Black ZnS	T1100	1.0			110°
		2.0			110°
		5.0	-40°	-24°	
		1.0	-40°	-24°	97°

Crystal Type	Sample No.	% Volume	Te	Tm	Th
Early Calcite	1254-407	2.0		-15.5°	
		5.0	-55°	-23.5°	126°
		1.0			75°
		1.0			90°
		1.0			90°
		1.0			107°
		1.0			112°
		1.0	-62°	-17°	109°
		1.0	-62°	-17°	105°
		1.0	-66°	-17°	111°
		1.0	-58°	-17°	
		1.0		-16°	
		1.0	-60°	-20°	115°
		2.0	-52°	-34°	93°
		1.0	-50°	-18°	119°
		2.0	-64°	-18°	
Dolomite III(?)	492-74	1.0		-25°	77°
or		1.0			77°
Late Dolomite		0.5			75°
	Tbx				78°
					78°
					78°
			-60°	-13°	78°

Crystal Type	Sample No.	% Volume	Te	Tm	Th
Saddle Dolomite A (next to ZnS)	L7500-2C	0.5			144°
		0.5			120°
		0.5			127°
		0.5			100°
		1.0			147°
		0.5			128°
		0.5	-55°	-32°	
		0.5			65°
		0.5			137°
Saddle Dolomite A	L-10	1.0			115°
		1.0			117°
Saddle Dolomite A	L7500-1	2.0	-58°	-28°	97°
		2.0			126°
		0.5			92°
		1.0			110°
Saddle Dolomite A	K1060-11C	3.0	-33°	-10°	48°
		2.0			110°
		2.0			130°
		1.0			73°
		2.0			82°
		1.0			78°
		3.0	-47°	-23°	
		3.0	-47°	-18°	70°

Crystal Type	Sample No.	% Volume	Te	Tm	Th
Saddle Dolomite A (Continued)		5.0	-36°	-12°	127°
		5.0			70°
		2.0			120°
		1.0			115°
		0.5			110°
		2.0			105°
		0.5			117°
		0.5			117°
Saddle Dolomite A	L-10	0.5			100°
		0.5			95°
		0.5			107°
Saddle Dolomite A	T1100	0.5			91°
		2.0			125°
	L7500-1	1.0			97°
		0.5			80°
		0.5			109°
		0.5			118°
Late Saddle Dolomite A	K-1060-11D	0.5			97°
		0.5			101°
		1.0			110°
		1.0			112°
		1.0			121°
		1.0			164°

Crystal Type	Sample No.	% Volume	Te	Tm	Th
Late Saddle Dolomite A (continued)	K-1060 11D	2.0	-57°	-24°	101°
		1.0	-48°	-28°	97°
		0.5			133°
Late Saddle Dolomite A	L10	0.5			100°
		0.5			137°
Late Saddle Dolomite A	T100	1.0			135°
		1.0			133°
		0.5			99°
Saddle Dolomite B	L-10	1.0			107°
		1.0			110°
Late Calcite	K1060-11B	3.0	-58°	-40°	53°
		2.0		-10°	165°
		2.0	-50°	-33°	
		3.0	-50°	-38°	59°
		3.0	-58°	-40°	
		2.0	-55°	-36°	105°
		2.0			25°
		3.0	-55°	-36°	45°
		2.0	-55°	-36°	65°
Late Calcite	K1060-11C	2.0	-48°	-34°	76°
		2.0	-48°	-34°	50°
		10.0	-55°	-38°	<20°

Crystal Type	Sample No.	% Volume	Te	Tm	Th
Late Calcite (continued)	K1060-11C	1.0			56°
		0.5			95°
		0.5			58°
		1.0			77°
		1.0			75°

APPENDIX G

Lead Isotope Data from Cambro-Ordovician Carbonate Hosted Galena Crystals

collected and analyzed by Swinden, Thorpe and Lane (1988)

SAMPLE LOCATION, FORMATION (FM)	206/204	207/204	208/204
Daniel's Harbour 84-132	17.857	15.475	38.438
Upper Catoche Formation 84-133	18.124	15.471	38.680
Upper Catoche Formation 84-134	18.116	15.515	38.663
Upper Catoche Formation 84-135	17.983	15.490	38.607
Piccadilly-Table Head Fm.	18.204	15.575	38.292
Frying Pan Pond-Catoche Fm.	17.777	15.462	38.490
Beaver Brook-Petit Jardin Fm.	17.574	15.425	38.231
Cook's Harbour-Catoche Fm.	17.772	15.462	38.517
Hodder-Rattling Brook Fm.	18.436	15.626	38.266
St. John Islands-Table Head Fm.	18.506	15.568	39.299
River of Ponds-Table Head Fm.	19.339	15.613	39.901
Pikes Feeder Road-Petit Jardin Fm.	17.294	15.388	37.871
Eddies Cave-Petit Jardin Fm.	17.431	15.418	37.878

APPENDIX II

STRATIGRAPHIC KEY TO PHOTOGRAPHIC LOGS OF COLLINS (1971)

DRILL HOLE 482, SOUTH OF THE L ZONE, FIG. 1.4

Upper member / Aguathuna Fm. 77 - 83.5 ft. (23.5 - 25.5 m)

Middle member / 83.5-96 ft. (25.5 - 29.5 m)

Lower member / 96 -270.5 ft. (29.3 - 82.5 m)

Markers -

Thick burrowed interval 96 - 137 ft. (25.5 - 41.8 m)

Upper argillite 137.5-140 ft. (42 - 42.7 m)

Breccias above burrowed beds -

at 163.5, 171, 181, 188-193, 215.5, 240.5, 252 ft.

DRILL HOLE 490, SOUTH OF THE L ZONE, FIG. 1.4

Top of the Catoche Fm. 306 ft. (93.3 m)

Worms marker 321-323.5 ft. (97.9 - 98.6 m)

"30" ft. bed below "w. m" 372-376 ft. (113.4-114.6 m)

"66" ft, bed below "w.m." 391-394.5 ft. (119.4-120.3 m)

end of core, 146 ft. below "w.m." 460 ft. (140 m)